

CRYSTALLIZATION AND SEPARATION OF PENTAERYTHRITOL
FROM LUBRICATING OIL DISPERSANT ADDITIVES

A thesis submitted

by

Nadim Abdul Rasool Najim

for the Degree of Doctor of Philosophy

DEPARTMENT OF CHEMICAL ENGINEERING
UNIVERSITY OF ASTON IN BIRMINGHAM

JUNE 1984

THE UNIVERSITY OF ASTON IN BIRMINGHAM
CRYSTALLIZATION AND SEPARATION OF PENTAERYTHRITOL
FROM LUBRICATING OIL DISPERSANT ADDITIVES

N.A.R. NAJIM

Ph.D.

1984

SUMMARY

In the industrial production of a lubricating oil dispersant additive pentaerythritol (PE) is reacted with polyisobutenyl succinic anhydride (PIBSA). The sediment obtained is difficult to separate due to many factors also there is usually an increase in the sediment level during the storage of the product. The main objectives of this work were to improve the solid/liquid separation and to identify and eliminate the cause of the sediment formation during storage. During the course of the investigation the kinetics of the PIBSA/PE reaction were studied in a stirred, 1 dm³ reaction vessel and the results were used to develop an approximate rate expression of the form

$$(-r_A) = k_o \cdot e^{-\frac{E}{RT}} \cdot C_A^a \cdot C_B^b = (r_T)$$

where $(-r_A)$ is the rate of conversion of PIBSA to esters, (r_T) is the rate of formation of esters, C_A and C_B are the concentrations of PIBSA and PE respectively, E is the activation energy of the reaction, and k_o , a , and b are constants. The values of these parameters were found to be as follows: $a = 1.465$, $b = 0.149$, $n = a+b = 1.614$ the overall order of reaction, $E = 7.767$ kcal/gmole, and $k_o = 15312$. Infrared spectroscopy was also used in the kinetic study and the values obtained for the parameters n and a were $n = 1.522$, and $a = 1.283$ which agrees well with the above values.

In the sediment formation investigation the effect of many production variables such as reaction temperature, cooling rate, seeding with PE crystals, holding time at filtration temperature and other factors, on the filtrability of the product, the final CSD of the sediment, and the sediment formation during storage were all investigated. From the results it was concluded that the source of the sediment formation was the unreacted excess pentaerythritol a large portion of which crystallized out on cooling as very fine thin square like plates which were stable at lower storage temperature but which agglomerate at higher temperatures whilst the rest of the PE remained in solution, probably as hydrogen bonded PE.

Among the successfully tested means of producing stable products at storage were; the use of high cooling rates of up to 4.5°C/min., the use of lower reaction temperatures, the use of an extended holding time of up to 65 hrs at the filtration temperature and reheating of the final product before storage to react the small amounts of the excess PE.

Key Words

Pentaerythritol
Polyisobutenyl succinic anhydride
Reaction kinetics
Crystallization from viscous solutions

ACKNOWLEDGEMENT

I would like to express my sincere thanks to Professor P. E. Barker for his invaluable supervision, encouragement, and stimulating advice throughout the entire period of this research, and for the valuable help he provided in the initiation and the continuation of this project.

I would also like to express my appreciation and thanks to the following:

Dr. E. Smith of the Department of Chemical Engineering for his constructive discussions and valuable suggestions during the performance of the reaction kinetic study.

Dr. P. C. Anson of the Esso Research Centre at Abingdon for his help, suggestions and discussions for the major part of this project.

Mr. J. G. Gardiner of the Esso Research Centre in Abingdon, who took over the task from Dr. Anson during the final stages of this work and continued in providing the necessary help.

Mr. R. W. Russell of the Esso Research Centre for his continuous help and cooperation during the whole period of the project, and for his assistance in the performance of the IR spectroscopy analysis at the Esso Research Centre in Abingdon.

The staff at the Esso Research Centre in Abingdon for performing the GC analysis on the sediment samples, and for providing photographs of the sediment using the electron microscope.

The staff of the Paramins plant of Esso Chemicals Ltd. at Fawley Refinery for their help and cooperation provided during the monitoring of the industrial production run of the dispersant additive (6-10/8/1982).

The Department of Chemical Engineering for providing the necessary facilities; in particular the technical staff for their efficient service.

The staff of the Department of Chemistry for their assistance in using the NMR and IR equipment of their department.

The Department of Biology for the use of their ultra-centrifuge equipment.

TABLE OF CONTENTS

	<u>Page</u>
TABLE OF CONTENTS	v
LIST OF TABLES	x
LIST OF FIGURES	xv
CHAPTER ONE - INTRODUCTION	1
CHAPTER TWO - LITERATURE SURVEY	3
2.1 Introduction	3
2.2 Literature on dispersant additives	3
2.2.1 Acylating agents/alcohol dispersants	5
2.2.2 Acylating agents/amine dispersants	7
2.2.3 Acylating agents/reactive metal compound dispersants	9
2.3 Theoretical aspects of reaction kinetics	10
2.3.1 Kinetics of homogeneous reactions	11
2.3.2 Treatment of data from a batch reactor	15
2.4 Crystallization literature	19
2.4.1 Solubility	20
2.4.2 Nucleation	25
2.4.2.1 Primary homogeneous nucleation	25
2.4.2.2 Primary heterogeneous nucleation	26
2.4.2.3 Secondary nucleation	27
2.4.2.3.1 Collision breeding	28
2.4.2.3.2 Dendritic and polycrystalline breeding	30
2.4.2.3.3 Crystal breakage	30
2.4.2.3.4 Other types of secondary nucleation	30
2.4.3 Crystal growth	31
2.4.3.1 Nucleation controlled growth	31
2.4.3.2 Surface dislocation controlled growth	32
2.4.3.3 Diffusion theories	33
2.4.3.4 Factors effecting crystal growth	36
CHAPTER THREE - PREVIOUS WORK ON PENTAERYTHRITOL	39
3.1 Introduction	39
3.2 Crystal morphology and habit	39
3.3 Physical properties	41
3.4 Functionality and chemical reactivity	43
3.5 Chemical analysis	45
3.6 Crystal growth rate	46

	<u>Page</u>
CHAPTER FOUR - PROCESS DESCRIPTION OF PIBSA/PE DISPERSANT ADDITIVES PRODUCTION	49
4.1 Introduction	49
4.2 Raw materials	49
4.2.1 Pentaerythritol	49
4.2.2 Polyisobutenyl succinic anhydride (PIBSA)	50
4.2.3 150 stock diluent base oil	51
4.2.4 Sulphonic acid catalyst	52
4.2.5 Filter aid and filter paper	52
4.2.6 Other chemicals used	54
4.3 PIBSA/PE reaction mechanism	55
4.4 Summary of process description	59
CHAPTER FIVE - THE EXPERIMENTAL RIG	62
5.1 Introduction	62
5.2 Reaction and crystallization section	62
5.2.1 Reaction flask and accessories	62
5.2.2 Heating system and temperature control	63
5.2.3 Temperature measurement	64
5.2.4 Agitation	64
5.3 Filtration section	65
5.3.1 Pressure filter and accessories	65
5.3.2 Heating system and temperature control	66
5.3.3 Temperature measurement	66
CHAPTER SIX - EXPERIMENTAL WORK	74
6.1 Introduction	74
6.2 Reaction kinetics investigation	74
6.2.1 Conditions of kinetic runs	74
6.2.2 Experimental procedure for kinetic runs	76
6.3 Sediment formation investigation	77
6.3.1 Laboratory production of PIBSA/PE dispersant	77
6.3.1.1 Production procedure	77
6.3.1.2 Production variables and conditions	80
6.3.1.3 Product analysis	81
6.3.2 Effect of storage temperature on sediment formation	82
6.3.3 Effect of product dilution on sediment formation	82
6.3.4 Sediment analysis	83
6.3.5 Reheating and refiltration of the final product	84
6.3.6 Refiltration of the product after storage	85
6.3.7 Sediment investigation using an ultra-centrifuge	85
6.3.8 Sediment investigation using Nuclear Magnetic Resonance (NMR)	85
6.4 Infra-red spectroscopy analysis	86
6.4.1 Infra-red spectroscopy in sediment formation investigation	86
6.4.2 Infra-red spectroscopy in reaction kinetic studies	87
6.5 Industrial production run of PIBSA/PE dispersant	87
6.6 Measurement of PE solubility in dilution oil	88
6.7 Microscopic studies of the sediment	90

	<u>Page</u>
CHAPTER SEVEN - PARTICLE SIZE MEASUREMENT	91
7.1 Introduction	91
7.2 Sediment preparation for size measurement	91
7.3 Sieve analysis	93
7.4 Coulter counter analysis	94
7.5 Laser particle size analysis	95
7.6 Ratio of particle sizes measured by laser and sieves	97
CHAPTER EIGHT - RESULTS OF REACTION KINETIC STUDY	98
8.1 Analysis using Total Acid Number (TAN)	98
8.1.1 Theoretical treatment	98
8.1.2 Calculation of reaction mixture density	106
8.1.3 Calculation of the overall order of reaction (n)	108
8.1.4 Calculation of the order of reaction with respect to PIBSA (a)	114
8.1.5 Calculation of the rate constant (k)	121
8.1.6 Calculation of the activation energy of the reaction (E)	124
8.1.7 Water evolved during the esterification reaction	128
8.1.8 Summary of results of TAN method analysis	130
8.2 Analysis using IR spectroscopy	132
8.2.1 Theoretical treatment	132
8.2.2 Calculation of (n) from IR spectroscopy analysis	136
8.2.3 Calculation of (a) from IR spectroscopy analysis	145
CHAPTER NINE - RESULTS OF SEDIMENT FORMATION INVESTIGATION	155
9.1 Product preparation and analysis	155
9.2 Sediment analysis results	164
9.3 Results of the effect of production and storage variables	165
9.3.1 Effect of storage temperature	166
9.3.2 Effect of dilution of product samples with solvents	172
9.3.3 Effect of cooling rate	172
9.3.4 Effect of mixing rate during the cooling stage	172
9.3.5 Effect of mixing during storage	172
9.3.6 Effect of PE/PIBSA equivalent ratio	178
9.3.7 Effect of reaction temperature	178
9.3.8 Effect of reaction time	178
9.3.9 Effect of reheating of final product	178
9.3.10 Effect of refiltration after long storage periods	182
9.3.11 Effect of extended time at filtration temperature	184
9.4 Results of IR spectroscopy in sediment investigation	184
9.5 Results of solubility measurements of PE in the dilution oil	195
9.6 Results of crystal size distribution (CSD) measurements	198
CHAPTER TEN - DISCUSSION OF KINETIC INVESTIGATION RESULTS	211
10.1 Discussion of Total Acid Number method results	211
10.2 Discussion of IR spectroscopy analysis results	228

	<u>Page</u>
CHAPTER ELEVEN - DISCUSSION OF SEDIMENT INVESTIGATION RESULTS	232
11.1 Sediment analysis and possible formation routes	232
11.2 Effect of storage temperature	236
11.3 Effect of product sample dilution with solvents	240
11.4 Effect of reaction time	241
11.5 Effect of reaction temperature	242
11.6 Effect of refiltration after long storage periods	244
11.7 Effect of reheating of the final product	245
11.8 Effect of extended time at filtration temperature	246
11.9 Effect of cooling rate	247
11.10 Discussion of the ultra-centrifuge results	250
11.11 Discussion of IR spectroscopy analysis results	253
11.12 Discussion of crystal size distribution (CSD) results	256
CHAPTER TWELVE - CONCLUSIONS AND SUGGESTIONS FOR FUTURE WORK	266
12.1 Conclusions of the reaction kinetic study	266
12.2 Conclusions of the sediment formation investigation	268
12.3 Suggested methods for the elimination of the sediment formation	270
12.4 Matters worthy of future investigation	271
APPENDICES	
APPENDIX 1 - Production of PIBSA/PE dispersant at Fawley	274
APPENDIX 2 - Conditions of sediment investigation runs	286
APPENDIX 3 - Procedure for the Total Acid Number calculation	294
APPENDIX 4 - Outline of the sediment test method	305
APPENDIX 5 - Kinematic viscosity measurement	307
APPENDIX 6 - Detailed calculations performed on a number of kinetic runs	313
APPENDIX 7 - Calculation of the theoretical projected area diameter of pentaerythritol crystal	365
APPENDIX 8 - Experimental measurement results for crystal size distribution analysis	370
APPENDIX 9 - Listing of the computer program developed for the evaluation of the final crystal size distribution and its parameters for the final crystalline sediment	375
APPENDIX 10 - Graphs of crystal size distribution of the sediment for a chosen number of runs	383

	<u>Page</u>
APPENDIX 11 - Microscope photographs of the dispersant product from different production runs	392
APPENDIX 12 - Electron microscope photographs of the sediment from different production runs	397
APPENDIX 13 - Nomenclature used in the thesis	409
REFERENCES	416

LIST OF TABLES

		<u>Page</u>
Table 3.1	Reticular densities of PE crystals.	41
Table 4.1	Properties of PIBSA used in the laboratory preparations of PIBSA/PE dispersant.	51
Table 4.2	Properties of the diluent base oil used in the laboratory preparations of the dispersant.	52
Table 6.1	Summary of conditions of all the kinetic runs.	75
Table 7.1	Main features of the different techniques of particle size measurement.	91
Table 8.1	Densities of reaction mixtures of different runs carried out at different reaction temperatures.	109
Table 8.2	Sample weight measurements and titration results for run 39.	109
Table 8.3	The slope of TAN vs. time curve at different points, for run 39.	110
Table 8.4	Sample weight measurements and titration results for run 44.	116
Table 8.5	The slope of TAN vs. time curve at different points for run 44.	118
Table 8.6	The values obtained for the order of reaction with respect to PIBSA (a).	119
Table 8.7	Summary of the values obtained for the constants (a) and (k) at 200°C.	124
Table 8.8	Summary of the rate constant (k) values obtained at different temperatures.	125
Table 8.9	Water evolved during the esterification reaction in some of the kinetic runs.	129
Table 8.10	Summary of some of the results obtained from all the kinetic runs using the Total Acid Number method analysis.	131
Table 8.11	Characteristic peak heights of run 45 samples analysed by IR spectroscopy.	138
Table 8.12	Final summary of characteristic peak heights for run 45 samples analysed by IR spectroscopy.	139

		<u>Page</u>
Table 8.13	The slope of the ester peak height vs. time curve, measured at five different points for run 45 samples.	143
Table 8.14	Characteristic peak heights for run 43 samples analysed by IR spectroscopy.	147
Table 8.15	Final summary of characteristic peak heights for run 43 samples analysed by IR spectroscopy.	148
Table 8.16	The slope of the ester peak height vs. time curve measured at five different points, together with corresponding values of y and x for run 43.	152
Table 9.1	Run 29 sample weight measurements and titration results.	156
Table 9.2	Run 29 filtration results.	158
Table 9.3	Results of product analysis of all the runs.	162
Table 9.4	Results of sediment analysis by gas chromatography.	165
Table 9.5	Results of melting point measurement for the sediment obtained.	165
Table 9.6	Effect of storage temperature on sediment formation for Fawley Batch.	167
Table 9.7	Centrifuge test results for samples with two successive storage periods.	170
Table 9.8	Summary of results of viscosity changes during storage.	171
Table 9.9	Summary of centrifuge test results for product samples diluted with, dilution oil, heptane or chlorobenzene.	173
Table 9.10	Summary of centrifuge test results for undiluted product samples of runs 13, 21, 34, 35, 52 and 54.	174
Table 9.11	Centrifuge test results for product samples of runs 55, 56 and 57.	176
Table 9.12	Centrifuge test results for product samples of runs 58, 59 and 60.	177
Table 9.13	Sediment test results for Fawley Batch, using mixing during storage.	178
Table 9.14	Centrifuge test results for product samples of runs 27 and 28.	179
Table 9.15	Centrifuge test results for product samples of runs 30, 31 and 32.	180
Table 9.16	Centrifuge test results for product samples of runs 6, 15 and 16.	181

		<u>Page</u>
Table 9.17	Conditions and product analysis of the reheating stage of runs 33, 34 and 35.	182
Table 9.18	Centrifuge test results for the reheated products of runs 33, 34 and 35.	183
Table 9.19	Centrifuge test results for refiltered product samples of run 14 and a mixture of runs 17, 18 and 19 products.	184
Table 9.20	Centrifuge test results for product samples of runs 9, 26, 29, 51 and 53.	185
Table 9.21	Approximate solubility of PE in the diluent oil.	195
Table 9.22	Results of laser analysis for the eight samples of known sieve fraction.	200
Table 9.23	Summary of the values obtained for the ratio of (d_s/d_p) for the eight samples of known sieve fractions.	201
Table 9.24	Calculation of the ratio of (d_s/d_p) for Sample No. 3 from laser analysis results.	202
Table 9.25	Sieve analysis results for run 34 large crystals fraction.	203
Table 9.26	Malvern laser analysis results for run 34 fine crystals.	204
Table 9.27	The final crystal size distribution for run 34 sediment.	207
Table 9.28	Summary of the results and parameters of the final crystal size distribution obtained for the sediment of the fourteen runs.	210
Table 10.1	The slope of TAN vs. time curve at different points for run 39 assuming an initial TAN value, TAN^0 , of 28.2 mgkoH/g.	213
Table 10.2	The values of the slope of TAN vs. time curve measured at five different points, together with the calculated values of y and x for run 42, with $\alpha = 1.25$, $n = 2.52$ and $TAN^0 = 28.2$ mgkoH/g.	216
Table 10.3	The slope of TAN vs. time at different points for run 39, with an initial TAN value of 28.2 mgkoH/g.	219
Table 12.1	The approximate solubility of PE in the dilution oil.	269

		<u>Page</u>
Table A1.1	Samples taken and analysis results for kinematic viscosity, for Fawley Batch.	278
Table A1.2	First filtration run details and conditions for Fawley Batch.	279
Table A1.3	Filtration rates for successive increments of first filtration run for Fawley Batch.	280
Table A2.1	Conditions of runs carried out during the sediment investigation experimental program.	288
Table A3.1	Sample size required for each TAN mgkoH/g range expected.	295
Table A3.2	pH titration of the blank 50cm ³ chlorobenzene with 0.1 N base.	296
Table A3.3	pH titration of Benzoic acid sample in 50cm ³ chlorobenzene against the 0.1 N base.	298
Table A3.4	Summary of the titration methods used and of the standardisation results of TBAH base.	303
Table A5.1	Summary of viscometers calibration results.	312
Table A6.1	Sample weight measurements and titration results for run 36.	314
Table A6.2	The slope of TAN vs. time curve at different points for run 36.	316
Table A6.3	Weight measurements of samples and their titration results for run 42.	320
Table A6.4	The values of the slope of TAN vs. time curve measured at five different points, together with the calculated values of y and x for run 42.	323
Table A6.5	Weight measurements of samples and their titration results for run 43.	326
Table A6.6	The values of the slope of TAN vs. time curve measured at five different points, together with the calculated values of y and x for run 43.	329
Table A6.7	Weight measurements of run 46 samples and their titration results.	333
Table A6.8	The slope of TAN vs. time curve measured at five different points for run 46.	332
Table A6.9	Weight measurements of run 47 samples and their titration results.	338

		<u>Page</u>
Table A6.10	The slope of TAN vs. time curve measured at five different points for run 47.	340
Table A6.11	Weight measurements for run 48 samples and their titration results.	343
Table A6.12	The slope of TAN vs. time curve measured at five different points for run 48.	345
Table A6.13	Run 49 samples and their potentiometric titration results.	348
Table A6.14	The slope of TAN vs. time curve measured at five different points for run 49.	350
Table A6.15	Comparison between run 39 and run 49 sample TAN values.	353
Table A6.16	Comparison between the values of (n) and (k) obtained from runs 39 and 49.	354
Table A6.17	Weight measurements of run 50 samples and their titration results.	355
Table A6.18	The slope of TAN vs. time curve measured at five different points for run 50.	357
Table A6.19	Weight measurements for run 63 samples and their titration results.	360
Table A6.20	The slope of TAN vs. time curve measured at five different points for run 63.	362
Table A8.1	Weight measurements of large and fine crystals fractions carried out for the sediment of all fourteen runs for CSD analysis.	370
Table A8.2	Sieve analysis results for the sediment of runs 34, 35, 51, 52, 53, 54 and 55.	371
Table A8.3	Sieve analysis results for the sediment of runs 56, 57, 58, 59, 60, 61 and 62.	372
Table A8.4	Lazer analysis results for the sediment of runs 34, 35, 51, 52, 53, 54 and 55.	373
Table A8.5	Lazer analysis results for the sediment of runs 56, 57, 58, 59, 60, 61 and 62.	374

LIST OF FIGURES

	<u>Page</u>	
Figure 2.1	Saturation-supersaturation diagram	21
Figure 3.1	Pentaerythritol crystal shape and structure	42
Figure 5.1	The schematic diagram of the experimental rig	68
Figure 5.2	Overall view of the experimental rig used in the laboratory preparation of the PIBSA/PE dispersant	71
Figure 5.3	Close-up view of the reaction and crystallization vessel and the heated pressure filter	72
Figure 5.4	Close-up view showing the details of the inside of the pressure filter top and bottom flanges	73
Figure 8.1	Graph of density of initial reaction mixture g/cm ³ vs. temperature °C	107
Figure 8.2	Graph of run 39 of TAN mgkoH/g vs. time hr since PE addition	111
Figure 8.3	Graph for run 39 of log (-d(TAN)/dt) vs. log(TAN-3.0)	112
Figure 8.4	Graph for run 39 of log(-d(TAN)/dt) vs. log(TAN)	113
Figure 8.5	Graph for run 44 of TAN mgkoH/g vs. time hr from PE addition	117
Figure 8.6	Graph for run 44 of log [$\frac{-d(\text{TAN})/dt}{(\text{TAN}_R + (\alpha-1)\text{TAN}_R^0)^n}$]	120
	vs. log [$\frac{\text{TAN}_R}{\text{TAN}_R + (\alpha-1)\text{TAN}_R^0}$]	
Figure 8.7	Graph of lnk vs. 1/T k ⁻¹	127
Figure 8.8	IR traces for samples No. 2 and No. 5, and the trace of their difference, for run 45	137
Figure 8.9	Graph for run 45 of ester peak height vs. time hr after PE addition, using IR spectroscopy analysis	140
Figure 8.10	Graph for run 45 of total acid (anhydride + free acid) peak height mm vs. time hr after PE addition, using IR spectroscopy analysis	141

	<u>Page</u>	
Figure 8.11	Graph for run 45 of hydroxyl peak height mm vs. TAN mgkoH/g using IR spectroscopy analysis	142
Figure 8.12	Graph for run 45 of $\log (dP_e/dt)$ vs. $\log (P_a)$ (dP_e/dt) is the slope of the ester peak height P_e mm vs. time hr. P_a is the total acid peak height mm	144
Figure 8.13	IR traces for samples No. 2 and No. 4, and the trace of their difference for run 43	146
Figure 8.14	Graph for run 43 of ester peak height P_e mm vs. time hr, using IR spectroscopy	149
Figure 8.15	Graph for run 43 of total acid peak height P_a mm vs. time hr, using IR spectroscopy analysis	150
Figure 8.16	Graph for run 43 of hydroxyl peak height mm vs. TAN mgkoH/g, using IR spectroscopy analysis	151
Figure 8.17	Graph for run 43 of $\log \left[\frac{(dP_e/dt)}{(P_a + (\alpha-1)P_a^0)^n} \right]$ vs. $\log \left[\frac{P_a}{(P_a + (\alpha-1) P_a^0)} \right]$	154
Figure 9.1	Graph for run 29 of TAN mgkoH/g vs. time hr after PE addition	157
Figure 9.2	Graph for run 29 of filtrate volume cm^3 vs. filtration time (min)	159
Figure 9.3	Graph for Fawley Batch of sediment content volume % vs. storage period (days)	168
Figure 9.4	Graph for Fawley Batch of sediment level volume % attained after 62 days of storage vs. storage temperature $^{\circ}\text{C}$	169
Figure 9.5	IR traces of samples No. 1 and No. 2 and their difference trace. Sample No. 1 is Fawley Batch stored at ambient for 168 days, sample No. 2 is Fawley Batch stored at 50°C for 168 days	187
Figure 9.6	IR traces of samples No. 1 and No. 3 and their difference trace. Sample No. 1 is Fawley Batch stored at ambient for 168 days, sample No. 3 is Fawley Batch stored at 90°C for 168 days	188
Figure 9.7	IR traces of samples No. 1 and No. 4 and their difference trace. Sample No. 1 is Fawley Batch stored at ambient for 168 days, sample No. 4 is Fawley Batch stored at 120°C for 95 days	189

	<u>Page</u>	
Figure 9.8	IR traces of sample No. 1 and No. 5 and their difference trace. Sample No. 1 is Fawley Batch stored at ambient for 168 days, sample No. 5 is Run 33 product stored at ambient for 69 days	190
Figure 9.9	IR traces of samples No. 1 and No. 6 and their difference trace. Sample No. 1 is Fawley Batch stored at ambient for 168 days, sample No. 6 is Run 33 reheated product stored at 90°C for 69 days	191
Figure 9.10	IR traces of samples No. 1 and No. 7 and their difference trace. Sample No. 1 is Fawley Batch stored at ambient for 168 days, sample No. 7 is Run 31 product stored at 50°C for 90 days	192
Figure 9.11	IR traces of samples No. 1 and No. 8 and their difference trace. Sample No. 1 is Fawley Batch stored at ambient for 168 days, sample No. 8 is a standard dispersant produced at Fawley	193
Figure 9.12	IR traces of samples No. 5 and No. 6 and their difference trace. Sample No. 5 is run 33 product stored at ambient for 69 days, sample No. 6 is Run 33 reheated product stored at 90°C for 69 days	194
Figure 9.13	Graph of solubility of PE in dilution oil $\times 10^2$, as gPE/100g oil vs. temperature °C	196
Figure 9.14	Graph for run number 34 of mass fraction in band vs. mean of band μm	208
Figure 9.15	Graph for run number 34, of cumulative undersize fraction vs. aperture size μm	209
Figure 10.1	Graph for run 39 of $\log(-d(\text{TAN})/dt)$ vs. $\log(\text{TAN})$ for initial TAN value of 28.2 mgkoH/g	215
Figure 10.2	Graph for run 42 of $Y = \log \left[\frac{-d(\text{TAN})/dt}{(\text{TAN} + (\alpha-1)\text{TAN}^0)^n} \right]$ vs. $X = \log \left[\frac{\text{TAN}}{\text{TAN} + (\alpha-1)\text{TAN}^0} \right]$, with $n = 2.52$, and $\text{TAN}^0 = 28.2 \text{ mgkoH/g}$	217
Figure 10.3	Graph for run 39 of $\log(-d(\text{TAN})/dt)$ vs. $\log(\text{TAN} - 3.0)$, with $\text{TAN}^0 = 28.2 \text{ mgkoH/g}$	220
Figure A1.1	Schematic diagram of reactor vessel and its associated pipework	281
Figure A1.2	Graph of kinematic viscosity $\text{m}^2/\text{s} \times 10^{-6}$ at 100°C vs. time hr from end of PE addition, for the Fawley Batch production	282

	<u>Page</u>	
Figure A1.3	Graph of kinematic viscosity $m^2/s \times 10^{-6}$ at $100^\circ C$ vs. time hr from start of PE addition, for the Fawley Batch production	283
Figure A1.4	Graph of filtrate volume m^3 vs. time hr, for filtration run No. 1, for Fawley Batch production	284
Figure A1.5	Graph of filtration rate m^3/hr vs. time hr, for filtration No. 1, for Fawley Batch production	285
Figure A3.1	Graph of pH vs. volume of (TBAH) base added cm^3 , for blank titration of $50 cm^3$ of chlorobenzene	297
Figure A3.2	Graph of pH vs. volume of base added cm^3 , for the standardisation of the (TBAH) base with Benzoic acid	299
Figure A6.1	Graph for run 36 of TAN mgkoh/g vs. time hr	315
Figure A6.2	Graph for run 36 of $\log (-d(TAN)/dt)$ vs. $\log (TAN-2.0)$	317
Figure A6.3	Graph for run 36 of $\log (-d(TAN)/dt)$ vs. $\log(TAN)$	318
Figure A6.4	Graph for run 42 of TAN mgkoh/g vs. time hr	321
Figure A6.5	Graph for run 42 of $Y = \log \left[\frac{-d(TAN)/dt}{(TAN_R + (\alpha-1)TAN_R^0)^n} \right]$	
	vs. $X = \log \left[\frac{TAN_R}{TAN_R + (\alpha-1) TAN_R^0} \right]$	324
Figure A6.6	Graph for run 43 of TAN mgkoh/g vs. time hr	328
Figure A6.7	Graph for run 43 of $Y = \log \left[\frac{-d(TAN)/dt}{(TAN_R + (\alpha-1)TAN_R^0)^n} \right]$	
	vs. $X = \log \left[\frac{TAN_R}{TAN_R + (\alpha-1)TAN_R^0} \right]$	331
Figure A6.8	Graph for run 46 of TAN mgkoh/g vs. time hr	334
Figure A6.9	Graph for run 46 of $\log (-d(TAN)/dt)$ vs. $\log (TAN-3.0)$	335
Figure A6.10	Graph for run 47 of TAN mgkoh/g vs. time hr	339
Figure A6.11	Graph for run 47 of $\log (-d(TAN)/dt)$ vs. $\log (TAN-3.0)$	341
Figure A6.12	Graph for run 48 of TAN mgkoh/g vs. time hr	344

	<u>Page</u>	
Figure A6.13	Graph for run 48 of $\log(-d(\text{TAN})/dt)$ vs. $\log(\text{TAN}-3.0)$	346
Figure A6.14	Graph for run 49 of TAN mgkoH/g vs. time hr	349
Figure A6.15	Graph for run 49 of $\log(-d(\text{TAN})/dt)$ vs. $\log(\text{TAN}-3.0)$	351
Figure A6.16	Graph for run 50 of TAN mgkoH/g vs. time hr.	356
Figure A6.17	Graph for run 50 of $\log(-d(\text{TAN})/dt)$ vs. $\log(\text{TAN}-3.0)$	358
Figure A6.18	Graph for run 63 of TAN mgkoH/g vs. time hr	361
Figure A6.19	Graph for run 63 of $\log(-d(\text{TAN})/dt)$ vs. $\log(\text{TAN}-3.0)$	364
Figure A7.1	Two pyramids of the total eight in each PE crystal	365
Figure A7.2	The projected area of a PE crystal	366
Figure A7.3	The estimation of the value of the unknown y in the projected area of the PE crystal	367
Figure A7.4	The estimation of the value of the unknown x in the projected area of the PE crystal	369
Figure A10.1	Graph for run No. 51 of mass fraction in band vs. mean of band μm	384
Figure A10.2	Graph for run No. 51 of cumulative under size fraction vs. aperture size μm	385
Figure A10.3	Graph for run No. 52 of mass fraction in band vs. mean of band μm	386
Figure A10.4	Graph for run No. 52 of cumulative under size fraction vs. aperture size μm	387
Figure A10.5	Graph for run No. 55 of mass fraction in band vs. mean of band μm	388
Figure A10.6	Graph for run No. 55 of cumulative under size fraction vs. aperture size μm	389
Figure A10.7	Graph for run No. 59 of mass fraction in band vs. mean of band μm	390
Figure A10.8	Graph for run No. 59 of cumulative under size fraction vs. aperture size μm	391
Figure A11.1	A 1mm scale of 0.01 mm subdivisions. Each subdivision of the superimposed scale represents 1.175 μm	393
Figure A11.2	Run 33 product sample, each subdivision represents 1.175 μm	393

	<u>Page</u>
Figure A11.3 Run 33 reheated product sample, each subdivision represents 1.175 μm	394
Figure A11.4 Run 52 product sample, showing agglomerates of PE crystals, each subdivision represents 1.175 μm	394
Figure A11.5 Run 55 product sample, each subdivision represents 1.175 μm	395
Figure A11.6 Run 59 product sample, showing agglomerates of PE crystals, each subdivision represents 1.175 μm	395
Figure A11.7 Fawley Batch product sample, each subdivision represents 1.175 μm	396
Figure A12.1 Run 33 large crystals fraction sediment	398
Figure A12.2 Run 33 large crystals fraction sediment	398
Figure A12.3 Run 33 fine crystal fraction sediment	399
Figure A12.4 Run 33 fine crystal fraction sediment	399
Figure A12.5 Run 51 large crystals fraction sediment	400
Figure A12.6 Run 51 large crystals fraction sediment	400
Figure A12.7 Run 51 large crystals fraction sediment	401
Figure A12.8 Run 51 large crystals fraction sediment	401
Figure A12.9 Run 51 fine crystals fraction sediment	402
Figure A12.10 Run 52 fine crystals fraction sediment	402
Figure A12.11 Run 53 fine crystals fraction sediment	403
Figure A12.12 Run 54 fine crystals fraction sediment	403
Figure A12.13 Run 55 fine crystals fraction sediment	404
Figure A12.14 Run 56 fine crystals fraction sediment	404
Figure A12.15 Run 57 fine crystals fraction sediment	405
Figure A12.16 Run 58 fine crystals fraction sediment	405
Figure A12.17 Run 59 fine crystals fraction sediment	406
Figure A12.18 Run 59 fine crystals fraction sediment	406
Figure A12.19 Run 59 large crystals fraction sediment	407
Figure A12.20 Run 60 fine crystals fraction sediment	407
Figure A12.21 Sediment collected from centrifuge tubes after tests carried out on stored products	408
Figure A12.22 Sediment collected from centrifuge tubes after tests carried out on stored products	408

CHAPTER ONE

INTRODUCTION

Pentaerythritol, $C(CH_2OH)_4$, is a polyhydric alcohol which has four primary hydroxyl groups arranged compactly around a central carbon atom⁽¹⁾. Pentaerythritol is a unique and superior member of the polyol family, which includes the glycols, glycerine, and sorbitol, due to its structural configuration and its functionality. Pentaerythritol is mainly used in the production of alkyd resins, which are polymers of polybasic acids and polyhydric alcohols, modified with drying or non-drying oils or fatty acids to produce the final desired properties⁽²⁾. Soluble carboxylic esters of pentaerythritol have a large industrial application, some of these esters can act as non-corrosive, oil soluble dispersants and detergents, which retard piston ring sticking and prevent the deposition of lacquer in engines^(1,3). The natural properties of lubricating oils are greatly improved and their active life is prolonged by the use of additives in general. The functions of dispersant additive in particular are to suspend the sludge, markedly reduce the size of the sludge particles, minimize varnish deposits, and neutralize combustion acids.

In the industrial production of certain dispersant additives for lubricating oils, Pentaerythritol (PE) is reacted with Polyisobutenylsuccinic anhydride (PIBSA), which is an important intermediate in the manufacture of lube oil additives and in its own right since it is used as an oil soluble corrosion inhibitor⁽⁴⁾. These raw PIBSA/PE dispersants contain sediment characterised by the following

- a - The sediment level is high, 1-3 volume %.
- b - The sediment is partially soluble in the product at high temperatures.
- c - The raw product viscosity is high at lower temperatures.

- d - The bulk of the sediment is crystalline and the particle size distribution depends on the cooling profile after the reaction stage.

These factors combine to make the solid/liquid separation more difficult than for other dispersants.

Another problem encountered with these PIBSA/PE dispersants is that the sediment level of the finished dispersant product increases with time during the storage of the product in tanks. This increase of the sediment level together with the difficulty of the solid/liquid separation⁽⁵⁾ warrant special attention to be given to these PIBSA/PE dispersants.

The main objectives of this research work were:

- 1 - To study the crystallization characteristics of pentaerythritol in the reaction product with a view to improving the filtrability of the dispersant product.
- 2 - To identify the cause of the sediment formation during the storage of the final dispersant product.
- 3 - To propose and test means for the elimination of this sediment formation.

CHAPTER TWO
LITERATURE SURVEY

2.1 Introduction

Polyisobutenyl succinic anhydride esters of pentaerythritol (PIBSA/PE) esters) are one type of oil soluble dispersants in lubricating oils. Their production involves, apart from the PIBSA/PE esterification reaction, the crystallization and separation of the excess pentaerythritol from the reaction mixture. In this chapter the literature review will be focussed on:

1. Dispersant additives and methods for their formulation.
2. Theoretical aspects of reaction kinetics.
3. Theoretical aspects of crystallization.

2.2 Literature on dispersant additives

Well refined lubricating oils which contain oil-soluble carboxylic acids or their substituted derivatives such as anhydrides, acid chlorides or esters, are remarkably stable in addition to having a valuable property of positively retarding piston ring sticking as well as being carbon softeners⁽³⁾. The oil soluble carboxylic dispersants have a characterising feature, with respect to molecular structure, which is the presence of a hydrocarbon-based radical having a number average molecular weight of over 1000 attached to a polar group^(6,7). The mechanism by which the dispersant acts is primarily a physical process, and that is by attracting the sludge particle by polar forces. The oil solubility of the dispersant keeps the sludge suspended.

The carboxylic acids or polycarboxylic acids substituted with

a fairly saturated hydrocarbon chain containing at least 30 to 50 carbon atoms, or their substituted derivatives such as anhydrides, acid chlorides, and esters are termed acylating agents, and are prepared by reacting an ethylenically unsaturated carboxylic acid, or an anhydride, an halide, or an alkyl ester of the acid, with an unsaturated polyolefin chain^(7,8). The requirement that the acylating agent have at least 30 aliphatic carbon atoms is based not only upon the consideration of oil solubility but also upon the effectiveness of the dispersant as an additive for the purpose indicated, e.g., a dispersant having improved demulsifying characteristics^(9,10,11). Moreover it is preferred also that the hydrocarbon substituent of the acylating agent be substantially saturated, e.g., at least about 95% of the total number of carbon-to-carbon covalent linkages are substantially saturated linkages^(8,9,10,11,12). Preferred olefin polymers for reaction with the unsaturated carboxylic acids or their derivatives are polymers comprising a major molar amount of C₂ to C₅ monoolefin, e.g., ethylene, propylene, butylene, isobutylene and pentene^(8,11,12). The polymers can be homopolymers such as polyisobutylene, as well as copolymers of two or more of such olefins⁽¹²⁾. An especially valuable starting material for a highly potent dispersant additive are polyalkenes with an average molecular weight of about 1200 to 5000 with approximately one terminal double bond per polymer chain, e.g., polyisobutylene^(7,8,11,12).

As the carboxylic acid moiety, ethylenically unsaturated carboxylic compounds may be employed including monoacids, such as acrylic acid; diacids, such as maleic acid, fumaric acid, their anhydrides or their chlorinated derivatives. Succinic anhydride and succinic acid both substituted by a fairly saturated hydrocarbon group containing at least

50 carbon atoms (as was discussed above) are the preferred acylating agents^(7,8,11,12). They are easily obtained by reaction of maleic acid or anhydride with a polyolefin, such as polybutylene, polyisobutylene, polypentene, etc.^(7,8).

An important example of an acylating agent is polyisobutylene succinic anhydride (PIBSA) which is the reaction product of polyisobutylene with maleic anhydride⁽⁴⁾ (see also Chapter Four). Although the acylating agents (including PIBSA) can be used in their own right as oil soluble additives, but their principle use is as intermediates in processes for preparing carboxylic derivative compositions as dispersant additives. These carboxylic dispersant additives are most often prepared by reacting one or more acylating agents with a reactant selected from the following groups^(6,7,11)

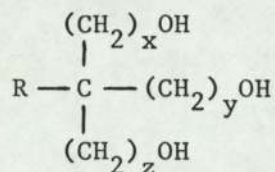
- a - alcohol
- b - amine characterised by the presence within its structure of at least an H-N< group
- c - reactive metal or reactive metal compounds
- d - a combination of two or more of (a) through (c), the components of (d) being reacted with said acylating agents simultaneously or sequentially in any order.

2.2.1 Acylating agents/alcohol dispersants

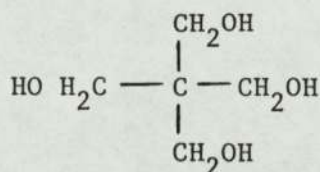
Alcohols which can be used as (a) above include the monohydric and polyhydric alcohols. The polyhydric alcohols are preferred since they usually result in carboxylic derivative compositions which are more effective dispersant/detergents relative to carboxylic derivative compositions derived from monohydric alcohols^(3,6,7). These alcohols as esterification agents for the acylating reagents may vary greatly

and may include aliphatic monoalcohols, such as methyl, ethyl, propyl alcohols, fatty alcohols, etc.; aromatic or cycloaliphatic monoalcohols, such as benzyl alcohol, cyclohexanol, etc.; polyalcohols, such as ethylene glycol, propylene glycol, diethylene glycol, glycerol, pentaerythritol, sorbitol, etc.; and partially esterified esters of those polyols. Hydroxyaromatic compounds, such as the phenolic compounds, may be employed as esterification agents, they include phenol, the cresols, naphols, alkylphenols, halogenated phenols, and diphenols^(6,7,8).

These esters are desired by esterification of at least one and preferably more of the hydroxy radicals for the polyhydric alcohols having a neo-carbon atom; a neo-carbon atom being defined as one that is attached directly to four other carbon atoms⁽³⁾. Symmetrical alcohols having short equal length carbon chains linking hydroxyl radicals to the neo-carbon atom appear to be the most effective carbon softeners. Alcohols containing a neo-carbon atom are represented by the formula:



where x, y and z are whole numbers, preferably one, and R may be aliphatic, aromatic, alicyclic or hetrocyclic..., preferably x, y and z = 1, and the R group is the carbinol group as is the case in pentaerythritol which is especially preferred^(3,6,12).

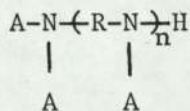


(pentaerythritol)

2.2.2 Acylating agents/amine dispersants

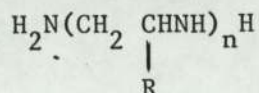
The amine that can be used for preparing carboxylic derivative compositions, characterised by the presence within its structure of at least one H-N< group, can be a monoamine or polyamine compound. Polyamines are preferred to monoamines especially if they contain at least two H-N< groups, either or both of which are primary or secondary amines. The polyamines not only result in carboxylic acid derivative compositions which are usually more effective as dispersant/detergent additives, but these preferred polyamines result in carboxylic derivative compositions which exhibit more pronounced V.I. improving properties^(6,7,11). The amines can be aliphatic, cycloaliphatic, aromatic or heterocyclic, including also any of these types substituted with any one of the others listed. Examples of suitable monoamines are ethylamine, diethylamine, n-butylamine, di-n-butylamine, isobutylamine, etc., aniline, methylaniline, diphenylamine, benzylamine, etc.^(6,7).

Among the preferred polyamines are alkylene polyamines, including those having the formula

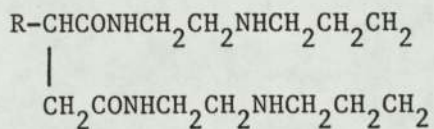


where n is an integer preferably between 2 and 8; each A is independently hydrogen or a hydrocarbon or hydroxy-substituted hydrocarbon radical; and R is a divalent hydrocarbon radical, preferably a lower alkylene radical having 2 - 6 carbon atoms. Especially preferred are the alkylene polyamines wherein each A is hydrogen. Such alkylene polyamines include methylene polyamines, ethylene polyamines, butylene polyamines, etc. The ethylene polyamines are especially useful for reasons of cost and

effectiveness and are most conveniently prepared by the reaction of an alkylene chloride with ammonia. The reaction results in the production of the somewhat complex mixtures of alkylene polyamines, including cyclic condensation products such as piperazines. Because of their availability, these mixtures are particularly useful in preparing the dispersants^(6,7,11). The acylating agent (e.g. PIBSA) is usually reacted directly with the ethylene amine although it may be first converted to the diacid before the reaction. The term "ethylene amine" is used here in a generic sense to denote a class of polyamines conforming for the most part with the structure



in which n is an integer and R is hydrogen or a low molecular weight alkyl radical.^(4,6) The reaction can result in a simple acyclic diamide, a cyclic diamide, a polymeric amide or a combination of these types of products. The amide groups may further react to form imide groups and it is believed that a substantial amount of imide formation takes place in the process. An appreciable amount of amine carboxylate salt is also believed to be present. The reaction involves the removal of water which is distilled off as an azeotrope as it is formed. Presumably the first principle reaction that occurs is the formation of a half amide followed then by salt formation and finally dehydration of this salt to form the product having the structure in the case of diethylene triamine⁽⁴⁾:



where R is the polyisobutenyl group.

2.2.3 Acylating agents/reactive metal compound dispersants

Reactive metal compounds useful for the formation of complexes with the acylating agents include the nitrates, nitrites, halides, carboxylates, phosphates, phosphites, sulphates, sulphites, carbonates, borates, and oxides of cadmium as well as metals having atomic numbers from 24 to 30 (including chromium, manganese, iron, cobalt, nickel, copper and zinc). These metals are the so-called transition or co-ordination metals, i.e., they are capable of forming complexes by means of their secondary or co-ordination valence. There are numerous specific examples of the complex-forming metal compounds, which may be used to produce dispersants, given in the patent literature^(6,7,11,12,13,14). Some of these compounds are, cobaltous nitrate, cobalt nitrite, chromic bromide, chromic sulphite, chromic phosphite, manganese dichloride, manganic phosphate, ferrous carbonate, ferrous nitrate, nickel nitrate, zinc borate, zinc chromate, zinc nitrate, cadmium benzoate, cadmium sulphite, and cadmium oxide. Hydrates of the above compounds are especially convenient for their use in this process.

From what has been stated above, it is seen that the amines used for preparing carboxylic derivative compositions may contain alcoholic hydroxy substituents, and also the alcohols used may contain primary, secondary, or tertiary amino substituents. Thus amino alcohols can fall into both categories (a) and (b) provided they contain at least one primary or secondary amino group. Amino alcohols contemplated as suitable for use as (a) and/or (b) have one or more amine groups and one or more hydroxy groups, examples of which are the N-(hydroxy-lower alkyl) amines and polyamines^(7.11). Especially preferred are the polyhydroxy-substituted alkanol primary amines corresponding to R_a-NH_2 where R_a is a polyhydroxy-

substituted alkyl group. U.S.Pat. No. 1, 441,600 (reference(11)) illustrates the method of preparing such dispersants by reacting polyisobutenyl succinic anhydride (component A) with pentaerythritol (component B), then adding polyoxypropylene di-amine (component C), and finally adding a mixture of polyethylene diamine and polyamine-H (component D).

Reactive metal compounds are also used together with the polyhydric alcohols and polyamines in forming complexes with the acylating agents. EUR. PAT. No. 0051998 (reference (14)) illustrates the method of preparing such dispersants by reacting PIBSA (A) with PE (B), then adding a polyamine mixture comprising polyoxypropylene amine and polyethylene amines (C and D), and adding the resultant product to a prepared automotive engine oil containing 1.5% by wt., of zinc dialkyl dithiophosphate.

As mentioned previously, in order to achieve the requisite degree of viscosity index improving capabilities in the carboxylic derivative compositions, it has been found necessary to react the acylating agents with polyfunctional reactants. For example, polyamines, polyhydric alcohols, amino alcohols, and polyvalent metal or polyvalent metal compounds. It is believed that the polyfunctional reactants serve to provide "bridges" or cross-linking in the carboxylic derivative compositions and this, in turn, is responsible for the viscosity index-improving properties.

2.3 Theoretical aspects of reaction kinetics

Reaction kinetics is the study of the factors influencing the rate of a chemical reaction. It measures this rate and proposes explanations for the values found. The satisfactory design of equipment to effect any chemical reaction on a technical scale cannot be carried out without a

knowledge of the kinetics of that reaction.

Reaction kinetics is a very vast and involved subject. Some of its theoretical aspects and fundamental concepts have been reviewed by, Prigogine⁽¹⁵⁾, Lewis⁽¹⁶⁾, Pilling⁽¹⁷⁾, Sharp⁽¹⁸⁾ and Jones⁽¹⁹⁾. Experimental techniques and methods of rate measurements have been reviewed by, Caneda⁽²⁰⁾, Townshend⁽²¹⁾ and Lin⁽²²⁾.

In this section some theoretical aspects of reaction kinetics reviewed in the above references and some others, relevant to this work, will be presented.

2.3.1 Kinetics of homogeneous reaction^(23,24,25,26,27,28)

For homogeneous systems the intensive measure based on unit volume of reacting fluid is used practically exclusively for defining the rate of reaction, thus the rate of reaction of any reacting component A is defined as

$$(-r_A) = \frac{1}{V} \cdot \left(\frac{-dN_A}{dt} \right) = \frac{\text{(moles of A which disappear by reaction)}}{\text{(unit Volume)(unit time)}} \quad (2.1)$$

In general the rate of reaction is a function of the state of the system, hence

$$\begin{aligned} (-r_A) &= f(\text{state of the system}) \\ &= f(\text{temperature, pressure, composition}) \end{aligned}$$

but these variables are interdependent, hence

$$(-r_A) = f(\text{temperature, composition}) \quad (2.2)$$

in the following section the form of this fundamental relationship will be considered.

For many reactions the rate expression can be written as a product of a temperature-dependent term and a composition-dependent term, or

$$(-r_A) = f_1(\text{temperature}) \cdot f_2(\text{composition})$$

and
$$(-r_A) = k \cdot f_2(\text{composition}) \tag{2.3}$$

where k is the reaction rate constant which is the temperature-dependent term. It has been found that this dependency of k on temperature can be well represented by the Arrhenius law:

$$k = k_0 \cdot e^{-\frac{E}{RT}} \tag{2.4}$$

where k_0 is the frequency factor and E is the activation energy of the reaction. The Arrhenius law is strongly supported by the collision theory of molecules and also by the transition-state theory. The collision theory predicts that the temperature dependence of the rate constant is given by

$$k \propto T^{\frac{1}{2}} \cdot e^{-\frac{E}{RT}} \tag{2.5}$$

while the transition theory predicts that

$$k \propto T \cdot e^{-\frac{E}{RT}} \tag{2.6}$$

or summarising for both theories in general terms,

$$k \propto T^m \cdot e^{-\frac{E}{RT}}$$

and
$$k = k_0' \cdot T^m \cdot e^{-\frac{E}{RT}}, \quad 0 \leq m \leq 1 \tag{2.7}$$

But since the exponential term is very much more temperature sensitive than T^m term, the variation of k caused by the latter is effectively masked, and hence in effect

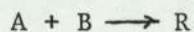
$$k \propto e^{-\frac{E}{RT}}$$

and
$$k = k_0 \cdot e^{-\frac{E}{RT}} \tag{2.4}$$

which is equivalent to the Arrhenius law. It can be seen from equation (2.4) that the activation energy E of a reaction can be determined by

measuring the rate constant at different temperatures. The plot of $\ln k$ versus $1/T$ should yield a straight line with a slope equal to $(-E/R)$. Wold and Ahlberg^(29,30) made the task of measuring the activation energy E considerably easier by the development of the 'vary-temp' method in which a reaction is studied under conditions where the temperature is varied in a controlled way, and E can be measured by carrying out a single kinetic experiment. Details of error analysis and computer programs for the method have also been published⁽³¹⁾.

The composition-dependent term of the rate expression depends very much on the type of reaction involved; whether the reaction is single or multiple reactions, elementary or nonelementary, and reversible or irreversible reaction. As an example consider the single irreversible reaction

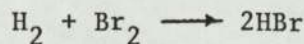


if the rate controlling mechanism involves the collision of a single molecule of A with a single molecule of B , then the rate of reaction is proportional to the number of collisions of molecules A with B which in turn is proportional to the concentrations of reactants A and B in the mixture at a given temperature, hence

$$(-r_A) = k \cdot C_A \cdot C_B \quad (2.8)$$

this is an elementary reaction since the rate equation corresponds to the stoichiometric equation.

A nonelementary reaction is one having a rate expression that has no correspondance with the stiochiomtry. A very well known example of a nonelementary reaction is

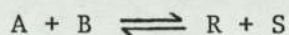


Bodenstein and Lind⁽³²⁾ studied the above reaction and found experimentally that the kinetics were well represented by the following expression,

$$(-r_{H_2}) = \frac{k_1 \cdot C_{H_2} \cdot C_{Br_2}^{\frac{1}{2}}}{k_2 + (C_{HBr}/C_{Br_2})} \quad (2.9)$$

Non elementary reactions are assumed to be the overall effect of a sequence of elementary reactions.

For reversible elementary reactions such as



both forward and reverse reactions rates must be considered. At equilibrium the rate of disappearance of A by the forward reaction must equal the rate of appearance by the reverse reaction, hence

$$(-r_A) = k_1 C_A C_B = (r_A) = k_2 C_R C_S, \text{ at equilibrium}$$

$$\therefore \frac{k_1}{k_2} = \frac{C_R C_S}{C_A C_B} = k_c \text{ equilibrium constant.} \quad (2.10)$$

For nonelementary reversible reactions no such simple relationships exist; however Denbigh⁽²⁴⁾ presented a more comprehensive treatment to this situation.

For complex nonelementary reactions, of an unknown mechanisms, involving say materials A, B, ..., D, the rate of progress can be approximated by an expression of the following type.

$$(-r_A) = k C_A^a C_B^b \dots C_D^d, \quad a+b+\dots+d = n \quad (2.11)$$

where a, b, ..., d, are the orders of reaction with respect to A, B, ..., D,

respectively, and are not necessarily related to the stoichiometric coefficients, and where n is termed the overall order of reaction.

2.3.2 Treatment of data from a batch reactor (23,32,33)

The equipment used to obtain experimental data for the determination of the rate equation can be divided into two types, the flow and batch reactor. The flow reactor is used primarily in the study of the kinetics of heterogeneous reactions while the batch reactor is used for obtaining homogeneous kinetic data. The data obtained from kinetic runs carried out in an experimental batch reactor operated isothermally and at a constant volume are usually easy to interpret. Thus the isothermal constant volume batch reactor is used whenever possible for obtaining homogeneous kinetic data.

There are two procedures for analysing kinetic data from a batch reactor, the integral and the differential methods. In the integral method of analysis a rate expression is put forward, then after appropriate integration and mathematical manipulations, prediction is made that a straight line should be obtained if the plot of a certain concentration function versus time is carried out. The data are plotted, and if a good straight line is obtained then the rate expression is a good fit to the data, but if not then a new rate expression is introduced and integrated, this procedure is continued until a rate expression is found that fits the data obtained satisfactorily. The integral method can only test specific mechanisms, or relatively simple rate expressions that can easily be integrated.

The differential method of analysis deals directly with the differential rate equation to be tested and without any integration, by

evaluating all terms in the equation including the rate of the reaction at chosen values of the concentration, and testing the goodness of fit of the equation with experiment. The differential method is very useful in complicated situations where the mechanism of reaction is unknown, and can be used to develop or build up a rate equation to fit the data. A summary of the differential method is given below,

for a constant volume batch reactor equation (2.1) holds, hence

$$(-r_A) = \frac{1}{V} \left(\frac{-dN_A}{dt} \right) = \frac{-d(N_A/V)}{dt} = - \frac{dC_A}{dt} \quad (2.12)$$

then as before

$$(-r_A) = - \frac{dC_A}{dt} = k \cdot f(C) \quad (2.13)$$

from the kinetic experiment, concentration-time data are obtained and then plotted, and a smooth curve is drawn through the data points. The slope of this curve is determined at suitably chosen concentration values.

These slopes are the rates of reactions at these points, (dC_A/dt) . By plotting $(-dC_A/dt)$ versus $f(C)$ for each composition a straight line through the origin should be obtained, if not then another form of $f(C)$ should be tested. Variations to this procedure can be introduced so that not only certain forms of $f(C)$ can be tested, but the parameters of a model for $f(C)$ can be evaluated and a model is developed to fit the experimental data.

Another technique that can be used for analysing the experimental data is the method of "least squares" which is specially useful for fitting equations of the type

$$(-r_A) = - \frac{dC_A}{dt} = k C_A^a C_B^b \dots\dots\dots (2.14)$$

where the parameters of the equation, k, a, b,... are to be determined.

Taking logarithms of equation (2.14),

$$\log \left(- \frac{dC_A}{dt}\right) = \log k + a \log C_A + b \log C_B + \dots\dots\dots$$

which is of the form

$$y = a_0 + a_1 x_1 + a_2 x_2 + \dots\dots\dots$$

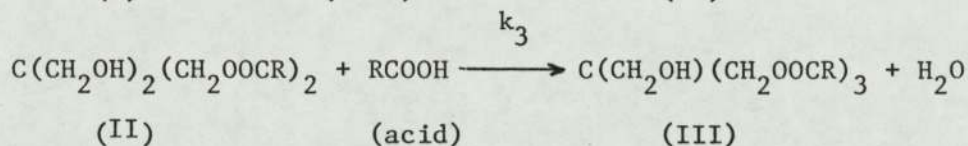
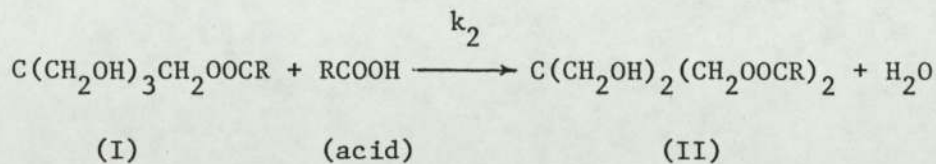
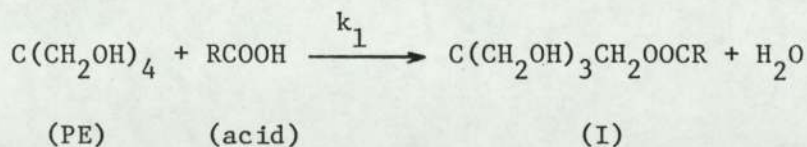
This can be solved^(33,34) to yield the values of best fit for $a_0 = \log k$, $a_1 = a$, $a_2 = b$, etc.

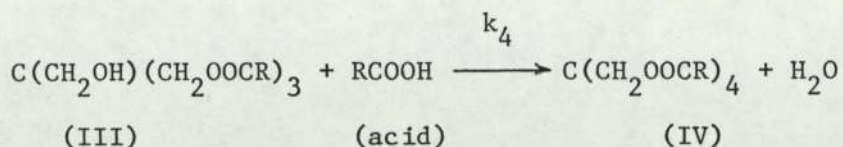
With this method all the individual orders of reaction are found at one time without any biases in fitting lines to experimental points. But without any additional statistical analysis this method gives no indication of how good the fit is. While with the graphical method the goodness of fit of the rate equation to the data is estimated at each step.

In Section 2.2 above the literature surveyed showed that dispersant additives are produced by reacting acylating agents with amines or alcohols. Most of the published literature on the kinetics of these acylating and esterification reactions is foreign, namely Russian or East European. Orudzheva, Guseinov and Gasarova⁽³⁵⁾ studied the synthesis of monoesters of ethylene glycol with carboxylic acid and formulated a kinetic model from the results, while Belov, Zavorotnyi and Korenev⁽³⁶⁾ assumed a second order rate expression for the monoesterification of maleic anhydride by 2-ethyl-1-hexanol (alcohol). The second order rate constant was evaluated at different temperatures from which the activation energy of the reaction was also determined. A second order kinetic model

was also assumed by Arranz, Sanchez and Gil⁽³⁷⁾ for the partial esterification of poly(vinyl alcohol) with acid chloride (n-butyroyl chloride). The activation energy of the reaction for <50% conversion was found to be equal to 9.9 k cal/mol. The kinetics of the acylating of aniline by phthalic anhydride in amide solvents were studied⁽³⁸⁾, and the rate constant and activation energy of the reaction were both determined. Khardin, et al.,⁽³⁹⁾ studied the kinetics of the acylation of monosubstituted aromatic amines by acid chlorides and formulated a mathematical model from which the rate constant and the activation energy of the reaction (using the Arrhenius equation) were estimated. Bouvier and Bruneau⁽⁴⁰⁾ developed a kinetic model to be used for the monoesterification of anhydride groups in ethylene-maleic anhydride copolymers.

Pentaerythritol esterification with phthalic anhydride,⁽⁴¹⁾ and acetic acid⁽⁴²⁾ were investigated. Popov, Nazarov, Kuznetsova, and Leshchiner^(43,44) developed a mathematical model for the kinetics of pentaerythritol ester synthesis which permitted the calculations of the rate constants for each carboxylic acid mixture used. The chemical equations and the differential equations presented were as follows





where R can be $\text{C}_n \text{H}_{2n+1}$, $3 \leq n \leq 9$.

An excess of RCOOH was used and pseudo first order reactions were assumed, hence assuming that the concentrations of PE, (I), (II), (III), and (IV) were C_0 , C_1 , C_2 , C_3 , and C_4 respectively, and k_1 , k_2 , k_3 , and k_4 are the rate constants for the reaction steps, then

$$(dC_0/dt) = -k_1 C_0$$

$$(dC_1/dt) = -k_2 C_1 + k_1 C_0$$

$$(dC_2/dt) = -k_3 C_2 + k_2 C_1$$

$$(dC_3/dt) = -k_4 C_3 + k_3 C_2$$

$$(dC_4/dt) = k_4 C_3$$

and the overall rate of the reaction ($-r_A$) equals to

$$(-r_A) = - (k_1 C_0 + k_2 C_1 + k_3 C_2 + k_4 C_3)$$

Although the equations and the assumptions are quite simple, however in this type of analysis all the concentrations of the intermediate compounds need to be followed and evaluated. There are many techniques for following up the kinetics of a reaction including infrared spectroscopy^(45a,b,c,d,46), and spectrophotometry^(47,48). Townshend⁽²¹⁾ presented a good review on rate measurements and calculations in spectrometry.

2.4 Crystallization literature

In any crystallization process two basic steps are involved, namely nucleation of crystal embryos, and their subsequent growth. However the state of supersaturation is an essential feature for both

steps, nucleation and crystal growth. The review presented in this Chapter is focussed on

- a - solubility
- b - nucleation
- c - crystal growth

2.4.1 Solubility

The first requirement in the analysis of any crystallization process is a knowledge of the phase equilibrium diagram (solubility diagram). The curve AB in figure 2.1 represents a typical solubility curve for the system of pure solute dissolved in pure solvent, which defines the mass of the solute at equilibrium with a given mass of the solvent at different temperatures. Supersaturated solutions are those solutions containing more dissolved solid than that represented by the saturation (equilibrium) conditions. Wilhelm Oswald⁽⁴⁹⁾ first introduced the terms "labile" (unstable) and 'Metastable' supersaturation; they refer to supersaturated solutions in which spontaneous deposition of the solid phase, in the absence of solid nuclei, may, and may not occur respectively⁽⁵⁰⁾.

Meirs⁽⁵¹⁾ carried out extensive research into the relationship between supersaturation and spontaneous crystallization by studying the refractive index of solutions, and his results can be summarised as follows:

- a - Crystallization is impossible in unsaturated solutions.
- b - Metastable supersaturated solutions do exist, in which spontaneous crystallization cannot occur, but crystal growth would occur if a crystal seed is introduced.
- c - Labile (unstable) supersaturated solutions do exist where spontaneous crystallization can occur.

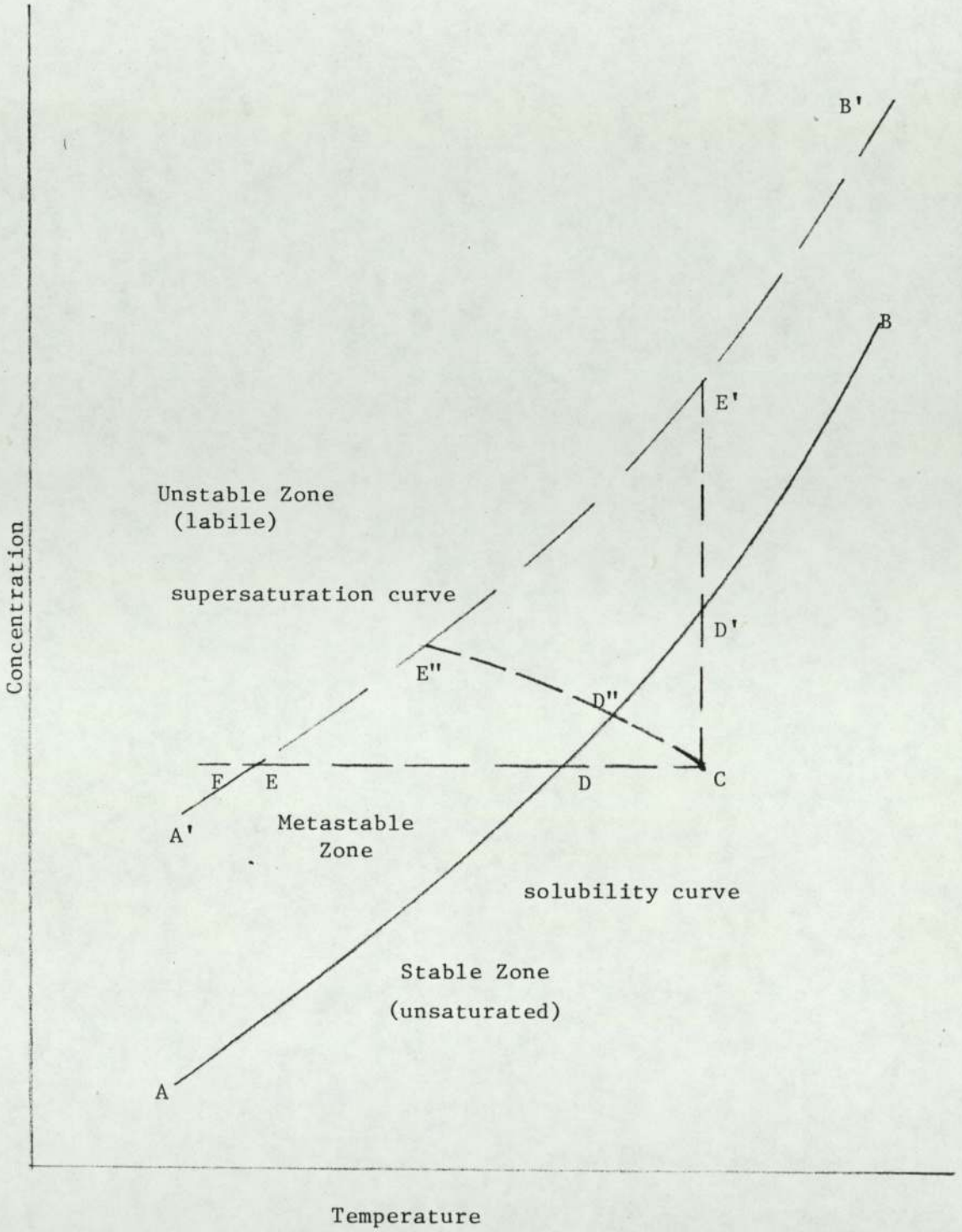


Figure 2.1

Saturation - Supersaturation diagram

On the solubility - supersolubility diagram, Figure 2.1, the metastable zone and the labile zone are separated by the supersolubility curve, the broken curve A'B' in Figure 2.1, (sometimes called the ghost curve). This curve is not well defined as the solubility curve, and it does not represent an equilibrium condition. The width of the metastable zone has been found to decrease with increasing temperature, decreasing cooling rate, and increasing concentration of seed crystals^(52,53). A direct dependence of the metastable zone width on solvent viscosity, molecular weight and density, and an inverse dependence on surface tension, dielectric constant and solute concentration was demonstrated by Storm et al.⁽⁵⁴⁾ Impurities can also affect the position of the ghost curve and hence the width of the metastable zone⁽⁵⁵⁾.

The state of supersaturation is sometimes produced by cooling, and sometimes by solvent evaporation. If a solution in state C (Figure 2.1) is cooled down it remains unsaturated until point D is reached, and spontaneous crystallization cannot occur until before point E is reached (and in many cases not before point F is reached). If solvent evaporation is chosen as a method for producing supersaturation then path CD'E' is followed at a constant temperature. In practice, a combination of both techniques is used, the operation is represented by the path CD''E''.

Ostwald⁽⁴⁹⁾ attempted to explain the phenomenon of supersolubility by correlating the relationship between solubility and particle size. He derived an equation by thermodynamical considerations, which was later corrected by Freundlich⁽⁵⁶⁾

$$\ln \frac{C_r}{C_\infty} = \frac{2\sigma_s V_m}{RT_r} \quad (2.15)$$

where C_r and C_∞ are the solubilities of spherical particles of radius r

and of large particles ($r \rightarrow \infty$) respectively, σ_s is the surface energy of the solid particle in contact with the solution, V_m is the molar volume of solute, T is the absolute temperature, and R is the gas constant. A number of assumptions were made in the derivation of the Ostwald-Freundlich equation namely, the particles were spherical, the gas laws were obeyed, and that σ_s and V_m were independent of particle size. Corrections to the Ostwald-Freundlich equation have been postulated by a number of workers⁽⁵⁰⁾, however the equations deduced all postulated a continual increase in solubility with reduction in particle size. To overcome this problem Knapp⁽⁵⁷⁾ showed that, if the opposing effect of the electric charge on the surface tension of a particle was considered, the particles being assumed to be isolated charged spheres and their charge independent of size, then the Ostwald-Freundlich equation is modified to:

$$\ln \frac{C_r}{C_\infty} = \frac{V_m}{RT} \left(\frac{2\sigma_s}{r} - \frac{q^2}{8\pi\psi r^4} \right) \quad (2.16)$$

where q is the particle charge and ψ the dielectric constant of the medium in which they are dispersed. It can be shown from equation (2.16) that the solubility have a maximum when

$$r^* = \left(\frac{q^2}{4\pi\sigma_s\psi} \right)^{\frac{1}{3}}$$

where r^* represents the critical radius for the maximum solubility C_r^* .

The solubilities of PbI_2 , Ag_2CrO_4 , PbF_2 , $SrSO_4$, $BaSO_4$, CaF_2 were studied by Dundon⁽⁵⁸⁾. He found large increases in the solubilities of small particles, in the range of 0.2 μm to 0.5 μm diameter, he also found that the solubility rose to a maximum on decreasing the particle size further. The solubility of gypsum was studied by Roller⁽⁵⁹⁾ who found that; at sizes above 25 μm the solubility rate was proportional to the

specific area; at sizes in the range of 25 μm and 2.8 μm the solubility rate increased more rapidly than the surface exposed; and at sizes below 2.8 μm the solubility rate began to decrease again. The solubility of gypsum in water was also studied by Hulett⁽⁶⁰⁾ who found that the solubility was increased by 19% for 0.4 μm particles.

In the experimental determination of solubility, its dependency on particle size of the solute is a complication that might affect the determined value. It may be safer to reach true equilibrium by over heating the system, although in some systems supersaturation may be quite stable.

The time needed to reach equilibrium in solid-liquid systems is usually much longer than in either gas-liquid or liquid-liquid systems. For example equilibrium is attained after 20h at room temperature in the iodine-perfluoroheptane system⁽⁶¹⁾, in which a continuously stirred saturator was employed, while up to ten days may be needed for dimethylglyoxime-alcohol systems⁽⁶²⁾. In practice solubility determination is checked by approaching equilibrium from both sides, the unsaturated state and the supersaturated state^(50,62). Zimmerman⁽⁶³⁾ has made an extensive review of the literature on experimental solubility determination up to 1950. A more recent comprehensive review on solubility determination has been presented by Kertes et al.⁽⁶²⁾. Two main categories of methods exist based on whether sampling from the equilibrium system is involved or not. Methods commonly used with low solubility materials are either electrical methods requiring no sampling⁽⁶⁴⁾ or spectrophotometric methods⁽⁶⁵⁾. which depend on analysis of samples. The residue weight method is normally used for high solubility materials, but there have been times when it was used for low solubility materials⁽⁶⁶⁾.

2.4.2 Nucleation

Nucleation is the phenomenon of the birth of new crystals. It involves the activation of small unstable particles called embryos. An embryo formed in the metastable region is very small and will dissolve on account of the increased solution potential. As the degree of supersaturation is increased the size of the embryo which can be tolerated by the solution decreases to a critical size where the embryo becomes a nucleus possessing sufficient surface energy to form a new phase and growth begins. Different modes of nucleation are recognised, and generally these are, primary homogeneous nucleation, primary heterogeneous nucleation, and secondary nucleation. The mechanism of nucleation and nucleation models have been reviewed by many authors including De Jong⁽⁶⁷⁾, Mullin^(50,68), Nielsen⁽⁶⁹⁾, and Ohara⁽⁷⁰⁾, while secondary nucleation has been reviewed by Strickland-Constable^(71,72), Garside and Davey⁽⁷³⁾, and Botsaris⁽⁷⁴⁾.

2.4.2.1 Primary homogeneous nucleation

Homogeneous nucleation is considered to be the result of an agglomeration or ordering process of solute molecules or ions. A stable nucleus is formed when the diameter of such an agglomerate or cluster, formed by a random process, becomes larger than a certain critical diameter (d_{crit}) which is given by the following equation^(50,67)

$$d_{crit} = \frac{4 \sigma_s V_m}{RT \ln S} \quad (2.18)$$

where σ_s is the surface energy, V_m is the molecular volume, R is the gas constant, T is the absolute temperature and S is the supersaturation ratio.

Nucleation occurs when clusters grow from a "subcritical" size to a "supercritical" size, with a net rate equal to the net flux of clusters passing the critical nucleus size. The derivation for the steady state homogeneous nucleation rate (B_H) leads to Becker-Döring equation⁽⁶⁷⁾:

$$B_H = K_H \exp \left(\frac{-\Delta G_{\text{crit}}}{RT} \right) \quad (2.19)$$

where K_H is a constant, and (ΔG_{crit}) is the free energy of formation of a critical nucleus, which for spherical clusters is given by^(50,67)

$$(\Delta G_{\text{crit}}) = \frac{16 \pi \sigma_s^3 V_m^2}{3(RT \ln S)^2} \quad (2.20)$$

Equation (2.20) is extremely important, it shows that when the system is just saturated ($S = 1$, $\ln S = 0$), the free energy of formation of a critical nucleus is infinite, hence a saturated solution cannot nucleate spontaneously. Homogeneous nucleation has been found to take place at a significant rate only above a certain limiting supersaturation^(50,67), which is normally higher than that required for heterogeneous nucleation⁽⁶⁷⁾. Because of that homogeneous nucleation rarely occurs in practice, except under experimental conditions.

2.4.2.2 Primary heterogeneous nucleation

This type of nucleation is induced by the presence of foreign bodies (e.g. atmospheric dust) which reduces to some extent the energy barrier required for nucleation at homogeneous conditions. Since real systems always contain extraneous bodies, homogeneous nucleation is practically impossible. Much lower supersaturations are required for primary heterogeneous nucleation due to the catalytic action of the

foreign bodies. Its critical free energy of formation can be related to that for homogeneous nucleation by the following equation^(50,67):

$$\Delta G_{\text{crit}}^* = \phi \cdot \Delta G_{\text{crit}} \quad (2.21)$$

where ϕ can take on any value between zero and unity. When there is no affinity between the substrate and the clusters, then $\phi = 1$, and when there is complete affinity (e.g. seeding the supersaturated solution with the same solute crystals), then $\phi = 0$. The value of ϕ can be related to the affinity between the substrate and the crystalline substance^(50,67,69). Since the estimation of ϕ for different systems is a very complicated, if not impossible, process, it has become a standard practice to use a power law model^(67,75), for primary heterogeneous nucleation (B_p) (briefly called primary nucleation),

$$B_p = K_p (\Delta C)^{m_p} \quad (2.22)$$

where K_p is the primary nucleation rate constant, and m_p is the order of primary nucleation. Relative supersaturation, or supersaturation ratio is frequently used instead of supersaturation term (ΔC) in equation (2.22).

2.4.2.3 Secondary nucleation

Secondary nucleation results by definition from the presence of crystals of the solute being crystallized. It involves the dislodgement of nuclei from a parent crystal at supersaturation at which primary (heterogeneous) nucleation would not occur. In most industrial crystallizers, secondary nucleation always accompanies primary nucleation, and is apt to be the predominant mechanism of nucleation^(67,74). Secondary nucleation can occur in a variety of different ways that can all be operational

simultaneously. The subdivisions of secondary nucleation are discussed below.

2.4.2.3.1 Collision breeding

Also known as collision nucleation or contact nucleation is by far the most important type of secondary nucleation and is normally the dominating mechanism for producing new crystals in any stirred crystallizer already containing suspended crystals^(71,72,76,77). New nuclei are formed due to, the crystal-crystal collisions, the crystal-impeller collisions, or the crystal-vessel collisions. Denk and Botsaris⁽⁷⁸⁾ showed that under a wide range of conditions, nuclei originated from the crystal surface rather than from the solution. Many suggestions have been put forward for the mechanism of collision nucleation^(71,72,76,79), these include:

- a - The cluster of molecules which already exist in solution are attracted into a surface adsorption layer, or alternatively, the supersaturation may be higher in the adsorption layer which may give rise to the formation of clusters. In either case disturbance of the layer due to impact with another body might cause the clusters to form nuclei.
- b - The protuberances and other forms of roughness may exist on the crystal surface, which are easily rubbed off on collision.
- c - The collision simply fractures the surface locally in such a way as to produce tiny nuclei of microscopic size.

Other suggestions for the mechanism, favouring the solution as the source of new nuclei in contact nucleation have also been advanced^(71,72,78).

Ottens et al.⁽⁸⁰⁾ proposed a model for the nucleation in suspensions in agitated vessels based on collision breeding. Garabedian and Stickland-Constable^(81,82) studied collision nucleation with sodium chlorate crystals, they reported that the number of new nuclei increased rapidly with the supersaturation. They used the Oswald-Freundlich equation for the enhanced solubility of small crystals (equation 2.15) to determine the proportion of these nuclei that survive and to establish the dependency on supersaturation.

In their study of contact nucleation of potash alum crystals, Rusli, Larson and Garside⁽⁸³⁾ reported that many nuclei of sizes smaller than about 4 μ m appear either not to grow or to grow at an immeasurably slow growth rate. In an earlier work carried out on pentaerythritol crystals, Bujac⁽⁸⁴⁾ reported that small fragments of PE crystals were stable over a wide range of supersaturations, and they only grew when the supersaturation was raised to >35%. Similar results were reported by van't Land and Wienk⁽⁸⁵⁾ in their investigation of particle size control in industrial NaCl-crystallization, they reported that small fragments (<40 μ m) of NaCl crystals do not grow. Garside⁽⁸⁶⁾ reported that potash alum crystals smaller than 20 μ m did not appear to grow, he suggested that secondary nuclei formed by contact nucleation have rough surfaces on the microscopic level and probably have the appearance of a sequence of 'hills' and 'valleys'. In the vicinity of the 'hills' the curvature will be such that the Oswald-Freundlich equation predicts a significant increase in the solubility, while in the 'valleys' the curvature is in the opposite direction and so the solubility will be lower. The 'hills' will then tend to dissolve while the valleys grow and the overall result will be that the surfaces become flat. During this process, however, the overall size of the crystal

will not change and so little or no growth will be observed. Contact nucleation has recently been reviewed in detail by Garside and Davey⁽⁷³⁾.

2.4.2.3.2 Dendritic and polycrystalline breeding^(71,72)

In the high range of supersaturation needles sometimes grow out of a crystal. In stirred systems such crystals can easily break giving secondary crystals of visible size. Under similar conditions polycrystals are sometimes formed, these can also break up rather easily giving macroscopic crystals. Both these mechanisms are probably of little significance in industrial crystallizers since collision nucleation would be dominant.

2.4.2.3.3 Crystal breakage⁽⁷¹⁾

If agitation is sufficiently violent crystals can be broken into macroscopic pieces. At the same time a shower of sub-microscopic nuclei are produced. Breakage depends on the violence of stirring and on the bed density.

2.4.2.3.4 Other types of secondary nucleation

If a dry crystal is introduced into any supersaturated solution 'initial nucleation' is observed, this is caused by the crystal dust present on the surface of the dry crystal. Denk and Botsaris⁽⁷⁸⁾ in their study of seeded sodium chlorate solutions concluded that secondary nucleation can occur because of an impurity concentration gradient in the boundary layer resulting from the uptake of impurities by the growing seed crystals. Finally fluid shear is sometimes claimed to cause nucleation, however, experimental evidence seems to indicate that at lower supersaturations fluid shear alone cannot cause secondary nucleation⁽⁷²⁾.

2.4.3 Crystal growth

As soon as stable nuclei have been formed in a supersaturated solution, they begin to grow into crystals of visible size. The addition of a new solute on the face of a crystal is considered to take place by a series of stages as follows:

- a - transport of the solute from the bulk of solution to the crystal surface.
- b - physical or chemical adsorption on the crystal surface.
- c - diffusion on the surface to a more favourable position.
- d - incorporation into the crystal lattice.

Many theories have been presented to explain the mechanism and the rate of crystal growth^(50,69,70,75). All these theories are mathematically complex and none of them yield results that can predict the rate of crystal growth as a simple function of the parameters of the system⁽⁷⁰⁾.

Recent developments in the theories of crystal growth have been reviewed by Mullin^(68,87) and Bennema^(88,89). Most of the theories of crystal growth assume that one of the many steps required for the deposition of solute on the crystal surface is usually the rate controlling step, theories presented below are based on this classification.

2.4.3.1 Nucleation controlled growth^(69,70,90)

These theories assume that the rate controlling step is nucleation. O'hara and Ried⁽⁷⁰⁾ present different mechanisms proposed for the growth mechanism of a nuclei. It is assumed that in mononuclear two dimensional nucleation, once a nucleus is formed it has an infinitely rapid rate of lateral growth across the surface, in this case growth rate (R_G) normal to any crystal face of total area, A and having a stepheight h is given by:⁽⁷⁰⁾

$$R_G = A \cdot h \cdot B_N \quad (2.23)$$

where B_N is the nucleation rate.

If the spreading velocity is assumed to be zero, growth then occurs by the accumulation of critical nuclei. This model is called the polynuclear two dimensional model, and the growth rate is given by:⁽⁷⁰⁾

$$R_G = a_n \cdot h \cdot B_N \quad (2.24)$$

where a_n is the surface area occupied by a single nucleus.

Different 'birth' and 'spread' models are possible for intermediate spreading velocities, but in these models the growth rate is a complex function of supersaturation and temperature.

All nucleation controlled growth models predict very low crystal growth rates at low supersaturation. This is not supported by experimental evidence, but in fact is contrary to it^(70,90).

2.4.3.2 Surface dislocations controlled growth^(50,69,70,90)

Most crystals contain dislocations, which cause steps to be formed on the faces. Of these the screw dislocation is considered to be important for crystal growth since it renders the requirement of surface nucleation unnecessary. Once a screw dislocation has been formed growth can take place on stepped growth spirals on the crystal surface, in such a manner that the spiral sources are self perpetuating. Burton, Cabrera and Frank⁽⁹¹⁾ developed a kinetic model (BCF model) in which the curvature of the spiral near its origin was related to the spacing of successive turns, and the level of supersaturation. The BCF relationship may be written as:

$$R_G = AS_r^2 \tanh(B/S_r) \quad (2.25)$$

where R_G is the crystal growth rate, S_r is the relative supersaturation,

and A and B are complex temperature-dependent constants which include parameters depending on step spacing. At low supersaturations the BCF model approximate to $R_G \propto S_r^2$, but at high supersaturations $R_G \propto S_r$.

The BCF theory was originally derived for crystal growth from the vapour. However, it can also be applied to growth from solutions, but more complex relationships are obtained due to the complex nature of these systems. This is the main shortcoming of the BCF model since it cannot be tested directly because of these complex expressions.

2.4.3.3 Diffusion theories (50,69,70,92)

Early diffusion models assumed that crystallization was governed by the difference between concentration at the solid surface and in the bulk of solution. An equation was proposed in the form of⁽⁵⁰⁾,

$$\frac{dm}{dt} = k_m \cdot A \cdot (C - C^*) \quad (2.26)$$

where m is the mass of solute deposited in time t; A is the surface area of the crystal; C is the solute concentration in the bulk of the supersaturated solution; C^* is the saturation concentration; and k_m is the coefficient of mass transfer. Equation (2.26) assumes that the solution which is in contact with the crystal surface is saturated. But Miers (1904) showed that the solution in contact with a growing crystal face is not saturated but in fact supersaturated. In view of this fact considerable modifications were made to the diffusion theory, and it was suggested that there were two steps involved in the deposition of solute mass, namely, the diffusion of solute from the bulk of the fluid to the solid surface, followed by a surface reaction step when the solute molecules arrange themselves into the crystal lattice. These two stages can be represented by the following equations⁽⁵⁰⁾:

$$\frac{dm}{dt} = k_d A (C - C_i) \quad (\text{diffusion}) \quad (2.27)$$

and

$$\frac{dm}{dt} = k_r A (C_i - C^*)^{m_r} \quad (\text{reaction}) \quad (2.28)$$

where k_d is the mass transfer coefficient by diffusion; k_r is the rate constant for the surface reaction; C_i is the solute concentration in the solution at crystal-solution interface; and m_r is the surface reaction order ($m_r = 1$) for first order surface reaction). It is usually more convenient to eliminate C_i by considering an 'overall' concentration deriving force $(C - C^*)$ which is easy to measure, hence a general equation for crystallization can be written as,

$$\frac{dm}{dt} = K_G \cdot A \cdot (C - C^*)^n \quad (2.29)$$

where K_G is an overall crystal growth coefficient; and n is the 'order' of the overall crystal growth process.

If $n = 1$ and $m_r = 1$ also, then C_i can be eliminated from equations (2.27) and (2.28) to give

$$\frac{dm}{dt} = \frac{A(C - C^*)}{\left(\frac{1}{k_d}\right) + \left(\frac{1}{k_r}\right)} \quad (2.30)$$

i.e.

$$\frac{1}{K_G} = \frac{1}{k_d} + \frac{1}{k_r} \quad (2.31)$$

It can be seen from equation (2.31) that for large k_r (rapid surface reaction), $K_G \approx k_d$ and the process is diffusion controlled. Similarly if k_d is large, $K_G \approx k_r$ and the process is surface reaction controlled. Garside⁽⁹³⁾ used the concept of effectiveness factors to calculate how closely measured growth rates approach the surface integration rate.

Mass transfer of solute from bulk of solution to the surface of the crystal does not involve molecular diffusion only, but it involves eddy diffusion also^(50,70). Hence for mass transfer limited growth, the use of general relations involving empirical mass transfer coefficients usually results in a more reliable rate equations for crystal growth⁽⁷⁰⁾. Therefore from equation (2.29) if bulk diffusion controls ($K_G \approx K_d$), then

$$R_G = \frac{dm}{dt} = k_d \cdot A \cdot (\Delta C)^n \quad (2.32)$$

where R_G is the rate of crystal growth, and (ΔC) is the supersaturation driving force. The mass transfer coefficient k_d depends on the fluid dynamics and other relevant physical properties involved, and is estimated from semi-empirical relationships.

It was suggested that the following dimensionless correlation can be used for the evaluation of k_d for regular geometric systems⁽⁹⁴⁻⁹⁸⁾:

$$Sh = F_1 + F_2 \cdot Re^{Z_1} \cdot Sc^{Z_2} \quad (2.33)$$

where Sh , Re and Sc are the Sherwood, Reynolds, and Schmidt numbers respectively; and F_1 , F_2 , Z_1 and Z_2 are constants. For spheres, tetrahedra and octahedra the value of F_1 is 2, $2\sqrt{6}$ and $2\sqrt{2}$ respectively. Ranz et al.^(94,95) reported that for spheres,

$$Sh = 2 + 0.60 Re^{0.5} \cdot Sc^{0.33} \quad (2.34)$$

A value for F_2 of 0.69 in air and 0.79 in water was presented by Rowe et al.⁽⁹⁷⁾ Levin et al.⁽⁹⁸⁾ reported a slightly different correlation for mass transfer to suspended particles in an agitated vessel

$$Sh = 2 + 0.44 Re^{0.5} Sc^{0.38} \quad (2.35)$$

2.4.3.4 Factors affecting crystal growth

There are many factors that may influence the process of crystal growth including solvent, crystal size, temperature, agitation and impurities, these are discussed below.

a - Solvent

Bourne and Davey^(99,100,101) in their investigation of the role of solvent-solute interactions on crystal growth mechanism reported different mechanisms and different rates associated with crystallization of the same substance from different solvents. Experimental evidence to this effect was reported⁽⁸⁷⁾. The molecular roughness of the crystal-solution interface has been presented for the explanation of this effect^(89,102).

b - Crystal size

Practically all crystal growth rates are particle size dependent. The effect of size may be quite insignificant for macro-crystals, but the situation is very much different for crystals of microscopic size⁽⁵⁰⁾. In their study of growth kinetics of potash alum crystals, Rusli, Larson and Garside⁽⁸³⁾ reported that growth rates were strongly size dependent for sizes above 4 μ m while no growth was noticed for sizes below 4 μ m. Similar results were also reported by Garside⁽⁸⁶⁾ in his study of the growth of small crystals of potash alum. Many empirical growth models make allowance for crystal size. Tavare et al.^(103,104) have analysed different modes of operation of batch crystallizers using both size independent and linear size-dependent power law growth model. Mullin and Nyvlt⁽¹⁰⁵⁾ and Jones⁽¹⁰⁶⁾ in their analyses of batch cooling crystallizer also used linear size-dependent growth models.

c - Temperature

Nucleation is much more affected by temperature than crystal growth, but it has been found that in mass transfer limited growth processes, the

mass transfer coefficient depends on temperature in accordance with an Arrhenius type equation⁽⁵⁰⁾. In general it can be stated that the growth rate increases with increasing temperature⁽⁷⁰⁾.

d - Agitation

For any given size of a solid particle, a maximum relative velocity exists between the particle and the fluid at a critical degree of agitation⁽¹⁰⁷⁾. This maximum velocity corresponds to higher rates of crystal growth. Nienow et al.⁽¹⁰⁸⁾, have described the use of slip velocities to correlate agitated vessel crystal growth data with single crystal and fluidised bed growth, while the same concept was applied to particle-liquid mass transfer in a stirred vessel by Levins and Glastonbury⁽⁹⁸⁾. Apart from the effect of agitation on crystal growth, agitation has a very strong effect on secondary nucleation. Because of that, Nienow^(109,110) suggested that optimum impeller speed should be the minimum required for the suspension to be effectively dispersed.

e - Impurities

Impurities can have a profound effect on crystal growth. Some impurities may suppress growth, while others can enhance it or can exert a selective effect with the net results of crystal habit modification⁽⁵⁰⁾. Numerous studies have been carried out on the effects of impurities on crystal growth, these have been discussed in a recent review by Mullin⁽⁸⁷⁾.

In a recent paper, Botsaris⁽¹¹¹⁾ discussed the mechanisms by which impurities effect nucleation, growth and 'growth dispersion' phenomenon in crystallization process. In their study of growth inhibiting impurities on the crystallization of pentaerythritol, Rehmatullah et al.⁽¹¹²⁾ reported that concentrations of formaldehyde as low as 5 parts/10⁶ in solution reduced the growth rate of PE crystals by one order of magnitude. Ziak⁽¹¹³⁾ reported similar inhibitions of PE crystal growth caused by the presence of formaldehyde as a trace impurity in solution.

The observed effects of impurities are thought to be due either to its influence on the nucleation rate or, in the case of non-nucleation controlled growth, to the blocking of active sites thereby preventing the advance of growth steps. Mullin^(50,87) pointed out that the solvent from which the crystals are grown can be considered as an impurity and is capable of interaction with the solute.

CHAPTER THREE

PREVIOUS WORK ON PENTAERYTHRITOL

3.1 Introduction

Pentaerythritol (tetramethylolmethane) is a polyhydric alcohol which has four primary hydroxyl groups arranged compactly around a central carbon atom. The high melting point of the compound, its slight solubility in water and the ready reactivity of its four hydroxyl groups have been attributed to the compact symmetrical structure of the molecule.⁽¹⁾ Pentaerythritol is an important organic compound, it is used in the manufacture of the explosive PETN (pentaerythritol tetranitrate), also its soluble carboxylic esters have a large industrial application. In this chapter, work done on its crystal morphology and habit, crystal growth rates, and physical and chemical properties will be presented.

3.2 Crystal Morphology and Habit

The original data on pentaerythritol crystals were obtained by Martin and were included in the Tollens et al. paper on pentaerythritol.⁽¹⁾ Since then a number of studies of the properties of pentaerythritol crystals have been reported.

Pentaerythritol ($C(CH_2OH)_4$; 2,2-bis(hydroxymethyl)-1,3-propanediol) crystal lattice is body-centred tetragonal (2nd order hol class 4/mmm) with two molecules to the unit cell.^(114,115) Figure 3.1 shows a sketch of a tetragonal bipyramid in the 2nd order (hol) orientation where the Miller indices of the main faces and also of the minor ones which sometimes appear are clearly marked. The values of the unit cell axes are recorded⁽¹¹⁵⁾ as $a_o = 6.083 \pm 0.002 \text{ \AA}$ and $c_o = 8.726 \pm 0.002 \text{ \AA}$ which give the equivalent axes ratio $c_o/a_o = 1.4345$.

On a microscope slide the silhouette of a crystal of only (101) faces appears as an almost regular hexagon since the ratio $C/a \approx \sqrt{2}$ to within 1.5%, and hence the distance across any pair of flats gives the size of the bipyramid base, λ .⁽¹¹⁴⁾ Pentaerythritol exhibits a polymorphic transformation at a temperature variously reported⁽¹⁾ as 180°C, 181.1°C, 184°C, 187.7°C, and 192°C at which point the crystal undergoes a change from a tetragonal to a cubic lattice. Wyckoff⁽¹¹⁵⁾ states that this transformation occurs at 179.5°C with $a_0 = 8.963 \text{ \AA}$ for the cubic cell above 179.5°C. Pentaerythritol has a pronounced layer-type of structure.⁽¹¹⁶⁾ The central carbon atom of one molecule in the unit cell is located at (0,0,0) and that of the other at $(\frac{1}{2}, \frac{1}{2}, \frac{1}{2})$. The molecular units are so arranged that the oxygen atoms are in planes perpendicular to the C-axis. The oxygen atoms of four neighbouring molecules are arranged in the form of a square whose sides are inclined 10° to the a_1 and a_2 -axes. In pentaerythritol the C-C bond length is 1.5 \AA , the C-O bond length is 1.46 \AA and the O-O bond length is 2.69 \AA .⁽¹¹⁷⁾

Wells⁽¹¹⁸⁾ found that when pentaerythritol is crystallized from aqueous solutions slowly, tetragonal bipyramid crystals bounded by (101) faces are obtained. But when a saturated aqueous solution of pentaerythritol is poured into acetone, thin square plates with predominant (001) faces are produced. Similar plates were obtained when pentaerythritol crystallized from β -ethoxyethanol on rapid cooling, whereas crystals grown slowly from this solvent are bipyramid. Frevel⁽¹¹⁹⁾ also noted similar results during crystallization of pentaerythritol from aqueous solutions.

In the investigation of the esterification reaction of pentaerythritol (PE) with polyisobutenylsuccinic anhydride (PIBSA) to produce a lubricating oil dispersant additive, thin square plates were obtained when the excess PE was crystallized from the non-aqueous reaction mixture.⁽¹²⁰⁾ Occasional occurrence of (001) faces was reported when

crystals were grown from pentaerythritol purified from ethers by hydrolysis with hydrochloric acid.⁽¹²¹⁾ These crystals were transparent and had a rectangular base. Well developed platelets with predominant (001) faces were also obtained together with small octahedra crystals bounded by (101) type planes when aqueous solutions of pentaerythritol were slowly evaporated.⁽¹²²⁾ The (101) and (001) faces are much more likely to appear than the (111) and (100) faces when PE is crystallized from solutions because of the law of reticular densities given in Table 3.1 below.⁽¹¹⁴⁾

TABLE 3.1

Reticular densities of PE Crystals

Tetragonal bipyramid (class 4/mmm), 2nd order (hol) $\frac{C_0}{\alpha_0} = 1.4345$.

<u>Face</u>	<u>Reticular Density</u>
[101]	1.000
[001]	0.873
[110]	0.860
[111]	0.613
[100]	0.609

3.3 Physical Properties

Pentaerythritol is an odourless, tasteless, white crystalline compound which is non-hygroscopic, burns with a luminous flame and without fumes, practically non-volatile and stable in air. Berlow et al.⁽¹⁾ collected all the published work on pentaerythritols up to 1958. They stated that various melting points ranging from 256°C to 265.5°C have been recorded for pure pentaerythritol with 261-262°C most often mentioned. Wyler and Warnett⁽¹²³⁾ reported that pentaerythritol forms an eutectic with 35% di-pentaerythritol melting at 190°C, while Rogers⁽¹²¹⁾ observed that

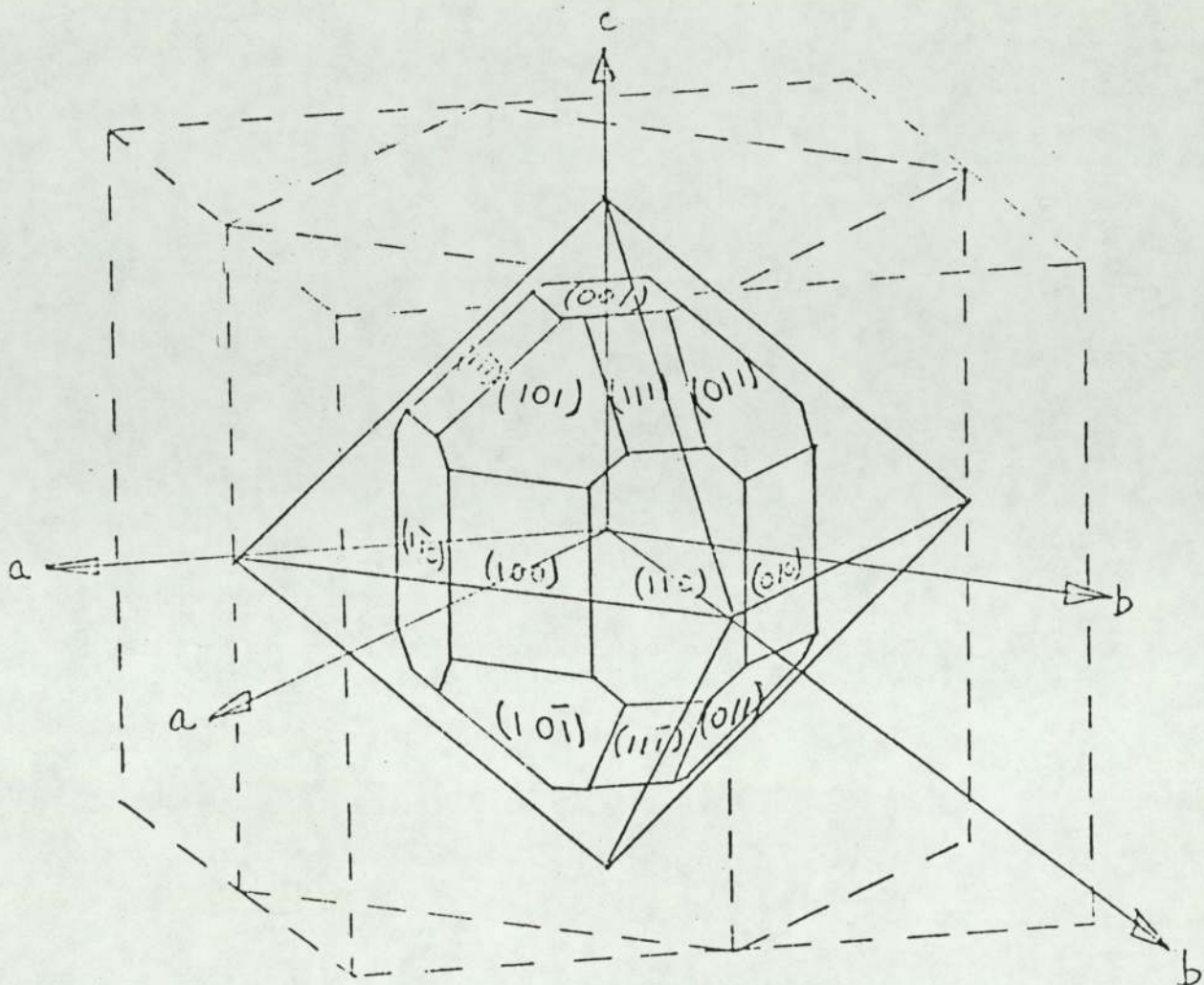


Figure 3.1 Pentaerythritol crystal shape and structure
Tetragonal bipyramid (class $4/mmm$)
2nd order (hol), $C_0/a_0 = 1.4345$

an eutectic with 40% di-pentaerythritol melting at 185.5°C is formed. The presence of 4% formal in the di-pentaerythritol source "Dipentek" used by Rogers, could have been the source of discrepancy between the two results.

Pentaerythritol is moderately soluble in cold water, freely soluble in hot water.⁽¹²⁴⁾ The solubility data have been reported by Cook,⁽¹²⁴⁾ Kunetsova and Gavrilova,⁽¹²⁵⁾ and Rogers et al.⁽¹²⁶⁾ The empirical correlation of Rogers et al. is

$$\log_{10} X_1 = 2.980 - 1242/T \quad (3.1)$$

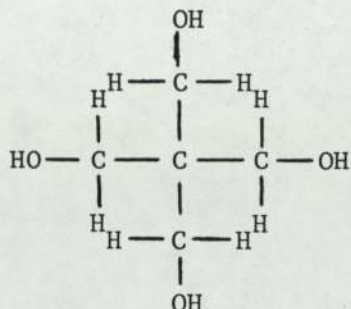
with standard deviation of $\pm 2.6\%$; where X_1 is the concentration of pentaerythritol (mass fraction), and T is the absolute temperature, °K. The heat of solution was determined from their data⁽¹²⁶⁾ to be 6.1K cal/mol at 30°C and 7.3K cal/mol at 75°C. The solubility of pentaerythritol in organic solvents and alcohols is very small.⁽¹⁾

The vapour pressure of pentaerythritol was reported by Bradley and Cotson⁽¹²⁷⁾ to range from 2.12×10^{-5} cm Hg at 106.4°C to 52.4×10^{-5} cm. cm Hg at 135.1°C. There is some discrepancy between their vapour pressure-temperature correlation and that reported by Nitta et al.⁽¹²⁸⁾

Pentaerythritol sublimes on heating under reduced pressure and boils at 276°C/30 mm Hg.⁽¹⁾ Its density was estimated by Llewellyn⁽¹²⁹⁾ to be 1396 Kg/m³. The diffusivity of pentaerythritol in water at 25°C was reported⁽¹³⁰⁾ to be equal to 0.76×10^{-9} (m²/s).

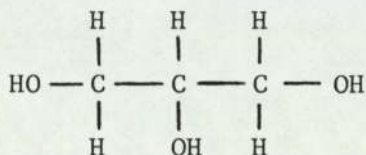
3.4 Functionality and Chemical Reactivity

Pentaerythritol is a member of the polyol family which includes the glycols, glycerine and sorbitol. It is a unique and superior member of the family due to its structural configuration and its functionality.^(1,2,3)



Pentaerythritol (PE)

The unique configuration of pentaerythritol consists of four methylol groups distributed symmetrically around the central carbon atom, all groups are equivalent and equidistant from each other, with all four hydroxyl groups being primary. This molecular structure makes for fast esterification since the hydroxyl groups are readily available for reaction.⁽²⁾ This is not so with glycerine



Glycerine

The central secondary hydroxyl group in glycerine slows down esterification and results in longer processing times. The secondary hydroxyl is also more susceptible to dehydration forming undesirable by-products. Such side reactions, plus the slower reaction rate contribute to higher colour of resin. Furthermore the secondary hydroxyl decreases the practical functionality of glycerine, i.e. the number of available groups is lower than the theoretical value and a greater excess of glycerine is required when formulating alkydes. These disadvantages also apply to other polyols containing secondary hydroxyl groups such as sorbitol.⁽²⁾

Esterification of pentaerythritol can be carried out by the usual methods using acids, acid chlorides, or acid anhydrides to yield simple esters some of which can act as a non-corrosive oil soluble detergents used as dispersant additives for lubricating oils,⁽³⁾ or to produce alkyd resins, which are polymers of a polybasic acid and polyhydric alcohol, modified with drying or non-drying oils as fatty acids to give the final derived properties.^(1,2) About 95% of the commercially produced pentaerythritol is consumed in the production of alkyd resins because superior products are obtained with pentaerythritol than with glycerine or with other members of the polyol family.⁽²⁾

3.5 Chemical Analysis

As pentaerythritol became a major organic compound and its use in the production of alkyd resins became more widespread, it became necessary to formulate an accurate procedure for its analysis. A number of analytical procedures have been suggested in the literature but only a few of these have proven to be sufficiently accurate and convenient for the routine analysis of pentaerythritol.

One of the most accurate and reliable procedures for the quantitative determination of pentaerythritol is the Benzol method⁽¹⁾ which is based on the formation of its dibenzylidene acetal, a well defined crystalline compound which is relatively insoluble in a dilute aqueous methanolic solution of hydrochloric acid containing benzaldehyde. The acetal is then determined gravimetrically. However Sporek and Williams⁽¹³¹⁾ reported that as little as 4% of di-pentaerythritol in a technical grade of pentaerythritol interferes with the accuracy of the pentaerythritol analysis as does the presence of liquid hydroxy compounds formed as by-products of the condensation of formaldehyde and acetaldehyde.

They recommend the use of chromatographic procedure to separate pentaerythritol from commercial samples and from reaction liquors prior to the application of the benzal procedure.

Another important technique is gas chromatography which is impossible to use directly because of the high melting point and the low vapour pressure of pentaerythritol, but can be used indirectly by converting the mono-, di-, and tri-pentaerythritols (if any) into their volatile derivatives such as their acetate esters before analysis. This can be achieved by refluxing the pentaerythritol samples with p-toluene sulphonic acid and acetic anhydride mixture for more than six hours then cooling to ambient temperature before analysis.⁽¹³²⁾

Gas chromatography is an important technique not only in determining the mono-pentaerythritol content but also in determining the di- and tri-pentaerythritol contents.⁽¹³²⁾ Apart from gas chromatography, there has been no specific method reported for the determination of the di- and tri-pentaerythritols in the presence of monopentaerythritol. The methods used commercially for their determination are based on the different solubilities of these alcohols or their derivatives, and usually do not distinguish between the di- and tri-pentaerythritols.⁽¹⁾

3.6 Crystal Growth Rate

Very little work has been published on the crystallization of pentaerythritol, most of which is on crystallization from aqueous solutions. No quantitative data has been found although the difficulties in growing large crystals have been emphasized.^(112,113,114,121,125,129,133,134)

Bujac⁽⁸⁴⁾ found in his small particle growth studies that small pentaerythritol particles produced by attrition in an agitated vessel showed no significant change in size (growth rate $<0.01 \mu\text{m}/\text{min}$) over a

wide range of relative supersaturations (5-30%). Although stable these particles were not capable of growth at all supersaturations likely to be found in crystallizers. Crash nucleation occurred at a relative supersaturation of >35% and many large particles were formed, the growth rate was estimated at >10 $\mu\text{m}/\text{min}$. He also showed experimentally that the crystals produced at the crash point were derived from the original fragments, indicating that all pentaerythritol fragments were capable of growing at sufficiently high supersaturation.

Rogers⁽¹²¹⁾ calculated the growth rate of pentaerythritol crystals by measuring the change in refractive index of a suspension of stirred crystals over a temperature range of 30 to 70°C. He also calculated the growth rate in fluidised beds by measuring the increase in crystal mass but these were very difficult to control.

The results obtained from both techniques,⁽¹²¹⁾ the stirred cells and the fluidised beds were in agreement but they were several order of magnitude lower than those values calculated from Nielsen's Correlation assuming that the crystallization process was diffusion controlled through the boundary layer surrounding the crystal.⁽¹¹⁴⁾ The growth rate estimated from Nielsen's equation was equal to 1.1×10^{-6} (m/s), while the highest growth rates measured at the same supersaturation (of $\Delta x = 0.025$ mass fraction) even at 70°C were only of the order of 10^{-9} (m/s), because of that it was suggested that the growth mechanism was surface integration controlled and was second order with respect to concentration over the range considered.⁽¹¹⁴⁾

In a later study it was found that very low concentrations of formaldehyde, as low as 5 parts/ 10^6 in solution, reduced the growth rate of PE crystals by one order of magnitude.⁽¹¹²⁾ At 10 parts/ 10^6 concentration of formaldehyde in solution, the growth rate was reduced by over two orders of magnitude.⁽¹¹²⁾ With chemical scavenging of

formaldehyde in the purification process, crystal growth rates approaching the diffusion control limit of 10^{-6} m/s were obtained exceeding earlier results under corresponding conditions by nearly three orders of magnitude. It is interesting to note that all samples of commercial pentaerythritol analysed were found to contain ≥ 20 parts/ 10^6 of formaldehyde which was more than enough to cause very serious growth inhibition.⁽¹¹²⁾ This growth inhibition of pentaerythritol crystals due to the presence of formaldehyde as trace impurity was also demonstrated by a very recent study by Ziak, Jozef.⁽¹¹³⁾ Chemical scavenging of this trace of formaldehyde is essential if reasonable growth rates are to be achieved in industrial crystallizers.

CHAPTER FOUR

PROCESS DESCRIPTION OF PIBSA/PE DISPERSANT ADDITIVES PRODUCTION

4.1 Introduction

In the production of lube oil dispersant additives, Pentaerythritol (PE) is reacted with Polyisobutenylsuccinic anhydride^(7,9,13) termed (PIBSA), which is an important intermediate in the manufacture of lube oil additives. A slight molar excess of pentaerythritol is reacted with one mole of PIBSA in a portion of a diluent oil and in the presence of a catalyst which can be either acidic or basic.⁽¹³⁵⁾ At the end of the reaction the mixture is cooled and then filtered to remove the sediment. During this finishing stage more diluent oil is added to bring the product to the desired dilution level.

4.2 Raw Materials

The raw materials that are used in the laboratory preparation of the dispersant were similar to those used in the industrial production. Some of the properties of these materials used in the laboratory preparations are given below.

4.2.1 Pentaerythritol

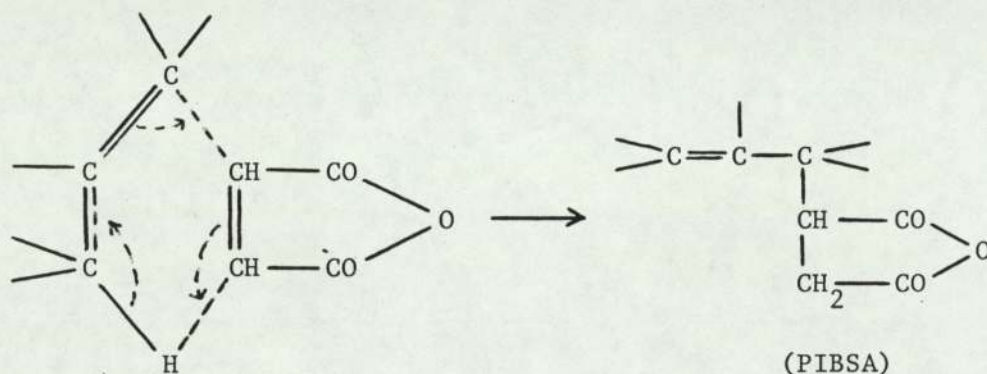
The monopentaerythritol used in the laboratory had a high hydroxyl content and low ash. Some of its important properties are as follows:⁽²⁾

MONO-PE content % (Dibenzal method)	99.0
Hydroxyl content, % min	49.5
Moisture content, % by wt., max	0.2
Ash content, % by wt., max	0.03
Initial melting point, °C, min	250.0

Details of physical and chemical properties of pentaerythritol are all given in Chapter Three.

4.2.2 Polyisobutenyl succinic anhydride (PIBSA)

This is an important intermediate in the manufacture of lube oil additives or in its own right since it is used as an oil soluble corrosion inhibitor. PIBSA is the reaction product of polybutene with maleic anhydride.⁽⁴⁾ The composition of the main "backbone" of the polybutene has been shown by N.M.R. to be largely isobutylene units for the higher molecular weight grades whilst the amount of butene-1 and butene-2 present increase with decreasing molecular weight. The reaction with maleic anhydride takes place via the Four Centre Type mechanism,⁽⁴⁾ e.g.



The reaction does not go to completion when polybutene is employed and some of the polymer is present in the product and can only be separated by tedious methods. PIBSA is also made commercially via chlorinated polybutene; a typical procedure involves chlorination at 100°C until approximately 4% chlorine is absorbed, followed by addition of a molar proportion of maleic anhydride and reaction at 190°C for several hours. The PIBSA so obtained contains very little chlorine and is usually better in colour than PIBSA prepared directly from maleic anhydride.

PIBSA is produced with different molecular weights and saponification numbers. The saponification number of the PIBSA specifically prepared for the laboratory preparation of PIBSA/PE dispersant was 103. Some of the important properties of the PIBSA used in the laboratory are given in Table 4.1.

TABLE 4.1

Properties of the PIBSA used in the laboratory preparations of PIBSA/PE dispersant.

Chlorine content wt. %	0.30
Maleic Anhydride wt. %	0.10
Saponification No. mgKOH/g	103
Sulphated Ash wt. %	0.20
Viscosity at 98.9°C $\text{m}^2/\text{s} \times 10^{-6}$	1820
Sediment Vol. %	<0.25

The test methods used in these analyses were all developed by Exxon Research Company. The PIBSA used in the laboratory preparations was prepared by the paramins plant of Esso Chemicals Limited at Fawley Refinery specifically for the purpose of this project of the sediment investigation.

4.2.3 150 Stock diluent base oil

It is a solvent extracted hydrofined and ketone dewaxed distillate from light crudes, used as a diluent oil for the reactants. This diluent base oil was also prepared at Fawley Refinery specifically for the purpose of this project and has the following properties.

TABLE 4.2

Properties of the diluent base oil used in the laboratory preparations of
the dispersant

Carbon Residue % mass	0.01
Cloud Point °C	-8
Colour ASTM	1.0
Flash Point COC °C	210
Pour Point °C	-9
Kinematic Viscosity m ² /s x 10 ⁻⁶ at 37.8°C	33
Viscosity Index	105

The test methods used in these analyses were again developed
By Exxon Research Company.

4.2.4 Sulphonic acid catalyst

Sulphonic acid is used as a catalyst for the production of
PIBSA/PE dispersant in both industrial and laboratory scales. The
acid is used after mixing it in a portion of the diluent base oil stock.
Two concentrations of sulphonic acid in oil were used in the laboratory
preparations.

- a - Concentrated catalyst grade containing 90% by wt.
active ingredients (90% A.I.)
- b - Less concentrated catalyst grade containing 70% by wt.
active ingredients (70% A.I.)

4.2.5 Filter aid and filter paper

To improve the filtration process filter aid is used in
two ways:

- a - Precoat to the filter (fixed bed): The filter is precoated with a fixed bed of filter air.
- b - Body aid (body feed filtration): The filter aid is added to the main body of the liquid.

The recommended filter aid used as Precoat and as body aid is Dicalite Special Speedflow which has the following properties:^(5,136)

Pore size, μm	4.3
Relative permeability	10*
Mean Particle Size, μm	4.8
Relative flow rate	3*

A coarser filter aid was used in a plant trial (Dicalite Speed plus) with the benefit of increased filtration rates, however, the sediment of the filtered product was slightly above the target value of <0.05 .

The recommended filter paper used for the separation is Eaton-Dikeman grade 654 (E-D 654) which has a high retention time as shown in the following listing of its main properties:⁽⁵⁾

Unit weight g/m^2	296
Thickness μm	1070
Surface	creped
Permeability	slow
Relative Retention Value**	2

* Relative permeability and relative flowrate should be similar, however, data is from two different sources.

** Retention is the filtration efficiency expressed differently by every manufacturer. In the scale used above, "1" indicates excellent retention while "6" indicates medium retention and "2,3,4 and 5" indicate intermediate values. These numbers are based on tests with a Coulter counter carried out by the manufacturers.

4.2.6 Other chemicals used

Other chemicals, such as organic solvents, are used in some of the tests carried out on the reactants or on the product. The chemicals used in the tests carried out on the laboratory preparations of the dispersant were as follows:

1. n-Heptane general purpose reagent (GPR) grade obtained from B.D.H. Chemicals Ltd., specifications as follows:

$\text{CH}_3(\text{CH}_2)_5\text{CH}_3$	M.W. 100.21
Minimum assay (GLC)	99.5%
Wt. per cm^3 at 20°C	0.682-0.684g
Boiling range not more than 1°C between 97 and 99°C	
Refractive index	1.3880-1.3885
2. Chlorobenzene GPR grade obtained from BDH Chemicals Ltd., specification as follows:

$\text{C}_6\text{H}_5\text{Cl}$	M.W. 112.56
Wt. per cm^3 at 20°C	1.105-1.108g
Boiling range (95%)	$130-133^\circ\text{C}$
Refractive index	1.5235-1.5250
3. White Spirit (BSS 245) equivalent to Stoddard Solvent (ASTM D484), suitable for use in the testing of petroleum products by ASTM methods.

Wt. per cm^3 at 20°C	About 0.77g
---	-------------
4. Tetra-n-butylammonium Hydroxide, 0.1N solution in toluene-methanol, obtained from BDH Chemicals Ltd., standardised by using benzoic acid.

5. Benzoic acid GPR obtained from BDH Chemicals Ltd.,
specification:

C_6H_5COOH	M.W. 122.12
Minimum assay (acidimetric)	99.5%
Melting point	121-122.5°C
Sulphated ash max.	0.05% by wt.
Total chlorine	0.1% by wt.

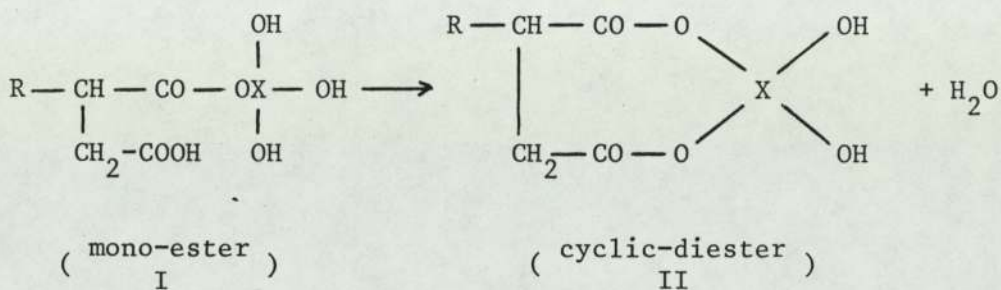
4.3 PIBSA/PE Reaction Mechanism

The initial attack of the pentaerythritol PE on the PIBSA (9,137) anhydride ring produces a half ester (Structure I in the equations to follow). Subsequently intermolecular esterification occurs to give the cyclic-diester (Structure II).^(7,9) However, since there is a slight molar excess of PE to PIBSA, there is also a small amount of di-PE substituted PIBSA molecules (III). There are also small amounts of other side products mainly because of the polyfunctional nature of both PIBSA and PE. The side products are mainly polymers and branched chains.

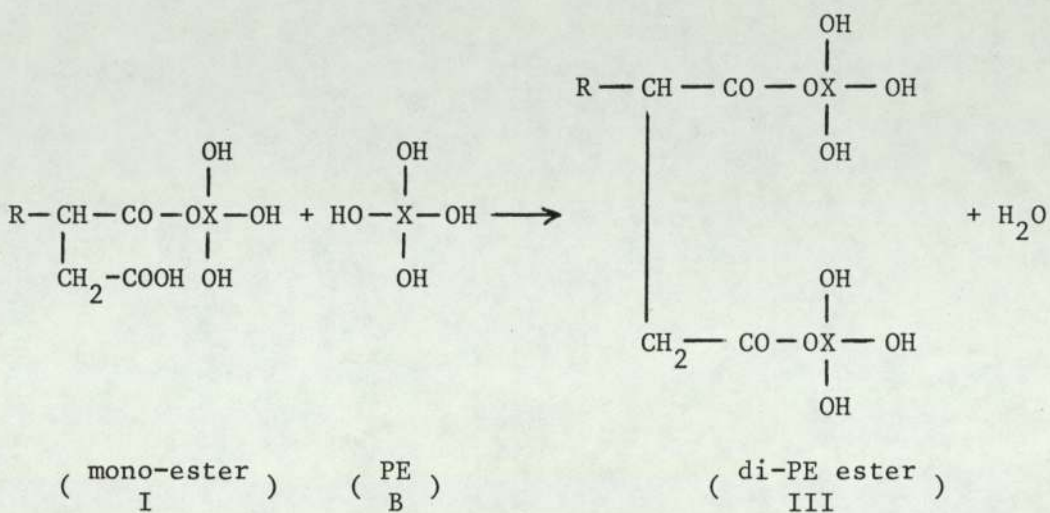
One type of a side product is 2:1 PIBSA:PE represented by structures (IV) and (V). Further successive addition of PE and PIBSA leads to linear polymers such as structure (VI). PE ether linkages may also produce side products such as structure (VII). Cross-linked structures occur through the reaction of free carboxylic acid group on one chain reacting with a free hydroxyl group on another chain (VII). Branching occurs through growth at two sites on the same chain as represented by structure (IX). Also since a large fraction of the PIBSA is in the form of $PIB(SA)_2$, branched products can be formed through reaction of both - SA molecules as represented by structure (X).^(138,139)

Evidence of these structures are obtained from literature sources, potency considerations and analytical data which are in agreement

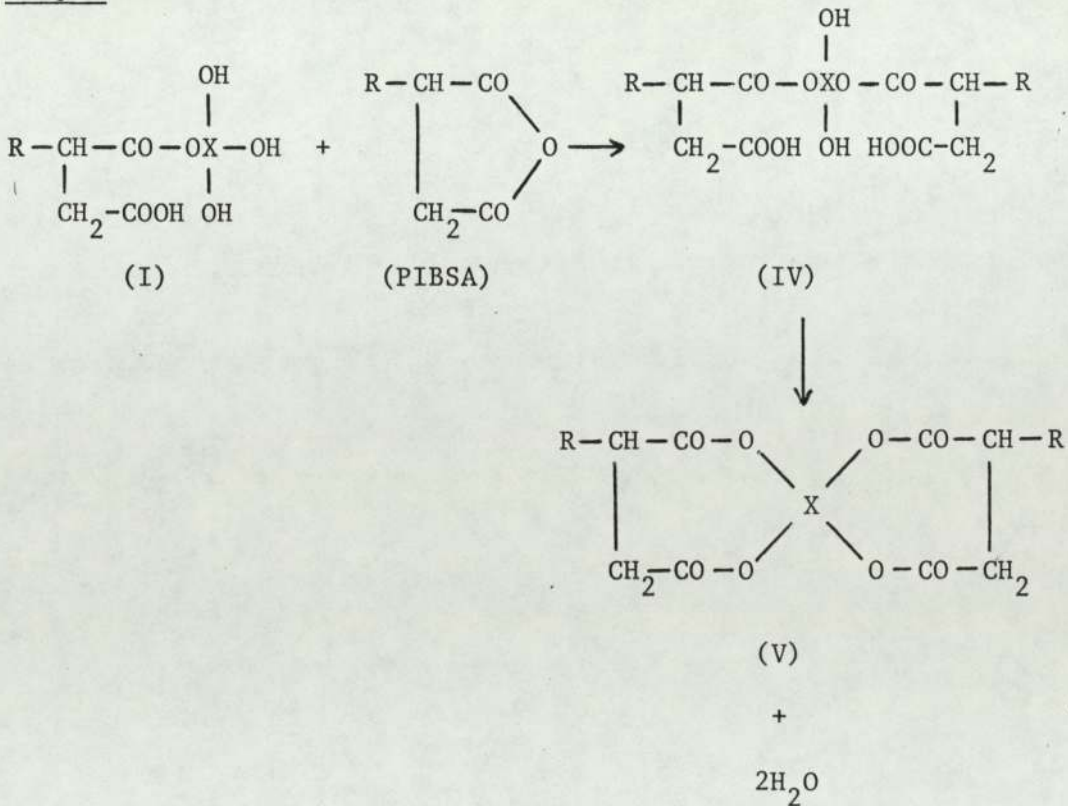
Step 2



Step 3



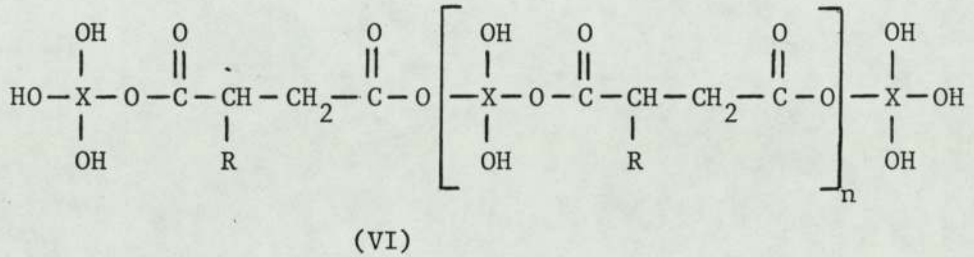
Step 4



Other side reactions do exist depending on the ratio of PE/PIBSA used and on other production conditions, they are mainly:

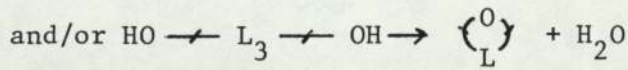
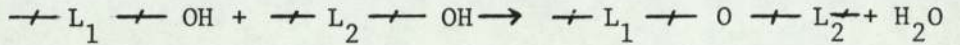
a. Linear polymer formation

As an example of this the following is presented:

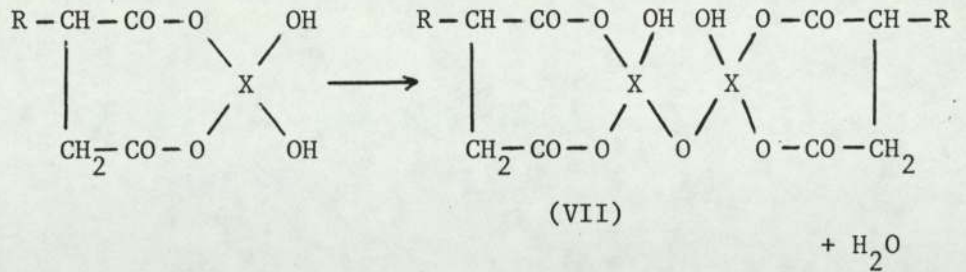


b. Etherification or ether formation

If $\text{---} L_1 \text{---}$, $\text{---} L_2 \text{---}$, $\text{---} L_3 \text{---}$, etc. are liquid phase moieties, then

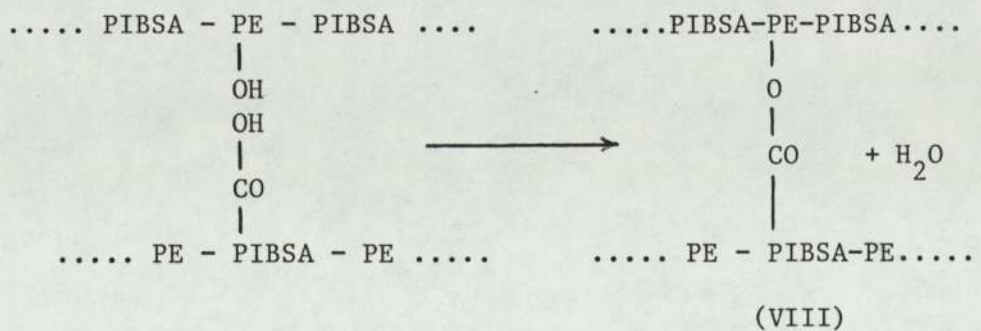


an example of ether formation ³ is



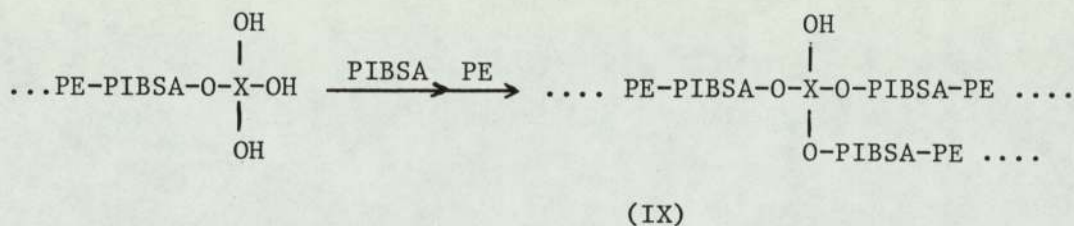
c. Cross-linking

(e.g.)

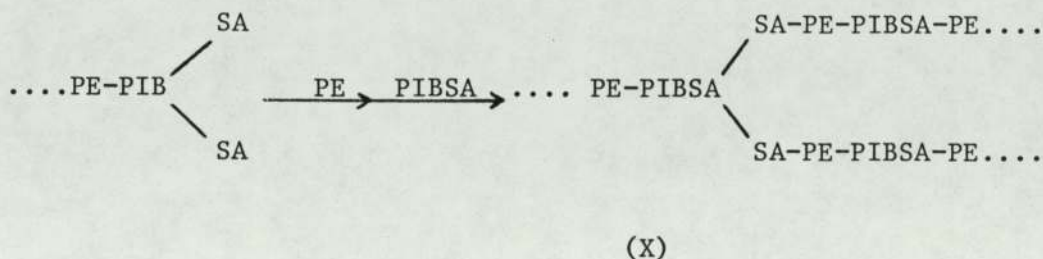


d. Branching

Two examples are given here on branching:



and



4.4 Summary of Process Description

A summary of the steps carried out in the industrial production of PIBSA/PE dispersant is given below. This would enable a comparison to be made between industrial production and laboratory preparations of the dispersant. The steps are very briefly as follows:⁽¹³⁵⁾

(See also Appendix 1).

1. A nominal rate of nitrogen sparge is used to maintain an inert atmosphere during charging of materials and the heat up stage of the reaction.
2. The initial dilution oil in the reaction is charged into the reaction vessel first, followed by the hot PIBSA.
3. When the temperature of the PIBSA/oil mixture is low enough, the catalyst mixture is then charged to the vessel.
4. Pentaerythritol is then charged to the vessel at a low enough temperature and at a fast rate while keeping

that temperature nearly constant.

5. The nitrogen sparge rate is increased to about double the volume of the reaction mixture per hour.
6. Heating is started after pentaerythritol addition at a slow rate to the required reaction temperature.
7. Samples are withdrawn periodically and analysed for the Total Acid Number (TAN) during the heating and reaction stages. When the TAN becomes lower than a certain set value, cooling of the reaction mixture is started.
8. The nitrogen sparge rate is reduced to about a third of its value during the cooling stage.
9. Cooling is carried out very slowly from the reaction temperature to the filtration temperature, increments of oil are added during the less critical stages of the cooling period to speed up the cooling process.
10. When the raw product temperature is steady at the filtration temperature the body aid is added to it and mixed thoroughly until uniformly dispersed.
11. For precoating and preheating the filter, the required amount of the precoat is mixed thoroughly with oil in the precoat drum, the slurry is then circulated through the filter via a preheater and then back to the drum.
12. When the filter temperature is nearly equal to filtration temperature and the sediment test on its outlet gives a satisfactory result, the filter is assumed ready for filtration.

13. The precoat circulation is stopped and the raw product is directed to the filter, the filtrate being sent to the product tank directly. Tests are carried out every hour on filtrate samples for sediment and haze checks. This is continued until the rate of filtration falls down below the minimum acceptable rate, then the filter is stopped, washed, blown and made ready for a new filtration cycle.

CHAPTER FIVE

THE EXPERIMENTAL RIG

5.1 Introduction

A rig was constructed in a fume cupboard in the laboratory to enable the following investigations to be carried out.

1. Reaction kinetic studies
2. Laboratory preparation of PIBSA/PE dispersant to investigate the sediment formation during storage.

There are two main sections in the rig, they are as follows:

- a. The reaction and crystallization section.
- b. The filtration section.

Photographs of the rig and of both sections are given in Figures 5.2, 5.3 and 5.4, also a schematic diagram of the whole rig is shown in Figure 5.1 with the component numbers marked on it. Details of these components in each section are given below.

5.2 Reaction and Crystallization Section

This is the top part of the schematic diagram in Figure 5.1, equipment details are as follows:

5.2.1 Reaction flask and accessories

A Quickfit, type FRILF, spherical glass reaction flask of nominal capacity 1 dm³ was used (item No. 1 in Figure 5.1). The vessel was fitted with a Quickfit, type MAF3/52, multi-socket, flat flange, glass lid having one central and four peripheral openings. A Quickfit, type JC100F, metal clip was used to clamp the lid to the vessel using a P.T.F.E. gasket. The overhead glass lid was heated from the outside by an electrical heating tape (heat by the yard tape, from Electrothermal

Engineering Ltd., Cat. No. CC501), and was fully insulated by glass wool to prevent condensation of water of reaction on its inner surface. The voltage to the heating tape was regulated by a variac, Cressall Torovolt model 64 Zp, and a maximum voltage of 15 volts per 300 mm tape length was used.

The flow of the low pressure nitrogen sparge was measured by a glass flowmeter (item No. 4) calibrated with air at STP and had a range of 0 to 3.7 dm³/min. A Quickfit glass distribution tube Cat. No. 232/2061, porosity 2, overall length 310 mm (item No. 5) was used to disperse the nitrogen into the reaction mixture. A Quickfit water cooled condenser Cat. No. C4/12 was used to condense the water of reaction (item No. 12). The condenser was fitted with two independent cooling coils and has an approximate surface area of 0.055 m² and overall length of 395 mm. Different types of Quickfit adaptors were used to connect these items to the peripheral openings in the overhead glass lid.

5.2.2 Heating system and temperature control

A type MUL/IL, 240V, 300W, isomantle laboratory heater was used to achieve heating and operating temperature (item No. 6). The heater was connected to a Stanton Redcroft programmable temperature controller model 681 (item No. 8) which controlled the rate of heating or cooling at the required preset value by regulating the voltage to the heater. The controller employed a platinum resistance sensor (item No. 7) introduced into the reaction vessel through one of the peripheral openings in the overhead glass lid using Quickfit cone/screwthread adaptor for the connection. The controller had a sensitivity of less than 0.5°C and a nominal working range of 0° to 350°C.

5.2.3 Temperature measurement

The temperature of the reaction mixture was measured by means of a Ni-Cr thermocouple introduced into the mixture directly through the same peripheral opening used for the platinum resistance sensor (item No. 9). The thermocouple was connected to a Comark electronic thermometer type 1601 which had its own cold junction compensator and had a built-in selector unit for ten thermocouples (item No. 10). It had a very wide temperature range and its indicator had three scales A, B and C to cover this range. Scale C was used which had an intermediate temperature range of 0 to 320°C and an accuracy of $\pm 0.5^{\circ}\text{C}$. The electronic thermometer was connected to a potentiometric recorder type RE 541.20 (item No. 11) so as to keep a permanent record of the temperature change during the whole production cycle, and to make sure that the temperature remained steady during the reaction, crystallization and filtration stages.

5.2.4 Agitation

Three types of stirrers were used during the performance of the experimental program (item No. 2), they were:

- a. A six blade turbine impeller made of brass of 32 mm diameter.
- b. A stainless steel three blade propellor of 50 mm diameter and a pitch of 45° .
- c. A stainless steel six blade turbine impeller of 60 mm diameter.

In all three cases a stainless steel shaft of 6 mm diameter was used which was inserted into the reaction vessel through the central opening in the glass lid. Two types of stirrer glands were used, one was a Quickfit stuffing box type, P.T.F.E., Cat. No. ST3/2F, to fit stirrer guide ST2/2, cone size 19/26, and the other was also from Quickfit, but ground sleeve type

Cat. No. ST20/2, to fit shaft size 6 mm, cone size 19/26, thread size 13 mm. A Voss electric motor of type S8, Cat. No. K867/18 with variable speed was used to drive the stirrer (item No. 2A). Although the stirrer speed was controlled directly by setting the Voss motor to the required speed, it was found that a better speed control was obtained when a Cressall Torovolt voltage regulator model 55Zp was included in the circuit especially at lower speeds.

The stirrer speed was measured using a Comark stroboscopic tachometer type 2101 which could have measured speeds up to 30000 r.p.m. Speed measurements were made on an intermediate scale with full scale deflection corresponding to 3000 r.p.m. On this scale the measurements were accurate to within ± 10 r.p.m.

5.3 Filtration Section

This is the bottom part of Figure 5.1, equipment details are given below:

5.3.1 Pressure filter and accessories

The main body of the filter was a hollow cast iron cylinder of 132 mm inner diameter and a height of about 132 mm (item No. 14 in Figure 5.1). The filter had a bottom flange (item No. 18) that had a grooved inner surface with an outlet in its centre for the collection and withdrawal of the filtrate (item No. 19) (see also Figure 5.4 for details of the grooves). In each run the bottom flange was removed momentarily to place the new filter paper and its support the filter cloth on top of the grooved surface (item No. 17); after that the flange was tightened up in place ready for heating up and then filtration. The product to be filtered was introduced manually from the top of the filter after removing the top flange momentarily, then tightening it in place

afterwards (item No. 15). Filtration was carried out by pressurising the filter with nitrogen from a high pressure cylinder using a 0 to 250 psig pressure regulator.

5.3.2 Heating system and temperature control

Two electric heaters were used to heat up the filter, they were as follows:

- a. A Hedin 1250W electric metal heater type BH 1637 was used to heat the main body of the metal filter and was heavily insulated with glass wool (item No. 20A).
- b. A Hedin 300W electric heater was used to heat the bottom flange of the filter (item No. 20B).

Both heaters were connected to a Diamond H proportional temperature controller model DH 82 (item No. 22) which controlled the temperature by regulating the voltage to both heaters directly or through the use of a Cressall Torovolt voltage regulator model 66Zp (item No. 23). The nominal working range of the temperature controller was 0 to 250°C and it had a sensitivity of 1°C. The temperature sensor of the controller was a Ni-Cr thermocouple in direct contact with the mixture as explained in the next section.

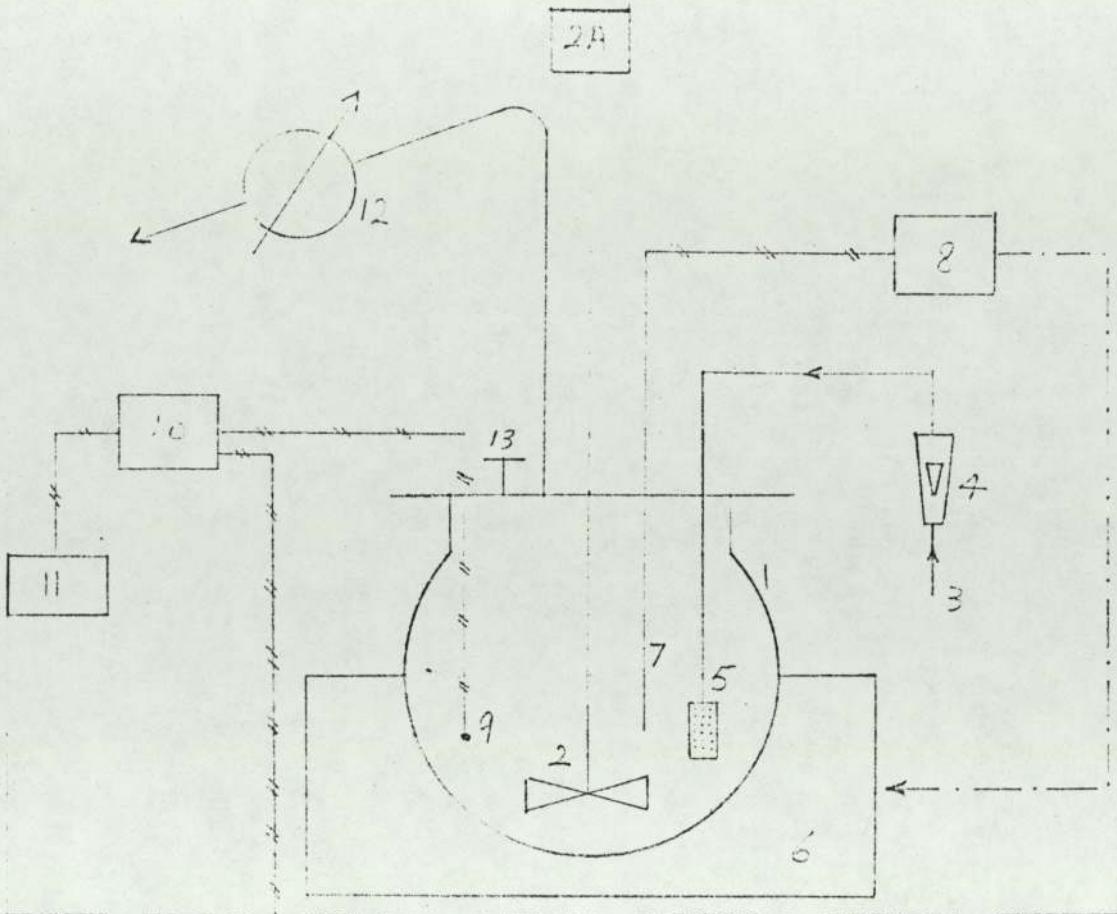
5.3.3 Temperature measurement

Two Ni-Cr thermocouple leads were passed through a piece of stainless steel tubing and glued to its end forming a thermocouple probe, one was used to measure the temperature, the other was the controller sensor. Originally the filter had a thermowell in place of the probe but temperature control was not accurate enough, so the thermowell was removed and the probe prepared and introduced in its place. The thermocouples were about 2 mm above the filter paper, and hence were measuring the raw product temperature directly. Araldite was used to glue the thermocouples

to the stainless steel tube end because it had a good resistance to the operating temperatures and pressures (and in fact proved very successful). One of the thermocouples was connected to the proportional temperature controller of the filter (item No. 22) to complete the control circuit, while the other thermocouple was connected to the electronic thermometer indicator (item No. 10) described in the reaction equipment section. This way a permanent record of the filtration temperature was obtained through the potentiometric recorder (item No. 11) which was connected to the Comark electronic thermometer as was explained in the reaction equipment section.



Reaction section



Filtration section

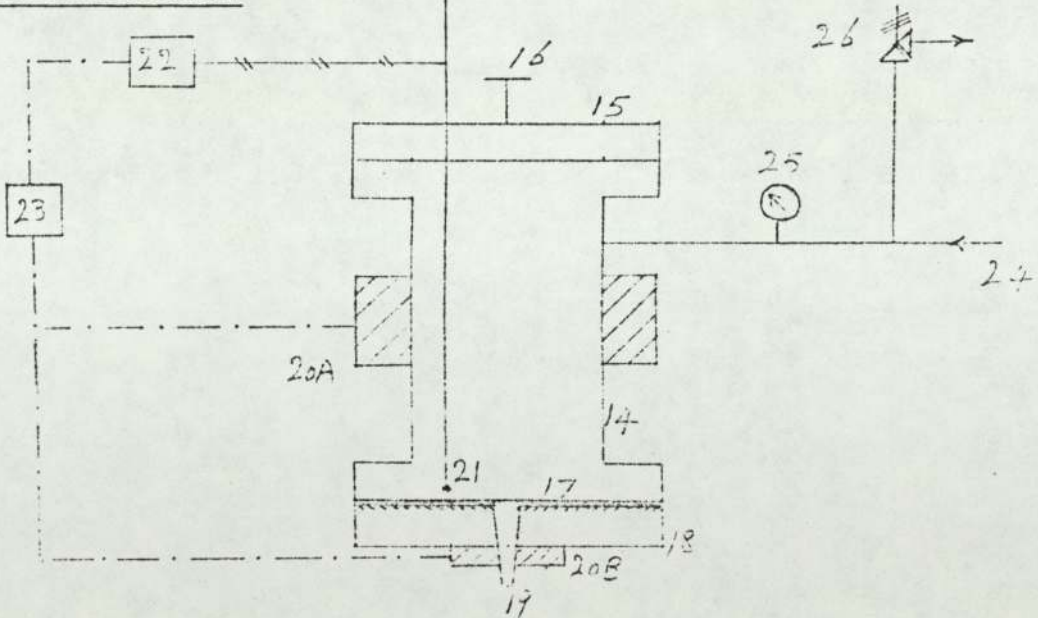


Figure 5.1: The schematic diagram of the experimental rig, reaction section (top), and filtration section (bottom)

Figure 5.1 (continued)

Reaction and crystallization section

1. Glass Reaction Flask
2. Six blade stirrer turbine impeller
- 2A. Stirrer Motor
3. Low pressure nitrogen sparge
4. Nitrogen flowmeter
5. Gas distribution tube
6. Electrical heating mantle
7. A platinum resistance sensor
8. Stanton Redcroft temperature controller
9. Ni-Cr thermocouple
10. Comark electronic thermometer
11. Potentiometric Recorder
12. Water cooled condenser
13. Large peripheral opening for charging materials and
sampling

Filtration section

14. A hollow metal cylinder (Filter body)
15. Removable filter top flange
16. Top flange handle
17. Filter paper and its support the filter cloth
18. Removable grooved bottom flange
19. Filtrate outlet
- 20A. Filter body electric belt heater
- 20B. Bottom flange electric heater

Figure 5.1 (continued)

21. Ni-Cr thermocouple probe
22. Filter temperature proportional controller
23. Voltage regulator
24. High pressure nitrogen gas
25. Pressure gauge
26. A pressure safety valve

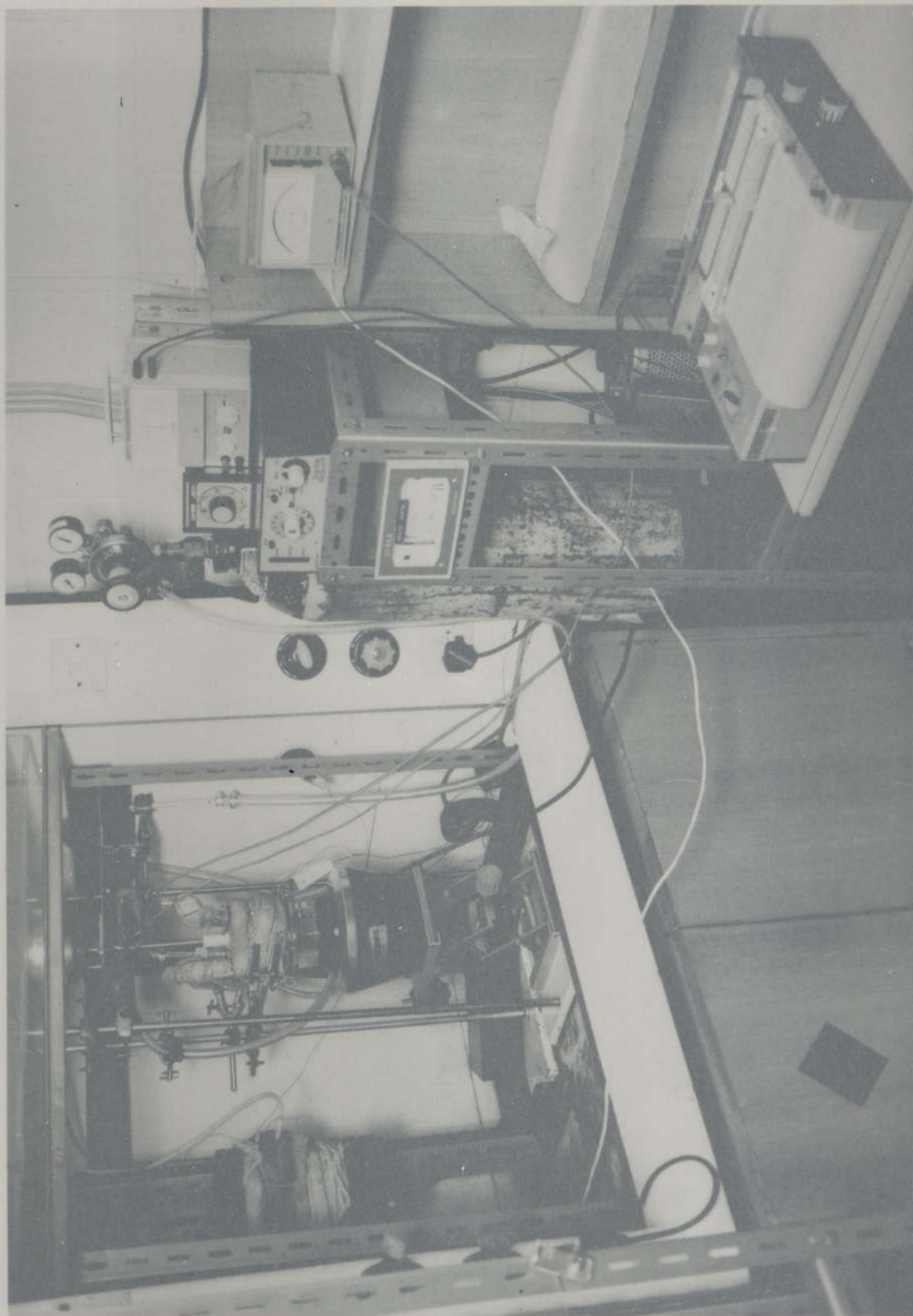
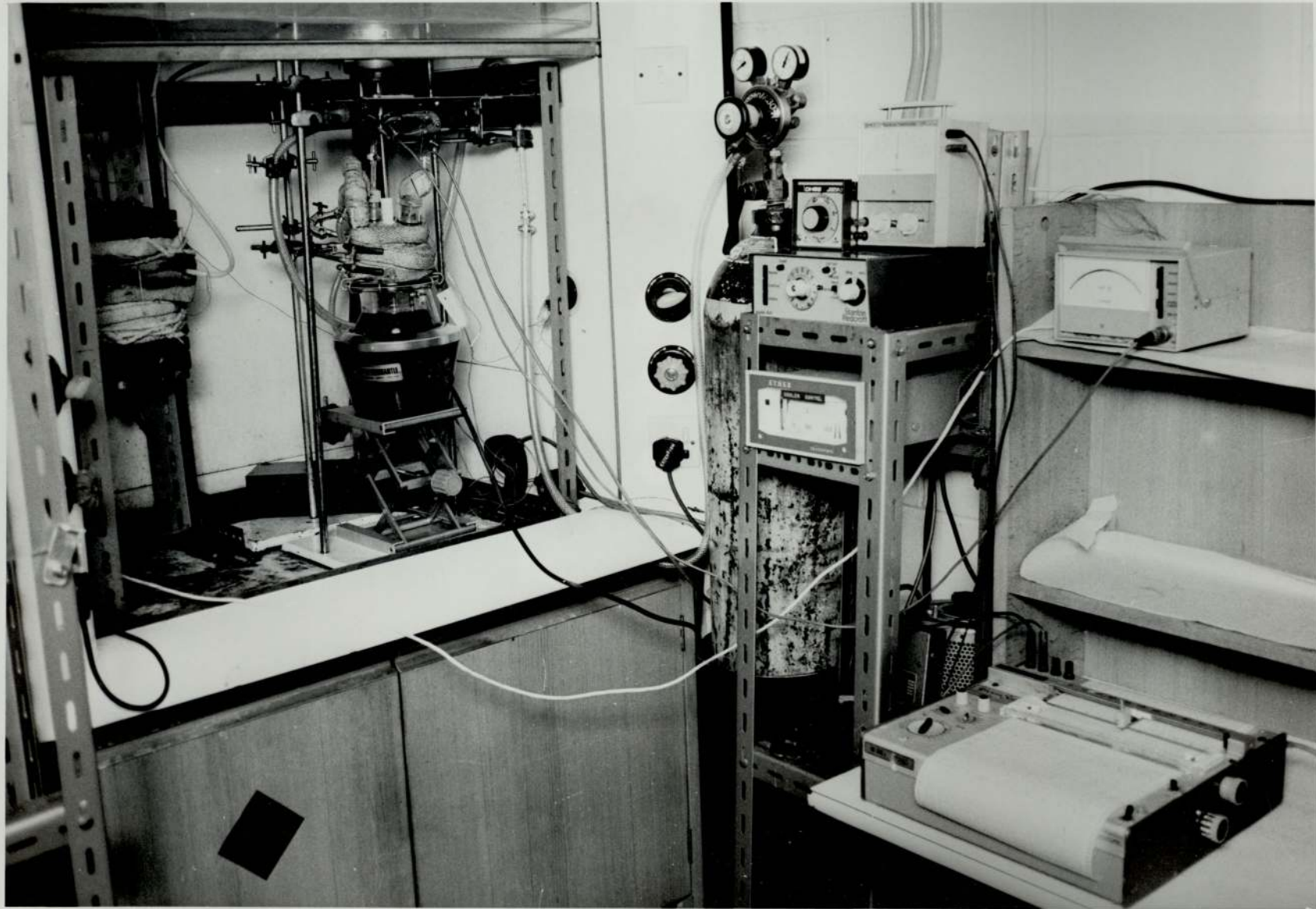


Figure 5.2: Overall view of the experimental rig used in the laboratory preparation of the PIBSA/PE dispersant additive



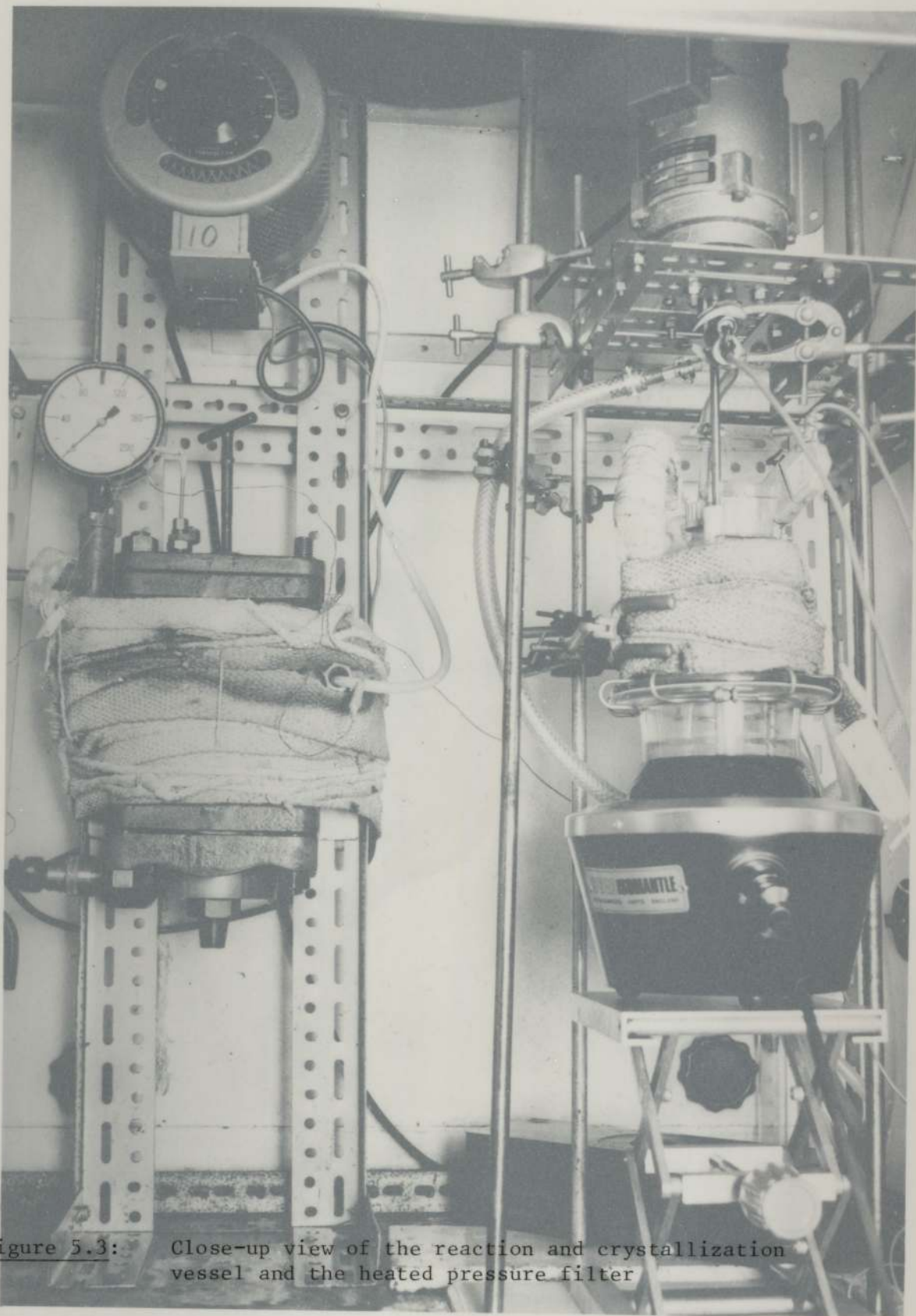
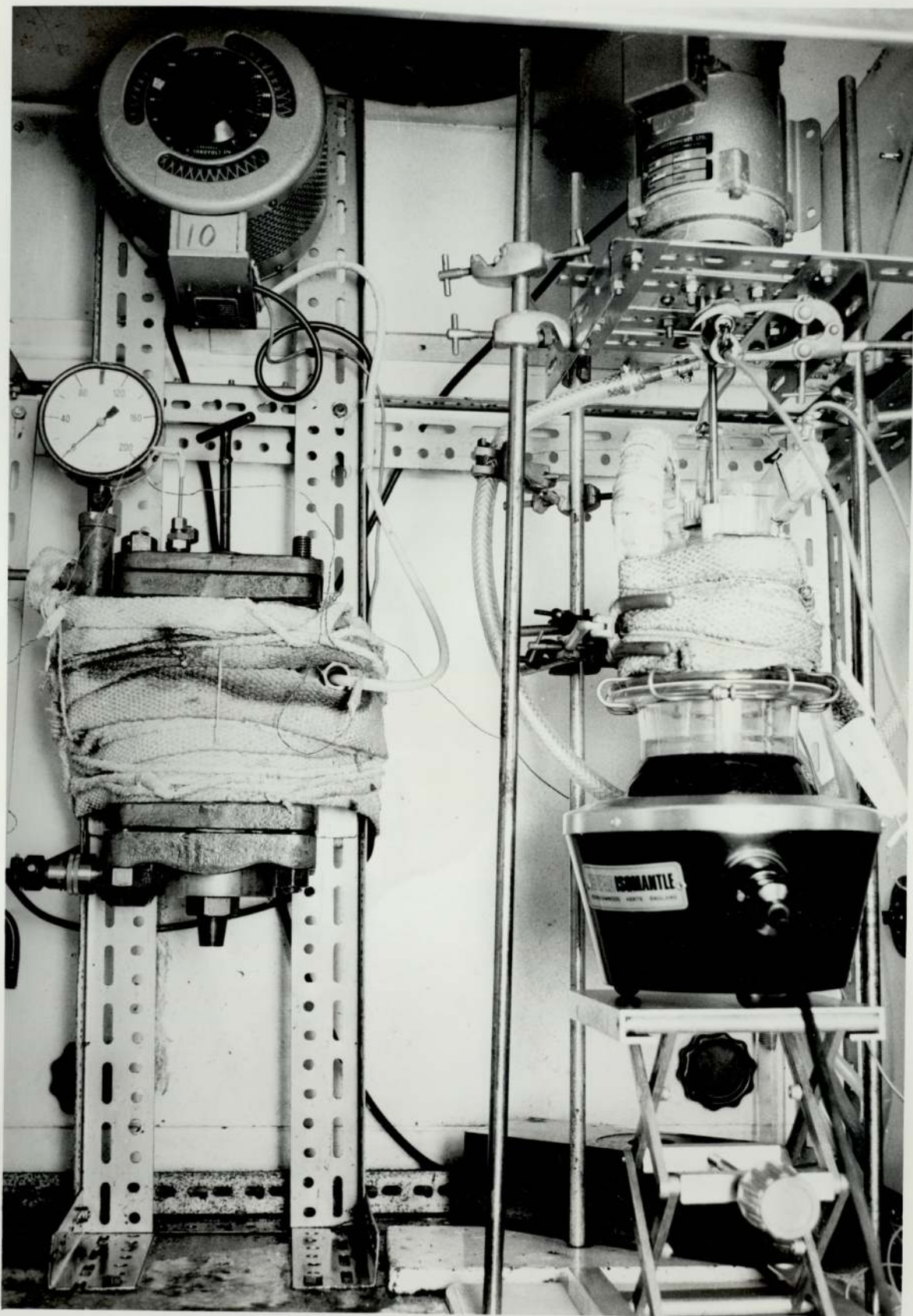


Figure 5.3: Close-up view of the reaction and crystallization vessel and the heated pressure filter



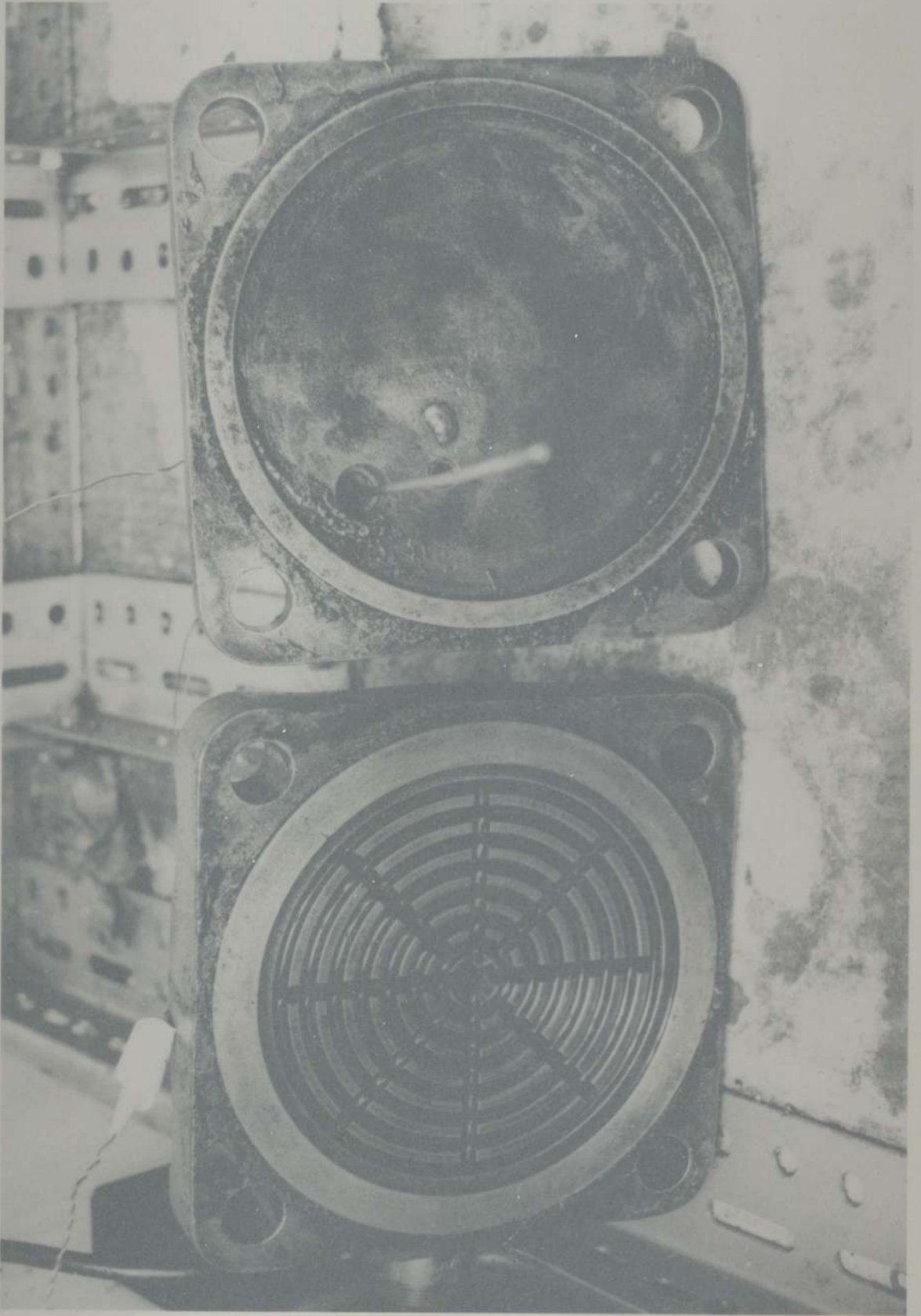
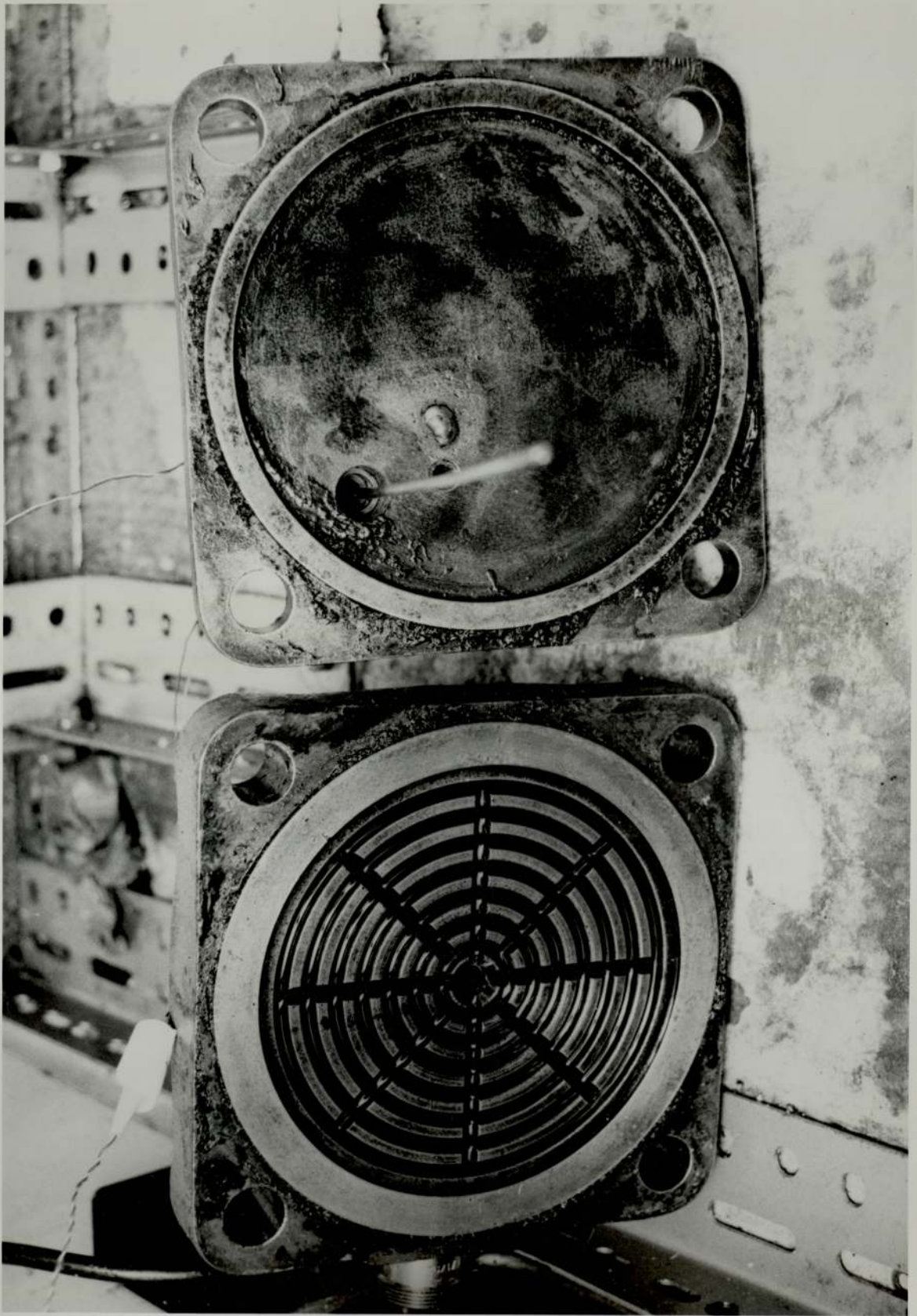


Figure 5.4: Close-up view showing the details of the inside of the pressure filter top and bottom flanges



CHAPTER SIX
EXPERIMENTAL WORK

6.1 Introduction

The two main areas of the experimental work were:

- a. the study of PIBSA/PE reaction kinetics
- b. the investigation of the sediment formation in the product.

An experimental rig was constructed in the laboratory for this purpose, details of which were given in Chapter Five. In the course of this investigation several techniques were used namely, Nuclear Magnetic Resonance (NMR), ultracentrifugation and Infra-Red Spectroscopy (IR). Detailed size analysis of pentaerythritol crystals was also carried out in which sieve analysis and the Malvern lazer size analyser were used. Particle size analysis will be dealt with in the next chapter, while all the rest of the investigation will be considered in this chapter.

6.2 Reaction Kinetics Investigation

The object of this investigation was the development of an approximate rate equation for the esterification reaction of PIBSA with pentaerythritol (PE). The rate expression that was assumed by considering the overall esterification reaction (see chapter eight for assumptions and justifications) was,

$$(-r_A) = k_o \cdot e^{\frac{-E}{RT}} \cdot C_A^a \cdot C_B^b \quad 6.1$$

6.2.1 Conditions of kinetic runs

The kinetic runs were carried out in such a manner so as to evaluate the parameters of the rate expression given in equation (6.1) above. A total number of sixteen kinetic runs were carried out (runs 36 to 50 and

also run 63) with different values of PE/PIBSA equivalent ratio and temperature, but in all these runs the following were kept constant.

- a. Nitrogen sparge into reaction mixture ($0.1 \text{ dm}^3/\text{min}$)
- b. Stirrer speed (700 r.p.m.)
- c. The percent oil dilution used with the PIBSA (77.68% wt. on PIBSA)
- d. The catalyst ratio (except in three runs only where it was nearly doubled, see Table 6.1)

Table 6.1

Summary of conditions of all the kinetic runs

Run No.	Weight of PIBSA (g)	PE/PIBSA equivalent ratio (α)	Catalyst		Reaction Temperature $^{\circ}\text{C}$
			Type	% wt. on PIBSA	
36	405.17	1.0	90% A.I.	2.2	200
37	405.09	0.5	"	2.2	200
38	399.18	0.25	"	2.2	200
39	402.82	1.0	70% A.I.	1.18	200
40	406.69	0.5	"	1.18	200
41	401.08	0.25	"	1.18	200
42	401.47	1.25	"	1.18	200
43	404.10	1.5	"	1.18	200
44	403.59	2.0	"	1.18	200
45	402.00	1.0	"	1.18	200
46	404.31	1.0	"	1.18	180
47	401.90	1.0	"	1.18	190
48	405.13	1.0	"	1.18	210
49*	404.25	1.0	"	1.18	200
50	405.64	1.0	"	1.18	150
63	404.95	1.0	"	1.18	220

* Run 49 was a repeat of run 39 but the reaction was followed using a potentiometric titrator to enable a comparison to be made between the two sets of results obtained.

6.2.2 Experimental procedure for kinetic runs

The same procedure was carried out in all the kinetic runs. The required amounts of PIBSA, dilution oil and catalyst were weighed in the reaction flask first, then nitrogen sparge and the stirring speeds were started at the required rates, $0.1 \text{ dm}^3/\text{min}$ and 700 r.p.m. respectively. The PIBSA/oil/catalyst mixture was heated up gradually to the required reaction temperature and was kept there. Then the calculated amount of pentaerythritol was weighed and added to the mixture at the reaction temperature with great speed (in about 30 seconds only) and a sample was drawn immediately to calculate the initial TAN (at $t=0$). Then samples were taken out every six minutes for the initial half hour since the catalysed reaction was very fast especially at higher temperatures. After that samples were withdrawn every fifteen minutes, then every thirty minutes and finally every hour up to about a total of six hours or more, in fact until the change in TAN became very small and a final residual TAN estimation was possible.

To calculate the Total Acid Number TAN, each sample was weighed, dissolved in 75 cm^3 of chlorobenzene and then titrated with standardised 0.1N solution of tetra-n-butylammonium-hydroxide using thymol blue as an indicator solution. An outline of the method used for the TAN calculations is given in Appendix 3. A potentiometric titrator model E536 (Metrohm series) was used in measuring the TAN of samples from the last six runs (46 to 50 and run 63 also). Colour titration was also used in these six runs and results of both methods were compared.

The density of the initial reaction mixture was measured at different temperatures, and the density of the reaction product at the end of each run was also measured. This enabled an average density to be used over the reaction period in the evaluation of the parameters of the rate expression.

Infrared spectroscopy was also used in the analysis of two runs for the reaction kinetic study. An account of the technique and procedure used is given below in Section 6.4.

6.3 Sediment Formation Investigation

To carry out this investigation the dispersant had to be prepared successfully in the laboratory. Many variables were used in the dispersant preparation runs, and several procedures were carried out on the prepared samples of the dispersant from different runs. As a result of this the effect of production variables and storage conditions on sediment formation was studied successfully.

6.3.1 Laboratory Production of PIBSA/PE dispersant

Sixty three production runs were carried out. Sixteen of these runs were kinetic runs for the purpose of the evaluation of the approximate rate expression, while the remaining 47 runs were performed for the purpose of the sediment investigation. The production procedure, production variables and product analysis are summarised below.

6.3.1.1 Production procedure

The same procedure was carried out in most of the production runs for sediment investigation. In a few runs some variations were made which will be discussed when considering those specific runs. The following were the main steps of this procedure:

1. The required amount of PIBSA at a temperature of about 80°C was weighed in the reaction flask (1) (see Figure 5.1).
2. The preliminary amount of dilution oil was then weighed in the flask followed by the catalyst, both being at ambient temperature.

3. The reaction flask was then placed back in its heating mantle (6) and the system was set as shown in the top section of Figure 5.1.
4. Nitrogen sparge was then started at a rate of $0.1 \text{ dm}^3/\text{min}$ and kept at this value during the whole cycle.
5. Cooling water was commissioned to the overhead condenser.
6. The electric stirrer was started at speeds varying between 700 r.p.m. and 900 r.p.m. depending on the type of impeller used in that specific run.
7. Controlled heating of the mixture was started at a set rate of about $2^\circ\text{C}/\text{min}$, using the programmable controller (8), up to 140°C , the temperature was then held at 140°C ready for Pentaerythritol addition.
8. The required amount of PE was weighed in a separate beaker, then added directly into the reaction flask from the overhead inlet (13) at the temperature of 140°C . The addition time of PE was about two minutes.
9. Heating was started again at a set rate of $0.5^\circ\text{C}/\text{min}$ up to the reaction temperature and then held at that temperature. During this heating period samples were taken from the reaction mixture through inlet (13) using a specially constructed stainless steel sampling pot, and were then analysed for the total acid number (TAN) using the method outlined in Appendix 3. In addition a pH meter with the appropriate glass electrode was used and a pH titration also carried out.
10. When the TAN of the reaction mixture fell below about 8 mgkoH/g sample, cooling of the reaction mixture was started from reaction temperature to filtration temperature (about 140°C). The cooling rate was varied depending on the actual run, and was

carried out by the same programmable controller (8) which was used for cooling as well as heating.

11. The required amount of the dilution oil was weighed, heated to 140°C then added to the reaction mixture in flask (1) through inlet (13). The whole system was left at filtration temperature of about 140°C for a long period of time depending on the run itself (in some runs it was left overnight, in others it was left for more than 60 hours at filtration temperature). The temperature of the whole cycle was measured by the electronic thermometer (10) and recorded by the recorder (11). At the end of this period and just before filtration was started, a 50 cm^3 sample was withdrawn from the mixture to be analysed for sediment content of the raw product; an outline of the method used is given in Appendix 4.
12. At this stage the pressure filter was prepared for filtration which was achieved by setting the filter as shown in the bottom section of Figure 5.1. The bottom flange was tightened up, with the filter paper and cloth acting as gasket to prevent leakage to the outside. The top cover of the filter was removed and some dilution base oil was introduced from the top, then the top cover was placed back and tightened up. Heating of the filter was started gradually to about 140°C and the temperature was kept at 140°C under the influence of the proportional controller (22) by controlling the power input to the metal heaters (20A) and (20B).
13. The filter was then pressurised with nitrogen gradually and the oil was collected from the filter outlet (19) into a beaker. The filter was then ready to be used, so the reaction section apparatus was dismantled and the reaction mixture in the

flask was poured manually into the top of the metal filter (after removing its top cover). When this was carried out, the filter top cover was tightened up again, nitrogen was introduced to raise the pressure gradually to the required value and filtration started. The filtrate obtained was then collected from the filter outlet (19) into a tall graduated beaker and a stop clock was used to time the flow of filtrate. The filtration temperature was kept between 135°C to 140°C by the proportional controller (22), and it was recorded using the electronic thermometer (10) and the recorder (11).

14. When filtration was completed a 25 cm³ sample was taken from the filtrate to be analysed for kinematic viscosity of the filtrate. Then the filtrate was weighed and the final amount of the dilution base oil was then added and mixed thoroughly with the filtrate to obtain the final dispersant product.

The above procedure was carried out in production runs using no filter aid. Filter aid was used in few runs only, in which case the body aid was added with the dilution oil to the reaction mixture just before filtration and the precoat was added with the oil into the pressure filter during filter preparation (point No. 12 in this production procedure).

6.3.1.2 Production variables and conditions

The effect of some production variables on sediment formation and also on crystal size distribution (CSD) of pentaerythritol crystals (which in turn will effect filtrability of the product) was studied by making certain changes in these variables in different production runs.

The main variables were:

- a. Reaction temperature
- b. Reaction time
- c. PE/PIBSA equivalent ratio
- d. Catalyst type and ratio
- e. Cooling rate from reaction temperature to filtration temperature
- f. Mixing rate during cooling stage
- g. Seeding with PE crystals during the cooling stage
- h. The time the reaction mixture is left at filtration temperature before filtration was started
- i. Filtration temperature.

Some other changes in certain runs were also made like the changing of the stirrer impeller and speed, and also the use of filter aid. Details of these changes with the production conditions for all the runs are presented in Appendix 2.

6.3.1.3 Product analysis

The following tests were carried out on product preparations from all the runs:

- a. Total Acid Number (TAN). A 5g sample was weighed and then tested for the final TAN. An outline of the method used is presented in Appendix 3.
- b. Sediment content. A 50 cm³ sample was centrifuged with 50 cm³ n-Haptane in a special graduated 100 cm³ centrifuge tube. An outline of the method used is presented in Appendix 4.

- c. Kinematic viscosity. A 20 cm³ sample was taken from the product and was tested for kinematic viscosity at 100°C. An outline of the method, together with viscosity calculations and viscometer calibrations are all presented in Appendix 5.
- d. Water content. This fourth test was performed only a limited number of times, and was carried out by dissolving 150g sample into 150 cm³ of a mixed solvent (60% white spirit and 40% n-Heptane), then distilling the solution and collecting the water in a special trap. The test method used for the determination of percent water by weight in the final product was ASTM D95.

6.3.2 Effect of storage temperature on sediment formation

To be able to assess this effect the product of each run was divided into four portions, each of which was stored at a different temperature namely, ambient, 50°C, 90°C and 150°C. A storage temperature of 120°C was also investigated at a later stage because of the big difference obtained between the results of storage at 90°C and 150°C. Centrifuge tests for sediment level checks were carried out periodically on these portions and the results were tabulated for each run separately.

Apart from this some product portions were stored at high temperature first (150°C) then shifted to lower storage temperature afterwards, while the reverse was done with other portions. In both cases periodical centrifuge tests were carried out for sediment level checks.

6.3.3 Effect of product dilution on sediment formation

To distinguish between viscosity effects and temperature effects product samples of different runs were diluted with oil, n-Heptane or

chlorobenzene and were stored at different temperatures. The following is a summary of these samples:

- a. Samples from runs 13 and 21, diluted with base oil, also other samples were diluted with n-Heptane. All samples were stored at ambient temperature.
- b. Samples from runs 34 and 35, diluted with n-Heptane and stored at ambient and at 50°C.
- c. Samples from runs 52 and 54, diluted with chlorobenzene and stored at ambient, 50°C and 90°C. The viscosities of all these samples were measured at the actual storage temperature so that comparison could be made between the results at similar storage conditions. Periodical centrifuge tests were carried out on all of these samples and results tabulated.

6.3.4 Sediment analysis

The sediment obtained needed to be analysed if a theoretical explanation was to be formulated. Some of the sediment originated from the PIBSA and had to be removed. Hence in runs 13, 14 and 15 the PIBSA was filtered first and no filter aid was used during the filtration in these runs. The sediment from these runs was washed with oil, purged with nitrogen, washed with heptane, filtered and finally dried, ready for analysis.

A second type of sediment was that obtained during storage of the product at slightly higher temperatures. Hence when centrifuge tests were carried out on stored product samples, the sediment obtained at the bottom of the centrifuge tubes was collected, washed with n-Heptane many times, filtered and finally dried, ready for analysis.

The melting points of the two types of sediment collected were measured using a melting point apparatus from Townson and Mercer Ltd., model No. 66/01313. Also the two types of sediment were studied under the microscope and photographs of its crystalline structure were obtained.

Apart from the melting points measurement, four sediment samples were analysed using Gas Chromatography. The samples were:

- a. Sediment obtained at the end of run 13
- b. Sediment obtained at the end of run 14
- c. Sediment obtained from the bottom of centrifuge tubes
- d. High purity monopentaerythritol supplied by ICI.

The analysis by gas chromatography was carried out by converting the mono-, di-, and tri-pentaerythritols (if any) into their volatile acetate esters by refluxing for 6 hrs a mixture of 1g of compound 10 mg p-toluene sulphonic acid, and 5 cm³ of acetic anhydride. The solution was analysed by GC after cooling to ambient temperature. The GC analysis was carried out at the Esso Research Centre in Abingdon.

6.3.5 Reheating and refiltration of the final product

One possible reason for the formation of sediment at storage was the presence of very fine pentaerythritol crystals which were very difficult to separate from the product during filtration. To investigate this possibility the product of runs 33, 34 and 35 were divided into two halves, one half was stored at 120°C while the other half was reheated again to reaction temperature to try and react these pentaerythritol particles again. The reheated product was refiltered again and the new product was analysed for TAN and kinematic viscosity then divided into portions each of which was stored at different temperature. Periodical centrifuge tests were carried out on all the products and reheated products and the results were tabulated.

6.3.6 Refiltration of the product after storage

One suggested method of stabilising the product was the removal of the sediment after its formation at storage. Products of different runs were refiltered again at a temperature of about 88°C after being stored at 90°C for periods ranging from 20 days to 100 days. The refiltered products were again stored at 90°C for a second period. Periodical centrifuge tests were carried out on the products and the refiltered products during the first and second storage periods and results were tabulated.

Apart from refiltration after long storage periods, viscosity checks were carried out also on some product portions after long storage periods at temperatures of 50°C, 90°C, and/or 150°C.

6.3.7 Sediment investigation using an Ultra-Centrifuge

Studying the same possibility of the presence of very fine particles of pentaerythritol in the product which was difficult to detect using the centrifuge test outlined in Appendix 4, products from different runs, stored at different temperatures were centrifuged at 30000 r.p.m. for more than three hours using the ultra-centrifuge. The samples tested by the ultra-centrifuge represented a very wide cross section of the products (e.g. crash cooled, slow cooled, high reaction temperature, low reaction temperature, reheated, and different storage temperatures). A product sample from the industrial run carried out at Fawley was also included in the test.

6.3.8 Sediment investigation using Nuclear Magnetic Resonance (NMR)

The same samples that were tested by the ultra-centrifuge were also tested by Nuclear Magnetic Resonance (NMR) techniques. It was thought that if the source of the sediment formation at storage was a back

reaction then the change in structure might be shown by this NMR analysis. An NMR trace for tetramethylsilate, $\text{Si}(\text{CH}_3)_4$, dissolved in carbon tetrachloride, was obtained first. The peak obtained was used to identify the zero starting point on the chart. Then an NMR trace of each sample was obtained by dissolving a small amount in carbon tetrachloride CCl_4 , in the presence of about two drops of tetramethylsilate (TMS) and running it in the proper equipment for about 160 seconds. The NMR traces obtained for these samples were not very encouraging and hence attention was directed towards Infra-Red spectroscopy.

6.4 Infra-Red Spectroscopy Analysis

Infra-red spectroscopy is one of the most powerful tools available for the solution of problems concerning molecular structure, molecular behaviour and identification of organic chemical substances and mixtures. In this work this technique was used in both studies, the sediment investigation, and also the esterification reaction kinetic study for the development of a rate expression.

6.4.1 Infra-red spectroscopy in sediment formation investigation

Because the results from the NMR traces were not very encouraging the same samples were tested again but this time using IR spectroscopy. The analysis was carried out at Esso Research Centre in Abingdon and monitored by the author.

The equipment used was:

- a. Perkin Elmer Spectrophotometer model 682.
- b. Perkin Elmer Printer model 660.
- c. Perkin Elmer Data station model 3600.

A thin film of the sample was smeared on the spectrophotometer cell and an IR trace of this film was obtained, and was fed directly to the

data station which was connected to the spectrophotometer. Traces of all the samples were obtained this way, also by focusing on one single wavelength all the traces were compared, between themselves, and also with the IR trace of a standard dispersant product. The resultant traces of the differences were collected and studied carefully.

6.4.2 Infra-red spectroscopy in reaction kinetic studies

Infra-red spectroscopy was also used to study the esterification reaction by following the increase in the height of the characteristic ester peak and the decrease in the height of the characteristic anhydride peak. Samples of two runs, run 43 and run 45 with PE/PIBSA equivalent ratios of 1.5/1.0 and 1.0/1.0, were analysed by IR spectroscopy at the Esso Research Centre in Abingdon, using the same Perkin Elmer equipment mentioned above. A thin film of each sample was smeared on the cell of the spectrophotometer and an IR trace of this film was obtained and was fed directly to the connected data station. Traces of all the samples were obtained this way. Also as before, by focusing on one single wavelength, all the traces of one run were compared with the IR trace of the first sample at time $t = 0$ of that particular run. The IR traces of the differences were obtained and the ester and acid peak heights were measured and recorded for each run.

6.5 Industrial Production Run of PIBSA/PE Dispersant

One industrial production run of the dispersant at Fawley Refinery was monitored by the author. The esterification and filtration stages took more than four days to be completed. All stages of production were followed carefully by the author and details of the production run, conditions, and results with analysis, graphs, and discussions are presented in Appendix 1.

6.6 Measurement of Pentaerythritol Solubility in Dilution Oil

In this work only an approximate value of the solubility of PE in the dilution oil was required. Hence none of the standard equipment for solid-liquid solubility measurements were purchased and the same constructed rig shown in Figure 5.1 was used for the solubility work. Four runs were carried out for measurement of the solubility of PE in the dilution oil at four different temperatures namely, 160°C, 140°C, 100°C, and at ambient temperature. The following procedure was carried out in all four runs.

About one litre of dilution base oil was poured into the reaction flask (1)(refer to Figure 5.1), the flask was then placed back in its heating mantle (6) and the system was set as shown in the top section of Figure 5.1. Nitrogen sparge was then started at a rate of 0.1 dm³/min and kept at this value during the whole cycle. Cooling water was then commissioned to the overhead condenser, and the electric stirrer was started at a speed of 400 r.p.m. Controlled heating of the oil was started at a set rate of about 2°C/min, using the programmable temperature controller (8), up to the required temperature for that particular run. The temperature was then held at this value till the end of the run. A certain amount of Pentaerythritol, which was assumed to be more than the solubility value, was weighed accurately to four decimal places in a separate beaker, then added directly into the reaction flask from the overhead inlet (13) at the temperature of that run. The beaker was weighed again after PE addition and the exact amount of PE added was calculated accurately to four decimal places. The whole rig was left overnight to allow equilibrium to be reached. The next morning the pressure filter was prepared for filtration (see point number 12 in the production procedure) by setting the filter as shown in the bottom section of Figure 5.1. The bottom flange was tightened up with the filter paper

and cloth acting as gasket; the filter paper used in the solubility work was Whatman laboratory filter paper with slow filtration speed and a retention of fine crystalline material. The oil was introduced from the top and heating of the metal filter was started gradually to the required temperature which was the same as that of the rig, at which the solubility was to be measured. When the filter was at the required temperature, it was pressurised with nitrogen gradually and the oil was collected from the filter outlet (19) into a beaker. The reaction section apparatus was then dismantled and the PE/oil mixture in the flask was poured manually into the top of the metal filter and filtration was started as before (point No. (13) of the production procedure). The filtrate obtained was then collected from the filter outlet (19) into another beaker, then weighed and the filtrate weight was then calculated. The filtration temperature was kept at the required value by the proportional controller (22) and was also recorded, as part of the whole cycle temperature, using the electronic thermometer (10) and the recorder (11).

After filtration was completed, the pentaerythritol crystals that were collected on the filter paper were washed many times with warm chlorobenzene then filtered at 80°C , dried in an oven at 90°C for about 3 hours and finally left at ambient to cool down.

Some of the pentaerythritol was left at the bottom of the reaction flask when the mixture was poured into the filter. This PE was treated in exactly the same manner, washed with warm chlorobenzene, filtered at 80°C , dried in an oven at 90°C then left at ambient to cool down. The filter papers with PE crystals were weighed, then weighed without the PE crystals and the total PE crystal weight was calculated, from which the solubility of PE in the dilution oil at that temperature was calculated.

6.7 Microscopic Studies of the Sediment

Two types of microscopes were used in this study as follows:

a. Optical microscope study: In this microscopic study not only the sediment obtained at the end of many runs was photographed, but samples of the dispersant product from different runs covering a wide cross section of the experimental work were studied under the microscope in search of the possible presence of very fine pentaerythritol crystals in the product. Some of the photographs obtained are presented in Appendix 11.

b. Electron microscope study: In this study the sediment obtained at the end of many runs, again covering a wide cross section of the experimental work, was studied using the electron microscope to search mainly for the presence of different habits of PE crystals, and also to check the effect of many production conditions on the type of crystal habit obtained and its relation to filtrability of the product. Some of the photographs obtained for these sediment samples are presented in Appendix 12. The photographs were taken using the electron microscope at the Esso Research Centre in Abingdon.

CHAPTER SEVEN

PARTICLE SIZE MEASUREMENT

7.1 Introduction

A wide range of measuring techniques is available both for single particles and for systems of particles. The applicability of each method depends on the size range of the sample to be analysed and the quantity of sample available. Each technique gives a particular equivalent size, also its cost depends on its complexity. In a series of reviews Hawksley^(140, 141,142), Allen^(143,144) and Haywood⁽¹⁴⁵⁾, examined the main physical principles of the different techniques available for particle size analysis. Table 7.1 below summarises the main features of these techniques.

The techniques that were used successfully in analysing the sediment obtained at the end of each run were sieve analysis and laser analysis by using the Malvern laser analyser. An attempt to use the Coulter counter was not successful because of two main reasons; the wide range of crystal sizes present causing the continuous blockage of the orifice tube, and the difficulty of preparing an adequate electrolyte for the system under study. Sieve analysis, when tried alone, was not successful, due to the sticking and caking of the fine sediment present, and some kind of a preliminary separation of the very fine sediment had to be carried out before any successful size analysis could have been made.

7.2 Sediment Preparation for Size Measurement

Size analysis was carried out on the sediment obtained at the end of fifteen runs, they were runs 33, 34, 35 and runs 51 to 62 inclusive. In the first run, run 33, the fine crystals were not separated first and all the crystals were sieved, but the results were not encouraging and a lot of sticking and caking occurred on the sieves causing the results

TABLE 7.1

Main features of the different techniques of particle size measurement (143,144,146).

Technique	Size Range (μm)	Measured Dimension	Sample Required	Ease and Cost
Sieving	38 μm to 13mm	Second largest dimension	Large	Easy and cheap
Microscopic analysis	1 to 100	Projected area diameter	Very small	Tedious and costly
Sedimentation	>1	Stokes diameter	Small	Slow but cheap
Elutriation	>1 to 200	Stokes diameter	Moderate	Easy and cheap
Electrical sensing zone	1 - 100 Can be extended to 1000	Volume diameter	Small	Complicated and expensive instrument
Permeametry	>1	Specific surface diameter	Small	Easy and cheap
Light scattering and field scanning	<1 to 1000	Projected area diameter	Small	Complicated, very expensive equipment

to be inaccurate. In the runs that followed the sediment collected at the end of the run on the filter paper was washed with warm heptane at a temperature of around 40°C to try and dissolve all the oil with the crystals in the heptane. Then after shaking the mixture well and letting the larger crystals settle first, most of the heptane, which contained practically all the very fine crystals, was poured into another beaker or crucible. The two fractions were both treated in a similar manner, washed with warm heptane and separated into two more fractions each. The fractions containing the larger crystals were combined and the fractions containing the fines were also combined. This settling and separation was repeated two or three times until a very satisfactory separation was obtained.

Apart from the sediment obtained on the filter paper there was also some sediment which remained at the bottom of the reaction flask. This sediment consisted mainly of larger crystals and was treated in exactly the same manner as explained above.

The two final fractions obtained of the larger crystals and the finer crystals were then filtered from the heptane at a temperature of about 60°C, washed again with warm heptane, filtered again and finally dried in an oven for a few hours then left at ambient to cool down. The fraction containing the larger crystals was weighed and analysed by sieving while the other fraction was weighed and analysed using the Malvern laser analyser model 2200, after the unsuccessful attempt to use the Coulter counter for the analysis.

7.3 Sieve Analysis

Sieve analysis is one of the cheapest methods of particle size analysis. The lower limit of size which can be used is determined by two principal factors, the first is that the proportion of free space on the screen surface becomes very small as the size of the aperture is

reduced, and the second is that attractive forces between particles become larger at small particle sizes and consequently the particles tend to stick together and block the screen.⁽¹⁴⁶⁾ But with the use of electroformed or micromesh sieves the lower limit of size used can be lowered down to about 5.5 μm .⁽¹⁴⁷⁾

In conducting the analysis, a nest of sieves, each lower sieve being of smaller aperture size, conforming to BS 410,⁽¹⁴⁸⁾ arranged so that the ratio of aperture sizes on consecutive sieves was $2^{\frac{1}{4}}$, was mounted on an Endecott mechanical sieve vibrator. The guidelines in British Standards, BS 1796⁽¹⁴⁹⁾ were followed when using these sieves in the size analysis. The sieve apertures used ranged from 1405 μm (12-mesh) to 44 μm (350-mesh) and were used in two stages. In the first stage the sieve apertures used ranged from 1405 μm to 295 μm (52-mesh) and were used to sieve the fraction of sediment containing the larger crystals. After 45 minutes of mechanical sieving the individual sieve fractions were weighed to the nearest 0.1 mg which was within the specified precision of $\pm 0.1\%$ by BS 1796.⁽¹⁴⁹⁾ The -295 μm sieve fraction obtained from the first stage was mechanically sieved for another 45 minutes in the second stage using sieve apertures ranging from 251 μm (60-mesh) to 44 μm (350-mesh). Again the individual sieve fractions were weighed to the nearest 0.1 mg and combining the results from both stages the size distribution for the full range of sieve apertures considered, was obtained. The mass of the larger crystals fraction of a typical run was about 12g which represented about 80% of the total crystal mass of that run. Losses during sieving were comparatively very low and were typically about 0.1% by mass.

7.4 Coulter Counter Analysis^(150,151)

This is an electrical sensing zone method of determining the number and equivalent volume diameter of particles suspended in an

electrolyte solution. By forcing the particles through a small orifice the resistance between two electrodes, one on either side of the orifice, changes hence generating a voltage pulse proportional to the particle volume. By counting and scaling these pulses the total number and equivalent volume diameter of the particles are obtained.

The instrument used for the analysis of the fine crystals fraction was a Coulter counter model Z_B (industrial). The fine crystals were suspended in an electrolyte solution specifically developed for this purpose. The electrolyte solution was made by preparing first a saturated solution of monopentaerythritol in distilled water at ambient temperature, then dissolving 10% (by mass) sodium chloride (Analar grade, from Hopkins and Williams) in the solution. The solution was kept well stirred for more than 48 hours before vacuum filtration was carried out to separate the undissolved pentaerythritol, using a very fine filter paper which separates particles down to 0.2 μm size. The fine crystals were suspended in this electrolyte solution using a round bottomed, 400 cc sample beaker fitted with a single glass baffle.⁽¹⁵²⁾ A 50 μm orifice tube was used first then switched with a 100 μm orifice tube because of orifice blocking problems. Even then results were not encouraging, and it was decided to analyse the sample using instead, the laser particle analyser.

7.5 Laser Particle Size Analyses^(153,154,155)

This is a light scattering technique based on the formation of Fraunhofer diffraction ring pattern when a spherical particle is illuminated by a parallel beam of monochromatic, coherent light. If a lens is placed in the light path after the particle, and a screen is placed at the focal plane of the lens, then the undiffracted light is focussed to a central spot and the diffracted light forms a 'far field' Fraunhofer pattern of rings around it. The relative volume and weight distribution of the

variously sized particles can be found from the diffraction pattern since the measured obscuration of light at the central spot is related by the Beer-Lambert law to the total projected cross-section area of the particles.

The instrument used in the analysis of the fine crystals fraction was the Malvern laser particle size model 2200/3300. Two Fourier transform lenses were used during the analysis having two different focal lengths of 64 mm and 300 mm, each with 15 measured size classes, ranging from 1.2 μm to 118.4 μm for the 64 mm lens and from 5.8 μm to 564.0 μm for the 300 mm lens. The lenses focussed the diffraction pattern on to a multi-element photoelectric detector which produced an analogue signal proportional to the received light intensity. This detector was interfaced directly to a desk computer allowing it to read the diffraction pattern and perform the necessary integration digitally. The analysis was carried out by suspending the fine crystals fraction in Heptane, then taking a sample of two to three drops from the suspension and placing the small sample in the instrument cell and diluting it again with Heptane to the required level. Two samples were analysed for each fraction as a check. It was important to keep the particle concentration in the sample below about 0.1% by volume, otherwise multiple scattering of the light resulted and the performance of the instrument deteriorated.⁽¹⁵³⁾ Each time the instrument was used the required lens was fitted, alignment was carried out with the sample cell removed, then a background reading was obtained with the cell in place containing only the heptane solvent. Only then was the sample placed in the cell and the particles kept in suspension using the magnetic stirrer. Each particle scattered light in a forward direction with intensity and angle which depended on its size. With particles of many sizes present in the laser beam, the relative intensities at various angles were manipulated to give the size distribution. These calculations were performed digitally within the instrument's microprocessor and a printed

output of the tabulated results with cumulative undersize and oversize wts. % plots were obtained. The data was also stored on a tape for future work if needed.

7.6 Ratio of Particle Sizes Measured by Laser and Sieves

The equivalent particle size measured by the Malvern laser analyser was the projected area diameter^(143,144,154), while the equivalent particle size measured by the sieve analysis was the second largest dimension of the particle^(143,144) (Table 7.1). Because about 80% by weight of the total sediment was analysed by sieving, it was decided to convert the projected area diameter obtained by laser analysis into the particle equivalent size measured by sieving. The conversion ratio was found experimentally by taking eight samples of the crystalline sediment of different sieve fractions after sieving was completed, and analysing them by the Malvern laser particle analyser using the procedure outlined in Section 7.5 above. For each sieve fraction size, a mean value of the projected area diameter was obtained which corresponded to one experimental value of the ratio. Eight such values for the ratio were obtained and their mean was taken to represent the final value of the experimental ratio of the second largest particle size (measured by sieving) to the projected area diameter (measured by the Malvern laser analyser).

CHAPTER EIGHT

RESULTS OF REACTION KINETIC STUDY

One of the main areas of the experimental work was the investigation of the kinetics of the PIBSA/PE esterification reaction. The results of this investigation, together with its theoretical treatment are presented in this chapter.

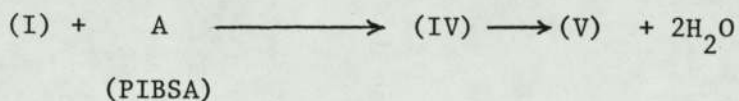
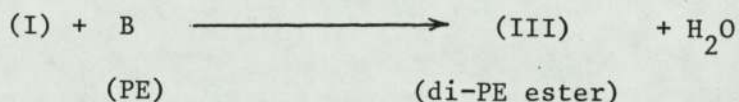
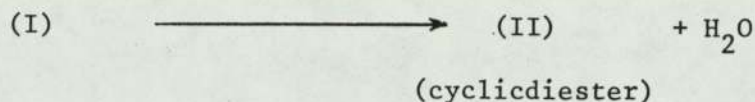
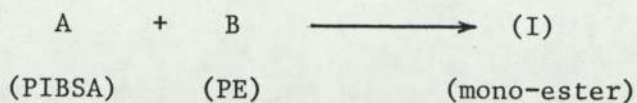
Two methods were used in the analysis of the kinetic runs performed during this study namely, using the Total Acid Number (TAN), and using Infra-red spectroscopy. Their theoretical treatment and results obtained are presented below separately.

8.1 Analysis Using Total Acid Number (TAN)

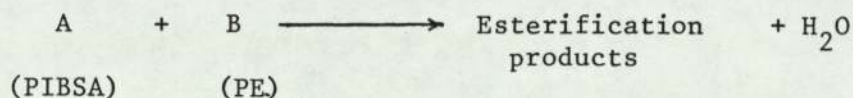
This was the main method used in following the PIBSA/PE esterification reaction carried out by taking periodical samples and measuring their Total Acid Number. The results were analysed in a manner consistent with the theoretical treatment given below to yield the parameters of the assumed rate expression.

8.1.1 Theoretical treatment

In Chapter Four Section 4.3 the main steps of the PIBSA/PE esterification reaction mechanism were presented. One of the main esterification products is the cyclic diester, structure II (see Chapter Four, Section 4.3), but the degree of presence of the other structures depends largely on the ratio of PE/PIBSA used and also on reaction temperature, hence the main steps of the reaction can be summarised as follows:

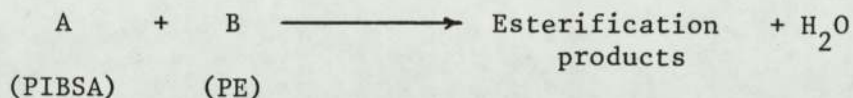


The structures (I), (II), (III), (IV), and (V) (see Chapter Four, Section 4.3) are all esterification products and it is very difficult to distinguish between them without detailed kinetic and analytic study, hence the overall esterification reaction can be written as



In the forthcoming analysis certain simplifying assumptions were made, these assumptions are mainly as follows:

1. The general form of the reaction will be assumed, hence



also, since the actual reaction is between pentaerythritol and the succinic anhydride ring, it will be assumed that one equivalent of pentaerythritol reacts with one equivalent of succinic anhydride. The following rate expression will be assumed to represent the reaction,

$$(-r_A) = k \cdot C_A^a \cdot C_B^b = (r_T) \quad 8.1$$

where:

- $(-r_A)$ = The rate of conversion of PIBSA to esters
- (r_T) = The total rate of formation of esters
- C_A, C_B = Concentrations of PIBSA and PE (equivalents/dm³)
- k = Reaction rate constant
- a, b = Constant indices

The reaction was catalysed but the catalyst concentration will be included with the rate constant k . The indices (a) and (b) are assumed to be constants but k varies with temperature.

2. An Arrhenius type of equation will be assumed for the variation of k with temperature

$$k = k_o \cdot e^{-\frac{E}{RT}} \quad 8.2$$

where:

- k_o = Frequency factor
- E = Activation energy of the reaction
- R = The gas constant
- T = Absolute temperature

This is supported by the kinetic theory and has been shown to be the case in many reactions.⁽²³⁾

3. The rate of conversion of the PIBSA to esters is assumed to be proportional to the drop in the Total Acid Number (TAN) of the reaction mixture.

4. It was noticed that in each kinetic run that was carried out there was a residual TAN (which will be termed as TAN^∞), the value of which

depended mainly on PE/PIBSA equivalent ratio used and can be estimated from the plot of TAN vs. time curves. The significance of this residual TAN (TAN^{∞}) is not very clear at this stage but it could be partly due to the residual acidity of the sulphonic acid catalyst used in the reaction. Attempts to analyse the results obtained using absolute TAN values were not successful as will be shown later, hence an empirical approach was decided on, and relative TAN values (TAN_R) were used in the analysis rather than absolute TAN values. The relative TAN values were obtained from the following expression

$$TAN_R = TAN - TAN^{\infty} \quad 8.3$$

where the subscript (R) represent the relative value. Relative TAN values (TAN_R), were used in all the calculations carried out in the analysis that follows.

Analysis

Let X_A be the fractional conversion of PIBSA (A) into esterification products, then

$$X_A = \frac{TAN_R^0 - TAN_R}{TAN_R^0} \quad 8.4$$

and also

$$X_A = \frac{C_A^0 - C_A}{C_A^0} \quad 8.5$$

where:

TAN_R^0 = Initial relative TAN of the mixture mg KOH/g sample

C_A^0 = Initial PIBSA concentration equivalents of succinic anhydride/dm³

$$\therefore \frac{\text{TAN}_R^{\circ} - \text{TAN}_R}{\text{TAN}_R^{\circ}} = \frac{C_A^{\circ} - C_A}{C_A^{\circ}}$$

$$\therefore 1 - \frac{\text{TAN}_R}{\text{TAN}_R^{\circ}} = 1 - \frac{C_A}{C_A^{\circ}}$$

rearranging and cancelling the unity from both sides,

$$\text{hence } \frac{C_A}{\text{TAN}_R} = \frac{C_A^{\circ}}{\text{TAN}_R^{\circ}} = \text{constant} = \gamma \quad 8.6$$

Now let $\alpha = \frac{C_B^{\circ}}{C_A^{\circ}}$ = the initial PE/PIBSA equivalent ratio

then two main cases will be considered, they are:

$$\alpha = 1.0 \text{ and } \alpha > 1.0$$

PE/PIBSA equivalent ratio (α) = 1.0

In this case $C_A^{\circ} = C_B^{\circ}$ and also $C_A = C_B$ at any time because one equivalent of PE reacts with one equivalent of succinic anhydride in the overall esterification reaction

hence from equation (8.1) we have

$$(-r_A) = kC_A^a \cdot C_B^b = kC_A^{a+b} = kC_A^n \quad 8.7$$

where: $n = a+b$ = overall order of the reaction

also for a batch reactor with a constant volume V, we have,

$$(-r_A) = -\frac{1}{V} \cdot \frac{dN_A}{dt} = -\frac{dC_A}{dt} \quad 8.8$$

hence from equations (8.7) and (8.8) we have

$$-\frac{dC_A}{dt} = kC_A^n \quad 8.9$$

$$\text{but } C_A = \gamma \cdot \text{TAN}_R \quad 8.6$$

$$\text{hence } \frac{dC_A}{dt} = \gamma \cdot \frac{d(\text{TAN}_R)}{dt} \quad 8.10$$

$$\text{also } \text{TAN}_R = \text{TAN} - \text{TAN}^\infty \quad 8.3$$

$$\text{hence } (-r_A) = -\frac{dC_A}{dt} = -\gamma \frac{d(\text{TAN}_R)}{dt} = -\gamma \frac{d(\text{TAN})}{dt} \quad 8.11$$

substituting equations (8.6) and (8.11) into equation (8.9) we have

$$-\gamma \cdot \frac{d(\text{TAN})}{dt} = k \cdot (\gamma \cdot \text{TAN}_R)^n \quad 8.12$$

rearranging and taking logarithms to base 10, we get

$$\log \left[\frac{-d(\text{TAN})}{dt} \right] = \log k + (n-1) \log \gamma + n \log(\text{TAN}_R) \quad 8.13$$

In equation (8.13), the term $\frac{d(\text{TAN})}{dt}$ represents the slope of the TAN vs. time curve (which is a negative quantity) measured at different TAN values. Hence by plotting $\log \left[\frac{-d(\text{TAN})}{dt} \right]$ against $\log(\text{TAN}_R)$ a straight line should be obtained with a slope of (n) and an intercept equal to $[\log k + (n-1) \log \gamma]$ from which (k) can be estimated. Hence the overall order of the reaction (n) can be found directly by carrying out kinetic runs with equal concentrations of PIBSA and PE and following the above analysis.

PE/PIBSA equivalent ratio (α) > 1.0

From the above analysis for $\alpha = 1.0$ the overall order of

reaction (n) is obtained, hence making use of this, (b) is eliminated as follows

from equation (8.1) we have

$$(-r_A) = kC_A^a \cdot C_B^b = kC_A^a \cdot C_B^{(n-a)} = k \cdot C_B^n \cdot \left(\frac{C_A}{C_B}\right)^a$$

$$\therefore \left[\frac{(-r_A)}{C_B^n} \right] = k \left(\frac{C_A}{C_B}\right)^a \quad 8.14$$

$$\text{but } C_B^0 = \alpha C_A^0, \text{ and } C_A^0 = \gamma \cdot \text{TAN}_R^0$$

$$\therefore C_B^0 = \alpha \cdot \gamma \cdot \text{TAN}_R^0 \quad 8.15$$

$$\text{but } C_B = C_B^0 - B \text{ reacted} = C_B^0 - A \text{ reacted} = C_B^0 - (C_A^0 - C_A) \quad 8.16$$

substituting for C_B^0 , C_A^0 and C_A in equation (8.16) we get

$$\therefore C_B = \alpha \cdot \gamma \cdot \text{TAN}_R^0 - \gamma \text{TAN}_R^0 + \gamma \text{TAN}_R$$

$$\therefore C_B = \gamma [\text{TAN}_R + (\alpha-1) \text{TAN}_R^0] \quad 8.17$$

$$\text{and hence } \left(\frac{C_A}{C_B}\right) = \frac{\text{TAN}_R}{[\text{TAN}_R + (\alpha-1) \text{TAN}_R^0]} \quad 8.18$$

Substituting equations (8.17) and (8.18) into equation (8.14) we get

$$\frac{(-r_A)}{\gamma^n [\text{TAN}_R + (\alpha-1) \text{TAN}_R^0]^n} = k \left[\frac{\text{TAN}_R}{(\text{TAN}_R + (\alpha-1) \text{TAN}_R^0)} \right]^a \quad 8.19$$

$$\text{but } (-r_A) = -\gamma \frac{d(\text{TAN})}{dt} \quad 8.11$$

substituting equation (8.11) into equation (8.19), then rearranging and taking logarithms to base ten we get,

$$\log \left[\frac{-\frac{d(\text{TAN})}{dt}}{(\text{TAN}_R + (\alpha-1)\text{TAN}_R^0)^n} \right] = [\log k + (n-1) \log \gamma] + a \cdot \log \left[\frac{\text{TAN}_R}{\text{TAN}_R + (\alpha+1)\text{TAN}_R^0} \right] \quad 8.20$$

Knowing (α) and (n) and measuring the slope of the TAN curve vs. time at different TAN values equation (8.20) can be plotted. Hence by plotting the L.H.S. of equation (8.20) against the last term of the R.H.S. of the equation, a straight line should be obtained of slope (a) and an intercept equal to $[\log k + (n-1) \log \gamma]$ from which the value of (k) can be estimated. Hence by carrying out different kinetic runs with varying values of (α) $>$ 1.0 but at the same reaction temperature, an average value of (a) and (k) can be estimated at that reaction temperature.

Variation of the rate constant (k) with temperature

The variation of (k) with temperature is given by equation (8.2)

$$k = k_0 \cdot e^{-\frac{E}{RT}} \quad 8.2$$

taking logarithms to base (e) we get

$$\ln k = \ln k_0 - \frac{E}{RT} \quad 8.21$$

equation (8.21) suggests that if a plot of $\ln k$ against $\frac{1}{T}$ is carried out a straight line should be obtained with a slope of $(-\frac{E}{R})$ and an intercept of $(\ln k_0)$. Hence the values of the frequency factor (k_0) and the

activation energy of the reaction (E) can be estimated with this type of analysis by carrying out different kinetic runs with the same value of (α) but at different reaction temperatures and then plotting the estimated values of $\ln k$ against ($\frac{1}{T}$) as suggested by equation (8.21) above.

All the parameters of the rate expression can now be estimated according to the above analysis, hence the rate of reaction can be evaluated at any stage and temperature from

$$\underline{(-r_A) = k_o \cdot e^{-\frac{E}{RT}} \cdot C_A^a \cdot C_B^b}$$

8.1.2 Calculation of reaction mixture density

The density of the reaction mixture was needed for the calculation of the concentrations of PIBSA and PE. A density flask of about 50 cm³ capacity was used and the following measurements were made,

weight of density flask (D.F.) + water at ambient (15°C) = 75.0742 g

" " " " " empty = 25.8019 g

" " " " + initial oil mixture (at 15°C) = 70.5403 g

weight of (D.F.) + initial oil mixture at 120°C = 68.0197 g

" " " + " " " " 160°C = 66.7828 g

" " " + " " " " 200°C = 65.3714 g

but the density of water at 15°C⁽¹⁶⁰⁾ = 0.99913 g/cm³

hence the volumes of the (D.F.) = $\frac{75.0742-25.8019}{0.99913}$ = 49.3152 cm³

∴ density of oil mixture at (15°C) = $\frac{70.5403-25.8019}{49.3152}$ = 0.9072 g/cm³

" " " " " (120°C) = $\frac{68.0197-25.8019}{49.3152}$ = 0.8561 "

" " " " " (160°C) = $\frac{66.7828-25.8019}{49.3152}$ = 0.8310 "

" " " " " (200°C) = $\frac{65.3714-25.8019}{49.3152}$ = 0.8024 "

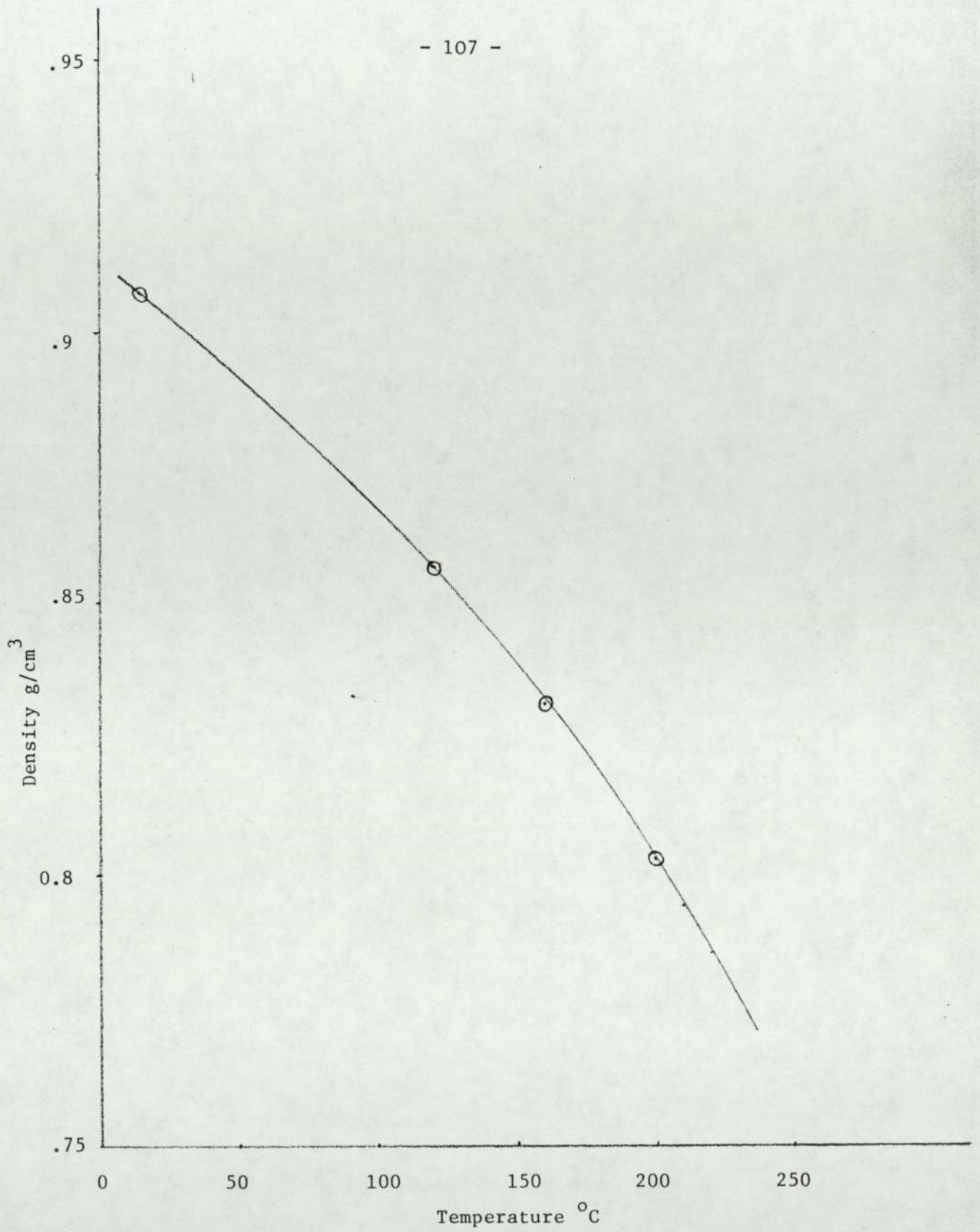


Figure 8.1

Graph of density of initial reaction mixture g/cm³

vs. temperature °C

Figure 8.1 was obtained by plotting the density of the initial oil mixture g/cm^3 vs. the temperature $^{\circ}\text{C}$, from which the density of the initial oil mixture at any reaction temperature can be found. From Figure 8.1 and from the values of the measured product densities given in Table 8.1 below, average densities were estimated and tabulated also in Table 8.1. It was assumed that reaction mixtures of runs carried out at the same temperatures had the same average densities.

8.1.3 Calculation of the overall order of reaction (n)

As was shown in the theoretical treatment given above, the overall order of reaction (n) can be found from the slope of the line obtained by plotting equation (8.12) for a kinetic run with $\alpha = 1.0$. Run 39 was such a run, its results and calculations are presented here as sample calculation for other runs with $\alpha = 1.0$. Table 8.2 contains details of the measurements carried out during the run with the calculated TAN values of each sample. The values of TAN tabulated in Table 8.2 were calculated using equation (A3.1) given in Appendix 3

$$\text{TAN} = \frac{(v-b) \times N \times 56.1}{w} \quad \text{A3.1}$$

the values of N and b used were those given in Table A3.4 for method No. 3 (the modified colour titration method) hence as an example, for sample No. 1 in Table 8.2 the TAN is given by

$$\text{TAN}_1 = \frac{(5.475-0.075) \times 0.1014 \times 56.1}{1.2287}$$

$$\therefore \text{TAN}_1 = 25.00$$

TABLE 8.1

Densities of reaction mixtures of different runs carried out at different reaction temperatures.

Number of Run	Reaction Temperature °C	Density of Initial Mixture g/cm ³	Density of Final Product g/cm ³	Average Density During Reaction g/cm ³
39	200	0.8024	0.826	0.814
46	180	0.8180	0.842	0.830
47	190	0.8104	0.8338	0.822
48	210	0.7940	0.818	0.806
49	200	0.8024	0.826	0.814
50	150	0.8380	0.862	0.850
63	220	0.7855	0.8065	0.796

TABLE 8.2

Sample weight measurements and titration results for run 39.

No. of Sample	Time After PE Addition Min.	Weight of Empty Beaker g	Weight of Beaker + Sample g	Weight of Sample g	Starting Level of Base Volume cm ³	Level of Base Volume at End of Titration cm ³	Volume of Base Used in Titration cm ³	TAN mg KOH / g sample
1	0.5	124.2888	125.5175	1.2287	8.975	14.45	5.475	25.0
2	6.0	125.8182	126.8943	1.0761	14.45	18.375	3.925	20.4
3	12.0	125.1537	126.2953	1.1416	18.55	21.925	3.375	16.4
4	18.0	116.2405	117.3611	1.1206	21.925	24.80	2.875	14.2
5	30.0	51.0343	51.9933	0.9590	6.85	8.75	1.90	10.8
6	45.0	117.5892	118.6779	1.0887	8.925	10.70	1.775	8.9
7	60.0	125.3711	127.1196	1.7485	10.750	13.250	2.50	7.9
8	90.0	116.3528	118.1323	1.7795	13.25	15.325	2.075	6.4
9	120.0	116.0000	117.5612	1.5612	15.40	16.975	1.575	5.5
10	150.0	124.2663	126.2715	2.0052	17.05	18.825	1.775	4.8
11	180.0	116.4322	118.3826	1.9504	18.85	20.50	1.65	4.6
12	240.0	124.1865	126.1374	1.9509	20.55	22.00	1.45	4.0
13	290.0	122.9667	124.8047	1.8380	22.175	23.375	1.20	3.5

all the other tabulated TAN values were calculated in the same way. Also the density of the product was calculated using the following measurements,

$$\begin{aligned} \text{weight of density flask (D.F.) empty} &= 25.7050 \text{ g} \\ \text{" " " " + reaction product at } 200^{\circ}\text{C} &= 66.4596 \text{ g} \\ \text{but volume of (D.F.) was found above to be} &= 49.3152 \text{ cm}^3 \\ \text{hence density of product at } 200^{\circ}\text{C} &= \frac{66.4596-25.7050}{49.3152} = 0.826 \text{ g/cm}^3 \end{aligned}$$

$$\begin{aligned} \text{but density of initial mixture at } 200^{\circ}\text{C (from Figure 8.1)} &= 0.8024 \text{ g/cm}^3 \\ \therefore \text{average density of mixture at } 200^{\circ}\text{C} &= 0.814 \text{ g/cm}^3 \end{aligned}$$

The TAN values tabulated in Table 8.2 were plotted against time (hr) and Figure 8.2 was obtained. The slope of the curve in Figure 8.2 was measured, by drawing tangents, at different points along the curve and these are tabulated below in Table 8.3. The initial slope at $t = 0$ could have been measured by drawing the tangent to the curve at $t = 0$, or from the drop in the TAN value over the first two sample periods (i.e. over twelve minutes), the later method was used⁽²³⁾ in the calculation of the initial slope in all the kinetic runs. The value of TAN^{∞} was estimated from Figure 8.2 to be equal to 3.0 mg KoH/g for run 39.

TABLE 8.3

The slope of TAN vs. time curve at different points for run 39.

TAN mg KoH/g	slope = $\frac{d(\text{TAN})}{dt}$ TAN/hr	$\log \left[\frac{-d(\text{TAN})}{dt} \right]$ = y_i	$\log(\text{TAN}-3.0)$ = x_i	$\log(\text{TAN})$
25.0	-43.000	1.633	1.342	1.3980
13.0	-20.2272	1.306	1.000	1.1139
10.0	-6.944	0.8416	0.845	1.000
7.0	-2.703	0.4318	0.602	0.845
5.0	-1.084	0.035	0.301	0.699

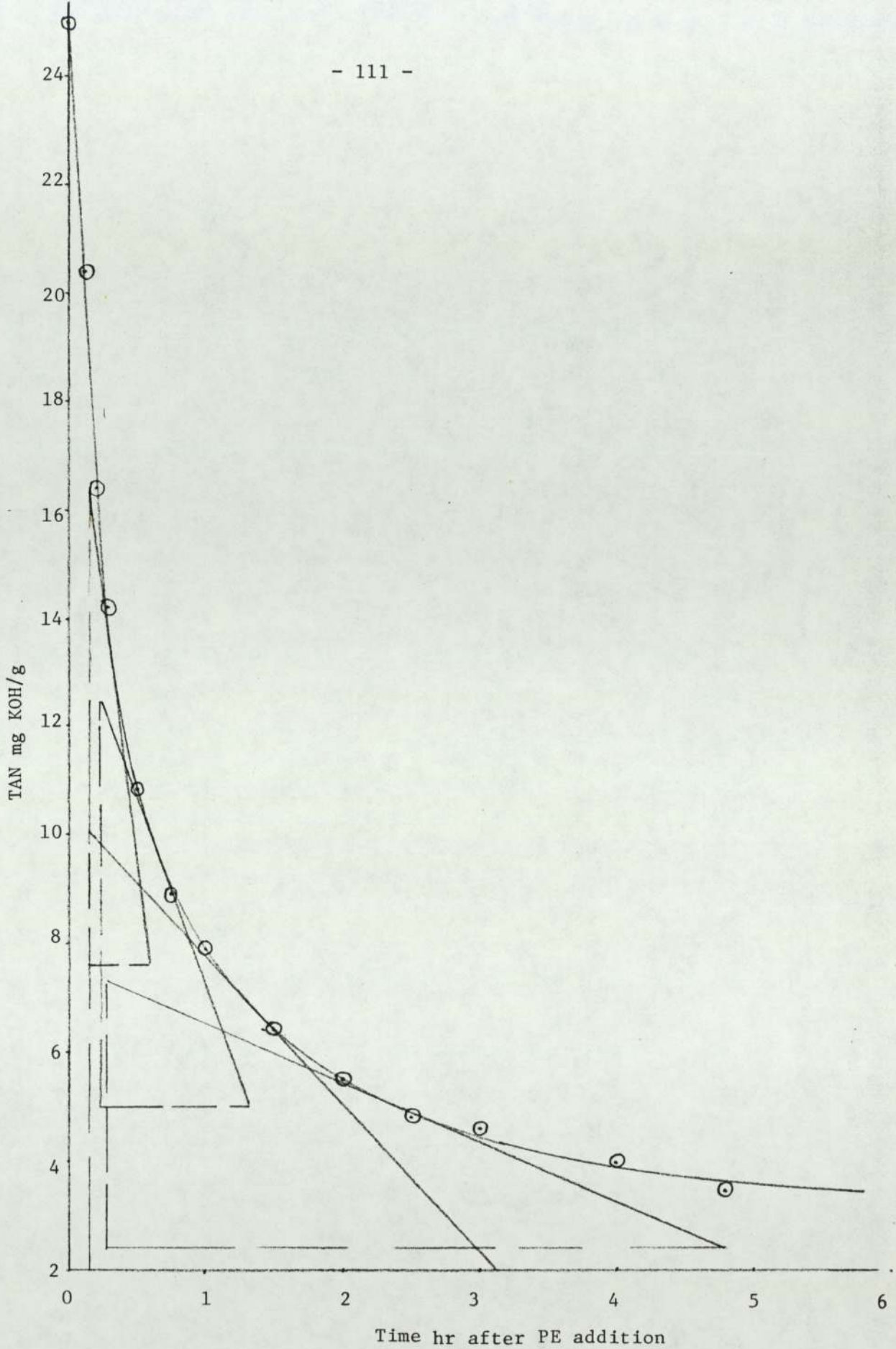


Figure 8.2

Graph of Run 39 of TAN mgKOH/g sample vs. time hrs since PE addition

PE/PIBSA ratio (α) = 1.0

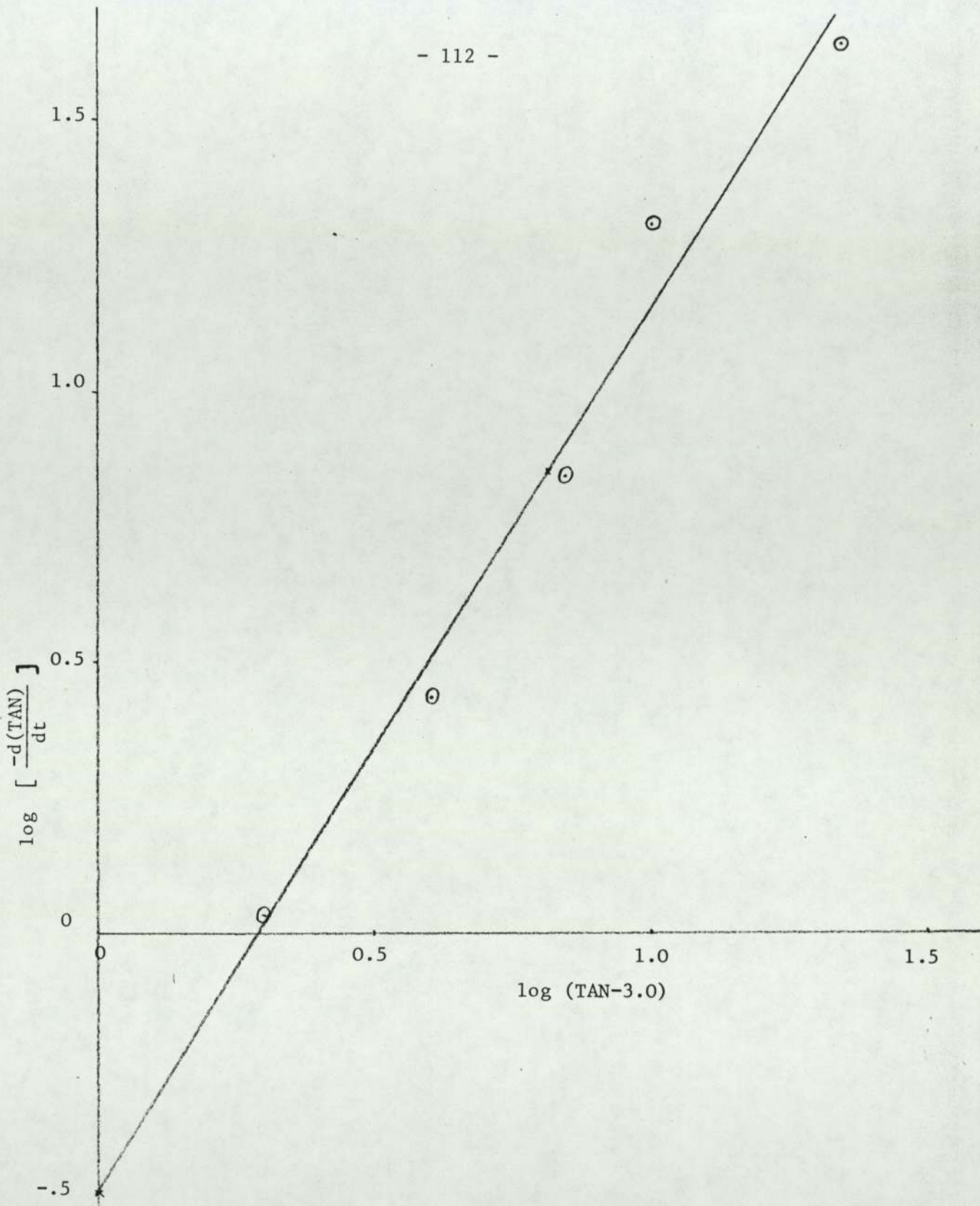


Figure 8.3

Graph for run 39 of $\log \left[\frac{-d(TAN)}{dt} \right]$ vs $\log(TAN-3.0)$

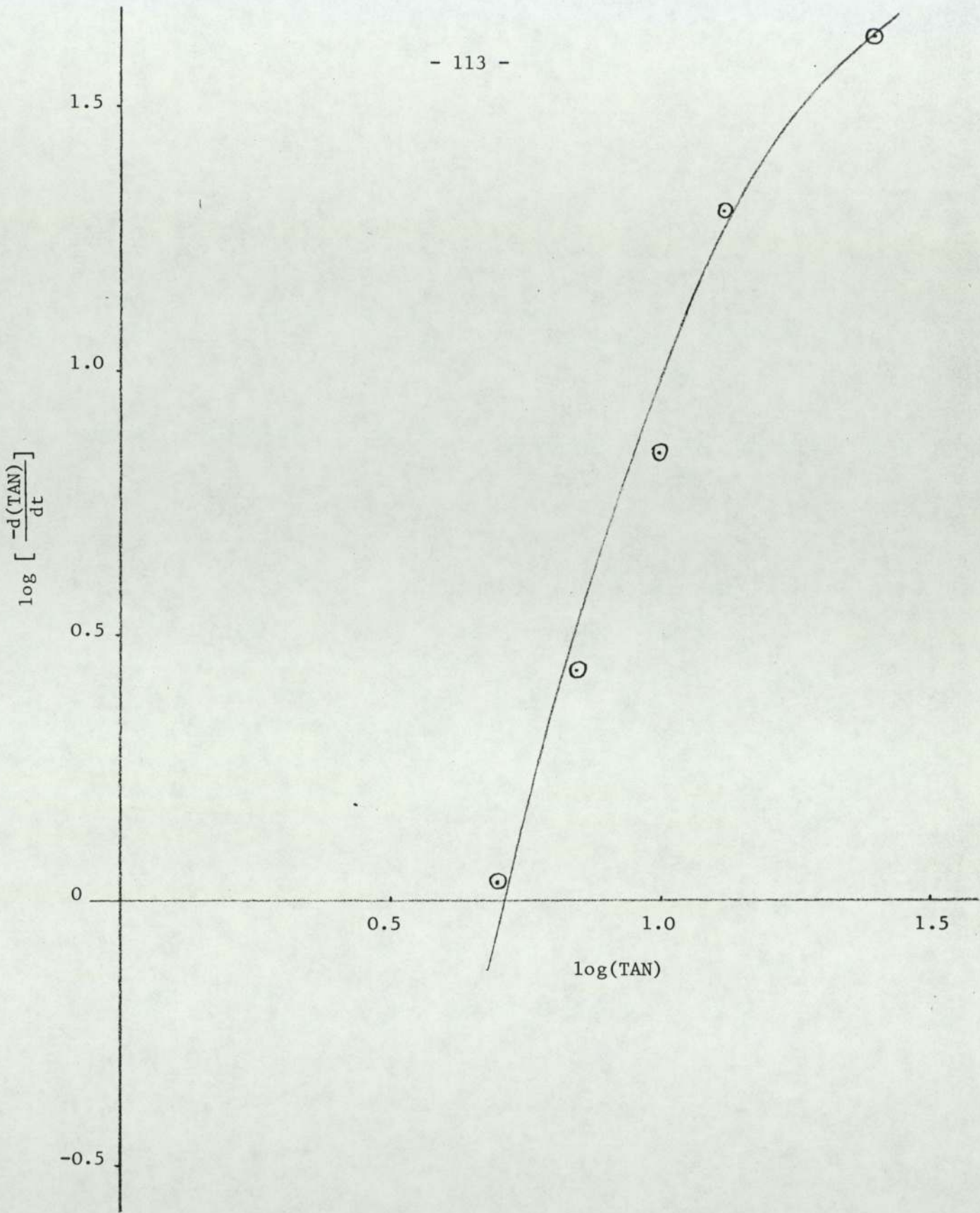


Figure 8.4

Graph for run 39 of $\log \left[\frac{-d(\text{TAN})}{dt} \right]$ vs. $\log(\text{TAN})$

From Table 8.3 we have,

$$\Sigma x_i = 4.0900, (\Sigma x_i)^2 = 16.7281, \Sigma x_i^2 = 3.9680,$$

$$\Sigma y_i = 4.2474, \Sigma x_i y_i = 4.4791, N = 5$$

hence for the least square best fit straight line of the plot of $\log \left[-\frac{d(\text{TAN})}{dt} \right]$ vs. $\log(\text{TAN}-3.0)$ we have,⁽³⁴⁾

$$\text{slope} = \frac{\Sigma x_i y_i - [\Sigma x_i \Sigma y_i / N]}{\Sigma x_i^2 - [(\Sigma x_i)^2 / N]} \quad 8.22$$

and

$$\text{intercept} = \frac{\Sigma y_i \Sigma x_i^2 - \Sigma x_i \Sigma x_i y_i}{N \Sigma x_i^2 - (\Sigma x_i)^2} \quad 8.23$$

substituting the values obtained above from Table 8.3 into equations (8.22) and (8.23) we get,

$$\text{slope} = \frac{4.4791 - [4.09 \times 4.2474/5]}{3.9680 - [16.7281/5]} = \underline{1.614}$$

and

$$\text{intercept} = \frac{4.2474 \times 3.968 - 4.09 \times 4.4791}{5 \times 3.968 - 16.7281} = \underline{-0.471}$$

but the slope is equal to the overall order of the reaction (n) (equation 8.13)

∴ the overall order of the reaction (n) = 1.614

The actual plot of $\log \left[-\frac{d(\text{TAN})}{dt} \right]$ vs. $\log(\text{TAN}-3.0)$ is given in

Figure 8.3. A plot of $\log \left[-\frac{d(\text{TAN})}{dt} \right]$ vs. $\log(\text{TAN})$ was also carried out and Figure 8.4 was obtained.

8.1.4 Calculation of the order of reaction with respect to PIBSA (a)

It was shown above in the theoretical treatment section that a plot of equation (8.20) would enable the order of reaction with respect to PIBSA (a) to be found from the slope of the line obtained. Different

runs with varying values of (α) were carried out. As a sample calculation the estimation of (α) for run 44 of $\alpha = 2.0$ will be carried out here. Table 8.4 contains details of the measurements carried out during the run. The tabulated TAN values were calculated as shown before in run 39 by using equation (A3.1) in Appendix 3,

$$\text{TAN} = \frac{(v-b) \times N \times 56.1}{w} \quad \text{A3.1}$$

hence to calculate the TAN of the first sample in Table 8.4, we have

$$\text{TAN}_1 = \frac{(5.55 - .075) \times 0.1014 \times 56.1}{1.3644} = 22.8 \text{ mg KOH/g}$$

all the other TAN values were calculated in a similar way.

The TAN values given in Table 8.4 were plotted against time (hr) and Figure 8.5 was obtained. The slope of the curve in Figure 8.5 was measured at different points by drawing tangents to the curve, and the results are tabulated in Table 8.5. The value of TAN^∞ was estimated from Figure 8.5 to be equal to 1.5 mg KOH/g for run 44.

To be able to plot equation (8.20), let

$$Y = \log \left[\frac{- \frac{d(\text{TAN})}{dt}}{[\text{TAN}_R + (\alpha-1)\text{TAN}_R^0]^n} \right]$$

$$X = \log \left[\frac{\text{TAN}_R}{\text{TAN}_R + (\alpha-1)\text{TAN}_R^0} \right]$$

where: $\text{TAN}_R = \text{TAN} - \text{TAN}^\infty = \text{TAN} - 1.5$

$\alpha = 2.0$

$n = 1.614$

TABLE 8.4

Sample weight measurements and titration results for run 44.

No. of Sample	Time After PE Addition Min.	Weight of Empty Beaker g	Weight of Beaker + Sample g	Weight of Sample g	Starting Level of Base Volume cm ³	Level of Base Volume at End of Titration cm ³	Volume of Base Used in Titration cm ³	TAN $\frac{\text{mg KOH}}{\text{g sample}}$
1	1	116.3605	117.7249	1.3644	9.95	15.50	5.55	22.8
2	6	115.9995	117.3050	1.3055	15.575	19.8	4.225	18.1
3	12	124.2656	125.6111	1.3455	19.825	23.125	3.3	13.6
4	18	116.4358	117.7113	1.2755	23.2	25.75	2.55	11.0
5	30	124.1871	125.5167	1.3296	25.825	27.8	1.975	8.1
6	45	122.9706	124.3852	1.4146	27.825	29.45	1.625	6.2
7	60	124.8740	126.2211	1.3471	29.55	30.825	1.275	5.1
8	75	124.2922	125.7995	1.5073	30.825	32.125	1.30	4.6
9	90	125.8224	127.1433	1.3209	32.15	33.125	0.975	3.9
10	125	125.1564	126.4588	1.3024	33.15	33.95	0.80	3.2
11	150	116.2424	117.6379	1.3955	33.975	34.725	0.75	2.7
12	181	51.0394	52.4634	1.4240	34.775	35.475	0.70	2.5
13	240	117.6038	118.9639	1.3601	35.525	36.125	0.60	2.2
14	300	125.3850	126.9753	1.5903	36.175	36.8	0.625	2.0
15	360	116.3629	117.9820	1.6191	36.875	37.45	0.575	1.8

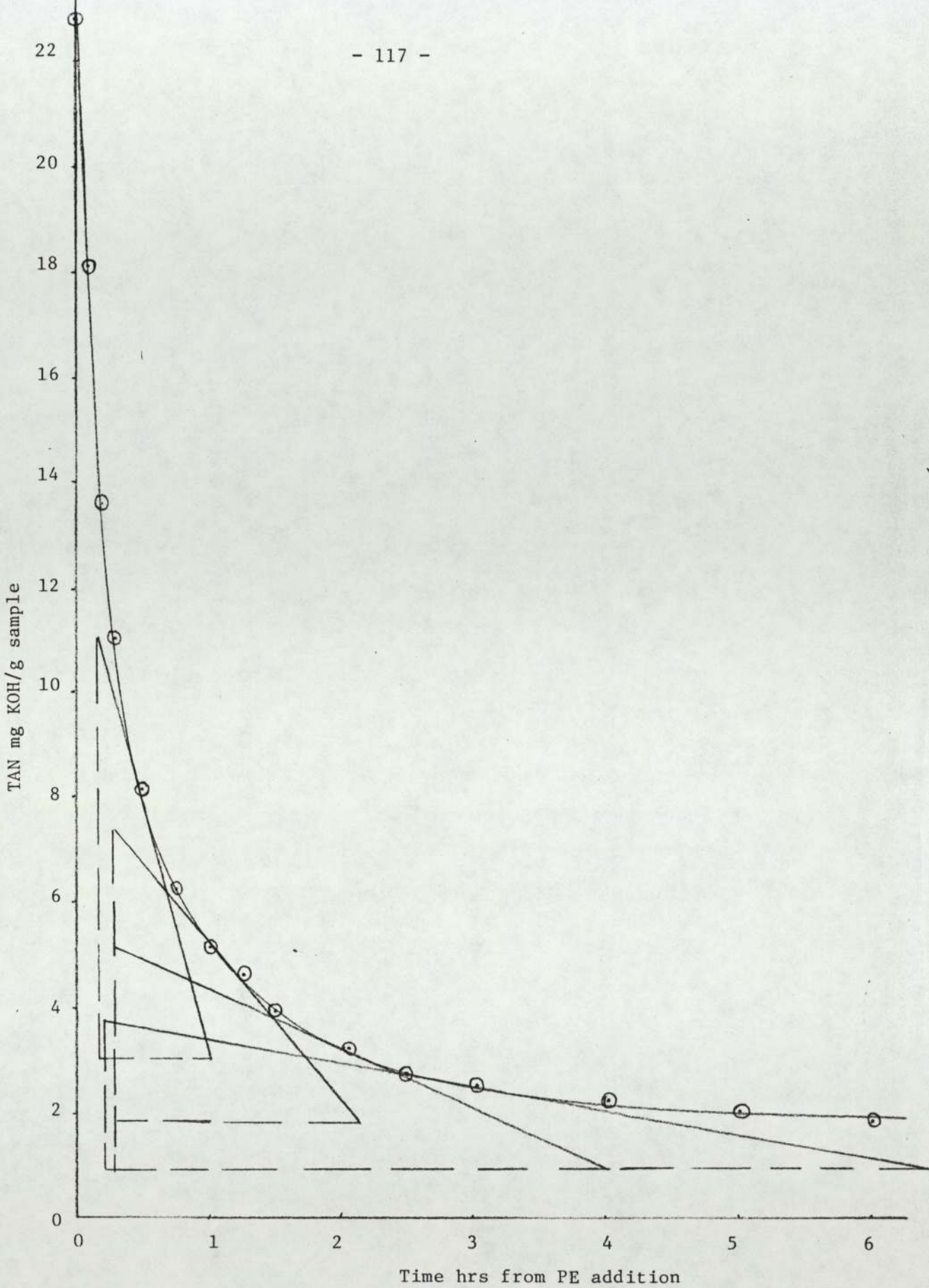


Figure 8.5

Graph for run 44 of TAN mg KOH/g vs. time hrs from PE addition

PE/PIBSA ratio $\alpha = 2.0$

$\frac{d(\text{TAN})}{dt}$ = The slope of the TAN vs. time curve hence the values of (y_i) and (x_i) at those points, at which the slope was calculated, were found and tabulated in Table 8.5 also.

TABLE 8.5

The slope of TAN vs. time curve at different points for run 44.

TAN mg KOH/g	TAN _R mg KOH/g	$\frac{d(\text{TAN})}{dt}$ TAN/hr	Y	X
22.8	21.3	-46.000	-0.9671	-0.301
8.1	6.6	-9.524	-1.3544	-0.6261
5.0	3.5	-2.989	-1.7751	-0.8504
3.15	1.65	-1.129	-2.1436	-1.1433
2.5	1.0	-0.457	-2.5163	-1.3483

As a sample calculation the values of y_i and x_i for the second point in Table 8.5 will be given here

$$y_2 = \log \left[\frac{-(-9.524)}{[6.6 + (2.0-1.0) \times 21.3]^{1.614}} \right]$$

$$\therefore \underline{y_2 = -1.3544.}$$

and $x_2 = \log \left[\frac{6.6}{6.6 + (2.0-1.0) \times 21.3} \right]$

$$\therefore \underline{x_2 = -0.6261}$$

all the other values of x_i and y_i in Table 8.5 were calculated in the same way.

From Table 8.5 we have,

$$\Sigma x_i = -4.2691, (\Sigma x_i)^2 = 18.2252, \Sigma x_i^2 = 4.3308,$$

$$\Sigma y_i = -8.7565, \Sigma x_i y_i = 8.4921, N = 5$$

hence for the least square best fit straight line of the plot of Y vs. X we have as before,

$$\text{slope} = \frac{\sum x_i y_i - [\sum x_i \sum y_i / N]}{\sum x_i^2 - [(\sum x_i)^2 / N]} \quad 8.22$$

$$\text{intercept} = \frac{\sum y_i \sum x_i^2 - \sum x_i \sum x_i y_i}{N \sum x_i^2 - (\sum x_i)^2} \quad 8.23$$

$$\therefore \text{slope} = \frac{8.4921 - [(-4.2691)(-8.7565)/5]}{4.3308 - [18.2252/5]} = 1.481$$

$$\text{and intercept} = \frac{(-87565)(4.3308) - (-4.2691)(8.4921)}{5(4.3308) - (18.2252)} = -.4868$$

hence slope = a = 1.481

and intercept = -0.4868

The actual plot of Y vs. X for run 44 is given in Figure 8.6. Two more runs with $\alpha > 1.0$ were carried out at the same reaction temperature of 200°C, they were runs 42 and 43 with $\alpha = 1.25$ and $\alpha = 1.5$ respectively. Their detailed calculations and analysis with the corresponding graphs are presented in Appendix 6. The values obtained for (a) from these three runs are tabulated below in Table 8.6.

TABLE 8.6

The values obtained for the order of reaction with respect to PIBSA (a)

Run No.	α	a
42	1.25	1.419
43	1.5	1.496
44	2.0	1.481
average value of (a)		1.465

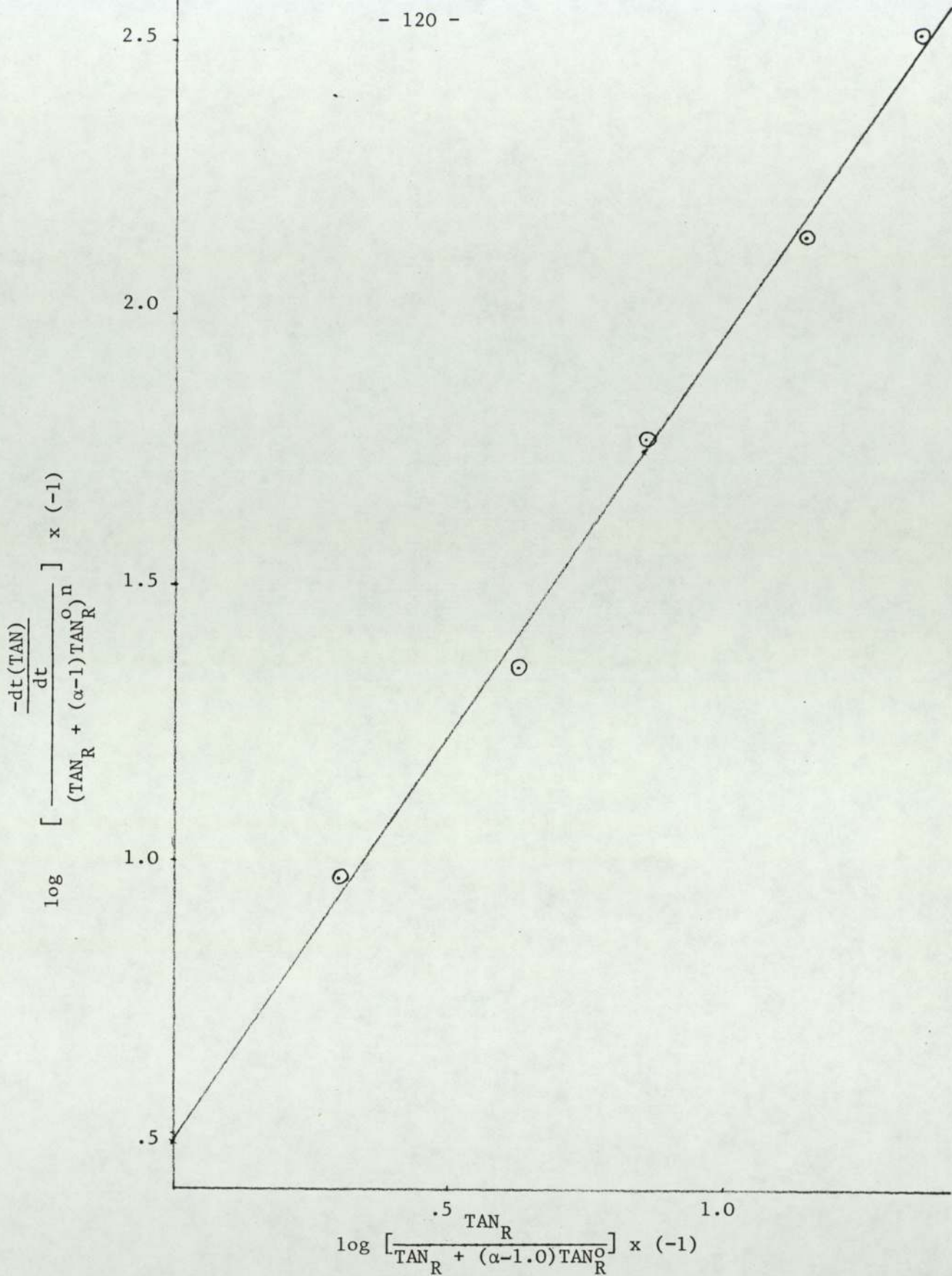


Figure 8.6

Graph for run 44 of $\log \left[\frac{-d(\text{TAN})}{dt} \cdot \frac{1}{[\text{TAN}_R + (\alpha-1)\text{TAN}_R^0]^n} \right] \text{ vs. } \log \left[\frac{\text{TAN}_R}{\text{TAN}_R + (\alpha-1)\text{TAN}_R^0} \right]$

8.1.5 Calculations of the rate constant (k)

In the theoretical treatment section it was shown that for both types of analysis with $\alpha \geq 1.0$ the intercept of the straight line obtained by plotting equation (8.13) and also equation (8.20) was given by

$$\text{intercept} = \log k + (n-1) \log \gamma \quad 8.24$$

where; $n = 1.614$, and $\gamma = C_A^0 / \text{TAN}_R^0$

hence the initial concentration of the PIBSA C_A^0 must be calculated before an estimation of the value of (k) can be made from equation (8.24). As a sample calculation let us calculate the value of the rate constant (k) for run 39 in this section.

The initial concentration of PIBSA C_A^0 is given by

$$C_A^0 = (\text{equivalents/g PIBSA}) \times (\text{wt. of PIBSA}) \times \frac{\text{Average density} \times 1000}{\text{Total wt. of mixture}} \quad 8.25$$

the units of C_A^0 from equation (8.25) are equivalents/dm³. To evaluate the number of equivalents of succinic anhydride per gram of PIBSA, use is made of the data given in reference (135) and that is 0.1376 g of pentaerythritol to 1 g of PIBSA represent a 1.1/1.0 equivalents ratio, hence since the equivalent weight of PE is equal to 136 then,

$$\underline{\text{equivalents of S.A./g. PIBSA}} = \frac{0.1376}{136 \times 1.1} = \underline{0.9198 \times 10^{-3}}$$

This can also be obtained from the saponification number of the PIBSA used in the laboratory investigation, which was given in Chapter Four to be equal to 103 mg KOH/g sample of PIBSA, hence

$$\underline{\text{equivalent of S.A./g PIBSA}} = \frac{103 \times 10^{-3}}{56.1 \times 2} = \underline{0.918 \times 10^{-3}}$$

and from this a 1.1/1.0, PE/PIBSA equivalents ratio represents

$$0.918 \times 10^{-3} \times 136 \times 1.1 = 0.1373 \text{ gPE/g PIBSA}$$

the difference between both calculations is very small, and hence the value of the No. of equivalents of S.A./g PIBSA that will be used in the calculations to follow is 0.9198×10^{-3} .

For run 39 from Table 6.1 in Chapter Six

$$\text{Weight of PIBSA} = 402.82\text{g}$$

$$\text{Weight of dilution oil} = 0.7768 \times 402.82 = 312.91\text{g}$$

$$\text{weight of catalyst} = 0.0118 \times 402.82 = 4.75\text{g}$$

$$\therefore \text{Total mixture weight} = 720.48\text{g}$$

the concentration can now be obtained using equation (8.25)

$$\therefore C_A^o = (0.9198 \times 10^{-3})(402.82) \times \frac{0.814}{720.48} \times 1000$$

$$\therefore C_A^o = 0.4186 \text{ equivalents of S.A./dm}^3$$

the constant γ can now be evaluated for run 39,

$$\therefore \gamma = \frac{C_A^o}{\text{TAN}_R^o} = \frac{0.4186}{22.0} = 0.01903 \left(\frac{\text{equivalents}}{\text{dm}^3} \right) \cdot \left(\frac{\text{g sample}}{\text{mg KOH}} \right)$$

hence (k) can now be estimated from equation (8.24) by substituting the values of n, γ , and the intercept in the equation,

$$\therefore -0.471 = \log k + (1.614 - 1.0) \log(0.01903)$$

$$\therefore k = 3.8497 \left(\frac{\text{equivalents}}{\text{dm}^3} \right)^{1-n} \cdot \text{hr}^{-1}$$

the units of k are obtained from the rate expression

$$(-r_A) = k C_A^a \cdot C_B^b, \quad \therefore k = \frac{(-r_A)}{C_A^a \cdot C_B^b} = \left(\frac{\text{equivalents}}{\text{dm}^3} \right)^{1-n} \cdot \text{hr}^{-1}$$

In the previous section the calculations for run 44 were presented and the value of the intercept of the straight line plot of

Y vs. X in Figure 8.6 was found to be equal to (-0.4868). The value of (k) for run 44 is calculated from this intercept in a similar manner as follows,

from Table 6.1 for run 44

weight of PIBSA	=	403.59g
weight of dilution oil = 0.7768 x 403.59	=	313.51g
weight of catalyst = 0.0118 x 403.59	=	4.76g
∴ Total weight of mixture	=	721.86g

$$\therefore C_A^o = (0.9198 \times 10^{-3})(403.59) \times \frac{0.814 \times 10^3}{721.86} = 0.4186$$

$$\therefore C_A^o = 0.4186 \text{ equivalents/dm}^3$$

$$\therefore \gamma = \frac{C_A^o}{\text{TAN}_R^o} = \frac{0.4186}{21.3} = 0.0197 \left(\frac{\text{equivalents}}{\text{dm}^3} \right) \cdot \left(\frac{\text{g sample}}{\text{mg KOH}} \right)$$

substituting back into equation (8.24), we get

$$-0.4868 = \log k + (1.614 - 1.0) \log(0.0197)$$

$$\therefore k = 3.634 \text{ (equivalent/dm}^3\text{)}^{1-n} \cdot \text{hr}^{-1}$$

Detailed calculations for the values of the rate constant (k) for runs 42 and 43 were carried out and presented in Appendix 6.

Table 8.7 summarises the results obtained for the constants (a) and (k) at 200°C.

TABLE 8.7

Summary of the values obtained for the constants (a) and (k) at 200°C.

Number of run	PE/PIBSA equivalents ratio α	Intercept of Y vs. X st. line plot	k $(\frac{\text{equivalents}}{\text{dm}^3})^{1-n} \cdot \text{hr}^{-1}$	a
39	1.0	-0.471	3.8497	-
42	1.25	-0.445	4.014	1.419
43	1.5	-0.434	4.130	1.496
44	2.0	-0.487	3.634	1.481
Average values of k and a			3.907	1.465

The above values for the constants (a) and (k) were obtained from runs carried out at 200°C and using a catalyst ratio of 1.18% by weight on PIBSA. Runs 36, 37 and 38 were also carried out at 200°C but the catalyst used was nearly doubled and of a more concentrated type (see Table 6.1 in Chapter Six). The reaction rates were definitely higher than those of the corresponding runs with the lower catalyst ratio. Detailed calculations performed on run 36 with $\alpha = 1.0$ are presented in Appendix 6, and the values obtained for the constants (n) and (k) were

$n = 1.588$ the overall order of reaction

$k = 5.545 (\text{equivalents}/\text{dm}^3)^{1-n} \cdot \text{hr}^{-1}$.

8.1.6 Calculation of the activation energy of the reaction

In the theoretical treatment section it was shown that the variation of the rate constant (k) with the temperature is given by the following equation,

$$\ln k = \ln k_o - \frac{E}{RT} \quad 8.26$$

and a plot of $\ln k$ vs. $\frac{1}{T}$ should yield a straight line of slope equal to $(-\frac{E}{R})$, and an intercept equal to $\ln k_o$.

Six runs were performed at different reaction temperatures, but all with $\alpha = 1.0$. Their detailed calculations, plots of TAN vs. time, plots of $\log [\frac{-d(\text{TAN})}{dt}]$ vs. $\log(\text{TAN}-\text{TAN}^\infty)$, and finally the estimation of the rate constant (k) are all presented in Appendix 6. Table 8.8 below gives a summary of these runs and the estimated (k) values.

TABLE 8.8

Summary of the rate constant (k) values obtained at different temperatures

Number of run	Reaction temperature °C	Reaction temperature °K	k ($\frac{\text{equivalents}}{\text{dm}^3}$) ¹⁻ⁿ .hr ⁻¹	$\ln k$ = y_i	$\frac{1}{T}$ °K ⁻¹ = x_i
39	200	473	3.907 (av.)	1.3628	2.114×10^{-3}
46	180	453	2.434	0.8895	2.208×10^{-3}
47	190	463	2.9075	1.0673	2.1598×10^{-3}
48	210	483	4.7005	1.5477	2.0704×10^{-3}
50	150	423	0.542	-0.6125	2.364×10^{-3}
63	220	493	5.4570	1.6969	2.0284×10^{-3}

At first a plot of $\ln k$ vs. $\frac{1}{T}$ for the first four runs tabulated above, with reaction temperatures of 200°C, 180°C, 190°C and 210°C, was carried out and the continuous straight line of Figure 8.7 was obtained. Hence if only the first four points are considered we have,

$$\begin{aligned} \sum x_i &= 8.5522 \times 10^{-3}, (\sum x_i)^2 = 73.1401 \times 10^{-6}, \\ \sum x_i^2 &= 1.8296 \times 10^{-5}, \sum y_i = 4.8673, \sum x_i y_i = 0.01035 \end{aligned}$$

substituting these values into equations (8.22) and (8.23), the values of the slope and the intercept of the least square best fit line of the plot can be obtained, hence

$$\text{slope} = \frac{0.01035 - [8.5522 \times 10^{-3} \times 4.8673/4]}{1.8296 \times 10^{-5} - [73.1401 \times 10^{-6}/4]}$$

$$\therefore \text{slope} = -5136.364^{\circ}\text{K}$$

and

$$\text{intercept} = \frac{(4.8673 \times 1.8296 \times 10^{-5}) - (8.5522 \times 10^{-3} \times 0.01035)}{4 \times 1.8296 \times 10^{-5} - 73.1401 \times 10^{-6}}$$

$$\therefore \text{intercept} = 12.230$$

$$\text{but } \ln k_0 = \text{intercept} = 12.230$$

$$\therefore \underline{k_0 = 204843 \text{ the frequency factor}}$$

also from the slope,

$$\left(-\frac{E}{R}\right) = \text{slope} = -5136.364^{\circ}\text{K}$$

$$\text{but } R = 1.989 \text{ cal./g.mole.}^{\circ}\text{K}$$

$$\therefore E = 5136.364 \times 1.989 \text{ cal/g.mole}$$

$$\therefore \underline{E = 10.216 \text{ kcal/g.mole}} \quad \text{the activation energy}$$

At a much later stage in the experimental program run 63 was carried out at a higher temperature of 220°C, and it was decided to consider the three runs, 39, 48 and 63 only which were carried out at the higher temperatures of 200°C, 210°C and 220°C. So if only these three points in Table 8.8 are considered we have,

$$\Sigma x_i = 6.2128 \times 10^{-3}, \quad (\Sigma x_i)^2 = 3.8599 \times 10^{-5},$$

$$\Sigma x_i^2 = 1.2870 \times 10^{-5}, \quad \Sigma y_i = 4.6074, \quad \Sigma x_i y_i = 9.5273 \times 10^{-3},$$

$$N = 3$$

and the slope and the intercept of the least square best fit straight line are given by

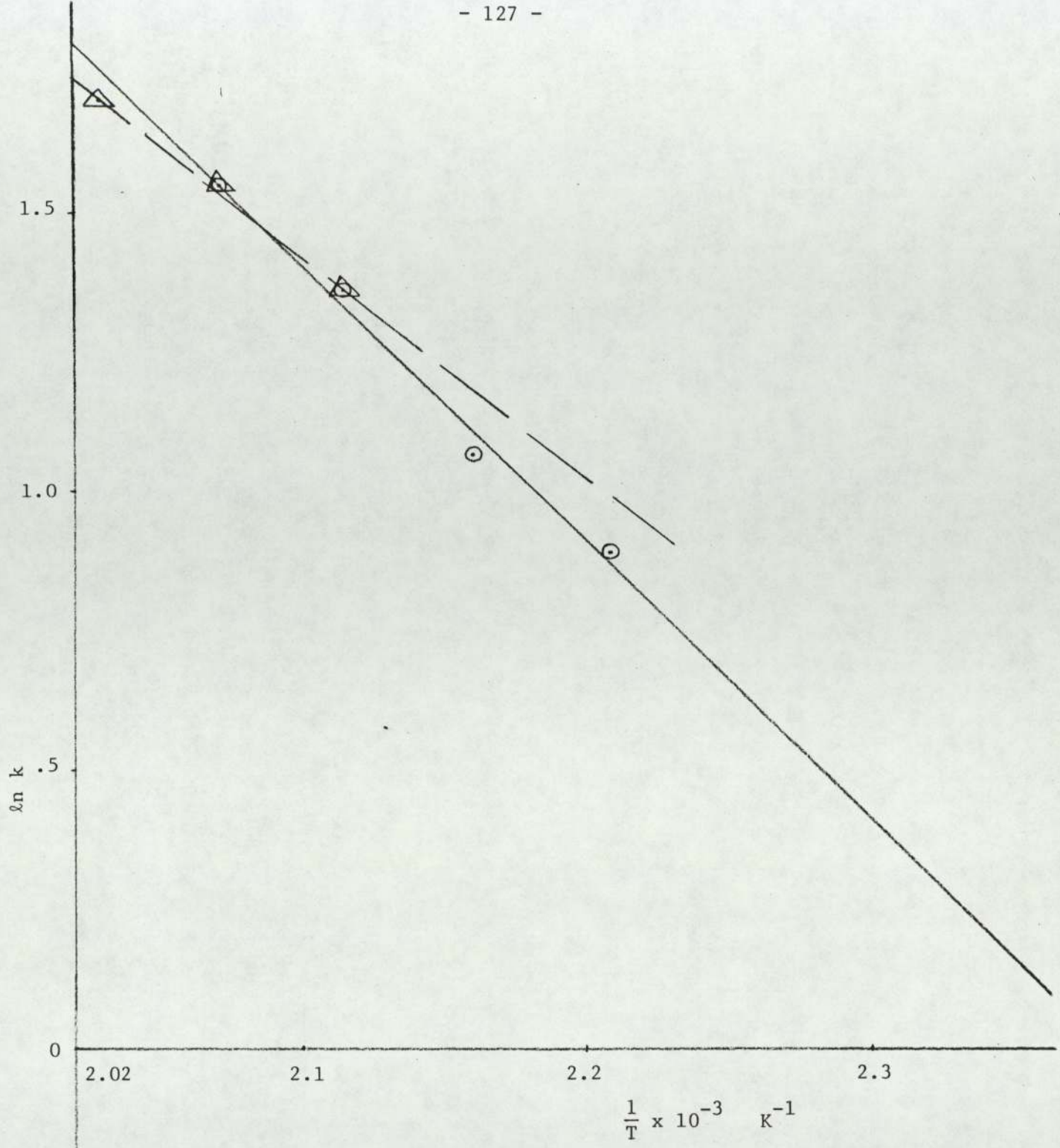


Figure 8.7

Graph of $\ln k$ vs. $\frac{1}{T} k^{-1}$

The continuous line is the plot of the four ⊙ points

The dotted line is the plot of the three △ points

-0.5

⊙

TABLE 8.9

Water evolved during the esterification reaction in some of the kinetic runs.

Run No.	α	Reaction Temperature °C	Total Reaction Time hr	Light Hydro-Carbon Collected cm ³	Approximate Volume of H ₂ O Collected cm ³	Approximate Volume of H ₂ O Lost with N ₂ Flow cm ³	Total Volume of H ₂ O (Collected + Lost with N ₂) cm ³
39	1.0	200	5.0	1.0	3.0	0.75	3.75
40	0.5	200	6.0	1.0	1.0	0.9	1.9
41	0.25	200	5.0	0.25	0.25	0.75	1.0
42	1.25	200	5.5	1.0	3.0	0.83	3.83
43	1.5	200	5.0	1.0	5.0	0.75	5.75
44	2.0	200	6.0	2.0	6.0	0.9	6.9
46	1.0	180	6.0	-	0.5	0.9	1.4
47	1.0	190	6.0	-	1.5	0.9	2.4
48	1.0	210	6.0	1.0	3.0	0.9	3.9
49	1.0	200	6.0	1.0	3.0	0.9	3.9
50	1.0	150	30	-	Traces	4.5	4.5
63	1.0	220	6.0	1.0	3.0	0.9	3.9

∴ Nitrogen flow rate = 0.1251 g/min = 7.51 g/hr.

∴ Water vapour leaving with nitrogen = 0.02 x 7.51 = 0.15 g/hr

Table 8.9 gives the approximate amounts of water collected at the outlet of the overhead condenser in some of the kinetic runs, it also gives the amounts of some light hydrocarbon distillate collected with the water in runs carried out at higher reaction temperatures. The amount of water vapour lost with the nitrogen flow was calculated assuming that the nitrogen leaving at the outlet of the overhead condenser was fully saturated. This may not have been the case in runs with prolonged reaction times, carried out at lower reaction temperatures (for example run No. 50).

8.1.8 Summary of results of TAN method analysis

The parameters of the approximate rate expression

$$\underline{(-r_A)} = k_o \cdot e^{-\frac{E}{RT}} \cdot C_A^a \cdot C_B^b$$

have all been evaluated above using the Total Acid Number method analysis.

A list of their values is given below.

k_o	=	15312	frequency factor
E	=	7.767	k.cal/g.mole activation energy of the reaction
n	=	1.614	overall order of reaction (a + b)
a	=	1.465	order of reaction with respect to PIBSA
b	=	0.149	order of reaction with respect to PE

Plots of TAN vs. time for all the kinetic runs were carried out, and from each of these plots the slope of the curve was measured, by drawing tangents to the curve, at five different points covering most of the reaction range. The plots of $\log \left[\frac{-d(\text{TAN})}{dt} \right]$ vs. $\log (\text{TAN}_R)$ for all these runs were carried out (together with plots of $\log \left[\frac{-d(\text{TAN})}{dt} \right]$ vs. $\log(\text{TAN})$ for some runs only), and the slopes and intercepts using equations

TABLE 8.10

Summary of some of the results obtained from all the kinetic runs using the Total Acid Number method analysis.

Number of Run	PE/PIBSA Equivalent Ratio α	Reaction Temperature $^{\circ}\text{C}$	TAN mg KOH/g sample		Results of the Straight Line Plot of Log $[-d(\text{TAN})/dt]$ vs. Log $(\text{TAN} - \text{TAN}^{\infty})$	
			TAN ^o at t=0	TAN [∞] at t→∞	Slope	Intercept
36	1.0	200	24.5	2.0	1.588	-0.275
37	0.5	"	25.9	6.0	1.481	-0.249
38	0.25	"	25.2	13.0	1.587	-0.221
39	1.0	"	25.0	3.0	1.614	-0.472
40	0.5	"	25.6	7.0	1.514	-0.408
41	0.25	"	26.3	14.0	1.435	-0.189
42	1.25	"	23.9	2.5	1.496	-0.289
43	1.5	"	23.5	2.0	1.524	-0.307
44	2.0	"	22.8	1.5	1.505	-0.309
45*	1.0	"	-	-	-	-
46	1.0	180	25.5	3.0	1.626	-0.6916
47	1.0	190	24.5	3.0	1.563	-0.497
48	1.0	210	24.6	3.0	1.611	-0.3769
49 ⁺	1.0	200	25.0	3.0	1.659	-0.521
50	1.0	150	25.5	4.0	1.641	-1.351
63	1.0	220	24.5	3.0	1.5701	-0.2438

*Run 45 was a repeat of run 39 carried out to prepare samples for IR analysis.

⁺Run 49 was also a repeat of run 39 but the results of run 49 were obtained using the potentiometric titrator. A comparison between run 49 and run 39 results is presented in Appendix 6.

(8.22) and (8.23) were calculated. Table 8.10 below summarised these and some other results obtained from these plots for all the kinetic runs. Appendix 6 contains the plots and detailed calculations of these results for few runs only (as was mentioned before).

8.2 Analysis Using Infra-Red (IR) Spectroscopy

Infra-red spectroscopy is a very useful tool for the solution of problems having to do with molecular structure and the identification of unknown organic chemical substances and mixtures. Infra-red radiation is electromagnetic in origin just like x-rays, ultra-violet, and visible radiation and is governed by the same mathematical laws. The infra-red spectrum of a material which absorbs this radiation constitutes a "finger print" of the material; an analytical study of such a spectrum helps a great deal in the solution of molecular structure and identification problems.

8.2.1 Theoretical treatment

The functional relationship between energy transmitted by a chemical mixture containing an absorbing component and the concentration of the component in the mixture is the well-known Beer's law⁽¹⁵⁶⁾

$$T = \frac{I}{I_0} = 10^{-\ell \cdot S \cdot C} \quad 8.27$$

where:

- I = radiation (or light) intensity transmitted by the sample
- I_0 = radiation (or light) intensity incident upon the sample
- T = transmittance, the fraction of incident radiation (or light) transmitted by the sample
- ℓ = the length of the absorption cell
- S = absorptivity, a constant depending on the identity of the absorbing molecule and the wavelength absorbed

C = concentration of the absorbing molecule

from equation (8.27) we have,

$$\log T = -\ell SC$$

$$\therefore \log \frac{1}{T} = \ell SC$$

$$\therefore A = \log \frac{1}{T} = \ell SC \quad 8.28$$

equation (8.28) is another form of equation (8.27), but now a new quantity, the absorbance A is defined which is equal to $\log \left(\frac{1}{T}\right)$ and is directly proportional to the concentration C. Spectrometer graphs are printed with a logarithmic absorbance scale for the ordinate to facilitate measurement of (A) directly. Absorbances are additive because A is directly proportional to C and the absorptivity is the proportionality factor. Because of this, absorbances can be estimated directly by measuring the height of peaks in the infra-red spectrum using the base-line method. ⁽¹⁵⁶⁾

The following analysis is based on the assumption that Beer's law is applicable which means that the absorbance is directly proportional to the concentration and its value is estimated directly by measuring the height of the respective peak using the base-line method, hence

$$C_e = Z_e P_e \quad (8.29)$$

and

$$C_A = Z_a P_a \quad (8.30)$$

where:

C_e = total product esters concentration

C_A = total acid concentration

P_e = height of the ester peak

P_a = height of the acid peak

Z_e, Z_a = proportionality constant

but from the rate expression we have

$$(-r_A) = kC_A^a \cdot C_B^b = (r_T) \quad 8.1$$

where (r_T) is the total rate of ester formation for a constant volume batch reactor we have

$$(r_T) = \frac{1}{V} \cdot \frac{dN_e}{dt} = \frac{dC_e}{dt}$$

and from equation (8.29) we have

$$(r_T) = Z_e \cdot \frac{dP_e}{dt} \quad 8.31$$

As in the previous section, two cases will be considered here,

$\alpha = 1.0$ and $\alpha > 1.0$ where $\alpha = C_B^0/C_A^0$

PE/PIBSA equivalent ratio $\alpha = 1.0$

$C_A^0 = C_B^0$ and $C_A = C_B$ because one equivalent of pentaerythritol is assumed to react with one equivalent of succinic anhydride (S.A.), hence as before,

$$\therefore (r_T) = kC_A^a \cdot C_B^b = kC_A^{(a+b)} = kC_A^n \quad 8.32$$

substituting equations (8.30) and (8.31) in (8.32), then rearranging and taking logarithms to base 10 we get,

$$\log (dP_e/dt) = [\log k + n \log Z_a - \log Z_e] + n \log(P_a) \quad 8.33$$

hence a plot of $\log(dP_e/dt)$ against $\log(P_a)$ should yield a straight line of slope (n) and intercept equal to $(\log k + n \log Z_a - \log Z_e)$, where

dP_e/dt is the slope of the plot of the height of ester peak vs. time, and P_a is the height of the acid peak. In this way the overall order of reaction (n) can be estimated and compared with its value found by the previous TAN analysis method.

PE/PIBSA equivalent ratio $\alpha > 1.0$

In a similar manner to the previous TAN analysis method for the case of $\alpha > 1.0$, from the rate expression we have,

$$(r_T) = kC_A^a \cdot C_B^b = kC_A^a \cdot C_B^{(n-a)} = k \cdot C_B^n \cdot \left(\frac{C_A}{C_B}\right)^a.$$

$$\therefore \left[\frac{(r_T)}{C_B^n} \right] = k \cdot \left(\frac{C_A}{C_B}\right)^a \quad 8.34$$

but $C_B^0 = \alpha C_A^0 = \alpha Z_a P_a^0$

and $C_B = C_B^0 - (C_A^0 - C_A) = \alpha Z_a P_a^0 - Z_a P_a^0 + Z_a P_a \quad 8.35$

$$\therefore (C_A/C_B) = \frac{P_a}{[P_a + (\alpha-1) P_a^0]} \quad 8.36$$

substituting equations (8.31), (8.35) and (8.36) into equation (8.34), rearranging and taking logarithms to base 10 we get,

$$\log \left[\frac{\frac{dP_e}{dt}}{[P_a + (\alpha-1)P_a^0]^n} \right] = [\log k + n \log Z_a - \log Z_e] + a \cdot \log \left[\frac{P_a}{[P_a + (\alpha-1)P_a^0]} \right] \quad 8.37$$

hence a plot of the L.H.S. of equation (8.37) against the last term of the R.H.S. should yield a straight line of slope equal to (a) the order of reaction with respect to PIBSA.

The samples of two runs only were analysed by IR spectroscopy, run 45 with $\alpha = 1.0$ for the estimation of the overall order of reaction (n), and run 43 with $\alpha = 1.5$ for the estimation of the order of reaction with respect to PIBSA (a).

8.2.2 Calculation of (n) from IR spectroscopy analysis

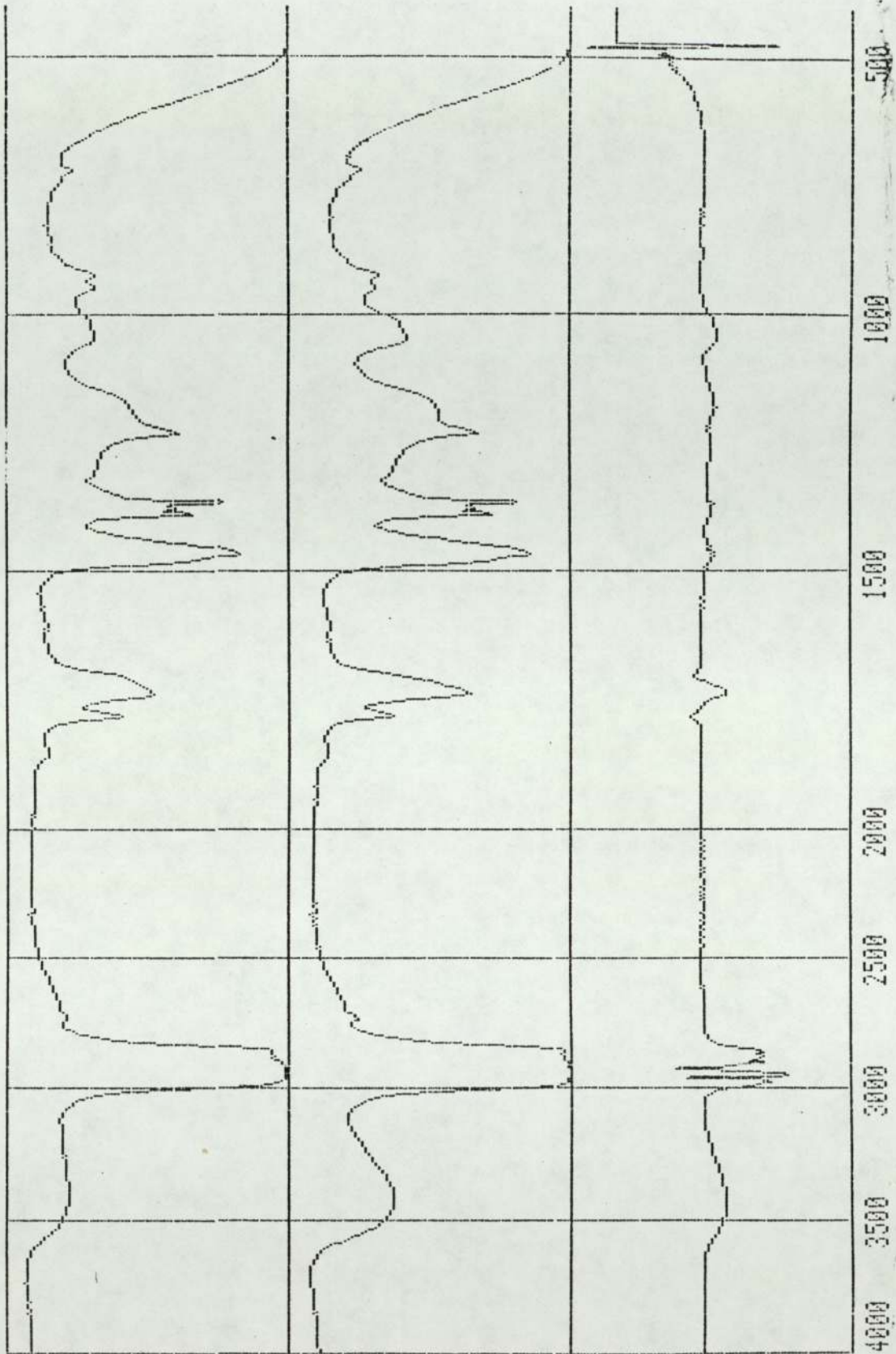
Samples of run 45 with $\alpha = 1.0$ were analysed by IR spectroscopy. The IR traces of the samples obtained from the spectrophotometer were fed directly into a connected data station and were all compared to the trace of the second sample, which in turn was compared with the trace of the first sample taken at $t=0$. The IR traces obtained for the differences were studied and the heights of the characteristic peaks representing the following were measured in mm

a - Hydroxyl group	at WN 3400 cm^{-1}
b - Ester group	at WN 1730 cm^{-1}
c - Anhydride group	(two peaks at WN 1860 and 1780 cm^{-1})
d - Free acid peak	at WN 1710 cm^{-1}
e - Ether group	at WN 1100 cm^{-1}
f - Ether group	at WN 1170 cm^{-1}

Figure 8.8 shows a sample of the IR traces and their comparison and gives the IR traces of samples No. 2 and No. 5 with their difference trace for run 45. Table 8.11 and Table 8.12 were formulated for run 45 from these peak height measurements. The following plots were carried out from Table 8.12,

1. Ester peak height (P_e) mm vs. time (hr) in Figure 8.9
2. Total acid peak height (P_a) mm vs. time (hr) in Figure 8.10.
3. Hydroxyl peak height (mm) vs. TAN mg KOH/g in Figure 8.11.

For run 45 equation (8.33) is applicable because $\alpha = 1.0$, hence the slope of the curve in Figure 8.9 for the plot of P_e vs. time was



Sample 2
IR trace

Sample 5
IR trace

The difference
between Samples
5 and 2
IR traces

Figure 8.8: IR traces for samples No.2 and No.5 and the trace of their difference for run 45

TABLE 8.11

Characteristic peak heights of run 45 samples analysed by IR spectroscopy

Number of Sample	Time After PE Addition (hr)	Hydroxyl Peak Height WN 3400 cm ⁻¹ (mm)	Ester Peak Height WN 1730 cm ⁻¹ (mm)	Acid Peak Heights (mm)		Total Available Acid (mm)	Ether Peak Heights (mm)		TAN mg KOH / g sample
				1780 + 1860 WN (cm ⁻¹)	1710 WN (cm ⁻¹)		WN 1100 cm ⁻¹	WN 1170 cm ⁻¹	
1	0	0	0	0	0	0	0	0	24.4
2	0.1	2.1	4.0	-4.0	0	-4.0	0.3	1.6	21.4
2	0.1	0	0	0	0	0	0	0	21.4
3	0.2	1.9	2.0	-1.0	0	-1.0	0.2	1.0	16.4
4	0.3	2.7	3.0	-1.4	-0.7	-2.1	0.8	1.5	14.2
5	0.5	3.8	4.0	-1.9	-1.0	-2.9	0.8	2.0	10.8
6	0.75	3.9	5.0	-2.3	-1.1	-3.4	1.0	3.1	8.9
7	1.0	4.0	5.8	-2.5	-1.2	-3.7	1.1	3.4	7.9
8	1.5	4.0	6.5	-3.0	-1.5	-4.5	1.1	3.4	6.4
9	2.0	3.8	7.0	-3.2	-1.8	-5.0	1.5	3.5	5.5
10	3.2	3.75	7.8	-3.6	-2.0	-5.6	2.0	4.0	4.5
11	4.2	3.5	8.0	-3.9	-2.1	-6.0	2.1	4.1	3.9

TABLE 8.12

Final summary of characteristic peak heights for run 45 samples analysed by IR spectroscopy

Number of Sample	Time After PE Addition (hr)	TAN mg KOH g sample	Hydroxyl		Ester Peak Height WN 1730 cm ⁻¹ (mm)	Total Acid Peak Height (1780+1860+1710) cm ⁻¹		Ether Peak Height		Total Ether Peak Height (mm)
			Peak Height WN 3400 cm ⁻¹ (mm)	Peak Height WN 1730 cm ⁻¹ (mm)		Negative Scale (mm)	Positive Scale (mm)	Ether Peak Height (mm)		
								WN 1100 cm ⁻¹	WN 1170 cm ⁻¹	
1	0	24.4	0	0	0	10.0	0	0	0	0
2	0.1	21.4	2.1	4.0	-4.0	6.0	0.3	1.6	1.9	1.9
3	0.2	16.4	4.0	6.0	-5.0	5.0	0.5	2.6	3.1	3.1
4	0.3	14.2	4.8	7.0	-6.1	3.9	1.1	3.1	4.2	4.2
5	0.5	10.8	5.9	8.0	-6.9	3.1	1.1	3.6	4.7	4.7
6	0.75	8.9	6.0	9.0	-7.4	2.6	1.3	4.7	5.0	5.0
7	1.0	7.9	6.1	9.8	-7.7	2.3	1.4	5.0	6.4	6.4
8	1.5	6.4	6.1	10.5	-8.5	1.5	1.4	5.0	6.4	6.4
9	2.0	5.5	5.9	11.0	-9.0	1.0	1.8	5.1	6.9	6.9
10	3.2	4.5	5.8	11.8	-9.6	0.4	2.3	5.6	7.9	7.9
11	4.2	3.9	5.6	12.0	-10.0	0	2.4	5.7	8.1	8.1

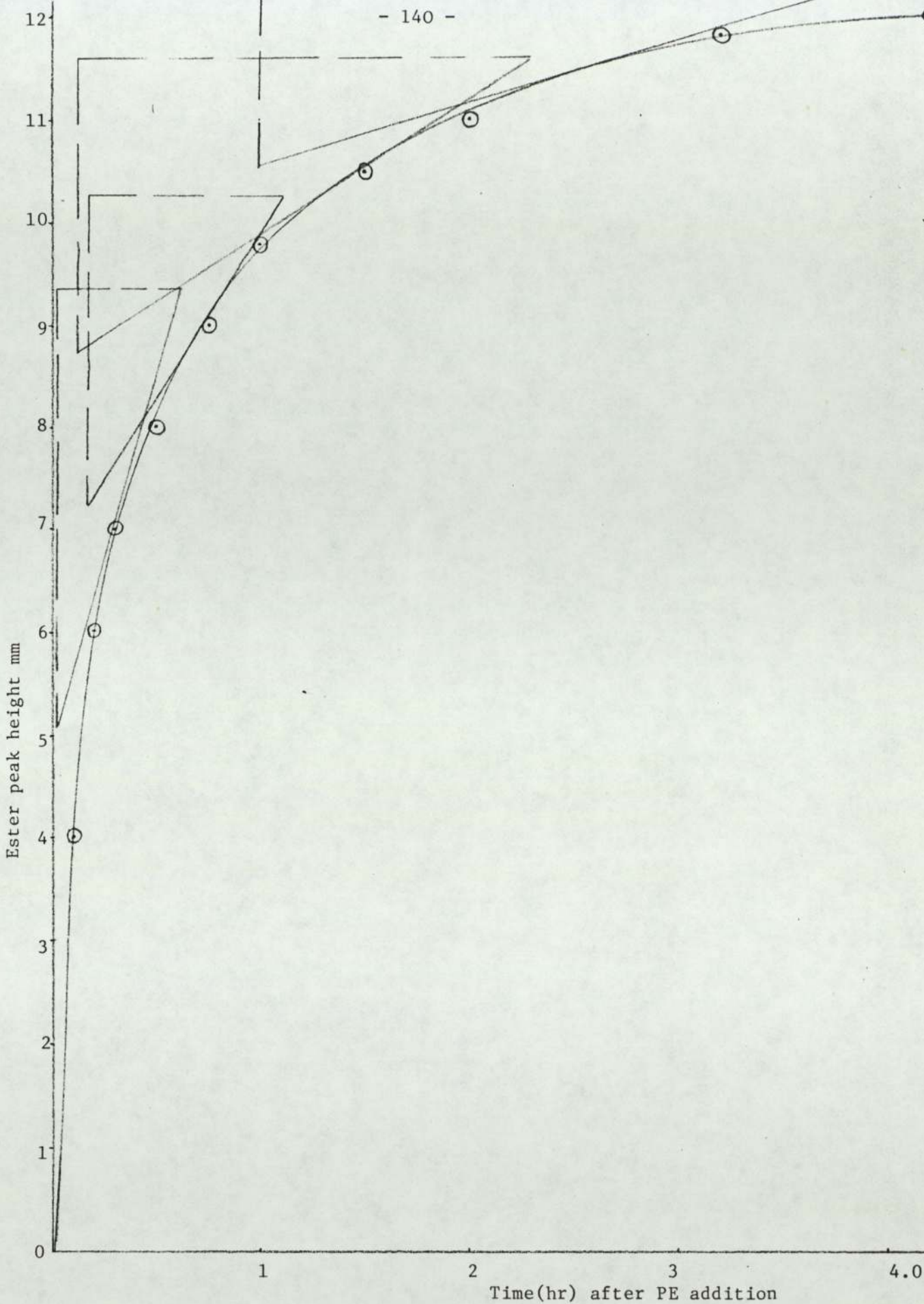


Figure 8.9

Graph for run 45 of Ester peak height mm vs. time hr after PE addition

Analysis by IR spectroscopy

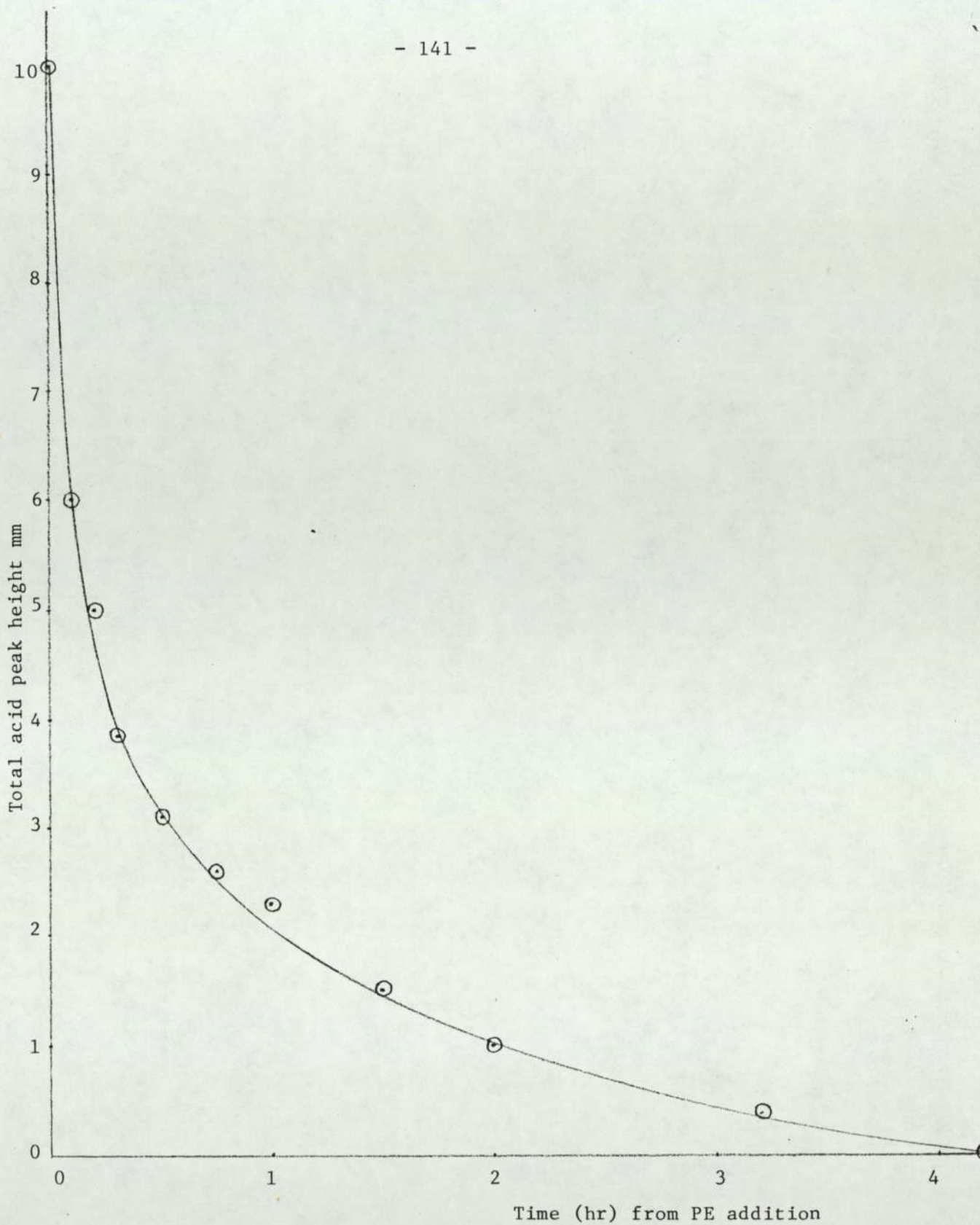


Figure 8.10

Graph for run 45 of total acid (anhydride + free acid) peak height mm vs. time (hr) after PE addition

Analysis by IR spectroscopy

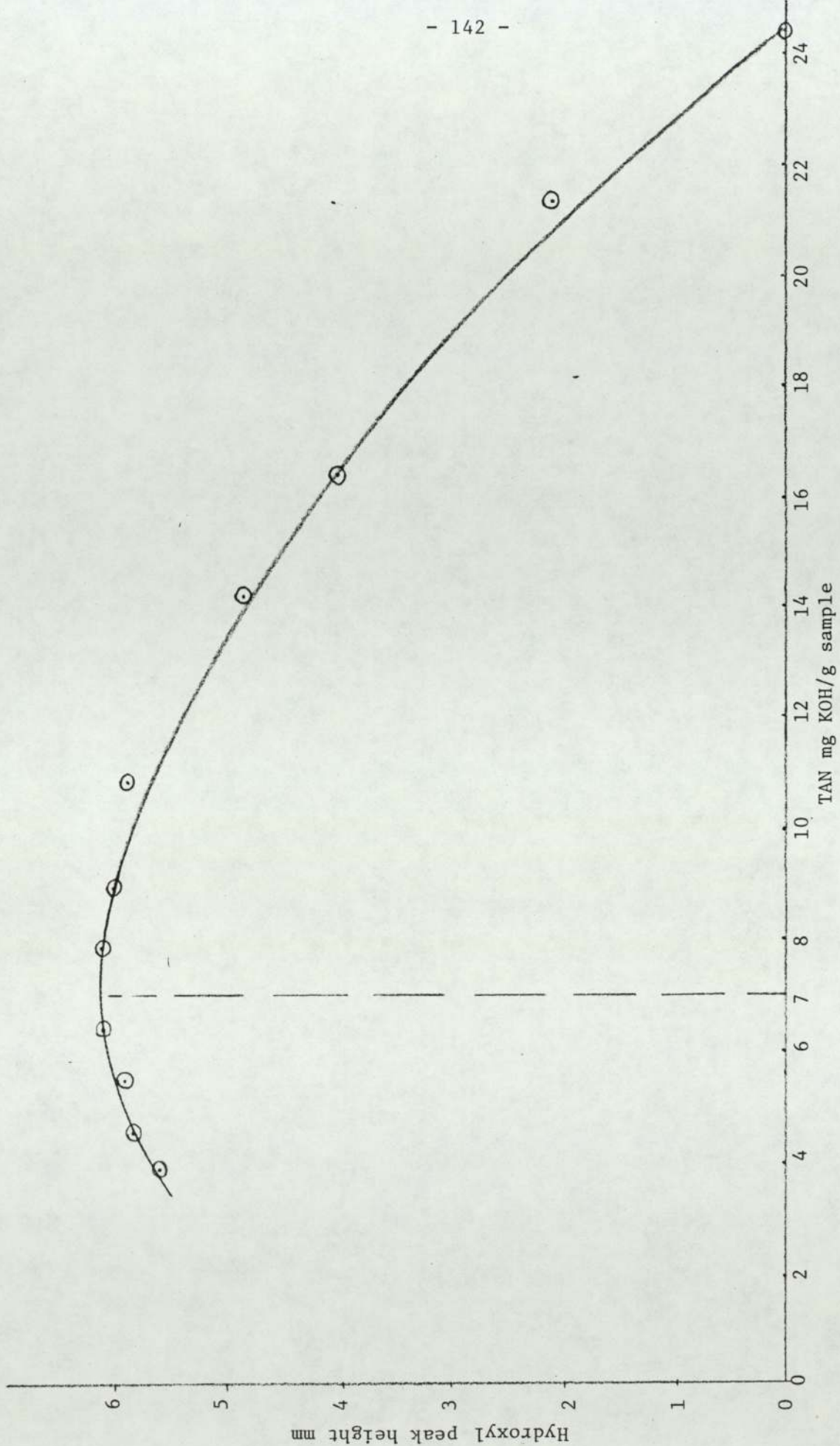


Figure 8.11 Graph for run 45 of hydroxyl peak height mm vs. TAN mg KOH/g sample. Analysis by IR spectroscopy

measured at five different points covering the whole reaction range. The initial slope was estimated from the increase in peak height over the first two intervals as before. These values were tabulated in Table 8.13, together with the corresponding values of the total acid peaks height (P_a) which were found from Figure 8.10 for (P_a) vs. time.

TABLE 8.13

The slope of the ester peak height vs. time curve, measured at five different points for run 45 samples

Time hr	Ester peak height P_e mm	slope = (dP_e/dt) mm/hr	$\log[dP_e/dt]$ = y_i	Total acid peak height P_a (mm)	$\log(P_a)$ = x_i
0	0	30.000	1.477	10.0	1.000
0.3	7.0	7.250	0.860	3.85	0.5855
0.725	9.05	3.243	0.511	2.57	0.4099
1.5	10.55	1.3103	0.117	1.50	0.1761
2.5	11.45	0.618	-0.209	0.725	-0.1397

and from Table 8.13 we have,

$$\Sigma x_i = 2.0318, (\Sigma x_i)^2 = 4.1282, \Sigma x_i^2 = 1.5614$$

$$\Sigma y_i = 2.756, \Sigma x_i y_i = 2.2400, \text{ and } N = 5$$

The slope and intercept of the least square best fit straight line of the plot of $\log(dP_e/dt)$ vs. $\log P_a$ are given by equations (8.22) and (8.23),

$$\therefore \text{ slope} = \frac{[2.2400 - 2.0318 \times 2.756/5]}{1.5614 - [4.1282/5]}$$

$$\therefore \text{ slope} = 1.522$$

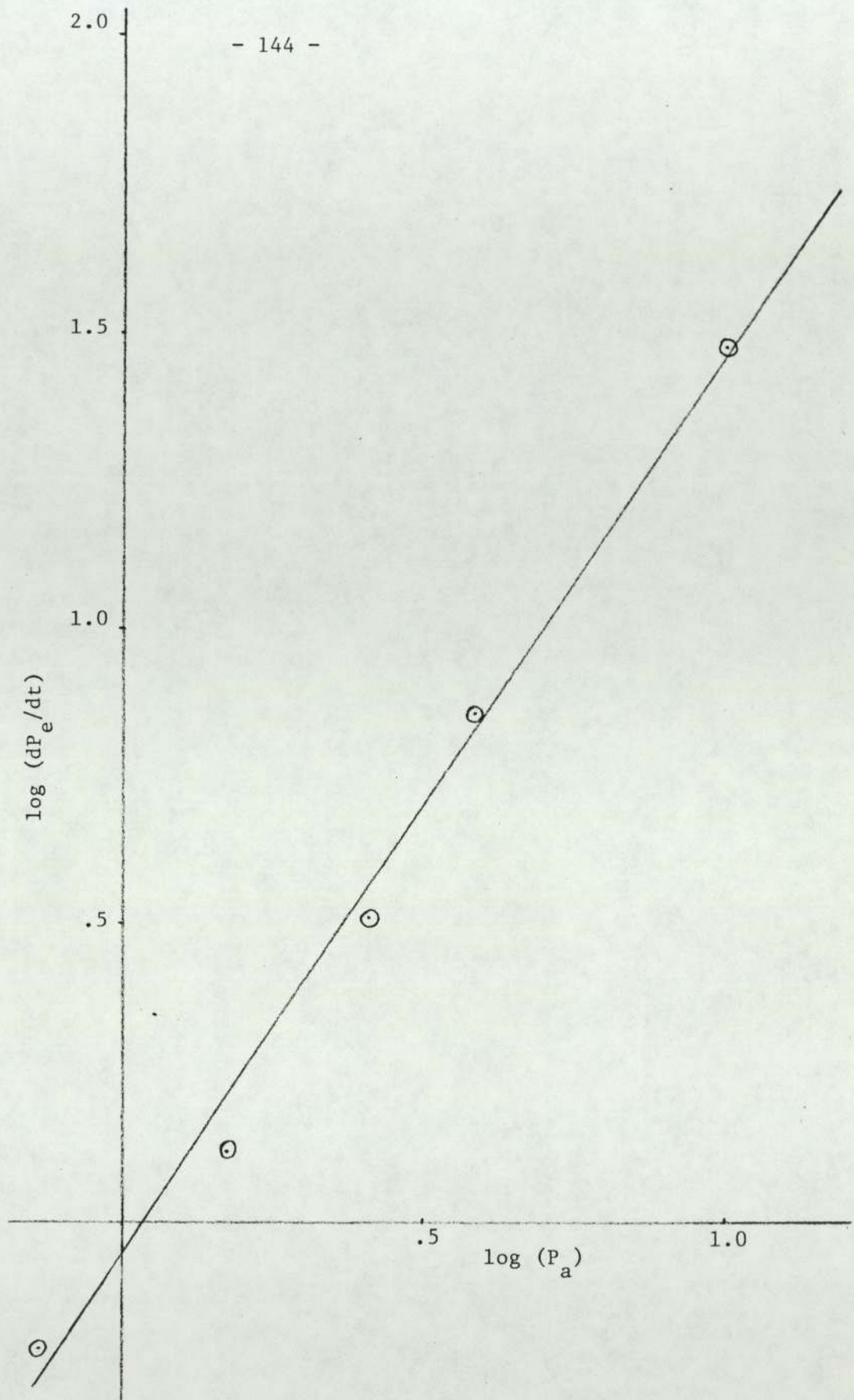


Figure 8.12

Graph for run 45 of $\log (dP_e/dt)$ vs. $\log (P_a)$

(dP_e/dt) = the slope of the ester peak height P_e (mm) vs. time (hr)

(P_a) = the total acid peak height (mm)

hence, the overall order of reaction (n) = slope = 1.522

also,

$$\text{intercept} = \frac{2.756 \times 1.5614 - 2.0318 \times 2.2400}{5 \times 1.5614 - 4.1282}$$

∴ intercept = -0.0674

the actual plot of $\log (dP_e/dt)$ vs. $\log (P_a)$ is given in Figure 8.12.

8.2.3 Calculation of (a) from IR spectroscopy analysis

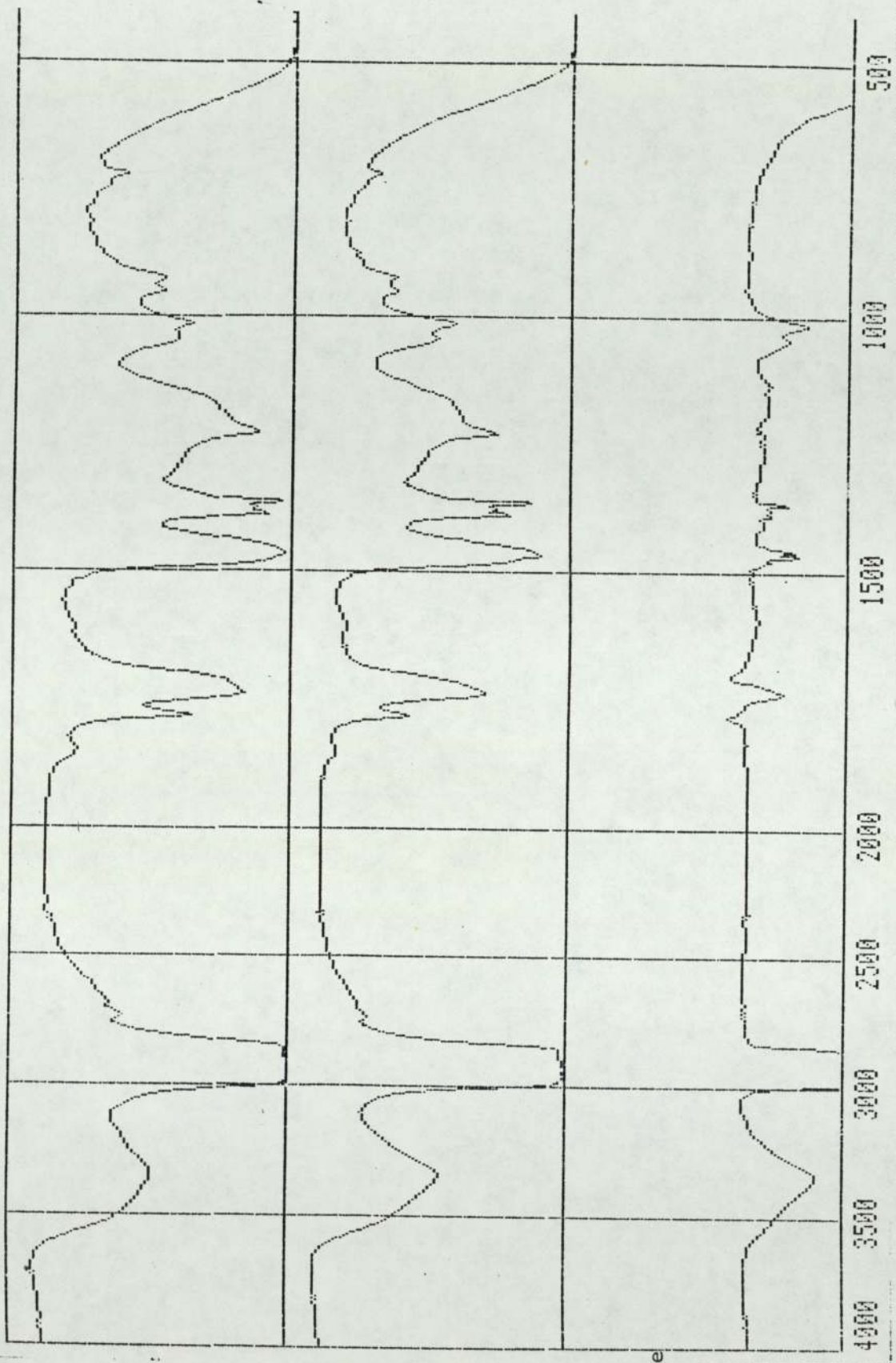
Samples of run 43 with $\alpha = 1.5$ were analysed by IR spectroscopy.

In a similar manner to that of run 45, the IR traces of the samples obtained from the spectrophotometer were fed directly into the connected data station and were all compared to the trace of the second sample, which in turn was compared with the trace of the first sample taken at $t = 0$. The IR traces obtained for the differences were studied and the heights of the characteristic peaks representing the following were measured in mm

a - Hydroxyl group	at WN 3400 cm^{-1}
b - Ester group	at WN 1730 cm^{-1}
c - Anhydride group	(two peaks at WN 1860 and 1780 cm^{-1})
d - Free acid peak	at WN 1710 cm^{-1}
e - Ether group	at WN 1100 cm^{-1}
f - Ether group	at WN 1170 cm^{-1}

Figure 8.13 is presented as a sample for the IR traces and their comparison and gives the IR traces of samples No. 2 and No. 4 with their difference trace for run 43. Table 8.14 and Table 8.15 were formulated for run 43 from these peak height measurements. The following plots were carried out from Table 8.15,

1. Ester peak height (P_e) mm vs. time hr in Figure 8.14.
2. Total acid peaks height (P_a) mm vs. time hr in Figure 8.15.
3. Hydroxyl peak height mm vs. TAN mg KOH/g in Figure 8.16.



I R trace
of sample
No.2

I R trace
of sample
No.4

I R trace of
the difference
between
samples 2 and
4

Figure 8.13: IR traces for samples No.2 and No.4 and the trace of their difference for tun 43.

TABLE 8.14

Characteristic peak heights for run 43 samples analysed by IR spectroscopy

Number of Sample	Time After PE Addition (hr)	TAN mg KOH g sample	Hydroxyl Peak Height 3400 cm ⁻¹ (mm)	Ester Peak Height 1730 cm ⁻¹ (mm)	Acid Peak Heights (mm)		Total Available Acid (mm)	Ether Peak Height (mm)
					Anhydride (cm ⁻¹)	Free Acid (cm ⁻¹)		
1	0	23.5	0	0	0	0	0	0
2	0.1	18.7	5.0	6.5	-4.3	0	-4.3	0.5
2	0.1	18.7	0	0	0	0	0	0
3	0.2	14.5	7.3	2.5	-2.2	-2.0	-4.2	1.0
4	0.3	12.6	11.1	5.8	-3.3	-2.5	-5.8	1.3
5	0.5	9.5	17.0	7.3	-5.5	-4.2	-9.7	3.0
6	0.75	7.2	20.0	11.0	-7.0	-4.4	-11.4	3.0
7	1.0	6.0	22.5	12.0	-9.1	-5.0	-14.1	3.3
8	1.5	4.5	19.0	12.7	-10.5	-5.0	-15.5	4.0
9	2.0	3.7	17.0	13.5	-10.8	-5.0	-15.8	5.0
10	2.55	3.3	16.0	14.0	-11.0	-5.0	-16.0	8.0
11	3.5	3.0	13.0	14.5	-11.1	-5.0	-16.1	9.0
12	5.05	2.5	12.0	15.3	-11.6	-5.3	-16.9	10.0

TABLE 8.15

Final summary of characteristic peak height for run 43 samples analysed by IR spectroscopy

Number of Sample	Time After PE Addition (hr)	TAN mg KOH g sample	Hydroxyl Peak Height 3400cm ⁻¹ (mm)	Ester Peak Height 1730cm ⁻¹ (mm)	Acid Peak Heights (1780+1860+1710)cm ⁻¹ (mm)		Ether Peak Height (mm)		Total Ether Peak Height (mm)
					Negative Scale	Positive Scale	WN 1100cm ⁻¹	WN 1170cm ⁻¹	
1	0	23.5	0	0	0	21.2	0	0	0
2	0.1	18.7	5	6.5	-4.3	16.9	0.5	2.0	2.5
3	0.2	14.5	12.3	9.0	-8.5	12.7	1.5	4.0	5.5
4	0.3	12.6	16.1	12.3	-10.1	11.1	1.8	4.0	5.8
5	0.5	9.5	22.0	13.8	-14.0	7.2	3.5	6.0	9.5
6	0.75	7.2	25.0	17.5	-15.7	5.9	3.5	7.2	10.7
7	1.0	6.0	27.5	18.5	-18.4	2.8	3.8	7.3	11.1
8	1.5	4.5	24.0	19.2	-19.8	1.4	4.5	8.5	13.0
9	2.0	3.7	22.0	20.0	-20.0	1.2	5.5	10.8	16.3
10	2.55	3.3	21.0	20.5	-20.3	0.9	8.5	13.0	21.5
11	3.5	3.0	18.0	21.0	-20.4	0.8	9.5	13.0	22.5
12	5.05	2.5	17.0	21.8	-21.2	0	10.5	14.0	24.5

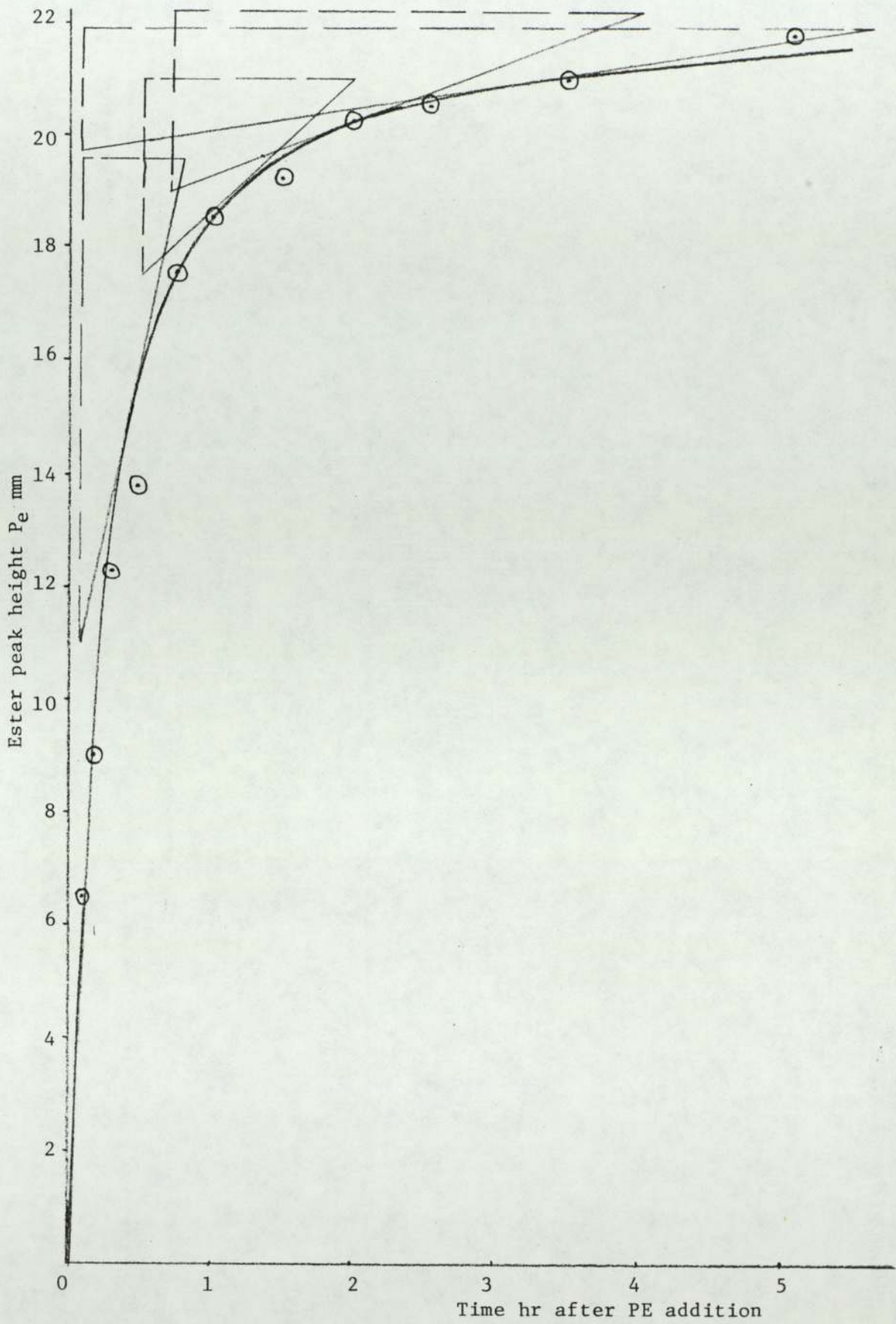


Figure 8.14

Graph for run 43 of ester peak height P_e (mm) vs. time hr
using IR spectroscopy analysis

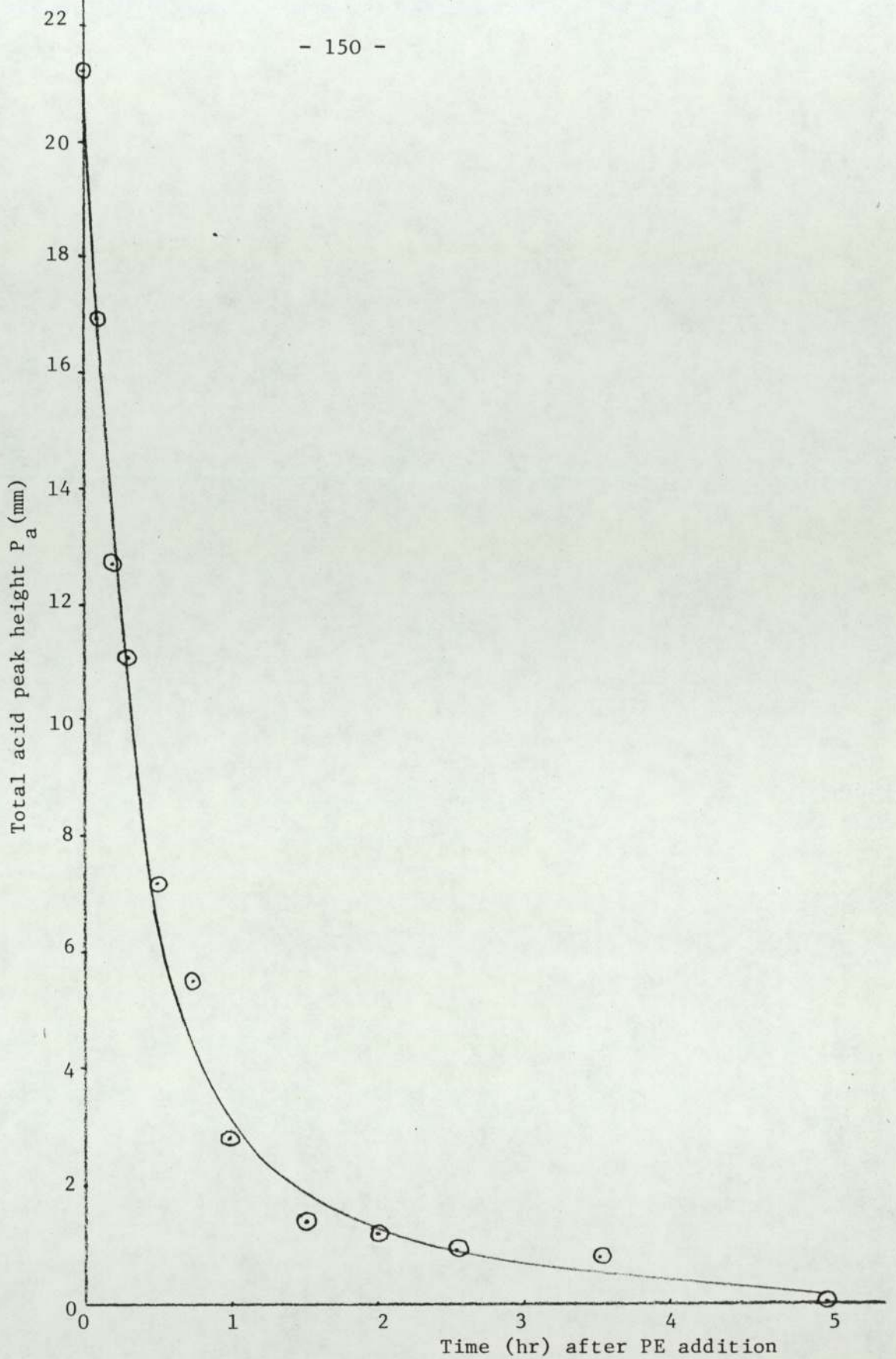


Figure 8.15

Graph for run 43 of total acid peak height P_a (mm) vs. time (hr) using

IR spectroscopy analysis

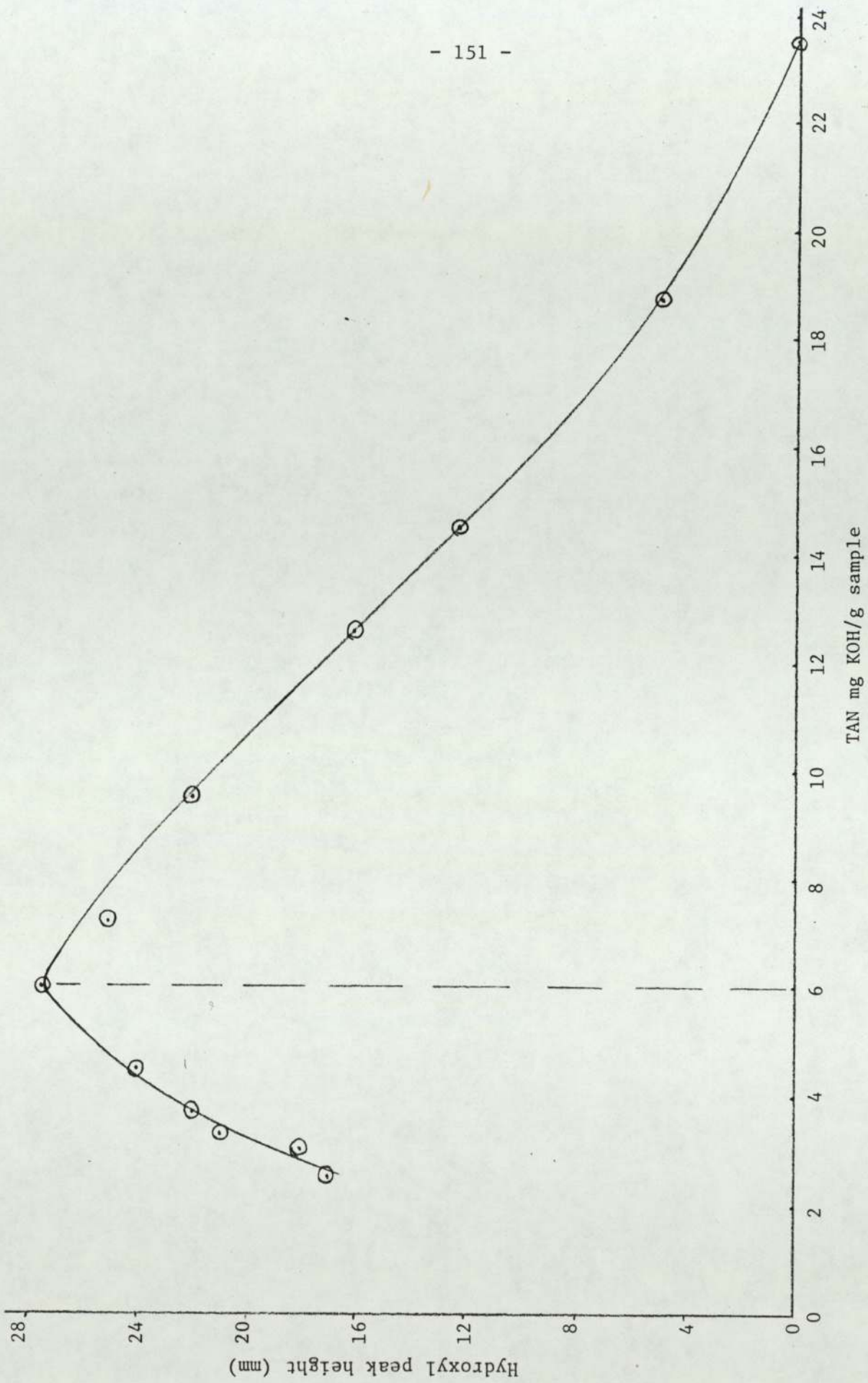


Figure 8.16

Graph for run 43 of hydroxyl peak height mm vs. TAN mg KOH/g samples, using I.R. spectroscopy analysis

For run 43 equation (8.37) is applicable because $\alpha > 1.0$, hence the slope of the curve in Figure 8.14 for the plot of P_e vs. time was measured at five different points covering the whole reaction range. These values were tabulated in Table 8.16, together with the corresponding values of the total acid peaks height (P_a) which were found from Figure 8.15 for (P_a) vs. time. Table 8.16 also contains the corresponding individual values of Y and X, (y_i and x_i) calculated from the following expressions,

$$Y = \log \left[\frac{\left(\frac{dP_e}{dt} \right)}{(P_a + (\alpha-1) P_a^0)^n} \right]$$

and

$$X = \log \left[\frac{P_a}{(P_a + (\alpha-1) P_a^0)} \right]$$

where: $n = 1.522$ and $\alpha = 1.5$.

TABLE 8.16

The slope of the ester peak height vs. time curve measured at five different points, together with corresponding values of Y and X for run 43.

Time (hr)	Ester peak height P_e (mm)	Slope = (dP_e/dt) (mm/hr)	Acid peak height (P_a) (mm)	Y	X
0	0	45.000	21.20	-0.6335	-0.1761
0.4	14.70	11.944	8.45	-0.8709	-0.353
1.2	19.10	2.3649	2.50	-1.3267	-0.7193
2.0	20.20	0.9756	1.30	-1.6477	-0.9616
3.2	20.90	0.3986	0.65	-2.0000	-0.1238

As a sample calculation let us calculate the values of Y and X for the second point in Table 8.16 (y_2 and x_2), hence

$$y_2 = \log \frac{11.944}{[8.45 + (1.5-1.0) \times (21.2)]^{1.522}} = -0.8709$$

and

$$x_2 = \log \frac{8.45}{[8.45 + (1.5 - 1.0)(21.2)]} = -0.353$$

all the other values of Y and X in Table 8.16 were calculated in the same way, also from these values we have,

$$\Sigma x_i = -3.4482, (\Sigma x_i)^2 = 11.8901, \Sigma x_i^2 = 3.1308,$$

$$\Sigma y_i = -6.4788, \Sigma x_i y_i = 5.4341, \text{ and } N = 5$$

The slope and intercept of the least square best fit straight line plot of Y vs. X are given by equations (8.22) and (8.23),

$$\therefore \text{ slope} = \frac{5.4341 - [(-3.4482)(-6.4788)/5]}{3.1308 - [11.8901/5]}$$

$$\therefore \text{ slope} = 1.283$$

but from equation (8.37) the slope is equal to (a), hence

$$\underline{a = \text{ slope} = 1.283.} \quad \text{Order of reaction with respect to PIBSA}$$

also,

$$\text{intercept} = \frac{(-6.4788)(3.1308) - (-3.4482)(5.4341)}{(5 \times 3.1308) - 11.8901}$$

$$\therefore \text{ intercept} = -0.411$$

the plot of Y vs. X of Table 8.16 is given in Figure 8.17.

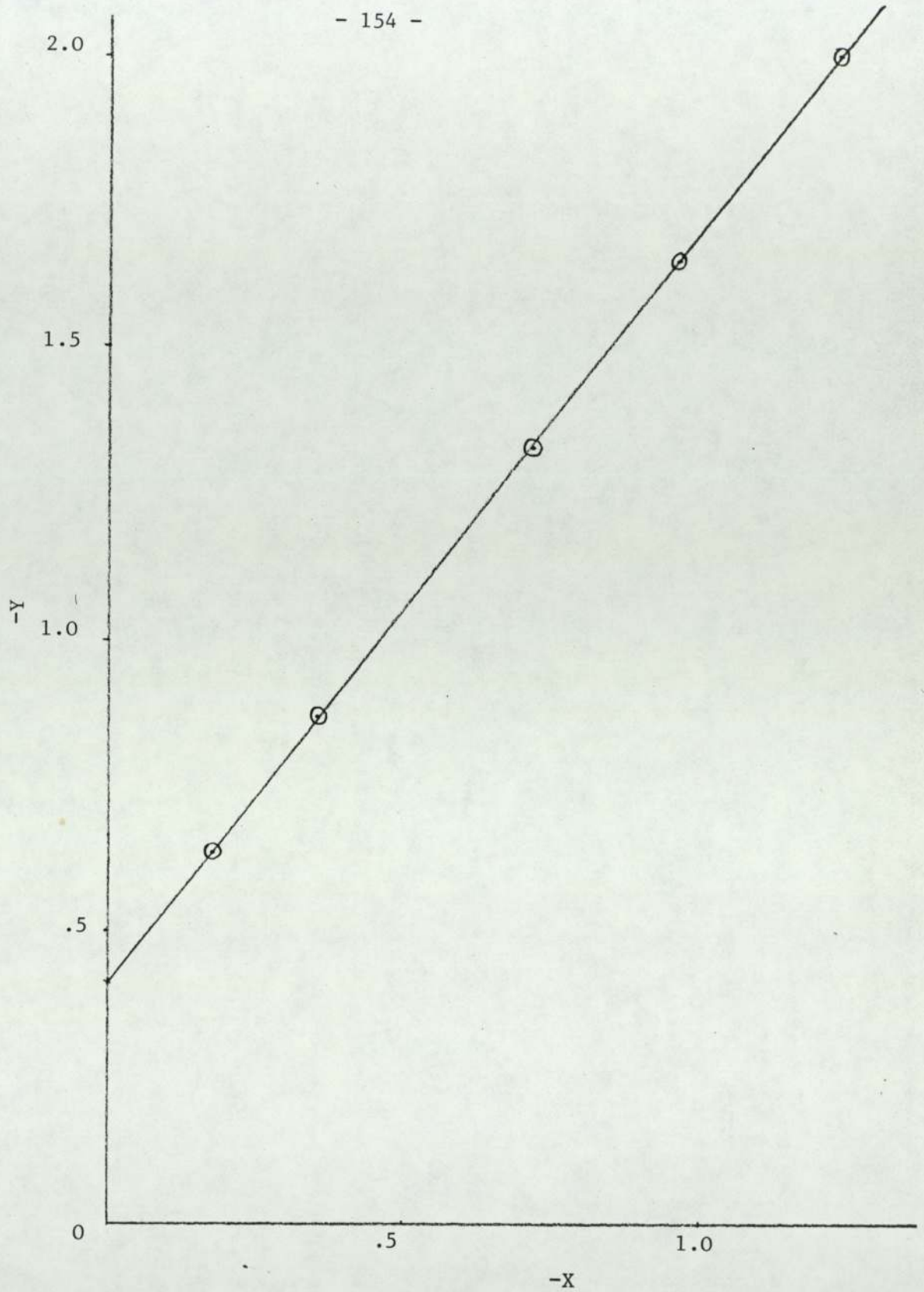


Figure 8.17

Graph for run 43 of $\log \left[\frac{(dP_e/dt)}{(P_a + (\alpha-1)P_a^0)^n} \right] = Y$ vs.

$\log \left[\frac{P_a}{(P_a + (\alpha-1)P_a^0)} \right] = X$

CHAPTER NINE

RESULTS OF SEDIMENT FORMATION INVESTIGATION

In the course of the sediment formation investigation the dispersant had to be prepared on a laboratory scale. Many procedures and tests were carried out during and after the preparation of the dispersant, the results of which are all presented in this chapter.

9.1 Product Preparation and Analysis

The calculations and product analysis of run 29 will be presented in this section as a sample calculation of all other preparation runs. Table 9.1 below contains details of the measurements carried out during run 29. The tabulated TAN values were calculated using equation (A3.1) in Appendix 3,

$$\text{TAN} = \frac{(v-b) \times N \times 56.1}{w} \quad \text{A3.1}$$

with $b = 0.075 \text{ cm}^3$ and $N = 0.01014$, as given in Table A3.4 in Appendix 3.

The first sample at $t = 0$ was in fact taken just before PE addition. Also cooling of the reaction mixture was started just after the withdrawal of sample 8, and the second portion of the dilution oil was added then. Hence the relatively larger drop in TAN between sample 8 and sample 9 was partly due to the increased percentage of the dilution oil. The variation of TAN with time during the heating and reaction stages for run 29 is presented in Figure 9.1, the last three samples given in Table 9.1 were not included in the plot. The second portion of the dilution oil added was 0.175% by weight of total dilution oil in all the runs so as to bring the level of the dilution oil at the filtration stage to 75% by weight of total dilution oil. Hence from Table A2.1 in Appendix 2 for run 29,

TABLE 9.1

Run 29 sample weight measurements and titration results.

No. of sample	Time after PE addition (hr)	Temperature of reaction mixture °C	Time at reaction temperature of 170°C (hr)	Weight of empty beaker g	Weight of beaker plus sample g	Weight of sample g	Volume of base used in titration cm ³	TAN mg KOH / g sample
0	0	140	-	47.25	47.77	0.52	2.675	28.5
1	0.833	160	-	46.24	47.15	0.91	3.10	18.9
2	1.217	169	-	45.98	46.94	0.96	2.80	16.2
3	1.40	170	0.15	48.44	49.31	0.87	2.375	15.0
4	2.25	170	1.00	46.24	47.39	1.15	2.275	10.9
5	2.75	170	1.50	45.81	46.99	1.18	2.10	9.8
6	3.083	170	1.833	46.24	47.14	0.90	1.525	9.2
7	3.75	170	2.50	45.96	47.06	1.10	1.725	8.5
8	4.15	170	3.00	45.84	46.98	1.14	1.70	8.1
9	22.0	136	-	45.78	47.32	1.54	1.325	4.6
10	45.0	136	-	48.41	49.94	1.53	1.15	4.0
11	68.5	136	-	48.39	49.99	1.60	1.15	3.8

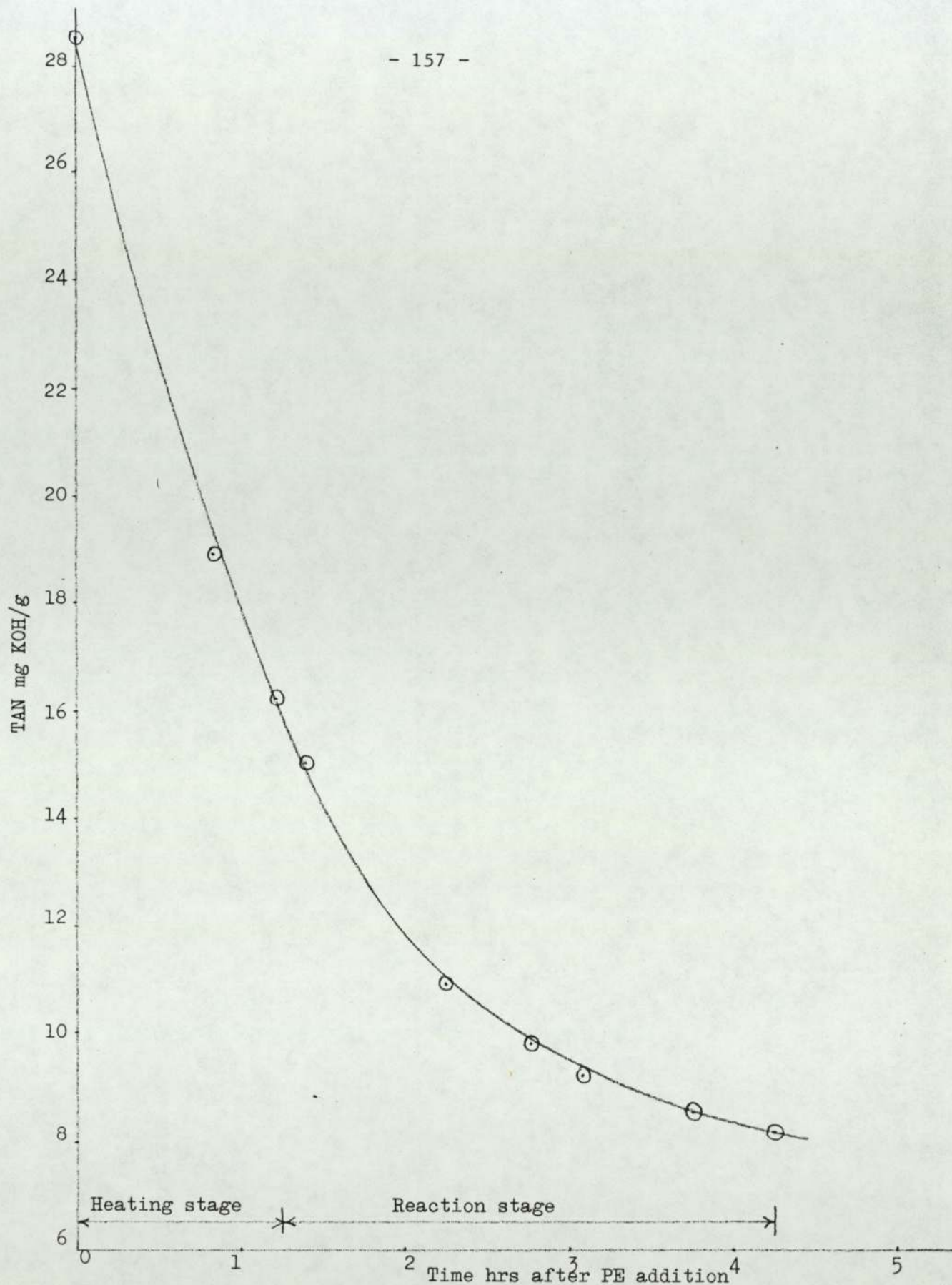


Figure 9.1

Graph for run 29 of TAN mg KOH/g vs. time (hrs) after PE addition

Weight of PIBSA = 403.07g

Weight of total dilution oil (O_t) = $1.351 \times 4.03.07 = 544.55g$

Weight of oil in reaction stage (O_r) = $0.575 \times 544.55 = 313.12g$

Weight of second portion of dilution oil to be added before filtration stage (O_f) = $0.175 \times 544.55 = 95.30g$

This amount of (O_f) was weighed in a beaker, heated to about $169^{\circ}C$ and then added directly into the reaction mixture when cooling was just started from $170^{\circ}C$ to a filtration temperature of about $136^{\circ}C$. The reaction mixture was left at $136^{\circ}C$ for about 65 hours (see Table A2.1).

Filtration stage

Filter aid was used in run 29 in two forms namely, as body aid, and as precoat. 4.03g of filter aid (1% by weight of PIBSA) was weighed and added to the mixture directly as body aid. Also about 1.2g of filter aid was mixed with oil and introduced into the filter as precoat. The filter was prepared and filtration was carried out as explained in Chapter 6. Table 9.2 presents the filtration results for run 29.

TABLE 9.2

Run 29 filtration results

Time (min)	Filtrate volume (cm ³)	Filtration temperature (°C)	Filtration pressure bar/gauge
0	0	130	0
1.45	200	131	1.655
2.17	300	132	2.758
2.73	400	133	4.137
3.45	500	133	4.137
4.20	600	133	4.137
5.35	700	132	4.137
6.82	800	126	4.137
7.70	8 40	125	4.137

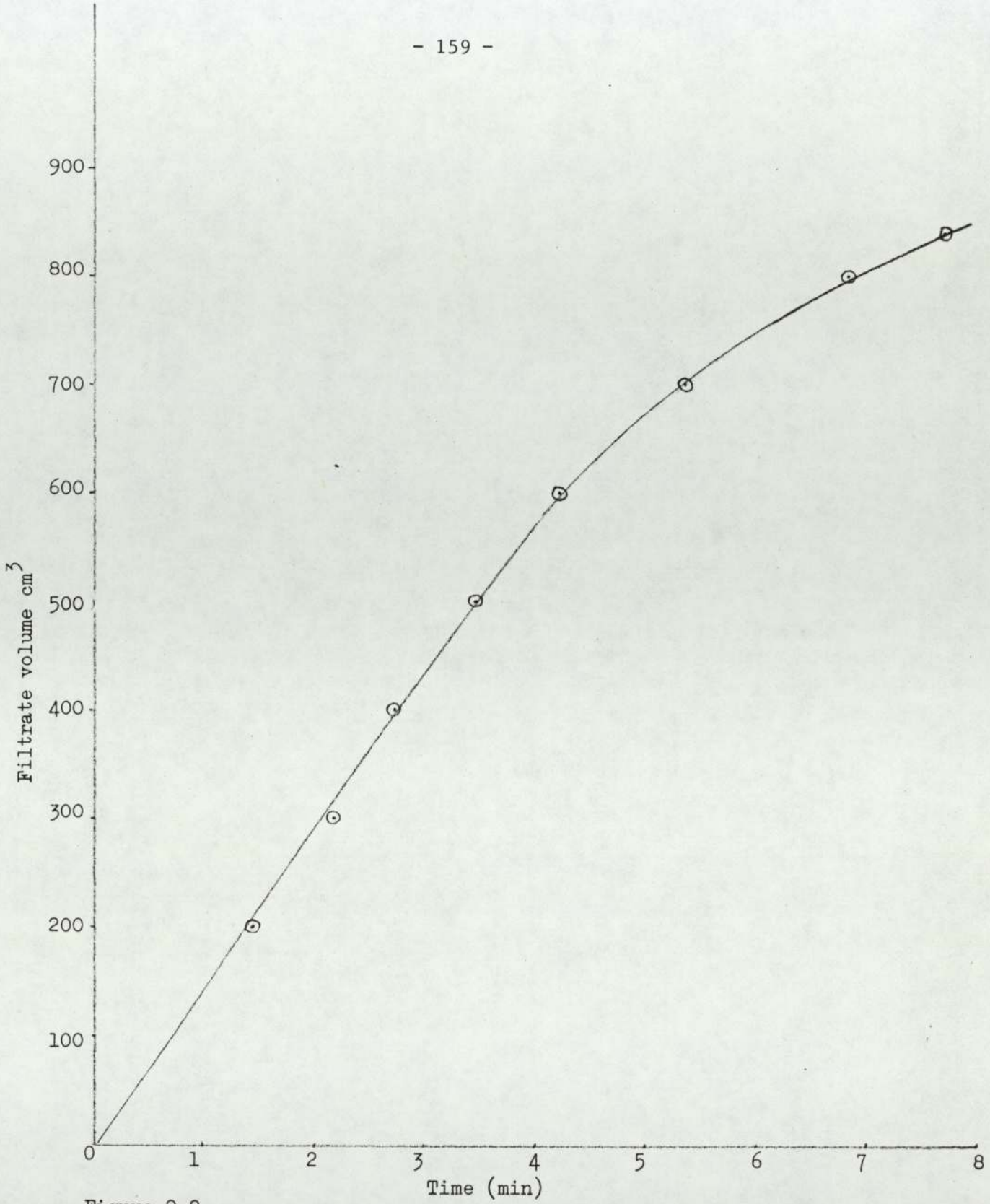


Figure 9.2

Graph for run 29 of filtrate volume cm³ vs. filtration time (min)

The filtration was very fast compared to other runs due to the use of filter aid (see Table A2.1). A plot of the filtrate volume against time is presented in Figure 9.2. The overall filtration rate in $\text{dm}^3/\text{m}^2\cdot\text{hr}$ units can be calculated from the data in Table 9.2 knowing the filtration area. For the laboratory filter used,

$$\text{filtration area} = 0.01368 \text{ m}^2$$

$$\therefore \text{Overall filtration rate} = \frac{840}{7.7} \times \frac{60}{1000 \times 0.01368} = \underline{478.5} \frac{\text{dm}^3}{\text{m}^2\cdot\text{hr}}$$

Also to calculate the third and final amount of the dilution oil after making corrections for the samples withdrawn, the following calculations were carried out

$$\text{Weight of the empty graduated beaker} = 286.85\text{g}$$

$$\text{Weight of beaker + total filtrate} = 1023.60\text{g}$$

$$\therefore \text{Weight of filtrate} = 736.75\text{g}$$

the approximate % of PIBSA in this filtrate was estimated from all the initially present weights and also the added (O_f), hence

$$\% \text{ PIBSA in filtrate} = \frac{403.07 \times 100}{403.07+313.12+95.30+4.77+55.46} = 46.23\%$$

$$\text{and } \% \text{ oil in filtrate} = \frac{313.12+95.30}{871.72} \times 100 = 46.9\%$$

$$\therefore \text{total PIBSA in filtrate} = 340.60\text{g}$$

$$\text{and total oil in filtrate} = 345.54\text{g}$$

$$\text{but total dilution oil } (O_T) \text{ for this PIBSA} = 460.15\text{g}$$

$$\therefore \text{the final dilution oil to be added } (O_p) = 114.61\text{g}$$

This amount of oil (O_p) was weighed separately heated and added to the filtrate while mixing thoroughly. Three main tests were performed on the product, the results were as follows:

Centrifuge test results

The test was carried out as outlined in Appendix 4 on two samples namely, raw product sample taken just before the addition of the body aid, and final dispersant product sample, the results were,

- a. Raw product sediment = 2.4 volume %
- b. Final product sediment = .01 dark sediment + .04 white haze
= 0.05 volume % total sediment

Viscosity measurements results

The viscosity of both the filtrate (with 75% by weight of the dilution oil) and of the final product (with all the dilution oil) were measured. The method used is outlined in Appendix 5, and the viscometer used was viscometer D with a factor of $1.3684 \times 10^{-6} \text{ (m}^2/\text{s}^2)$ (see Table A5.1 in Appendix 5).

a. Viscosity of filtrate:

1st run flowing time = 5 min + 42.5s

2nd run flowing time = 5 min + 42.5s

$$\therefore \text{Viscosity of filtrate} = 1.3684 \times 10^{-6} \times 342.5 = 468.7 \times 10^{-6} \text{ m}^2/\text{s} \\ \text{at } 100^{\circ}\text{C}$$

b. Viscosity of product:

1st run flowing time = 2 min + 46.5s

2nd run flowing time = 2 min + 46.5s

$$\therefore \text{Viscosity of product} = 1.3684 \times 10^{-6} \times 166.5 = 227.8 \times 10^{-6} \text{ m}^2/\text{s} \\ \text{at } 100^{\circ}\text{C}$$

Total Acid Number measurement

The TAN of the final product was calculated as outlined in Appendix 3,

TABLE 9.3

Results of product analysis of all the runs

No. of run	Sediment of raw product volume %	Sediment of final product volume %			Viscosity $\times 10^{-6}$ (m ² /s) at 100°C		TAN
		Actual sediment	Haze	Total sediment	Filtrate	Product	mg KOH g sample
1	2.0	0.03	-	0.03	268.9	-	2.7
2	1.4	< 0.01	-	< 0.01	-	129.7	2.4
3	1.4	< 0.02	-	< 0.02	-	-	2.3
4	1.2	< 0.01	-	< 0.01	-	104.4	2.0
5	-	< 0.01	-	< 0.01	-	152.6	3.7
6	0.2	0.06	-	0.06	-	1032.1	0.8
7	2.0	0.09	-	0.09	-	291.2	2.0
8	0.9	0.04	-	0.04	-	340.4	1.7
9	0.6	0.01	-	0.01	-	363.6	1.9
10	0.7	0.04	-	0.04	-	451.1	1.4
11	0.7	0.03	-	0.03	-	352.7	1.7
12	0.5	0.05	0.02	0.07	-	414.2	1.5
13	2.2	0.06	-	0.06	-	142.2	3.9
14	1.4	0.12	-	0.12	-	150.1	2.7
15	0.3	0.04	0.02	0.06	-	153.0	1.4
16	1.4	0.02	0.04	0.06	291.2	-	1.3
17	1.4	0.2	-	0.2	-	132.6	2.7
18	2.0	0.2	-	0.2	-	114.8	2.6
19	2.0	0.15	-	0.15	-	142.2	2.5
20	1.4	0.2	-	0.2	-	132.6	2.7
21	2.0	< 0.01	-	< 0.01	-	125.8	1.9
22	1.0	< 0.01	0.01	< 0.02	370.0	-	2.2
23	0.8	0.2	-	0.2	797.0	372.5	1.0
24	1.4	0.01	0.03	0.04	-	210.5	2.9
25	1.0	< 0.01	-	< 0.01	-	337.7	1.7
26	2.0	< 0.01	-	< 0.01	-	250.6	2.2
27	8.0	0.02	0.04	0.06	-	336.3	1.9
28	6.5	< 0.01	-	< 0.01	-	278.4	2.2
29	2.4	0.01	0.04	0.05	468.7	227.8	3.4
30	4.0	0.01	0.03	0.04	345.2	181.2	4.6
31	5.0	< .01	-	< .01	261.3	148.6	6.3
32	4.0	0.01	0.01	0.02	196.4	117.8	3.7
33	3.0	0.01	0.02	0.03	190.4	-	4.3
34	3.4	0.01	-	0.01	176.0	-	5.1
35	2.8	0.01	0.03	0.04	359.0	189	4.9

TABLE 9.3 (Continued)

Results of product analysis of all the runs

No. of run	Sediment of raw product volume %	Sediment of final product volume %			Viscosity $\times 10^{-6}$ (m^2/s) at 100°C		TAN
		Actual sediment	Haze	Total sediment	Filtrate	Product	mg KOH / g sample
51	2.8	<.01	-	<.01	502.8	256.2	3.2
52	3.0	<.02	-	<.02	443.9	244.4	3.7
53	3.2	<.01	-	<.01	520.9	248	3.2
54	2.4	<.01	-	<.01	423	246.6	3.7
55	3.6	<.01	-	<.01	370	210	4.7
56	3.0	<.01	-	<.01	391	216.5	4.3
57	3.2	<.01	-	<.01	426.1	213.3	4.1
58	2.7	<.01	-	<.01	437	222.7	4.1
59*	2.4	<.01	hazy liquid		530.2	235.7	3.3
60*	2.4	<.01	hazy liquid		494.6	223.1	3.6

*In runs 59 and 60, the sediment test result of the final product showed that the liquid above the sediment at the bottom of the centrifuge tube was hazy with no definite interface, hence no value was estimated for the haze.

Weight of empty beaker = 46.91g

Weight of beaker + sample = 49.18g

∴ Weight of sample = 2.27g

Titration results:-

Starting base level in burette = 26.1 cm³

Final level of base in burette = 27.525 cm³

∴ Volume of base used in titration = 1.425 cm³

hence using equation (A3.1) with N = 0.1014 and b = 0.075 cm³ we have,

$$\text{product TAN} = \frac{(1.425-0.075) \times 0.1014 \times 56.1}{2.27}$$

$$\underline{\therefore \text{TAN} = 3.4 \text{ mg KOH/g sample}}$$

Table 9.3 presents the product analysis results of all the runs performed during the sediment investigation program, calculated in a similar manner to that given above.

9.2 Sediment Analysis Results

Gas Chromatography (GC) was used in the analysis of sediment from different runs. The GC analysis was carried out at Esso Research Centre in Abingdon. Samples of mono-, di-, and tri-pentaerythritols were analysed first by GC to identify each of the peaks by determining the corresponding elution time in minutes for each peak. The elution time in minutes for the mono-, di-, and tri-PE peaks were found to be equal to 4.87, 9.83, and 14.10 respectively. Different sediment samples were then analysed by GC, and the final results are presented in Table 9.4, after taking the above elution times of the peaks concerned into consideration.

TABLE 9.4

Results of sediment analysis by Gas Chromatography

Sample No.	Sample source	mono-PE % by weight	di-PE % by weight	tri-PE % by weight
1	Pentaerythritol raw material	99.83	0.17	-
2	Sediment at the end of run 14	99.77	0.23	-
3	Sediment at the end of run 13	99.98	0.02	-
4	Sediment collected from residue in centrifuge tubes	98.45	0.92	0.63

Melting point measurements were also carried out, and the results obtained are given in Table 9.5

TABLE 9.5

Results of melting point measurements for the sediment obtained

Sample Number	Sample source	Melting point °C
1	Sediment at end of run 14	259.5
2	Sediment at end of run 13	260.0
3	Sediment collected from residue in centrifuge tubes	230.0

9.3 Results of the Effect of Production and Storage Variables

As was discussed in Chapter Six, many procedures were carried out on the dispersant products, during their production, and also during their storage, to study the effect of certain factors on the sediment

formation. The results obtained are given in this section for each factor separately.

9.3.1 Effect of storage temperature

Product samples were stored at different temperatures namely, ambient, 50°C, 90°C, 120°C, and 150°C. Periodical centrifuge tests were carried out and the sediment results were tabulated for each run separately. One of the samples investigated was that of a batch produced at Fawley, and its sediment formation results are presented below in Table 9.6 as a sample of other results.

A plot of sediment content vs. storage period was carried out and presented in Figure 9.3 for storage temperatures of 90°C and 120°C only, because there was no change in the sediment content at storage temperatures of ambient, 50°C and 150°C. Also a plot of the sediment level attained after a fixed storage period against the storage temperature was performed and is presented in Figure 9.4, the fixed stage period chosen was 62 days.

During the course of the investigation of the effect of storage temperature on sediment formation, some product samples from different runs were stored at certain temperatures in a 'first storage period', then shifted to other storage temperatures in a 'second storage period', and the results obtained are given in Table 9.7.

Also during the course of the investigation the viscosity of many product samples was measured after long storage periods at different temperatures. A summary of the results obtained are given in Table 9.8.

TABLE 9.6

Effect of storage temperature on sediment formation
for Fawley Batch

Storage at ambient (days)	Storage at 50°C (days)	Storage at 90°C (days)	Storage at 120°C (days)	Storage at 150°C (days)	Total sediment volume %
8	-	-	-	-	< .01
73	-	-	-	-	< .01
133	-	-	-	-	< .01
-	62	-	-	-	< .01
-	83	-	-	-	< .01
-	133	-	-	-	< .01
-	-	10	-	-	< .01
-	-	24	-	-	0.05
-	-	31	-	-	0.09
-	-	45	-	-	0.14
-	-	62	-	-	0.20
-	-	83	-	-	0.25
-	-	97	-	-	0.30
-	-	104	-	-	0.32
-	-	119	-	-	0.35
-	-	-	10	-	0.25
-	-	-	14	-	0.30
-	-	-	24	-	0.35
-	-	-	31	-	0.35
-	-	-	45	-	0.4
-	-	-	59	-	0.4
-	-	-	-	62	< 0.01
-	-	-	-	104	< 0.01

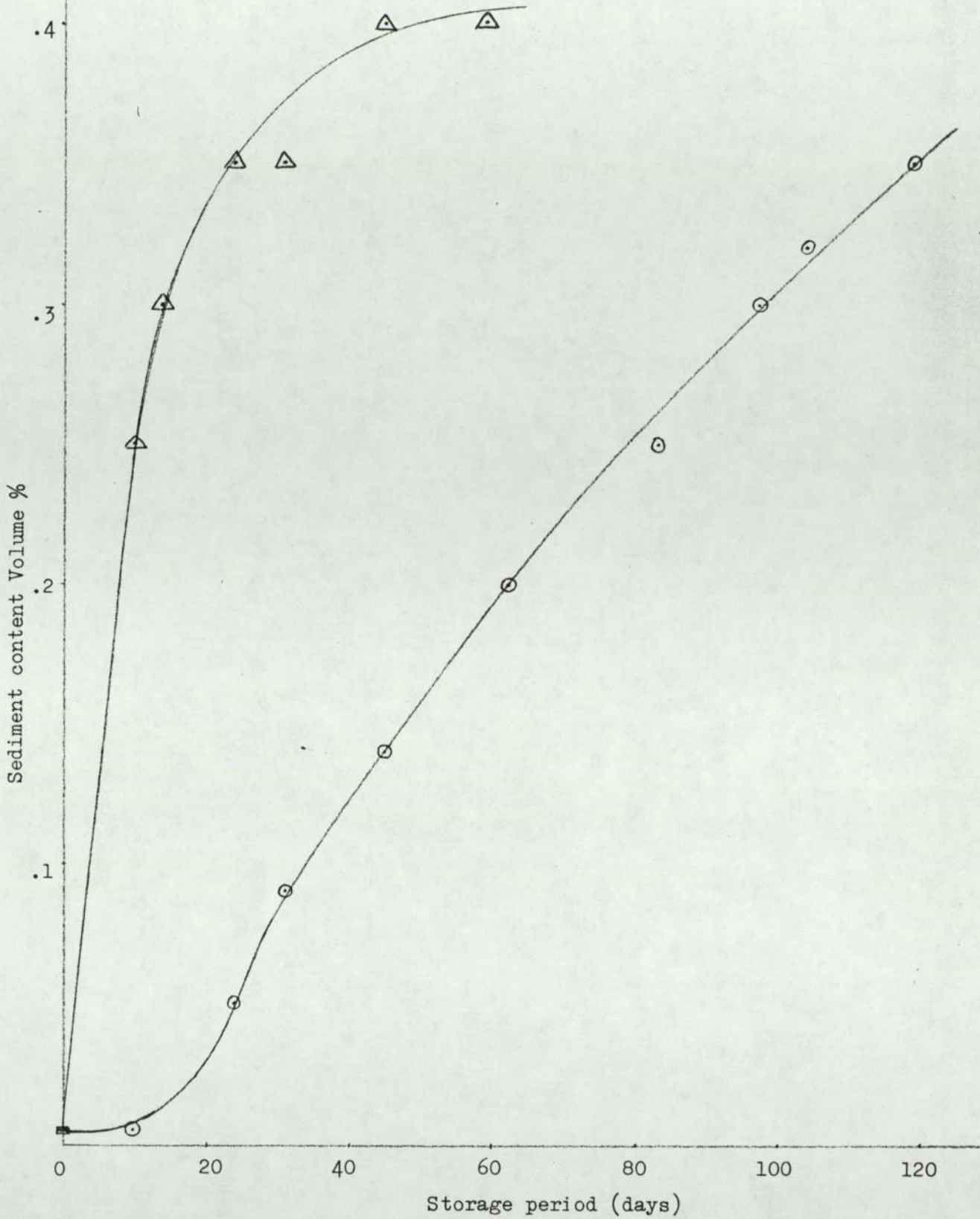


Figure 9.3

Graph for Fawley Batch of sediment content volume % vs. storage period (days). Points marked \circ are storage at 90°C , points marked \triangle are storage at 120°C

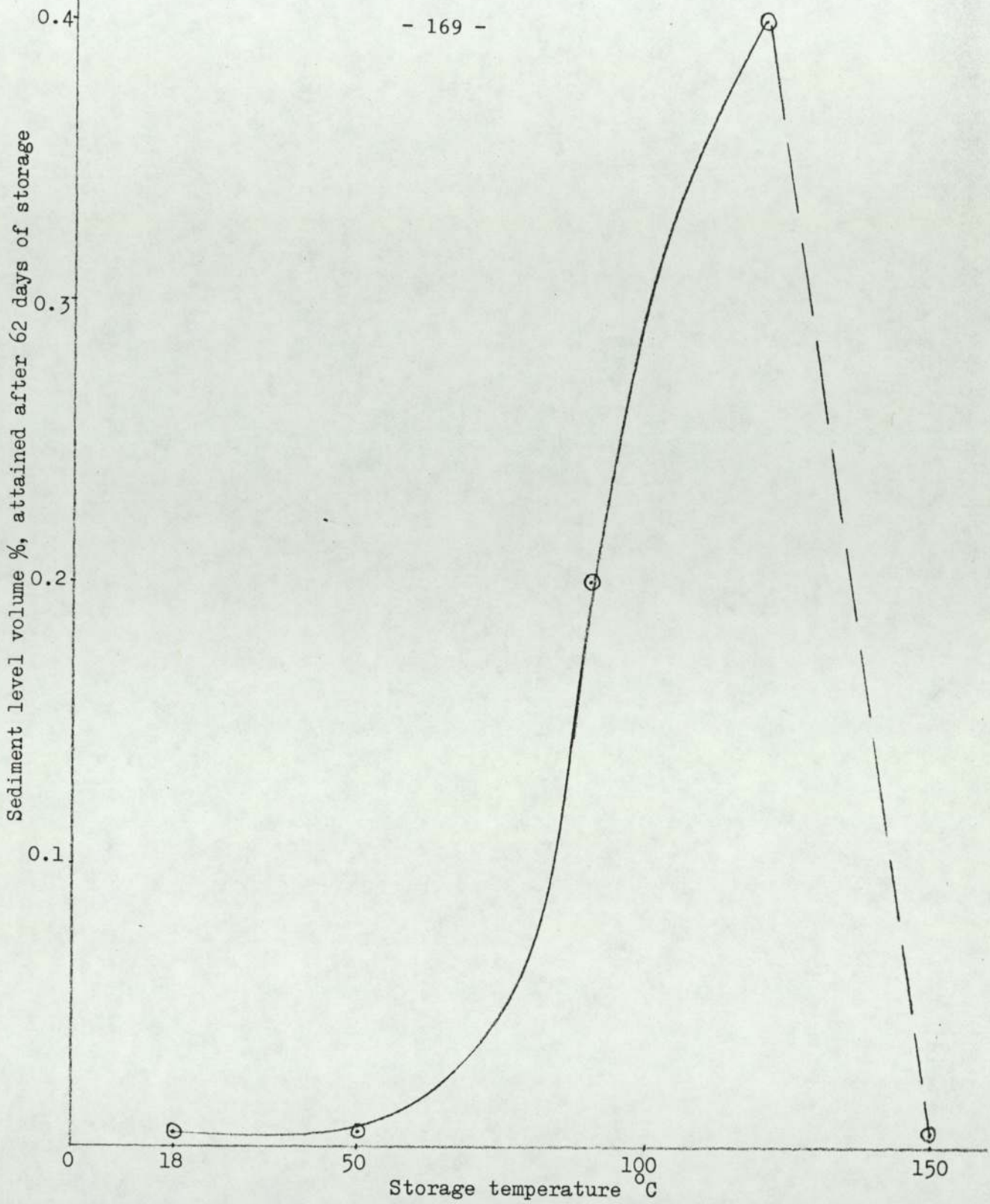


Figure 9.4

Graph for Fawley Batch of sediment level volume % attained after 62 days of storage vs. storage temperature °C

TABLE 9.7

Centrifuge test results for samples with two successive storage periods

Run number	First storage period			Second storage period		
	temp. °C	days	sediment volume %	temp. °C	days	sediment volume %
9	50	53	0.12	90	20	0.4
13	90	71	0.55	150	29	0.2
14	90	8	0.4	50	77	0.65
17	150	43	0.15	90	22 48	0.15 0.07
17	90	29	0.4	-	-	-
22	150	60	< .02	90	55	< .01
22	90	60	0.45	-	-	-
27	150	75	0.05	90	17	0.09
27	90	20	0.35	-	-	-
28	150	73	0.01	90	16	0.01
28	90	19	0.25	-	-	-

TABLE 9.8

Summary of results of viscosity changes during storage

Number of run	Storage period (days)			Viscosity $\times 10^{-6}$ (m ² /s) at 100°C
	at 50°C	at 90°C	at 150°C	
21	-	-	-	125.8
"	-	63	-	117.8
"	-	-	63	111.7
22	-	-	-	370
"	-	-	34	322.6
"	42	-	-	413
24	-	-	-	210.5
"	235	-	-	225.6
25	-	-	-	337.7
"	234	-	-	351.4
26	-	-	-	250.6
"	233	-	-	272.6
27	-	-	-	336.3
"	-	105	-	300.0
"	-	-	105	252.2
28	-	-	-	278.4
"	-	104	-	258.0
"	-	-	104	208.6
Fawley Batch	-	-	-	339.8
" "	-	-	70	324.7
" "	150	-	-	347.3

The effect of storage temperature on sediment formation in conjunction with other production variables (e.g. cooling rate, mixing rate, product dilution with heptane.... etc.) was also investigated, and the results will be presented in the following sections.

9.3.2 Effect of dilution of product samples with solvents

Product samples from runs 13, 21, 34, 35, 52, and 54 were diluted with dilution oil, n-Heptane, or chlorobenzene. Their viscosities were measured at ambient, and the samples were stored at different temperatures namely, ambient, 50°C, and 90°C. Periodical centrifuge tests were carried out and the results obtained are presented below in Table 9.9. Also for comparison reasons the centrifuge test results for the product samples from the above six runs, with no dilution solvent added, are presented in Table 9.10.

9.3.3 Effect of cooling rate

The cooling rates used in runs 34, 35, 55, 56, 57 and 58 were much higher than those used in other production runs (see Appendix 2). The centrifuge test results for runs 34 and 35 were given in Table 9.10, while those for runs 55, 56 and 57 are presented in Table 9.11.

9.3.4 Effect of mixing rate during the cooling stage

The speed of the electrical stirrer was reduced from 700 r.p.m. to 100 r.p.m. during the cooling stage of three production runs only 58, 59 and 60 (see Appendix 2), their centrifuge test results are given in Table 9.12.

9.3.5 Effect of mixing during storage

A sample of the Fawley Batch, after it was kept at ambient for about eight and a half months (253 days), was then stored at 50°C with continuous stirring. The sediment test results obtained are given in Table 9.13.

TABLE 9.9

Summary of centrifuge test results for product samples diluted with dilution oil, heptane, or chlorobenzene

Run number	Dilution solvent	Viscosity at ambient $\times 10^{-6}$ (m^2/s)	Storage period (days)			Total sediment volume %
			at ambient	at 50°C	at 90°C	
13	dilution oil 20% by weight	4239.6	15	-	-	0.055
			22	-	-	0.055
			37	-	-	0.05
			51	-	-	0.05
13	n-Heptane 20% by weight	395.0	15	-	-	0.03
			22	-	-	0.05
			37	-	-	0.04
21	n-Heptane 33% by volume	164.3	17	-	-	< .01
			37	-	-	< .01
			63	-	-	< .01
			118	-	-	< .01
			161	-	-	< .01
			275	-	-	< .01
			275	126	-	0.3 *
34	n-Heptane 20% by weight	-	102	-	-	< .01
35	n-Heptane 10% by weight	-	149	-	-	0.04
			-	149	-	0.07
			-	303	-	0.06
52	chloro- benzene 50% by weight	134.0	-	-	23	0.275
			38	-	-	< .02
			-	38	-	0.05
			-	-	38	0.4
			63	-	-	0.03
			-	63	-	0.06
54	chloro- benzene 50% by weight	130.0	-	-	14	0.175
			29	-	-	< .01
			-	29	-	0.05
			-	-	29	0.25
			54	-	-	< .01
			-	54	-	0.05
			-	-	54	0.35
			74	-	-	< .01
			-	74	-	0.06
			-	-	74	0.4

*The diluted product sample of run 21 after being stored for 275 days at ambient temperature, it was then transferred into storage at 50°C for another 126 days, and the final sediment test result was 0.3 volume %.

TABLE 9.10

Summary of centrifuge test results for undiluted product samples of runs 13, 21, 34, 35, 52 and 54

Run number	Storage period (days)					Total sediment volume %
	at ambient	at 50°C	at 90°C	at 120°C	at 150°C	
13	-	-	-	-	-	0.06
	15	-	-	-	-	0.06
	-	15	-	-	-	0.12
	-	-	15	-	-	0.5
	22	-	-	-	-	0.06
	-	22	-	-	-	0.16
	-	-	22	-	-	0.6
	37	-	-	-	-	0.065
	-	37	-	-	-	0.2
	51	-	-	-	-	0.06
-	-	51	-	-	0.55	
-	-	71	-	-	0.55	
21	-	-	-	-	-	<.01
	-	17	-	-	-	<.01
	-	-	17	-	-	0.2
	-	-	-	-	17	<.01
	37	-	-	-	-	<.01
	-	37	-	-	-	0.05
	-	-	37	-	-	0.3
	-	-	-	-	37	<.01
	63	-	-	-	-	<.01
	-	63	-	-	-	0.06
	-	-	63	-	-	0.3
	-	-	-	-	63	<.01
-	-	118	-	-	0.35	
-	-	139	-	-	0.38	
34	-	-	-	-	-	0.01
	-	-	-	17	-	0.04
	-	-	-	31	-	0.03
	-	-	-	46	-	0.03
35	-	-	-	-	-	0.04
	-	-	-	13	-	0.07
	-	-	-	27	-	0.08
	-	-	-	42	-	0.09

TABLE 9.10 (Continued)

Run number	Storage period (days)					Total sediment volume %
	at ambient	at 50°C	at 90°C	at 120°C	at 150°C	
52	-	-	-	-	-	<.02
	-	-	9	-	-	0.05
	-	-	23	-	-	0.15
	38	-	-	-	-	<.02
	-	38	-	-	-	<.02
	-	-	38	-	-	0.25
	63	-	-	-	-	<.02
	-	63	-	-	-	0.03
-	-	63	-	-	0.5	
54	-	-	-	-	-	<.01
	-	-	14	-	-	0.01
	29	-	-	-	-	<.01
	-	29	-	-	-	<.01
	-	-	29	-	-	0.08
	-	-	54	-	-	0.18
	74	-	-	-	-	<.01
	-	74	-	-	-	0.02
-	-	74	-	-	0.25	

TABLE 9.11

Centrifuge test results for product samples of runs 55, 56 and 57

Run number	Storage period (days)			Total sediment volume %
	at ambient	at 50°C	at 90°C	
55	-	-	-	< .01
	-	-	24	< .01
	49	-	-	< .01
	-	49	-	< .01
	-	-	49	< .01
	69	-	-	< .01
	-	69	-	< .01
56	-	-	69	< .01
	-	-	-	< .01
	-	-	23	< .01
	48	-	-	< .01
	-	48	-	< .01
	-	-	48	0.07
	68	-	-	< .01
57	-	68	-	< .01
	-	-	68	0.18
	-	-	-	< .01
	-	-	21	< .01
	46	-	-	< .01
	-	46	-	< .01
	-	-	46	0.04
57	66	-	-	< .01
	-	66	-	0.01
	-	-	66	0.15
	-	-	-	< .01

TABLE 9.12

Centrifuge test results for product samples of runs 58, 59 and 60

Run number	Storage period (days)			Total sediment volume %	Notes on sediment
	at ambient	at 50°C	at 90°C		
58	-	-	-	<.01	-
	-	-	14	0.01	hazy liquid
	39	-	-	<.01	-
	-	39	-	<.01	-
	-	-	39	0.1	-
	59	-	-	<.01	-
	-	59	-	0.01	-
59	-	-	59	0.2	-
	-	-	-	<.01	hazy liquid
	-	-	10	0.15	" "
	35	-	-	<.01	" "
	-	35	-	<.01	" "
	-	-	35	0.3	-
	55	-	-	<.01	hazy liquid
60	-	55	-	0.04	" "
	-	-	55	0.5	-
	-	-	-	<.01	hazy liquid
	-	-	8	0.01	" "
	33	-	-	<.01	" "
	-	33	-	<.01	" "
	-	-	33	0.16	-
53	-	-	<.01	hazy liquid	
-	53	-	0.02	" "	
-	-	53	0.25	-	

TABLE 9.13

Sediment test results for Fawley Batch, using mixing during storage.

Run number	Initial storage period at ambient (days)	Second storage period at 50°C with mixing (days)	Total sediment volume %
Fawley	-	-	<.01
Batch	253	-	<.01
	253	20	<.01
	253	60	0.01

9.3.6 Effect of PE/PIBSA equivalent ratio

Runs 27 and 28 were carried out using PE/PIBSA equivalent ratio of 1.9, which was higher than all the other runs (see Appendix 2). The sediment test results for both these runs are given below in Table 9.14.

9.3.7 Effect of reaction temperature

Runs 30, 31 and 32 were carried out at a much lower reaction temperature than other runs, which was about 140°C (see Appendix 2). The sediment test results for these runs are given in Table 9.15.

9.3.8 Effect of reaction time

Runs 6, 15, and 16 were carried out using relatively longer reaction times of 5.17 hr, 4.0 hr, and 5.0 hr respectively. Their centrifuge test results are given in Table 9.16.

9.3.9 Effect of reheating of final product

Portions of the products of runs 33, 34 and 35 were reheated and refiltered again (see Chapter Six, Section 6.3.5). The second

TABLE 9.14

Centrifuge test results for product samples of runs 27 and 28

Run number	Storage period (days)				Sediment volume %			Notes on sediment
	at ambient	at 50°C	at 90°C	at 150°C	actual sediment	haze	total	
27	-	-	-	-	0.02	0.04	0.06	hazy liquid
	-	20	-	-	0.04	0.06	0.1	" "
	-	-	20	-	0.35	-	0.35	-
	-	-	-	20	0.02	0.01	0.03	hazy liquid
	75	-	-	-	0.02	0.04	0.06	" "
	-	75	-	-	0.05	0.1	0.15	" "
	-	-	75	-	0.7	-	0.7	-
	-	-	-	75	0.01	0.04	0.05	-
	-	92	-	-	0.06	0.14	0.2	-
-	-	92	-	1.0	-	1.0	-	
28	-	-	-	-	<.01	-	<.01	clear liquid
	-	19	-	-	<.01	-	<.01	" "
	-	-	19	-	0.25	-	0.25	" "
	-	-	-	19	<.01	-	<.01	" "
	73	-	-	-	<.01	-	<.01	" "
	-	73	-	-	0.3	-	0.3	loose packing
	-	-	73	-	0.6	-	0.6	-
	-	-	-	73	0.01	-	0.01	-
	-	89	-	-	0.3	-	0.3	loose packing
-	-	89	-	0.7	-	0.7	-	

TABLE 9.15

Centrifuge test results for product samples of runs 30, 31 and 32

Run number	Storage period (days)			Sediment volume %			Notes on sediment
	at 50°C	at 90°C	at 120°C	actual	haze	total	
30	-	-	-	0.01	0.03	0.04	-
	10	-	-	0.01	0.03	0.04	-
	-	10	-	0.01	0.03	0.04	-
	-	-	10	0.01	0.05	0.06	-
	-	20	-	0.01	0.03	0.04	-
	-	-	20	0.01	0.03	0.04	hazy liquid
	-	27	-	0.01	0.01	0.02	-
	-	-	27	0.01	0.03	0.04	hazy liquid
	-	41	-	0.01	0.03	0.04	-
	-	-	41	0.01	0.04	0.05	hazy liquid
	55	-	-	0.01	0.03	0.04	-
	-	55	-	0.01	0.04	0.05	-
-	-	55	0.01	0.04	0.05	hazy liquid	
126	-	-	0.01	0.03	0.04	-	
31	-	-	-	< .01	-	<.01	clear liquid
	9	-	-	< .01	-	<.01	" "
	-	9	-	< .01	-	<.01	" "
	-	-	9	< .01	-	<.01	" "
	-	19	-	< .01	-	<.01	" "
	-	-	19	< .01	-	<.01	" "
	-	26	-	< .01	-	<.01	" "
	-	-	26	< .01	-	<.01	" "
	-	40	-	< .01	-	<.01	" "
	-	-	40	< .01	-	<.01	" "
	54	-	-	< .01	-	<.01	" "
	-	54	-	< .01	-	<.01	" "
-	-	54	< .01	-	<.01	" "	
125	-	-	< .01	-	<.01	" "	
32	-	-	-	0.01	0.01	0.02	-
	7	-	-	0.01	0.01	0.02	-
	-	7	-	0.01	0.03	0.04	-
	-	-	7	0.01	0.04	0.05	-
	-	17	-	0.01	0.01	0.02	-
	-	-	17	0.01	0.03	0.04	-
	-	24	-	0.01	0.03	0.04	-
	-	-	24	0.01	0.03	0.04	-
	-	38	-	0.01	0.02	0.03	-
	-	-	38	0.01	0.03	0.04	-
	52	-	-	0.01	0.01	0.02	-
	-	52	-	0.01	0.02	0.03	-
-	-	52	0.01	0.04	0.05	-	
123	-	-	0.01	0.01	0.02	-	
-	123	-	0.01	0.05	0.06	-	

TABLE 9.16

Centrifuge test results for product samples of runs 6, 15 and 16

Run Number	Storage period (days)			Sediment volume %		
	at ambient	at 50°C	at 90°C	sediment	haze	total
6	-	-	-	0.06	-	0.06
	-	12	-	0.06	0.02	0.08
	-	-	12	0.06	0.09	0.15
	-	18	-	0.06	-	0.06
	-	-	18	0.06	-	0.06
	-	26	-	0.06	0.02	0.08
	-	-	26	0.06	-	0.06
	-	42	-	0.06	-	0.06
	-	-	42	0.06	-	0.06
15	-	-	-	0.04	0.02	0.06
	-	-	7	0.04	-	0.04
	-	-	14	0.05	0.01	0.06
	43	-	-	0.04	-	0.04
	-	43	-	0.04	0.01	0.05
	-	-	43	0.09	-	0.09
	-	-	65	0.15	-	0.15
	85	-	-	0.04	-	0.04
-	85	-	0.05	-	0.05	
	-	-	85	0.4	-	0.4
16	-	-	-	0.02	0.04	0.06
	-	-	6	0.01	-	0.01
	-	-	34	0.01	0.08	0.09
	-	-	57	0.03	0.07	0.10
	-	-	77	0.01	0.02	0.03
	-	-	103	0.01	0.03	0.04
	-	-	157	0.01	0.01	0.02

filtration was just to prevent the contamination of the product dispersant with solid particles from the walls of the reaction flask, and it was very fast indeed. The product analysis after the reheating and refiltration stage, together with the conditions used are presented in Table 9.17.

TABLE 9.17

Conditions and product analysis of the reheating stage of runs 33, 34 and 35

Run number	Reheating stage		Product analysis after the reheating and refiltration stage				
	temperature °C	time hr	TAN mg KOH g sample	Viscosity $\times 10^{-6}$ (m ² /s) at 100°C	Sediment volume %		
					Sediment	haze	total
33	200	2	3.0	198*	0.01	0.02	0.03
34	202	4.1	3.3	171.3*	0.01	-	0.01
35	192	4.25	3.6	162	0.01	-	0.01

* The viscosities given for runs 33 and 34 were those of the filtrates with 75% of the dilution oil only.

The centrifuge test results for the reheated product samples of runs 33, 34 and 35 are presented together with the results of run 33 product (with no reheating) in Table 9.18. The centrifuge results for runs 34 and 35 products were given in Table 9.10 before.

9.3.10 Effect of refiltration after long storage periods

Samples of run 14 product and a mixture of runs 17, 18 and 19 products were refiltered at a temperature of about 90°C after storage at 90°C initially, then stored again at 90°C after refiltration (see Chapter Six, Section 6.3.6). The centrifuge test results obtained are presented in Table 9.19.

TABLE 9.18

Centrifuge test results for the reheated products of runs 33, 34 and 35

Run Number	Storage period (days)		Sediment volume %		
	at 90°C	at 120°C	sediment	haze	total
33	-	-	0.01	0.02	0.03
not reheated product	-	19	0.3	-	0.3
	-	33	0.3	-	0.3
	-	48	0.3	-	0.3
	-	-	0.01	0.02	0.03
	19	-	0.01	0.02	0.03
33 reheated product	-	19	0.01	0.02	0.03
	33	-	0.01	0.02	0.03
	-	33	0.01	-	0.01
	48	-	0.01	-	0.01
	-	48	0.015	-	0.015
	104	-	0.01	0.02	0.03
	-	104	< .01	-	< .01
	-	-	0.01	-	0.01
	17	-	< .01	-	< .01
	-	17	< .01	-	< .01
34 reheated product	31	-	< .01	-	< .01
	-	31	< .01	-	< .01
	46	-	< .01	-	< .01
	-	46	< .01	-	< .01
	102	-	< .01	-	< .01
	-	102	< .01	-	< .01
	-	-	0.01	-	0.01
	13	-	< .01	-	< .01
	-	13	< .01	-	< .01
35 reheated product	27	-	< .01	-	< .01
	-	27	< .01	-	< .01
	42	-	< .01	-	< .01
	-	42	< .01	-	< .01
	98	-	< .01	-	< .01
	-	98	< .01	-	< .01

TABLE 9.19

Centrifuge test results for refiltered product samples of run 14 and a mixture of runs 17, 18 and 19 products

Run number	Storage before refiltration		Storage after refiltration	
	days at 90°C	sediment volume %	days at 90°C	sediment volume %
14	51	0.45	-	0.12
			13	0.12
			34	0.12
			62	0.18
			116	0.14
A mixture of runs 17, 18 and 19 products	25	0.4	-	0.06
			13	0.15
			34	0.15
			62	0.15
			116	0.13
			141	0.1

9.3.11 Effect of extended time at filtration temperature

In many production runs, after cooling the reaction mixture down to filtration temperature, it was left at that temperature for an extended period of time (see Appendix 2). The centrifuge test results for runs 9, 26, 29, 51 and 53 are presented in Table 9.20 below as sample results. In these runs the reaction mixture was left at filtration temperature for different periods of time ranging from 2.72 hrs for run 9 to 66 hrs for run 51 (see Table 9.20).

9.4 Results of IR Spectroscopy in Sediment Investigation

A wide range of stored product samples were tested using the ultra-centrifuge at first, then using Nuclear Magnetic Resonance technique afterwards. But because the results were not very conclusive, the same

TABLE 9.20

Centrifuge test results for product samples of runs 9, 26, 29, 51 and 53

Run number	Time at filtration temperature (hr)	Storage period (days)				Sediment volume %		
		ambient	50°C	90°C	120°C	Sediment	Haze	Total
9	2.72	-	-	-	-	0.01	-	0.01
		11	-	-	-	0.02	-	0.02
		-	11	-	-	0.02	-	0.02
		-	-	11	-	0.2	-	0.2
		23	-	-	-	0.02	-	0.02
		-	23	-	-	0.03	0.07	0.1
		-	-	23	-	0.3	-	0.3
		31	-	-	-	0.02	-	0.02
		-	31	-	-	0.04	0.08	0.12
		-	-	31	-	0.4	-	0.4
		-	38	-	-	0.04	0.08	0.12
		-	-	38	-	0.45	-	0.45
		46	-	-	-	0.02	-	0.02
		-	46	-	-	0.04	0.08	0.12
-	-	46	-	0.45	-	0.45		
-	53	-	-	0.04	0.08	0.12		
26	15.8	-	-	-	-	<.01	-	<.01
		-	21	-	-	<.01	-	<.01
		-	-	21	-	0.07	0.01	0.08
		76	-	-	-	<.01	-	<.01
		-	76	-	-	<.01	-	<.01
		-	-	76	-	0.4	-	0.4
		-	93	-	-	<.01	-	<.01
		-	-	93	-	0.6	-	0.6
-	-	110	-	0.6	-	0.6		
29	64.7	-	-	-	-	0.01	0.04	0.05
		-	-	5	-	0.02	0.07	0.09
		-	-	-	5	0.02	0.08	0.1
		-	15	-	-	0.01	0.04	0.05
		-	-	15	-	0.02	0.07	0.09
		-	-	-	15	0.03	-	0.03
		-	-	25	-	0.02	0.03	0.05
		-	-	-	25	0.02	0.08	0.1
		-	-	32	-	0.02	0.01	0.03
		-	-	-	32	0.02	0.02	0.04
		-	-	46	-	0.03	-	0.03
		-	-	-	46	0.03	-	0.03
		-	60	-	-	0.01	0.04	0.05
		-	-	60	-	0.03	-	0.03
-	-	-	60	0.01	0.04	0.05		
-	-	-	75	0.01	0.02	0.03		
-	121	-	-	0.01	0.04	0.05		

TABLE 9.20 (Continued)

Run number	Time at filtration temperature (hr)	Storage period (days)				Sediment volume %		
		ambient	50°C	90°C	120°C	Sediment	Haze	Total
51	66	-	-	-	-	<.01	-	<.01
		28	-	-	-	<.01	-	<.01
		-	28	-	-	<.01	-	<.01
		-	-	28	-	<.01	-	<.01
		-	-	43	-	<.02	-	<.02
		68	-	-	-	<.01	-	<.01
		-	68	-	-	<.01	-	<.01
		-	-	68	-	0.06	0.06	
53	41	-	-	-	-	<.01	-	<.01
		-	-	21	-	<.01	-	<.01
		36	-	-	-	<.01	-	<.01
		-	36	-	-	<.01	-	<.01
		-	-	36	-	0.03	-	0.03
		61	-	-	-	<.01	-	<.01
		-	61	-	-	<.01	-	<.01
		-	-	61	-	0.12	0.12	

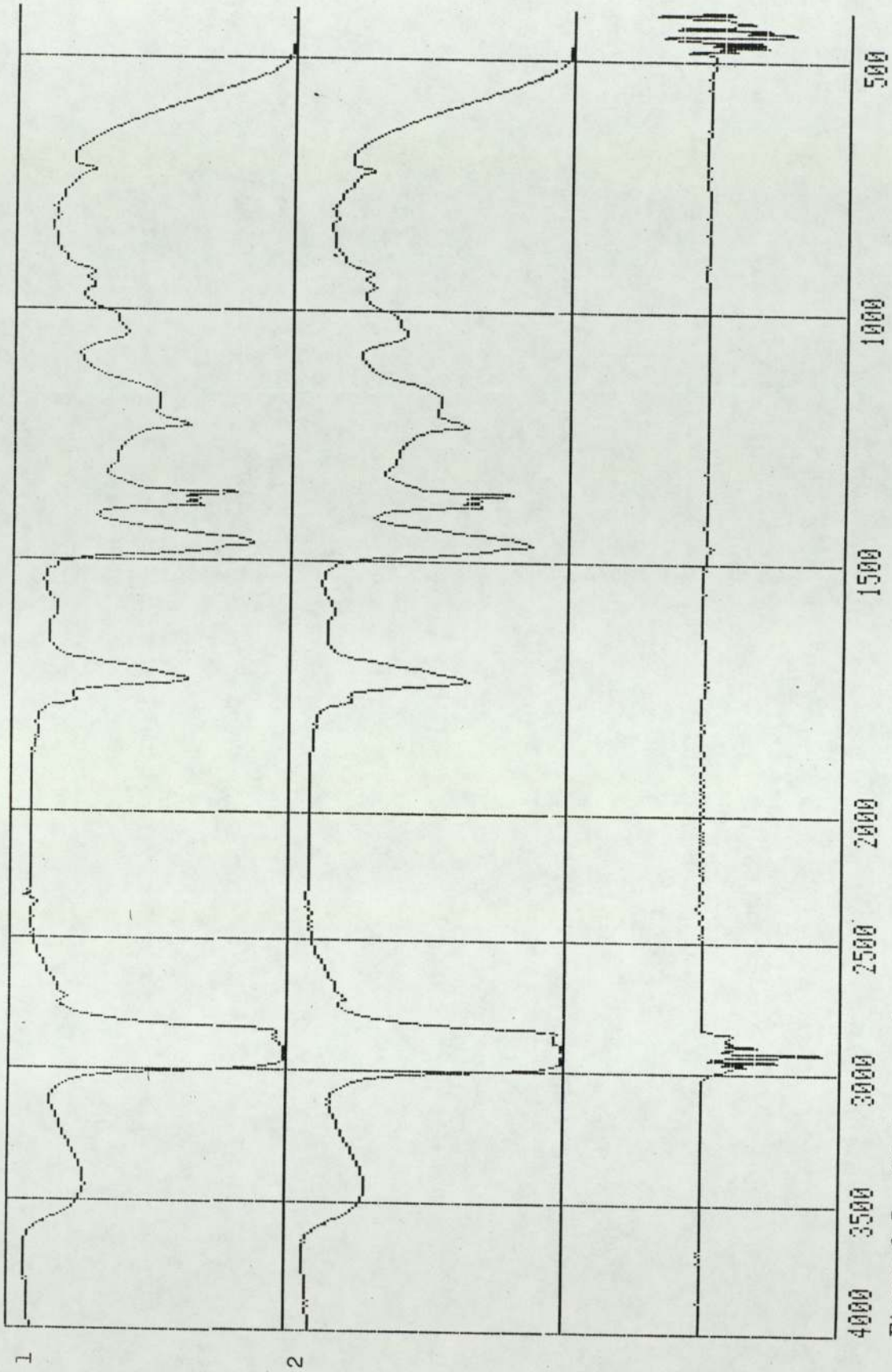


Figure 2.5: IR traces of samples No. 1 and No. 2 and their difference trace

No. 1 = Fawley Batch product stored at ambient for 168 days

No. 2 = " " " " 50°C

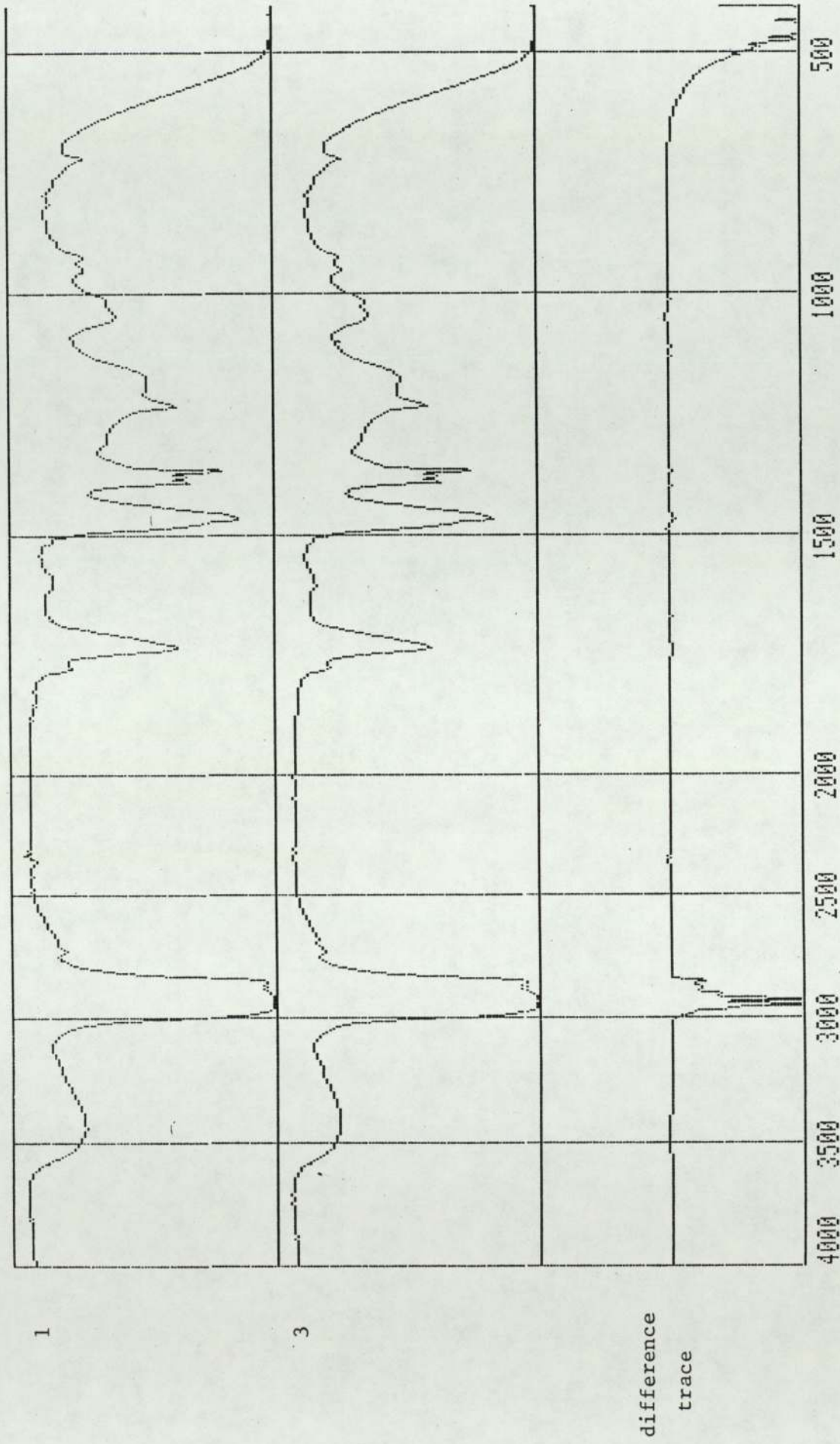


Figure 9.6: IR traces of samples No. 1 and No. 3 and their difference trace

No. 1 = Fawley Batch product stored at ambient for 168 days

No. 3 = " " " " 90°C " " "

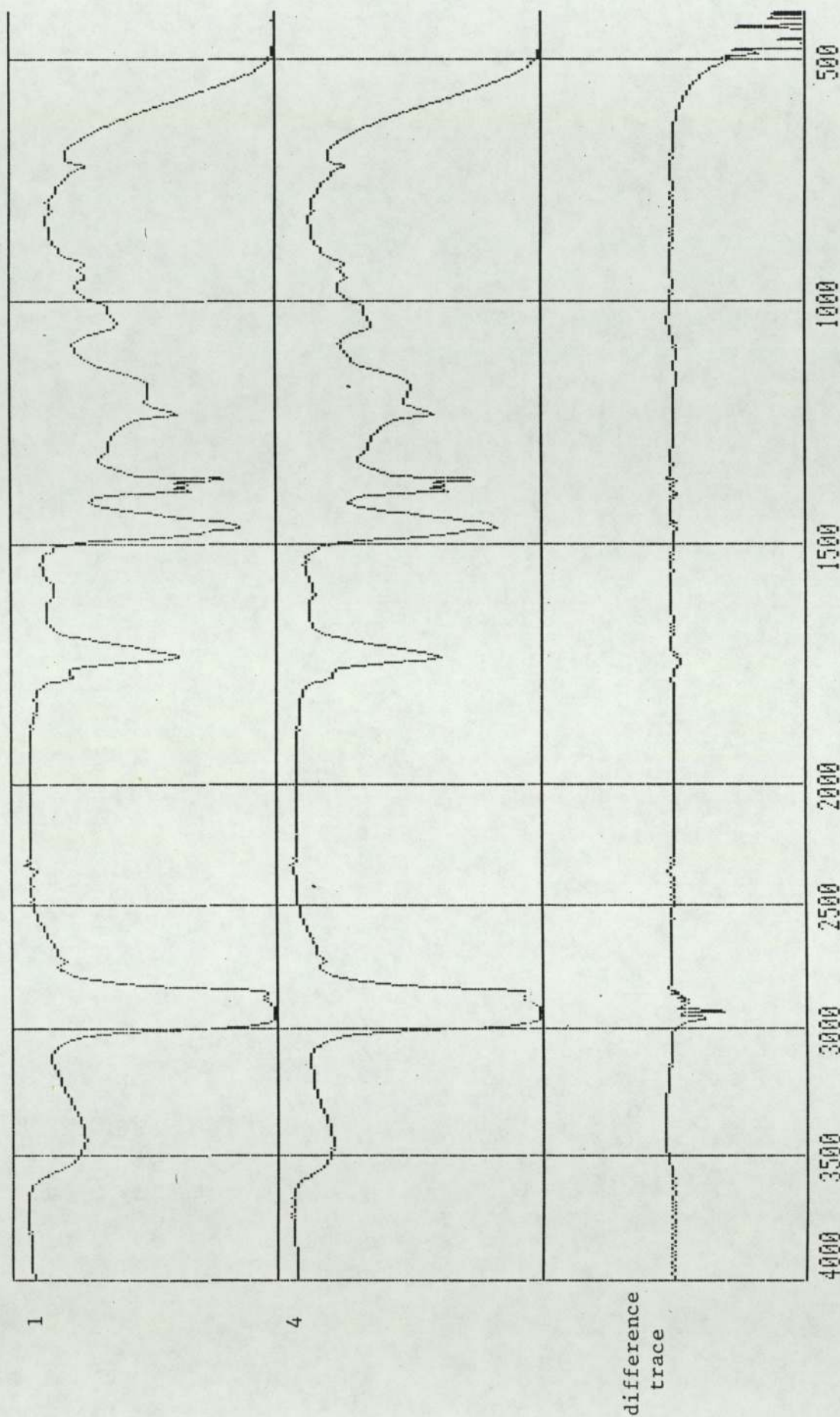


Figure 9.7: IR traces of samples No. 1 and No. 4 and their difference trace

No. 1 = Fawley Batch product stored at ambient for 168 days
No. 4 = " " " 120°C " 95 "

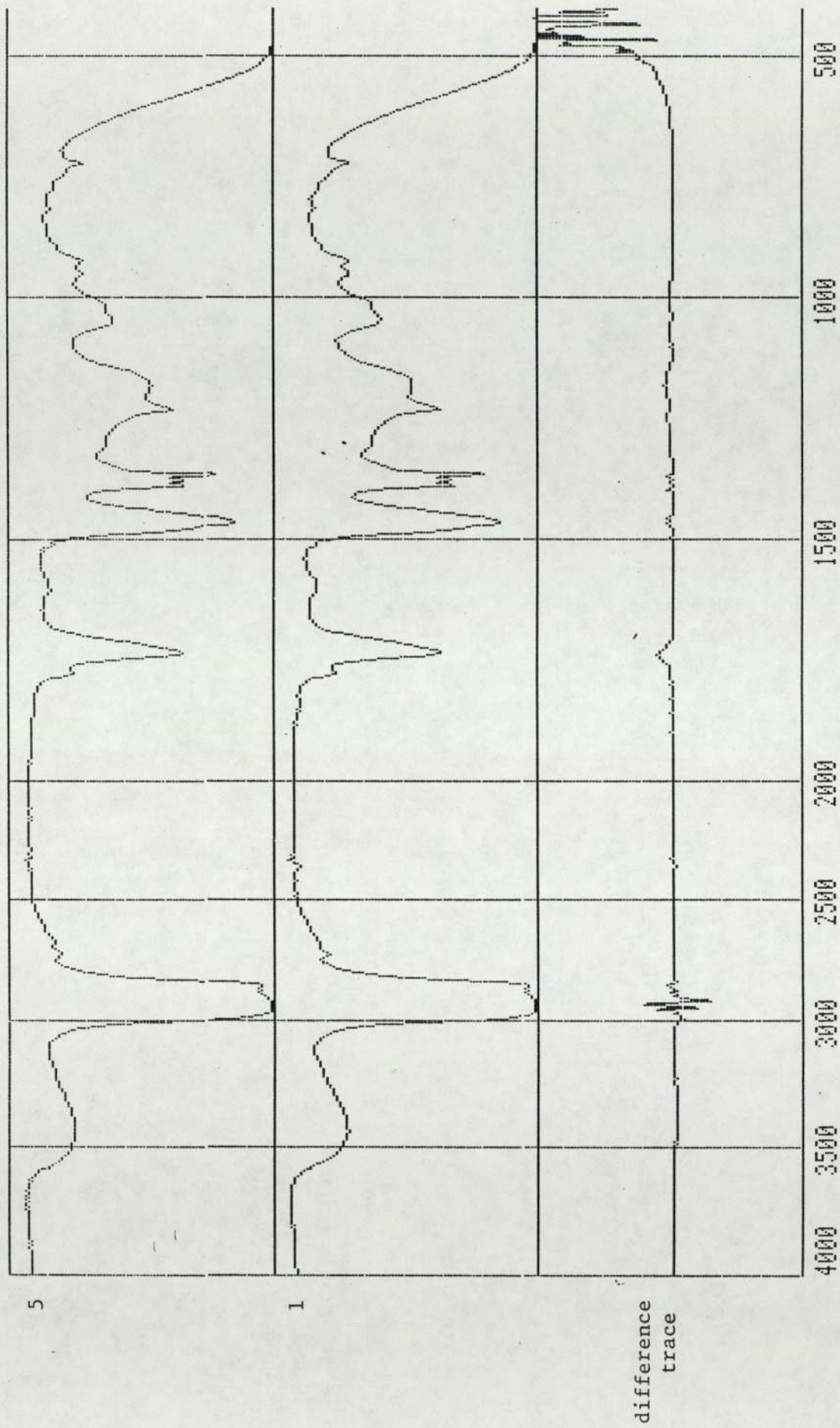


Figure 9.8: IR traces of samples No. 5 and No. 1 and their difference trace.

No. 5 = Run 33 product stored at ambient for 69 days

No. 1 = Fawley Batch product stored at ambient for 168 days

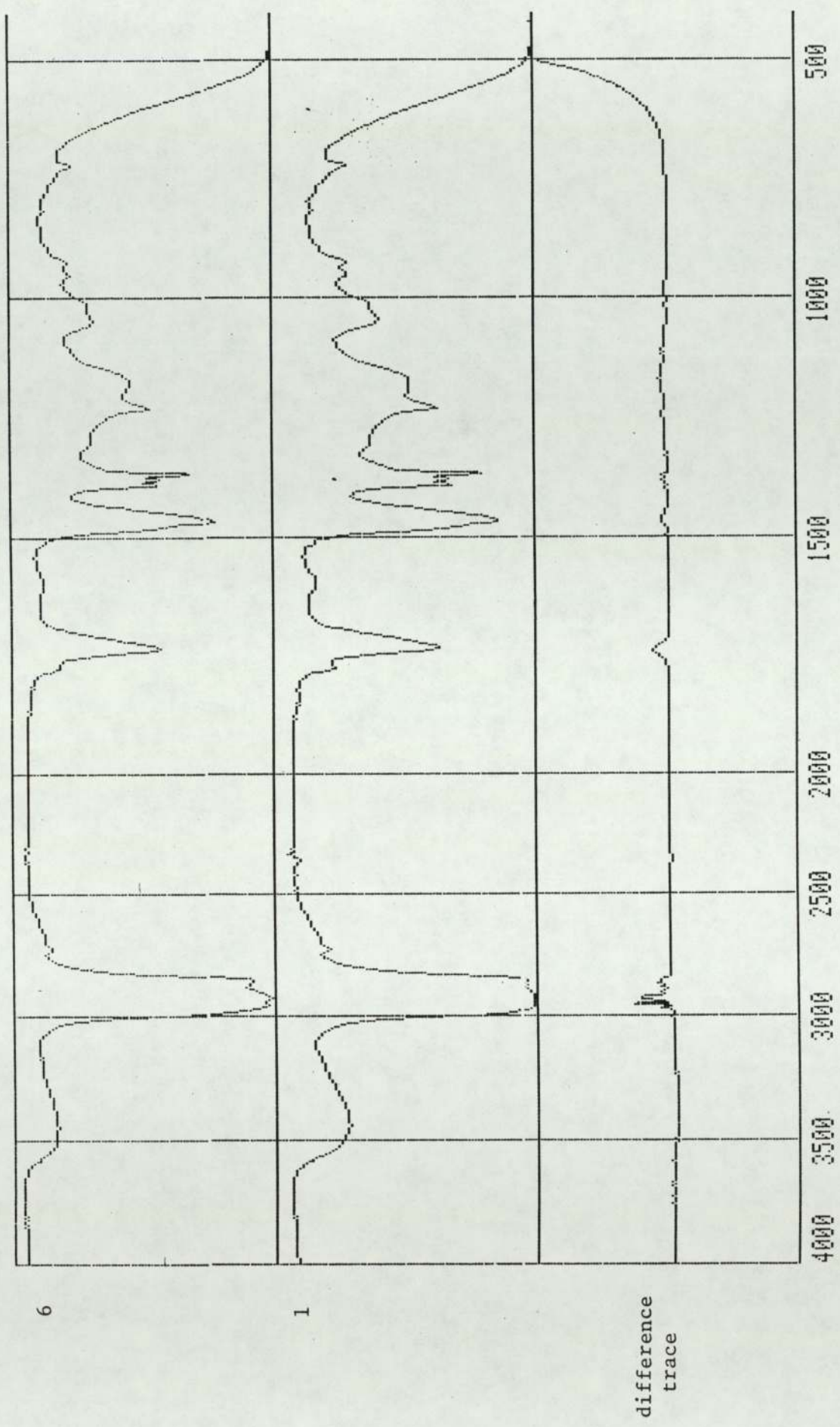


Figure 9.9: IR traces of samples No. 6 and No. 1 and their difference trace

No. 6 = Run 33 reheated and refiltered product stored at 90°C for 69 days

No. 1 = Fawley Batch product stored at ambient for 168 days

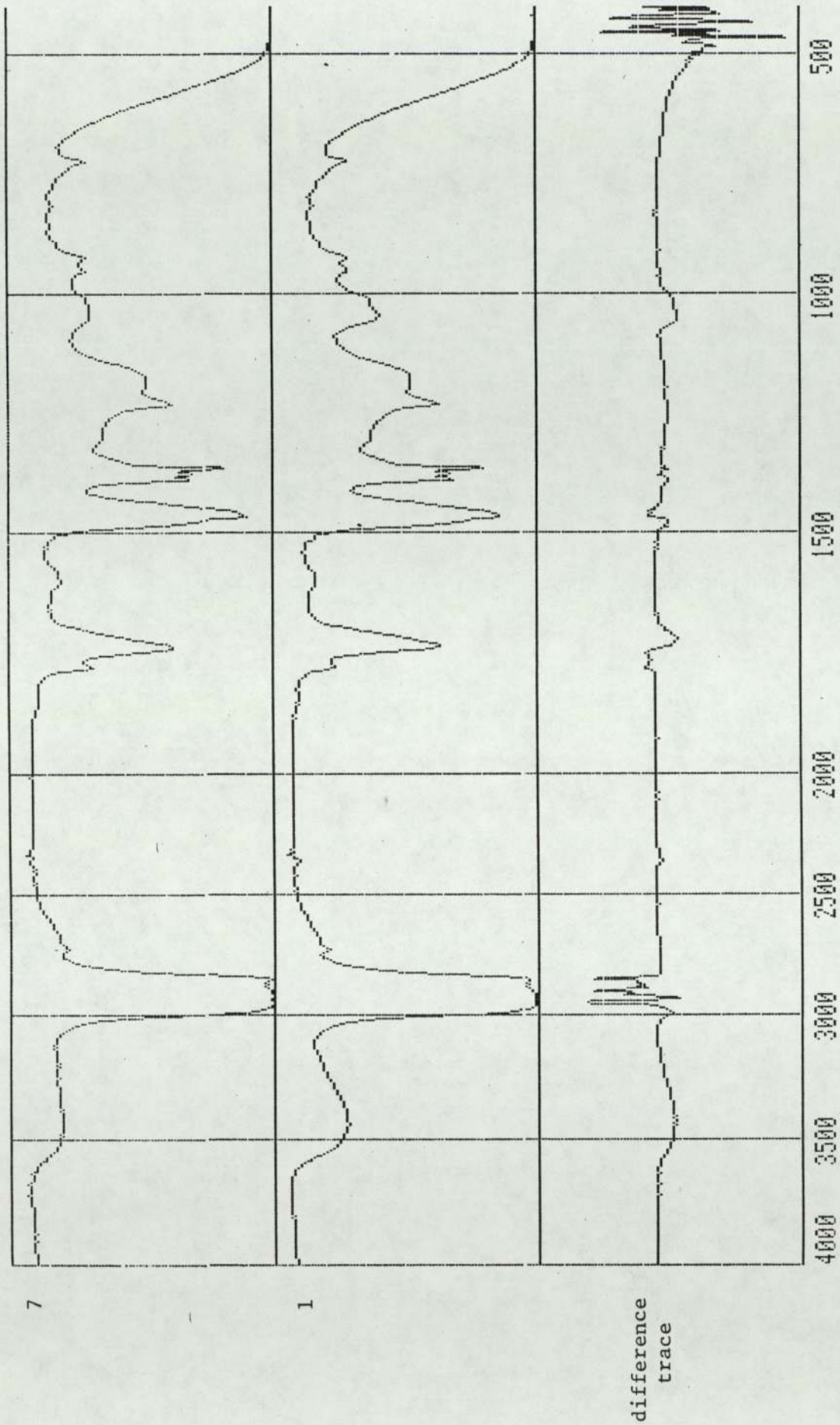


Figure 9.10: IR traces of samples No. 7 and No. 1 and their difference trace

No. 7 = Run 31 product stored at 50°C for 90 days

No. 1 = Fawley Batch product stored at ambient for 168 days

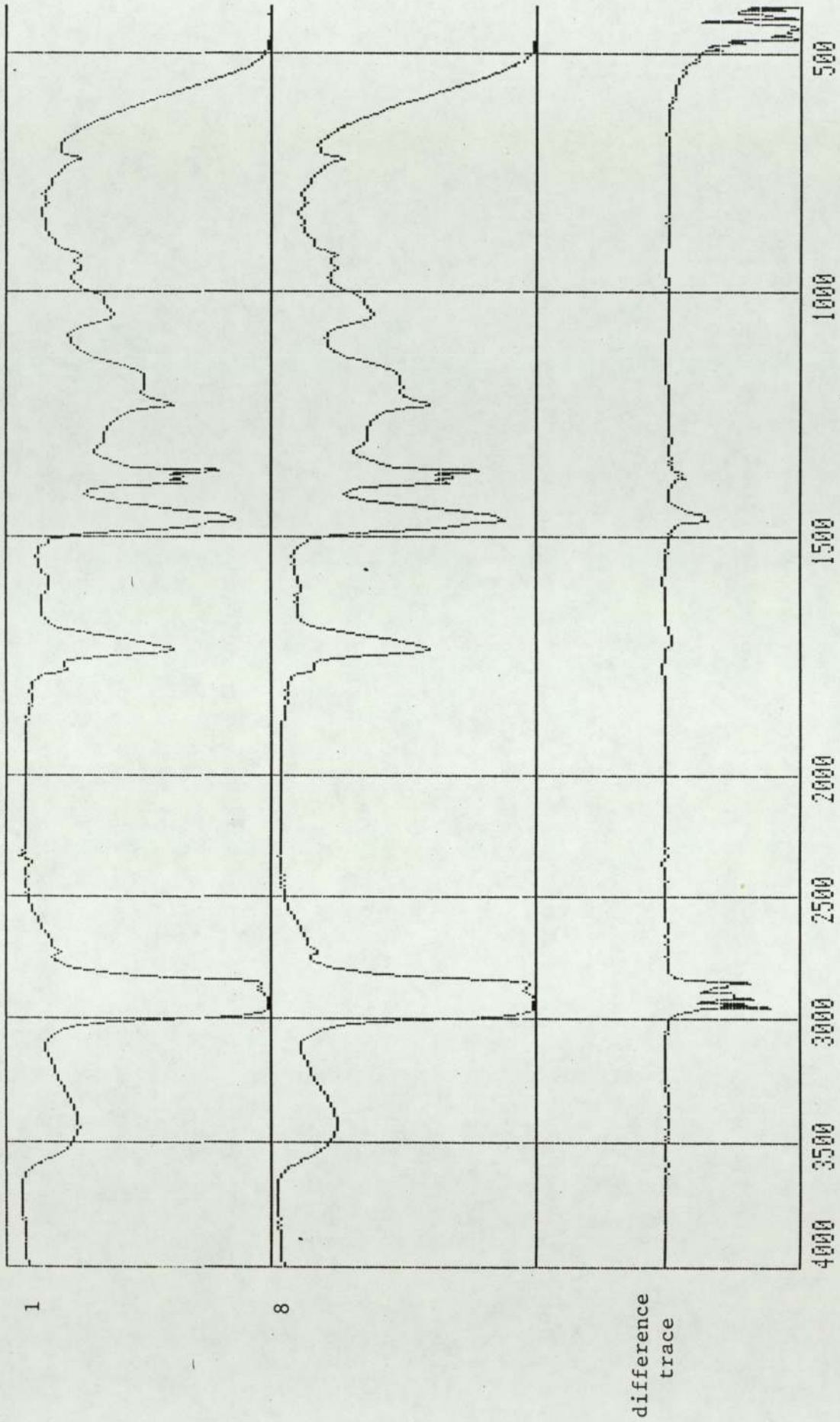


Figure 9.11: IR traces of samples No. 1 and No. 8 and their difference traces

No. 1 = Fawley Batch product stored at ambient for 168 days

No. 8 = Standard dispersant sample produced at Fawley Refinery

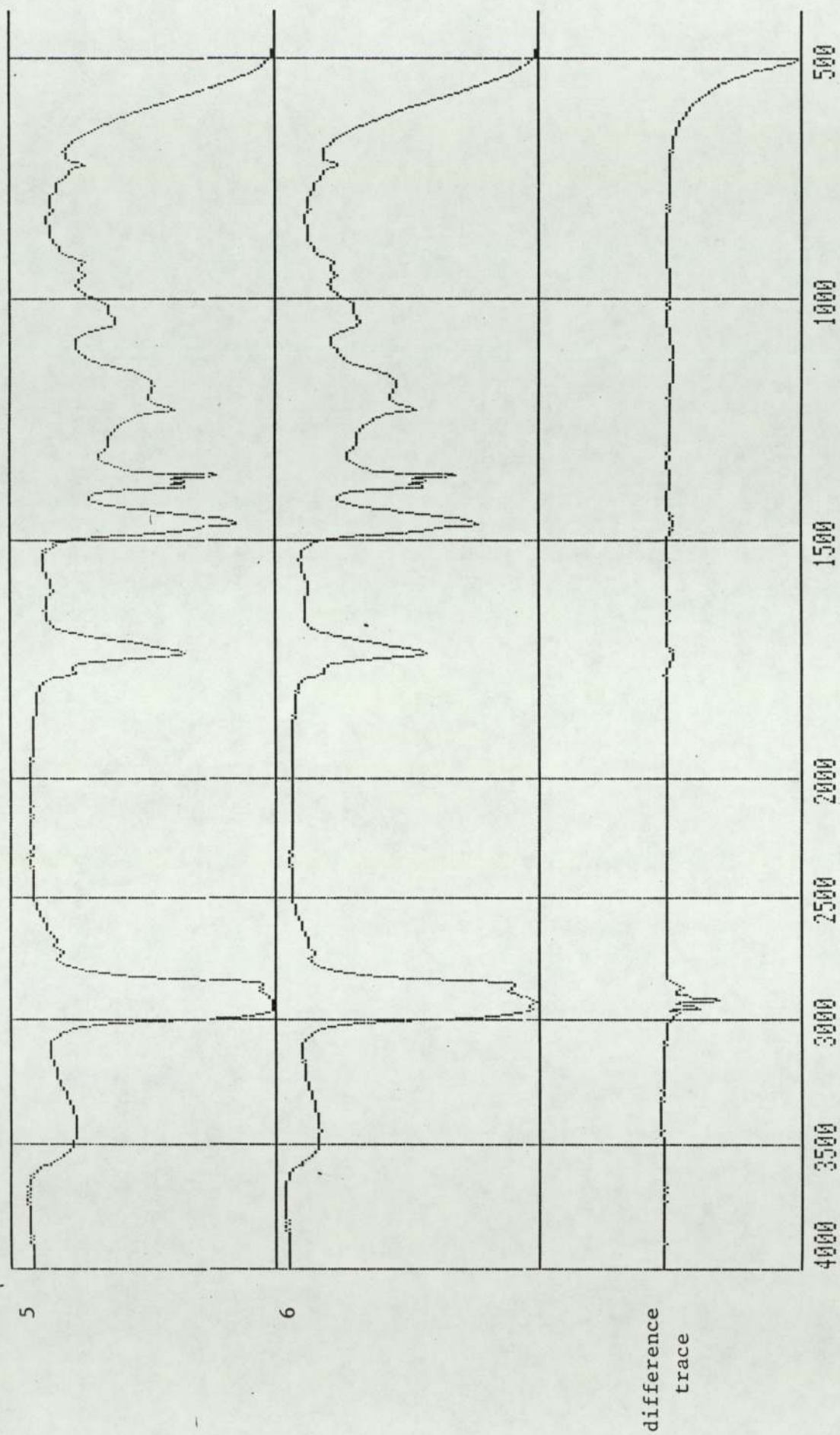


Figure 9.12: IR traces of samples No. 5 and No. 6 and their difference trace

No. 5 = Run 33 product stored at ambient for 69 days

No. 6 = Run 33 reheated and refiltered product stored at 90°C for 69 days

samples were analysed again using IR spectroscopy which was carried out at Esso Research Centre in Abingdon in association with Esso staff (see Chapter 6, Section 6.4.1).

These samples were as follows:

- Number 1 = Fawley Batch product stored at ambient for 168 days
- Number 2 = " " " " " 50°C for 168 days
- Number 3 = " " " " " 90°C for 168 days
- Number 4 = " " " " " 120°C for 95 days
- Number 5 = Run 33 product stored at ambient for 69 days
- Number 6 = Run 33 reheated and refiltered product stored at 90°C for 69 days
- Number 7 = Run 31 product stored at 50°C for 90 days
- Number 8 = A standard dispersant sample produced at Fawley

The IR traces of these samples and their difference traces obtained from their comparison with the IR trace of sample number 1 are all presented in Figure 9.5 to Figure 9.12 inclusive.

9.5 Results of Solubility Measurements of PE in the Dilution Oil

Four runs were carried out to measure the solubility of pentaerythritol in the dilution oil at different temperatures (see Chapter Six, Section 6.6). The results obtained are presented in Table 9.21 below.

TABLE 9.21

Approximate solubility of PE in the dilution oil

Temperature °C	Approximate solubility of PE in the dilution oil g/100g
160	0.114
140	0.067
100	0.014
25	0.000

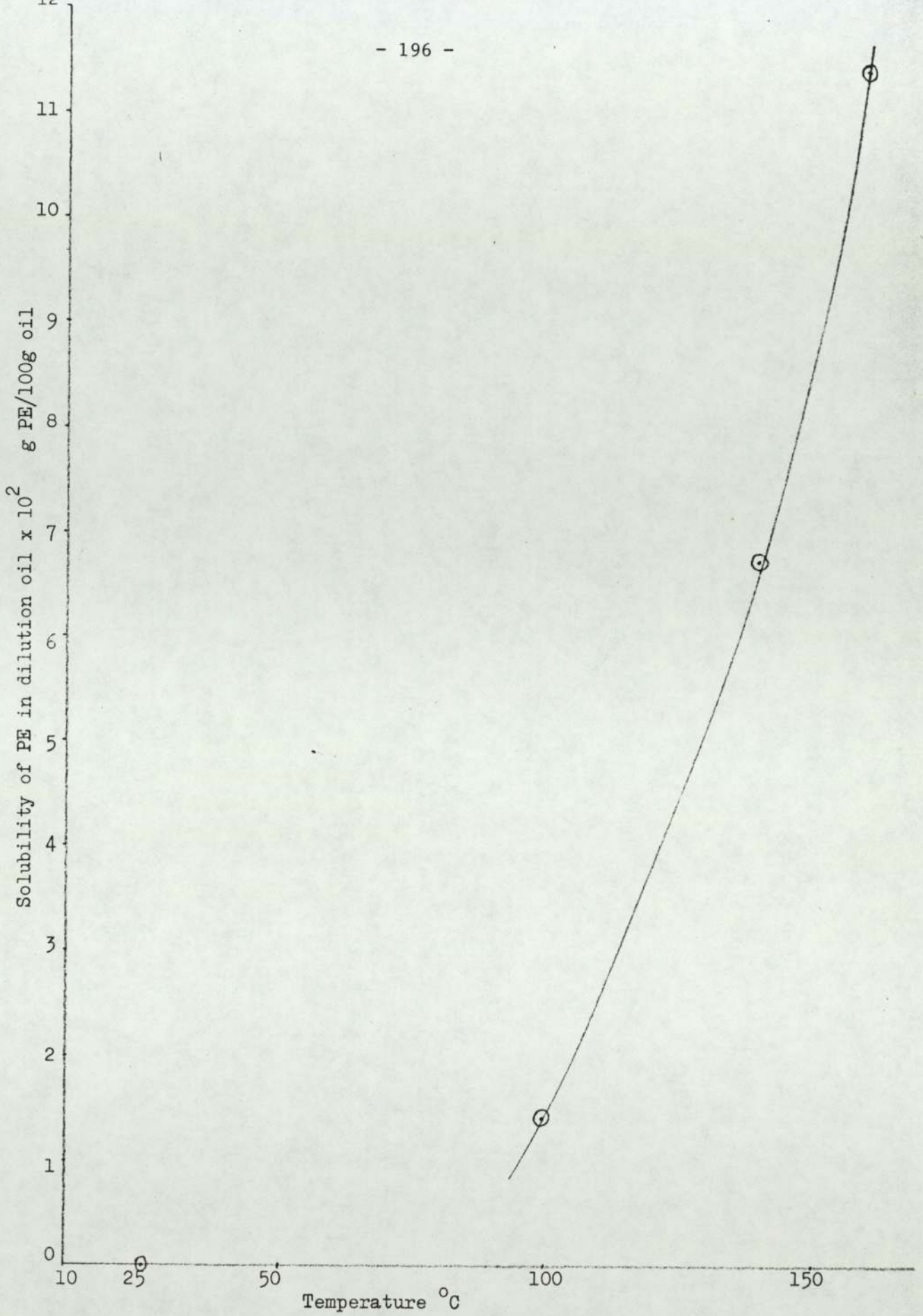


Figure 9.13

Graph of solubility of PE in dilution oil $\times 10^2$

as g PE/100g oil vs. temperature $^{\circ}\text{C}$

A plot of the solubility values given in Table 9.21 against the temperature is presented in Figure 9.13. The calculations of the solubility values obtained at 160°C and 140°C will be presented here as a sample calculation.

Run No. 1 at 160°C

Weight of empty beaker	= 17.7712g
Weight of beaker + PE	= 38.8136g
Weight of empty beaker after PE addition	= 17.7744g
∴ Weight of PE added to the oil	= 16.0392g

For filtration:

Weight of empty beaker	= 236.55g
Weight of beaker + filtrate	= 752.24g
∴ Weight of filtrate	= 515.69g

Also

Weight of filter paper No. 1 + PE crystals	= 3.2419g
Weight of filter paper No. 1 alone	= 2.0500g
∴ Weight of PE crystals from filter paper No. 1	= 1.1919g

and

Weight of filter paper No. 2 + PE crystals	= 16.2310g
Weight of filter paper No. 2 alone	= 1.9686g
∴ Weight of PE crystals from filter paper No. 2	= 14.2624g
∴ Total weight of undissolved PE crystals	= 15.4543g

assuming that the losses of PE crystals are negligible

$$\therefore \text{Weight of PE crystals in filtrate} = 16.0392 - 15.4543 = 0.5849\text{g.}$$

∴ Solubility of PE crystals in the dilution oil calculated

$$\text{at } 160^{\circ}\text{C as } \underline{\text{gPE/100g oil}} = \frac{0.5849}{515.69 - 0.5849} \times 100 = \underline{0.114}$$

Run No. 2 at 140°C

Weight of empty beaker	= 17.7704g
Weight of beaker + PE	= 67.7769g
Weight of empty beaker after PE addition	= 17.7755g
∴ Weight of PE added to the oil	= 50.0014g

For filtration:

Weight of empty beaker	= 230.77g
Weight of beaker + filtrate	= 1024.39g
∴ Weight of filtrate	= 793.62g

Also

Weight of filter paper No. 1 + PE crystals	= 2.0142g
Weight of filter paper No. 1 alone	= 1.9222g
∴ Weight of PE crystals from filter paper No. 1	= 0.0920g

and

Weight of filter paper No. 2 + PE crystals	= 51.3305g
Weight of filter paper No. 2 alone	= 1.9506g
∴ Weight of PE crystals from filter paper No. 2	= 49.3799g
∴ Total weight of undissolved PE crystals	= 49.4719g

assuming that the losses of PE crystals are negligible

$$\therefore \text{Weight of PE crystals in filtrate} = 50.0014 - 49.4719 = 0.5295\text{g}$$

∴ Solubility of PE crystals in the dilution oil calculated at 140°C

$$\text{as } \underline{\text{g PE/100g oil}} = \frac{0.5295}{793.62 - 0.5295} \times 100 = \underline{0.067}$$

9.6 Results of Crystal Size Distribution (CSD) Measurements

The crystal size distribution (CSD) of PE crystals was measured successfully at the end of fourteen production runs which were runs 34 and 35 and runs 51 to 62 inclusive (see Chapter 7). A value for the ratio of the

equivalent particle size measured by sieve analysis (d_s) to that measured by laser analysis (d_p) had to be found experimentally, which was performed by analysing eight samples of the crystalline sediment of known sieve fractions using the Malvern laser particle size analyser (see Chapter 7, Section 7.6); the results of these analyses are presented below in Table 9.22.

The values of the ratio of (d_s/d_p) calculated from these laser analysis results of Table 9.22 are present below in Table 9.23.

The experimental average value of the ratio (d_s/d_p) of 1.33 given in Table 9.23 is in a very good agreement with the theoretical value of the ratio calculated in detail in Appendix 7 which was found to be equal to 1.34.

As a sample calculation the third value of the ratio (d_s/d_p) given in Table 9.23 will be calculated here. From the results given in Table 9.22 for the third sample of 251-295 μm sieve fraction, Table 9.24 was constructed.

All the other mean projected area diameters (d_p) obtained by laser analysis and tabulated in Table 9.23 were calculated in a similar manner. The average value of the ratio (d_s/d_p) obtained in Table 9.23 was used to combine the two distributions obtained from sieve analysis for the large crystal fraction and from laser analysis for the fine crystals fraction (see Chapter 7), to give the final crystal size distribution (CSD) of the sediment of a particular run, from which the final parameters of the distribution were calculated. The method of calculation will be demonstrated by presenting the calculations of the parameters of the final distribution for run 34 sediment below. Appendix 8 gives the detailed experimental measurements and results for the sieve and laser analysis for both fractions of large and fine crystals carried out in all the fourteen runs.

TABLE 9.22

Results of laser analysis for the eight samples of known sieve fraction

Size band (μm)		Weight in band % for different sieve fractions (μm)							
		1	2	3	4	5	6	7	8
upper	lower	251- 295	355- 422	251- 295	105- 125	251- 295	105- 125	251- 295	75- 90
564.0	261.6	34.9	39.8	29.3	4.2	28.5	0.5	22.7	0.0
261.6	160.4	37.1	28.6	34.6	6.5	34.8	4.9	27.0	0.0
160.4	112.8	9.2	9.2	11.5	19.8	14.2	17.9	14.7	3.5
112.8	84.3	7.4	3.8	7.3	21.5	6.7	20.9	7.3	17.4
84.3	64.6	3.6	3.5	3.8	13.8	3.5	13.1	5.4	19.5
64.6	50.2	2.1	2.3	3.8	8.3	2.3	9.2	4.3	15.2
50.2	39.0	1.2	2.5	1.3	4.3	2.0	6.1	4.0	9.4
39.0	30.3	0.8	1.4	1.7	4.1	1.9	3.5	2.2	8.5
30.3	23.7	0.0	1.5	1.1	2.8	1.0	4.3	1.6	3.2
23.7	18.5	0.0	1.1	0.7	2.0	0.6	1.5	2.8	3.7
18.5	14.5	3.3	0.8	0.0	1.4	0.3	2.4	0.6	2.5
14.5	11.4	0.0	0.5	1.4	1.0	1.3	1.0	0.0	1.5
11.4	9.1	0.0	0.0	0.0	1.8	0.0	2.0	1.9	1.9
9.1	7.2	0.0	1.5	1.0	2.3	0.9	1.7	1.7	1.5
7.2	5.8	0.0	1.4	1.0	2.1	0.8	3.9	2.4	5.3
5.8	0.0	0.4	2.1	1.5	4.1	1.2	7.1	1.4	7.0

TABLE 9.23

Summary of the values obtained for the ratio of (d_s/d_p) for the eight samples of known sieve fractions

Sample number	Sieve fraction (μm)	Mean diameter (d_s) of sieve fraction (μm)	Mean diameter (d_p) calculated from lazer analysis (μm)	Ratio of (d_s/d_p)
1	251-295	273.5	246.8	1.10
2	355-422	388.5	247.6	1.57
3	251-295	273.5	223.9	1.22
4	105-125	115.0	100.0	1.15
5	251-295	273.5	222.4	1.23
6	105-125	115.0	79.3	1.45
7	251-295	273.5	188.7	1.40
8	75- 90	82.5	55.5	1.49
Average value of ratio of (d_s/d_p)				1.33

TABLE 9.24

Calculations of the ratio of (d_s/d_p) for sample No. 3 from laser analysis results

Upper	Size band (μm)		Weight fraction in band (f_i)	Mass weighted mean of band $\mu_i f_i$ (μm)
	Lower	Mean (μ_i)		
564.0	261.6	412.8	0.293	120.950
261.6	160.4	211.0	0.346	73.006
160.4	112.8	136.6	0.115	15.709
112.8	84.3	98.55	0.073	7.194
84.3	64.6	74.45	0.038	2.829
64.6	50.2	57.4	0.038	2.181
50.2	39.0	44.6	0.013	0.580
39.0	30.3	34.65	0.017	0.590
30.3	23.7	27.0	0.011	0.297
23.7	18.5	21.1	0.007	0.148
18.5	14.5	16.5	0.0	0.0
14.5	11.4	12.95	0.014	0.181
11.4	9.1	10.25	0.0	0.0
9.1	7.2	8.15	0.01	0.0815
7.2	5.8	6.5	0.01	0.065
5.8	0.0	2.9	0.015	0.0435
The weighted mean diameter (d_p) = $\sum_i (\mu_i f_i)$				223.9

Evaluation of the final CSD for run 34 sediment

From Table A8.1 in Appendix 8 the following were obtained for run 34 sediment,

Weight of large-crystals to be analysed by sieves	=	12.4600g
Weight of fine crystals to be analysed by laser	=	2.4643g
∴ Total weight of run 34 crystalline sediment	=	14.9243g

Sieve analysis

Table 9.25 below was constructed from calculations carried out on results presented in Table A8.2 in Appendix 8 for run 34.

TABLE 9.25

Sieve analysis results for run 34 large crystals fraction

Sieve details		Mass retained (g)	Cumulative mass retained (g)	Cumulative % oversize (% mass)
Mesh number	Aperture size (µm)			
10	1676	0.0000	0.0000	0.0000
12	1405	0.0823	0.0823	0.661
16	1003	0.7085	0.7908	6.348
18	853	0.8298	1.6206	13.009
22	699	1.3797	3.0003	24.085
25	599	1.4659	4.4662	35.852
30	500	1.4513	5.9175	47.503
36	422	1.6974	7.6149	61.129
44	355	1.4581	9.0730	72.833
52	295	0.8978	9.9709	80.041
60	251	0.8243	10.7952	86.658
72	210	0.5699	11.3651	91.233
85	180	0.5003	11.8654	95.249
100	150	0.2408	12.1062	97.182
120	125	0.1630	12.2692	98.491
150	105	0.1138	12.3830	99.404
170	90	0.0356	12.4186	99.690
200	75	0.0288	12.4474	99.921
240	63	0.0099	12.4572	100.000
300	53	0.0000	12.4572	100.000

and from Table 9.25,

Weight of large crystals after sieving = 12.4572g

∴ % Weight loss of crystals due to sieving = 0.022%

and % weight of crystals analysed by sieving = 83.49%

Laser analysis

The laser size bands were multiplied by the ratio (d_s/d_p) of 1.33 and hence were transformed into size bands compatible with sieve sizes. Also since the total weight of the fine crystals was found to be 2.4643g the weight % values given in Table A8.4 for run 34 were transformed into absolute weight (g) and tabulated in Table 9.26 below.

TABLE 9.26

Malvern laser analysis results for run 34 fine crystals

size band (μm)		size band x Ratio (d_s/d_p) (μm)		weight in band %	total weight in band (g)
upper	lower	upper	lower		
118.4	54.9	157.5	73.0	13.1	0.3228
54.9	33.7	73.0	44.8	10.6	0.2612
33.7	23.7	44.8	31.5	3.5	0.0863
23.7	17.7	31.5	23.5	3.5	0.0863
17.7	13.6	23.5	18.1	2.7	0.0665
13.6	10.5	18.1	14.0	3.9	0.0961
10.5	8.2	14.0	10.9	8.2	0.2021
8.2	6.4	10.9	8.5	16.9	0.4165
6.4	5.0	8.5	6.6	8.1	0.1996
5.0	3.9	6.6	5.2	1.4	0.0345
3.9	3.0	5.2	4.0	10.0	0.2464
3.0	2.4	4.0	3.2	4.4	0.1084
2.4	1.9	3.2	2.5	6.3	0.1553
1.9	1.5	2.5	2.0	3.7	0.0912
1.5	1.2	2.0	1.6	1.4	0.0345
1.2	0.0	1.6	0.0	2.6	0.0641

As can be seen from Table 9.25 and Table 9.26 there is an overlapping of the sieve and laser sizes between the ranges 157.5-73.0 μm and 73.0-44.8 μm . Hence to be able to add both size distributions it was decided to divide the size ranges in the overlapping area into the following ranges: 180-150 μm , 150-75 μm , and 75-44.8 μm . Also to be able to calculate the total weight of crystals in these new ranges it was assumed that the rate of change of crystal mass with size ($\Delta M/\Delta L$) in the laser size range of 157.5-73 μm was constant, hence from Table 9.26, ($\Delta M/\Delta L$) for the size range 157.5-73 μm = $\frac{0.3228}{157.5-73}$ = 0.00382 g/ μm and the weight of crystals in each of the new size bands was found as follows:

Size range 180-150 μm

$$\begin{aligned} \text{Weight of crystals from sieve analysis (from Table 9.25)} &= 0.2408\text{g} \\ \text{Weight of crystals from laser analysis} &= 7.5 \times 0.00382 = 0.0286\text{g} \\ \therefore \text{total crystal weight in range 180-150 } \mu\text{m} &= 0.2694\text{g} \end{aligned}$$

Size range 150-75 μm

$$\begin{aligned} \text{Weight of crystals from sieve analysis (from Table 9.25)} &= \\ 0.1630 + 0.1138 + 0.0356 + 0.0288 &= 0.3412\text{g} \\ \text{Weight of crystals from laser analysis} &= \\ 0.3228 - (7.5 \times 0.00382) - (2.0 \times 0.00382) &= 0.2865\text{g} \\ \therefore \text{total crystal weight in range 150-75 } \mu\text{m} &= 0.6277\text{g} \end{aligned}$$

Size range 75-44.8 μm

$$\begin{aligned} \text{Weight of crystals from sieve analysis (from Table 9.25)} &= 0.0099\text{g} \\ \text{Weight of crystals from laser analysis} &= \\ (2.0 \times 0.00382) + 0.2612 &= 0.2689\text{g} \\ \therefore \text{total crystal weight in the range 75-44.8 } \mu\text{m} &= 0.2787\text{g} \end{aligned}$$

The two size distributions can now be added and Table 9.27 was constructed for the final crystal size distribution for run 34 sediment. The final mass weighted mean diameter of the distribution $\bar{\mu}$ was calculated from the expression

$$\bar{\mu} = \frac{\sum_{\text{all } i\text{'s}} \mu_i \cdot f_i}{\sum_{\text{all } i\text{'s}} f_i}$$

and the standard deviation σ was calculated from

$$\sigma^2 = \frac{\sum_{\text{all } i\text{'s}} (\mu_i - \bar{\mu})^2 \cdot f_i}{\sum_{\text{all } i\text{'s}} f_i}$$

where: σ^2 = the variance of the distribution
 μ_i = mean of the size band concerned
 f_i = mass fraction in the size band concerned

The last column in Table 9.27 was constructed after the mean of the distribution $\bar{\mu}$ was calculated from the table in the column before last. Hence the parameters of the final distribution for run 34 sediment are

$\bar{\mu}$ = 456.5 μm mass weighted mean diameter
 σ^2 = 101536.3 (μm)² the variance
 σ = 318.6 μm the standard deviation

The size distribution results for run 34 sediment are also presented in a graphical form and the following plots were carried out.

- a. Crystal mass retained in band (g) vs. mean of size band (μm), a curve was forced through the plotted points.
- b. Cumulative undersize fraction retained vs. aperture size (μm) (or the lower limit of the size band (μm)).

These plots are presented in Figures 9.14 and 9.15 respectively.

TABLE 9.27
The final crystal size distribution for run 34 sediment

Size band (μm)		Mean of size band	Mass retained	Mass fraction	Cumulative undersize fraction	Mass weighted mean $\mu_i f_i$ (μm)	$(\mu_i - \bar{\mu})^2 \cdot f_i$
upper	lower	μ_i (μm)	(g)	f_i			
1676.0	1405.0	1540.5	0.0823	0.0055	0.9945	8.470	6462.8
1405.0	1003.0	1204.0	0.7085	0.0475	0.9470	57.19	26540.9
1003.0	853.0	928.0	0.8298	0.0556	0.8914	51.60	12360.6
853.0	699.0	776.0	1.3797	0.0924	0.7990	71.70	9432.2
699.0	599.0	649.0	1.4659	0.0982	0.7008	63.73	3638.9
599.0	500.0	549.5	1.4513	0.0972	0.6036	53.41	840.7
500.0	422.0	461.0	1.6974	0.1137	0.4899	52.42	2.3
422.0	355.0	388.5	1.4581	0.0977	0.3923	37.96	451.8
355.0	295.0	325.0	0.8978	0.0601	0.3321	19.53	1039.3
295.0	251.0	273.0	0.8243	0.0552	0.2769	15.07	1858.7
251.0	210.0	230.5	0.5699	0.0382	0.2387	8.81	1951.1
210.0	180.0	195.0	0.5003	0.0335	0.2052	6.53	2290.8
180.0	150.0	165.0	0.2694	0.0180	0.1872	2.97	1529.5
150.0	75.0	112.5	0.6277	0.0421	0.1451	4.74	4981.9
75.0	44.8	59.9	0.2787	0.0187	0.1264	1.12	2941.4
44.8	31.5	38.1	0.0863	0.0058	0.1207	0.22	1015.3
31.5	23.5	27.5	0.0863	0.0058	0.1149	0.16	1067.4
23.5	18.1	20.8	0.0665	0.0045	0.1104	0.094	854.3
18.1	14.0	16.0	0.0961	0.0064	0.1040	0.102	1241.9
14.0	10.9	12.4	0.2021	0.0135	0.0905	0.167	2662.5
10.9	8.5	9.7	0.4165	0.0279	0.0626	0.271	5569.7
8.5	6.7	7.6	0.1996	0.0134	0.0492	0.102	2700.3
6.7	5.2	5.9	0.0345	0.0023	0.0469	0.014	467.0
5.2	4.0	4.6	0.2464	0.0165	0.0304	0.076	3369.5
4.0	3.2	3.6	0.1084	0.0073	0.0231	0.026	1497.4
3.2	2.5	2.8	0.1553	0.0104	0.0127	0.029	2140.8
2.5	2.0	2.2	0.0912	0.0061	0.0066	0.013	1259.0
2.0	1.6	1.8	0.0345	0.0023	0.0043	0.004	475.5
1.6	0.0	0.8	0.0641	0.0043	0.0000	0.003	892.9
The mean $\bar{\mu} = \Sigma \mu_i f_i$						456.5	
The variance $\sigma^2 = \Sigma (\mu_i - \bar{\mu})^2 \cdot f_i$							101536.3

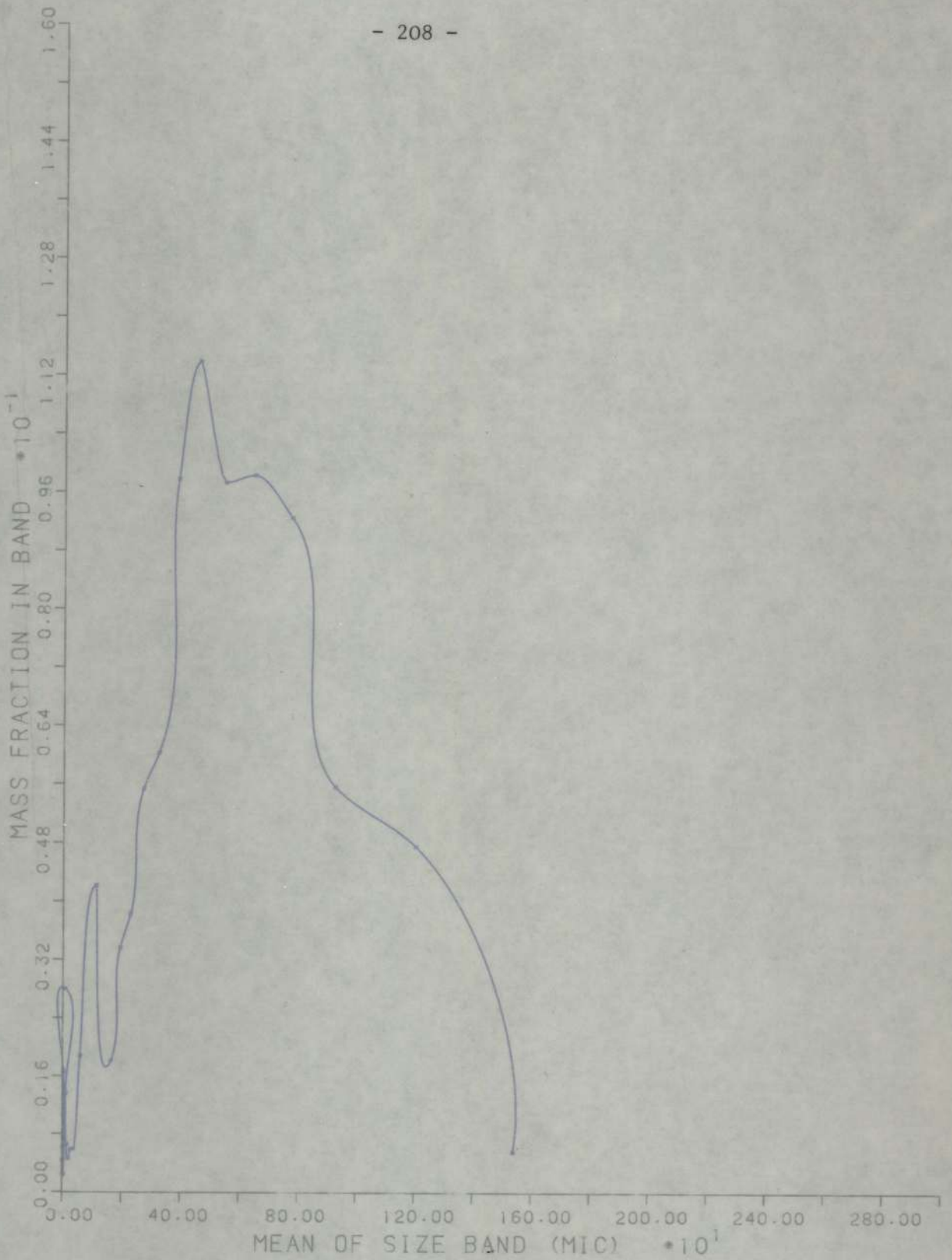


FIGURE 9.14

GRAPH FOR RUN NUMBER 34

MASS FRACTION IN BAND VS. MEAN OF BAND

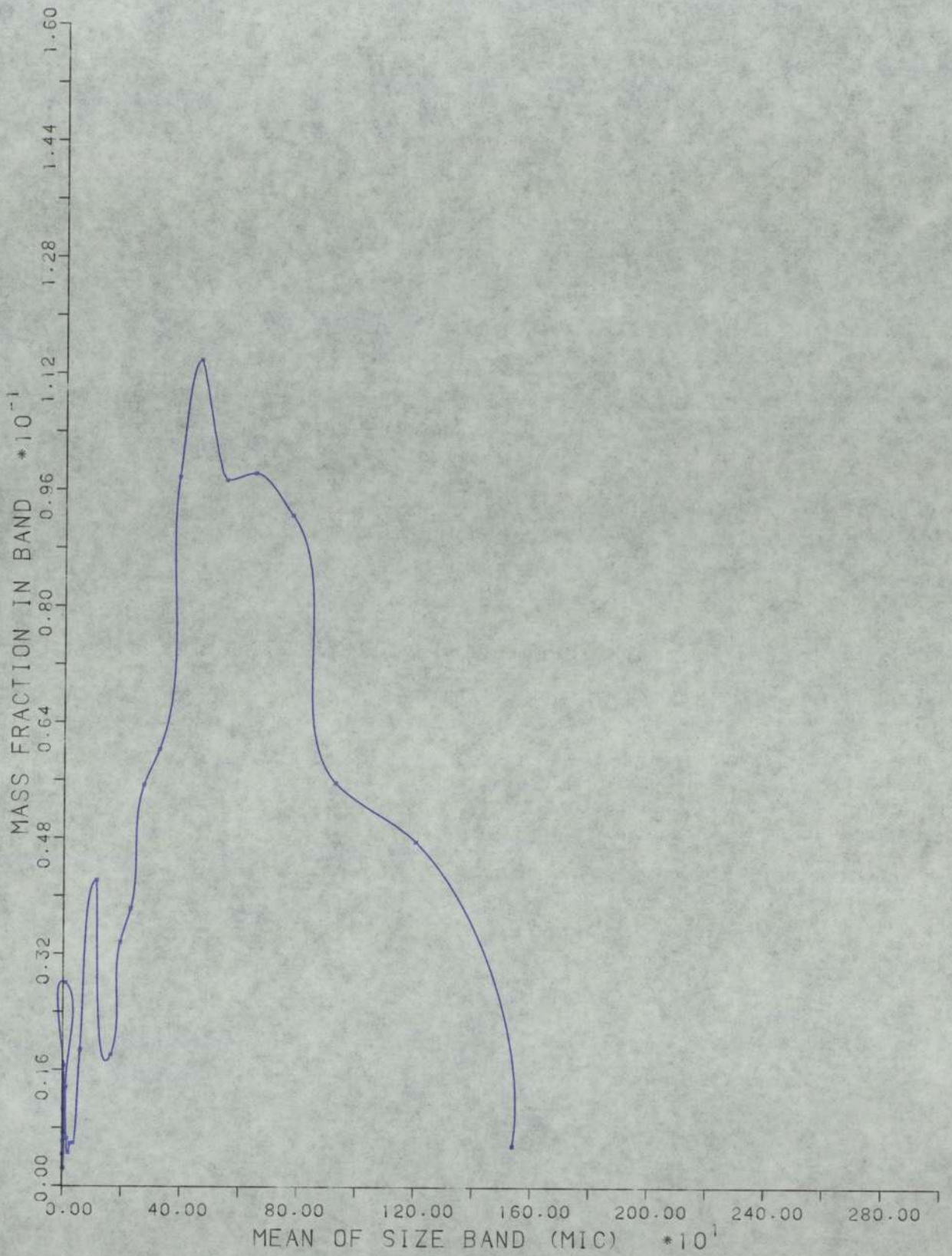


FIGURE 9.14

GRAPH FOR RUN NUMBER 34

MASS FRACTION IN BAND VS. MEAN OF BAND

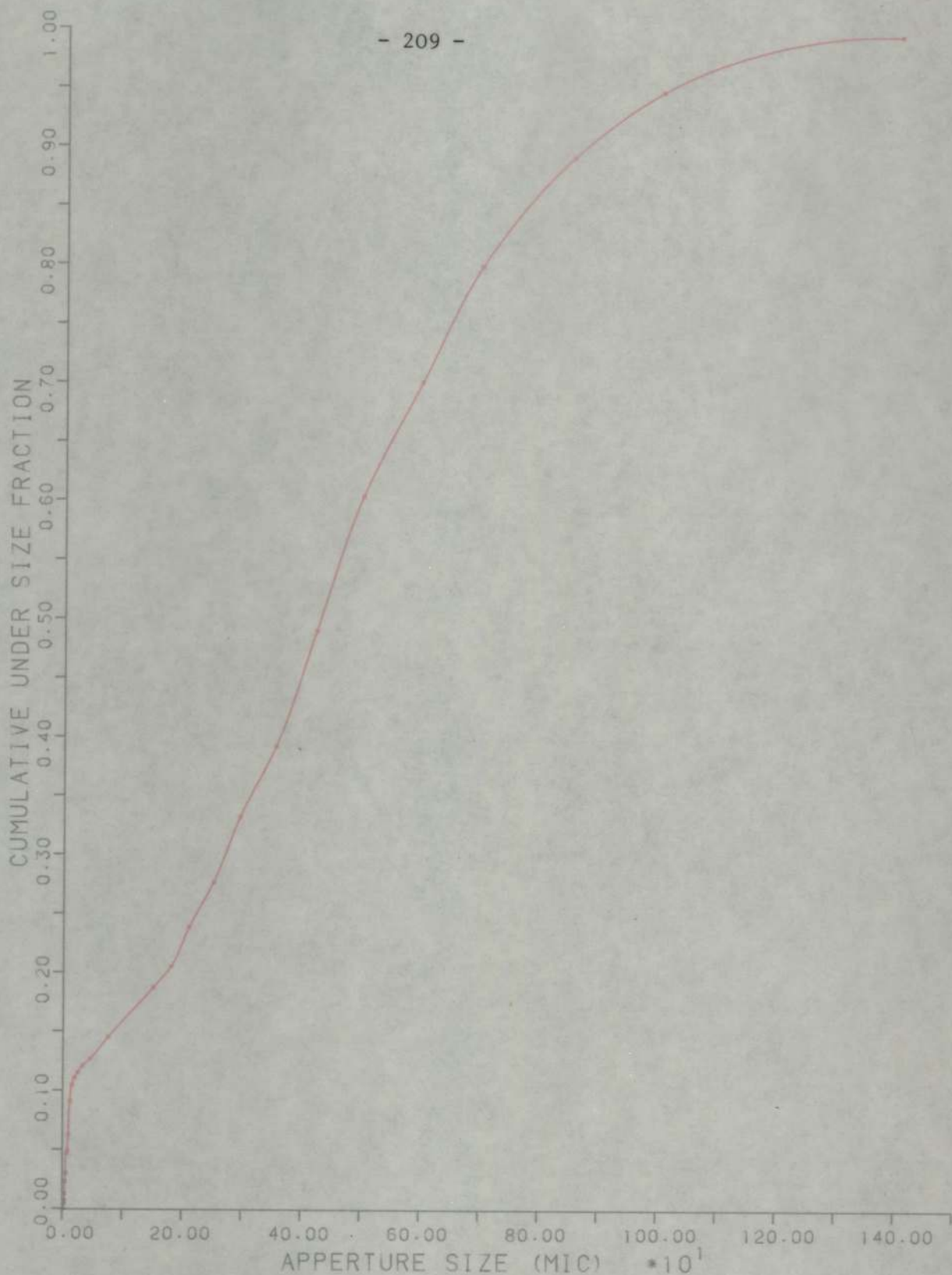


FIGURE 9.15

GRAPH FOR RUN NUMBER 34

CUMULATIVE UNDER SIZE FRACTION VS. APPERTURE SIZE

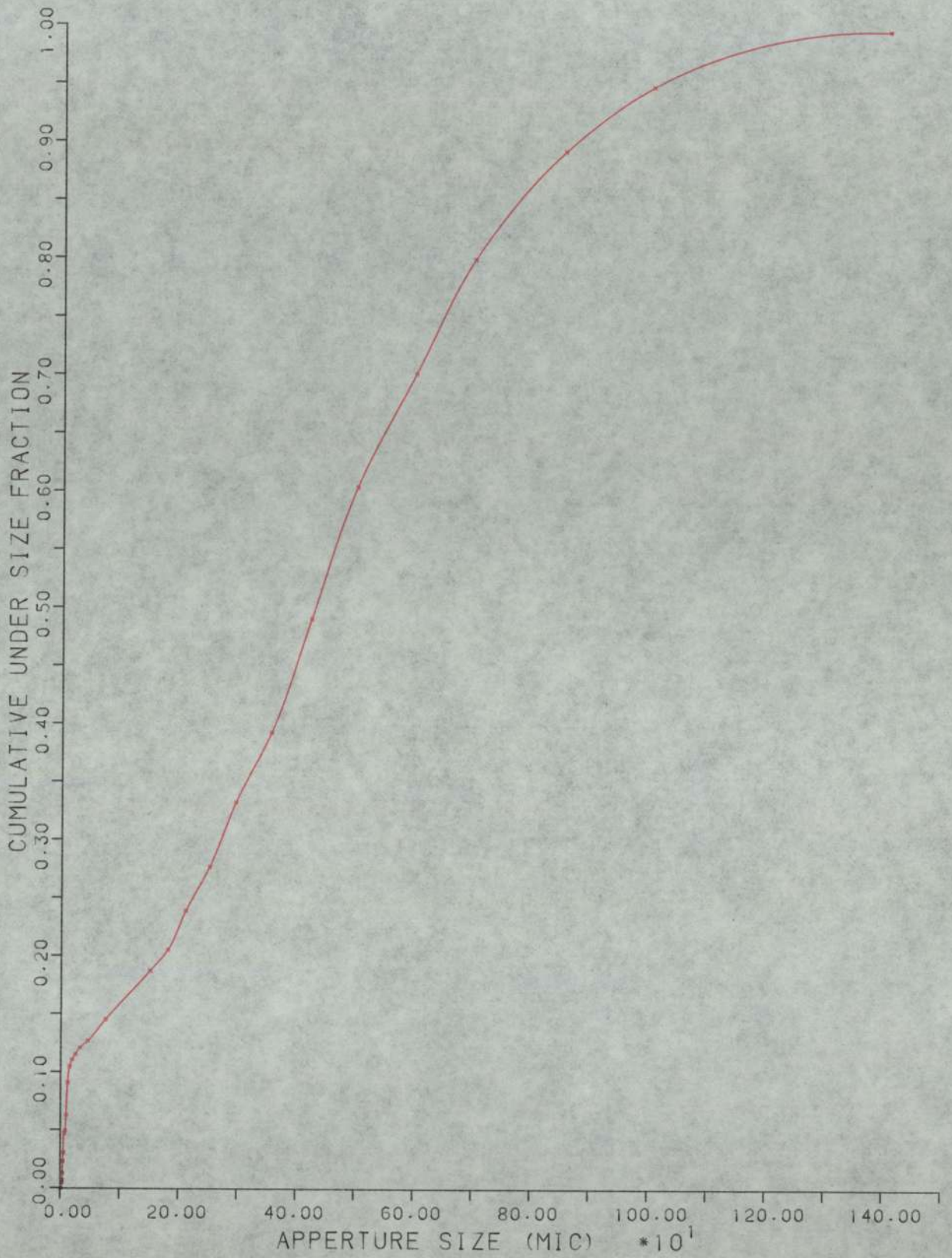


FIGURE 9.15

GRAPH FOR RUN NUMBER 34

CUMULATIVE UNDER SIZE FRACTION VS. APPERTURE SIZE

Summary of crystal size distribution results

A computer program was developed in Fortran 77 and was used to perform the calculations shown above for run 34 sediment on the experimental results obtained for the sediment of all the fourteen runs. Plots of crystal mass retained vs. mean of size band and of cumulative undersize fraction vs. aperture size were also carried out by the computer using the same program and also using the graphic package CALCOMP from Aston computer library. Appendix 9 presents the listing of this computer program which contains extensive comment statements to clarify the functions of the various program segments. The size distribution results, presented in a graphical form, for a chosen number of runs are presented in Appendix 10. A summary of some of the results and of the parameters of the final crystal size distribution obtained for the sediment of all the fourteen runs is given below in Table 9.28.

TABLE 9.28

Summary of the results and parameters of the final crystal size distribution obtained for the sediment of the fourteen runs

Number of run	Weight of large crystals analysed by sieves (g)	Weight of fine crystals analysed by laser (g)	Total weight of crystals (g)	Mass weighted mean diameter $\bar{\mu}$ (μm)	Standard deviation σ (μm)
34	12.4600	2.4643	14.9243	456.5	318.6
35	16.3300	0.7057	17.0357	541.7	319.7
51	8.4731	2.6823	11.1554	427.8	332.4
52	11.2590	3.6482	14.9072	412.5	323.5
53	8.2030	3.6688	11.8714	404.8	348.9
54	8.7213	4.5678	13.2891	404.3	346.8
55	12.8194	4.2928	17.1122	467.8	363.8
56	8.7535	5.2637	14.0172	410.2	374.6
57	8.2335	5.6030	13.8365	409.4	384.5
58	9.6547	4.8976	14.5523	420.6	368.6
59	7.7539	2.8934	10.6473	498.6	374.7
60	10.5551	2.2465	12.8016	553.1	366.9
61	14.5059	0.3628	14.8687	619.6	309.7
62	10.0171	0.0479	10.0650	628.8	295.5

CHAPTER TEN

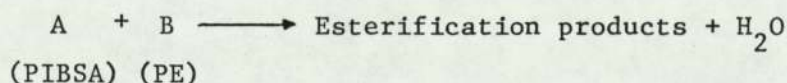
DISCUSSION OF KINETIC INVESTIGATION RESULTS

Two methods were used in the analysis of the kinetic investigation results presented in Chapter Eight, the Total Acid Number method, and infrared spectroscopy analysis. A detailed discussion of the results obtained by each of these two methods is presented separately in this chapter.

10.1 Discussion of Total Acid Number Method Results

The results obtained using this method of analysis depended to a large degree on the assumptions that were made and presented in the theoretical treatment section of Chapter Eight (Section 8.1.1). A discussion of these assumptions and of the results obtained is given below.

1. In considering the overall PIBSA/PE esterification reaction



it is inherently assumed that none of the four reaction steps presented in Section 8.1.1 is a reversible reaction. This assumption is made because in the reaction steps 2, 3 and 4 the water that is produced is being stripped by nitrogen gas; this would shift the equilibrium position of the reaction far to the right, and so these steps can be assumed irreversible. This does not apply to the first step of the reaction in which the mono-ester is formed. But it has been found⁽¹⁵⁷⁾ that although PIBSA has two acidic groups it titrates with tetra-n-butyl ammonium hydroxide solution as monoacidic (i.e. one mole of the quaternary base reacts with one mole of the anhydride)⁽¹⁵⁷⁾, so the first step in the reaction does not represent any drop in the value

of the Total Acid Number (TAN). But all the experimental results obtained showed that the drop in the value of the TAN was very fast indeed, this indicates that the forward esterification reaction is very much faster than any backward reaction that may be taking place due to the reversibility of the first step of the reaction, which is a justification to the assumption of the irreversibility of the reaction.

2. A second assumption was that the drop in the value of the TAN can be used to represent the conversion to esters; this assumption seems reasonable because practically all the esterification products of reaction steps 2, 3 and 4 have no theoretical acidity. The monoester produced in the first reaction step has a theoretical acidity, but as was shown above the very fast drop in TAN indicates that reaction steps 2, 3 and 4 are very fast indeed and hence the PIBSA is being esterified into formulas (II), (III) and (V), which are without theoretical acidity.

3. A third assumption was the use of the relative Total Acid Number (TAN_R) instead of the absolute TAN in the analysis of all the results. This assumption was decided on after an attempt to analyse the results of the kinetic runs using absolute TAN values was made and failed. Plots of $\log (d(TAN)/dt)$ vs. $\log (TAN)$ were carried out for different runs and all of them were not straight lines, figure 8.4 for run 39 and figure A6.3 for run 36 were presented as an example of these plots, while straight lines were obtained when the relative TAN, (TAN_R) was used instead of the absolute TAN in these plots. But the attempt did not stop at that. By studying figure 8.4 for run 39 it can be seen that the first point representing the initial slope was the one causing the curvature of the plot, and that could be due to the low initial slope calculated at $t = 0$. But the TAN at $t < 0$ (i.e. before PE addition) was about 28.2 mgkoH/g in practically all the runs, hence by assuming this value to be the initial

value of the TAN, and by considering the drop in the TAN over the first sample period of six minutes duration, a much higher initial slope of $(20.4-28.2)/0.1 = -78$ TAN/hr was obtained, then from these values of the initial TAN and initial slope, and from the data given in Table 8.3 for run 39, Table 10.1 was constructed.

TABLE 10.1

The slope of TAN vs. time curve at different points for run 39 assuming an initial TAN value TAN^0 of 28.2 mgkoH/g.

TAN mgkoH/g	Slope d(TAN)/dt TAN/hr	$\log \left(\frac{-d(TAN)}{dt} \right)$ = y_i	$\log (TAN)$ = x_i
28.2	- 78.000	1.892	1.450
13.0	- 20.227	1.306	1.114
10.0	- 6.944	0.842	1.000
7.0	- 2.703	0.432	0.845
5.0	- 1.084	0.035	0.699

with $\Sigma x_i = 5.108$, $(\Sigma x_i)^2 = 26.092$, $\Sigma x_i^2 = 5.546$

$\Sigma y_i = 4.507$, $\Sigma x_i y_i = 5.430$, $N = 5$

and using the least square best fit straight line method ⁽³⁴⁾ as before, we have,

$$\text{slope} = \frac{5.43 - (5.108 \times 4.507/5)}{5.546 - (26.092/5)} = 2.520 = n$$

and

$$\text{intercept} = \frac{(4.507 \times 5.546) - (5.108 \times 5.43)}{(5 \times 5.546) - 26.092} = -1.673$$

k is calculated from the intercept using equation 8.24 as was done before in Chapter Eight Section 8.1.5 but this time using $n = 2.52$ and

$$\gamma = \frac{C_A^0}{TAN^0} = \frac{0.4186}{28.2} = 0.01484$$

hence $-1.673 = \log k + (2.52 - 1.0) \log (0.01484)$

$$\therefore k = \underline{12.777 \text{ (equiv/dm}^3\text{)}^{1-n} \cdot \text{hr}^{-1}}$$

and $n = 2.520$ the overall order of reaction.

The plot of $\log (-d(TAN)/dt)$ vs. $\log (TAN)$ is presented in figure 10.1. It can be seen that the straight line obtained is a good fit for the data, hence because of that, although the values obtained for n and k differ quite a lot from those obtained using the value of the TAN_R instead of the TAN , the analysis using the absolute TAN values was continued. The next step was to use these values of n , TAN^0 and the absolute values of the TAN in the analysis of run 42 with $\alpha = 1.25$, for which equation (8.20) is applicable, hence by putting

$$Y = \log \left[\frac{-d(TAN)/dt}{(TAN + (\alpha - 1) TAN^0)^n} \right]$$

and

$$X = \log \left[\frac{TAN}{(TAN + (\alpha - 1) TAN^0)} \right]$$

with $\alpha = 1.25$, $n = 2.520$ and $TAN^0 = 28.2$ mgkoH/g, and by using the data given in Table A6.4 in Appendix 6 for run 42, Table 10.2 below was constructed.

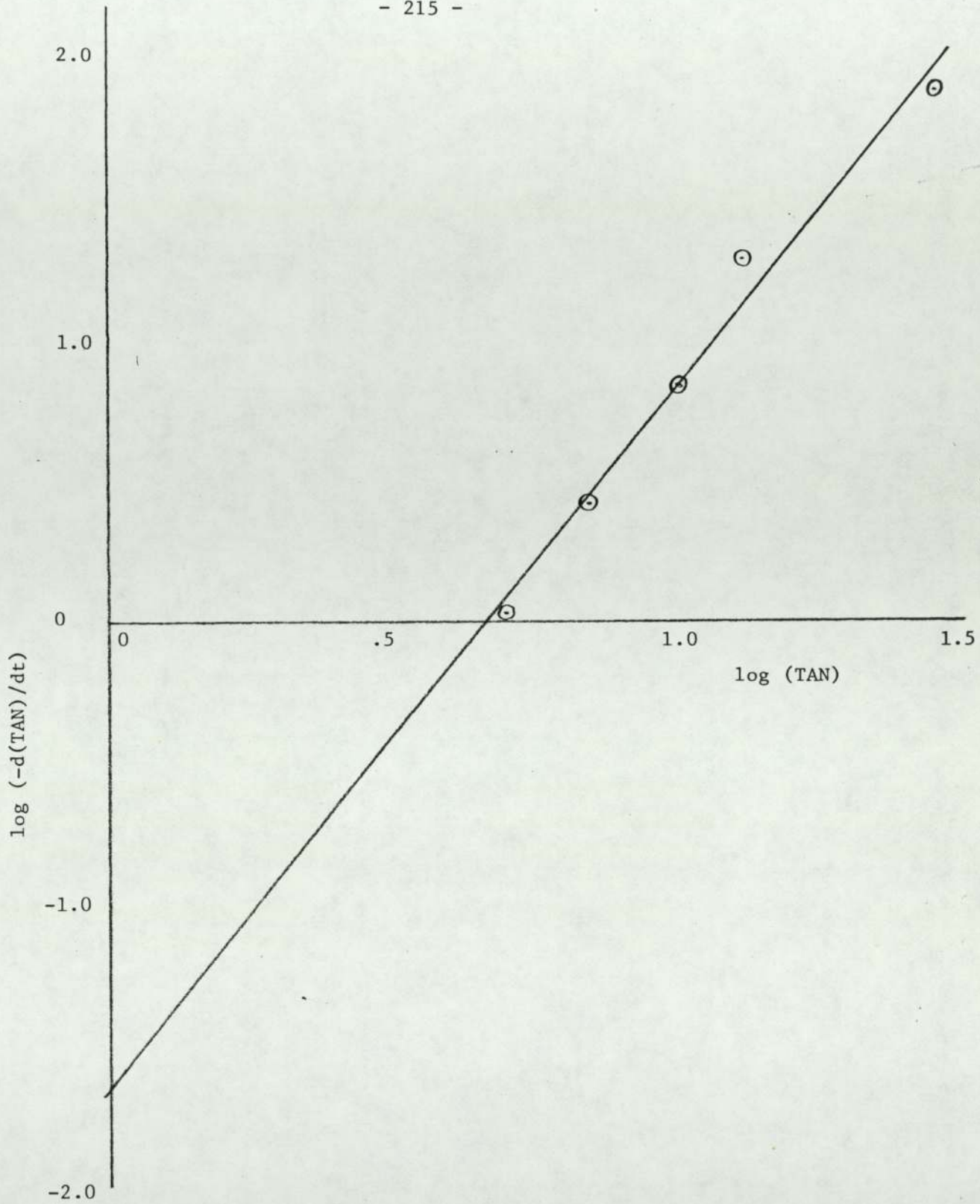


Figure 10.1

Graph for run 39 of $\log(-d(\text{TAN})/dt)$ vs. $\log(\text{TAN})$

for initial TAN value of 28.2 mgkoH/g.

TABLE 10.2

The values of the slope of TAN vs. time curve measured at five different points together with the calculated values of y and x for run 42, with $\alpha = 1.25$, $n = 2.52$, and $\text{TAN}^0 = 28.2 \text{ mgkoH/g}$.

TAN mgkoH/g	d(TAN)/dt TAN/hr	Y	X
28.2	- 93.000	- 1.9304	- 0.0969
13.2	- 20.000	- 1.9912	- 0.1859
9.6	- 10.761	- 2.0461	- 0.2391
6.0	- 2.972	- 2.3383	- 0.3375
3.4	- 0.441	- 2.9237	- 0.4876

with $\Sigma x_i = -1.347$, $(\Sigma x_i)^2 = 1.8144$, $\Sigma x_i^2 = 0.4528$

$\Sigma y_i = -11.2297$, $\Sigma x_i y_i = 3.2612$, $N = 5$

A plot of Y vs. X was carried out and is presented in figure 10.2. It can be seen that the plot does not represent a straight line at all and nothing can be done about it, but supposing that a straight line was forced through these data points then from the least square best fit method the slope of such a line is given by

$$\text{slope} = \frac{3.2612 - ((-1.347)(-11.2297)/5)}{0.4528 - (1.8144/5)} = 2.642$$

and

$$\text{intercept} = \frac{(-11.2297)(0.4528) - (-1.347)(3.2612)}{5(0.4528) - 1.8144} = -1.539$$

but the order of reaction with respect to PIBSA, a, is equal to the slope, hence

a = 2.624

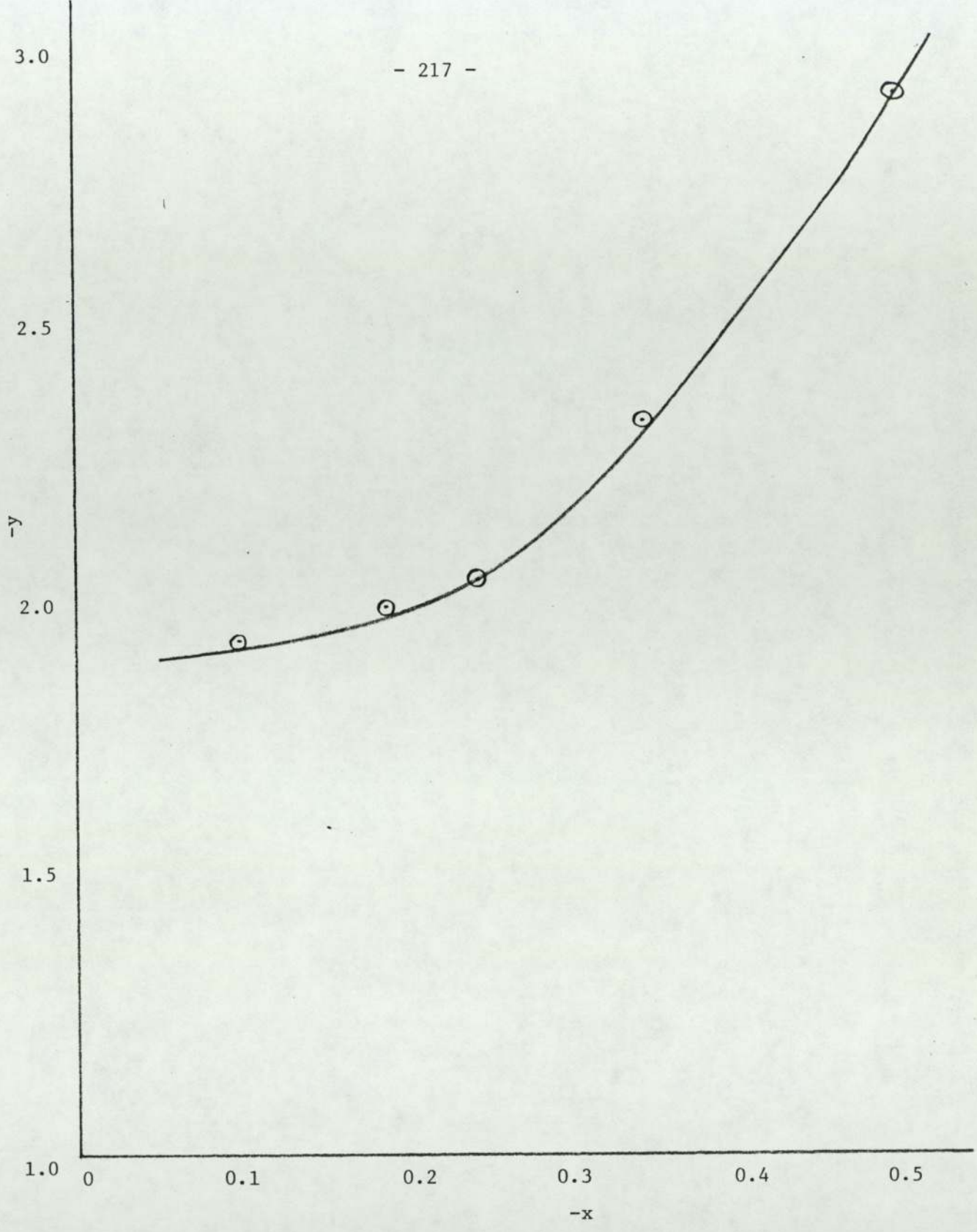


Figure 10.2

Graph for run 42 of $Y = \log \left(\frac{-d(\text{TAN})/dt}{(\text{TAN} + (\alpha - 1)\text{TAN}^0)^n} \right)$ versus

$X = \log \left(\frac{\text{TAN}}{(\text{TAN} + (\alpha - 1)\text{TAN}^0)} \right)$, with $n = 2.52$ and $\text{TAN}^0 = 28.2 \text{ mgkoH/g}$

This result did not seem to make any sense because the estimated value of a , equal to 2.624, is higher than that obtained for the overall order of reaction n , equal to 2.52. Because of that it was decided to use the value of TAN_R instead of the value of the TAN in the analysis of all the results. In fact this empirical transformation to TAN_R was the only way in which the results of the kinetic runs could have been analysed properly to yield sensible end results based on a theoretical treatment. It is also possible that this empirical approach has a theoretical explanation behind it because the residual TAN obtained at the end of each run TAN^∞ is partly due to the acidity of the sulphonic acid catalyst used in the reaction and does not represent the presence of PIBSA. The rest of the acidity could well be due to the presence of a by product which does not enter in to the calculations involved, in any case more work needs to be done to investigate the significance of this residual TAN and the possible theoretical explanation behind it in future research.

4. The value of the initial TAN used in the analysis was taken as TAN^0 at $t = 0$ immediately after PE addition and not as TAN^0 at $t < 0$ before PE addition. This was done because there was some drop in the TAN value after PE addition which was mainly due to the fact that the sample taken after PE addition had part of its weight as PE crystals which did not contribute to the TAN value in the titration, hence for consistency of results the initial TAN was taken at $t = 0$. But to check the effect of choosing one or the other as TAN^0 the overall order of reaction n was calculated again from run 39 results assuming an initial TAN value of 28.2 mgkoH/g. Hence from the data in Table 8.3 in Chapter Eight, Table 10.3 was constructed and presented below.

TABLE 10.3

The slope of TAN vs. time curve at different points for run 39, with an initial TAN value of 28.2 mgkoH/g.

TAN mgkoH/g	slope = d(TAN)/dt TAN/hr	$\log \left(\frac{-d(\text{TAN})}{dt} \right)$ = y_i	$\log (\text{TAN} - 3.0)$ = x_i
28.2	-59.000	1.771	1.401
13.0	-20.2272	1.306	1.000
10.0	- 6.944	0.842	0.845
7.0	- 2.703	0.432	0.602
5.0	- 1.084	0.035	0.301

with $\Sigma x_i = 4.149$, $(\Sigma x_i)^2 = 17.214$, $\Sigma x_i^2 = 4.130$

$\Sigma y_i = 4.386$, $\Sigma x_i y_i = 4.769$, $N = 5$.

hence for the least square best fit straight line of the plot of

$\log \left(\frac{-d(\text{TAN})}{dt} \right)$ vs. $\log (\text{TAN} - 3.0)$ we have,

$$\text{slope} = \frac{4.769 - 4.149 \times 4.386/5}{4.130 - 17.214/5} = 1.644 = n$$

and

$$\text{intercept} = \frac{4.386 \times 4.13 - 4.149 \times 4.769}{5 \times 4.130 - 17.214} = -0.487$$

the actual plot is given in figure 10.3.

Hence the value of n obtained = 1.644 when $\text{TAN}^0 = 28.2$ mgkoH/g while $n = 1.614$ when $\text{TAN}^0 = 25.0$ mgkoH/g. The difference in n is $\approx 1.9\%$ which did not seem to be high. Because of that and for consistency of results the value of TAN^0 was taken at $t = 0$ measured immediately after PE addition.

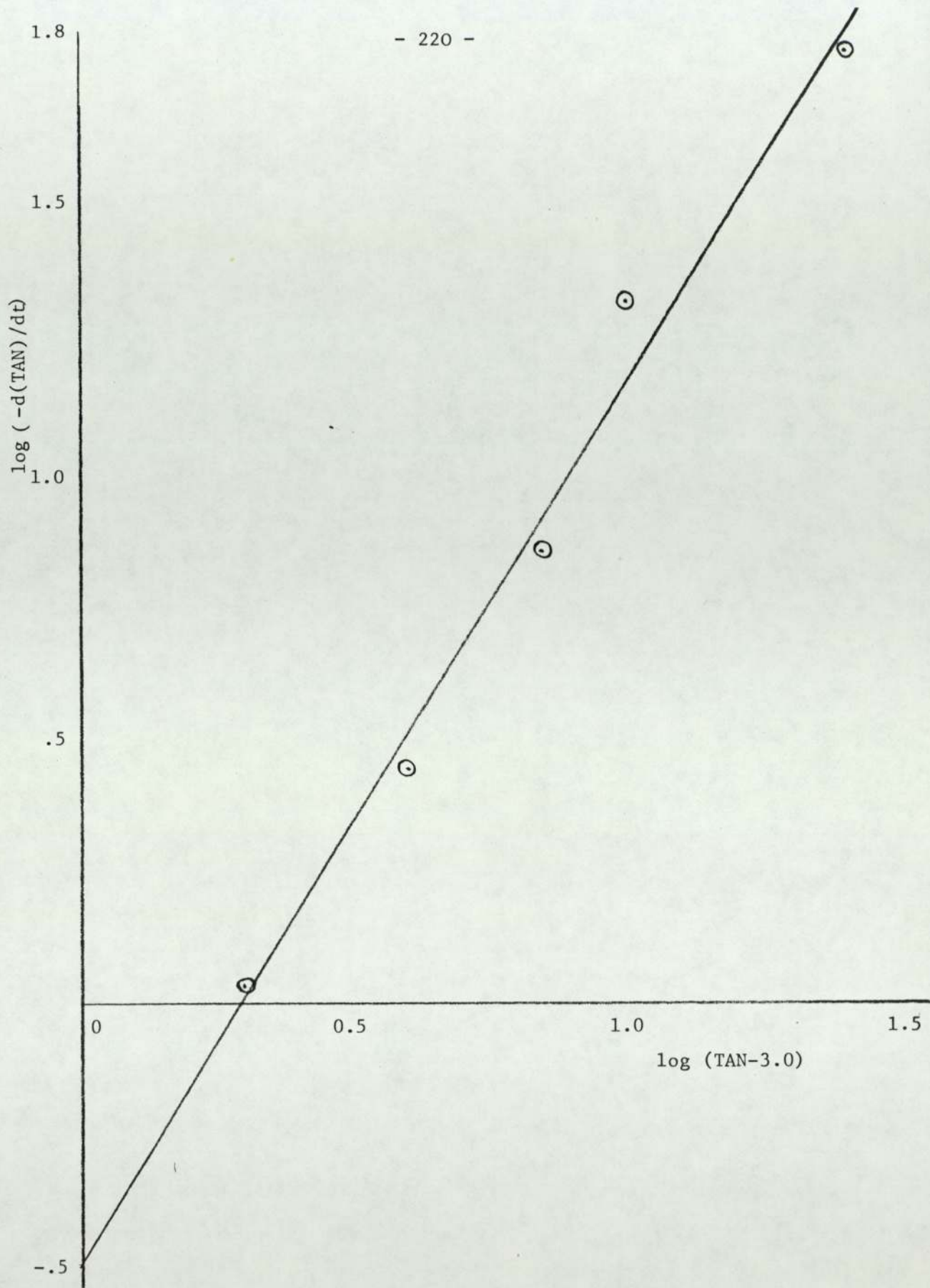


Figure 10.3

Graph for run 39 of $\log(-d(\text{TAN})/dt)$ vs. $\log(\text{TAN}-3.0)$

The value of $\text{TAN}^0 = 28.2 \text{ mgkoh/g}$

5. When the overall esterification reaction was considered it was assumed that one equivalent of PE reacted with one equivalent of succinic anhydride in the PIBSA, which seemed reasonable under the circumstances. But from Table 8.10 in Chapter Eight, it can be seen that for runs with $\alpha < 1.0$ the residual TAN (TAN^{∞}) was much lower than the value expected from the one to one PE to PIBSA reaction, for example for run 41 with $\alpha = 0.25$, the expected residual TAN was around 21 mgkoH/g, but the experimental value obtained was 14 mgkoH/g. This tends to indicate that for $\alpha < 1.0$ the ratio of PE to PIBSA in the overall reaction was less than the one to one value assumed in the analysis. This becomes very clear when the mechanism of the reaction is considered. When there is an excess of PIBSA (i.e. $\alpha < 1.0$), the fourth step of the esterification reaction becomes important and plays a bigger role in the overall esterification reaction with the net result that more equivalents of PIBSA are consumed in the reaction per one equivalent of PE (and less potent products are obtained). Because of that such runs with $\alpha < 1.0$ were not included in the analysis, and the assumption of the one to one PE/PIBSA reaction ratio was taken to be the case for runs with $\alpha \geq 1.0$ only.

6. The esterification reaction under study is a catalysed reaction, and so the concentration of the catalyst is an important factor in determining the speed of the reaction and hence the rate constant k , because of that the same ratio of the catalyst was used in runs 39 to 50, and run 63 also, hence the values of k obtained in these runs are associated with this catalyst ratio only, which was 1.18% by wt. on PIBSA of a catalyst type with 70% A.I. (see Table 6.1 in Chapter Six). The values of n and k obtained at 200°C from run 39 results associated

with this catalyst ratio are

$$\underline{n = 1.614, \quad k = 3.8497 \text{ (equiv./dm}^3\text{)}^{1-n} \cdot \text{hr}^{-1}}$$

The effect of the catalyst ratio on k was very apparent when three runs, 36, 37 and 38, were carried out at 200°C also but with about double the catalyst ratio and of a more concentrated catalyst type (2.2% by wt. on PIBSA of the catalyst with 90% A.I., see also Table 6.1). The values of n and k obtained from run 36 results (see appendix six), with $\alpha = 1.0$, associated with this high catalyst ratio are,

$$\underline{n = 1.588, \quad k = 5.545 \text{ (equiv./dm}^3\text{)}^{1-n} \cdot \text{hr}^{-1}}$$

The variation in n is only about 1.6% but the increase in k is very large, about 45%. In fact little or no change was expected in the value of n since the catalyst ratio does not affect the order of the reaction but it affects to a large degree its velocity, and hence this high increase in the value of k was obtained.

7. The average value of a , the order of reaction with respect to PIBSA, obtained by considering three runs, 42, 43 and 44, with $\alpha = 1.25, 1.5$ and 2.0 respectively was 1.465 , but the overall order of reaction n is $= 1.614$, hence the reaction order with respect to PE b is $= 0.149$. These values indicate that the reaction rate dependence on PIBSA concentration is much more pronounced than on PE concentration. This in fact does seem to agree with what was obtained when runs 39 to 44 were carried out covering a large range of α , 0.25 to 2.0 . These runs showed that the change in the reaction rate was much less pronounced than the change in α , and this may be because although α was changed by a factor of eight, the concentration of PIBSA was kept at the same value. The values of a , b and n obtained above indicate that the reaction has a

very complex mechanism. A thorough kinetic study with variations in PIBSA concentration as well as PE concentration needs to be carried out in future research to investigate this complex mechanism.

8. The value of n of 1.614 used in the analysis, was obtained from one run only, run 39 at 200°C, so it became necessary to check the values of n obtained from other runs with $\alpha = 1.0$ at different temperatures and compare them to the above value. From Table 8.10 the average value of n obtained from the results of runs 39, 46, 47, 48, 50 and 63 is equal to 1.604, this agrees very well with the above value of 1.614 (a difference of about 0.6%), and hence very little error was introduced in using the value 1.614 for n instead of the average value.

9. In the experimental measurement of the TAN in all the runs a colour titration method was employed using thymol blue solution as an indicator, then towards the end of the kinetic study, one potentiometric titrator became available and was borrowed from the Esso Research Centre at Abingdon, so the samples of the last six runs, 46 to 50, and run 63 were analysed for the TAN using both colour titration and also the potentiometric titrator, and it was noticed that the differences between the TAN results obtained from both methods ranged between 0 to about 7%. To check the effect of this difference on the values of n and k obtained in the analysis, run 49 was carried out as a repeat for run 39 with $\alpha = 1.0$ at 200°C, but this time the samples were analysed for TAN using the potentiometric titrator and the results obtained are presented in appendix six in detail. A comparison between the results of run 39 with those of run 49 is given in appendix six, Tables A6.15 and A6.16, from which it can be seen that the variation in the value of n is about

2.8% while it is higher for the value of k , which is about 6.5%.

These differences are quite low in the circumstances, and although the potentiometric titration results are more accurate it was decided to use the colour titration results all along for consistency of results in all the kinetic runs.

10. The values obtained for k at 200°C from runs 39, 42, 43 and 44 were presented in Table 8.7 in Chapter Eight. These values differed by a maximum of about 12% only, which was assumed to be acceptable in this analysis. Hence an average value of k at 200°C was obtained which is equal to $3.907 (\text{equiv./dm}^3)^{1-n} \cdot \text{hr}^{-1}$.

The plot of $\ln k$ vs. $\frac{1}{T}$ given in Figure 8.7 was carried out initially for only the first four data points given in Table 8.8. These four values of k were obtained from runs carried out at high reaction temperatures, 210, 200, 190 and 180 and it can be seen that the straight line fits these four data points quite well, giving support to the assumption that the variation of k with temperature T can be represented by an Arrhenius type of equation. The value of k obtained from run 50 which was carried out at the much lower reaction temperature of 150°C was way off from this straight line and was not included in the plot. This could well have been due to the largely reduced solubility of PE in the reaction mixture at the lower reaction temperature of 150°C, in fact it was possible to see that most of the PE crystals stayed as solid particles in suspension for a long time. This might have had two main effects on the reaction rate, the first one is that the actual ratio of PE to PIBSA, α , was much lower than the calculated value of 1.0, and the second is that the rate of the reaction was lower than expected due to the lower solubility of PE at 150°C. Because of that and to avoid any

errors that might have arisen due to the complications mentioned above, the value of k obtained at the reaction temperature of 150°C was not included in the plot of Figure 8.7.

When runs 61 and 62 were carried out towards the end of the sediment investigation experimental program, it was found out that not all the PE crystals dissolved in the reaction mixture even at 180°C . This would mean that the value of k obtained at the reaction temperature of 180°C is in fact lower than it should be which would tend to increase the slope of the straight line plot of Figure 8.7, giving rise to a higher activation energy of the reaction than the actual. Because of this complication it was decided to carry out another kinetic run at the higher reaction temperature of 220°C . This was performed and run 63 was carried out, detailed calculations of which are presented in appendix six. Also it was decided to plot the values of k obtained at the higher reaction temperatures of 200°C , 210°C and 220°C only, and not to include those values of k obtained at 180°C and even 190°C . This was carried out and the dotted (discontinuous) line of Figure 8.7 was obtained. As was anticipated, the new value of the activation energy obtained was lower than the first estimated value. The initial estimated values of the activation energy E and of the frequency factor k_0 , obtained from the slope and the intercept of the continuous line plot are

$$E = 10.216 \text{ kcal/g.mol}$$

$$k_0 = 204843$$

while the new values estimated from the slope and intercept of the dotted discontinuous line plot are

$$E = 7.767 \text{ kcal/g.mol}$$

$$k_0 = 15312$$

These new values of E and k_0 , obtained at the higher temperatures, are a much better estimate than the initial values for the reasons given above. The value 7.767 kcal/g.mol of E is of the right order of magnitude for liquid-liquid phase reactions carried out at such temperatures⁽²³⁾, and it is also in very good agreement with the activation energy value obtained for PIBSA/PE esterification reaction by an entirely different type of kinetic analysis⁽¹³⁸⁾. This is an important factor that tends to support this analysis and its results.

11. One of the by products of the esterification reaction was water, the removal of which was very important in shifting the reaction towards completion, and which was removed by nitrogen stripping. The amounts of water collected in the kinetic runs were presented in Table 8.9. In calculating the approximate amount of water lost with the nitrogen flow it was assumed that the nitrogen leaving the overhead condenser was fully saturated. This may have been the case with runs in which a relatively large amount of water was produced (e.g. runs carried out at higher reaction temperatures), but it may not be true in runs with prolonged reaction times or those carried out at lower reaction temperatures such as run 50. The amount of water produced in the reaction, taken together with the value of α and the reaction temperature can be used as a pointer to certain aspects of the esterification reaction. As an example consider runs 46, 47, 48 and 63 and their data given in Table 8.9. The value of α in all these runs was equal to 1.0, and the total reaction time in all of them was 6.0 hours, but they were carried out at different reaction temperatures, and as a result some of them gave rise to different amounts of water, possibly signifying different degrees of esterification. Runs 48, 49 and 63 were carried out at 210°C, 200°C and 220°C respectively, but the amount of water collected in each of them was 3cm³ possibly

indicating the same degree of esterification although the reaction temperatures were not the same, while runs 46 and 47 were carried out at 180°C and 190°C and the amounts of water collected in them were 0.5cm^3 , and 1.5cm^3 respectively which were quite different from what was collected in runs 48, 49 and 63, signifying this time different degrees of esterification. One possible explanation for these varying degrees of esterification is the change in the solubility of PE in the reaction mixture at different temperatures. As was mentioned above, it was found out that not all the PE crystals were dissolved in the reaction mixture at 180°C , which might have been the reason for the low amount of water collected. The increased amount of water collected in run 47 carried out at 190°C could well have been due to the increased solubility of PE. The fact that this amount of water increased further from 1.5cm^3 to 3.0cm^3 in run 49 performed at 200°C could mean that not all the PE crystals were in solution even at 190°C , and more of them dissolved as the temperature was raised to 200°C . As the temperature was raised still further to 210°C in run 48 and to 220°C in run 63 no change in the collected amount of water was noticed, possibly indicating that all the PE crystals did dissolve and were in solution at 200°C , and hence the increase in reaction temperature affected the rate of the reaction only. This is supported by previous work performed by the author⁽¹²⁰⁾ in which the PIBSA/PE reaction was studied under the microscope and photographs of undissolved PE crystals in the reaction mixture at 185°C were taken and presented, while above 200°C no PE crystals were noticed, and the reaction mixture was reported to be completely homogeneous at the uncatalysed reaction temperature of 218°C . This is the reason for not plotting the value of k obtained at 190°C and leaving it behind together with that obtained at 180°C in the estimation of the activation energy of the reaction.

10.2 Discussion of Infrared spectroscopy analysis results

The validity of the analysis and results obtained from infrared spectroscopy depended largely on the assumptions made. A discussion of these assumptions and the results obtained is given in this section.

1. In the theoretical analysis it was assumed that the concentration of a component is directly proportional to the peak height of the absorption band of the component at that specific wave length. This assumption is very reasonable because for infrared spectroscopy the functional relationship between the energy transmitted and the concentration of an absorbing component is given by Beer's Law ⁽¹⁵⁶⁾ from which equation (8.28) was obtained (see Chapter 8, Section 8.2.1).

$$A = \ell.S.C. \tag{8.28}$$

hence the absorbance A is directly proportional to the concentration C, ℓ and S being constants.

The computer data station which was connected to the spectrophotometer, when it compared the IR traces of the individual samples, it compared the absorbances of the different components and produced the IR traces of the differences which were the net differences in these absorbances, measured by the height of the peak in the absorption band. Moreover because absorbances are directly proportional to the concentrations, they are additive, and can be added or subtracted as required.

2. One of the difficulties encountered in setting up Tables 8.11 and 8.12 for run 45, and Tables 8.14 and 8.15 for run 43 was to decide the position of the base lines from which the height of the peaks were to be measured. The base line technique, which corrects for light attenuation (from causes other than absorption by the component, was used ⁽¹⁵⁶⁾. The base line was much easier to establish in the cases of:

the hydroxyl group, ester group and acid groups than in the cases of both ether groups at $WN\ 1100\text{cm}^{-1}$ and $WN\ 1170\text{cm}^{-1}$ as can be seen from Figures 8.8 and 8.13, (although the main ether group is at $WN\ 1100\text{cm}^{-1}$, but ether groups can show absorption in WN up to 1170cm^{-1} , and since it was noticed that some change seemed to have occurred at $WN\ 1170\text{cm}^{-1}$, it was decided to include it in the tables under the ether grouping).

Another problem was the actual measurements themselves since they were carried out manually which could have been another source of error. In any case these measurements were assumed to be accurate enough for this analysis which was conducted mainly to obtain approximate values of (n) and (a) and compare them with the values obtained by the previous analysis using the TAN method.

3. The values obtained for the overall order of the reaction n and for the order with respect to PIBSA a by IR analysis are,

$$\underline{n = 1.522}$$

$$\underline{a = 1.283}$$

these values are quite near to those obtained before using the TAN analysis method, and represent a difference of 5.7% in n , and of about 12.4% in a . These results seem to present another support to the analysis carried out previously and to their results, it also indicates the possibility of using this type of analysis for the determination of the order of reactions in general. In this case if IR spectroscopy is to be used for reaction kinetic studies and for the determination of the order of the reaction, a more accurate measurement needs to be done for the height of the peaks in the absorption bands. This can be achieved by the development of a computer program that does these measurements, so that when the computer data station compares the IR traces of the samples and gives out a trace of the difference, it also measures the peak heights of the difference

trace at the same time and hence similar tables to those given in 8.11, 8.12, 8.14 and 8.15 are obtained as outputs from the data station directly. Another way of improving the accuracy is to use a constant volume cell or a spacer, instead of the smeared film, in obtaining the IR traces of the samples, so that the same sample volume is analysed each time. Also by obtaining a proper calibration curve before analysing the samples, which can be carried out by measuring the absorbances of the peaks of samples of known concentrations, then the actual IR traces of the samples, and not their differences, may be used, and the absolute values of the concentrations can be worked out from the calibration curve. This is a very accurate way to carry out the IR analyses, but because we are dealing with a very viscous material, all samples will have to be diluted to a large degree to enable this type of analysis to be carried out, and this becomes very tedious and time consuming which is something that was not available at the time. Because of that this method of analyses was not used.

4. In the production of the PIBSA/PE dispersant it is suggested⁽¹³⁵⁾ that a specific target value of the product TAN should be aimed at, the reason given being product potency considerations, of which the hydroxyl number is a measure. Because of that the hydroxyl peak height at $WN\ 3400\ cm^{-1}$, which was assumed to be proportional to the hydroxyl number and hence becomes a measure of product potency, was plotted versus the TAN for both runs 45 and 43 with $\alpha = 1.0$, and $\alpha = 1.5$, and the results are presented in Figures 8.11 and 8.16 respectively, it is interesting to note the following:

a - A maximum for the hydroxyl number does seem to exist corresponding to a TAN value of 6.0 to 7.0 mgkoH/g. The reason given

for the drop in the hydroxyl number as the reaction proceeds further is the etherification of the hydroxyl groups to produce ether linkages, as was explained in the reaction mechanism section (Chapter Four, Section 4.3).

b - The actual height measurement of the hydroxyl peak for run 43 with $\alpha = 1.5$ (Figure 8.16) is a lot higher than that for run 45 with $\alpha = 1.0$ (Figure 8.11), also the shape and position of the maximum is much more pronounced for run 43 than run 45. One suggested reason is that the increase in the peak height was due to the increased amount of PE present since the hydroxyl number of the PE itself is quite high due to the presence of the four hydroxyl groups, but this seems very doubtful because sample No. 1 for both runs, taken at time $t = 0$ contain the maximum amount of unreacted PE compared to other samples but showed the lowest hydroxyl number of all the samples. This agrees well with the suggestion that the absorption bands of an IR trace of a liquid sample containing solid particles, are produced by the components in the liquid phase only because of the strong interactive forces between the molecules in the solid phase. Hence it is more likely that the increase in the peak height could be an indication that higher potency dispersant products are produced when higher PE/PIBSA ratios are used, which agrees well with what was suggested by the reaction mechanism and that was the formation of the di-PE ester, formula (III), which has a high hydroxyl number due to the six hydroxyl groups present, when an excess of PE was used in the reaction.

CHAPTER ELEVEN

DISCUSSION OF SEDIMENT INVESTIGATION RESULTS

One of the main objectives of this research program was to identify the cause of increased sediment formation during storage and to propose and test methods of eliminating it. Experiments were designed accordingly and the results obtained were presented in Chapter Nine. A detailed discussion of these results is presented in this chapter.

11.1 Sediment Analysis and Possible Formation Routes

The melting point measurement results given in Table 9.5 indicate that the sediment obtained at the end of runs 13 and 14 was very probably monopentaerythritol, since the melting point of monopentaerythritol reported in the literature⁽¹⁾ is 261°C (see Section 3.3 in Chapter 3), while the sediment collected from centrifuge tubes was a mixture of mono- and di-pentaerythritol. Mono-PE and di-PE form together a eutectic with a well defined melting point of 188°C⁽²⁾. Although the melting point of the mono-, and di-PE mixture is not very well defined (which was the case in measuring the melting point of the sediment from the centrifuge tubes), it is determined by the ratio of di-PE in the mixture. A melting point between 230 to 240°C could represent a di-PE content of 10 to 20% by wt. in the mixture⁽²⁾.

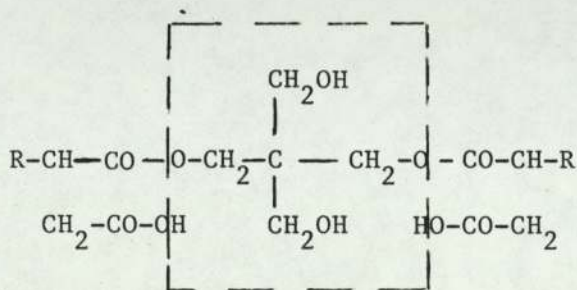
The more accurate GC analysis results given in Table 9.4 showed that even the sediment collected from the centrifuge tubes was mainly mono-PE, although with the centrifuge tubes sample the di-PE content was slightly higher than the rest. From this analysis it is concluded that the sediment was mainly monopentaerythritol.

There are two possible routes for the formation of pentaerythritol during the storage period, they are:

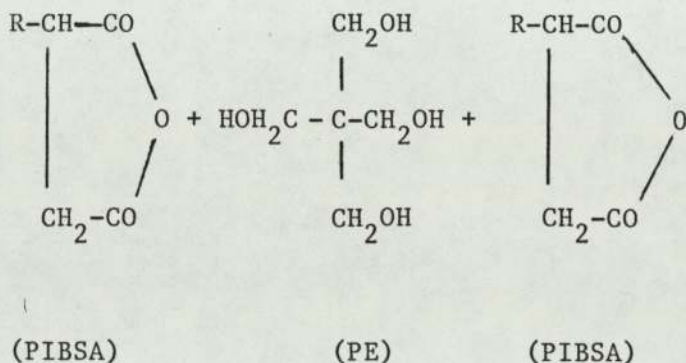
1. Back reaction

Due to the complexity of the PIBSA/PE esterification reaction and its complex products it is possible that the formation of PE during storage could be due to a back reaction caused by one of the following.

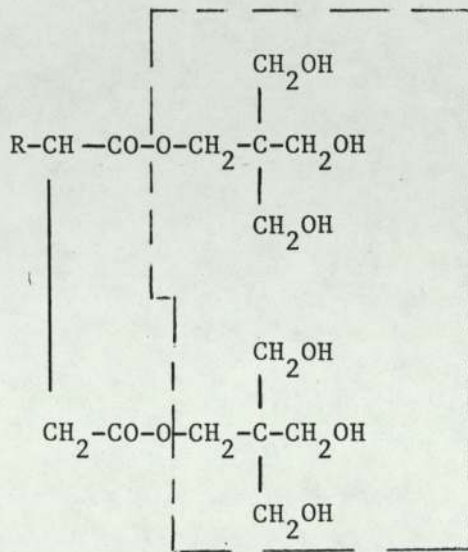
- a. Breaking down of large molecules, caused by high storage temperatures to give pentaerythritol which will then crystallize out as sediment; as an example consider the breaking down of formula (IV) (see Chapter 4, Section 4.3).



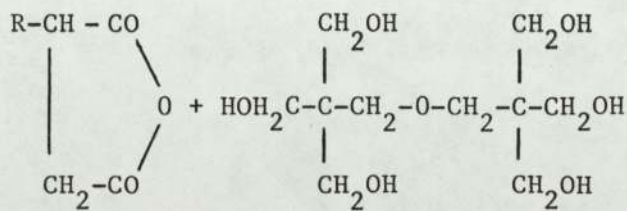
Breaking down may occur along the dotted line if heat is supplied.



The formation of the di-PE could be due to the polymerisation of the mono-PE although normally high temperatures are needed for this polymerisation or it could well be due to the breaking down of the di-PE substituted PIBSA molecules formula (III) given in Section 4.3, e.g.



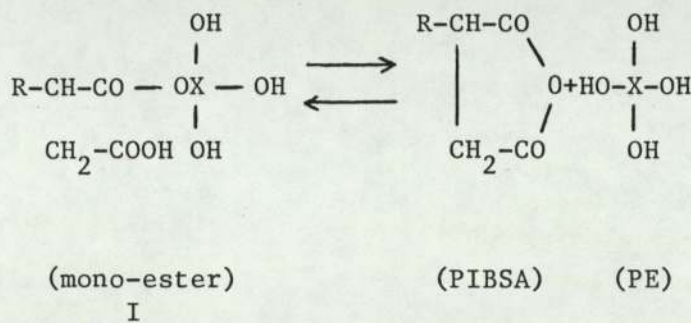
Breaking down may occur along the dotted line if heat is applied.



(PIBSA)

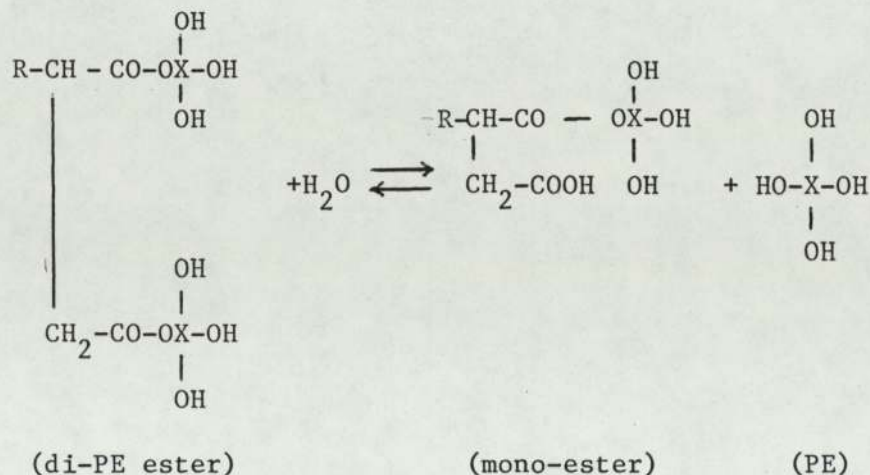
(di-PE)

b. It has also been suggested that the formation of the mono-PE could be due to the reversibility of the first step of the esterification reaction (see Section 4.3) in which the mono-ester is formed. At higher temperatures the reaction is shifted to the right and the mono-ester is reacted to give cyclic di-ester and the other esterification products while at lower temperatures the reaction is reversed and the mono-ester breaks down to yield PE and PIBSA, e.g.



hence at storage conditions the mon-ester present in the final product may break down to yield PE according to the above reaction.

c. The formation of PE can also be assumed to happen by a back reaction involving water if a small amount of water is present in the product. As an example consider the reverse of Step 3 in the reaction mechanism involving formula III (see Section 4.3).



This route involving water may be less probable than the others because of the difficulty of having water at higher storage temperatures.

2. Delayed desupersaturation

Another possible and very probable source of PE formation during storage is the excess unreacted pentaerythritol. This excess pentaerythritol does not come out of solution at the filtration stage due to many possible reasons one of which is the possibility of the enhanced solubility of PE caused by the presence of very fine PE particles, according to the Ostwald-Freundlick relationship given in Chapter Two. It is also possible that a large portion of the excess PE comes out of solution as very fine particles in a stable colloidal form that may not be separated by filtration which will agglomerate and precipitate at a later stage during the storage period.

Because of these two main possible routes for the sediment formation during storage, experiments and procedures were devised to give support or otherwise to these two hypotheses and the discussion of their results is presented in the following sections.

11.2 Effect of Storage Temperatures

Product samples from different runs were stored at different temperatures and a total of five storage temperatures were investigated; these temperatures were ambient, 50°C, 90°C, 120°C and 150°C. From the centrifuge test results obtained samples of which were presented in Tables 9.6, 9.10, 9.11, 9.12, 9.14, 9.15, 9.16 and 9.20, it was concluded that:

- a. there was no increase in the sediment level at ambient storage temperature
- b. there was little or no increase in the sediment level at a storage temperature of 50°C in most cases
- c. there was a high increase in the sediment level at a storage temperature of 90°C
- d. there was an even higher increase in the sediment level and its rate of formation at a storage temperature of 120°C
- e. there was no increase in the sediment level at a storage temperature of 150°C .

These results were very interesting and at first it was thought that a back reaction could have been the cause of the sediment formation. At storage temperatures of ambient and 50°C the rate of the back reaction was very low and little or no sediment was obtained while at 90°C and 120°C the rate was much higher and a high sediment level was obtained. At a storage temperature of 150°C it was suggested that the forward esterification reaction was faster than the back reaction and hence no increase in the sediment level was obtained. If this was the case then the viscosity of the product samples was expected to increase at the storage temperature of 150°C . But this was not the case and in fact the reverse happened, the results given in Table 9.8 show that the viscosity of the product decreased at higher storage temperatures, the per cent decrease in the viscosity being different from one run to the other. Also if the reason for not having sediment at 150°C was the faster forward esterification reaction then by lowering the storage temperature to 90°C (after the initial storage period at 150°C), the sediment level should have increased because of the higher rate of the back reaction at the lower temperature. But the results

given in Table 9.7 for runs 17, 22, 27 and 28 show that this was not the case. The products of these runs, when stored initially at 90°C for periods ranging from three weeks to eight weeks (see Table 9.7), had their sediment level increased to 0.4, 0.45, 0.35 and 0.25 volume % respectively, but when they were stored initially at 150°C for few weeks, then stored for a second period at 90°C, there was practically no increase in the sediment level. This indicates that storing at 150°C stabilises the product and prevents any sediment formation even at a storage temperature of 90°C. One suggested reason for the stabilisation of the product and for the lower viscosity obtained at a storage of 150°C is the possible pyrolysis of the excess pentaerythritol. Although normally higher temperatures of 200°C or above are needed for the pyrolysis of PE, it has been found by Muller (1956) that impurities present in the pentaerythritol, such as formate salts, catalyse its thermal decomposition on prolonged heating⁽¹⁾. Hence at such high storage temperatures and for long storage periods PE can lose one or more water molecules and give rise to lower viscosity products and soluble compounds. It is also possible for the excess PE to cause the formation of ether linkages (in contrast to cross-linking) by an etherification side reaction which occurs simultaneously with the esterification reaction and may be faster under these storage conditions^(138,159). The reduction in the sediment level of run 13 product sample from 0.55 volume % (obtained after an initial storage period at 90°C), to 0.2 volume % due to a second storage period at 150°C (Table 9.7) is a good support to the above suggestion. The increased solubility of PE at higher temperatures does not seem to be the reason for sediment level reduction because lowering the temperature again does not cause the increase of sediment level back again as was discussed above.

Another factor which seems to support this hypothesis is the drop in the viscosity of the product at 150°C storage temperature and its apparent dependence on the excess PE 'thought' to be present in the product sample, an example of this is a comparison between product samples of runs 27, 28 and the Fawley batch (see Table 9.8). The drop in the viscosities of runs 27, and 28 product samples was much higher than that for the Fawley batch sample, at the same time they gave a much higher rate of sediment formation than the Fawley batch sample, when stored at 90°C (see Table 9.14 and Table 9.6). A possible reason for this is the much higher PE/PIBSA ratio used in their production, of $\alpha = 1.9$ (see Table A2.1 in Appendix 2). Also if the back reaction is responsible for the sediment formation then products with a higher Total Acid Number (TAN) are expected to give rise to more sediment formation at storage than products with lower values of TAN because the former have a higher content of the mono-ester which may be responsible for the back reaction as was shown before. But this was not the case at all, since the TAN values for runs 27 and 28 products were 1.9, and 2.2 mgkoH/g respective, compared to 4.4 mgkoH/g for the Fawley batch. In fact by studying the results given in Table 9.3 and the other respective tables for the centrifuge test results it was concluded that there was no apparent dependence of the sediment formation on the TAN. The hypothesis of the pyrolysis and/or the reaction of PE on prolonged storage at higher temperatures predicts the formation of water, which in fact was suspected to be the case since an emulsion was noticed at the bottom of the centrifuge tube during the sediment test with many products and also the development of higher vapour pressure inside the storage sample bottles on prolonged storage at higher temperatures.

A possible reason for the dependance of the rate of sediment formation on the storage temperature was thought to be the viscosity of the product. At lower storage temperatures the dispersant product viscosity was very high, this viscosity decreased as the storage temperature was increased. In a stagnant viscous liquid, the viscosity plays a big role in controlling the diffusion process needed for the crystallisation and the formation of the sediment^(69,92). Hence at lower storage temperatures no sediment was formed due to the high viscosity, while at higher storage temperatures the increased rate of sediment formation was due to the reduction in the viscosity of the product. Hence experiments or procedures were to be devised, to find out whether the sediment formation is a temperature dependant process or a viscosity dependent process. An experiment was carried out to check the effect of mixing during storage on the sediment formation, and a sample of the Fawley batch was stored at 50°C with continuous mixing, the results obtained were presented in Table 9.13. Comparing these results with those given for the Fawley batch in Table 9.6 it was concluded that mixing had little or no effect on the sediment formation during storage.

11.3 Effect of Product Sample Dilution with Solvents

Product samples from runs 13, 21, 34, 35, 52 and 54 were diluted with oil, n-heptane, or chlorobenzene and stored at ambient, 50°C, and 90°C. Their centrifuge test results were given in Tables 9.9 and 9.10. The n-heptane and chlorobenzene were chosen as solvents because of the very low solubility of PE in them⁽¹⁾, and because they were used in the process itself (n-heptane was used for the centrifuge test, while chlorobenzene was used in the titration to measure the TAN value), also

the vapour pressure of chlorobenzene was lower than n-heptane, so it was possible to store its diluted samples at 90°C. From the results obtained it was concluded that:

- a. there was no increase in the sediment level during storage at ambient temperature even though the viscosities of the diluted samples at ambient temperature were even lower than those measured at 100°C for the undiluted samples of normal products.
- b. when storage temperatures were increased to 50°C and 90°C, the sediment formation also increased. In fact a comparison between the results given in Table 9.9 for the diluted samples with those given in Table 9.10 for the undiluted samples show that nearly the same level of the sediment increase was obtained with both samples at the same storage temperature. Hence it was concluded that the sediment formation process is definitely a temperature controlled process and not a viscosity controlled process which may indicate that a back reaction is responsible for the sediment formation.

11.4 Effect of Reaction Time

Three runs were carried out with prolonged reaction times compared to other runs, these were runs 6, 15 and 16 with reaction times, 5.17 hr, 4.0 hr and 5.0 hr respectively (see Appendix 2). The centrifuge test results were presented in Table 9.16. By studying these results the following points were noticed:

- a. Runs 6 and 16 products did not give rise to any sediment formation during storage, even at a storage temperature of 90°C. These runs were two of the very few runs which did not show any sediment formation during storage.

- b. Although the initial rate of the sediment formation in run 15 product during storage at 90°C was low but the final level attained was quite high, 0.4 vol.%.

The reason behind choosing a prolonged reaction time was to try and react most of the PE, this way reducing its supersaturation level, and to see the effect of that on the sediment formation. The results of run 6 and run 16 clearly indicate the success of this, and strongly supports the delayed desupersaturation hypothesis. The higher sediment formation in run 15 product was very probably caused by the higher filtration temperature of 156°C. Filtration temperatures above 150°C were found to cause some of the PE to dissolve in the product, and hence preventing its separation by filtration^(135,158,159). This by itself favours the delayed desupersaturation hypothesis, since it shows the dependance of the sediment formation on the filtration temperature.

Although using a prolonged reaction time may present a solution to the sediment formation problem but the end product is a dispersant with very low TAN, low hydroxyl number, and high ether/ester ratio, which all indicate a low potency product^(138,159). Hence this method cannot be proposed as a solution to the problem.

11.5 Effect of Reaction Temperature

It was reasoned that the supersaturated PE solution in the reaction mixture is being obtained during the cooling stage of the reaction due to the reduced solubility of PE at the lower temperatures. Hence if an experiment can be devised to do away with this cooling stage the results of such an experiment would give a very good indication as to the source of the sediment formation. Such an experiment was devised, and the reaction

was carried out at very low reaction temperatures. In fact the reaction temperature was the same as the filtration temperature, hence a higher catalyst ratio was used and much longer reaction times were needed. Three runs, 30, 31 and 32 were performed under such conditions (see Table A2.1 in Appendix 2), and their centrifuge test results were presented in Table 9.15. These results show very clearly that the products were very stable and that no sediment was formed during storage at 90°C, and even at 120°C. This is a very good indication that the source of the sediment formation is delayed desupersaturation and not a back reaction.

Performing the reaction in the above manner, at the filtration temperature, is an attractive idea and has many advantages, namely, it does away with the heating and cooling stages of the reaction and the problems associated with them; it reduces the reaction cycle time considerably, and it solves the problem of the sediment formation. But an analysis of run 31 product sample was carried out at Esso Research Centre in Abingdon, and it showed that the dispersant product had a lower hydroxyl number than the desirable value for the product, and so this method of solution was not accepted.

One possible reason for the low hydroxyl number could be the higher catalyst ratio used, since this would favour the etherification side reaction and would cause a considerable increase in the ether/ester ratio hence reducing the final hydroxyl number^(138,158,159); this may be overcome by using a lower catalyst ratio. Another way of increasing the hydroxyl number could be by using a higher PE/PIBSA ratio to compensate for the lower reaction temperature, or produce an end product with slightly lower TAN value, or use a slightly higher reaction temperature. In any

case, it is felt that due to the advantages of this method, more research work along these lines should be carried out in the future.

11.6 Effect of Refiltration After Long Storage Periods

It was reasoned that if the source of the sediment formation is a back reaction then the back reaction will continue until an equilibrium stage is reached, then if the sediment is removed from the product sample, the equilibrium position will be shifted and this would cause the back reaction to start again until the equilibrium position is established once again. Because of this samples of run 14 product, and of a mixture of runs 17, 18 and 19 products were refiltered again after long storage periods, and their centrifuge test results were presented in Table 9.19. From these results it can be seen that:

- a. The refiltered product of run 14 did not give rise to sediment formation when stored for a second period at 90°C. This is not what was expected and so it does not support the back reaction hypothesis.
- b. The refiltered mixture of runs 17, 18 and 19 products sediment level was increased slightly during the second storage period from 0.06 to 0.15 vol. %, but it did not go up to the 0.4 vol. % value obtained at the end of the first storage period. This slight increase in the sediment level was not taken to indicate a back reaction, but to indicate that equilibrium was not reached at the end of the first storage period. This is a logical deduction since the first storage period for this mixture was 25 days only compared to 51 days for the run 14 product sample, and also because the sediment level of the mixture during the

second storage period was increased to 0.15 rapidly in 13 days only (or maybe less, since no test was carried out during those 13 days), and remained at that value for over two months (see Table 9.19). These results were taken to indicate that the source of the sediment formation is the excess PE present, or its delayed desupersaturation.

11.7 Effect of Reheating of the Final Product

It was becoming more and more apparent that the source of the sediment formation was the presence of the excess PE either in the form of very fine particles or in solution as supersaturation. It was decided to react this excess, as a means of its elimination, in a way not to affect the final product greatly. Hence samples of runs 33, 34 and 35 final products were reheated for a few hours at the reaction temperature, and the results of their analysis and centrifuge tests were presented in Tables 9.17 and 9.18. From these results it can be seen that the reheated product samples were very stable at storage, and no sediment was formed at storage temperature of 90°C and even at 120°C. This result strongly favours the hypothesis of the presence of excess PE, and presents us with a very simple and efficient way of over-coming this sediment formation problem. However from studying the results given in Table 9.17 and those given in Table 9.3 for runs 33, 34 and 35, the following points can be raised:

- a. The viscosity of run 33 product was slightly raised after the reheating stage, while those for run 34 and 35 products were lowered. It is possible to explain this point by considering the reaction time for the reheating stage. In runs 34 and 35, it may be said that the longer than 'needed' reaction times were used in the reheating stage causing the

increased formation of ether-linkages, which was not the case with run 33, since its reaction time was less than half that used in the other two runs. In any case more research work needs to be done in analysing the products and optimizing the conditions of this reheating stage if this method is to be used as a solution to the problem.

11.8 Effect of Extended Time at Filtration Temperature

The problems associated with the growing of larger crystals of pentaerythritol were discussed in detail in Chapter 3 Section 3.6, and in Chapter 2 Section 2.4.2.3. Add to that the problems associated with crystallization from very viscous solutions^(160,161), it becomes apparent that very long periods are required for equilibrium to be established. Thinking along these lines experiments were performed in which the reaction mixtures were left at filtration temperatures for extended periods of time, and the results of these runs were presented in Table 9.20. From these results it can be seen that:

- a. Run 29 and run 51 products were very stable and gave rise to very little or no sediment formation at high storage temperatures. The reaction mixtures of these two runs were left at filtration temperature for 64.7 hr, and 66 hr respectively, much longer than all the other runs (see Table 9.20 and Appendix 2).
- b. Although run 53 product gave rise to a higher sediment level of about 0.12 vol. % compared to runs 29 and 51, it showed a much better stability than the products of runs 9 and 26.

From the above it was concluded that the stability of the product increased when the reaction mixture was kept at filtration temperature for

longer periods of time, and when this period of time was around 65 hr the products obtained were very stable and their sediment level did not rise by any appreciable amount during storage at higher temperatures. These results strongly favour the hypothesis of the presence of excess PE, and they also present us with a physical method for overcoming the sediment formation problem.

11.9 Effect of Cooling Rate

Since it has become apparent that the source of the sediment formation is the excess PE, and because of the many problems associated with its crystallization and growth in this viscous solution, it was decided to perform a certain number of runs in which crash cooling was carried out in an attempt to deplete the solution from its supersaturation. Such runs as 34, 35, 55, 56, 57 and 58 were performed, their production conditions were presented in Appendix 2, and the centrifuge test results were given in Tables 9.10 and 9.11. From these results the following points were deduced,

- a. Runs 34 and 55 products were very stable, and very little or no sediment formation was obtained during storage at 90°C and 120°C. Run 35 product was also stable although slightly more sediment was formed during storage at 120°C.
- b. Runs 56 and 57 products showed a much higher sediment level increase than those of runs 34, 35 and 55 products. The reason for this is not very clear but it is thought that the increased reaction time in runs 56 and 57 to 1.25 hr, compared to 0.33 hr, 0.37 hr and 0.5 hr in runs 34, 35 and 55, might have been responsible for this increased level of sediment formation because of two effects, namely, a higher viscosity

product was obtained, and also it might be possible that equilibrium was not attained at the reaction temperature in as short a period as 0.5 hr, so possibly more PE dissolved when the reaction time was increased to 1.25 hr, hence causing a higher supersaturation at later stages and a higher level of sediment formation. This assumption implied that not all the PE crystals were dissolved in solution at the reaction temperature of 180°C, which in fact will be shown to be the case in a later section.

The results given in Table 9.11 indicate very clearly that the products obtained with crash cooling rates were much more stable than those obtained in other runs with similar production conditions (apart from the cooling rate). It would be very interesting to investigate the effect of combining crash cooling, and leaving the reaction mixture at filtration temperature for an extended period of time. Crash cooling proved very successful because it was an important way to deplete the solution from its supersaturation, since the growth of PE crystals was probably very slow due to the presence of formaldehyde as a trace impurity^(112,113) (see Section 3.6 in Chapter 3). This success indicates very strongly that the source of the sediment formation is the presence of the excess PE in solution and not a back reaction, it also supplied us with a very good method for overcoming the problem of sediment formation at storage.

Apart from crash cooling, the effect of the mixing rate during the cooling stage was investigated. Runs 58, 59 and 60 were carried out using a very low stirrer speed compared to other runs (see Appendix 2), and the centrifuge test results for their products were presented in Table 9.12. These results show clearly that all three products gave rise

to sediment formation at storage even though crash cooling was used in run 58, and that the highest sediment level obtained was in run 59 product compared to runs 58 and 60 products. The reason behind this was probably because in run 59 two factors were combined namely, a slow cooling rate, and a longer reaction time of 1.25 hr, which caused an increased product viscosity and also probably more dissolved PE at the reaction temperature (as was explained above). The increased level of the sediment formation due to the reduction in stirrer speed suggests that the crystallization process is partly a diffusion process^(69,92). although this increase in the sediment level was not as bad as was expected for a completely diffusion controlled crystallization process.

The effect of seeding was also investigated. PE seed crystals were added during the cooling stage of run 52 (see Appendix 2), and the centrifuge test results were presented in Table 9.10. These results show that there was a high level of sediment formation at 90°C storage temperature, and seeding in no way reduced (if not increased) the sediment formation. This result was not easy to understand at first, but became clear when it was found out that not all the PE crystals were dissolved in solution at the reaction temperature of 180°C, which meant that seed crystals were already present when cooling was started.

The solubility of pentaerythritol in many organic solvents is quite low, Berlow et al.⁽¹⁾, presented many tables for its solubility in different organic solvents. The evaluation of the solubility of PE in the reaction mixture is not an easy task because of the reaction involved, but this evaluation must be carried out if quantitative analysis for the crystallization process is to be performed since the driving force of crystallization is related to the supersaturation which is the difference

between the actual amount of the dissolved PE and the equilibrium (solubility) value at that temperature. Optimization techniques may be used in such an evaluation, but in any case this was not part of this research project. An approximate value for the solubility of PE in the dilution oil was thought to be a useful thing to have, and it was decided to try and evaluate this value approximately using the available equipment at first. Because of that it was decided to use the residue weight method even though this method is normally used for high solubility materials. The results obtained were surprisingly consistent with each other and were correlated by a smooth curve given in Figure 9.13. The zero value of the solubility calculated at ambient temperature was not included in the plot because an extrapolation of the curve shows that the expected solubility at temperatures below about 80 to 85°C, is zero. These values of the solubility are the highest obtainable with these calculations because it was assumed that the losses of PE crystals were negligible.

11.10 Discussion of the Ultra-Centrifuge Results

Because it has become clear now that the source of the sediment formation at storage was the excess PE present as very fine dispersed particles or/and as soluble PE present in the supersaturated solution, it was decided to use the ultra-centrifuge as a means of deciding between these two possibilities. A list of the samples tested by the ultra-centrifuge (and also by the NMR and IR spectroscopy afterwards), is given in Chapter 9, Section 9.4; these samples were ultra-centrifuged at a speed of 30,000 r.p.m. for three hours. Small amounts of sediment were obtained at the end of the test in practically all the samples in varying degrees. Very little (just a shadow of) sediment was obtained with samples number 6 and 7 compared to the others, while sample number 5 gave rise to a much larger sediment level (see the sample list in Section 9.4).

Even the Fawley batch sample which was stored at ambient contained small amounts of sediment. The problem was that there was no quantitative way of knowing what the sediment level was in these samples. These results suggest the possibility that some of the excess PE could well be present as very fine dispersed colloidal particles, which cannot be detected by the normal centrifuge test method used in the analysis because of the much lower centrifugal force. Colloidal particle sizes normally range from $1 \mu\text{m}$ to $10^{+3} \mu\text{m}$ and cannot be retained by the conventional filter papers. Particles of colloidal dispersions have a tendency to aggregate. Encounters between these particles occur frequently as a result of Brownian motion, and the stability of the dispersion is determined by the interaction between the particles during these encounters^(162,163). The attraction forces between the particles are normally of the Van der Waals type, whereas the repulsion forces are due to electrostatic interaction between the electrically charged surfaces of the particles, at the same time the particle-solvent affinity (solvation) can play a big role in stabilizing the colloid dispersion in lyophilic (liquid loving) systems^(162,164). Also, the adsorption of polymeric material on to the particle surfaces will usually promote stability through increased particle-solvent affinity. In any case it can be seen that the aggregation of the particles depends largely on the collision rate of these particles, also particles repelled from one another must possess sufficient kinetic energy to overcome this repulsion, hence, although these colloid dispersions may be stable at ambient temperature, they will lose their stability at higher temperatures, and the particles will aggregate causing an increase in the particle size, and separates out when this size becomes sufficiently large^(162,163).

Since there was no quantitative way of measuring how much of the excess PE was present as colloidal particles, and visually it seemed that the sediment obtained using the ultracentrifuge was much less than that obtained after storage at higher temperatures, it was concluded that, although some of the excess PE could be present as colloidal particles, this was not the complete answer, and the rest of the excess PE could well be present as soluble PE in the supersaturated solution.

An attempt was made to try and photograph some of these fine particles using an optical microscope, and some of the results are presented in Appendix 11. These photographs are not very good because it was very difficult to focus on sediment in the oil sample, especially when the sediment was not stationary, also the presence of air bubbles made things even worse. But even though there were a lot of difficulties, certain points became apparent, and they are,

- a. Although the centrifuge test results of most of the product samples showed that the sediment levels were very low in these samples, these photographs showed that there was some sediment in practically all the samples, with runs 33, 52 and 59 product samples containing more than any of the rest, some of these particles were quite large, up to 13 μm or even more, which were not of colloidal dimensions. If such large particles existed in the product samples, then it is very probable that much smaller particles of colloidal dimensions existed also in these samples, which were not detected by the optical microscope due to their smaller dimensions. Other techniques, such as light scattering and dark field microscopy, are needed in the study of colloidal suspensions^(162,164).

- b. The sediment obtained in the reheated product sample of run 33, Figure All.3, was much finer and much less than that obtained for the product of the same run, presented in Figure All.2.
- c. There was also some sediment obtained in run 55 product sample, Figure All.5, even though the product of this run was very good and showed very high stability during storage at higher temperatures. The sediment shown in Figure All.5 is different from those obtained for the other runs, in that it is being very fine compared to the rest, which is expected due to the crash cooling rate used during the preparation of run 55 product.

11.11 Discussion of IR Spectroscopy Analysis Results

In an attempt to evaluate whether or not there is any chemical change in the product sample associated with the formation of the sediment at storage, the same list of samples given in Section 9.4 was analysed using the Nuclear Magnetic Resonance (NMR) technique. Although the results obtained indicate that there was no chemical change in the product associated with the sediment formation, but it was suggested that a small chemical change in the product, say less than about 10%, may not be detected by the NMR technique, while it may be detectable by IR spectroscopy analysis. Hence the same samples were analysed again, using IR spectroscopy and the IR traces were presented in Figures 9.5 to 9.12. In formulating these IR traces the smeared film method was used rather than the constant cell method due to the difficulties associated with the latter which were discussed in Section 10.2 in Chapter 10. Because of that it was difficult to reach definite conclusions from this analysis, especially since we were dealing with small changes. But by studying these traces and concentrating

on, the hydroxyl group at $WN\ 3400\ cm^{-1}$, the ester group at $WN\ 1730\ cm^{-1}$, the anhydride group at $WN\ 1780\ cm^{-1}$, and the ether groups at $WN\ 1100$ and $1170\ cm^{-1}$, it was possible to notice the following points:

- a. There was no change in the Fawley batch after long storage periods at ambient or at $50^{\circ}C$ (Figure 9.5), but as the storage temperature increased to $90^{\circ}C$ and $120^{\circ}C$, a slight decrease in the anhydride and the hydroxyl groups, with a slight increase in the ester and ether groups was noticed, Figures 9.6 and 9.7. This does not necessarily mean that there is a back reaction, but it may very well mean that the esterification and etherification reactions are still going on at very slow rates, during the higher temperature storage. This conclusion was reached before and was discussed before in Section 11.2.
- b. Run 33, product and reheated product samples are slightly more reacted products with higher ester content than the Fawley batch, Figures 9.8 and 9.9.
- c. From Figure 9.10 it can be seen that run 31 product sample is very much less reacted than the Fawley batch sample, with much lower hydroxyl and ester contents and higher anhydride content. This may well be the reason for the lower hydroxyl number obtained for this batch, and so, longer reaction time period may present a solution to this problem.
- d. A comparison between run 33 product and run 33 reheated product samples given in Figure 9.12 indicate that there is very little detectable change between the two samples apart from the slightly increased ester content of the run 33 reheated product sample, while the centrifuged test results showed that there was a very big difference between their

stability at higher temperature storage (see Section 11.7).

From these results and also all those discussed in the previous sections of Chapter Eleven it is concluded that the source of the sediment formation is not a back reaction but is the excess unreacted PE, partly present as very fine particles not separated during the filtration stage, while the rest is present as soluble PE in the supersaturated solution. But the centrifuge test results obtained from diluting the product samples with n-heptane, and chlorobenzene, which were discussed in Section 11.3, indicate clearly that this supersaturation was stable even though the solvent addition was expected to reduce it, and cause some sediment formation at ambient temperature. Additional energy, supplied by the higher storage temperatures, was needed to reduce this supersaturation, which is an indication of the strong interaction between the PE and the solvent. Boistelle⁽¹⁶⁵⁾ in his study of 'crystal growth from non-aqueous solutions' discussed the types of solvent and of the solute and the strong solvent-solute interactions that can exist between them. Hydrogen bonding between the solute and the solvent can play a big role in increasing the solubility of the solute^(165,166,167,168). Hydrogen bonding occurs between a proton donor group A-H and a proton acceptor group B, where A is an electronegative atom such as O, and the acceptor group is a lone electron pair of an electronegative atom^(166,167). The O-H group is a strong proton donor and can form hydrogen bonds with a very large range of compounds including carboxylic acids and their derivatives⁽¹⁶⁷⁾. Because of that the existence of such hydrogen bonds between PE, which contains four of these O-H groups, and some of the compositions of the reaction mixture is very likely. These bonds are much weaker than the normal chemical bonds, having strengths ranging between 1 to 10 Kcal/mole, $1/10$ to $1/50$ as strong as the more familiar chemical bonds^(166,167). Hence although these bonds are stable at ambient temperature, they become

unstable and break down at higher storage temperatures causing the formation of the sediment and the precipitation of the PE. More work needs to be done in future research in studying this possibility using the usual techniques of IR spectroscopy or Raman spectroscopy^(166,167).

11.12 Discussion of Crystal Size Distribution (CSD) Results

Continuous crystal size distributions (CSD) are normally represented by a continuous one-dimensional distribution function. The most widely used distribution functions are, the normal, the log-normal, and the gamma-type distribution functions, all with two adjustable parameters that characterise the distribution completely^(50,169). As an example, the normal distribution is given by,

$$f(L) = \left[\frac{1}{\sigma} (2\pi)^{\frac{1}{2}} \right] \exp \left[-(L-\bar{L})^2 / 2\sigma^2 \right] \quad (11.1)$$

the two parameters of the distribution are σ , and \bar{L} , given by

$$\sigma^2 = \int_{-\infty}^{\infty} (L-\bar{L})^2 f(L) dL \quad (11.2)$$

and

$$\bar{L} = \int_{-\infty}^{\infty} L \cdot f(L) dL \quad (11.3)$$

Although the normal distribution is widely used in engineering science but it is of little use in describing particle-size distributions simply because these distributions are typically very asymmetric and are poorly represented by the normal distribution, also it predicts finite crystal populations for negative values of the size coordinate L. These

difficulties are overcome by the use of the log-normal distribution, which is not symmetric about the mean but in fact skewed towards larger sizes, and also there is no problem associated with negative values of the size L . The log-normal distribution is very useful and often used for representing particle size distributions in crystallization and precipitation processes⁽¹⁶⁹⁾.

By the use of these distribution functions, the total crystal mass and the total crystal surface area can be calculated in any characterised system, as an example let $n(L)$ be the distribution function representing the crystal population about a size L for values of L in $(0, \infty)$. Further let $n(L)$ be the number of particles per unit volume of solid-free liquid, then $n(L)$ is defined as the population density of the particles in the system. If these particles are assumed to be geometrically similar, then the weight of each particle (m_s) is given by,

$$m_s = \rho k_v L^3 \quad (11.4)$$

where ρ is the density and k_v is a volumetric shape factor for the particles. The change in the total mass M with the size L is given by the differential equation

$$dM = \rho k_v L^3 n(L) dL \quad (11.5)$$

and so

$$M_T = \rho k_v \int_0^{\infty} L^3 n(L) dL \quad (11.6)$$

where M_T is the total crystal mass. Similarly for the total surface area of the crystals,

$$dA = k_a \cdot L^2 n(L) dL \tag{11.7}$$

and so

$$A_T = k_a \int_0^{\infty} L^2 n(L) dL \tag{11.8}$$

where k_a is the area shape factor, and A_T is the total surface area of the crystals (or particles)⁽¹⁶⁹⁾.

By substituting the given distribution function for $n(L)$ in equations (11.6) and (11.8), the total crystal mass and surface area can be evaluated by numerical integration (or area calculation). If on the other hand the distribution function is to be evaluated from sieve size analysis, the measured sieve equivalent diameter (second largest crystal dimension) is converted to the equivalent volume diameter, using the appropriate shape factor, the mass-size data are then fitted to the required empirical distribution for $n(L)$ in equation (11.6), using computer optimization techniques, to yield the two parameters of the distribution, the mean \bar{L} , and the standard deviation σ for a normal distribution, or the geometric mean and geometric standard deviation for a log-normal distribution⁽¹⁶⁹⁾.

The above quick outline is presented to indicate the procedure normally used in evaluating the two parameters of the CSD that fits the size analysis data obtained experimentally. In this research project such detailed size analysis and distribution model fitting was not required or needed, and the above procedure was not followed. The evaluation of the mean and the standard deviation of the final distribution can be very much simplified by assuming discrete distribution functions instead of continuous ones. In such a case, the arithmetic, mass weighted, mean equivalent diameter $\bar{\mu}$ can be evaluated from the expression⁽³⁴⁾

$$\bar{\mu} = \sum_{\text{all } i's} \mu_i \cdot f_i$$

and the standard deviation σ from the expression

$$\sigma^2 = \sum_{\text{all } i\text{'s}} (\mu_i - \bar{\mu})^2 \cdot f_i$$

where μ_i is the arithmetic mean of the size band, and f_i is the mass fraction in the band. This type of size analysis was performed and was assumed to give a good representation to the crystal size distribution obtained for the final sediment. Certain other assumptions were made in the CSD analysis performed in Section 9.6, a discussion of these and of the results obtained is given below,

- 1 - The sieve arrangement was assumed to be conforming to BS 410⁽¹⁴⁸⁾, and the ratio of aperture sizes on consecutive sieves was $2^{\frac{1}{4}}$. This assumption was true except that one sieve, of mesh No. 14 and nominal aperture 1204 μm was missing from the series.
- 2 - The average value of the ratio of (d_s/d_p) found experimentally was 1.33. This value agrees very well with the theoretical value of 1.34 calculated in Appendix 7. A value of 2.0 was also tried in carrying out another set of calculations but it did not make a big difference in the results of the final CSD, probably because of the low weight percentage of the fine crystals fraction.
- 3 - In combining both distributions, obtained by sieve and laser analysis, an assumption was made, that the rate of change of crystal mass with size $(\Delta M/\Delta L)$ in the laser size range of 157.5-73 μm was constant. Although this assumption is not strictly true but the error introduced was not high

since it was only used to calculate the crystal mass between 157.5 to 150 μm and between 75 to 73 μm , while the rest of the crystal mass between 150 to 75 μm were left as it was.

- 4 - At first the CSD analysis was carried out for twelve runs only, 34, 35, and 51 to 60 inclusive. These runs covered a very large range of production conditions (see Appendix 2), and the results obtained were presented in Table 9.28. These results show that the mass weighted mean diameter $\bar{\mu}$ values ranged between 400 μm to 550 μm in all the runs, no matter what production conditions were used. Also the values of $\bar{\mu}$ obtained for runs 34, 35, and 55 sediment were higher than those for runs 51, 52, 53, and 54 sediment, even though the formers were performed using a very high cooling rate which should result in the formation of a large number of small nuclei, leading to a lower value of $\bar{\mu}$. Because of these and other factors which were discussed before, like the failure in using seed crystals, it was suspected that some of the PE crystals did not dissolve at 180°C and existed as solid particles in suspension. Hence runs 61 and 62 were carried out. In these two runs the reactants were kept at the reaction temperature of 180°C for 0.5 hr, and 1.25 hr respectively, then the reactants were filtered at 180°C, in both runs, without allowing the mixture to cool down. The results obtained for these two runs were also presented in Table 9.28. These results are very astonishing, and they very clearly indicate that there are a lot of undissolved PE crystals

present at 180°C. The values obtained for $\bar{\mu}$ for runs 61 and 62 of 619.6 and 626.8 μm are very much higher than all the other values of $\bar{\mu}$, this indicates that the main source of the large PE crystals obtained in the final sediment was the undissolved PE present, and not nucleation and subsequent crystal growth.

- 5 - From the results of runs 55, 56 and 57 it can be seen that as the reaction time was increased from 0.5 hr in run 55 to 1.25 hr in runs 56 and 57, the per cent weight of the fine crystals in the final sediment increased appreciably, which may indicate that more PE must have dissolved due to the increased reaction time. This PE crystallized out as very fine crystals, causing a drop in the value of $\bar{\mu}$ and a slight increase in the value of the standard deviation σ .
- 6 - From the results of runs 58, 59 and 60, it can be seen that the reduction in the stirrer speed from 700 r.p.m. in previous runs, to 100 r.p.m. in these runs caused a high increase in the value of the mean $\bar{\mu}$. This may indicate the presence of a lot of crystal attrition and secondary nucleation due to the high stirrer speed of 700 r.p.m. in the other runs, which would result in the lower values obtained for $\bar{\mu}$. Secondary nucleation and crystal attrition were discussed in detail in Section 2.4.2.3 in Chapter Two. The very high value of $\bar{\mu}$ obtained in run 60 is due to the lower stirrer speed, while the slightly lower value of $\bar{\mu}$ obtained in run 59 could be due to the increased reaction time, and finally the still lower value of $\bar{\mu}$ for run 58 may well be due to the much higher cooling rate used (see Appendix 2 for production condition).

7 - It was very difficult to reach a clear cut conclusion about the effect of these crystal size distribution results on the filtration rate because the filtration rate was very sensitive to the filtration temperature, due to its effect on the viscosity of the filtrate. Keeping this temperature constant and the same for all the runs proved to be very difficult even though a proportional temperature controller was used to control the temperature. It is very possible that the filtration rate is much more sensitive to changes in temperature and viscosity than to the small changes obtained in the values of the mass mean diameter $\bar{\mu}$, and hence the effect of these changes in $\bar{\mu}$ are effectively masked and overshadowed by the other effects of viscosity and temperature. But generally it can be said that the larger the value of $\bar{\mu}$, the higher is the filtration rate. It must also be mentioned that it is important to keep the initial filtration pressure very low, and then let it build up very gradually, otherwise the holes of the filter paper will be plugged very soon and the filtration rate will drop very sharply, which was what happened in run 35.

Different techniques are used in industry to improve the filtrability of the PIBSA/PE esterification products. One such important technique is to wash the raw PIBSA/PE dispersant product with water⁽¹³⁷⁾. In this method, a water soluble organic solvent, such as pyridine, or methylisobutyl ketone, may be added to the water to promote contact between the water and the insoluble matter. The organic solvent can also be added during the esterification stage

and may be retained in the crude ester composition. The raw dispersant product is then washed thoroughly with water, which is believed to cause the aggregation of the finely divided pentaerythritol crystals to a readily filterable size. This water is then removed, before filtration, by vacuum stripping. More than 1000% increases in filtration rates were obtained by washing the raw dispersant products with water using the above technique⁽¹³⁷⁾.

- 8 - In the calculations of the parameters of the final CSD, $\bar{\mu}$ and σ , it was assumed that the distribution functions were discrete to simplify the calculations. Randolph⁽¹⁶⁹⁾ showed by mathematical treatment that these parameters can be obtained from the cumulative particle size distribution plots for normal and for log-normal continuous distributions. He showed mathematically that for a normal distribution

$$\bar{L} = L_{0.5} \quad (11.9)$$

and

$$\text{C.V.} \equiv \sigma/\bar{L} = (L_{0.841} - L_{0.159})/2L_{0.5} \quad (11.10)$$

where C.V. is the coefficient of variation of the distribution, and $L_{0.5}$, $L_{0.841}$ and $L_{0.159}$ are the aperture sizes corresponding to 0.5, 0.841 and 0.159 fractions of the material passing through the sieves respectively, and can be obtained easily from the cumulative particle size distribution plots.

For a log-normal distribution he showed that

$$\bar{L}' = L_{0.5} \quad (11.11)$$

and

$$\sigma' = L_{0.841}/L_{0.5} \quad (11.12)$$

where \bar{L}' and σ' are the two parameters of the log-normal distribution. The crystal size distribution results from run 34, presented in a graphical form, are given in Figures 9.14 and 9.15. Also, in Appendix 10, the graphical representation of the CSD results for a chosen number of runs are given. From these plots it can be seen that the normal and the log-normal distributions do not seem to fit these experimental results. But if such an assumption is made, then the cumulative under size fraction plots presented, can be used to find the two parameters of the continuous distributions, using either equations (11.9) and (11.10) or (11.11) and (11.12).

- 9 - Photographs of the sediment obtained from different runs were taken using the electron microscope at Esso Research Centre in Abingdon. These photographs, which are presented in Appendix 12, were examined to check the effect of different production conditions on the PE crystal habit obtained, and to relate that, if possible, to the effect on the filtration rate. They show that the fine sediment obtained in practically all the runs consists mainly of thin square plates which are probably the cause of the bad filtration. These PE platelets are very difficult to grow because of the presence of formaldehyde as a trace impurity in the technical grade PE used^(112,113), and also because of the difficulties associated with growing fine crystals^(81,82,83,85,86), which were discussed in detail in Section 2.4.2.3.1 of Chapter Two.

The photographs of the large crystals of run 51 presented in Figures A12.5, A12.6, A12.7 and A12.8 show that the growth process is being carried out by the deposition of layer after layer of the solute on the surface of a large PE crystal. This type of growth is not shown by run 33 large crystals or run 59 large crystals presented in Figures A12.2 and A12.18 respectively; this may be due to the much longer time given in run 51 for the crystal growth process. The fine crystals of run 59 sediment, presented in Figure A12.17, is much larger than those obtained in other runs probably due to the much lower stirring speed used in run 59, and the same applies to its large crystals given in Figure A12.18. Finally, Figures A12.21 and A12.22 for the sediment obtained during storage and collected from the centrifuge tubes indicate that this sediment is much finer than that obtained at the end of each run and it also consists mainly of very thin plates. The sediment obtained during storage is finer, probably due to the higher viscosity of the product because of the lower temperatures used for storage.

CHAPTER TWELVE

CONCLUSIONS AND SUGGESTIONS FOR FUTURE WORK

In this chapter the main conclusions deduced from the reaction kinetic study, and the sediment formation investigation are presented separately. The successfully tested methods for the elimination of the sediment formation are also reported together with matters worthy of future investigation.

12.1 Conclusions of the Reaction Kinetic Study

- 1 - The mechanism of the PIBSA/PE esterification reaction is very complex, but the rate of the reaction can be approximated by the following rate expression

$$\underline{(-r_A) = (r_T) = k \cdot C_A^a \cdot C_B^b = k_o \cdot e^{-\frac{E}{RT}} \cdot C_A^a \cdot C_B^b .}$$

- where: $(-r_A)$ = the rate of conversion of PIBSA to esters
 (r_T) = the rate of formation of the esters
 k = the rate constant of the reaction
 k_o = the frequency factor
 E = the activation energy of the reaction
 a = the order of reaction with respect to PIBSA
 b = the order of reaction with respect to PE
 n = $a+b$ = the overall order of reaction
 R = the universal gas constant
and T = the absolute temperature

- 2 - The dependence of the reaction rate on PIBSA concentration C_A is much more pronounced than on PE concentration C_B . The values obtained for the constants a , b and n are:

$$\underline{a = 1.465}, \quad \underline{b = 0.149}, \quad \underline{n = 1.614}.$$

- 3 - The values obtained for the activation energy of the reaction and for the frequency factor are,

$$\underline{E = 7.767 \text{ kcal./gmole}}, \quad \underline{k_o = 15312}$$

- 4 - The values of the rate constants obtained at 200°C for the two different catalyst ratios used, are as follows:

a - a catalyst ratio of 1.18% by wt. on PIBSA, the catalyst type is that containing 70% A.I.

$$\underline{k = 3.907 \text{ (equivalent/dm}^3\text{)}^{1-n} \cdot \text{hr}^{-1}}$$

b - a catalyst ratio of 2.2% by wt. on PIBSA, the catalyst type is that containing 90% A.I.

$$\underline{k = 5.545 \text{ (equivalents/dm}^3\text{)}^{1-n} \cdot \text{hr}^{-1}}$$

- 5 - Infra-red spectroscopy analysis was used successfully in the kinetic study. The values of n and a obtained by IR analysis for the PIBSA/PE reaction are as follows:

$$\underline{n = 1.522}, \quad \underline{a = 1.283}$$

these values agree very well with the values given above, which is a further support for the previous analysis.

- 6 - A maximum value for the hydroxyl number does seem to exist at a value of a Total Acid Number (TAN) between 6.0 to 7.0 mgkoH/g, and a target value for the product TAN of about 6.5 mgkoH/g is justified.

- 7 - It is very likely that higher potency products are produced when higher ratios of PE to PIBSA are used in the esterification reaction.

12.2

Conclusions of the Sediment Formation Investigation

- 1 - The sediment obtained at the end of the reaction stage, and also that formed during the storage of the dispersant product is mainly mono-pentaerythritol with very small amounts of di-PE, and traces of tri-PE.
- 2 - There is very little or no increase in the sediment level during storage of the product at ambient temperature, or at 50°C, while there is a very much higher level of sediment formation during storage at 90°C and 120°C.
- 3 - There is no increase in the sediment level during storage at 150°C, in fact sediment level is stabilised, and subsequent storage at different temperatures does not cause any increase in the sediment level. This stabilisation during the storage at 150°C is accompanied by a slight reduction in the viscosity which may be due to a side reaction involving pentaerythritol.
- 4 - There was little or no sediment formation during storage at ambient temperature and 50°C of product samples diluted with n-heptane and chlorobenzene, while the sediment formation was much higher at 90°C storage temperature. This leads to the conclusion that the sediment formation is not a viscosity dependent process but very much a temperature dependent process. The sediment formation increases with storage temperatures up to a temperature of about 120°C.
- 5 - Dispersant products produced at lower reaction temperatures as low as the filtration temperature are very stable during storage and show no sediment formation at high storage temperatures.

- 6 - It is concluded that the cause of the sediment formation during the storage of the product is not a back reaction, but is the presence of the excess unreacted pentaerythritol, partly present as very fine thin plates not separated during the filtration stage, while the rest is present as soluble PE in the supersaturated solution. This supersaturation is stable due to the strong interaction between the pentaerythritol and the reaction mixture. It is very probable that hydrogen bonding between the pentaerythritol and some of the compositions of the reaction mixture is responsible for this strong interaction. At higher storage temperatures the hydrogen bonds are broken causing the precipitation of PE and the sediment formation.
- 7 - The pentaerythritol crystal growth process is partly surface integration controlled and partly diffusion controlled. It is very probable that the presence of formaldehyde as a trace impurity in the technical grade pentaerythritol used is responsible for the slow growth process^(112,113) with the result that a lot of very fine PE crystals are obtained at the end of the cooling stage.
- 8 - Approximate values for the solubility of pentaerythritol in the dilution oil were estimated at different temperatures; these values are presented in Table 12.1 below:

TABLE 12.1

The approximate solubility of PE in the dilution oil

Temperature °C	Approximate solubility of PE in the dilution oil g/100g
160	0.114
140	0.067
100	0.014
25	0.000

- 9 - From the crystal size distribution results it is concluded that,
- a - a lot of undissolved pentaerythritol large crystals exist in the reaction mixture at 180^oC. These crystals are the source of the large PE crystals obtained at the end of the cooling stage.
 - b - a great deal of crystal attrition and secondary nucleation takes place during the cooling stage due to the high stirring rate resulting in a large number of very small nuclei not capable of growth and hence causing a large drop in the filtration rate.
 - c - most of the pentaerythritol which crystallizes out from the solution is obtained as very thin square like plates. These plates are responsible for the bad filtration characteristics exhibited by the PIBSA/PE dispersants in general.
- 10 - There are other conclusions concerning the sediment formation at storage and its elimination, these are presented in the following section.

12.3 Suggested Methods for the Elimination of the Sediment Formation

The following methods for the production of the PIBSA/PE dispersant were tested very successfully in the laboratory, the products obtained were stable during storage at higher temperatures and gave rise to little or no sediment formation.

- 1 - By using very fast cooling rates, up to 4.5^oC/min (crash cooling), during the cooling stage of the production. This would help to deplete the solution from its super-saturation very effectively.

- 2 - By keeping the reaction mixture for an extended period of time at the filtration temperature, prior to filtration, for up to 65 hrs. This extended period of time helps in letting the viscous solution approach equilibrium conditions.
- 3 - By reheating the dispersant product for a second period, for up to 2 or 3 hrs at the reaction temperature, to react all the excess PE present.
- 4 - By performing the production using the lowest allowable reaction temperature that would result in a potent dispersant product.

A combination of any two or more of these methods would even be more effective in producing very stable dispersant products during high temperature storage.

12.4 Matters Worthy of Future Investigation

The following points are thought to be worth investigating in future research.

- 1 - The development of a more comprehensive rate expression, based on a detailed kinetic study involving the main steps of the PIBSA/PE reaction mechanism. This would involve the determination of the relative amounts of the different formulas suggested by the reaction, by the use of the different available spectroscopic techniques. In such a detailed study, variations in the starting PIBSA concentration, as well as for that of the PE are required; this would even give a much clearer picture as to the real meaning of the value of the residual TAN, (TAN^{∞}), obtained at the end of each kinetic run.

- 2 - Investigation of the changes that are taking place at higher storage temperatures, especially at 150°C, since this would give a clearer insight to the problem of the sediment formation and its elimination. Spectroscopic techniques can be used in following these changes in the product at different intervals of time.
- 3 - More work needs to be carried out to evaluate properly the possibility of using a low reaction temperature, as low as the filtration temperature, in producing the dispersant product, since such products were found to be very stable during high temperature storage.
- 4 - More investigation work needs to be carried out in determining the optimum conditions needed to produce stable dispersant product by reheating the product for a second period of time to react the excess PE present.
- 5 - The evaluation of the solubility of pentaerythritol in the reaction mixture by using indirect methods, such as optimization techniques.
- 6 - Investigation of the possibility of the presence of some of the excess PE as very fine stable colloidal particles, by special techniques such as light scattering, and dark field microscopy.
- 7 - Investigation of the possible presence of hydrogen bonding between pentaerythritol and some of the compositions of the reaction mixture, using infra-red and Raman spectroscopy.
- 8 - When the solubility of pentaerythritol in the reaction mixture is determined, and when a more comprehensive rate expression is developed, then it becomes worthwhile to

investigate the crystallization characteristics of PE in the reaction mixture quantitatively by formulating nucleation and crystal growth models and evaluating their parameters experimentally.

APPENDIX 1

PRODUCTION OF PIBSA/PE DISPERSANT AT FAWLEY

during the period 6-10/8/82

BATCH No. 2610

Esterification stage

The esterification stage of the Fawley run was started on 6/8/82. This particular run being observed and monitored by the author. The production of the dispersant was carried out in the normal manner as shown in Chapter Four. Detailed material balances and production conditions are not presented here because it is proprietary information. Heating of the reactants started at the end of the pentaerythritol charge addition and samples were taken every hour from D114 to be analysed for Total Acid Number (TAN) and kinematic viscosity (KV). Cooling of the reactants from the reaction temperature to filtration temperature was started when the TAN reached the required value and four oil increments were carried out at different times during this cooling stage to speed up the cooling process and to bring the oil dilution to the required level before filtration. The results of the analysis for kinematic viscosity carried out on the hourly samples taken from D114 are given below in Table A1.1. The viscosity results were plotted against time and the profiles obtained are given in Figure A1.2 and A1.3.

Filtration stage

Filtration started on the morning of 8/8/82. F13 was precoated first with S.S.F. filter aid. Table A1.2 gives some of the details of the first filtration run which was treated as representative of the other filtration runs that followed. Also the actual volume of filtrate in the run down tank TK 128 had to be related to the level % so that

filtration rate plots can be obtained. This was done by measuring the actual level using a dip gauge and then calculating the actual volume from the calibration of the tank. Three such measurements were made, at the beginning of the run, middle and towards the end of the run; details of which are not presented here (together with some of the details of Table A1.2) because it is proprietary information.

Combining this data with that given in Table A1.2 we obtain Table A1.3 which contains the filtrate volume and filtration rate calculated at half hour intervals over the first filtration run. By plotting these data against time Figure A1.4 and Figure A1.5 were obtained.

Discussion of results obtained

Since details of the material balance and production conditions for the dispersant are not presented in this appendix, the discussion concerning them will also be omitted.

1. When the required end point of the reaction was reached, cooling of the reactants commenced. During the early stages of the cooling period the mixer of D114 was stopped. This may have had a large effect on the crystallization process of PE because diffusion becomes an important process in the growth of crystals from viscous mixtures, ^(69,92) hence mixing becomes an important factor in such processes.
2. To speed up cooling of material in D114 and to help mixing, the circulation around D114 via the fin atmospheric cooler using the bottom pump was kept on until a much later stage in the cooling period (Figure A1.1). This might have helped mixing but it might also have had the effect of breaking down crystals when passing through the pump due to the high impeller speed, and hence causing secondary

nucleation which was not desirable^(74,170,171,172). This combination of points (1) and (2) may have had the effect of causing a large number of very small crystals to be present, hence reducing the filtrability of the material to a large extent.

3. Filtration temperature had a big effect on filtration rate because of its effect on viscosity of the material, and since the only heat input to the filter was from the material in D114 flowing through the filter. So when filtration rate dropped due to build up of cake the flow rate decreased causing the filter temperature to be reduced, hence viscosity increased causing filtration rate to drop still further... and so on. This chain effect together with the presence of a large number of small crystals can explain the fast deterioration in filtration rate from an initial value of about $6 \text{ m}^3/\text{hr}$ to about $2.0 \text{ m}^3/\text{hr}$ in one and a half hours, then finally to about $0.8 \text{ m}^3/\text{hr}$ in four hours as can be seen from Table A1.3 and Figures A1.4 and A1.5.
4. The results of the analysis for TAN (not presented in this Appendix) and viscosity carried out at Fawley were used for comparison with the results of the analysis carried out at Aston. It was found that there was a slight difference in viscosity measurement of the same sample. Three samples of different viscosities were tested and the discrepancy between Aston and Fawley viscosities were about 1%. This is slightly higher than the 0.7% value allowed by the test method ASTM D974-80 and can readily be attributed to the more advanced equipment at Fawley compared to Aston.

To compare the TAN measurements, the last sample in Table A1.1 (after 12.5 hrs cooling) of TAN 4.4 mg KOH/g was taken. A pH titration was carried out at Aston and a plot of pH vs. base volume was obtained. Using the inflection point as the end point, the TAN value calculated was exactly 4.4 which shows that pH titration results for TAN calculations carried out at Aston agrees very well with results obtained by potentiometric titrations carried out at Fawley.^(173d) However when phenolphthalein indicator was used, the TAN calculated was 5.5 which was very high and inaccurate.

At Fawley laboratories, 0.3% thymol blue in dimethylformamide solution was used as an indicator even when carrying out potentiometric titration,^(173d) and it was noticed that the colour titration end point coincided with the potentiometric titration end point. Because of this, the same sample was titrated again using the modified test method and using thymol blue solution as an indicator and a colour titration was carried out; the TAN obtained this time was 4.4. This indicates that the results obtained from colour titrations using thymol blue as an indicator are satisfactory and coincide with pH titration results. Since this was found to be the case and because colour titrations are much faster than pH titrations, they will be used in monitoring the reaction in the future preparation of PIBSA/PE dispersant on a laboratory scale at Aston.

TABLE A1.1

Samples taken and analysis results for kinematic viscosity.

Sample type and condition	Kinematic viscosity* $\text{m}^2/\text{S} \times 10^{-6}$ at 100°C
Just before PE addition	85.7
End of PE addition, at 145°C (start of heating)	205
1 hr since start of heating, at 151°C	316
2 " " " " " " 158°C	358
3 " " " " " " 165°C	446
4 " " " " " " 171°C	513
5 " " " " " " 177°C	606
6 " " " " " " 181°C (Holding at 181°C)	685
$\frac{3}{4}$ hr at 181°C , final temp. (Start of cooling)	752
2 hrs since cooling started, 172°C	696
4 " " " " " 163°C	590
6 " " " " " 155°C	485
12.5" " " " " 138°C	385

*SI unit of kinematic viscosity is m^2/s which is equal to 10^6 cst. Hence the values of the viscosity tabulated above are given in $\text{m}^2/\text{s} \times 10^{-6}$, which is equal to cst.

TABLE A1.2

First filtration run for Batch 2610 details and conditions.

Date : 8/8/82 Admix mixed from 02.30 hrs.
 Batch No. : 2610 to 04.45 hrs
 Filtration run No. : 1 Precoat mixed
 from 08.30 hrs
 to 09.40 hrs

Operation	Time	Filter Temp. °C		Filter Pressure (psig)		D114 Temp. °C	Filter Outlet Sediment Level Vol. %
		Inlet	Outlet	Inlet	Outlet		
Pre-coat							
Start	08.30	85	80	15	10	137	
Finish	09.40	125	120	20	10	137	<.01
Filtration							
Start	09.45	126	120	99	8	137	
0.25 hr	10.00	125.5	124	100	8	137	
0.5 "	10.15	126	122	102	6	137	<.01
1.0 "	10.45	128	120	102	4.5	137	
1.25 "	11.00	130	110	102	2	136	
1.75 "	11.30	129	108	102	2	136	
2.25 "	12.00	129	106	102	2	136	
2.75 "	12.30	129	103	102	2	136	
3.25 "	13.00	129	102	102	2	136	
3.75 "	13.30	127	100	102	3	136	
4.25 "	14.00	127	99	102	3	136	

TABLE A1.3

Filtration rates for successive increments of first filtration run.

Time	Time From Beginning of Filtration No. 1 hrs	Volume of Filtrate Collected m ³	Increment In Filtrate Volume m ³	Filtration Rate m ³ /hr
09.45	0	-	-	-
10.00	0.25	1.448	1.448	5.792
10.15	0.5	2.896	1.448	5.792
10.45	1.0	4.344	1.448	2.896
11.00	1.25	4.996	0.652	2.606
11.30	1.75	5.792	0.796	1.592
12.00	2.25	6.661	0.869	1.738
12.30	2.75	7.240	0.579	1.158
13.00	3.25	7.964	0.724	1.448
13.30	3.75	8.362	0.398	0.797
14.00	4.25	8.761	0.398	0.797

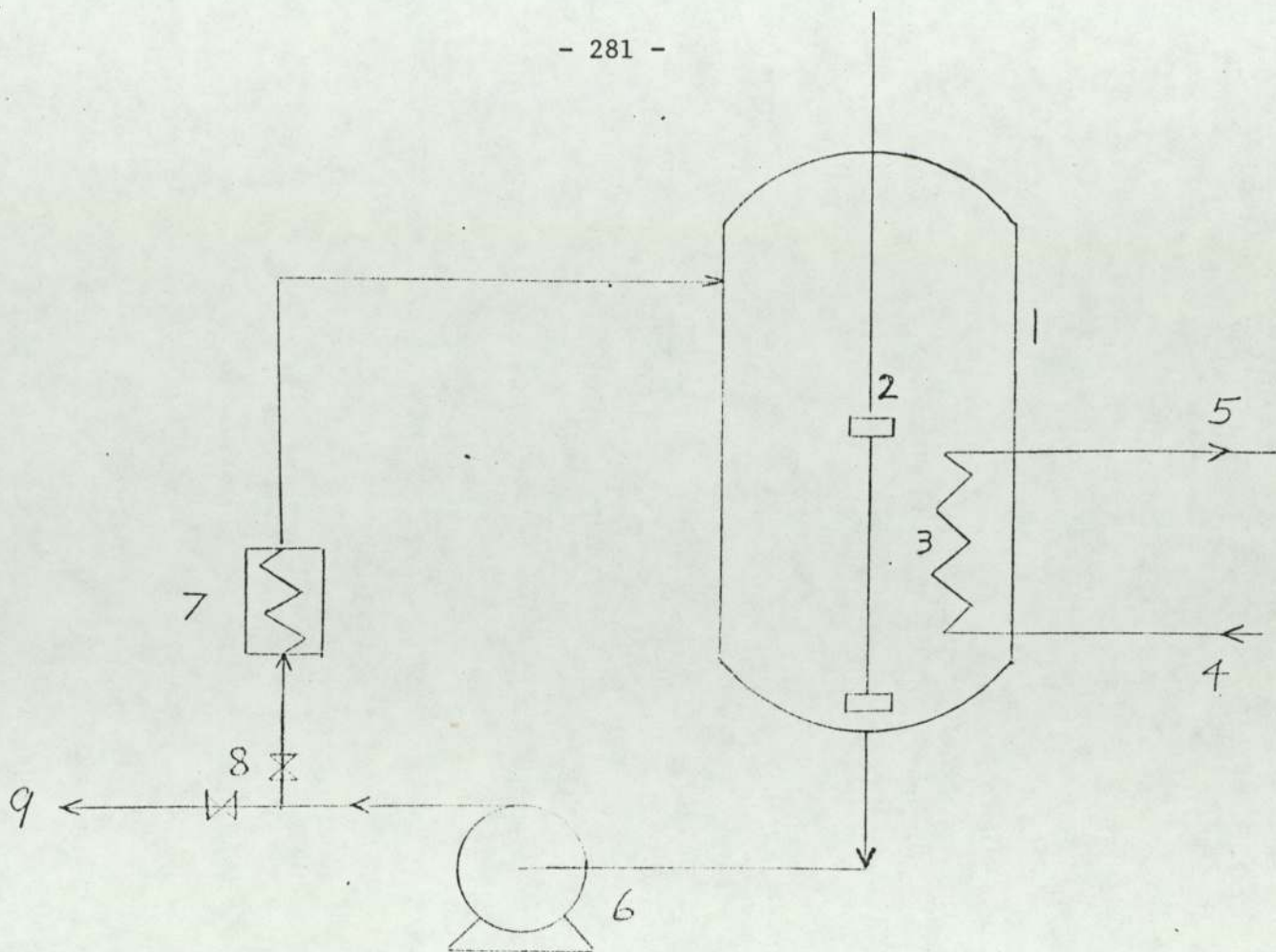


Figure A1-1- Schematic Diagram of Reactor Vessel and its Associated Pipework

- 1 - Reactor vessel D114
- 2 - Mixer
- 3 - Heating coil for hot oil circulation
- 4 - Hot oil from hot oil furnace
- 5 - Hot oil outlet to hot oil receiver
- 6 - Bottom centrifuge pump
- 7 - Atmospheric fin cooler
- 8 - Block valves
- 9 - To press and frame filter F.13

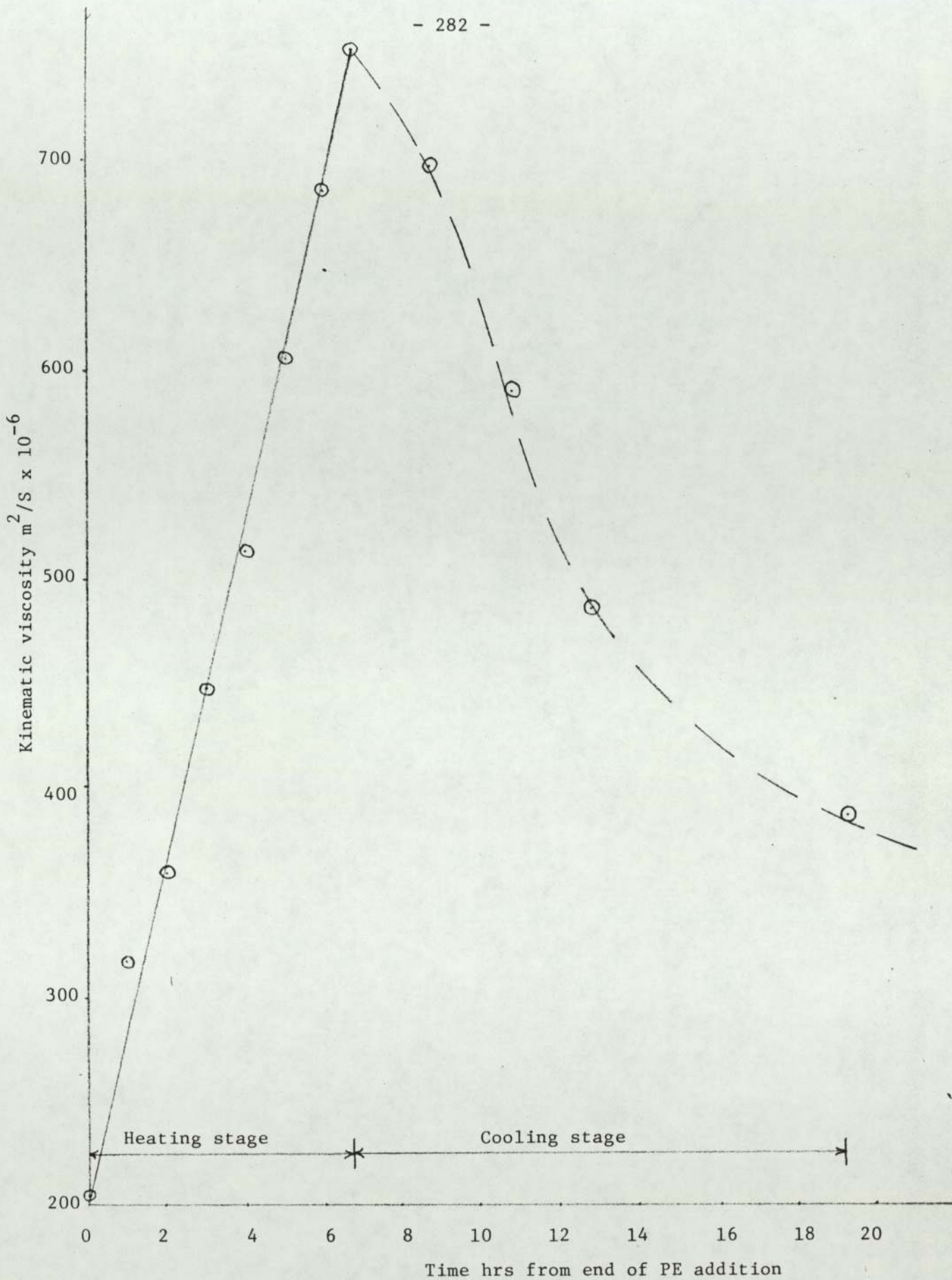


Figure A1.2

Graph of kinematic viscosity $m^2/S \times 10^{-6}$ at $100^{\circ}C$ vs. time hrs from end of PE addition

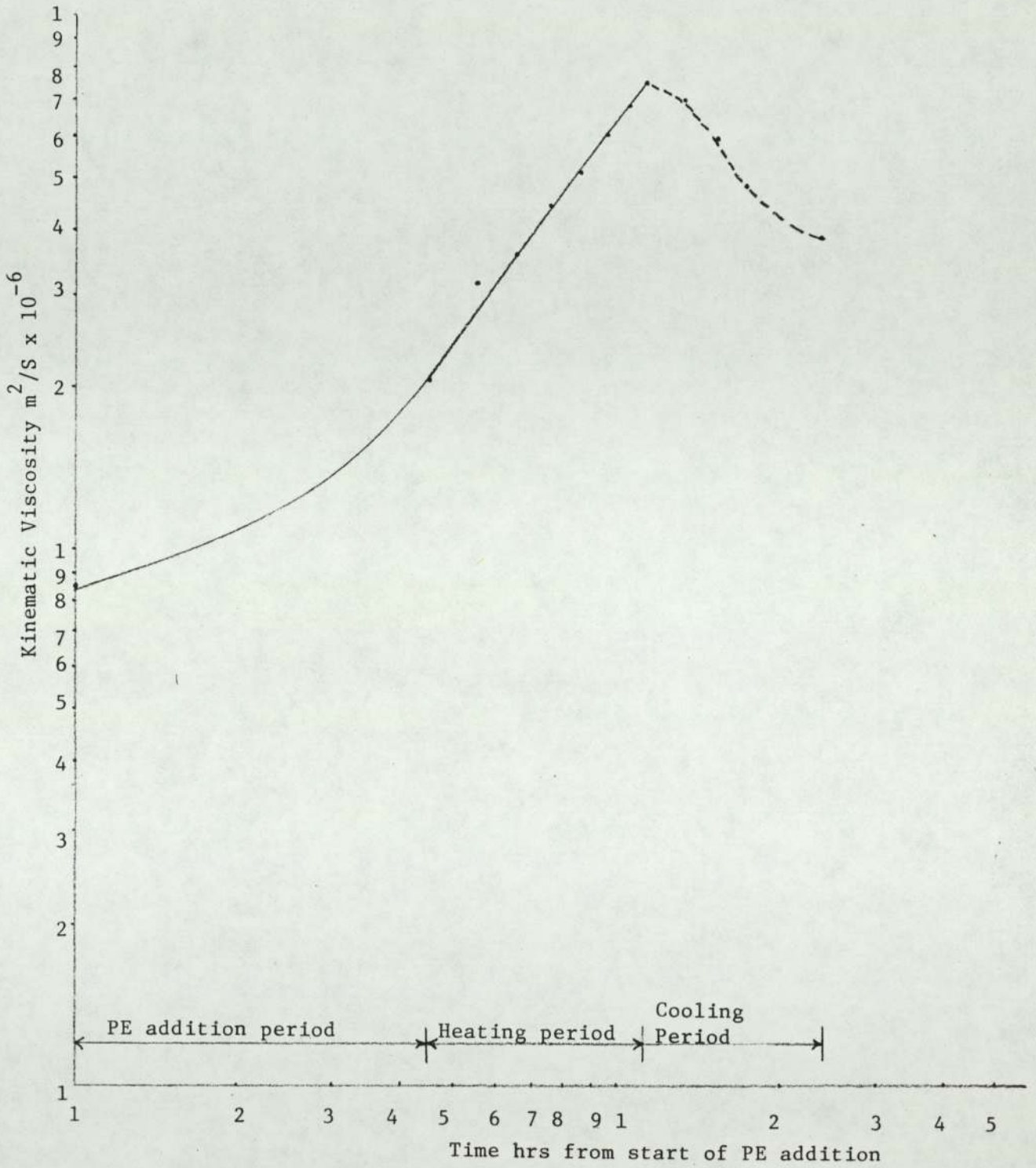


Figure A1.3

Graph of kinematic viscosity $\text{m}^2/\text{S} \times 10^{-6}$ vs. time hrs from start of PE addition

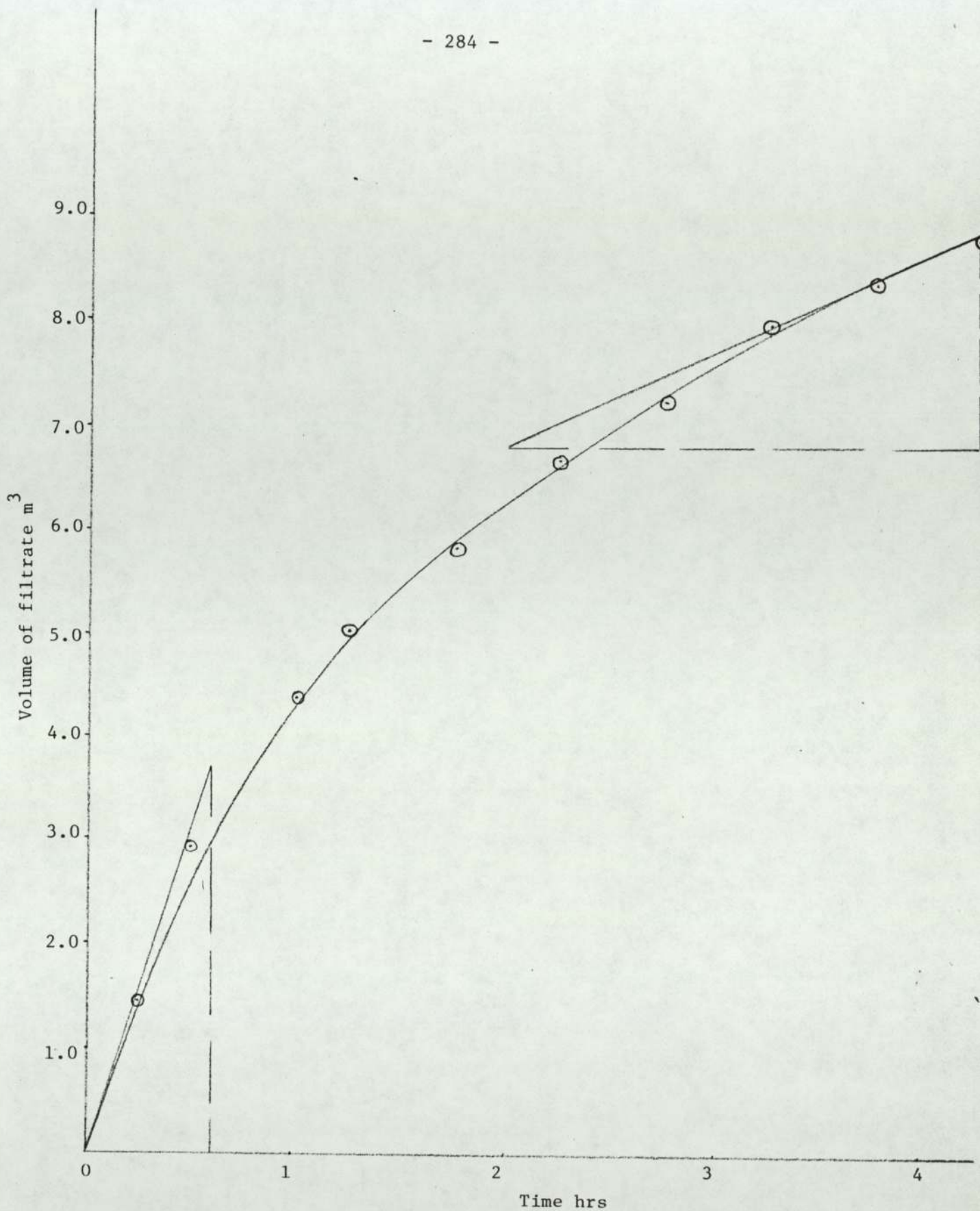


Figure A1.4

Graph of filtrate volume m³ vs. time hrs

Filtration run number one of Fawley batch 2610

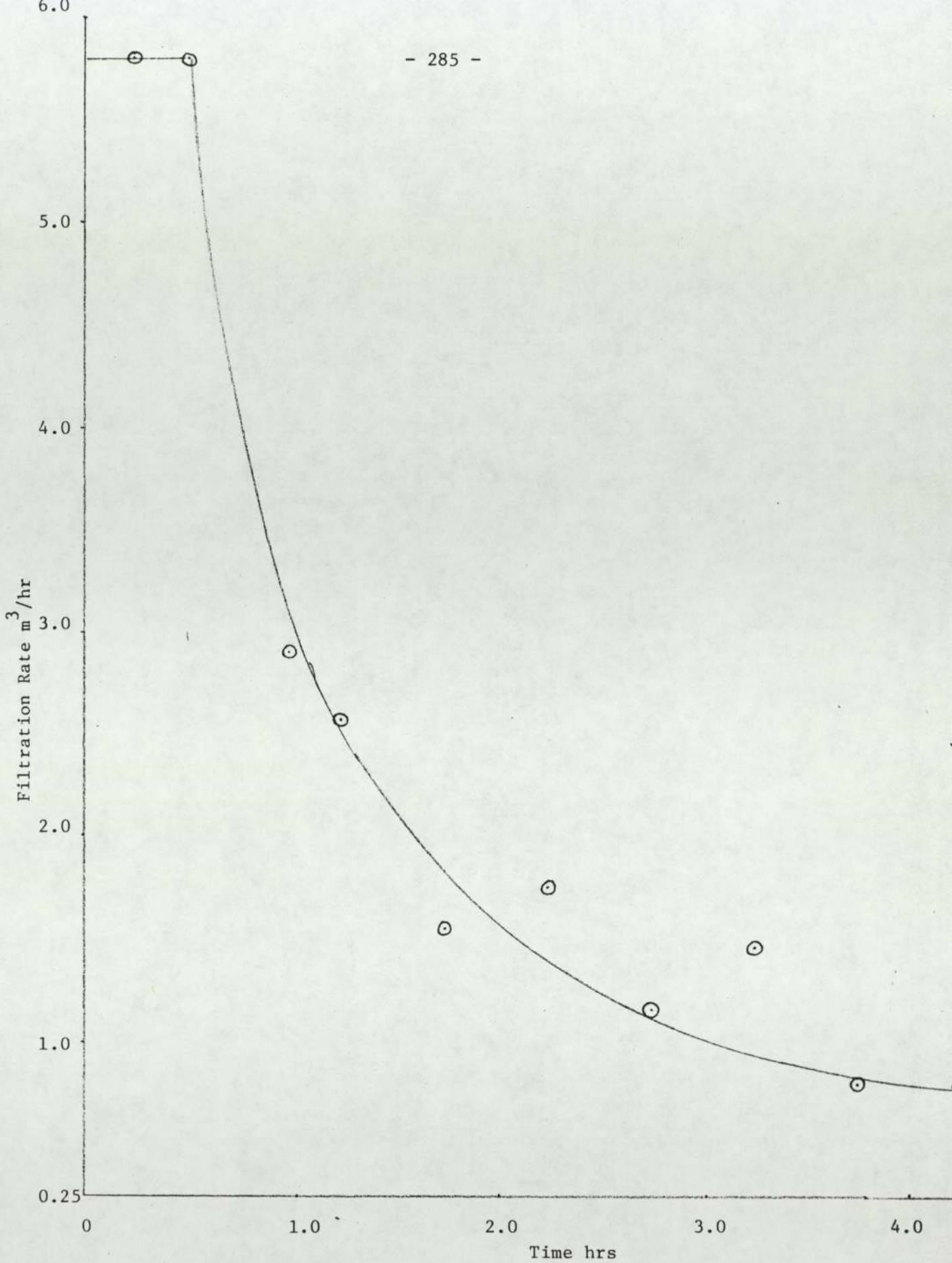


Figure A1.5

Graph of filtration rate m³/hr vs. time hrs

Filtration No.1 for Fawley batch No. 2610

APPENDIX 2

CONDITIONS OF SEDIMENT INVESTIGATION RUNS

Detailed conditions of the runs carried out during the sediment investigation experimental program are given below in Table A2.1. The following points are notes on other production conditions not mentioned in the table.

1. Heating rate from 140°C to reaction temperature was 0.5°C/min after pentaerythritol addition to reaction mixture in all the runs.
2. Nitrogen sparge rate was 0.1 dm³/min in all the runs.
3. About 57.5% by wt. of the total dilution oil was added to the PIBSA during the reaction stage in practically all the runs except runs 15, 16 and 24. This ratio was increased in run 15, lowered in run 16, and finally increased to 100% by wt. in run 24, i.e. all the dilution oil was added in the reaction stage in run 24. The second part of the dilution oil was added to the mixture before filtration to raise its ratio to 75% by wt., while the final part was added to the filtrate to raise the percentage to the full 100% by wt.
4. As was mentioned in Chapter Five, three types of stirrers were used during the performance of the experimental program, they were as follows:
 - a. A six blade turbine impeller of 32 mm diameter used in runs 1 to 12 inclusive and also in runs 21, 22 and 23. The speed of the stirrer during these runs was 900 r.p.m.
 - b. A three blade propeller of 50 mm diameter and a pitch of 45° used in runs 13 to 20 inclusive with stirrer speed of 800 r.p.m.

c. An ever larger, six blade turbine impeller of 60 mm diameter was used in run 24 and all the other runs that followed. A stirrer speed of 700 r.p.m. was used in these runs while using the larger impeller.

5. Filter aid was used in two runs only, run 5 and run 29.

Filtration in all the other runs was performed without the use of filter aid.

6. PE/PIBSA equivalent ratio employed in all the runs was 1.1/1.0 except in two runs only, run 27 and run 28, where the equivalent ratio of PE/PIBSA used was 1.9/1.0.

7. In the first four runs, 1, 2, 3 and 4, the reaction mixture was cooled to the filtration temperature at a rate of $0.3^{\circ}\text{C}/\text{min}$, kept at that temperature for about two hours, then the electrical power to the rig was switched off and the mixture was left at ambient temperature overnight. The next morning the mixture was heated gradually back to filtration temperature, kept at that temperature for about three hours and finally filtered.

8. In run 52, about 3g of pentaerythritol seed crystals of sieve fraction cut 355-422 μm were added to the reaction mixture at 170°C during the cooling stage.

9. In runs 55, 56, and 58 crash cooling was carried out using an external air jet, and the total cooling time was less than ten minutes.

10. In runs 58, 59 and 60 stirrer speed was reduced to 100 r.p.m. at the start of the cooling stage and kept at this value till the end of the run.

11. In runs 61 and 62, at the end of the reaction period, the reaction mixture was filtered at the reaction temperature and no cooling to filtration temperature was carried out.

TABLE A2.1

Conditions of runs carried out during the sediment investigation experimental program

Number of run	Weight of PIBSA g	Weight of oil in reaction stage g	Total oil dilution % wt. on PIBSA	Catalyst used		Reaction temperature °C	Time at reaction temperature hr	Cooling rate to filtration temperature °C/min	Time kept at final temperature hr	FILTRATION					
				Ratio % wt. on PIBSA	Type % A.I.					Temperature °C		Maximum pressure bar/gauge	Total time min.	Filtrate Volume cm ³	Rate $\frac{dm^3}{2m \cdot hr}$
										Max.	Min.				
1	366.70	289.00	137.08	2.2	90	190	3	0.3	14	140	135	1.379	8.5	850	438.6
2	419.40	330.57	137.08	2.2	90	190	3	0.3	13	137	133	1.724	9.0	900	438.6
3	349.04	275.11	137.08	2.2	90	190	3	0.3	14	128	124	1.172	8.0	800	438.6
4	421.57	332.28	137.08	2.2	90	190	3	0.2	14	128	124	3.034	9.0	900	438.6
5	445.14	350.86	137.08	2.2	90	190	0.7	0.2	2.5	144	138	0.345	3.5	900	1127.8
6	379.14	294.53	135.1	2.2	90	190	5.17	0.2	11.5	137	133	6.895	19.17	700	160.2
7	497.33	386.34	135.1	2.2	90	190	0.32	0.3	3.08	135	128	6.619	23.42	1080	102.7
8	420.19	326.42	135.1	2.2	90	189	2.0	0.3	2.72	140	130	5.378	7.0	900	563.9

TABLE A2.1 (continued)

Conditions of runs carried out during the sediment investigation experimental program

Number of run	Weight of PIBSA g	Weight of oil in reaction stage g	Total oil dilution % wt. on PIBSA	Catalyst used		Reaction temperature °C	Time at reaction temperature hr	Cooling rate to filtration temperature °C/min	Time kept at final temperature hr	FILTRATION						
				Ratio % wt. on PIBSA	Type % A.I.					Temperature °C		Maximum pressure bar/gauge	Total time min.	Filtrate Volume cm ³	Rate $\frac{\text{dm}^3}{\text{m}^2 \cdot \text{hr}}$	
										Max.	Min.					
9	448.84	348.67	135.1	2.2	90	190	2.0	0.3	2.72	139	140	135	4.482	7.37	1000	595.1
10	422.64	328.32	135.1	2.2	90	192	2.0	0.3	2.72	139	155	110	7.585	>60	-	-
11	450.88	350.26	135.1	2.2	90	191	1.25	0.3	2.7	139	140	120	8.550	>60	-	-
12	354.88	279.72	135.1	2.2	90	192	2.0	0.3	3.0	137	145	120	7.928	9.0	770	375.3
13	411.22	324.13	135.1	2.2	90	175	0.02	0.3	2.0	138	134.4	118	8.136	55.0	985	78.6
14	442.35	343.67	135.1	2.2	90	181	0.02	0.3	2.1	139	141	136	6.137	10.7	1000	409.9
15	411.90	378.95	137.08	2.2	90	189	4.0	0.3	15.8	138	156	139	6.206	7.6	900	519.4
16	446.79	347.08	137.08	2.2	90	190	5.0	0.2	11.6	138	139	134	4.827	4.7	1000	933.2

TABLE A2.1 (continued)

Conditions of runs carried out during the sediment investigation experimental program

Number of run	Weight of PIBSA g	Weight of oil in reaction stage g	Total oil dilution on PIBSA % wt.	Catalyst used		Reaction temperature °C	Time at reaction temperature hr	Cooling rate to filtration temperature °C/min	Time kept at final temperature hr	F I L T R A T I O N			Rate $\frac{\text{dm}^3}{\text{m}^2 \cdot \text{hr}}$		
				Ratio % wt. on PIBSA	Type % A.I.					Temperature °C		Maximum pressure bar/gauge		Total time min.	Filtrate Volume cm ³
										Max.	Min.				
17	394.28	306.29	135.1	2.2	90	190	0.02	0.3	1.5	135	130	6.619	8.5	900	464.4
18	351.88	475.39	135.1	2.2	90	190	0.02	0.3	1.5	130	126	5.378	6.25	900	631.6
19	346.21	467.73	135.1	2.2	90	189	1.0	0.3	1.0	124	121	6.206	7.0	900	563.9
20	399.41	310.27	135.1	2.2	90	190	1.0	0.3	1.5	129	124	4.896	10.25	900	385.1
21	399.27	310.16	135.1	2.2	90	191	1.0	0.3	17.3	130	125	2.758	10.0	900	394.7
22	399.27	310.16	135.1	2.2	90	190	1.0	0.3	16.75	129	124	4.551	9.33	900	423.1
23	401.60	311.97	135.1	2.2	90	190	2.0	0.3	16.5	129	125	5.516	9.83	900	401.6
24	363.84	491.55	135.1	1.0	90	189	0.62	0.3	17.8	134	130.6	4.137	18.0	-	-

TABLE A2.1 (continued)

Conditions of runs carried out during the sediment investigation experimental program

Number of run	Weight of PIBSA g	Weight of oil in reaction stage g	Total oil dilution % wt. on PIBSA	Catalyst used		Reaction temperature °C	Time at reaction temperature hr	Cooling rate to filtration temperature °C/min	Time kept at final temperature hr	F I L T R A T I O N					
				Ratio % wt. on PIBSA	Type % A.I.					Temperature °C		Maximum pressure bar/gauge	Total time min.	Filtrate Volume cm ³	Rate $\frac{dm^3}{m \cdot hr}$
										Max.	Min.				
25	406.73	315.96	135.1	1.0	90	190	0.1	6.0	135	130	4.137	41.83	900	94.37	
26	409.05	317.76	135.1	1.0	90	185	0.02	15.8	138	133	4.137	42.33	900	93.3	
27	402.97	313.04	135.1	1.0	90	187	0.02	16.4	143	135	4.137	9.17	890	425.7	
28	410.81	319.13	135.1	1.0	90	178	0.02	16.7	138	134	4.137	31.33	890	124.6	
29	403.07	313.12	135.1	1.18	70	170	3.0	64.7	133	125	4.137	7.7	840	478.5	
30	409.83	318.37	135.1	2.23	90	139	26.7	-	-	134	1.655	4.42	890	883.2	
31	399.80	310.57	135.1	2.2	90	130	20.5	-	-	124	4.827	25.75	800	136.26	
32	401.17	311.64	135.1	2.2	90	142	22.3	-	-	136	1.586	3.67	900	1075.6	

TABLE A2.1 (continued)

Conditions of runs carried out during the sediment investigation experimental program

Number of run	Weight of PIBSA g	Weight of oil in reaction stage g	Total oil dilution % wt. on PIBSA	Catalyst used		Reaction temperature °C	Time at reaction temperature hr	Cooling rate to filtration temperature °C/min	Time kept at final temperature hr	F I L T R A T I O N						
				Ratio % wt. on PIBSA	Type % A.I.					Temperature °C		Maximum pressure bar/gauge	Total time min.	Filtrate Volume cm ³	Rate $\frac{dm^3}{m^2 \cdot hr}$	
										Max.	Min.					
33	400.57	311.17	135.1	1.18	70	180	0.67	0.25	16.9	132	139	112	4.137	20.83	880	185.3
34	401.07	311.56	135.1	1.2	70	180	0.33	1.3	17.3	126	139	124	4.137	16.75	885	231.74
35	403.19	313.21	135.1	1.18	70	178	0.37	1.3	20.3	131	139	126	4.137	159.5	700	19.25
51	403.67	313.58	135.1	1.18	70	180	0.5	0.2	66	134	135	128	4.137	55.0	800	63.8
52	403.31	313.30	135.1	1.18	70	180	0.5	0.2	17.8	135	135	129	4.137	95.4	850	39.1
53	400.67	311.25	135.1	1.18	70	180	0.5	0.2	41	137	135	127	4.137	24.5	850	152.2
54	402.03	312.31	135.1	1.18	70	180	0.5	0.2	20.9	136	135	131	4.137	60.0	850	62.1
55	403.27	313.27	135.1	1.18	70	180	0.5	4.5	22.2	137	135	130	4.137	25.8	870	147.7

APPENDIX 3

PROCEDURE FOR THE TOTAL ACID NUMBER CALCULATION

In the first twenty eight runs of the experimental work the Total Acid Number (TAN) was calculated by dissolving a sample in 50 cm³ of chlorobenzene and then titrating the solution with standardised 0.1N tetra-n-butyl ammonium-hydroxide (in toluene-methanol) solution. The end point of the titration was determined using two methods namely, colour titration with phenolphthalein solution as an indicator, and pH titration using a pH meter model 7010 with a pH range of zero to 14 from Electronic Instruments Ltd., using a glass electrode as a pH probe which was a Pye-Unicam laboratory combined electrode (type: 405-60) of an operating range of 0 to 14 pH units. The pH titration end point was found from the inflection point of the graph of pH vs. volume of base used (cm³). Both of these methods were used in the calculations of the TAN in the first 28 runs because there were differences in the results obtained from both methods. In the other production and kinetic runs that followed, a slightly modified colour titration method was used which yielded a TAN value exactly the same as that obtained by using the pH titration (see Appendix 1, point No. 4 of the discussion). In the modified method the sample was dissolved in 75 cm³ of chlorobenzene and then titrated with standardised 0.1N tetra-n-butyl ammonium hydroxide (in toluene-methanol) solution using 0.3% thymol blue in dimethyl formamide solution as an indicator for the determination of the titration end point. Finally the modified method was used in conjunction with a potentiometric titrator model E536 (Metrohm series) which automatically plotted the titration, and the end point was found from the inflection point of the curve. This titrator became available and was borrowed from Esso

Research Centre at Abingdon towards the end of the kinetic study. In all these methods the TAN was calculated using the following formula

$$\text{TAN} = \frac{(v-b) \times N \times 56.1}{w} \quad \text{A3.1}$$

where: V = Volume of the standardised 0.1N base (TBAH) required to titrate the sample in cm³
b = Volume of the standardised base (TBAH) required to titrate the blank chlorobenzene solvent in cm³
N = Normality of the standardised base (TBAH)
w = Mass of the sample which was taken in accordance with the following Table A3.1.

TABLE A3.1

Sample size required for each TAN mg KOH/g range expected

TAN mg KOH/g	Sample size g	Sensitivity of weighing g
0.05-1.0	20 ± 2.0	0.1
1.0 -5.0	5 ± 0.5	0.02
5.0 -20	1.0 ± 0.1	0.005
20 -100	0.25 ± 0.02	0.001
100	0.1 ± 0.01	0.0005

Standardisation procedure

The standardisation of 0.1N tetra-n-butyl ammonium hydroxide (in toluene-methanol) solution (the base) was carried out by dissolving 0.06g of dried benzoic acid into 50 cm³ of chlorobenzene then titrating the solution with the base, using a pH meter for pH titrations, phenolphthalein solution as an indicator for colour titration, or thymol blue

solution as an indicator for the modified method. The standard normality was calculated from the following equation

$$N = \frac{w}{0.1221 (V-b)} \quad \text{A3.2}$$

where N, V and b have the same definitions as in equation (A3.1), with w representing the sample weight of benzoic acid.

Standardisation calculations using pH titration

Blank titration

A pH titration was carried out for the 50 cm³ of chlorobenzene against the 0.1N base in the presence of phenolphthalein indicator solution. The values of the pH corresponding to the added volume of the base are presented in Table A3.2 below.

TABLE A3.2

pH titration of the blank 50 cm³ chlorobenzene with the 0.1N base ,
 starting volume of base in the burette = 22.2 cm³
 starting pH of the solution = 4.2

Volume of 0.1N base (cm ³)	pH	Volume of 0.1N base (cm ³)	pH
22.2	4.2	22.5	12.85
22.225	8.8	22.525	13.1
22.25	8.9	22.55	13.35
22.3	9.35	22.6	13.5
22.35	10.1	22.625	13.5
22.41	11.39		

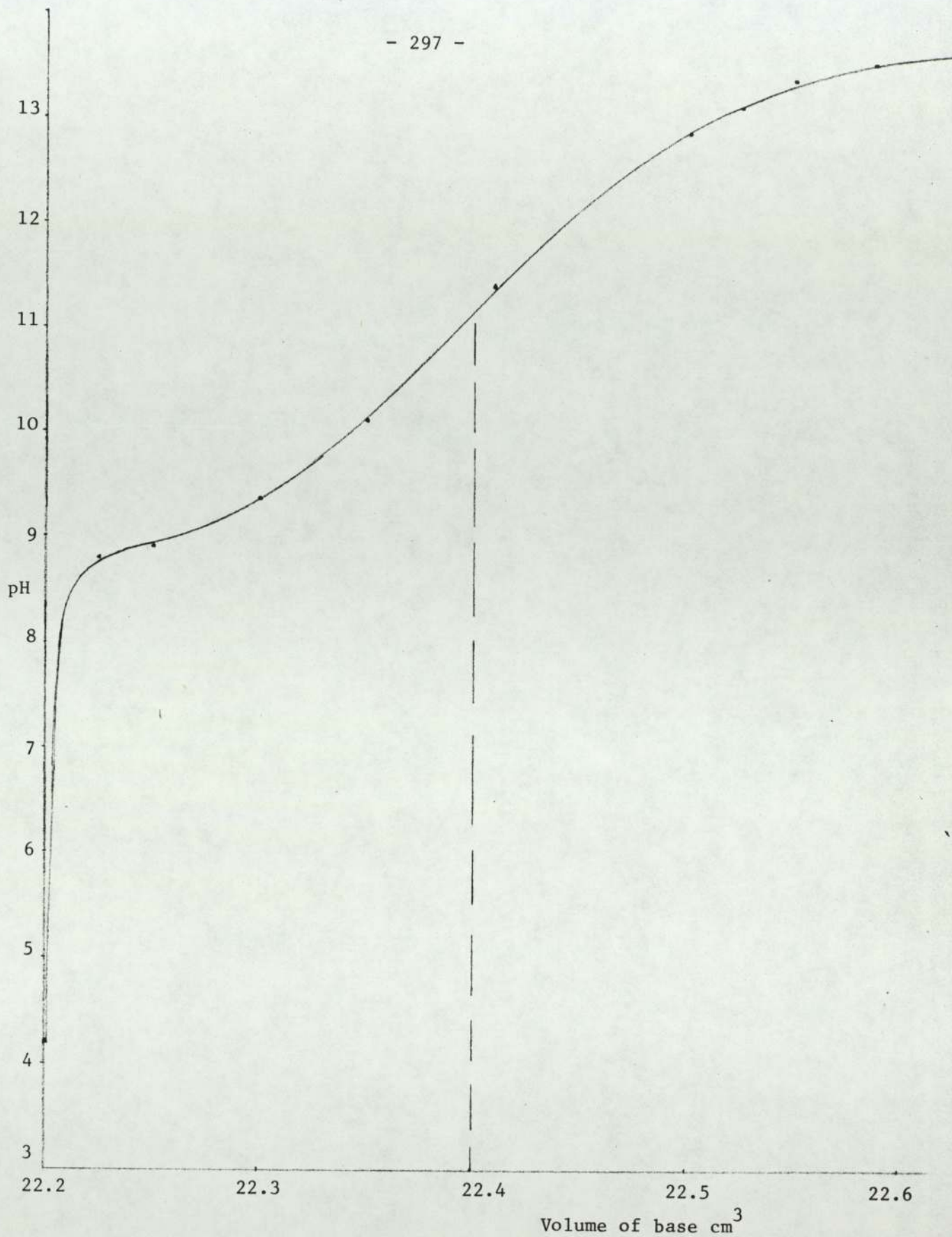


Figure A3.1

Graph of pH vs. volume of (TBAH) base added cm³ for blank titration of 50 cm³ of chlorobenzene

Figure A3.1 was obtained when a plot of the volume of base cm^3 vs. the pH, given in Table A3.2, was carried out. The titration end point was found to be 22.4 cm^3 from the inflection point of the curve.

$$\text{Hence base volume used} = 22.4 - 22.2 = 0.2 \text{ cm}^3$$

$$\therefore b = 0.2 \text{ cm}^3 \text{ for pH titration}$$

Titration with Benzoic acid

A sample of Benzoic acid was weighed, dissolved in 50 cm^3 of chlorobenzene then titrated against the 0.1N base in the presence of phenolphthalein indicator solution. The results of the pH titration are given below.

Weight of empty beaker	=	46.2213g
Benzoic acid sample in beaker	=	46.2828g
\therefore Weight of Benzoic acid sample	=	0.0615g
Starting volume of 0.1N base in the burette	=	5.95 cm^3
Starting pH of solution	=	3.9

TABLE A3.3

pH titration of Benzoic acid sample in 50 cm^3 chlorobenzene against the 0.1N base

Volume of base cm^3	pH	Volume of base cm^3	pH	Volume of base cm^3	pH
5.95	3.90	9.30	8.25	10.95	10.72
6.225	6.25	9.95	8.52	11.00	11.05
6.45	6.43	10.025	8.60	11.025	11.30
6.925	6.85	10.525	9.07	11.10	11.60
7.50	7.35	10.65	9.33	11.15	11.73
8.10	7.60	10.75	9.50	11.20	11.85
8.35	7.85	10.80	9.60	11.30	12.20
8.725	8.03	10.90	10.15	11.40	12.40

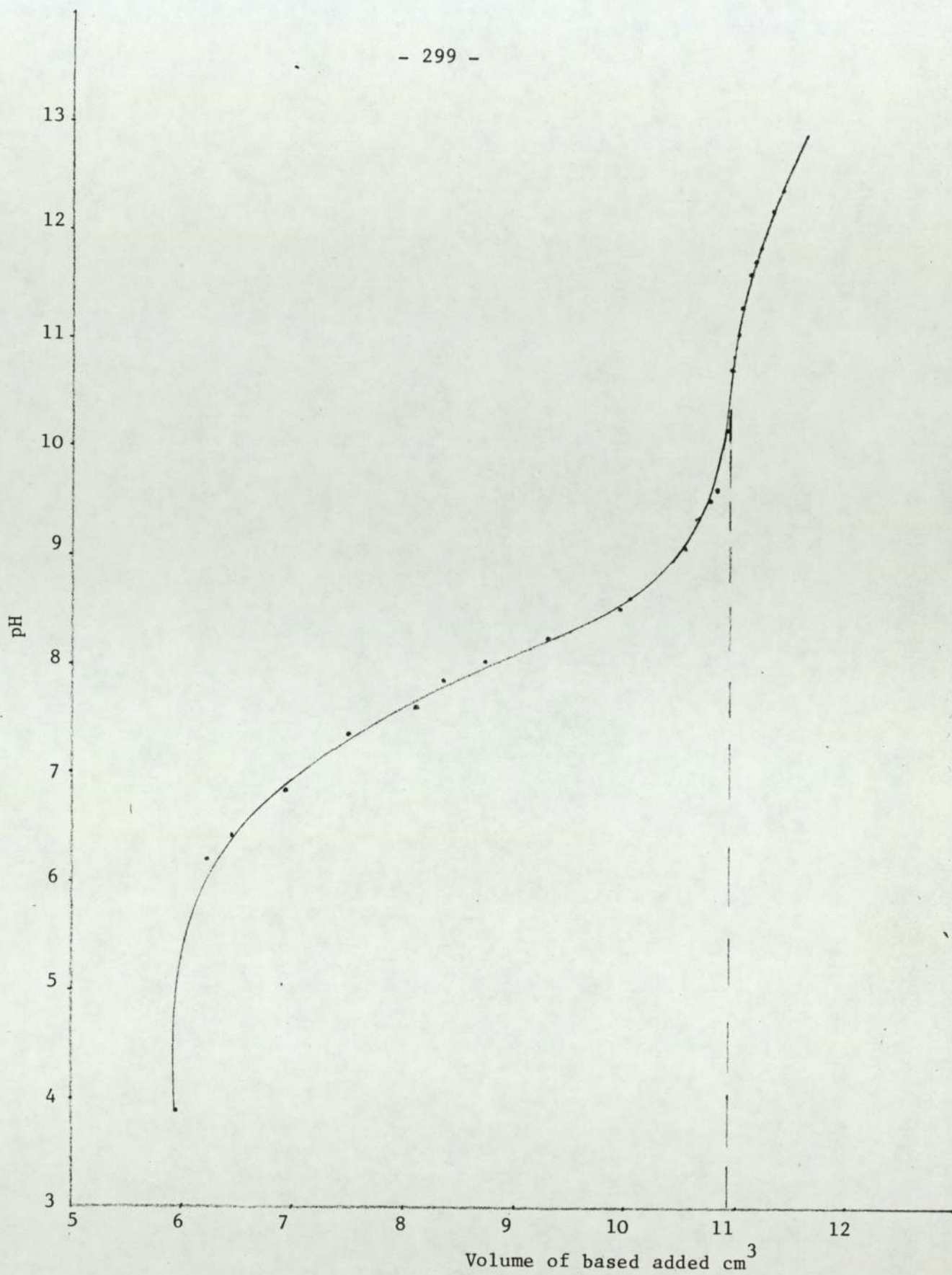


Figure A3.2

Graph of pH vs. volume of base added cm³ for the standardisation of the base with Benzoic acid

Figure A3.2 was obtained when a plot of the base volume vs. the pH listed in Table A3.3 was carried out. The titration end point was found from the inflection point of the curve to be equal to 10.93 cm^3

$$\therefore \text{Volume of base used} = 10.93 - 5.95 = 4.98 \text{ cm}^3$$

$$\therefore N = \frac{0.0615}{0.1221 (4.98-0.2)}$$

$\therefore N = 0.105$ The standardised normality of the 0.1N base.

Standardisation of the 0.1N tetra-n-butyl ammonium-hydroxide solution (TBAH) was carried out every two weeks to check for any changes in normality with time.

Standardisation calculations using colour titration

Blank titration

The 50 cm^3 of chlorobenzene was titrated against the base (TBAH) using phenolphthalein indicator solution for the determination of the titration end point. The results are given below.

First blank titration:

Starting volume of base in the burette	= 9.2 cm^3
End point volume of base in the burette	= 9.5 cm^3
\therefore Volume of base used for blank titration	= 0.3 cm^3

Second blank titration:

Starting volume of base in the burette	= 18.65 cm^3
End point volume of base in the burette	= 18.95 cm^3
\therefore Volume of base used for blank titration	= 0.3 cm^3

$\therefore b = 0.3 \text{ cm}^3$ for colour titration using phenolphthalein indicator

Titration with Benzoic acid

A sample of Benzoic acid was dissolved in 50 cm³ of chlorobenzene and titrated against the base (TBAH) using phenolphthalein indicator to determine the titration end point. Results of the titration were as follows:

Weight of empty beaker	=	45.9317g
Weight of Benzoic acid sample in beaker	=	45.9944g
∴ Weight of Benzoic acid sample	=	0.0627g

Titration results:

Starting volume of base in burette	=	9.6 cm ³
End point volume of base in burette	=	14.975 cm ³
∴ Volume of base used in the titration	=	5.375 cm ³
∴ Normality N =	$\frac{0.0627}{0.1221 (5.375-0.3)}$	

∴ N = 0.1012 standardised normality of the base if using phenolphthalein indicator

Standardisation calculations for the modified method

Blank titration

75 cm³ of chlorobenzene was titrated against the base (TBAH) using 0.3% thymol blue in dimethylformamide solution as an indicator.

Results were as follows:

Starting volume of base in the burette	=	4.0 cm ³
End point volume of base in the burette	=	4.075 cm ³
∴ Volume of base used for the blank titration	=	0.075 cm ³

∴ b = 0.075 cm³ for the modified method using thymol blue as an indicator

Titration with Benzoic acid

A sample of Benzoic acid was dissolved in 75 cm³ of chlorobenzene and titrated against the base using thymol blue as an indicator. Results were as follows:

Weight of empty beaker = 116.4330g

Weight of Benzoic acid sample in the beaker = 116.4989g

∴ Weight of Benzoic acid sample = 0.0659g

Titration results:

Starting volume of base in the burette = 19.2 cm³

End point volume of base in the burette = 24.6 cm³

∴ Volume of base used in the titration = 5.4 cm³

$$\therefore N = \frac{0.0659}{0.1221 (5.4-0.075)}$$

∴ N = 0.1014 Normality of the base when using the modified method with thymol blue as as indicator

Standardisation calculations using the potentiometric titrator

Blank titration

75 cm³ of chlorobenzene were titrated against the base (TBAH) using the potentiometric titrator. Thymol blue indicator solution was also added but the titration end point was found from the inflection point of the curve which was plotted automatically by the titrator. The volume of the base corresponded to the end point was = 0.16 cm³

∴ b = 0.16 cm³ for blank titration using the potentiometric titrator.

Titration with Benzoic acid

A sample of benzoic acid was dissolved in 75 cm³ of chlorobenzene

and titrated against the base using the titrator, and also adding a few drops of thymol blue indicator solution. Results were as follows:

Weight of empty beaker = 45.9213g
 Weight of Benzoic acid sample in beaker = 45.9911g
 ∴ Weight of Benzoic acid sample = 0.0698g

From the inflection point of the automatically plotted curve for the titration, the volume of the base corresponding to the end point was found to be = 5.850 cm³

$$\therefore N = \frac{0.0698}{0.1221(5.850-0.16)}$$

∴ N = 0.1005 The standardised normality of the base using the potentiometric titrator

Summary of standardisation results

As was shown above, four sets of values for (N) and (b) were calculated corresponding to the four methods used for the determination of the titration end point. These results are tabulated below in Table A3.4.

TABLE A3.4

Summary of the titration methods used and of the standardisation results of TBAH base

Method No.	Titration method	Indicator added	Titration end point	b cm ³	N
1	pH titration	phenol-phthalein	Inflection of pH vs. base vol. plot	0.2	0.105
2	colour titration	phenol-phthalein	colour change	0.3	0.1012
3	modified colour titration	thymol blue	colour change	0.075	0.1014
4	potentiometric titration	thymol blue	inflection of potential vs. base vol. plot	0.16	0.1005

Titration methods No. 1 and 2 were used in the determination of the TAN in the first 28 experimental runs while method No. 3 was used in all the runs that followed (runs 29 to 63). The potentiometric titration, method No. 4, was used with method No. 3 in calculating the TAN in the last 17 runs (runs 46 to 63).

APPENDIX 4

OUTLINE OF THE SEDIMENT TEST METHOD

The sediment test was carried out by centrifuging 50 cm³ of the sample with 50 cm³ of n-heptane at room temperature in a general purpose centrifuge at a speed of 1700 r.p.m. for two to three 20 minutes intervals. A special centrifuge tube of 100 cm³ capacity and a length of about 200 mm, cone shaped, with 0.005 cm³ subdivisions from 0 to 0.05 cm³; 0.05 cm³ subdivisions from 0.05 cm³ to 0.50 cm³; and 0.10 cm³ subdivisions above 0.50 cm³, was filled to the 50 cm³ mark with the sample, and then to the 100 cm³ mark with n-heptane. A stopper was inserted firmly in the tube and the contents were mixed thoroughly by inverting the tube repeatedly and also shaking it. The tube was centrifuged at room temperature using a special centrifuge that can handle such a long tube and was capable of providing a relative centrifugal force (rcf) of about 800 at the tip of the tube. The centrifuge was from Damon-Internation Equipment Company, Model CU-5000 general purpose centrifuge, having a six tube rotor head. The rotational speed necessary to give the required (rcf) was calculated from the following equation

$$\text{rpm} = 1325 \frac{(\text{rcf})}{d} \quad \text{A4.1}$$

where:

(rcf) = The relative centrifugal force

d = Diameter of swing in mm measured between
tips of tubes when in rotating position

and was found to be around 1700 r.p.m. for this centrifuge model to develop an (rcf) of about 800 as required by the test. The tube was spinned at 1700 r.p.m. for successive periods of 20 minutes intervals until the sediment level was nearly constant (three 20 minutes spins were found to be very satisfactory). The combined volume of sediment and water at the

bottom of the centrifuge tube was read and with it was included the volume of any emulsion or layer of haze that had a distinguishable top surface or interface. This observed volume of sediment, water and haze was multiplied by two and the result reported as sediment % by volume.

APPENDIX 5

KINEMATIC VISCOSITY MEASUREMENT

The kinematic viscosity of different product samples was measured mostly at a temperature of 100°C, but in some cases it was also measured at 50°C and ambient temperature. Two thermostat baths, and six U-shaped viscometer tubes of different capillary sizes were used in these measurements. One of the thermostat baths was used to measure viscosities at 100°C and contained a mixture of about 50% by volume of glycerol and 50% water, while the other bath was used to measure viscosities at 50°C and ambient temperatures and contained only water. The temperatures of both baths were controlled at the required setting to the nearest 0.05°C by two proportional feed back controllers. The viscosity of a sample was measured by introducing the sample in one of the U-shaped clean calibrated glass capillary viscometers which was then suspended in the bath using viscometer holders and was left for a sufficient time to establish a safe temperature equilibrium (about 30 minutes). Suction was used to raise the head level of the test sample to a position in the capillary arm of the instrument about 5 mm ahead of the first timing mark. With the sample flowing freely, the time required for the meniscus to pass from the first timing mark to the second was measured in seconds using a stop clock. This test was repeated a second and in some cases a third time, and the average value of passage time was taken. The kinematic viscosity was calculated from the following equation

$$v = Ct \qquad \qquad \qquad A5.1$$

where:

- v = kinematic viscosity cst ($10^{-6} \text{ m}^2/\text{s}$)
- C = calibration constant of the viscometer (cst/s)
- t = flow time in seconds

The calibration constant C of the viscometer was found by calibrating the viscometer with a standard fluid of a known viscosity at the required temperature. The above procedure was repeated using the standard fluid, and C was calculated from

$$C = \frac{v_s}{t_s} \quad \text{A5.2}$$

where:

- v_s = kinematic viscosity of the standard fluid in cst
($10^{-6} \text{ m}^2/\text{s}$)
- t_s = flow time of the standard fluid in seconds

Calibration of the viscometers used in the measurements

A total number of six viscometers were used in the measurements of viscosities at 100°C , 50°C and ambient temperatures. These viscometers were as follows:

- a. Viscometer A of capillary No. 300 used to measure viscosities at a temperature of 100°C .
- b. Viscometer B of capillary No. 350 (sub. No. 1407) used to measure viscosities at 100°C .
- c. Viscometer C of capillary No. 350 (sub. No. 1406) used to measure viscosities at 100°C .
- d. Viscometer D of capillary No. 400 used to measure viscosities at a temperature of 100°C .
- e. Viscometer E of capillary No. 400 (sub. No. 834) used to measure viscosities at ambient temperature (taken to be 18°C).
- f. Viscometer F of capillary No. 450 used to measure viscosities at a temperature of 50°C and also at ambient temperature.

The standard fluid used in the calibration of these viscometers was the 1000 cst Dow Corning 200 fluid (MS 200 fluid), the 1000 cst being the fluid viscosity at 25°C. The actual viscosity at 25°C of the fluid batch in question was found to be equal to 976 cst by checking the production records at the company through the batch number. A correlation was also obtained from the Company for calculating the viscosity of the MS 200 fluid at different temperatures, it is being

$$\log AV = \frac{722.5}{T} + \frac{0.000032\mu}{T} + 1.004 \log\mu - 2.447 \quad A5.3$$

where:

AV = Apparent viscosity in cst at temperature T

T = Temperature in °K

μ = Viscosity of the fluid in cst at 25°C

The viscosity of the fluid at three different temperatures namely, 100°C, 50°C and ambient were needed, hence,

at 100°C

$$\log AV = \frac{722.5}{373} + \frac{0.000032 \times 967}{373} + 1.004 \log 967 - 2.44$$

$$\therefore AV = \text{Viscosity at } 100^\circ\text{C} = 307.2 \text{ cst} = 307.2 \times 10^{-6} \text{ m}^2/\text{s}$$

at 50°C

$$\log AV = \frac{722.5}{323} + \frac{0.000032 \times 967}{323} + 1.004 \log 967 - 2.44$$

$$\therefore AV = \text{Viscosity at } 50^\circ\text{C} = 612.8 \text{ cst} = 612.8 \times 10^{-6} \text{ m}^2/\text{s}$$

and at 18°C (ambient)

$$\log AV = \frac{722.5}{291} + \frac{0.000032 \times 967}{291} + 1.004 \log 967 - 2.447$$

$$\therefore AV = \text{viscosity at } 18^\circ\text{C} = 1079.4 \text{ cst} = 1079.4 \times 10^{-6} \text{ m}^2/\text{s}$$

Calibration of viscometer A at 100°C

$$\text{1st run flowing time} = 21 \text{ min} + 7\text{s.}$$

$$\text{2nd run flowing time} = 21 \text{ min} + 3\text{s.}$$

$$\text{Average flow time} = 1265\text{s}$$

$$\therefore \text{factor C} = \frac{307.2}{1265} = 0.2428$$

$$\text{i.e. factor of viscometer A at } 100^\circ\text{C} = 0.2428$$

Calibration of viscometer B at 100°C

$$\text{1st run flowing time} = 10 \text{ min} + 3\text{s.}$$

$$\text{2nd run flowing time} = 10 \text{ min.}$$

$$\therefore \text{Average flowing time} = 601.5\text{s}$$

$$\therefore \text{factor C} = \frac{307.2}{601.5} = 0.5107$$

$$\text{i.e. factor of viscometer B at } 100^\circ\text{C} = 0.5107$$

Calibration of viscometer C at 100°C

$$\text{1st run flowing time} = 11 \text{ min} + 2\text{s.}$$

$$\text{2nd run flowing time} = 10 \text{ min} + 57\text{s.}$$

$$\therefore \text{Average flowing time} = 659.5\text{s}$$

$$\therefore \text{factor C} = \frac{307.2}{659.2} = 0.4658$$

$$\text{i.e. factor of viscometer C at } 100^\circ\text{C} = 0.4658$$

Calibration of viscometer D at 100°C

$$\text{1st run flowing time} = 3 \text{ min} + 45\text{s.}$$

$$\text{2nd run flowing time} = 3 \text{ min} + 44\text{s.}$$

$$\therefore \text{Average flowing time} = 224.5\text{s}$$

$$\therefore \text{factor } C = \frac{307.2}{224.5} = 1.3684$$

i.e. factor of viscometer D at 100°C = 1.3684

Calibration of viscometer E at ambient (18°C)

$$\text{1st run flowing time} = 16 \text{ min} + 30\text{s.}$$

$$\text{2nd run flowing time} = 16 \text{ min} + 34\text{s.}$$

$$\therefore \text{Average flowing time} = 992\text{s}$$

$$\therefore \text{factor } C = \frac{1079.4}{992} = 1.0881$$

i.e. factor of viscometer E at 18°C = 1.0881

Calibration of viscometer F at ambient (18°C)

$$\text{1st run flowing time} = 8 \text{ min} + 4\text{s.}$$

$$\text{2nd run flowing time} = 8 \text{ min} + 7.5\text{s.}$$

$$\therefore \text{Average flowing time} = 485.75\text{s.}$$

$$\therefore \text{factor } C = \frac{1079.4}{485.75} = 2.2221$$

i.e. factor of viscometer F at 18°C = 2.2221

Calibration of viscometer F at 50°C

$$\text{1st run flowing time} = 4 \text{ min} + 26\text{s.}$$

$$\text{2nd run flowing time} = 4 \text{ min} + 25\text{s.}$$

$$\text{3rd run flowing time} = 4 \text{ min} + 26\text{s.}$$

$$\therefore \text{Average flowing time} = 265.67\text{s}$$

$$\therefore \text{factor } C = \frac{612.8}{265.67} = 2.3066$$

i.e. factor of viscometer F at 50°C = 2.3066

Summary of calibration results

A summary of the calibration results of the six viscometers is given below in Table A5.1.

TABLE A5.1

Summary of viscometers calibration results

Viscometer code	Viscometer capillary number	Calibration temperature °C	Factor $\times 10^{-6}$ (m ² /s)/s
A	300	100	0.2428
B	350 (sub.No.1407)	100	0.5107
C	350 (sub.No.1406)	100	0.4658
D	400	100	1.3684
E	400 (sub.No.834)	18	1.0881
F	450	18	2.2221
F	450	50	2.3066

APPENDIX 6

DETAILED CALCULATIONS PERFORMED ON A NUMBER OF KINETIC RUNS

Detailed calculations of run 36

Table A6.1 contains the weight measurements of samples taken during the run and their titration results also.

The tabulated TAN values were calculated using equation (A3.1) in Appendix 3.

$$\text{TAN} = \frac{(v-b) \times N \times 56.1}{w} \quad (\text{A3.1})$$

and the values of (N) and (b) are given in Table A3.4 to be 0.1014 and 0.075 cm³ respectively. Hence as a sample calculation let the TAN of the first sample be calculated here,

$$\therefore \text{TAN}_1 = \frac{(4.875 - 0.075) \times 0.1014 \times 56.1}{1.1152}$$

$$\therefore \text{TAN}_1 = 24.5 \text{ mg KOH/g sample.}$$

All the other TAN values given in Table A6.1 were calculated in the same way, and were plotted against time (hr) to give Figure A6.1. The slope of the curve obtained in Figure A6.1 was measured at different points and the results are presented in Table A6.2 below. The value of TAN[∞] was estimated from Figure A6.1 to be equal to 2.0 mg KOH/g for run 36.

From Table A6.2 we have,

$$\Sigma x_i = 3.3538, (\Sigma x_i)^2 = 11.2480, \Sigma x_i^2 = 3.6436,$$

$$\Sigma y_i = 3.9468, \Sigma x_i y_i = 4.8603, N = 5.$$

TABLE A6.1

Sample weight measurements and titration results for run 36.

No. of sample	Time after PE addition min	Weight of empty beaker g	Weight of beaker plus sample g	Weight of sample g	Starting level of base volume cm ³	Level of base volume at end of titration cm ³	Volume of base used in titration cm ³	TAN $\frac{\text{mg KOH}}{\text{g sample}}$
1	0.5	116.3630	117.4782	1.1152	24.3	29.175	4.875	24.5
2	16.417	116.4273	118.3644	1.9371	5.725	9.75	4.025	11.6
3	31.25	115.9874	117.3875	1.4001	9.875	11.975	2.10	8.2
4	47.917	124.2525	125.4905	1.2380	11.975	13.375	1.40	6.1
5	61.833	124.1742	125.5267	1.3525	13.375	14.75	1.375	5.5
6	93.50	116.3513	117.6821	1.3308	14.75	15.80	1.05	4.1
7	123.25	116.4192	117.6637	1.2445	15.80	16.65	0.85	3.5
8	156.75	115.9873	117.3538	1.3665	16.80	17.575	0.775	3.0
9	183.50	124.2676	126.9131	2.6455	17.65	19.05	1.40	2.8
10	225.0	116.3630	119.3219	2.9589	19.125	20.55	1.425	2.6
11	287.0	124.1736	127.2100	3.0364	20.725	22.15	1.425	2.5
12	405.0	116.3592	119.0532	2.6940	24.225	25.325	1.10	2.2

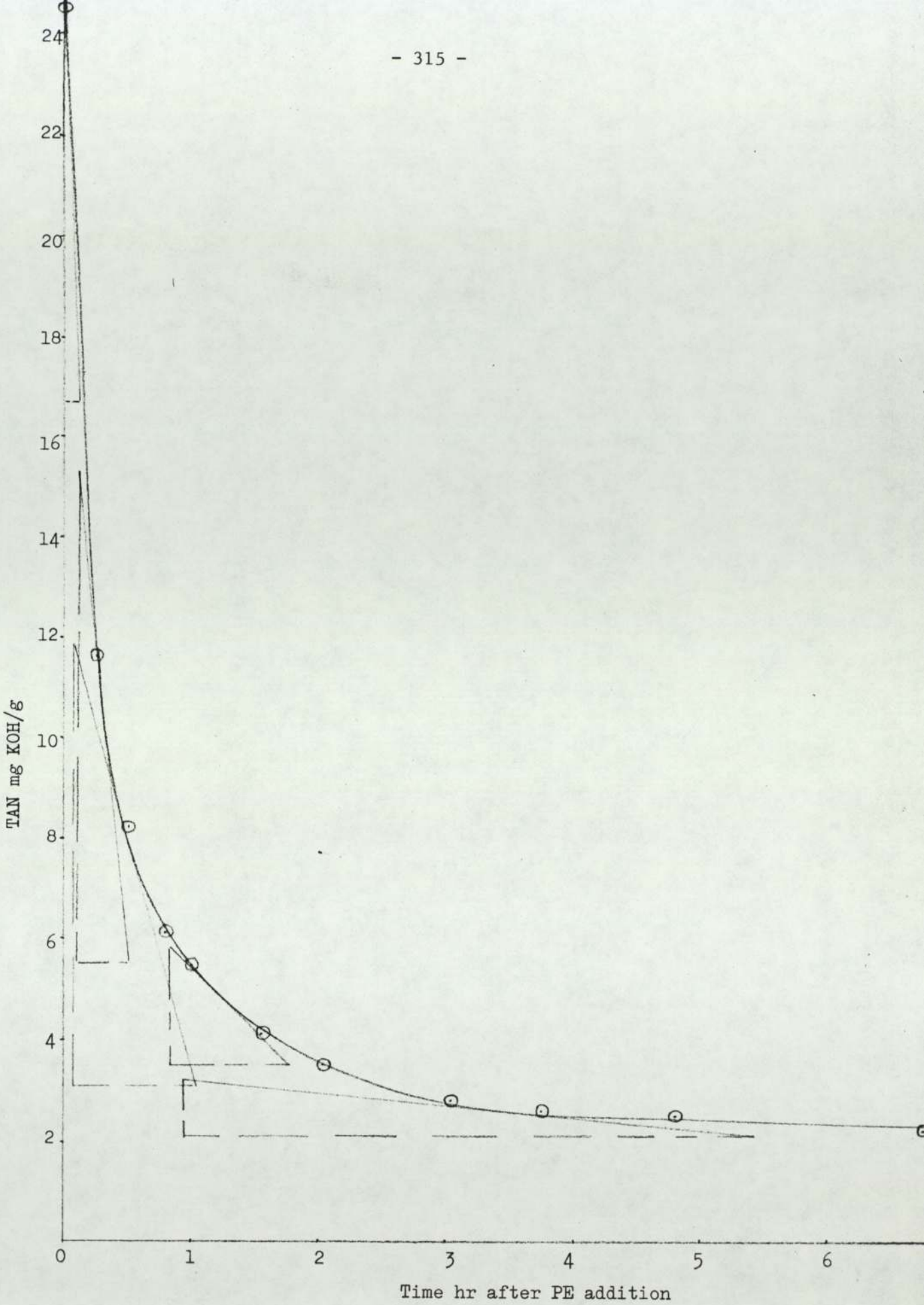


Figure A6.1

Graph for run 36 of TAN mg KOH/g vs. time hr after PE addition

PE/PIBSA ratio (α) = 1.0

Temperature = 200°C

TABLE A6.2

The slope of TAN vs. time curve at different points for run 36.

TAN mg KOH/g	slope = d(TAN)/dt TAN/hr	log [$\frac{-d(\text{TAN})}{dt}$] = y_i	log(TAN -2.0) = x_i	log (TAN)
24.5	-65.00	1.8129	1.3522	1.389
11.0	-24.50	1.389	0.9542	1.0414
8.2	-9.06	0.957	0.7924	0.914
5.0	-2.50	0.3979	0.477	0.699
2.6	-0.2455	-0.610	-0.222	0.415

hence for the least square best fit straight line of the plot of

$\log \left[\frac{-d(\text{TAN})}{dt} \right]$ vs. $\log(\text{TAN}-2.0)$, the slope and intercept are given by

equations (8.22) and (8.23) in Chapter 8, hence

$$\text{slope} = \frac{4.8603 - [3.3538 \times 3.9468/5]}{3.6436 - [11.2480/5]}$$

$\therefore \text{slope} = 1.588$

and intercept = $\frac{3.9468 \times 3.6436 - 3.3538 \times 4.8603}{5 \times 3.6436 - 11.2480}$

$\therefore \text{intercept} = -0.275$

but since the ratio of PE/PIBSA of run 36 (α) = 1.0 then equation (8.13) in Chapter 8 is applicable, hence

$n = \text{slope} = 1.588$ the overall order of reaction

and intercept = $\log k + (n-1.0) \log \gamma$

8.24

where $\gamma = C_A^0 / \text{TAN}_R^0$

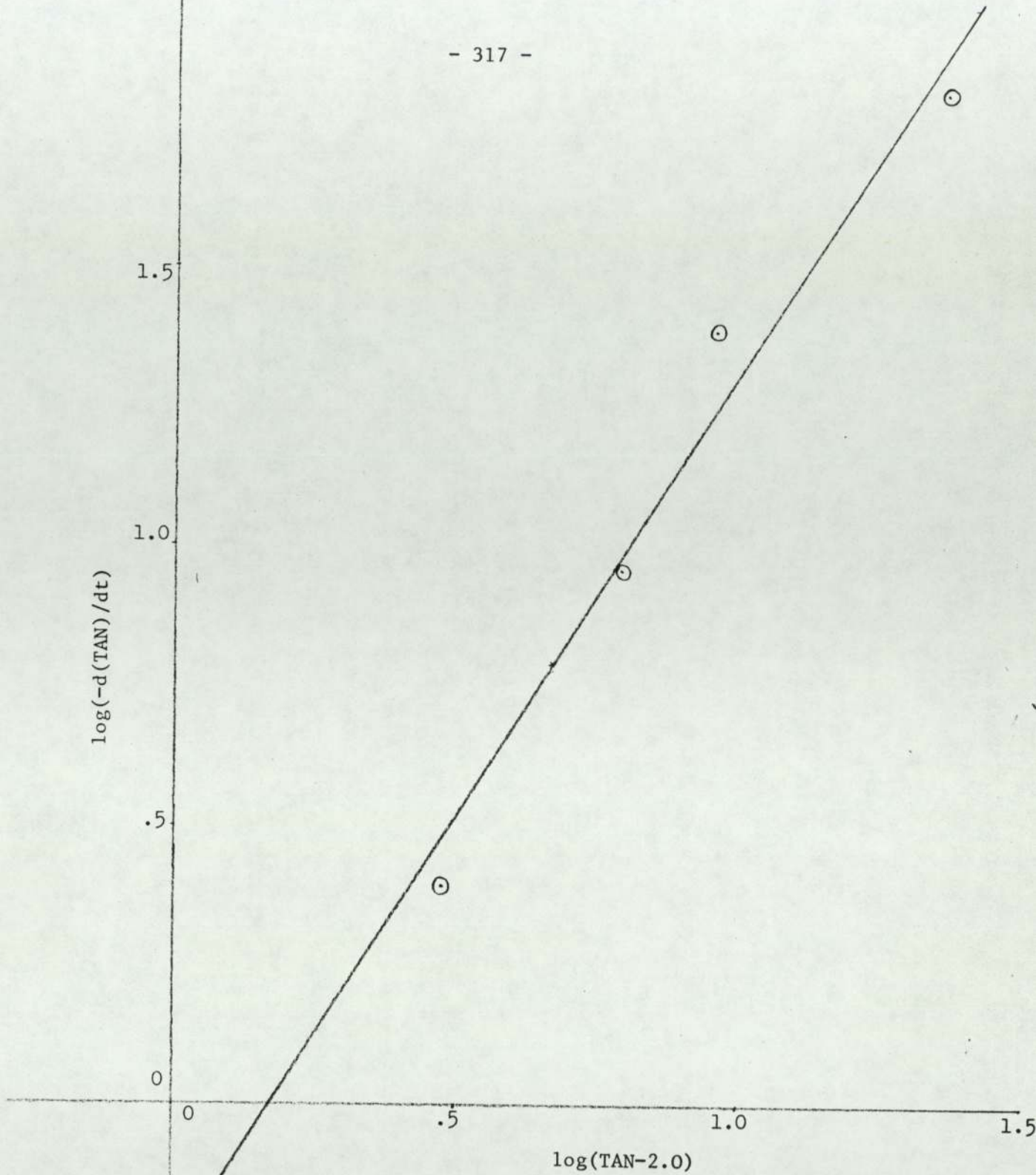


Figure A6.2
Graph for run 36 of $\log\left(\frac{-d(TAN)}{dt}\right)$ vs. $\log(TAN - 2.0)$

PE/PIBSA equivalent ratio $\alpha = 1.0$

Temperature = 200°C

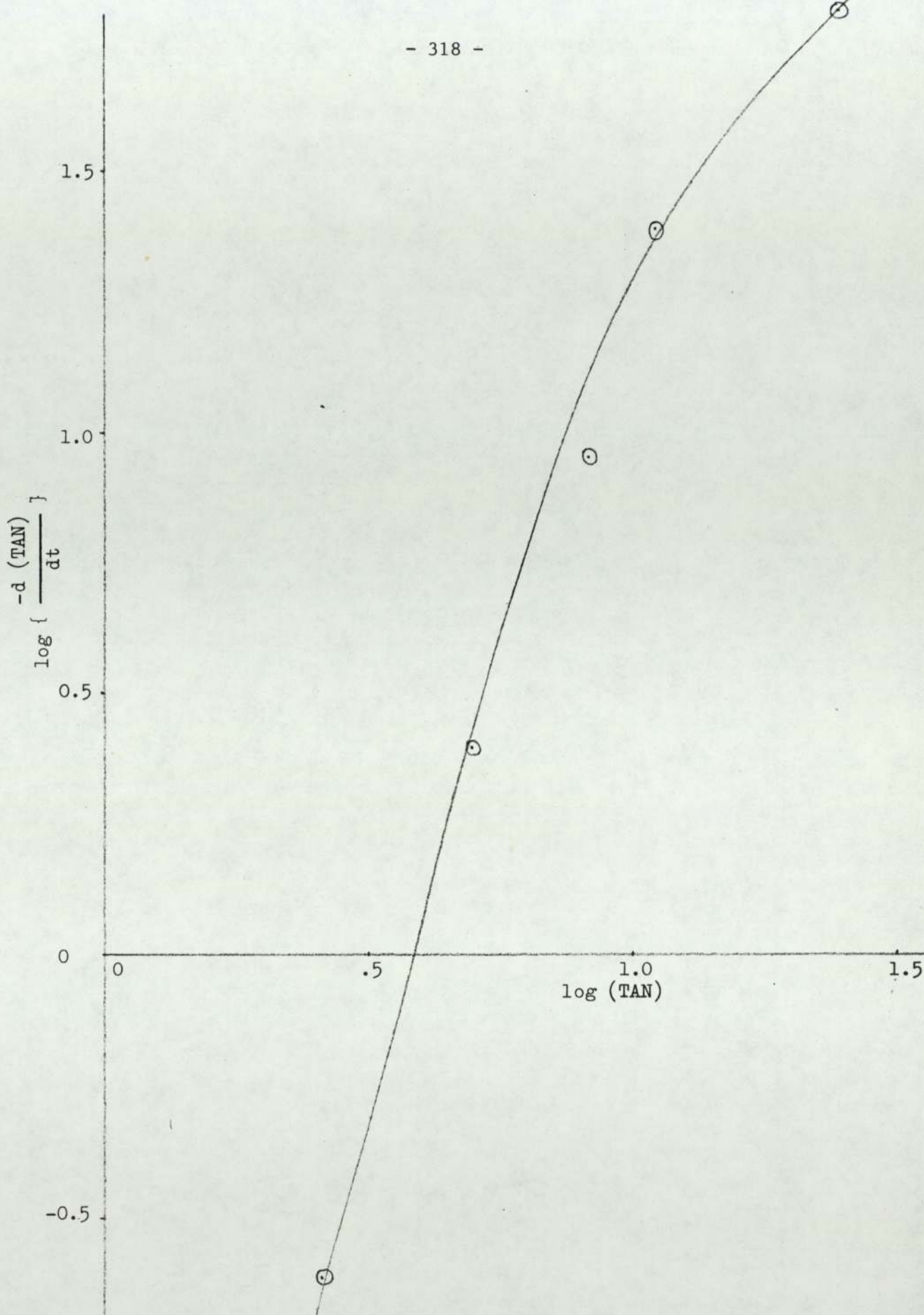


Figure A6.3

Graph for run 36 of $\log \left[\frac{-d(TAN)}{dt} \right]$ vs.

log (TAN), with $\alpha = 1.0$ and temperature = 200°C

For run 36 from Table 6.1 in Chapter Six.

$$\text{Weight of PIBSA} = 405.17\text{g}$$

$$\text{Weight of dilution oil} = 0.7768 \times 405.17 = 314.74\text{g}$$

$$\text{Weight of catalyst} = 0.022 \times 405.17 = 8.92\text{g}$$

$$\therefore \text{total mixture weight} = 728.83\text{g}$$

the initial concentration C_A^0 can now be obtained using equation (8.25)

$$\therefore C_A^0 = (0.9198 \times 10^{-3})(405.17) \times \frac{0.814 \times 10^3}{728.83}$$

$$\therefore C_A^0 = 0.4162 \text{ equivalents/dm}^3$$

$$\therefore \gamma = \frac{0.4162}{22.5} = 0.0185 \left[\frac{\text{equivalents}}{\text{dm}^3} \cdot \frac{\text{gsample}}{\text{mg KOH}} \right]$$

substituting the values of the intercept, n , and γ in equation (8.24) we have,

$$-0.275 = \log k + (1.588 - 1.0) \log (0.0185)$$

$$\therefore k = 5.545 \text{ (equivalents/dm}^3)^{1-n} \cdot \text{hr}^{-1} \text{ the rate constant}$$

The actual plot of $\log \left[\frac{-d(\text{TAN})}{dt} \right]$ vs. $\log(\text{TAN}-2.0)$ is given in Figure A6.2.

A plot of $\log \left[\frac{-d(\text{TAN})}{dt} \right]$ vs. $\log(\text{TAN})$ was also carried out and Figure A6.3 was obtained.

Detailed calculations of run 42

Table A6.3 below gives the weight measurements of the samples taken during run 42 with their titration results.

All the tabulated TAN values were calculated using equation (A3.1) in Appendix 3, as was shown before,

$$\text{TAN} = \frac{(v-b) \times N \times 56.1}{w} \quad \text{A3.1}$$

A plot of TAN vs. time (hr) was carried out and Figure A6.4 was obtained.

TABLE A6.3

Weight measurements of samples and their titration results, for run 42

No. of sample	Time after PE addition min.	Weight of empty beaker g	Weight of beaker plus sample g	Weight of sample g	Starting level of base volume in burette cm ³	Level of base volume at end of titration cm ³	Volume of base used in titration cm ³	TAN $\frac{\text{mg KOH}}{\text{g sample}}$
1	0.5	116.3606	117.5014	1.1408	5.025	9.90	4.875	23.9
2	6.0	115.9984	117.1827	1.1843	10.0	14.00	4.00	18.9
3	12.0	124.2641	125.4200	1.1559	14.05	17.15	3.10	14.9
4	18.0	116.4355	117.6145	1.1790	19.30	22.00	2.70	12.7
5	30.0	124.1770	125.3010	1.1240	17.275	19.25	1.975	9.6
6	45.0	122.9694	124.3230	1.3536	22.05	23.925	1.875	7.6
7	60.0	124.8730	125.9145	1.0415	3.60	4.80	1.20	6.2
8	75.0	124.2910	125.7007	1.4097	4.85	6.30	1.45	5.6
9	90.0	125.8212	127.0961	1.2749	6.325	7.525	1.20	5.0
10	120.0	125.1559	126.5817	1.4258	7.55	8.70	1.15	4.3
11	150.0	116.2420	117.6764	1.4344	8.725	9.80	1.075	4.0
12	210.0	51.0383	52.5766	1.5383	9.825	10.825	1.00	3.4
13	270.0	117.6034	119.1683	1.5649	10.975	11.875	0.90	3.0
14	330.0	125.3851	127.1268	1.7417	11.90	12.825	0.925	2.8

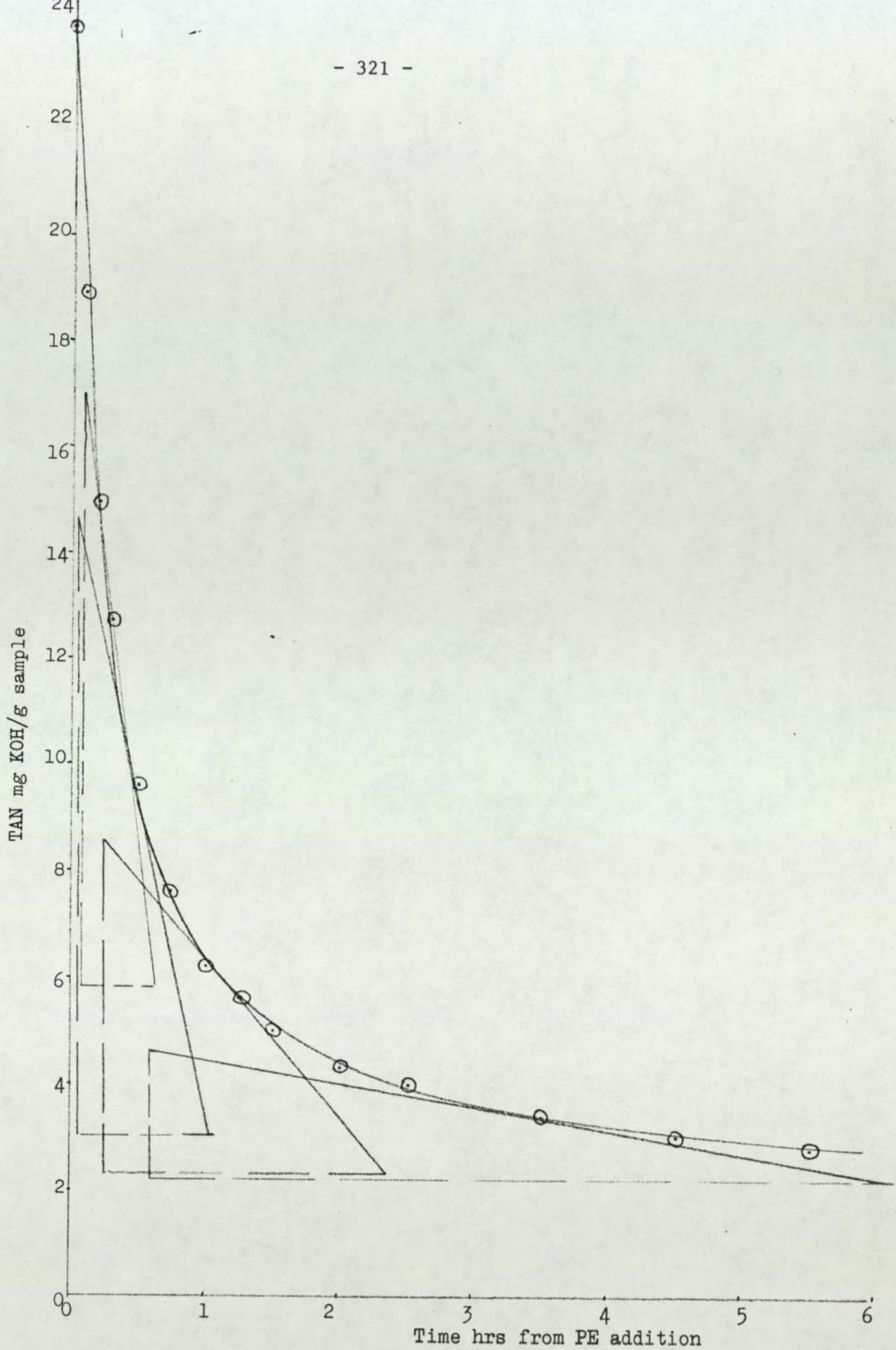


Figure A6.4

Graph for run 42 of TAN mg KOH/g vs. time hrs from PE addition

PE/PIBSA equivalent ratio $\alpha = 1.25$

The slope of the curve in Figure A6.4 was measured at five different points covering most of the reaction range, and the results were tabulated in Table A6.4. The value of the residual Total Acid Number, TAN^{∞} was estimated from the graph to be equal to 2.5 mg KOH/g for run 42. Also since α is larger than 1.0 ($\alpha = 1.25$) then equation (8.20) in Chapter 8 is applicable, hence let

$$Y = \log \left[\frac{-\frac{d(TAN)}{dt}}{[TAN_R + (\alpha - 1.0)TAN_R^0]^n} \right]$$

and

$$X = \log \left[\frac{TAN_R}{[TAN_R + (\alpha - 1)TAN_R^0]} \right]$$

where, for run 42:

$$TAN_R = (TAN - 2.5)$$

$$\alpha = 1.25$$

$$n = 1.614$$

and $\frac{d(TAN)}{dt}$ = The slope of the TAN vs. time curve

the individual values of Y and X (y_i and x_i) at those points, at which the slope was calculated, were evaluated and also tabulated in Table A6.4 below.

TABLE A6.4

The values of the slope of TAN vs. time curve measured at five different points, together with the calculated values of Y and X for run 42.

TAN mg KOH/g	TAN _R mg KOH/g	$\frac{d(\text{TAN})}{dt}$ TAN/hr	Y	X
23.9	21.4	-45.00	-0.6506	-0.09691
13.2	10.7	-20.00	-0.6446	-0.1761
9.6	7.1	-10.761	-0.7358	-0.2439
6.0	3.5	- 2.972	-1.0553	-0.4029
3.4	0.9	- 0.441	-1.6401	-0.8416

As a sample calculation let the values of y_i and x_i for the third point in Table A6.4 be given here, hence

$$y_3 = \log \left[\frac{-(-10.761)}{[7.1 + (1.25-1.0) \times 21.4]^{1.614}} \right] = -0.7358$$

and

$$x_3 = \log \left[\frac{7.1}{[7.1 + (1.25-1.0) \times 21.4]} \right] = -0.2439$$

all the other values of x_i and y_i in Table A6.4 were calculated in the same way. Also from the same table we have,

$$\Sigma x_i = -1.7614, (\Sigma x_i)^2 = 3.1025, \Sigma x_i^2 = 0.9705,$$

$$\Sigma y_i = -4.7263, \Sigma x_i y_i = 2.1616, \text{ and } N = 5$$

hence for the least square best fit straight line for the plot of Y vs. X, the slope and intercept can be calculated using equations (8.22) and (8.23) in Chapter 8,

$$\therefore \text{slope} = \frac{2.1616 - [(-1.7614)(-4.7263)/5]}{0.9705 - [3.1025/5]}$$

$$\therefore \text{slope} = 1.419$$

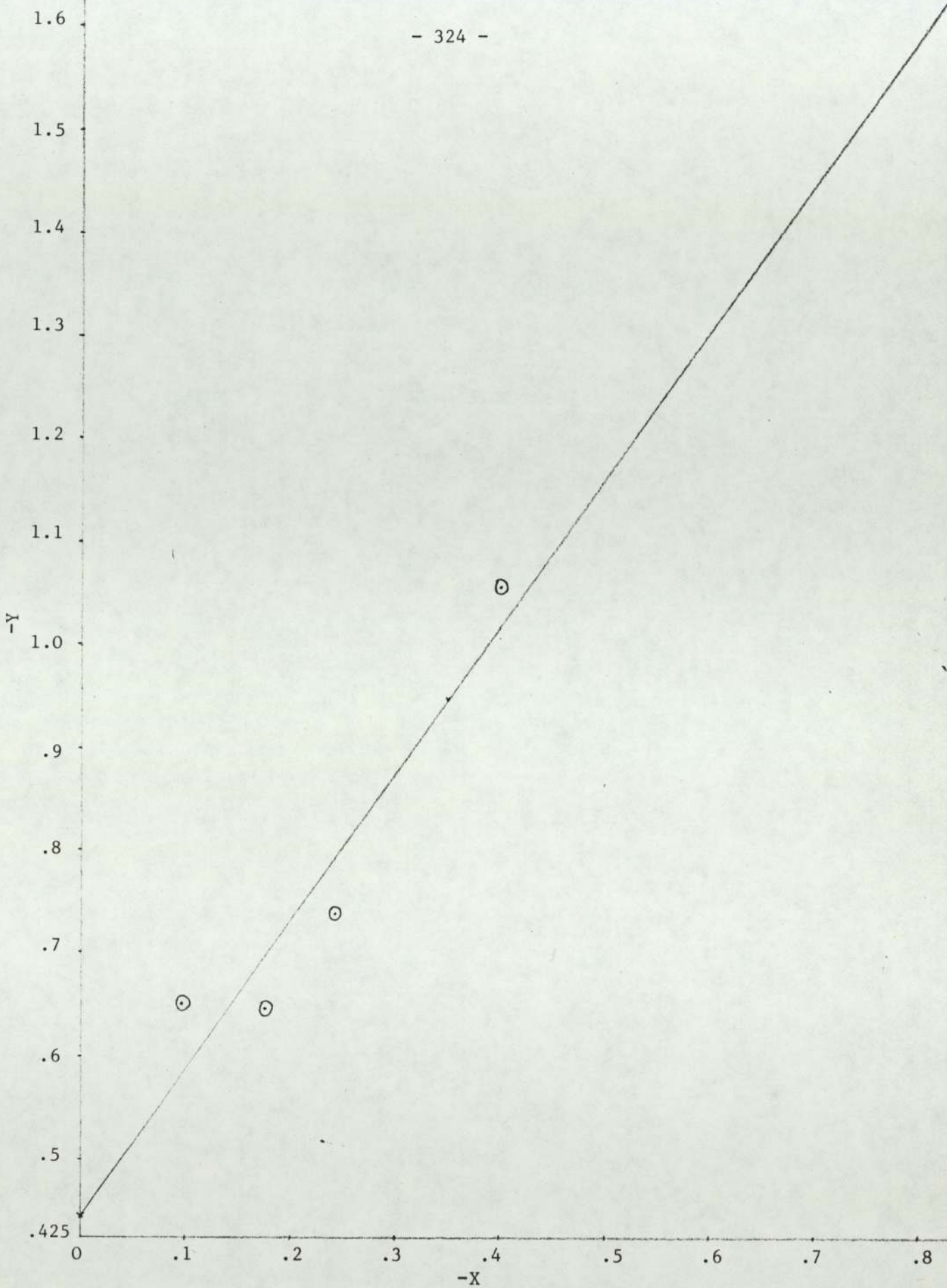


Figure A6.5

Graph for run 42 of $Y = \log \left[\frac{-d(\text{TAN})}{dt} \frac{1}{(\text{TAN}_R + (\alpha-1)\text{TAN}_R^0)^n} \right]$ vs. $X = \log \left[\frac{\text{TAN}_R}{\text{TAN}_R + (\alpha-1)\text{TAN}_R^0} \right]$

PE/PIBSA equivalent ratio $\alpha = 1.25$

$$\text{and intercept} = \frac{(-4.7263)(0.9705) - (-1.7614)(2.1616)}{(5 \times 0.9705) - 3.1025}$$

$$\therefore \text{intercept} = -0.445$$

but from equation (8.20), the slope of the line is equal to (a) the order of reaction with respect to PIBSA, and the intercept is equal to $[\ln k + (n-1)\log\gamma]$,

$$\therefore a = 1.419$$

$$\text{and intercept} = \ln k + (n-1)\log \gamma \quad 8.24$$

The actual plot of Y vs. X is given in Figure A6.5.

For run 42 from Table 6.1 in Chapter 6,

$$\text{Weight of PIBSA} = 401.47\text{g}$$

$$\text{Weight of dilution oil} = 0.7768 \times 401.47 = 311.86\text{g}$$

$$\text{Weight of catalyst} = 0.0118 \times 401.47 = 4.74\text{g}$$

$$\text{Total weight of mixture} = 718.07\text{g}$$

the initial concentration C_A^0 can now be obtained using equation (8.25)

$$\therefore C_A^0 = (0.9198 \times 10^{-3}) (401.47) \times \frac{0.814 \times 10^3}{718.07}$$

$$\therefore C_A^0 = 0.4186 \text{ equivalents/dm}^3$$

$$\therefore \gamma = \frac{C_A^0}{\text{TAN}_R^0} = \frac{0.4186}{21.4} = 0.0196 \left[\frac{\text{equivalents}}{\text{dm}^3} \cdot \frac{\text{g sample}}{\text{mg KOH}} \right]$$

substituting the values of the intercept, n, and γ in equation (8.24) we get,

$$-0.445 = \log k + (1.614-1.0) \log(0.0196)$$

$$\therefore k = 4.014 (\text{equivalents/dm}^3)^{1-n} \cdot \text{hr}^{-1} \text{ the rate constant}$$

Detailed calculations of run 43

Table A6.5 below gives the weight measurements of the samples taken during run 43 with their titration results.

TABLE A6.5

Weight measurements of samples and their titration results for run 43

No. of sample	Time after PE addition min.	Weight of empty beaker g	Weight of beaker plus sample g	Weight of sample g	Starting level of base volume in burette cm ³	Level of base volume at end of titration cm ³	Volume of base used in titration cm ³	TAN $\frac{\text{mg KOH}}{\text{g sample}}$
1	1	116.3611	117.6614	1.3003	3.15	8.60	5.45	23.5
2	6	115.9990	117.5163	1.5173	8.60	13.675	5.075	18.7
3	12	124.2653	125.7957	1.5304	13.675	17.65	3.975	14.5
4	18	116.4357	118.1284	1.6927	17.75	21.575	3.825	12.6
5	30	124.1763	126.0902	1.9139	21.60	24.875	3.275	9.5
6	45	122.9700	124.1104	1.1404	24.90	26.425	1.525	7.2
7	60	124.8731	126.0851	1.2120	26.45	27.80	1.35	6.0
8	90	124.2900	125.5388	1.2488	27.80	28.85	1.05	4.5
9	120	125.8204	127.2341	1.4137	28.90	29.90	1.00	3.7
10	153	125.1554	126.4513	1.3009	29.925	30.75	0.825	3.3
11	210	116.2426	117.6515	1.4089	30.825	31.65	0.825	3.0
12	303	51.0376	52.2613	1.2237	31.675	32.275	0.60	2.5

All the tabulated TAN values were calculated using equation (A3.1) in Appendix 3, as was shown before,

$$\text{TAN} = \frac{(v-b) \times N \times 56.1}{w} \quad \text{A3.1}$$

A plot of TAN vs. time (hr) was carried out and Figure A6.6 was obtained. The slope of the curve in Figure A6.6 was measured at five different points covering most of the reaction range, and the results were tabulated in Table A6.6 below. The value of TAN^∞ was estimated from the graph to be equal to 2.0 mg KOH/g for run 43. Also since $\alpha = 1.5$ then equation (8.20) is applicable, hence as in the calculations carried out for run 42, let

$$Y = \log \left[\frac{-\frac{d(\text{TAN})}{dt}}{[\text{TAN}_R + (\alpha - 1.0)\text{TAN}_R^0]^n} \right]$$

and

$$X = \log \left[\frac{\text{TAN}_R}{[\text{TAN}_R + (\alpha - 1.0)\text{TAN}_R^0]} \right]$$

where for run 43;

$$\text{TAN}_R = (\text{TAN} - 2.0)$$

$$\alpha = 1.5$$

$$n = 1.614$$

$$\text{and } \frac{d(\text{TAN})}{dt} = \text{The slope of the TAN vs. time curve}$$

the individual values of Y and X (y_i and x_i) at those points at which the slope was calculated were evaluated and also tabulated in Table A6.6.

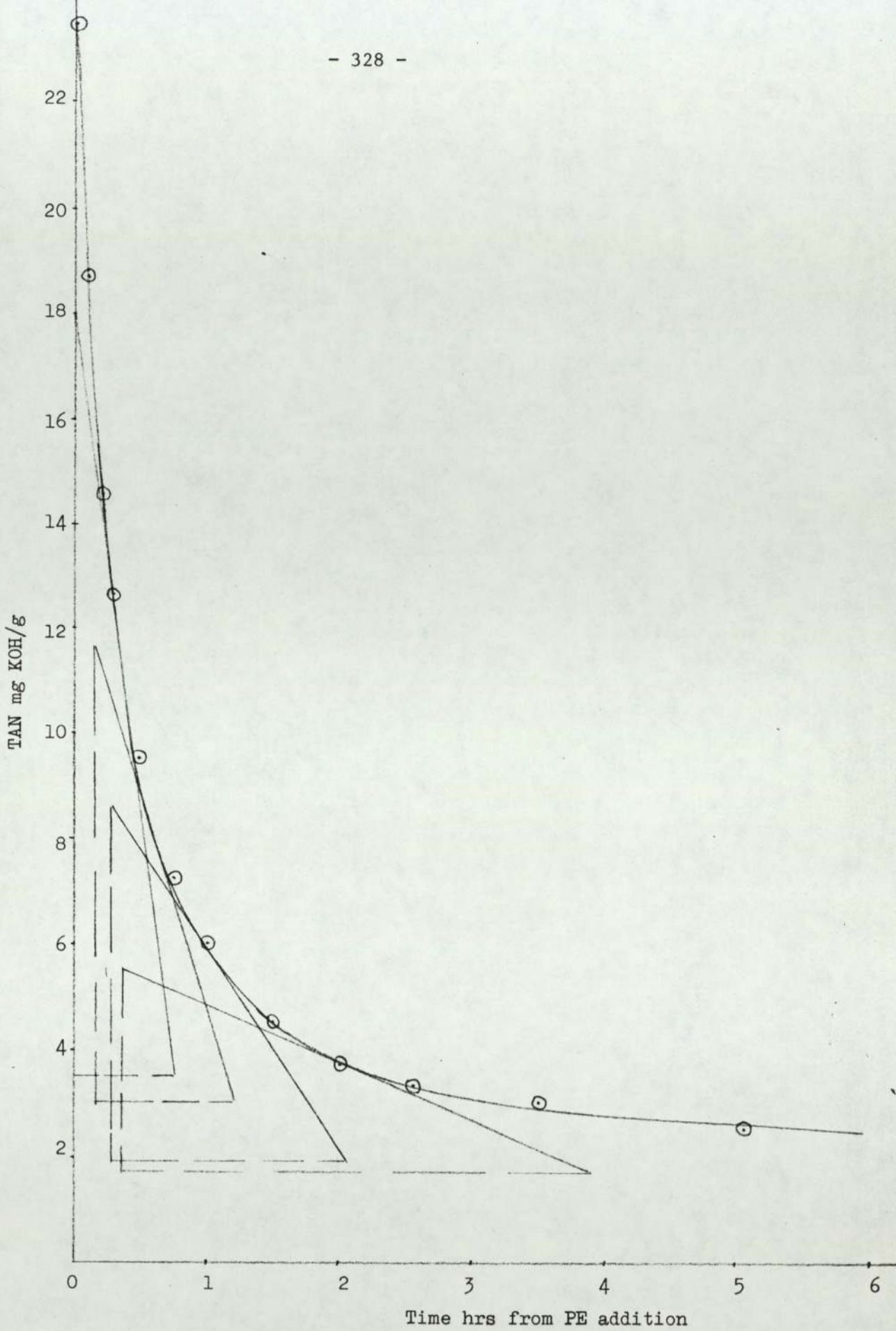


Figure A6.6

Graph for run 43 of TAN mg KOH/g sample vs. time hrs
PE/PIBSA equivalent ratio $\alpha = 1.5$

TABLE A6.6

The values of the slope of TAN vs. time curve measured at five different points, together with the calculated values of Y and X for run 43

TAN mg KOH/g	TAN _R mg KOH/g	$\frac{d(\text{TAN})}{dt}$ TAN/hr	Y	X
23.5	21.5	-45.000	-0.7816	-0.1761
11.0	9.0	-17.237	-0.8546	-0.3413
8.0	6.0	- 8.269	-1.0581	-0.4459
6.0	4.0	- 3.807	-1.3058	-0.5667
3.75	1.75	- 1.080	-1.7370	-0.8539

As a sample calculation let us calculate the values of y_i and x_i for the last point in Table A6.6, hence

$$y_5 = \log \left[\frac{-(-1.080)}{[1.75 + (1.5-1.0) \times 21.5]^{1.614}} \right]$$

$$\therefore \underline{y_5 = -1.7370}$$

and
$$x_5 = \log \left[\frac{1.75}{[1.75 + (1.5-1.0) \times 21.5]} \right]$$

$$\therefore \underline{x_5 = -0.8539}$$

All the other values of x_i and y_i in Table A6.6 were calculated in the same way. Also from the same table we have,

$$\Sigma x_i = -2.3839, (\Sigma x_i)^2 = 5.6830, \Sigma x_i^2 = 1.3966,$$

$$\Sigma y_i = -5.7371, \Sigma x_i y_i = 3.1243, \text{ and } N = 5$$

hence for the least square best fit straight line for the plot of

Y vs. X, the slope and intercept can be calculated using equations (8.22) and (8.23) as before,

$$\therefore \text{slope} = \frac{3.1243 - [(-2.3839)(-5.7371)/5]}{1.3966 - [5.6830/5]}$$

$$\therefore \text{slope} = 1.496 = a \quad \text{Order of reaction with respect to PIBSA}$$

$$\text{and intercept} = \frac{(-5.7371)(1.3966) - (-2.3839)(3.1243)}{(5 \times 1.3966) - 5.6830}$$

$$\therefore \text{intercept} = -0.4342 = \log k + (n-1) \log \gamma \quad 8.24$$

The plot of Y vs. X was carried out and Figure A6.7 was obtained.

Also for run 43, from Table 6.1 we have,

Weight of PIBSA	= 404.10g
Weight of dilution oil	= 313.91g
Weight of catalyst	= 4.77g
\therefore Total weight of mixture	= 722.78g

the initial concentration can be found by using equation (8.25),

$$\therefore C_A^0 = (0.9198 \times 10^{-3})(404.1) \times \frac{0.814 \times 10^3}{722.78}$$

$$\therefore C_A^0 = 0.4186 \text{ equivalents/dm}^3$$

$$\therefore \gamma = \frac{C_A^0}{\text{TAN}_R^0} = \frac{0.4186}{21.5} = 0.0195 \left[\frac{\text{equivalents}}{\text{dm}^3} \cdot \frac{\text{g sample}}{\text{mg KOH}} \right]$$

substituting the values of the intercept, n, and γ in equation (8.24)

we get

$$-0.4342 = \log k + (1.614 - 1.0) \log(0.0195)$$

$$\therefore k = 4.130 \text{ (equivalents/dm}^3)^{1-n} \cdot \text{hr}^{-1} \text{ the rate constant.}$$

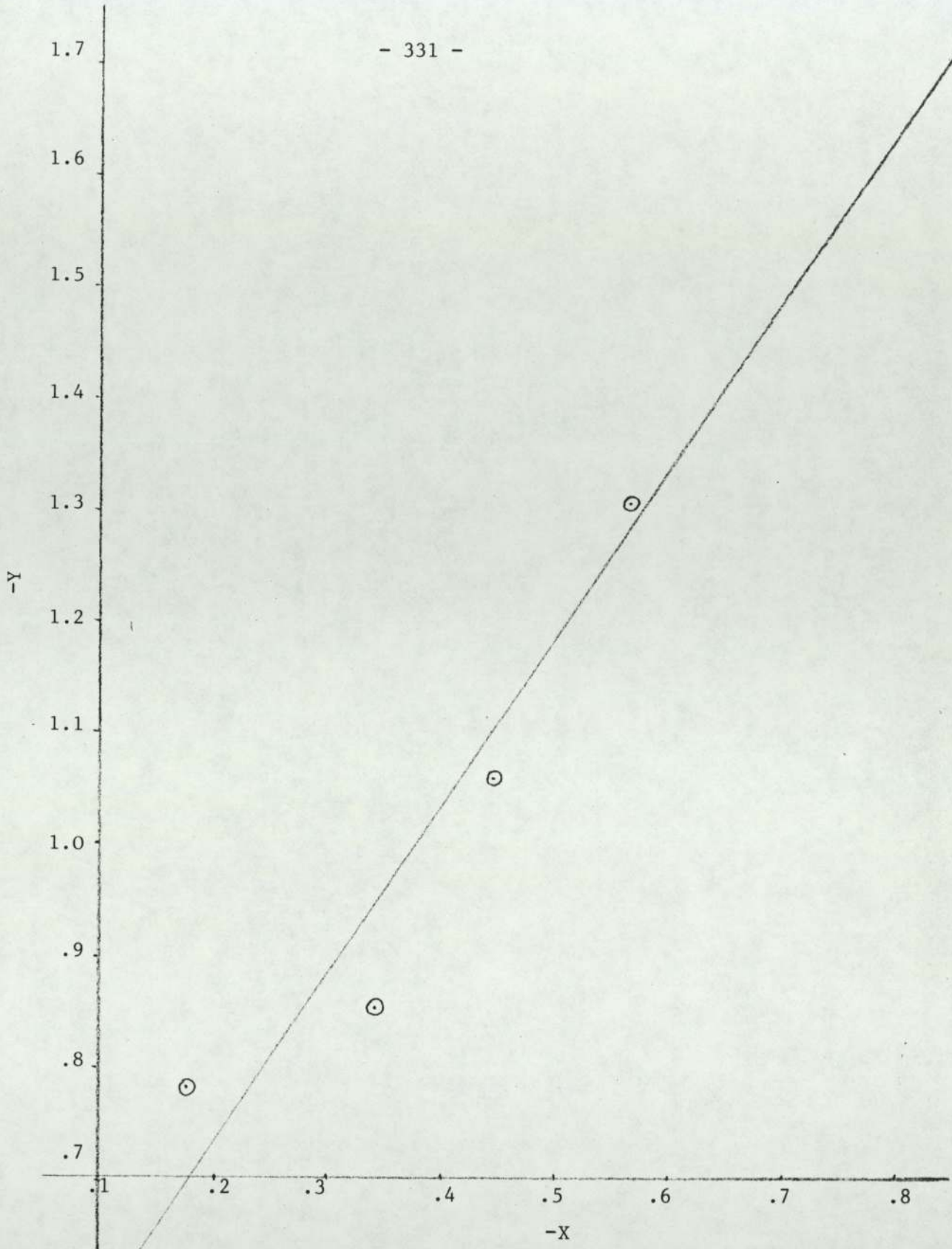


Figure A6.7

Graph for run 43 of $Y = \log \left[\frac{-d(\text{TAN})}{dt} \right]$
 $\left[\text{TAN}_R + (\alpha - 1) \text{TAN}_R^0 \right]^n$

vs. $X = \log \left[\frac{\text{TAN}_R}{\left[\text{TAN}_R + (\alpha - 1) \text{TAN}_R^0 \right]} \right]$, with $\alpha = 1.5$

Detailed calculations of run 46

Table A6.7 contains the weight measurements of samples taken during run 46 together with their titration results. The tabulated TAN values were calculated using equation (A3.1) as in previous runs,

$$\text{TAN} = \frac{(v-b) \times N \times 56.1}{w} \quad \text{A3.1}$$

A plot of TAN vs. time (hr) was carried out and Figure A6.8 was obtained. The slope of the curve in Figure A6.8 was measured at five different points and the results were tabulated in Table A6.8. The value of TAN^∞ was estimated from Figure A6.8 to be equal to 3.0 mg KOH/g for run 46.

Run 46 was carried out at 180°C with $\alpha = 1.0$, hence equation (8.13) in Chapter 8 is applicable. From the values of the slope of TAN vs. time curve tabulated in Table A6.8, the respective values of $\log \left[-\frac{d(\text{TAN})}{dt} \right]$ and $\log(\text{TAN}-3.0)$ were calculated and also tabulated in Table A6.8.

TABLE A6.8

The slope of TAN vs. time curve measured at five different points for run 46.

TAN mg KOH/g	slope $\frac{d(\text{TAN})/dt}{\text{TAN/hr}}$	$\log \left[-\frac{d(\text{TAN})}{dt} \right]$ = y_i	$\log(\text{TAN}-3.0)$ = x_i
25.5	-35.000	1.544	1.352
13.0	- 8.295	0.919	1.000
10.0	- 4.286	0.632	0.845
7.0	- 1.934	0.286	0.602
5.0	- 0.6739	-0.1714	0.301

hence for the least square best fit straight line of the plot of $\log \left[\frac{-d(\text{TAN})}{dt} \right]$ vs. $\log (\text{TAN}-3.0)$, we get from Table A6.8,

TABLE A6.7

Weight measurements of run 46 samples and their titration results

Number of sample	Time after PE addition min.	Weight of empty beaker g	Weight of beaker plus sample g	Weight of sample g	Volume of base used in titration cm ³	TAN $\frac{\text{mg KOH}}{\text{g sample}}$
1	0.5	116.3606	117.6055	1.2449	5.66	25.5
2	6.5	115.9981	116.8756	0.8775	3.38	21.4
3	12.0	124.2648	125.5328	1.2680	4.20	18.5
4	16.0	116.4339	117.6552	1.2213	3.88	17.7 *
5	18.0	124.1859	125.3657	1.1798	-	-
6	30.0	122.9725	124.1972	1.2247	3.22	14.6
7	45.0	124.8800	126.3652	1.4852	3.31	12.4
8	60.0	124.2827	125.6910	1.4083	2.65	10.4
9	90.0	125.8251	127.2702	1.4451	2.32	8.84
10	120.0	125.1550	126.5314	1.3764	1.83	7.25
11	180.0	116.2419	117.5431	1.3012	1.37	5.65
12	240.0	125.3892	126.8524	1.4632	1.37	5.0
13	300.0	117.6026	119.0682	1.4656	1.22	4.4
14	360.0	45.7688	47.0366	1.2678	0.91	3.75

* Sample five was taken but it was not titrated since there was only a small time gap between samples five and six.

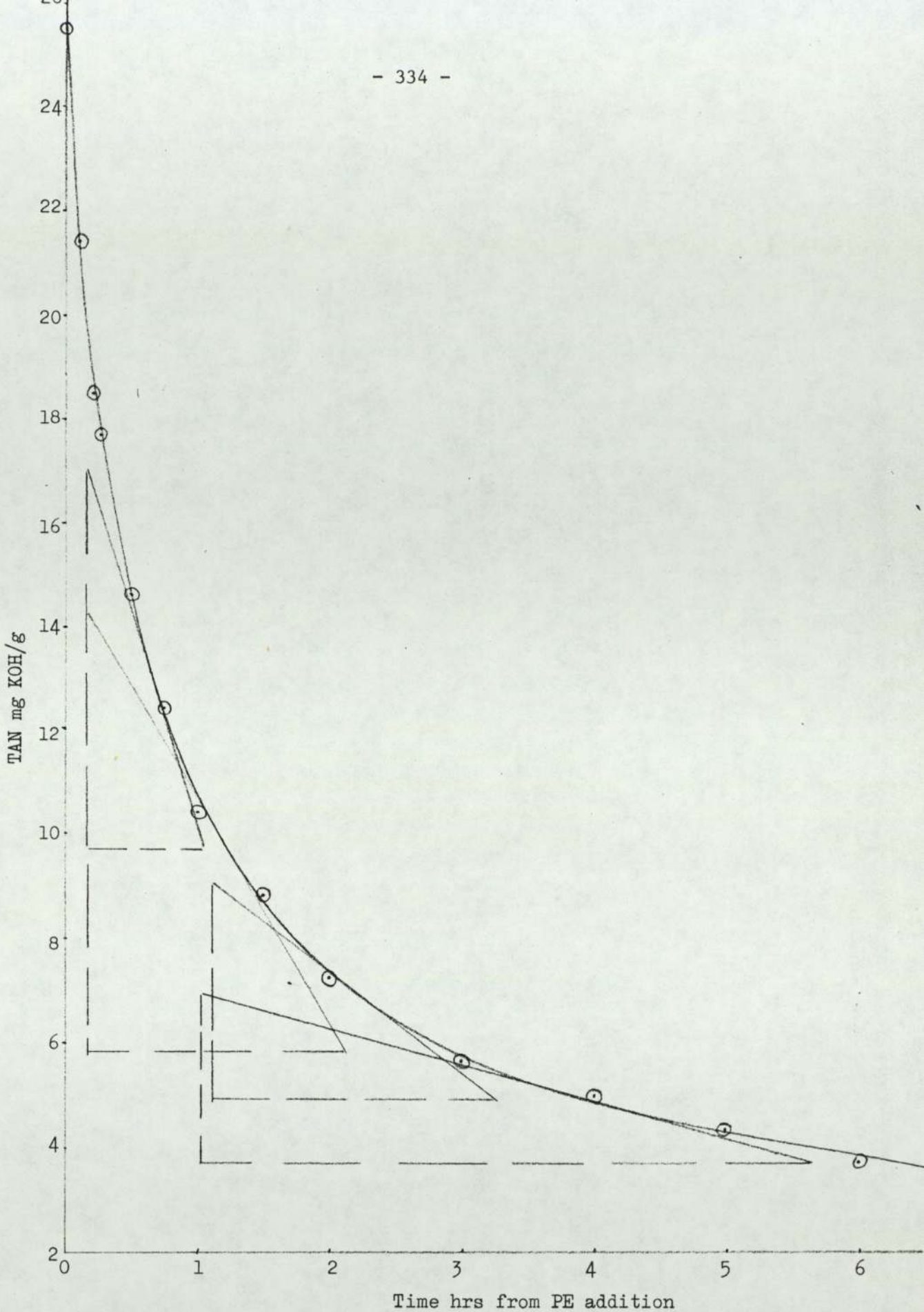


Figure A6.8

Graph for run 46 of TAN mg KOH/g vs. time hr after PE addition

PE/PIBSA equivalent ratio $\alpha = 1.0$

Temperature = 180°C

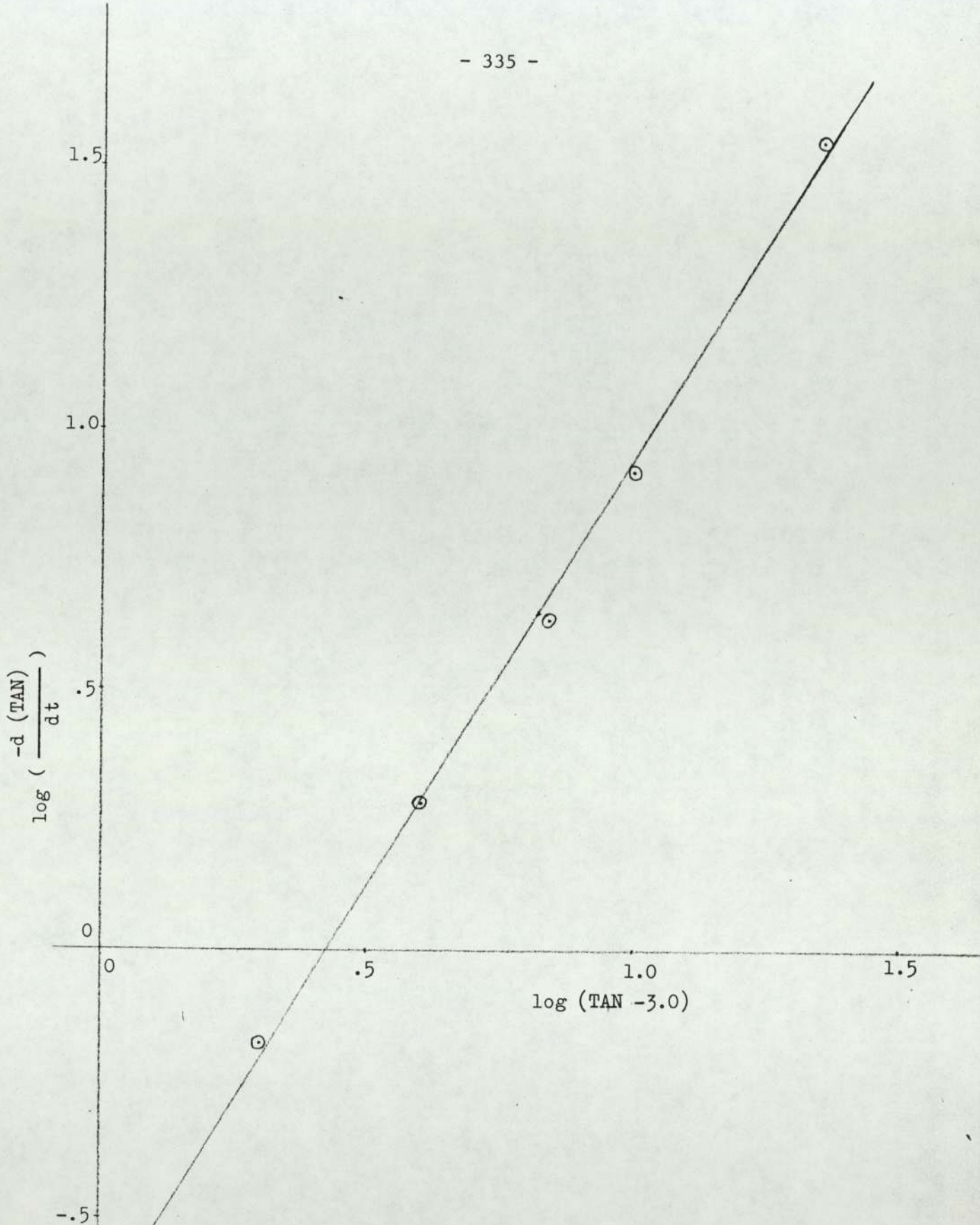


Figure A6.9

Graph for run 46 of $\log\left[\frac{-d(\text{TAN})}{dt}\right]$ vs. $\log(\text{TAN} - 3.0)$

Temperature = 180°C, and $\alpha = 1.0$

$$\Sigma x_i = 4.1000, (\Sigma x_i)^2 = 16.8100, \Sigma x_i^2 = 3.9949,$$

$$\Sigma y_i = 3.2096, \Sigma x_i y_i = 3.6611, \text{ and } N = 5$$

the slope and intercept of the best fit are given by equations (8.22)

and (8.23), therefore,

$$\text{slope} = \frac{3.6611 - [4.100 \times 3.2096/5]}{3.9949 - [16.810/5]}$$

$$\therefore \text{slope} = 1.626 = n \text{ over all order of reaction}$$

$$\text{and intercept} = \frac{3.2096 \times 3.9949 - 4.100 \times 3.6611}{5 \times 3.9949 - 16.810}$$

$$\therefore \text{intercept} = -0.6916 = \log k + (n-1) \log \gamma \quad 8.24$$

the plot of $\log \left[\frac{-d(\text{TAN})}{dt} \right]$ vs. $\log (\text{TAN}-3.0)$ is given in Figure A6.9.

From Table 6.1 for run 46 we have,

$$\text{Weight of PIBSA} = 404.31\text{g}$$

$$\text{Weight of dilution oil} = 314.07\text{g}$$

$$\text{Weight of catalyst} = 4.77\text{g}$$

$$\therefore \text{Total weight of mixture} = 723.15\text{g}$$

also the density of the final product was measured using the density flask D.F. as follows:

$$\text{Weight of D.F. + product at } 180^\circ\text{C} = 67.2251\text{g}$$

$$\text{but weight of the empty D.F.} = 27.7050\text{g}$$

$$\text{and volume of the D.F. (from before)} = 49.3152 \text{ cm}^3$$

$$\therefore \text{density of the product} = \frac{67.2251 - 27.7050}{49.3152} = 0.842 \text{ g/cm}^3$$

this value is tabulated in Table 8.1 in Chapter 8, and the average density for run 46 at 180°C is then obtained and also tabulated in Table 8.1 and is equal to 0.830 g/cm^3 . Equation (8.25) can now be used to calculate C_A^0 ,

$$\therefore C_A^0 = (0.9198 \times 10^{-3})(404.31) \times \frac{0.830 \times 10^3}{723.15}$$

$$\therefore C_A^0 = 0.4268 \text{ (equivalents/dm}^3\text{)}$$

$$\therefore \gamma = \frac{0.4268}{22.5} = 0.01897 \left[\frac{\text{equivalents}}{\text{dm}^3} \cdot \frac{\text{g sample}}{\text{mg KOH}} \right]$$

hence from equation (8.24) we have

$$-0.6916 = \log k + (1.626 - 1.0) \log (0.01897)$$

$$\therefore k = 2.434 \text{ (equivalents/dm}^3\text{)}^{1-n} \cdot \text{hr}^{-1} \text{ the rate constant.}$$

Detailed calculations of run 47

Table A6.9 contains the weight measurements of samples taken during run 47, together with their titration results. The tabulated TAN values were all calculated using equation (A3.1) as before

$$\text{TAN} = \frac{(v-b) \times N \times 56.1}{w} \tag{A3.1}$$

A plot of TAN vs. time (hr) was carried out and Figure A6.10 was obtained. The slope of the curve in Figure A6.10 was measured at five different points and the results were tabulated in Table A6.10 below. The value of TAN^∞ was estimated from Figure A6.10 to be equal to 3.0 mg KOH/g for run 47.

Run 47 was carried out at 190°C with $\alpha = 1.0$, hence equation (8.13) is applicable. From the values of the slope tabulated in Table A6.10, the respective values of $\log \left[\frac{-d(\text{TAN})}{dt} \right]$ and $\log(\text{TAN}-3.0)$ were calculated and also tabulated in Table A6.10.

TABLE A6.9

Weight measurements of run 47 samples and their titration results

Number of sample	Time after PE addition min.	Weight of empty beaker g	Weight of beaker plus sample g	Weight of sample g	Volume of base used in titration cm ³	TAN $\frac{\text{mg KOH}}{\text{g sample}}$
1	1	116.3610	117.5347	1.1737	5.13	24.5
2	6	115.9991	117.1745	1.1754	4.30	20.5
3	12	124.2650	125.4085	1.1435	3.50	17.04
4	18	116.4426	117.8788	1.4362	3.91	15.2
5	30	124.1856	125.4802	1.2946	2.85	12.2
6	45	122.9737	124.2597	1.2860	2.36	10.1
7	60	124.8811	126.2400	1.3589	2.1	8.5
8	90	124.2827	125.6804	1.3977	1.75	6.8
9	120	125.8101	127.1410	1.3309	1.45	5.9
10	180	125.1555	126.6046	1.4491	1.27	4.7
11	240	116.2422	118.7710	2.5288	1.94	4.2
12	300	125.3878	128.1768	2.7890	2.05	4.0
13	360	117.6030	120.5458	2.9428	2.0	3.7

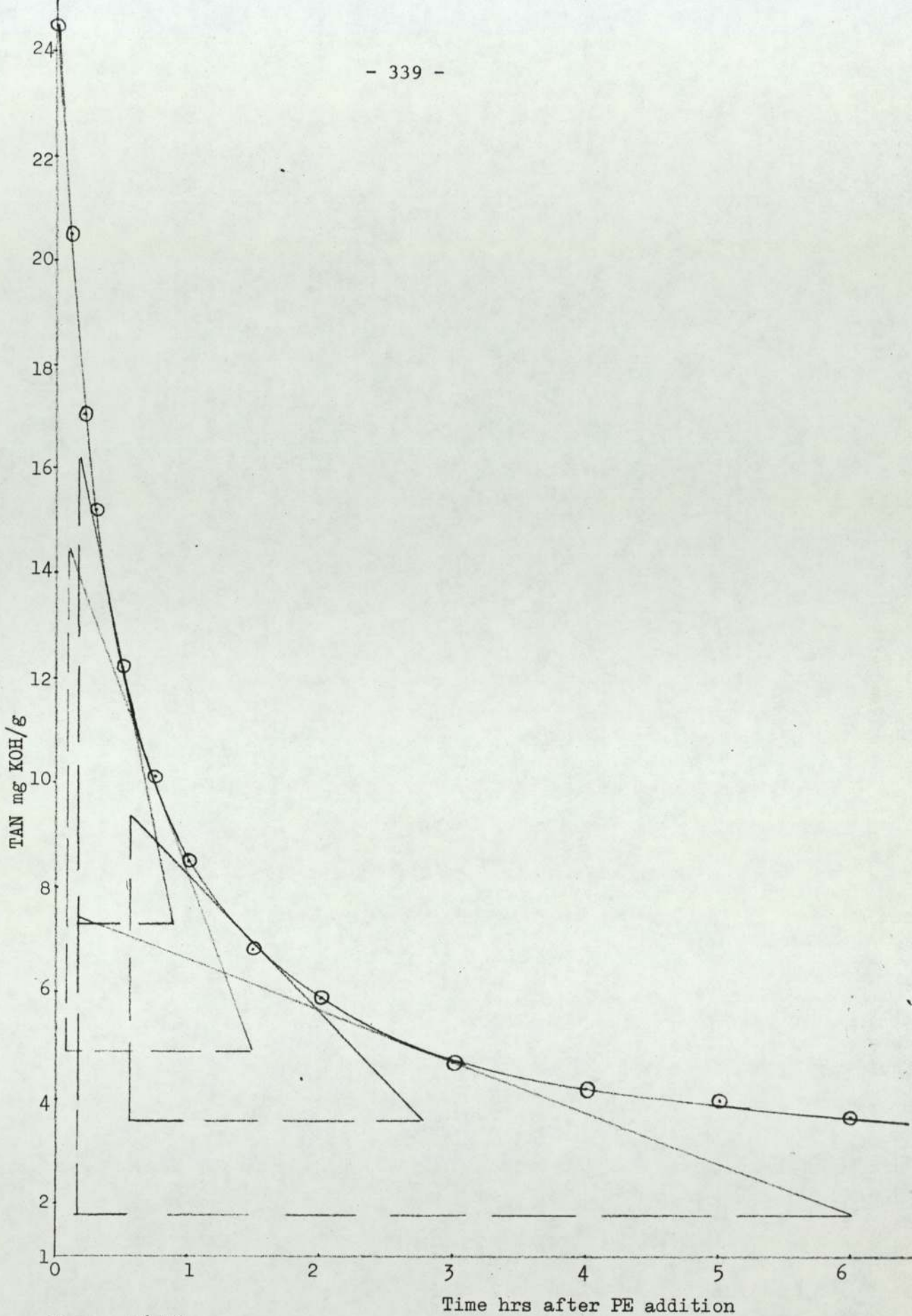


Figure A6.10

Graph for run 47 of TAN mg KOH/g vs. time hrs after PE addition

Temperature = 190°C, $\alpha = 1.0$

TABLE A6.10

The slope of TAN vs. time curve measured at five different points for run 47

TAN mg KOH/g	slope = d(TAN)/dt TAN/hr	$\log \left[\frac{-d(\text{TAN})}{dt} \right]$ = y_i	$\log(\text{TAN}-3.0)$ = x_i
24.5	-37.300	1.5717	1.3324
13	-12.361	1.0921	1.0000
10	- 6.7857	0.8316	0.8451
7	- 2.5909	0.4135	0.602
5	- 0.9589	-0.0182	0.301

with $\sum x_i = 4.0804$, $(\sum x_i)^2 = 16.650$, $\sum x_i^2 = 3.9425$

$\sum y_i = 3.8907$, $\sum x_i y_i = 4.1324$, and $N = 5$

The slope and intercept of the least square best fit straight line of the plot of $\log \left[\frac{-d(\text{TAN})}{dt} \right]$ vs. $\log(\text{TAN}-3.0)$ are given by equations (8.22) and (8.23), therefore

$$\text{slope} = \frac{4.1324 - [4.0804 \times 3.8907/5]}{3.9425 - [16.650/5]}$$

$$\therefore \text{slope} = 1.563 = n \text{ over all order of reaction}$$

$$\text{and intercept} = \frac{3.8907 \times 3.9425 - 4.0804 \times 4.1324}{5 \times 3.9425 - 16.650}$$

$$\therefore \text{intercept} = -0.4972 = \log k + (n-1) \log \gamma \quad 8.24$$

the actual plot of $\log \left[-\frac{d(\text{TAN})}{dt} \right]$ vs. $\log (\text{TAN}-3.0)$ is given in Figure A6.11.

From Table 6.1 for run 47 we have,

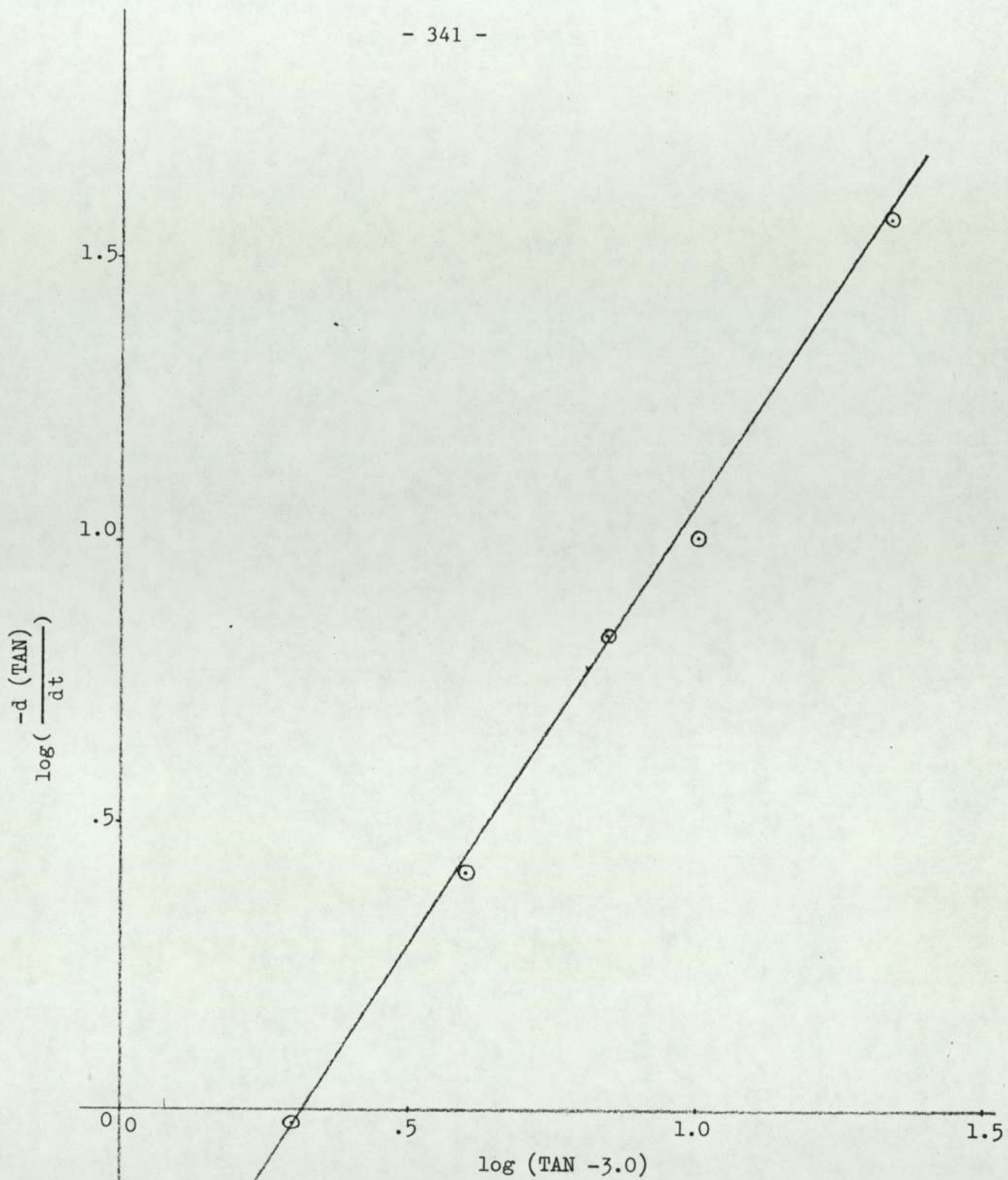


Figure A6.11
Graph for run 47 of $\log\left[\frac{-d(TAN)}{dt}\right]$ vs. $\log(TAN - 3.0)$
Temperature = 180°C, $\alpha = 1.0$

Weight of PIBSA	=	401.90g
Weight of dilution oil	=	312.20g
Weight of catalyst	=	4.74g
∴ Total mixture weight	=	718.84g

also the density of the final product was measured using the density flask (D.F.) as follows:

Weight of D.F. + product at 190°C	=	66.8240g
but Weight of D.F. empty	=	25.7050g
and Volume of D.F.	=	49.3152 cm ³
∴ density of the product at 190°C	=	0.8338 g/cm ³

this value is tabulated in Table 8.1 in Chapter 8, and the average density for run 47 at 190°C is then obtained and equal to 0.822 g/cm³.

Equation (8.25) can now be used to calculate C_A^0 ,

$$\therefore C_A^0 = (0.9198 \times 10^{-3})(401.90) \times \frac{0.822 \times 10^3}{718.84}$$

$$\therefore C_A^0 = 0.4227 \text{ (equivalents/dm}^3\text{)}$$

$$\therefore \gamma = \frac{0.4227}{21.5} = 0.01966 \left[\frac{\text{equivalents}}{\text{dm}^3} \cdot \frac{\text{g sample}}{\text{mg KOH}} \right]$$

hence from equation (8.24) we have

$$-0.4972 = \log k + (1.563 - 1.0) \log(0.01966)$$

$$\therefore k = 2.9075 \text{ (equivalents/dm}^3\text{)}^{1-n} \cdot \text{hr}^{-1} \text{ the rate constant}$$

Detailed calculations of run 48

Table A6.11 contains the weight measurements of samples taken during run 48, together with their titration results. The tabulated TAN values were all calculated using equation (A3.1) as before.

$$\text{TAN} = \frac{(v-b) \times N \times 56.1}{w} \quad \text{A3.1}$$

TABLE A6.11

Weight measurements of run 48 samples and their titration results

Number of sample	Time after PE addition min.	Weight of empty beaker g	Weight of beaker plus sample g	Weight of sample g	Volume of base used in titration cm ³	TAN $\frac{\text{mg KOH}}{\text{g sample}}$
1	1	116.3630	117.7153	1.3523	5.93	24.6
2	6	116.0039	117.2701	1.2662	4.25	18.8
3	12	124.2665	125.5888	1.3223	3.48	14.6
4	18	116.4445	117.7800	1.3355	2.97	12.3
5	30	124.1861	125.5577	1.3716	2.43	9.8
6	45	122.9735	124.3342	1.3607	1.90	7.6
7	60	124.8816	126.1723	1.2907	1.58	6.6
8	90	124.2846	125.5572	1.2726	1.25	5.3
9	120	125.8127	127.0377	1.2250	1.09	4.7
10	180	125.1563	127.8758	2.7195	2.13	4.3
11	240	116.2433	118.4683	2.2250	1.55	3.8
12	300	125.3892	128.1168	2.7276	1.77	3.5
13	360	117.6045	120.4844	2.8799	1.73	3.3

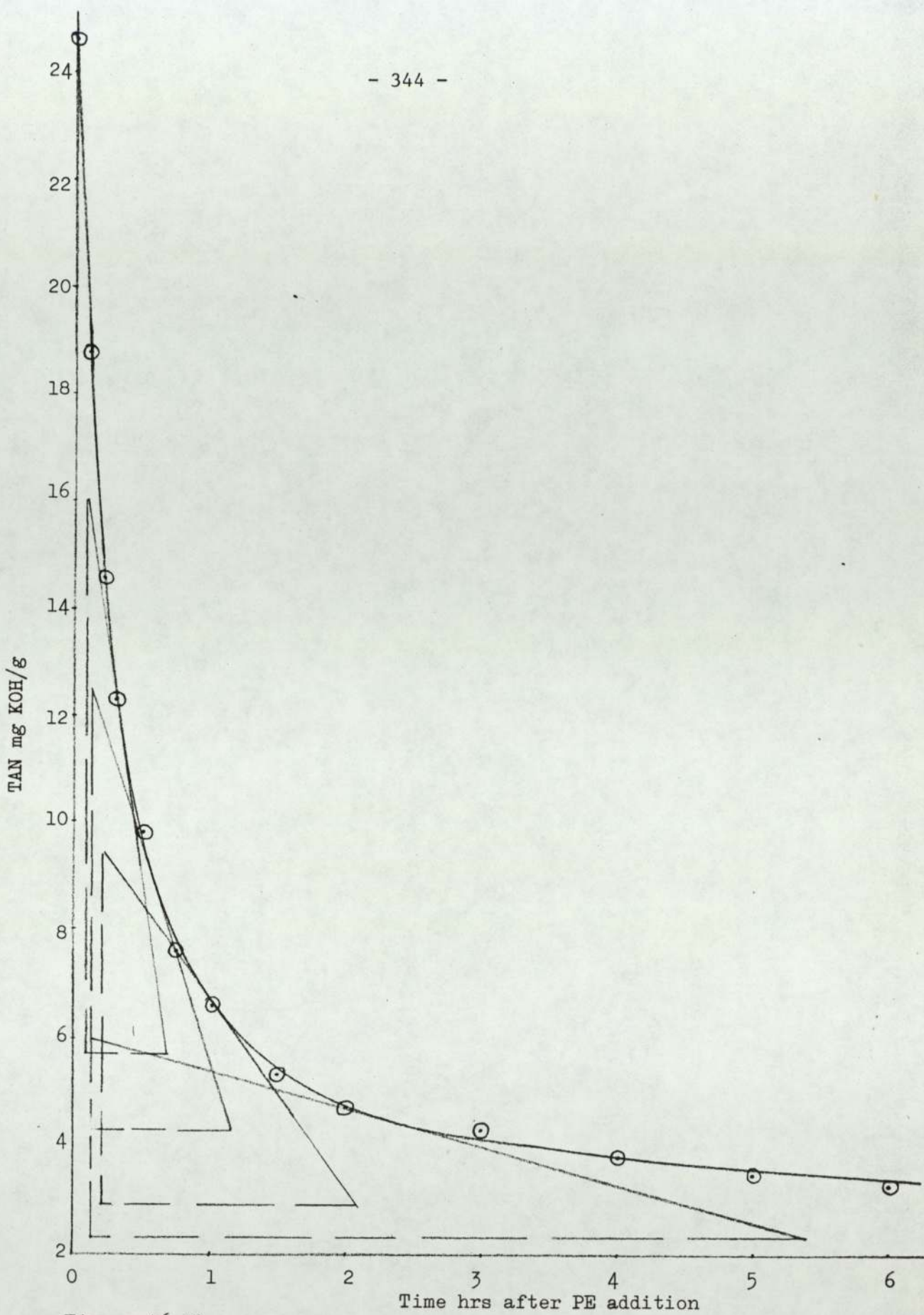


Figure A6.12

Graph for run 48 of TAN mg KOH/g vs. time hr after PE addition

Temperature = 210°C, $\alpha = 1.0$

A plot of TAN vs. time (hr) was carried out and Figure A6.12 was obtained. The slope of the curve in Figure A6.12 was measured at five different points and the results were tabulated in Table A6.12 below. The value of TAN^{∞} was estimated from Figure A6.12 to be equal to 3.0 mg KOH/g for run 48.

TABLE A6.12

The slope of TAN vs. time curve measured at five different points for run 48

TAN mg KOH/g	slope = $\frac{d(TAN)/dt}{TAN/hr}$	$\log \left[\frac{-d(TAN)}{dt} \right]$ = y_i	$\log (TAN-3.0)$ = x_i
24.6	-50.000	1.6990	1.3345
12.0	-17.167	1.2347	0.9542
9.0	- 7.885	0.8968	0.7782
6.5	- 3.457	0.5387	0.5441
4.5	- 0.7008	-0.1544	0.1761

and from Table A6.12 we have,

$$\Sigma x_i = 3.7871, (\Sigma x_i)^2 = 14.3421, \Sigma x_i^2 = 3.6240$$

$$\Sigma y_i = 4.2148, \Sigma x_i y_i = 4.4093, \text{ and } N = 5$$

Equation (8.13) is applicable for run 48 because $\alpha = 1.0$, hence the slope and intercept of the least square best fit straight line plot of

$\log \left[\frac{-d(TAN)}{dt} \right]$ vs. $\log (TAN-3.0)$ are given by equations (8.22) and (8.23)

$$\therefore \text{slope} = \frac{4.4093 - [3.7871 \times 4.2148/5]}{3.6240 - [14.3421/5]}$$

$$\therefore \text{slope} = 1.611 = n \text{ overall order of reaction}$$

$$\text{and intercept} = \frac{4.2148 \times 3.624 - 3.7871 \times 4.4093}{5 \times 3.624 - 14.3421}$$

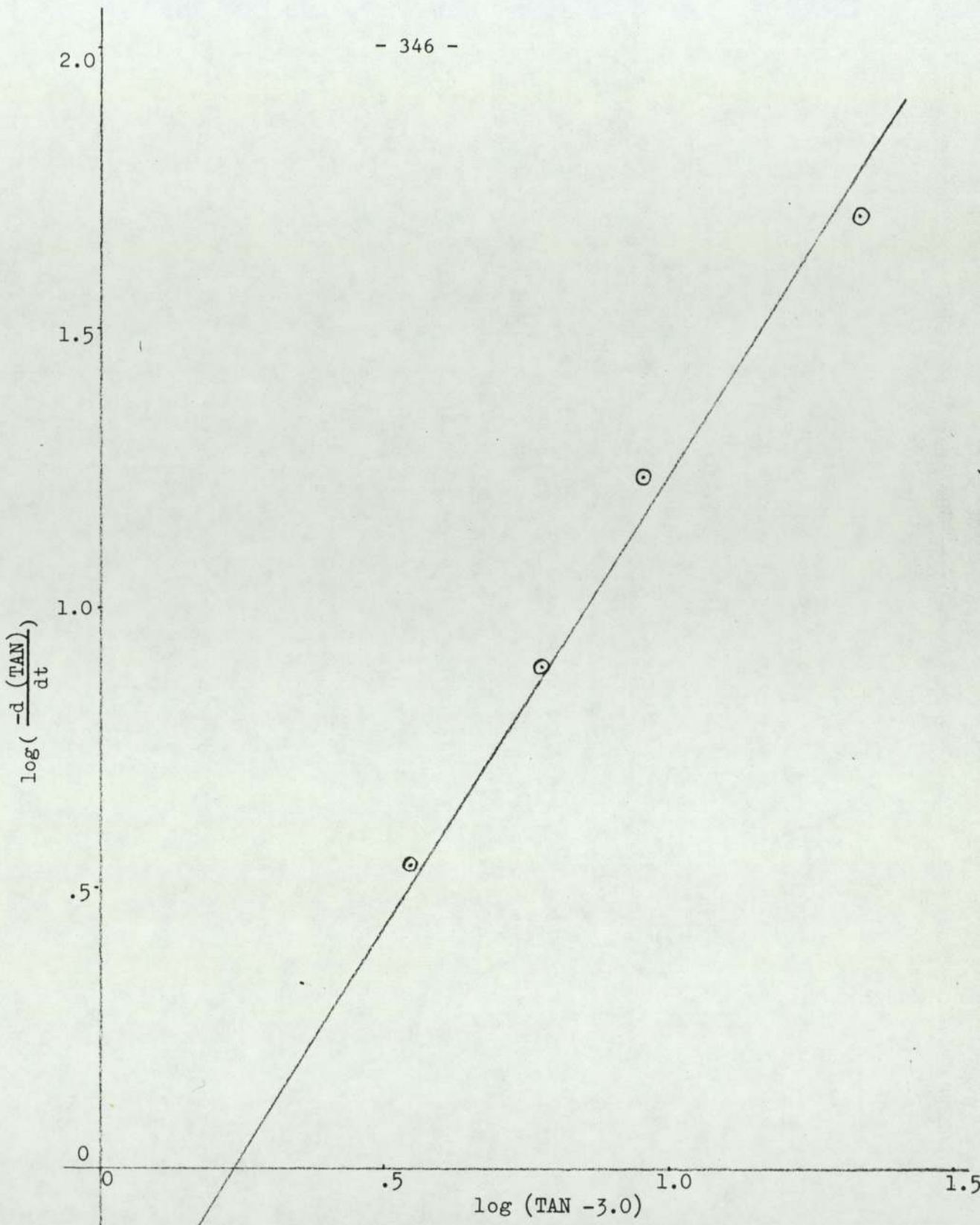


Figure A6.13

Graph for run 48 of $\log\left[\frac{-d(\text{TAN})}{dt}\right]$ vs. $\log(\text{TAN} - 3.0)$

Temperature = 210°C, $\alpha = 1.0$

$$\therefore \text{intercept} = -0.3769 = \log k + (n-1) \log \gamma$$

8.24

the actual plot of $\log \left[\frac{-d(\text{TAN})}{dt} \right]$ vs. $\log (\text{TAN}-3.0)$ is given in Figure A6.13.

From Table 6.1 for run 48 we have,

$$\text{Weight of PIBSA} = 405.13\text{g}$$

$$\text{Weight of dilution oil} = 314.71\text{g}$$

$$\text{Weight of catalyst} = 4.78\text{g}$$

$$\therefore \text{total weight of mixture} = 724.62\text{g}$$

$$\text{also, weight of density flask + product at } 210^{\circ}\text{C} = 66.0448\text{g}$$

$$\text{weight of empty D.F.} = 25.7050\text{g}$$

$$\text{volume of D.F.} = 49.3152 \text{ cm}^3$$

$$\therefore \text{density of product at } 210^{\circ}\text{C} = 0.818 \text{ g/cm}^3$$

$$\therefore \text{average density for run 48 (from Table 8.1)} = 0.806 \text{ g/cm}^3$$

\therefore from equation (8.25) for C_A° we have

$$C_A^{\circ} = (0.9198 \times 10^{-3})(405.13) \times \frac{0.806 \times 10^3}{724.62} = 0.4145 \left(\frac{\text{equivalent}}{\text{dm}^3} \right)$$

$$\text{hence } \gamma = \frac{C_A^{\circ}}{\text{TAN}_R^{\circ}} = \frac{0.4145}{21.6} = 0.01919$$

hence from equation (8.24), $-0.3769 = \log k + (1.611-1.0) \log (0.01919)$

$\therefore k = 4.7005 \text{ (equivalents/dm}^3)^{1-n} \cdot \text{hr}^{-1}$ the rate constant.

Detailed calculations of run 49

Run 49 was carried out at 200°C with $\alpha = 1.0$ and was a repeat for run 39 but the TAN results were calculated using a potentiometric titrator model E536 (Metrohm series), to enable a comparison to be made between colour titration results of run 39, and potentiometric titration results of run 49. Table A6.13 gives the weight measurements of run 49 samples with their potentiometric titration results.

TABLE A6.13

Run 49 samples and their potentiometric titration results

Number of sample	Time after PE addition min.	Weight of empty beaker g	Weight of beaker plus sample g	Weight of sample g	Volume of base used in titration cm ³	TAN $\frac{\text{mg KOH}}{\text{g sample}}$
1	1	116.3622	117.7084	1.3462	6.11	24.9
2	6	116.0044	117.1455	1.1411	4.23	20.1
3	12	124.2662	125.5896	1.3232	3.99	16.3
4	18	116.4443	117.6693	1.2250	3.20	14.0
5	30	124.1863	125.4959	1.3096	2.69	10.9
6	45	122.9738	124.3805	1.4067	2.36	8.8
7	60	124.8803	126.3175	1.4372	2.07	7.5
8	90	124.2833	125.5892	1.3059	1.60	6.2
9	120	125.8113	127.1706	1.3593	1.51	5.6
10	150	125.1570	126.5636	1.4066	1.38	4.9
11	180	116.2415	117.8407	1.5992	1.49	4.7
12	240	125.3885	128.3263	2.9378	2.40	4.3
13	288	117.6034	120.1362	2.5328	1.87	3.8
14	345	45.7739	48.3157	2.5418	1.78	3.6

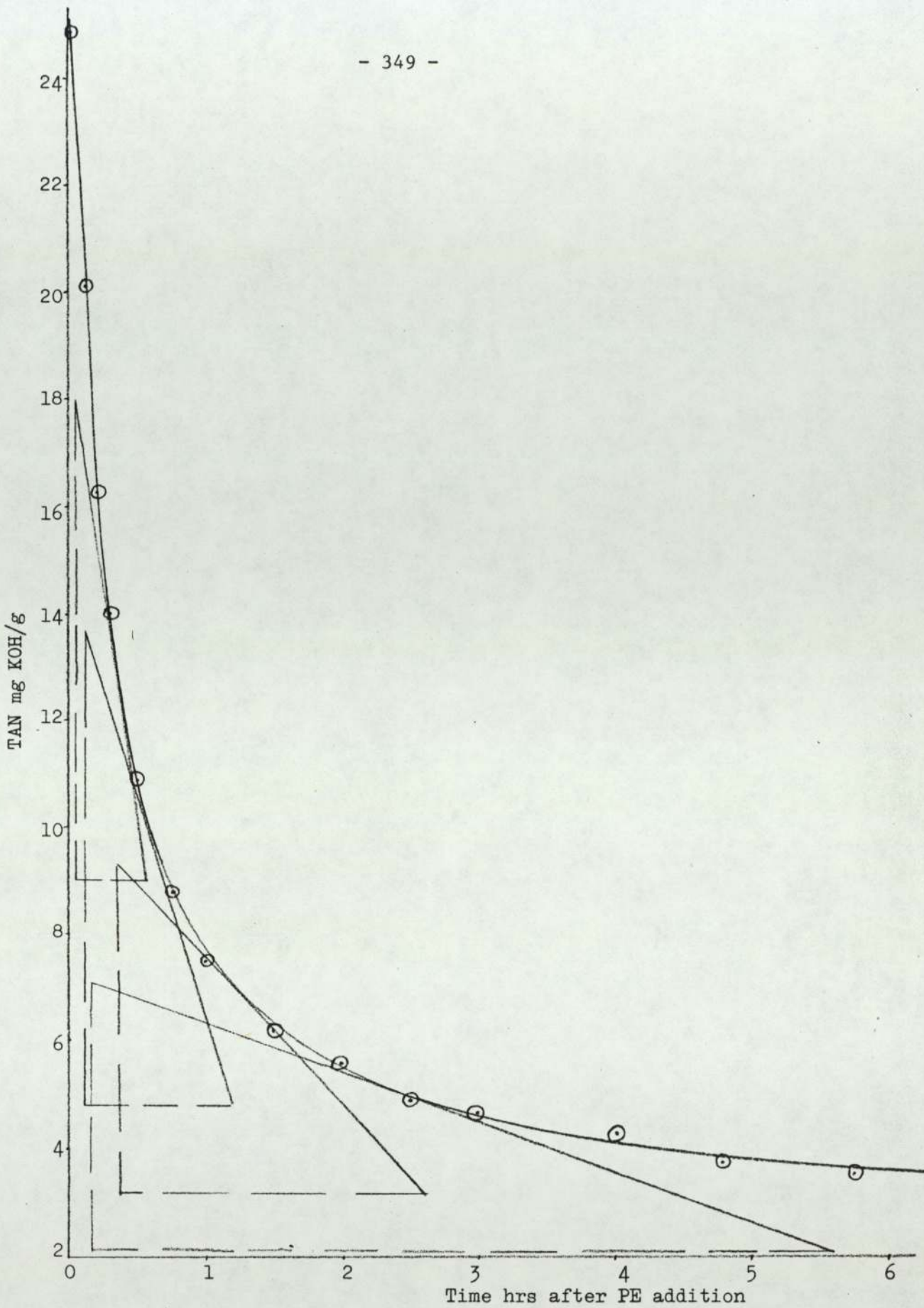


Figure A6.14

Graph for run 49 of TAN mg KOH/g vs. time hr after PE addition

Temperature 200°C, $\alpha = 1.0$, Potentiometric titration results

The tabulated TAN values were calculated using equation (A3.1) as before

$$\text{TAN} = \frac{(v-b) \times N \times 56.1}{w} \quad (\text{A3.1})$$

but in this case the values of (N) and (b) used in the equation were those obtained from Table A3.4 in Appendix 3, for potentiometric titration (method No. 4), which were, N = 0.1005 and b = 0.16 cm³, hence for the first sample in Table A6.13

$$\text{TAN}_1 = \frac{(6.11-0.16) \times 0.1005 \times 56.1}{1.3462} = 24.9 \text{ mg KOH/g}$$

all the other TAN values were calculated in the same manner. A plot of TAN vs. time (hr) was carried out and Figure A6.14 was obtained. The slope of the curve was measured at five different points and the results were tabulated in Table A6.14 below. The value of the TAN[∞] was estimated from Figure A6.14 to be equal to 3.0 mg KOH/g sample for run 49.

TABLE A6.14

The slope of TAN vs. time curve measured at five different points for run 49.

TAN mg KOH/g	slope = d(TAN)/dt TAN/hr	log [$\frac{-d(\text{TAN})}{dt}$] = y _i	log (TAN-3.0) = x _i
24.9	-43.000	1.6335	1.340
13	-17.300	1.238	1.000
10	- 8.148	0.9111	0.845
7	- 2.723	0.435	0.602
5	- 0.919	-0.0366	0.301

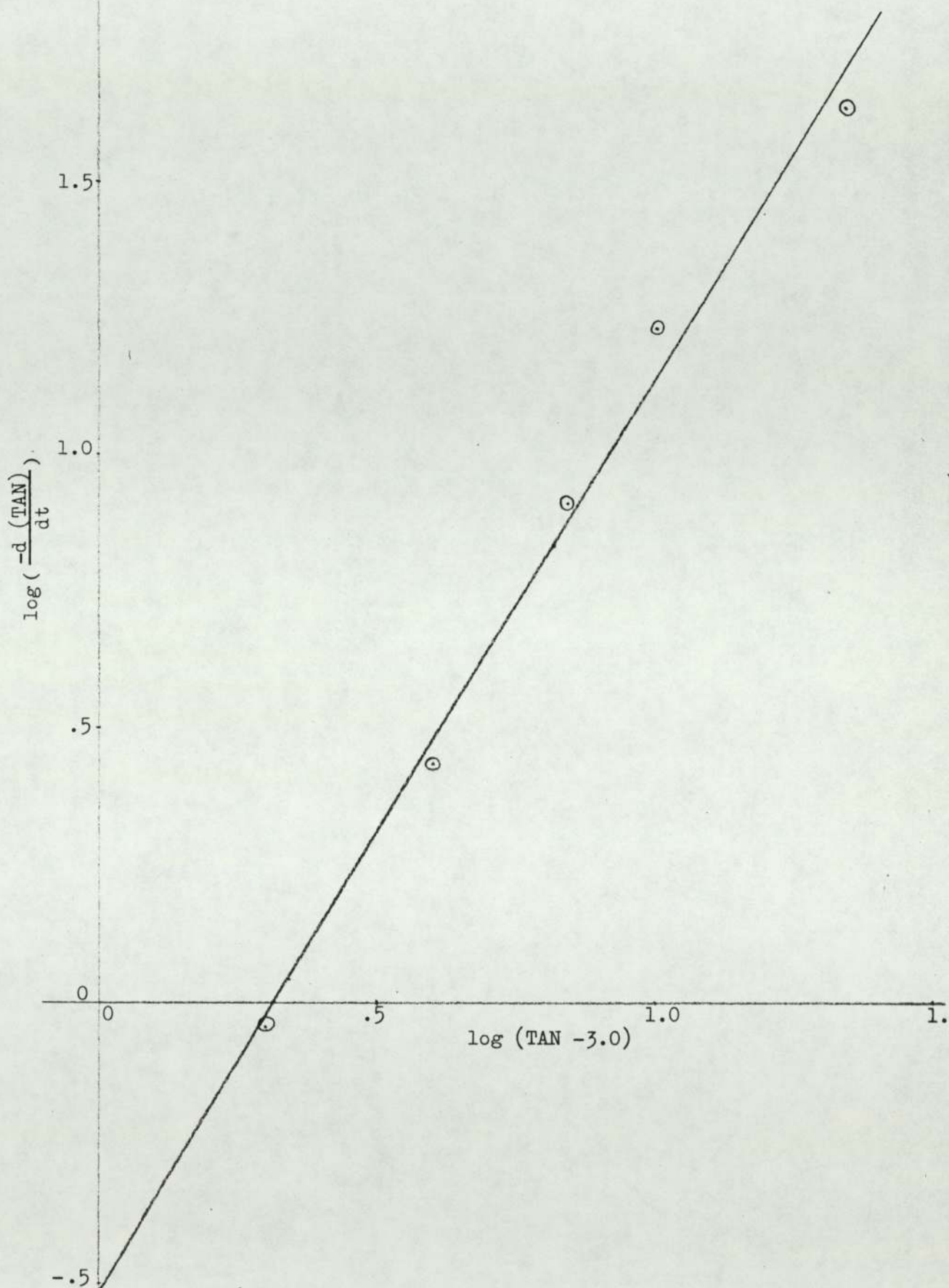


Figure A6.15

Graph for run 49 of $\log\left[\frac{-d(TAN)}{dt}\right]$ vs. $\log(TAN - 3.0)$

Results by potentiometric titration. Temperature = 200°C. $\alpha = 1.0$

and from Table A6.14 we have,

$$\Sigma x_i = 4.088, (\Sigma x_i)^2 = 16.7117, \Sigma x_i^2 = 3.9626$$

$$\Sigma y_i = 4.181, \Sigma x_i y_i = 4.4477, \text{ and } N = 5$$

Equation (8.13) is applicable for run 49 because $\alpha = 1.0$, hence the slope and intercept of the least square best fit straight line plot of $\log \left[\frac{-d(\text{TAN})}{dt} \right]$ vs. $\log (\text{TAN}-3.0)$ are given by equations (8.22) and (8.23)

$$\therefore \text{slope} = \frac{4.4477 - [4.088 \times 4.181/5]}{3.9626 - [16.7117/5]}$$

$$\therefore \text{slope} = 1.659 = n \text{ over all order of reaction}$$

$$\text{and intercept} = \frac{4.181 \times 3.9626 - 4.088 \times 4.4477}{5 \times 3.9626 - 16.7117}$$

$$\therefore \text{intercept} = -0.521 = \log k + (n-1) \log \gamma \quad 8.24$$

the actual plot of $\log \left[\frac{-d(\text{TAN})}{dt} \right]$ vs. $\log (\text{TAN}-3.0)$ is given in Figure A6.15.

From Table 6.1 for run 49 we have,

Weight of PIBSA	=	404.25g
Weight of dilution oil	=	314.02g
Weight of catalyst	=	4.77g
\therefore total weight of mixture	=	723.04g

also average density at 200°C (from Table 8.1) = 0.814 g/cm^3

hence from equation (8.25) for C_A^0 we have,

$$C_A^0 = (0.9198 \times 10^{-3})(404.25) \times \frac{0.814 \times 10^3}{723.04}$$

$$\therefore C_A^0 = 0.4186 \text{ (equivalents/dm}^3\text{)}$$

$$\therefore \gamma = \frac{C_A^0}{\text{TAN}_R^0} = \frac{0.4186}{21.9} = 0.019114 \left(\frac{\text{equivalent}}{\text{dm}^3} \cdot \frac{\text{g sample}}{\text{mg KOH}} \right)$$

and from equation (8.24) we have,

$$-0.521 = \log k + (1.659-1) \log(0.019114)$$

$$\therefore k = 4.089 \text{ (equivalent/dm}^3\text{)}^{1-n} \cdot \text{hr}^{-1} \text{ the rate constant.}$$

Comparison between run 39 and run 49 results

A comparison between the TAN values of run 39 samples, calculated using colour titration method, and the TAN values of run 49 samples, calculated using potentiometric titration, is presented in Table A6.15.

TABLE A6.15

Comparison between run 39 and run 49 samples TAN values

Number of sample	Time after PE addition (min.)	Run 39 TAN values using colour titration (mg KOH/g)	Run 49 TAN values potentiometric titration (mg KOH/g)	Deviation from run 39 results %
1	1	25.0	24.9	0.4
2	6	20.4	20.1	1.5
3	12	16.4	16.3	0.6
4	18	14.2	14.0	1.4
5	30	10.8	10.9	0.9
6	45	8.9	8.8	1.1
7	60	7.9	7.5	5.1
8	90	6.4	6.2	3.1
9	120	5.5	5.6	1.8
10	150	4.8	4.9	2.1
11	180	4.6	4.7	2.2
12	240	4.0	4.3	7.5
13	288	3.5	3.8	8.5
14	345	-	3.6	-

Also comparison between the values of (n) and (k) obtained from both runs is given in Table A6.16.

TABLE A6.16

Comparison between the values of (n) and (k) obtained from runs 39 and 49.

Parameter	Run No. 39 results	Run No. 49 results	Deviation from run 39 results %
n	1.614	1.659	2.8
k	3.8497	4.089	6.2

Detailed calculations of run 50

Table A6.17 gives the weight measurements of samples taken during run 50 together with their titration results. The tabulated TAN values were all calculated using equation (A3.1) as before

$$\text{TAN} = \frac{(v-b) \times N \times 56.1}{w} \quad \text{A3.1}$$

A plot of TAN vs. time (hr) was carried out and Figure A6.16 was obtained. The slope of the curve was measured at five different points and the results were tabulated in Table A6.18. The value of TAN^{∞} was estimated from Figure A6.16 to be equal to 4.0 mg KOH/g. Run 50 was the only kinetic run with $\alpha = 1.0$ which had an estimated value of TAN^{∞} not equal to 3.0 mg KOH/g, probably because of the much lower reaction temperature of 150°C.

TABLE A6.17

Weight measurements of run 50 samples and their titration results

Number of sample	Time after PE addition hr.	Weight of empty beaker g	Weight of beaker plus sample g	Weight of sample g	Volume of base used in titration cm ³	TAN mg KOH g sample
1	0.02	116.3613	117.7944	1.4331	6.50	25.5
2	0.25	116.0032	117.5721	1.5689	6.42	23.0
3	0.5	124.2652	125.9129	1.6477	6.05	20.6
4	0.75	116.4439	117.9760	1.5321	5.3	19.4
5	1.0	124.1858	125.7222	1.5364	5.15	18.8
6	1.5	122.9725	124.3816	1.4091	4.45	17.7
7	2.5	124.8795	126.4644	1.5849	4.36	15.4
8	3.5	124.2840	125.8306	1.5466	3.75	13.5
9	4.5	125.8110	127.4892	1.6782	3.77	12.5
10	6.0	125.1559	126.6327	1.4768	2.90	10.9
11	8.0	116.2417	117.8772	1.6355	2.78	9.4
12	23.75	125.3875	127.2037	1.8162	1.83	5.5
13	30.5	117.6028	119.2792	1.6764	1.55	5.0

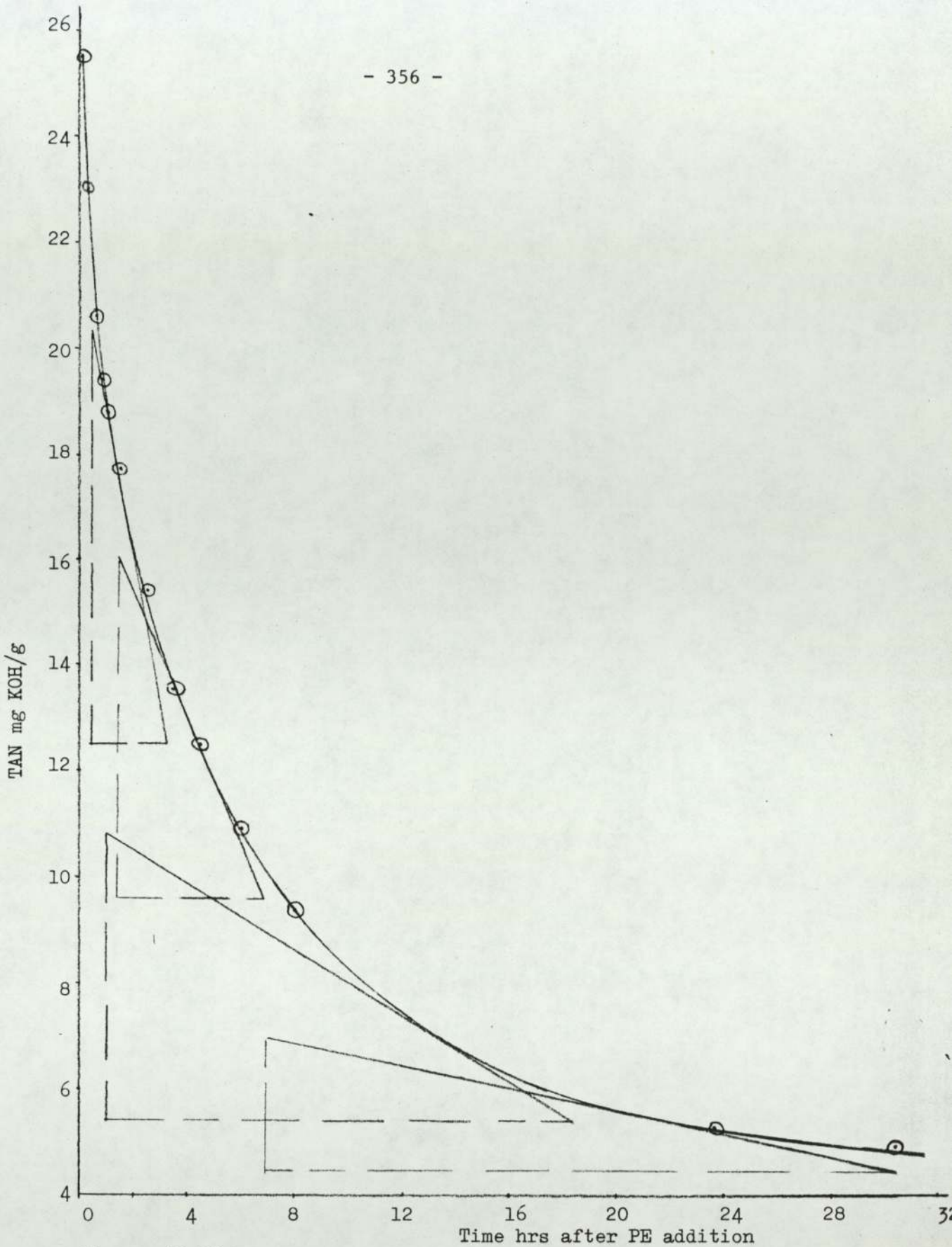


Figure A6.16

Graph for run 50 of TAN mg KOH/g vs. time hr after PE addition

Temperature = 150°C, $\alpha = 1.0$

TABLE A6.18

The slope of TAN vs. time curve measured at five different points for run 50

TAN mg KOH/g	slope = d(TAN)/dt TAN/hr	log [$\frac{-d(\text{TAN})}{dt}$] = y_i	log(TAN-4.0) = x_i
25.5	-10.000	1.000	1.3324
18.0	- 2.786	0.445	1.1461
13.0	- 1.185	0.0738	0.9542
7.0	- 0.2784	-0.5554	0.4771
5.5	- 0.0977	-1.0103	0.1761

and from Table A6.18 we have,

$$\Sigma x_i = 4.0859, (\Sigma x_i)^2 = 16.6946, \Sigma x_i^2 = 4.2580$$

$$\Sigma y_i = -0.0469, \Sigma x_i y_i = 1.4699, \text{ and } N = 5$$

Equation (8.13) is applicable for run 50 because $\alpha = 1.0$, hence the slope and intercept of the least square best fit straight line plot of $\log \left[\frac{-d(\text{TAN})}{dt} \right]$ vs. $\log(\text{TAN}-4.0)$ are given by equations (8.22) and (8.23)

$$\therefore \text{slope} = \frac{1.4699 - [4.0859 \times (-0.0469)/5]}{4.2580 - [16.6949/5]}$$

$$\therefore \text{slope} = 1.641 = n \text{ over all order of reaction}$$

$$\text{and intercept} = \frac{(-0.0469)(4.258) - 4.0859 \times 1.4699}{5 \times 4.258 - 16.6946}$$

$$\therefore \text{intercept} = -1.3504 = \log k + (n-1) \log \gamma \quad 8.24$$

the plot of $\log \left[\frac{-d(\text{TAN})}{dt} \right]$ vs. $\log (\text{TAN}-4.0)$ is given in Figure

A6.17.

From Table 6.1 for run 50 we have,

$$\text{Weight of PIBSA} = 405.64\text{g}$$

$$\text{Weight of oil} = 315.10\text{g}$$

$$\text{Weight of catalyst} = 4.79\text{g}$$

$$\therefore \text{total mixture weight} = 725.53\text{g}$$

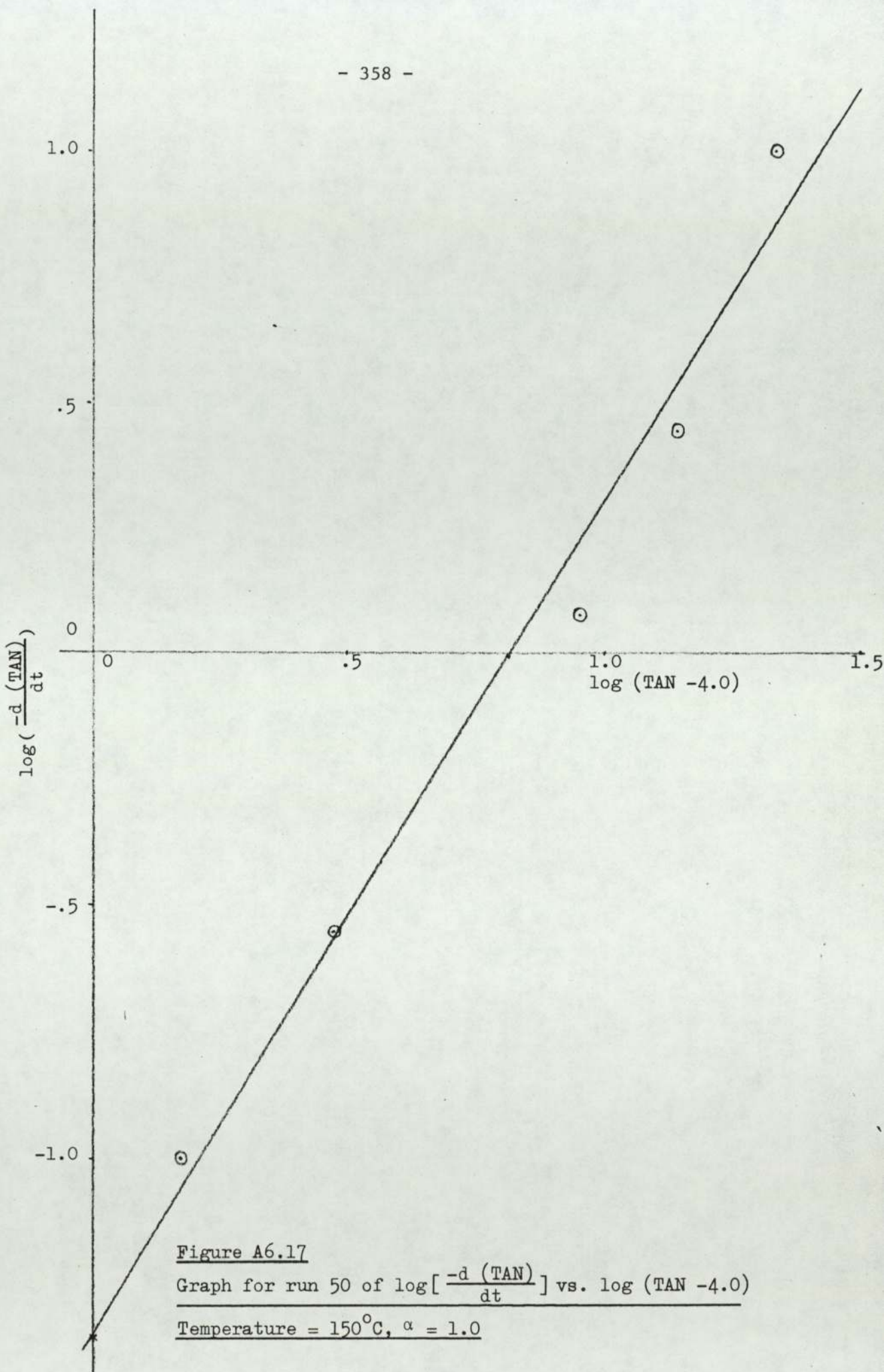


Figure A6.17

Graph for run 50 of $\log\left[\frac{-d(TAN)}{dt}\right]$ vs. $\log(TAN - 4.0)$

Temperature = 150°C, $\alpha = 1.0$

also weight of density flask + product at 150°C = 68.2147g
 ∴ weight of empty D.F. = 25.7050g
 Volume of D.F. = 49.3152g
 ∴ density of product at 150°C = 0.862 g/cm³
 and average density at 150°C (see Table 8.1) = 0.850 g/cm³
 ∴ from equation (8.25) for C_A^o we have,

$$C_A^o = (0.9198 \times 10^{-3}) \times (405.64) \times \frac{0.850 \times 10^3}{725.53} = 0.4371 \left(\frac{\text{equivalent}}{\text{dm}^3} \right)$$

$$\therefore \gamma = C_A^o / \text{TAN}_R^o = 0.4371 / 21.5 = 0.0203 \left[\frac{\text{equivalent}}{\text{dm}^3} \cdot \frac{\text{g sample}}{\text{mg KOH}} \right]$$

hence from equation (8.24),

$$-1.3504 = \log k + (1.641 - 1.0) \log (0.0203)$$

$$\therefore k = 0.5426 \text{ (equivalents/dm}^3\text{)}^{1-n} \cdot \text{hr}^{-1}$$

Detailed calculations for run 63

Table A6.19 gives the weight measurements of samples taken during run 63 together with their titration results.

The tabulated TAN values were all calculated using equation (A3.1) as before

$$\text{TAN} = \frac{(v-b) \times N \times 56.1}{w} \tag{A3.1}$$

A plot of TAN vs. time (hr) was carried out and Figure A6.18 was obtained. The slope of the curve was measured at five different points and the results were tabulated in Table A6.20. The value of TAN[∞] was estimated from Figure A6.18 to be equal to 3.0 mg KOH/g for run 63.

TABLE A6.19

Weight measurements of run 63 samples and their titration results

Number of sample	Time after PE addition min.	Weight of empty beaker g	Weight of beaker plus sample g	Weight of sample g	Volume of base used in titration cm ³	TAN mg KOH / g sample
1	0.5	116.3624	117.4980	1.1356	4.97	24.5
2	6	116.0000	117.2247	1.2247	3.93	17.9
3	12	124.2654	125.5013	1.2359	3.01	13.5
4	18	116.4432	117.8910	1.4478	2.95	11.3
5	30	124.1848	125.5790	1.3942	2.28	9.0
6	45	122.9743	124.4780	1.5037	1.93	7.0
7	60	124.8820	126.3612	1.4792	1.58	5.8
8	90	124.2855	125.8186	1.5331	1.42	5.0
9	120	125.8137	127.3120	1.4983	1.13	4.0
10	180	125.1554	126.7175	1.5621	1.15	3.9
11	240	116.2423	117.7701	1.5278	1.04	3.6
12	300	125.3884	126.8723	1.4839	0.96	3.4
13	360	117.6057	119.1720	1.5663	0.96	3.2

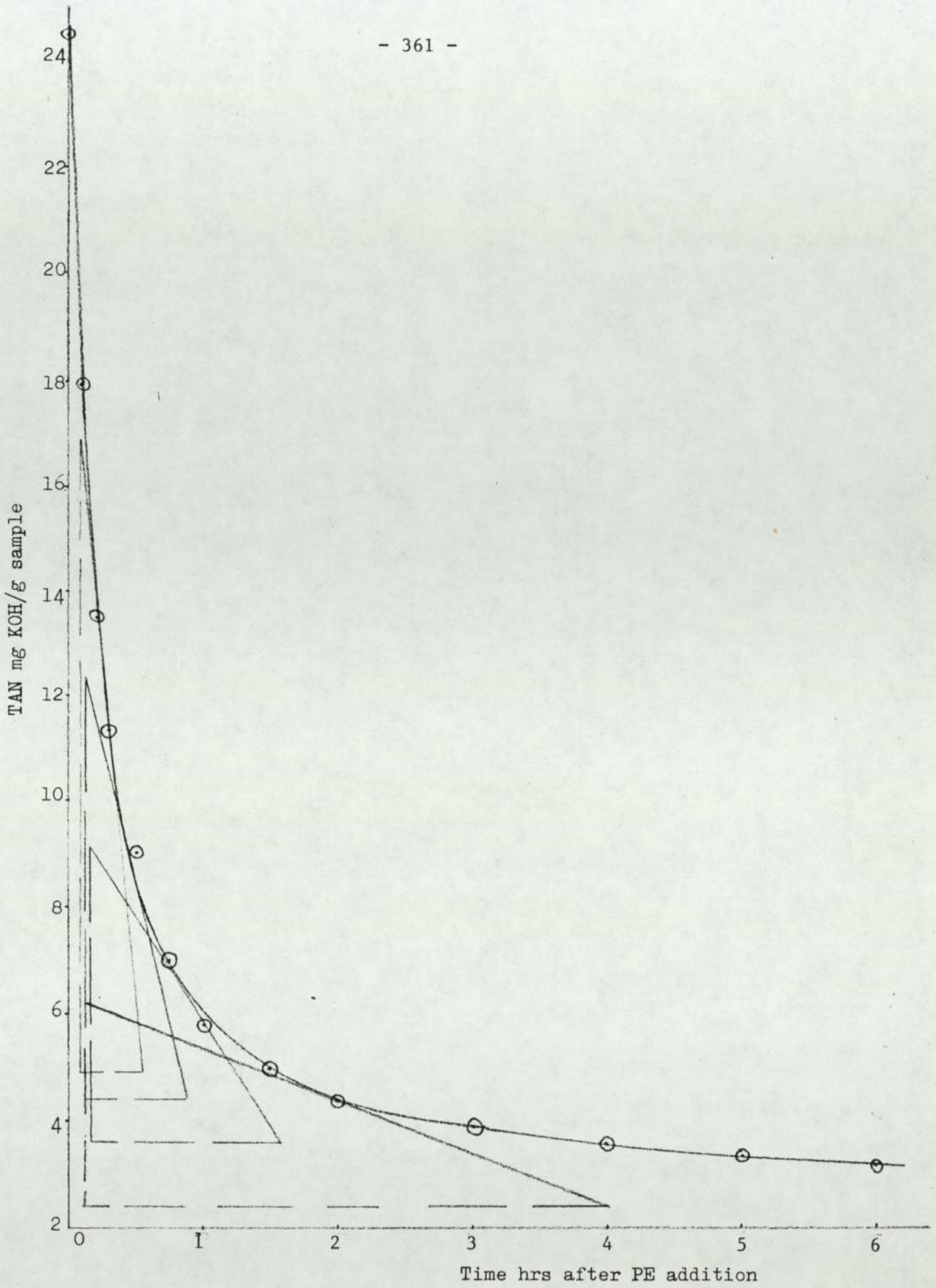


Figure A6.18

Graph for run 63 of TAN mg KOH/g vs. time hrs after PE addition

PE/PIBSA equivalent ratio $\alpha = 1.0$, temperature = 220°C

TABLE A6.20

The slope of TAN vs. time curve measured at five different points for run 63

TAN mg KOH/g	slope = d(TAN)/dt TAN/hr	$\log \left[\frac{-d(\text{TAN})}{dt} \right]$ = y_i	$\log(\text{TAN}-3.0)$ = x_i
24.5	-55.000	1.7404	1.3324
12.0	-25.000	1.398	0.954
9.0	-10.395	1.0168	0.7782
6.5	- 3.819	0.5820	0.5441
4.5	- 0.9694	-0.0135	0.1761

and from Table A6.20 we have,

$$\Sigma x_i = 3.7848, \quad (\Sigma x_i)^2 = 14.3247, \quad \Sigma x_i^2 = 3.6181$$

$$\Sigma y_i = 4.7237, \quad \Sigma x_i y_i = 4.7582, \quad \text{and } N = 5$$

Equation (8.13) is applicable for run 63 because $\alpha = 1.0$, hence the slope and intercept of the least square best fit straight line plot of $\log \left[\frac{-d(\text{TAN})}{dt} \right]$ vs. $\log(\text{TAN}-3.0)$ are given by equations (8.22) and (8.23)

$$\therefore \text{slope} = \frac{4.7582 - [3.7848 \times 4.7237/5]}{3.6181 - [14.3247/5]}$$

$$\therefore \text{slope} = 1.5701 = n \text{ over all order of reaction}$$

$$\text{and intercept} = \frac{4.7237 \times 3.6181 - 3.7848 \times 4.7482}{5 \times 3.6181 - 14.3247}$$

$$\therefore \text{intercept} = -0.2438 = \log k + (n-1) \log \gamma \quad 8.24$$

the plot of $\log \left[\frac{-d(\text{TAN})}{dt} \right]$ vs. $\log (\text{TAN}-3.0)$ is given in Figure A6.19.

From Table 6.1 for run 63 we have,

Weight of PIBSA	=	404.95g
Weight of oil	=	314.57g
Weight of catalyst	=	4.78g
∴ total weight of mixture	=	724.30g
also weight of density flask + product at 220°C	=	65.4777g
weight of empty D.F.	=	25.7050g
volume of D.F.	=	49.3152 cm ³
∴ density of product at 220°C	=	0.8065 g/cm ³
and average density at 220°C (see Table 8.1)	=	0.796 g/cm ³

$$\therefore C_A^0 = (0.9198 \times 10^{-3})(404.95) \times \frac{0.796 \times 10^3}{724.30} = 0.4093 \left(\frac{\text{equivalents}}{\text{dm}^3} \right)$$

$$\therefore \gamma = C_A^0 / \text{TAN}_R^0 = 0.4093 / 21.5 = 0.01904 \left[\frac{\text{equivalents}}{\text{dm}^3} \cdot \frac{\text{g sample}}{\text{mg KOH}} \right]$$

hence from equation (8.24)

$$-0.2438 = \log k + (1.5701 - 1.0) \log (0.01904)$$

$$\therefore k = 5.457 (\text{equivalents/dm}^3)^{1-n} \cdot \text{hr}^{-1}.$$

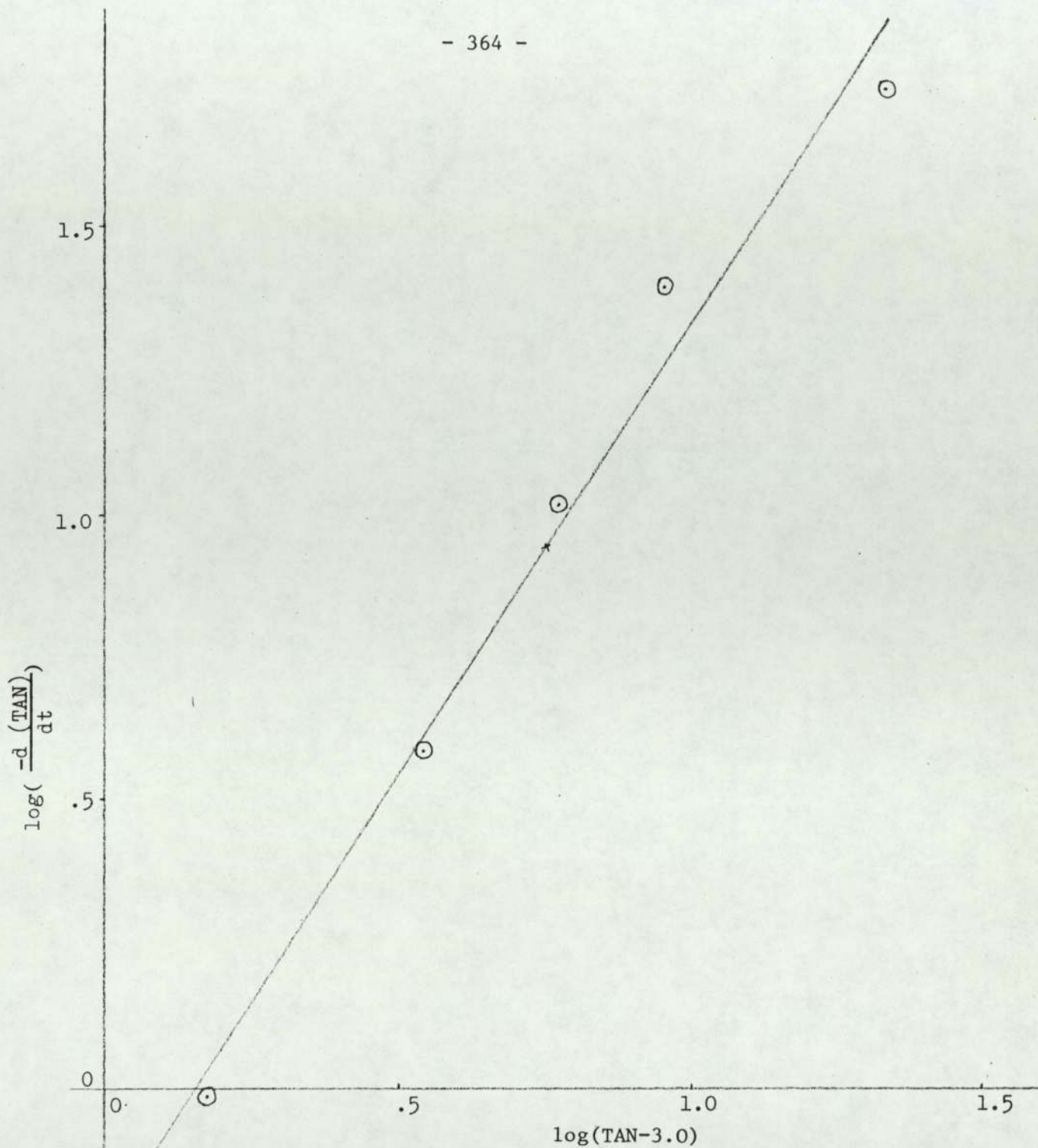


Figure A6.19

Graph for run 63 of $\log\left(-\frac{d(\text{TAN})}{dt}\right)$ vs. $\log(\text{TAN}-3.0)$

Temperature = 220°C, $\alpha = 1.0$

APPENDIX 7

CALCULATION OF THE THEORETICAL PROJECTED AREA DIAMETER OF PENTAERYTHRITOL

CRYSTAL

It was reported in Chapter 3 that the pentaerythritol crystal is an equilateral tetragonal bipyramid having (101) faces only (the silhouette of which under the microscope appears as an almost regular hexagonal)⁽¹¹⁴⁾. The values of the unit cell axes are recorded as $a_o = 6.083$ and $c_o = 8.726$ ⁽¹¹⁵⁾.

Consider the shape in Figure A7.1 of only two of the total eight pyramids

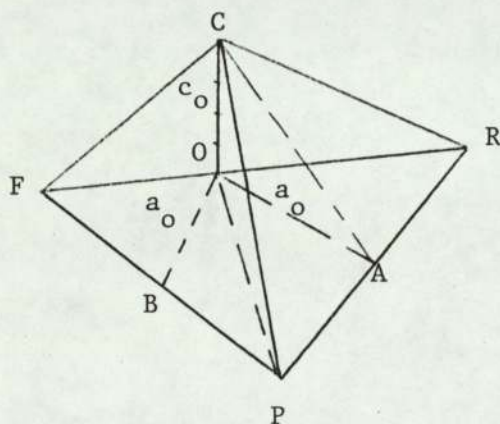


Figure A7.1: Two pyramids of the total eight in each PE crystal

$$OA = OB = a_o = 6.08 \text{ \AA}$$

$$OC = c_o = 8.73 \text{ \AA}$$

also from algebra and trigonometry we have

$$RA = AP = PB = BF = a_o = 6.08 \text{ \AA}$$

$$OR = OP = OF = a_o \sqrt{2} = 8.60 \text{ \AA}$$

$$CR = CP = CF = \sqrt{c_o^2 + 2a_o^2} = 12.2534 \text{ \AA}$$

$$CA = \sqrt{c_o^2 + a_o^2} = 10.634 \text{ \AA}$$

also $\angle OAC = \tan^{-1} \frac{c_o}{a_o} = 55.145^\circ$

To find the projected area, the crystal has to be looked at vertically downwards through the microscope while it is on its most stable position, resting on one face of the pyramid. In such a case the projected area is a hexagon with the following dimensions as given in Figure A7.2.

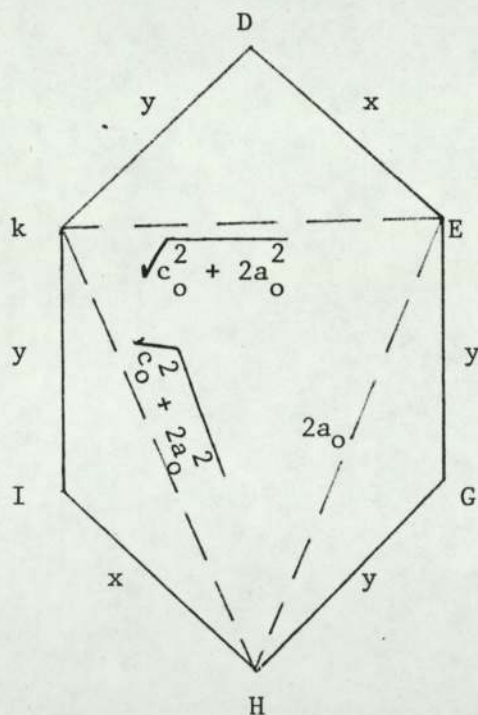


Figure A7.2: The projected area of a PE crystal

To evaluate the values of the unknowns x and y consideration must be given to the planes at angles to the hexagon plane by combining some parts of Figure A7.1 and Figure A7.2 as shown in Figure A7.3.

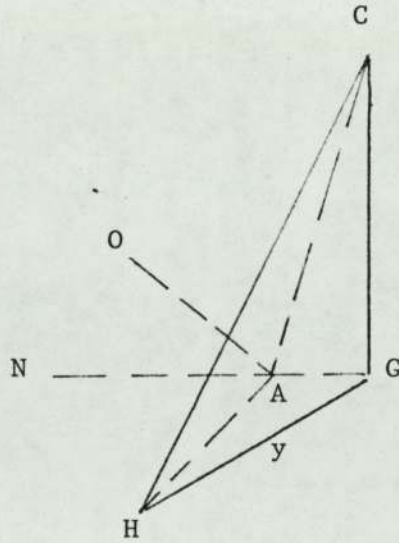


Figure A7.3: The estimation of the value of the unknown y

It was shown that $\angle OAC = 55.145^\circ$ (from Figure A7.1)

hence $\angle CAG = 180 - 2 \times 55.145^\circ = 69.71^\circ$

also it was shown that $CA = 10.634 \text{ \AA}$ (from Figure A7.1)

$$\therefore \text{in } \triangle CAG \text{ the side } CG = 10.634 \times \sin(69.71^\circ)$$

$$\therefore CG = 9.974 \text{ \AA}$$

also in $\triangle CGH$, the side CH represent the side of the pyramid which equals to 12.253 (Figure A7.1), hence $CG = 9.974$, $GH = y$, and $\angle CGH = 90^\circ$.

$$\therefore y^2 = (12.253)^2 - (9.974)^2$$

$$\therefore \underline{y = 7.118 \text{ \AA}}$$

The value of the unknown x can now be estimated by considering the L.H.S. of Figure A7.2. Assume that the point I is the projection of point L on the actual crystal pyramid, then Figure A7.4 may be drawn as follows:

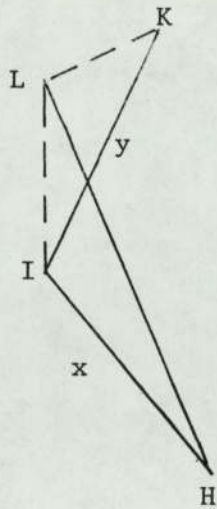


Figure A7.4: The estimation of the value of the unknown x.

In the figure, $\angle LIH = \angle LKH = 90^\circ$

and $LH = 2a_o = 12.16 \text{ \AA}$ (base of pyramid)

also $LK = \sqrt{c_o^2 + 2a_o^2} = 12.2534 \text{ \AA}$ (side of pyramid)

$$\therefore (12.16)^2 - x^2 = (12.2534)^2 - y^2 = (12.2534)^2 - (7.118)^2$$

$$\therefore \underline{x = 6.956 \text{ \AA}}$$

The projected area in Figure A7.2 can now be evaluated using the following formula for the area of a triangle with sides a, b, and c

$$\text{Area of } \Delta = \sqrt{s(s-a)(s-b)(s-c)}$$

$$\text{where } S = \frac{1}{2}(a+b+c)$$

Now in Figure A7.2, the sides of the four triangles shown are as follows:

$$x = 6.956 \text{ \AA}, y = 7.118 \text{ \AA}, 2a_o = 12.16 \text{ \AA}, \sqrt{c_o^2 + 2a_o^2} = 12.253$$

hence using the above formula for the area we have

APPENDIX 8

EXPERIMENTAL MEASUREMENT RESULTS FOR CRYSTAL SIZE DISTRIBUTION ANALYSIS

Table A8.1 gives the details of the weight measurements of the two filter papers with the two fractions of large crystals and fine crystals carried out on the sediment of the fourteen runs.

TABLE A8.1

Weight measurements of large and fine crystals fractions carried out for the sediment of all fourteen runs for CDS analysis

Run number	Weight of filter paper No.1 + large crystals (g)	Wt. of filter paper No.1 + some fines left over after removal of large crystals (g)	Weight of filter paper No.1 alone (g)	Weight of filter paper No.2 + fine crystals (g)	Weight of filter paper No.2 alone (g)
34	14.6588	2.1988	2.1032	4.6002	2.2315
35	18.6961	2.3661	2.2130	2.6636	2.1110
51	10.5462	2.0731	2.0060	4.7614	2.1462
52	13.8600	2.6010	2.3541	5.5313	2.1300
53	10.6730	2.4700	2.2488	5.6500	2.2024
54	11.3029	2.5816	2.4033	6.7863	2.3968
55	15.37760	2.5582	2.2092	6.2438	2.3000
56	11.3882	2.6347	2.2817	7.1298	2.2191
57	11.7057	3.4722	2.1882	6.7139	2.3949
58	12.1502	2.4955	2.2285	6.9889	2.3583
59	10.1681	2.4142	2.1348	4.6884	2.0744
60	12.7056	2.1505	1.9937	4.1496	2.0599
61	16.7277	2.2218	2.0715	2.2724	2.0599
62	11.9759	1.9588	1.9588	2.2342	2.1863

Sieve analysis

Table A8.2 presents the sieve analysis results of the large crystals fraction for the first seven runs of Table A8.1, while Table A8.3 gives the results for the last seven runs.

TABLE A8.2

Sieve analysis results for the sediment of runs 34, 35, 51, 52, 53, 54 and 55

Sieve details	Weight of crystals retained on each sieve presented as cumulative weight in beaker for different runs (g)								
	Mesh No.	Mesh size (µm)	34	35	51	52	53	54	55
-	-	-	116.1262	116.1375	124.5732	124.5742	124.5733	124.5746	124.5737
10	1676	116.1262	116.1375	124.5732	124.5742	124.5733	124.5746	124.5746	124.5737
12	1405	116.2085	116.3206	124.6086	124.6520	124.6253	124.6171	124.6171	124.6835
16	1003	116.9170	117.6903	125.1796	125.3183	125.2752	125.1806	125.1806	125.8695
18	853	117.7468	118.8892	125.7560	125.9944	125.8630	125.8756	125.8756	127.0478
22	699	119.1265	120.5316	126.6744	127.0515	126.8035	126.9602	126.9602	128.7817
25	599	120.5924	122.3690	127.8254	128.3016	127.9799	128.4319	128.4319	130.8787
30	500	122.0437	124.1880	128.7633	129.2857	128.8228	129.9572	129.9572	132.4678
36	422	123.7411	126.3113	129.7810	130.4800	129.8103	131.4890	131.4890	133.6187
44	355	125.1992	128.1352	131.0000	133.7523	130.9493	132.3327	132.3327	134.7928
52	295	126.0970	128.2805	131.6282	134.6002	131.1301	132.5765	132.5765	135.6203
60	251	126.9213	130.2100	132.1482	134.9888	131.9758	132.8833	132.8833	136.2796
72	210	127.4912	131.0848	132.5515	135.3642	132.3585	133.0705	133.0705	136.6744
85	180	127.9915	131.6717	132.7850	135.5904	132.5610	133.1714	133.1714	136.9612
100	150	128.2323	132.0242	132.9002	135.6986	132.6654	133.2258	133.2258	137.1560
120	125	128.3953	132.2277	132.9694	135.7667	132.7222	133.2604	133.2604	137.2711
150	105	128.5091	132.3743	133.0165	135.8096	132.7570	133.2830	133.2830	137.3442
170	90	128.5447	132.4243	133.0322	135.8221	132.7673	133.2907	133.2907	137.3658
200	75	128.5737	132.4496	133.0416	135.8281	132.7717	133.2944	133.2944	137.3755
240	63	128.5834	132.4600	133.0433	135.8310	132.7740	133.2950	133.2950	137.3790
300	53	128.5834	132.4600	133.0433	135.8310	132.7740	133.2950	133.2950	137.3790

* The first line in the Table represents the weight of the empty beaker

TABLE A8.3

Sieve analysis results for the sediment of runs 56, 57, 58, 59, 60, 61 and 62

Sieve details		Weight of crystals retained on each sieve presented as cumulative weight in beaker for different runs (g)						
Mesh No.	Mesh size (μm)	56	57	58	59	60	61	62
-	-	124.5753	124.5737	135.0650	124.5752	135.0642	135.0644	135.0644
10	1676	124.5753	124.5737	135.0650	124.5752	135.0642	135.0644	135.0644
12	1405	124.6627	124.6433	135.1804	124.6664	135.2425	135.2783	135.1800
16	1003	125.4659	125.5052	136.0029	125.4579	136.5114	136.7011	136.1737
18	853	126.2916	126.3885	136.8568	126.4782	137.5439	137.9932	137.0265
22	699	127.6068	127.8001	138.2152	127.6532	138.9657	139.8762	138.3442
25	599	129.1442	129.3255	139.7479	129.0006	140.7001	142.1324	139.9277
30	500	130.2612	130.3864	140.9259	129.9141	141.9338	143.8477	141.0673
36	422	131.4264	131.3768	142.1245	130.7298	143.0956	145.4093	142.2198
44	355	132.3408	132.0641	143.2543	131.3553	144.1690	146.9879	143.3533
52	295	132.6478	132.3301	143.7001	131.6673	144.6093	147.7862	143.9714
60	251	132.8865	132.4984	144.0727	131.8385	144.9793	148.4470	144.3515
72	210	133.0832	132.6479	144.3730	132.0239	145.2348	148.8306	144.6291
85	180	133.1918	132.7206	144.5353	132.1205	145.3884	149.1096	144.7868
100	150	133.2486	132.7530	144.6155	132.1819	145.4669	149.2218	144.8661
120	125	133.2753	132.7704	144.6601	132.2227	145.5166	149.2993	144.9036
150	105	133.2953	132.7816	144.6922	132.2589	145.5530	149.3341	144.9253
170	90	133.3030	132.7849	144.7025	132.2803	145.5667	149.3424	144.9311
200	75	133.3074	132.7864	144.7080	132.2953	145.5736	149.3445	144.9328
240	63	133.3090	132.7870	144.7080	132.3010	145.5760	149.3455	144.9328
300	53	133.3090	132.7870	144.7080	132.3010	145.5760	149.3455	144.9328

* The first line in the Table represents the weight of the empty beaker

Malvern laser analysis

Table A8.4 gives the Malvern laser analysis results of the fine crystals fraction for the first seven runs in Table A8.1 while Table A8.5 gives the results for the last seven runs.

TABLE A8.4

Laser analysis results for the sediment of runs 34, 35, 51, 52, 53, 54 and 55

Size band (μm)		Weight in size band % for the different runs						
Upper	Lower	34	35	51	52	53	54	55
118.4	54.9	13.1	16.7	6.3	4.8	10.0	4.7	6.2
54.9	33.7	10.6	17.9	4.4	3.9	8.0	0.7	0.0
33.7	23.7	3.5	10.7	0.7	0.0	0.8	0.0	0.0
23.7	17.7	3.5	8.3	2.1	1.1	5.1	1.9	6.7
17.7	13.6	2.7	6.5	14.8	5.6	11.7	12.9	16.4
13.6	10.5	3.9	5.2	17.8	13.5	15.1	19.8	26.4
10.5	8.2	8.2	4.0	14.4	13.0	11.7	12.2	16.9
8.2	6.4	16.9	6.1	10.8	12.2	7.3	7.7	8.6
6.4	5.0	8.1	6.1	7.4	10.0	7.8	7.2	7.4
5.0	3.9	1.4	5.0	5.0	8.4	5.0	6.5	1.6
3.9	3.0	10.0	5.3	5.3	5.5	4.6	6.3	2.8
3.0	2.4	4.4	2.4	2.9	5.4	3.2	5.3	2.2
2.4	1.9	6.3	1.7	2.1	4.2	2.9	4.4	1.8
1.9	1.5	3.7	1.7	1.4	4.4	2.3	3.5	0.0
1.5	1.2	1.4	0.6	1.6	3.2	1.8	2.8	0.0
1.2	0.0	2.6	1.7	3.0	4.8	2.8	4.2	3.0

TABLE A8.5

Laser analysis results for the sediment of runs 56, 57, 58, 59, 60, 61 and 62

Size band (μm)		Weight in size band % for the different runs						
Upper	Lower	56	57	58	59	60	61	62
118.4	54.9	6.0	2.8	3.0	9.0	10.3	16.1	15.3
54.9	33.7	0.0	0.0	0.0	25.5	16.8	17.2	14.2
33.7	23.7	0.0	0.0	3.3	18.7	15.1	13.3	11.5
23.7	17.7	2.6	22.8	16.4	10.2	9.2	10.5	9.6
17.7	13.6	14.4	23.2	19.2	6.0	9.4	6.1	8.4
13.6	10.5	21.5	13.8	24.4	7.0	11.6	4.3	7.1
10.5	8.2	16.0	11.3	13.5	3.1	5.0	3.8	5.6
8.2	6.4	14.1	7.0	7.3	4.2	4.9	5.2	6.1
6.4	5.0	7.8	7.4	4.5	5.3	4.8	4.9	4.8
5.0	3.9	6.9	2.9	3.1	1.8	3.3	3.8	3.7
3.9	3.0	3.1	3.3	2.1	2.6	3.8	2.9	2.8
3.0	2.4	1.6	0.8	0.6	1.3	0.6	2.5	2.5
2.4	1.9	1.6	0.9	0.0	1.6	1.2	2.1	2.1
1.9	1.5	0.9	1.3	0.0	1.2	1.4	2.1	1.9
1.5	1.2	0.5	1.0	1.5	1.0	1.1	2.8	2.0
1.2	0.0	2.9	1.5	1.2	1.5	1.7	2.4	2.3

APPENDIX 9

LISTING OF THE COMPUTER PROGRAM DEVELOPED FOR THE EVALUATION OF THE FINAL
CRYSTAL SIZE DISTRIBUTION AND ITS PARAMETERS FOR THE FINAL CRYSTALLINE
SEDIMENT

This appendix presents the listing of the computer program that was developed for the evaluation of the final crystal size distribution CSD for the crystalline sediment by combining the two separate distributions obtained by sieve analysis and lazer analysis. The program was written in Fortran 77 suitable for an ICL 19045 computer. Extensive comment statements in the body of the listing were used to clarify the function of the various program segments.

PROGRAM CSD

C THIS PROGRAM WAS FORMULATED TO EVALUATE THE CRYSTAL SIZE
C DISTRIBUTION (CSD) OF EXCESS PENTAERYTHRITOL CRYSTALLIZED OUT
C FROM LUBE. OIL DISPERSANT ADDITIVE SOLUTIONS. THE CRYSTAL MASS
C WAS SEPARATED INTO TWO FRACTIONS, LARGE CRYSTALS AND FINE ONES,
C BY MEANS OF SETTLING. THE LARGE CRYSTALS WERE ANALYSED BY
C SIEVES WHILE THE FINE CRYSTALS WERE ANALYSED BY THE MALVERN
C LAZER SIZE ANALYSER. THE FINAL CSD IS OBTAINED BY COMBINING
C BOTH OF THESE DISTRIBUTIONS USING THE FOLLOWING PROGRAM.

C -----
C DEFINITIONS OF VARIABLES
C -----

C FLPL = WT. OF FILTER PAPER PLUS ALL THE LARGE CRYSTALS IN GRAMS.
C FLPF = WT. OF FILTER PAPER PLUS SOME FINE CRYSTALS LEFT ON THE
C PAPER AFTER REMOVING THE LARGE CRYSTALS TO THE SIEVES.
C FL = WT. OF FILTER PAPER USED FOR LARGE CRYSTALS.
C FFPF = WT. OF FILTER PAPER PLUS THE FINE CRYSTALS FRACTION.
C FF = WT. OF FILTER PAPER USED FOR FINE CRYSTALS.

C B(I) = ARRAY OF SIEVED CRYSTAL WTS.
C SIEVED = TOTAL WT. OF SIEVED CRYSTALS.
C CLOSS = PERCENT LOSS OF CRYSTAL WT. DUE TO SIEVING.
C SIVSIZ = ARRAY FOR STORING SIEVE SIZES.
C BLAZER = ARRAY FOR STORING LAZER ANALYSER SIZES.
C FLAZER = ARRAY FOR STORING LAZER ANALYSER SIZES AFTER
C MAKING THEM COMPATIBLE WITH SIEVE SIZES.

C RATIO = IT IS THE RATIO OF PARTICLE SIZES MEASURED BY
C SIEVES TO THAT MEASURED BY LAZER ANALYSER.
C AF(I) = ARRAY OF WTS. OF FINE CRYSTALS MEASURED BY LAZER
C ANALYSER IN EACH SIZE BAND.
C Z = THE UNIFORM RATE OF CHANGE OF CRYSTAL MASS WITH
C SIZE IN GIVEN SIZE BAND.
C SIZE = ARRAY FOR STORING THE SIZES OF THE FINAL DISTRIBUTION
C CBMEAN = ARRAY FOR STORING THE MEAN OF THE FINAL DISTRIBUTION
C SIZE BANDS.
C WTS. = ARRAY FOR STORING THE WTS. OF CRYSTALS IN EACH SIZE
C BAND OF THE FINAL DISTRIBUTION.
C CUSF = CUMULATIVE UNDER SIZE WT. FRACTION OF THE CRYSTALS.
C DAV = MASS MEAN CRYSTAL SIZE OF THE FINAL DISTRIBUTION.
C VAR = VARIANCE OF THE FINAL DISTRIBUTION.
C X(I) = X-COORDINATES FOR THE PLOTTER.
C Y(I) = Y-COORDINATES FOR THE PLOTTER.
C

+ REAL B(18),SIVSIZ(19),FLAZER(17),BLAZER(17),X(31),Y(31),
AF(16),SIZE(30),CBMEAN(29),WTS(29),CUSF(29)

+ DATA SIVSIZ/1676.,1405.,1003.,853.,699.,599.,500.,422.,355.,
295.,251.,210.,180.,150.,125.,105.,90.,75.,63./
+ RATIO/1.33/BLAZER/118.4,54.9,33.7,23.7,17.7,13.6,10.5,8.2,
+ 6.4,5.0,3.9,3.0,2.4,1.9,1.5,1.2,0.0/
+ SIZE/1676.,1405.,1003.,853.,699.,599.,500.,422.,355.,
+ 295.,251.,210.,180.,150.,75.,44.8,31.5.,23.5.,18.1
+ 14.0,10.9,8.5,6.7,5.2,4.0,3.2,2.5,2.0,1.6,0.0/

C TO TRANSFORM THE PARTICLE SIZE MEASURED BY LAZER ANALYSER INTO
C A SIZE COMPATIBLE WITH THOSE SIZES MEASURED BY SIEVES THE
C CONVERSION RATIO (WHICH WAS OBTAINED EXPERIMENTALLY) IS USED.

DO 5 I=1,17
FLAZER(I)=RATIO*BLAZER(I)
5 CONTINUE

C TO BE ABLE TO PLOT THE FINAL RESULTS OBTAINED, THE FOLLOWING
C CALL STATEMENTS ARE INTRODUCED.

CALL OPENW
CALL PLOT(5.0,5.0,-3)

C TO REPEAT THE CALCULATIONS FOR 14 RUNS THE FOLLOWING LOOP IS
C INTRODUCED

DO 500 NUMBER =1,14
IF(NUMBER.GT.14) THEN
PRINT*,'NO MORE DATA',NUMBER
STOP
END IF

C TO CALCULATE THE WTS. OF THE TWO CRYSTAL FRACTIONS AND
C HENCE THE TOTAL WT. OF CRYSTAL MASS COLLECTED AT THE
C END OF RUN

```
READ*,NRUN
READ*,FLPL,FLPF,FL,FFPF,FF
SLARGE = FLPL - FLPF
FINES = (FFPF - FF)+(FLPF - FL)
TOTALC = FINES + SLARGE
```

```
READ*,BEAKER,B
SIEVED =B(18)-BEAKER
CLOSS =(SLARGE-SIEVED)*100./SLARGE
```

```
PRINT 300,NRUN
300 FORMAT('1'//T50,'CSD ANALYSIS FOR RUN NUMBER',13/
+ T10,110('=')/T10,110('=')/T10,110('='))
PRINT*
PRINT*
PRINT*
PRINT 301
301 FORMAT(T46,'THE FOLLOWING IS THE SET OF INPUT DATA'
+ /T31,68('-'))
PRINT*
PRINT*
PRINT*
PRINT*
PRINT*
PRINT*
PRINT*, 'RUN NO. =',NRUN
PRINT*
PRINT*, 'FLPL =',FLPL,'GRMS', ' WT. OF FILTER PAPER ',
+ 'PLUS LARGE CRYSTALS'
PRINT*
PRINT*, 'FLPF =',FLPF,'GRMS', ' WT. OF FILTER PAPER ',
+ 'PLUS SOME FINES LEFT AFTER REMOVAL OF LARGE CRYSTALS'
PRINT*
PRINT*, 'FL =',FL,'GRMS', ' WT. OF FILTER PAPER ',
+ 'FOR LARGE CRYSTALS'
PRINT*
PRINT*, 'FFPF =',FFPF,'GRMS', ' WT. OF FILTER PAPER ',
+ 'PLUS FINE CRYSTALS'
PRINT*
PRINT*, 'FF =',FF,'GRMS', ' WT. OF FILTER PAPER ',
+ 'FOR FINE CRYSTALS'
PRINT*
PRINT*
PRINT*
PRINT*
PRINT*, 'WT. OF BEAKER FOR SIEVE ANALYSIS =',BEAKER,'GRMS'
PRINT*
PRINT*
```

```
PRINT*
PRINT*
PRINT 302, (SIVSIZ(I), SIVSIZ(I+1), B(I), I=1, 18)
302  FORMAT(T10, 'SIEVE SIZE BANDS, IN MICRS.', T48,
+      'CUMULATIVE WT. OF CRYSTALS IN BEAKER' /
+      T13, 'UPPTER', T27, 'LOWER', T62, 'IN GRMS' / T10, 11('-'), T24,
+      11('-'), T40, 53('-')) / (' ', T12, F7.2, T26, F7.2, T62, F8.4))

PRINT*
PRINT*
PRINT*
DO 10 I=18, 2, -1
      B(I)=B(I)-B(I-1)
10  CONTINUE
      B(1) = B(1)-BEAKER

PRINT*

READ*, AF

PRINT 303, (BLAZER(I), BLAZER(I+1), AF(I), I=1, 16)
303  FORMAT('1' // T10, 'LAZER ANALYSER SIZE BANDS, IN MICRS.', T54,
+      'WEIGHT IN BAND' / T13, 'UPPER', T36, 'LOWER', T58
+      'PERCENT' / T10, 11('-'), T33, 11('-'), T50, 22('-')
+      / (' ', T13, F5.1, T36, F5.1, T58, F5.1))

PRINT*
PRINT 304
304  FORMAT(T5, 125('-'))

PRINT*
PRINT*
PRINT*
PRINT 305, NRUN
305  FORMAT(T50, 'CALCULATIONS AND RESULTS OF RUN', 13/T30, 74('-'))
PRINT*
PRINT*
PRINT*, 'SLARGE =', SLARGE, 'GRMS', ' WT. OF LARGE CRYSTALS'
PRINT*
PRINT*, 'FINES =', FINES, 'GRMS', ' WT. OF FINE CRYSTALS.
PRINT*
PRINT*, 'TOTALC =', TOTALC, 'GRMS', ' TOTAL WT. OF CRYSTALS'
PRINT*
PRINT*, 'SIEVED =', SIEVED, 'GRMS', ' WT. OF SIEVED CRYSTALS'
PRINT*
PRINT*, 'CLOSS =', CLOSS, ' PERCENT WT. LOSS DUE TO SIEVING'
PRINT*
PRINT*
PRINT*
PRINT*
PRINT 306, (SIVSIZ(I), SIVSIZ(I+1), B(I), I=1, 18)
```

```
306      FORMAT(T10,'SIEVE SIZE BANDS,IN MICRS.',T47,
+          'CRYSTAL MASS RETAINED IN BAND'/T13,'UPPER',T27,
+          'LOWER',T57,'IN GRMS'/T10,11('-'),T24,11('-'),T40,
+          44('-')/(' ',T12,F7.2,T26,F7.2,T57,F7.4))
      PRINT*
      PRINT*
      PRINT*
      PRINT*
      PRINT*
      DO 50 I=1,16
          AF(I) = 0.01*AF(I)*FINES
50      CONTINUE
      PRINT*
      PRINT*
      PRINT*
      PRINT*
      PRINT*

      PRINT 307,(FLAZER(I),FLAZER(I+1),AF(I),I=1,16)
307     FORMAT(T10,'LAZER ANALYSER SIZE BANDS,IN MICRS.',T54,
+         'TOTAL WEIGHT IN BAND'/T13,
+         '(CORRECTED FOR COMPATIBILITY)'/T13,'UPPER',T36,
+         'LOWER',T60,'IN GRMS'/T10,11('-'),T33,11('-'),T50,
+         28('-')/(' ',T13,F5.1,T36,F5.1,T60,F7.4))

      PRINT*
      PRINT*
      PRINT*

      Z =AF(1)/(FLAZER(1)-FLAZER(2))
      V1 =Z*(FLAZER(1)-SIVSIZ(14))
      V2 =Z*(SIVSIZ(18)-FLAZER(2))
      V3 =AF(1)-V1-V2

      DO 60 I=1,29
          CBMEAN(I) =(SIZE(I)+SIZE(I+1))/2.
60      CONTINUE

      DO 70 I=1,12
          WTS(I) =B(I)
70      CONTINUE

      WTS(13) =V1+B(13)
      WTS(14) =V3+B(14)+B(15)+B(16)+B(17)
      WTS(15) =V2+AF(2)+B(18)

      DO 80 I=3,16
          WTS(I+13) =AF(I)
80      CONTINUE
```

```
      SUM = 0.0
      DO 90 I=1,29
        SUM = SUM+WTS(I)
90     CONTINUE

      TOTALC = SUM

      SUM = 0.0
      DO 100 I=1,29
        SUM = SUM+(WTS(I)/TOTALC)
        CUSF(I) = 1.0 -SUM
100    CONTINUE
```

C TO CALCULATE THE AVERAGE MASS DIAMETER (D AV.) AND THE
C VARIANCE (VAR) OF THE FINAL CSD ASSUMING DISCRETE DISTRIBUTION

```
      DAV = 0.0
      DO 110 I=1,29
        DAV = DAV+(CBMEAN(I)*WTS(I)/TOTALC)
110    CONTINUE

      VAR = 0.0
      DO 120 I=1,29
        VAR = VAR+((CBMEAN(I)-DAV)**2)*WTS(I)/TOTALC
120    CONTINUE
```

```
      PRINT 308, NRUN
308    FORMAT('1'//T45, 'THE FINAL DISTRIBUTION OF CRYSTAL MASS FOR RUN'
+         , I3/T10, 120('-'))
```

```
      PRINT*
      PRINT 309, (SIZE(I), SIZE (I+1), CBMEAN(I), WTS(I), WTS(I)/TOTALC,
+         CUSF(I), I=1, 29)
309    FORMAT(T10, 'THE FINAL DISTRIBUTION', T36, 'MEAN OF BAND',
+         T52, 'TOTAL CRYSTAL MASS', T74, 'MASS FRACTION', T91,
+         'CUMULATIVE UNDER SIZE'/T11, 'SIZE BANDS, IN MICRS.',
+         T53, 'RETAINED IN BAND', T77, 'IN BAND', T97, 'FRACTION'
+         /T12, 'UPPER', T25, 'LOWER', T39, 'MICRS.', T58, 'IN GRMS'
+         /T10, 9('-'), T23, 9('-'), T35, 14('-'), T51, 20('-'), T73,
+         15('-'), T90, 23('-'))/(' ', T10, F7.1, T23, F7.1, T38, F7.1,
+         T58, F7.4, T77, F6.4, T98, F6.4))
      PRINT*
      PRINT*
      PRINT*
      PRINT*
      PRINT*
```

```
PRINT*, 'THE MASS MEAN DIAMETER OF THE DISTRIBUTION =', DAV, 'MIC'

PRINT*
PRINT*
PRINT*, 'THE STANDARD DEVIATION OF THE DISTRIBUTION =', SQRT(VAR)
+      , 'MIC'

PRINT*
PRINT*
PRINT*
PRINT*
PRINT*
PRINT*
PRINT 310
310  FORMAT(T5,125('-'))

C      TO PLOT THE CUMULATIVE UNDER SIZE FRACTION AGAINST
C      THE APERTURE SIZE (LOWER VALUE OF THE SIZE BAND)
      DO 130 I=1,29
          Y(I) =CUSF(I)
130    CONTINUE

      DO 140 I=1,29
          X(I) =SIZE(I+1)
140    CONTINUE

      CALL NEWPEN(1)
      CALL SCALE(X,15.0,29,1)
      CALL AXIS(0.,0., 'APERTURE SIZE (MIC)', 20,15.,0.,X(30),X(31),
+          -1)
      CALL CHARPT(0.,-3.,.3, 'FIGURE 2 FOR RUN NUMBER', 0.0,23)
      CALL SCALE(Y,20.0,29,1)
      CALL AXIS(0.,0., 'CUMULATIVE UNDER SIZE FRACTION', 30,20.0,90.0,
+          Y(30),Y(31),1)
      CALL NEWPEN(2)
      CALL FLINE(X,Y,-29,1,1,10)
      CALL PLOT(0.0,0.0,3)
      CALL PLOT(0.0,50.0,-3)

C      TO PLOT THE MASS FRACTION IN EACH SIZE BAND AGAINST
C      THE MEAN OF THAT SIZE BAND ON THE SAME PAPER

      DO 150 I=1,29
          Y(I) =WTS(I)/TOTALC
150    CONTINUE
```

```
DO 160 I=1,29
  X(I) =CBMEAN(I)
160 CONTINUE
```

```
CALL NEWPEN(1)
CALL SCALE(X,15.0,29,1)
CALL AXIS(0.0,0.0,'MEAN OF SIZE BAND (MIC)',23,15.0,
+         0.0,X(30),X(31),-1)
CALL CHARPT(0.0,-3.0,.3,'FIGURE 1 FOR RUN NUMBER',
+          0.0,23)
CALL SCALE(Y,20.0,29,1)
CALL AXIS(0.0,0.0,'MASS FRACTION IN BAND',21,20.0,
+         90.0,Y(30),Y(31),1)
CALL NEWPEN(3)
CALL FLINE(X,Y,29,1,1,10)
CALL PLOT(0.0,0.0,3)
CALL PLOT(20.0,-50.0,-3)
```

```
500 CONTINUE
```

```
CALL CLOSE
```

```
STOP
```

```
END
```

APPENDIX 10

GRAPHS OF CRYSTAL SIZE DISTRIBUTION OF THE SEDIMENT FOR A CHOSEN NUMBER OF RUNS

This appendix presents the crystal size distribution results obtained for the sediment of a number of runs presented in the form of computer plots of cumulative under size fraction vs. aperture size and of crystal mass retained vs. mean of size band. The plots were carried out using the same computer program that was developed to perform the CSD calculations and also using the graphic package CALCOMP from Aston University computer library.

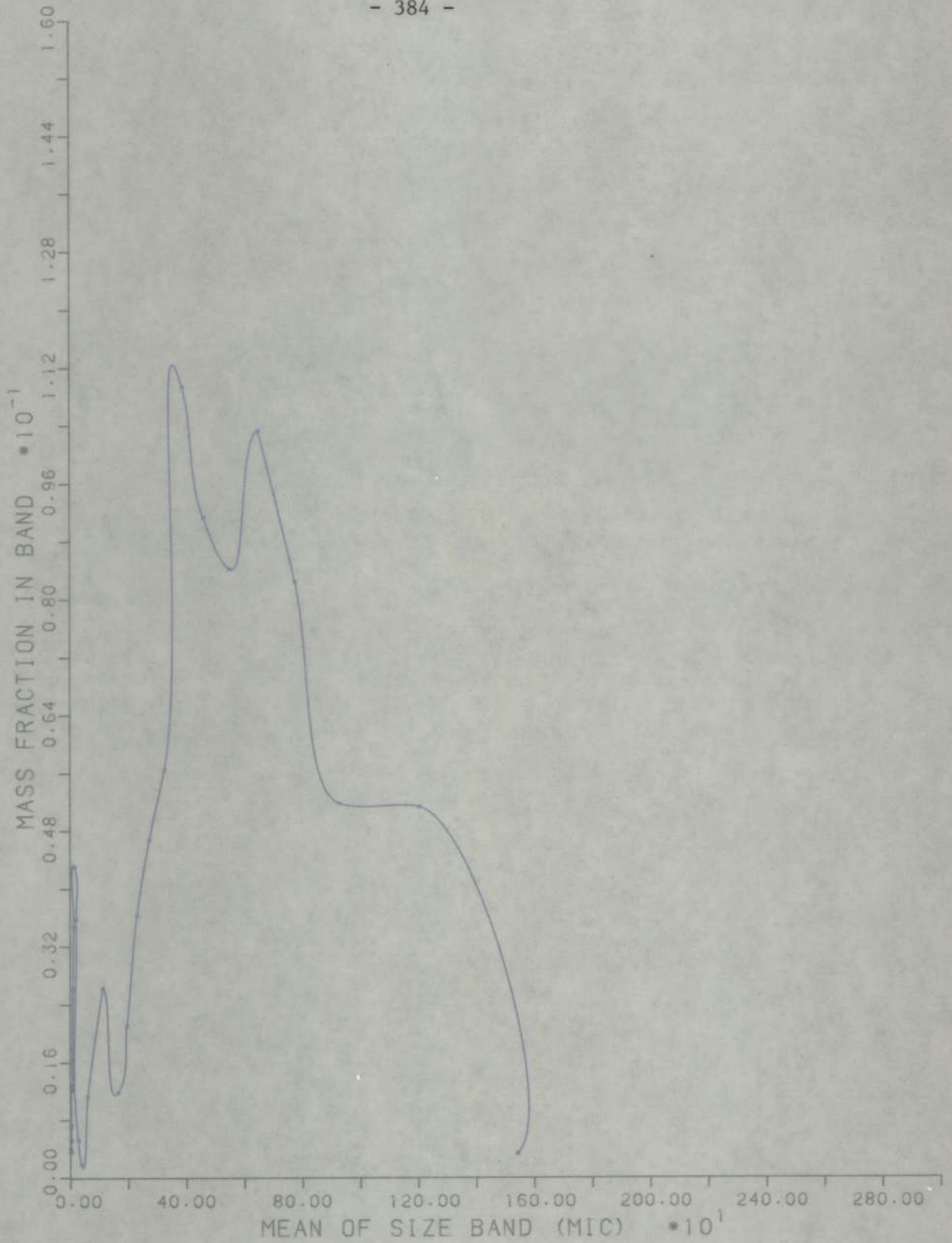


FIGURE A10.1

GRAPH FOR RUN NUMBER 51

MASS FRACTION IN BAND VS. MEAN OF BAND

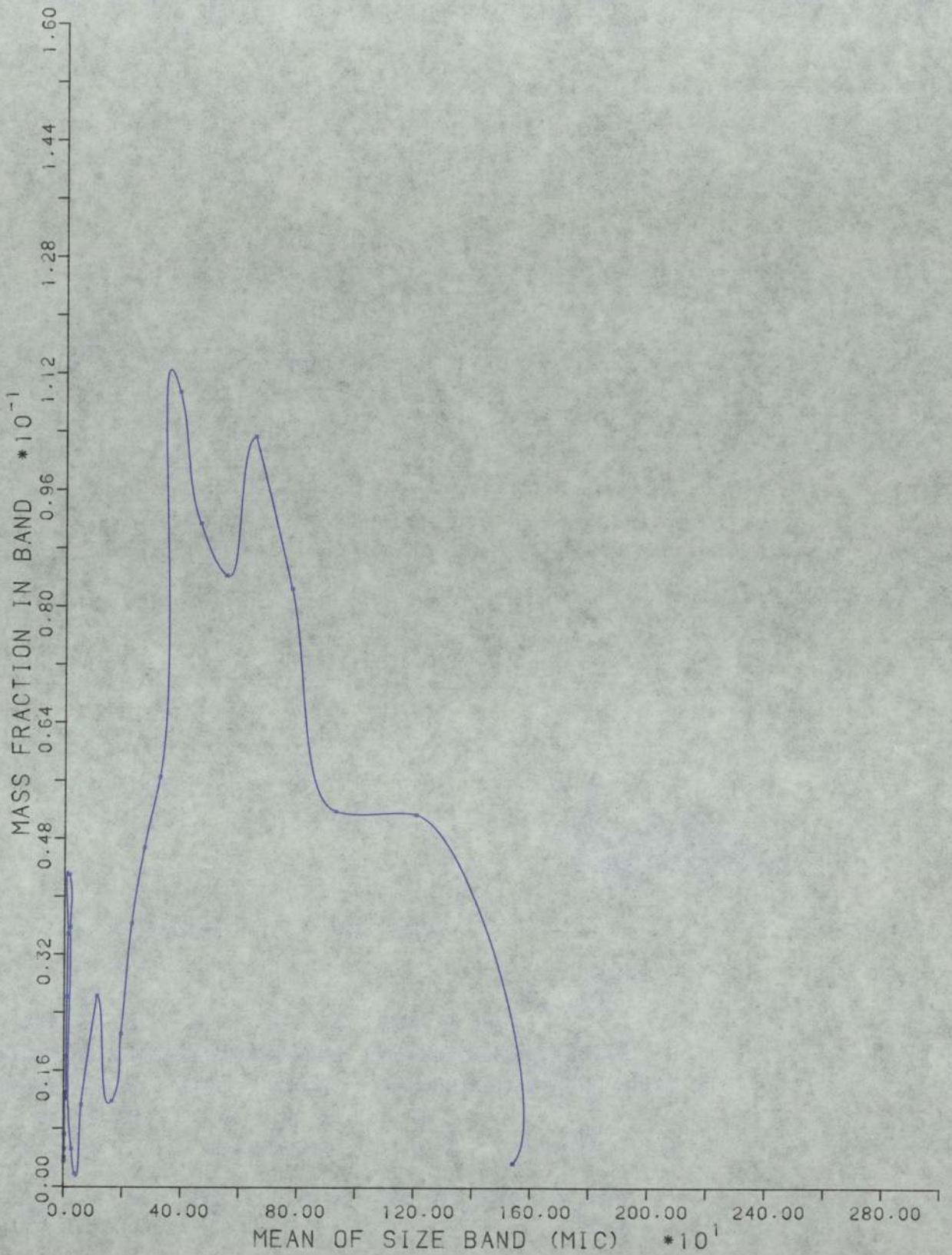


FIGURE A10.1

GRAPH FOR RUN NUMBER 51

MASS FRACTION IN BAND VS. MEAN OF BAND

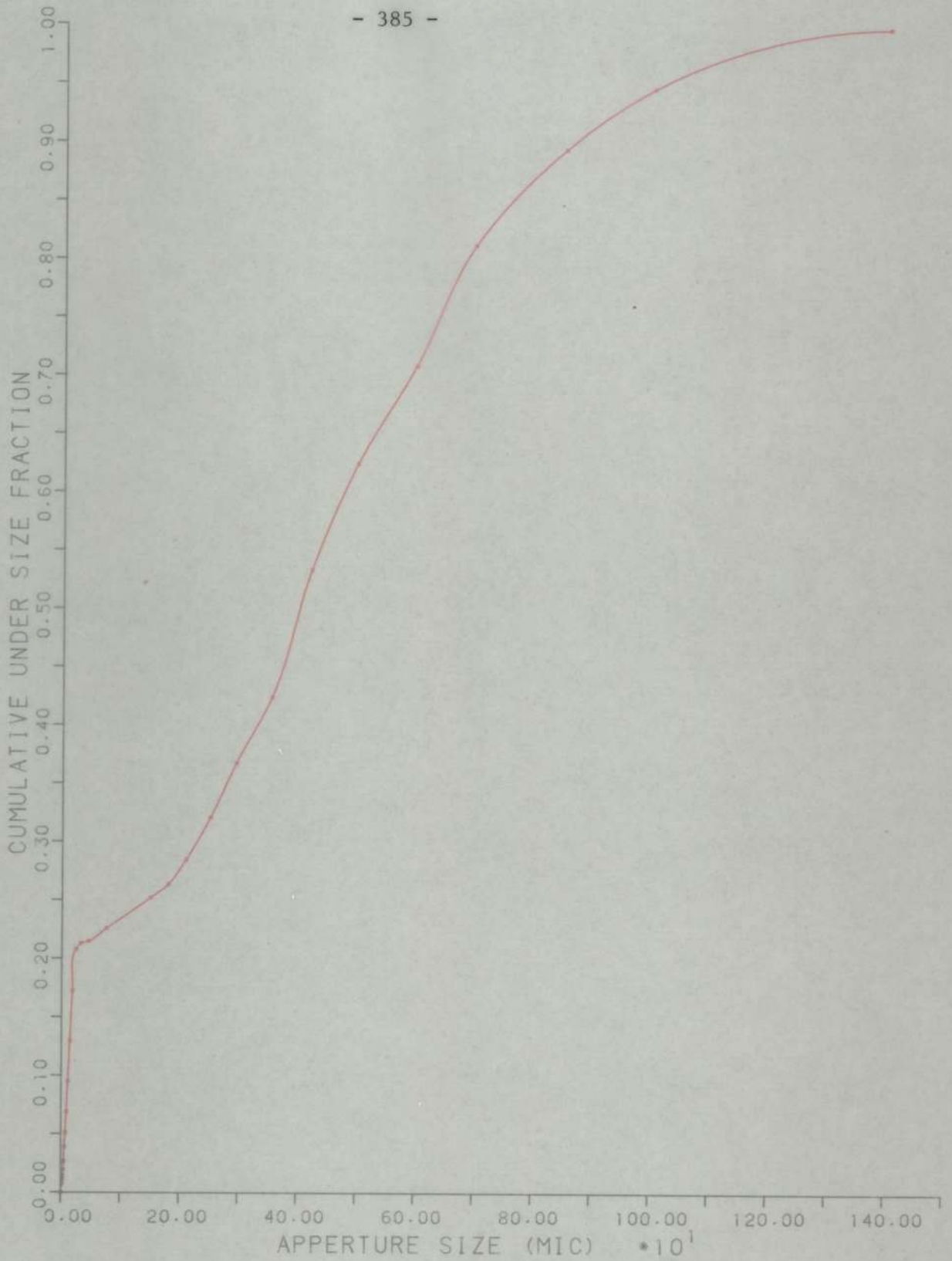


FIGURE A10.2

GRAPH FOR RUN NUMBER 51

CUMULATIVE UNDER SIZE FRACTION VS. APPERTURE SIZE

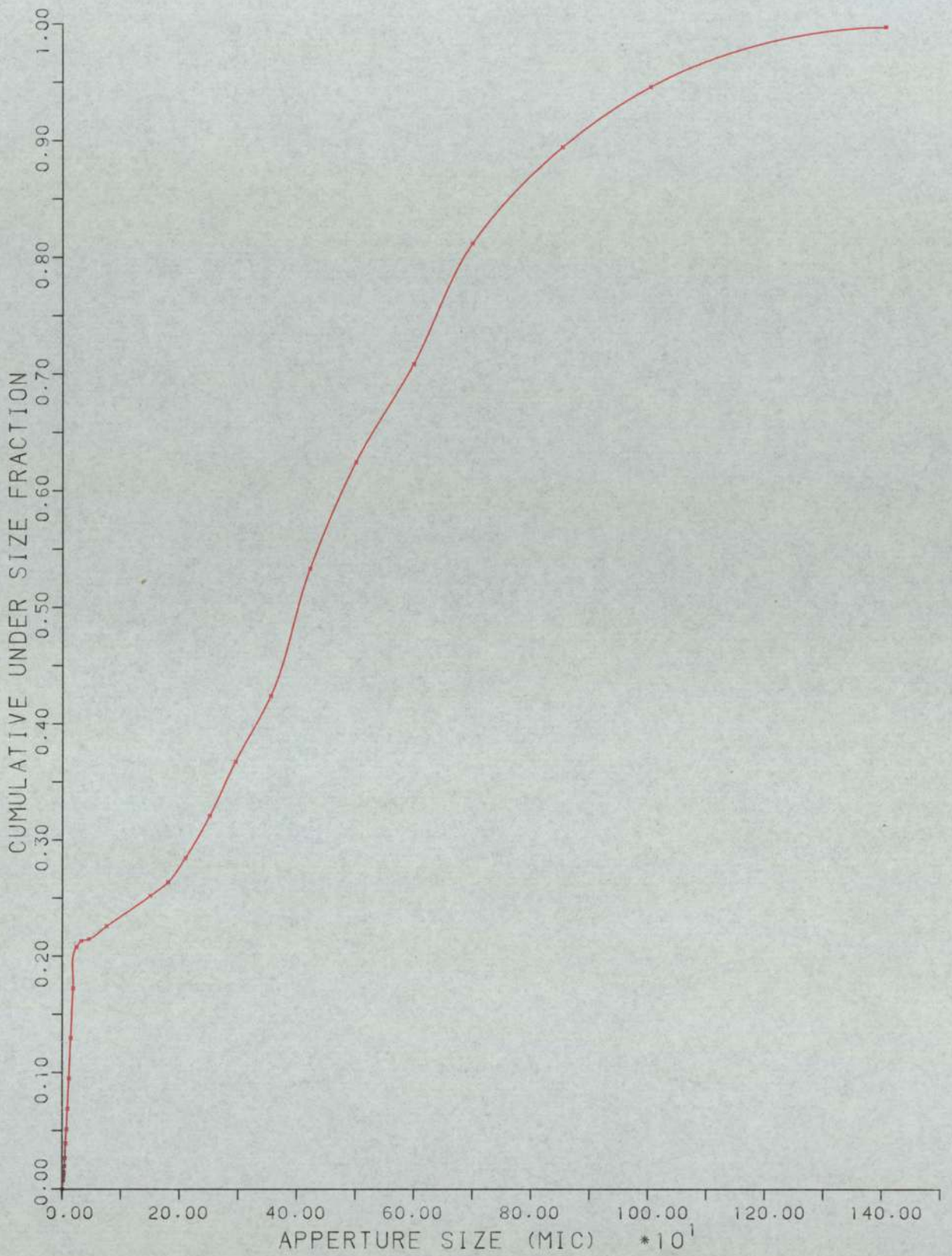


FIGURE A10.2

GRAPH FOR RUN NUMBER 51

CUMULATIVE UNDER SIZE FRACTION VS. APPERTURE SIZE

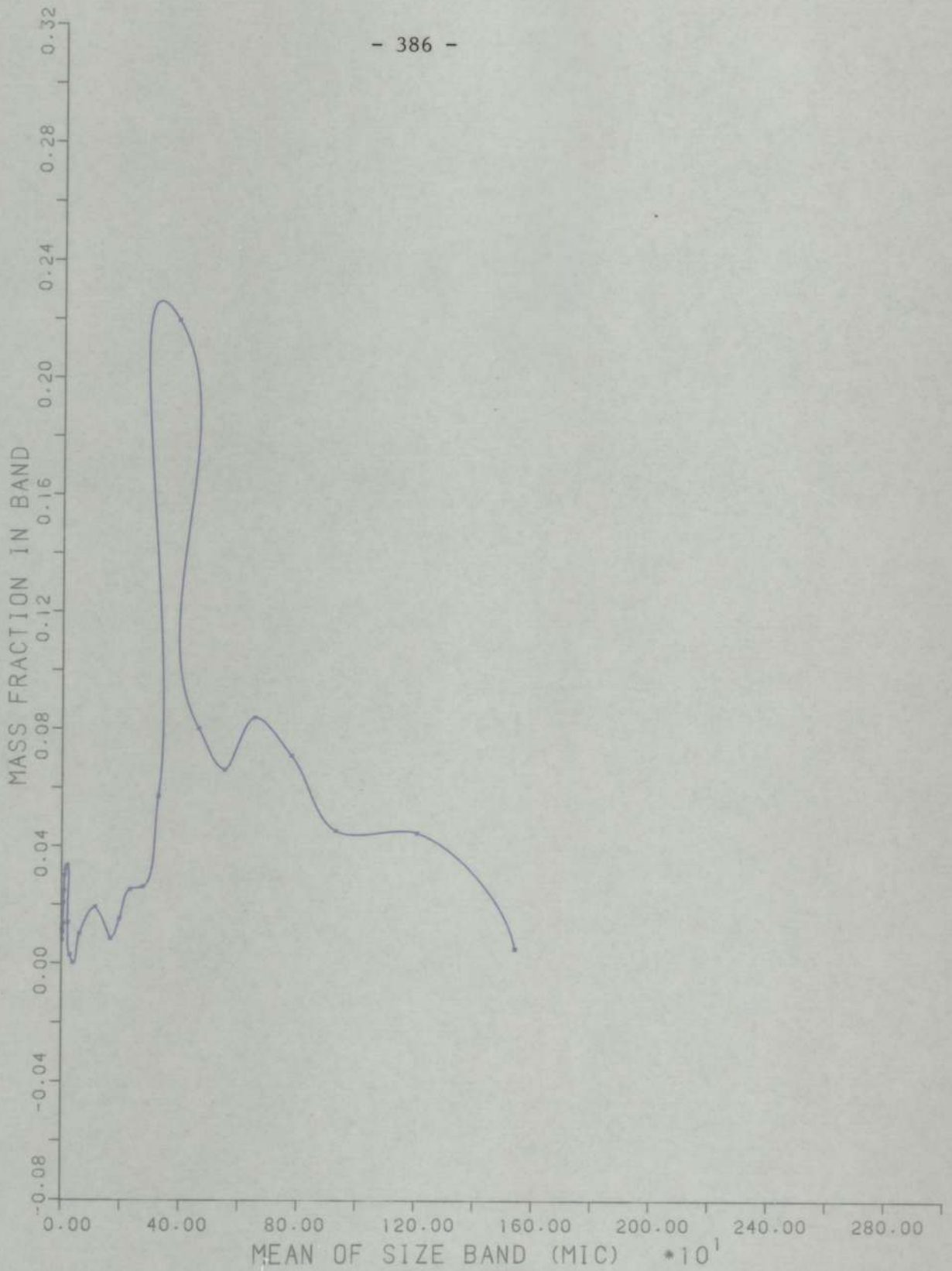


FIGURE A10.3

GRAPH FOR RUN NUMBER 52

MASS FRACTION IN BAND VS. MEAN OF BAND

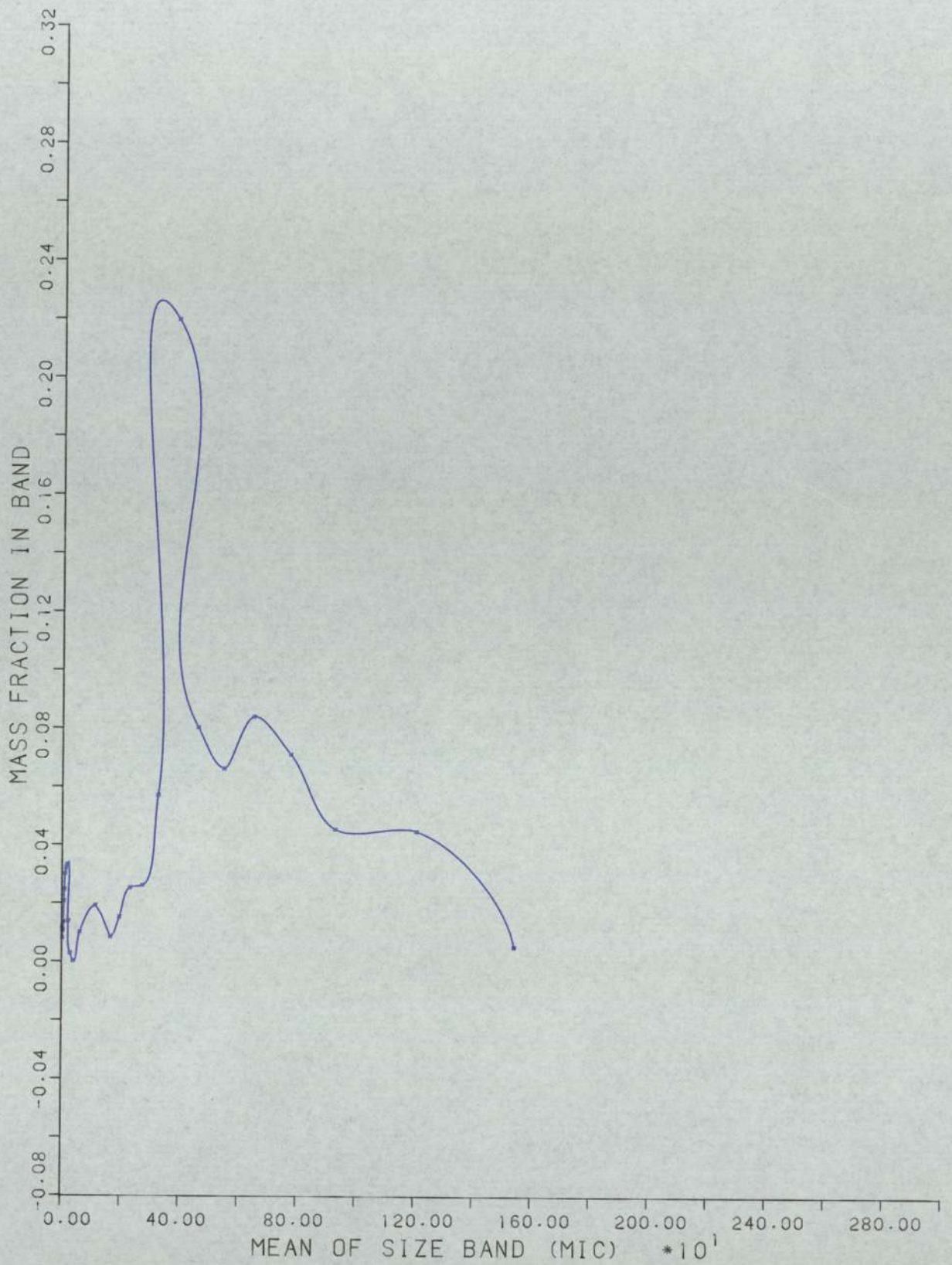


FIGURE A10.3

GRAPH FOR RUN NUMBER 52

MASS FRACTION IN BAND VS. MEAN OF BAND

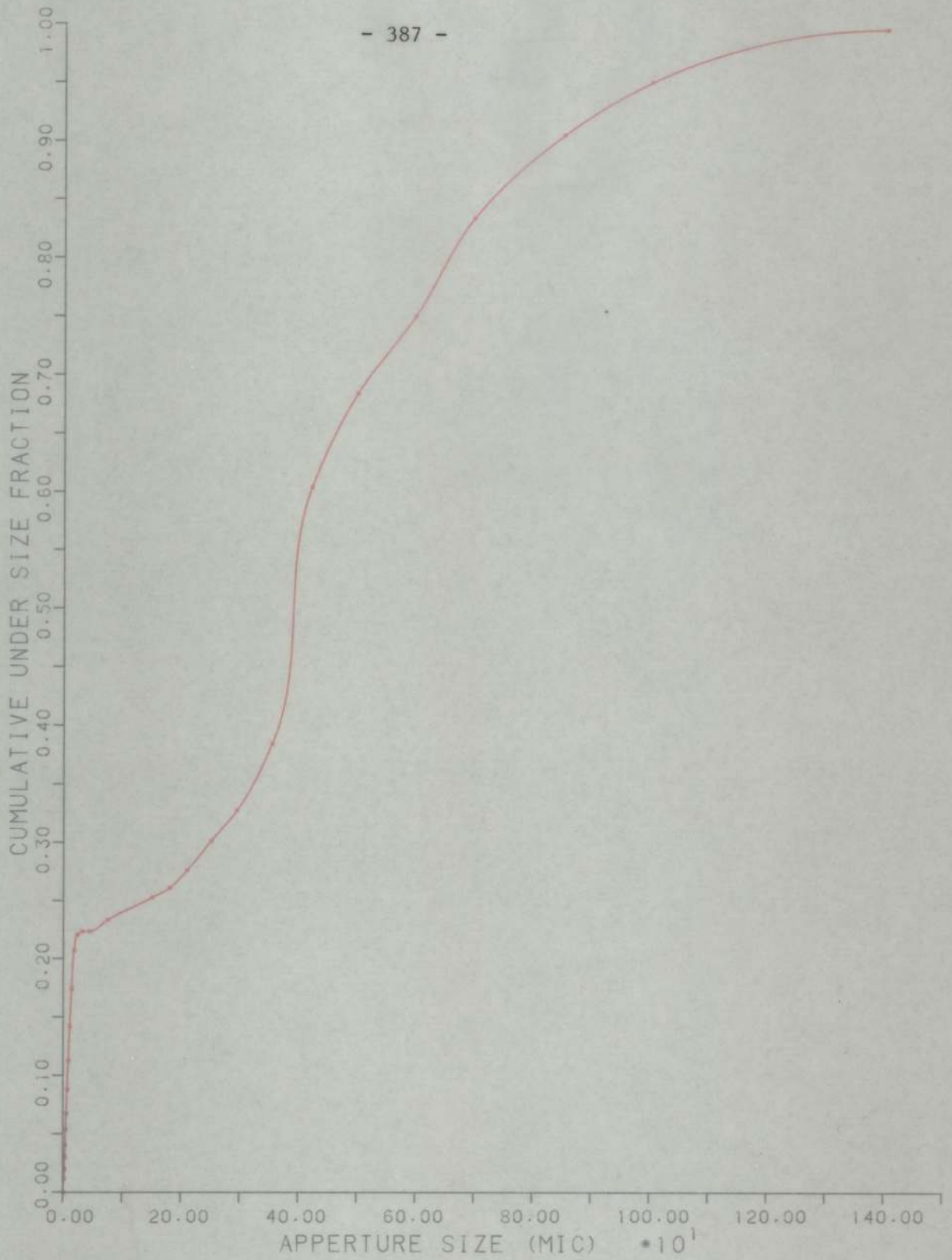


FIGURE A10.4

GRAPH FOR RUN NUMBER 52

CUMULATIVE UNDER SIZE FRACTION VS. APPERTURE SIZE

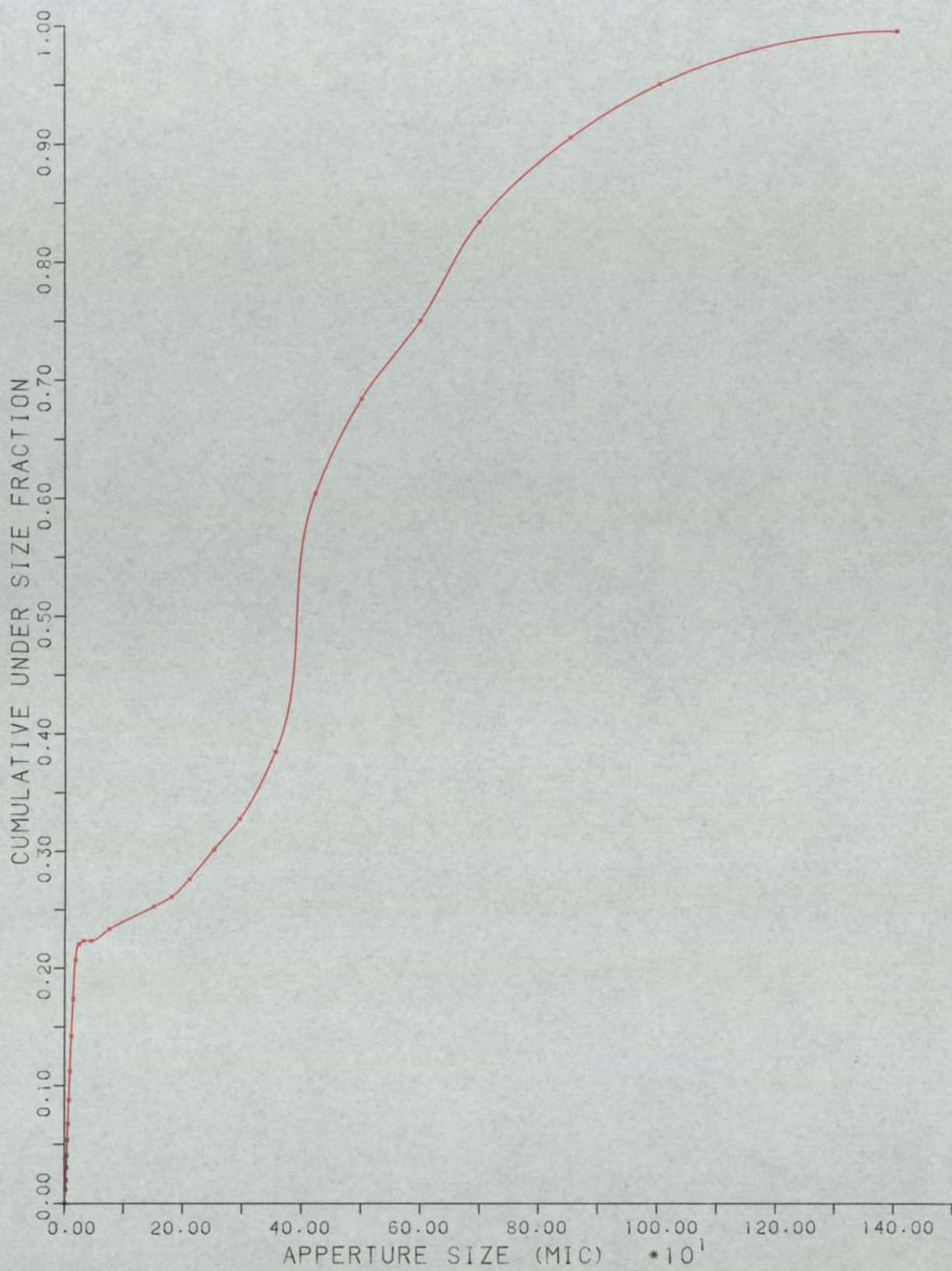


FIGURE A10.4

GRAPH FOR RUN NUMBER 52

CUMULATIVE UNDER SIZE FRACTION VS. APPERTURE SIZE

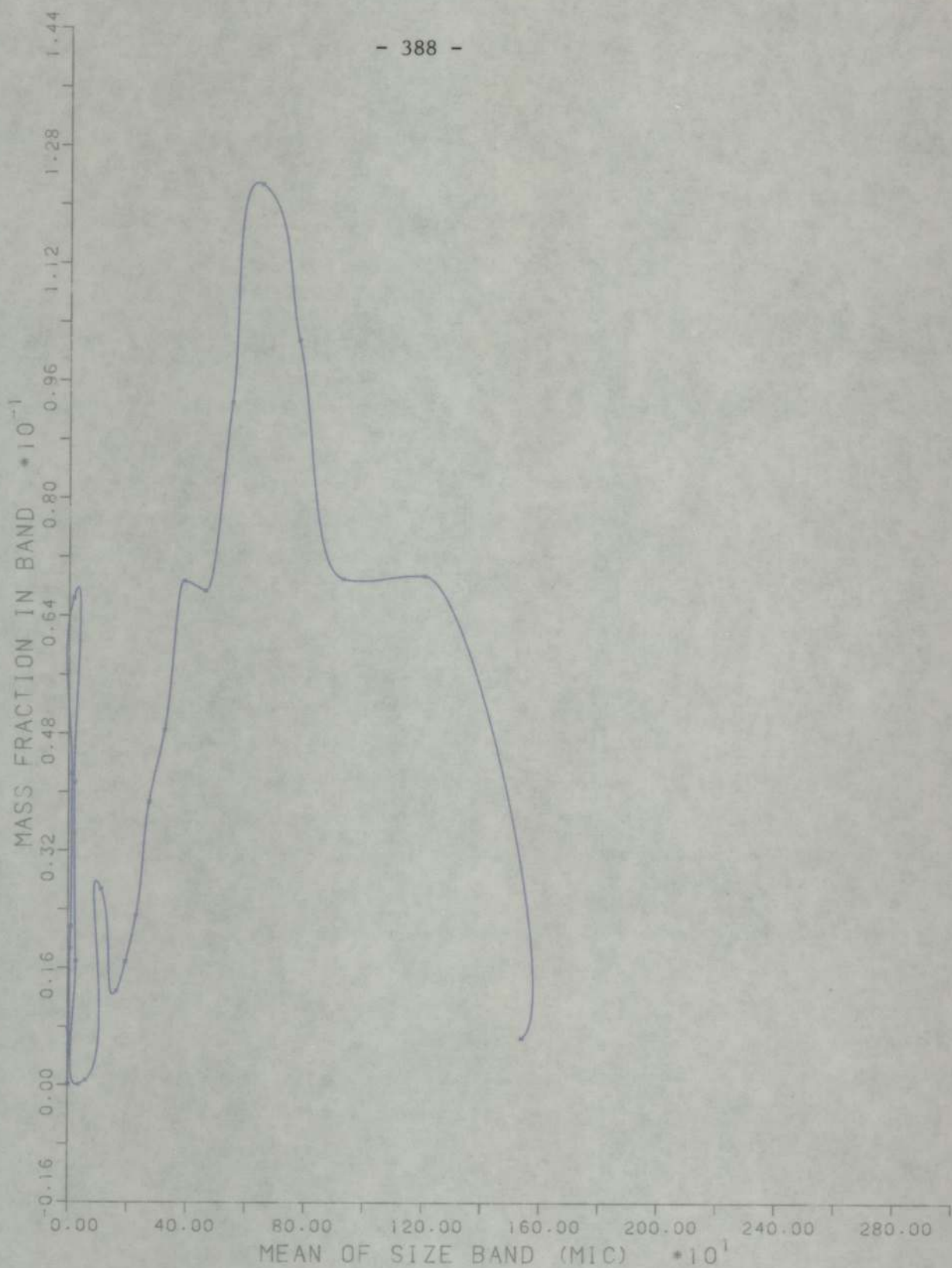


FIGURE A10.5

GRAPH FOR RUN NUMBER 55

MASS FRACTION IN BAND VS. MEAN OF BAND

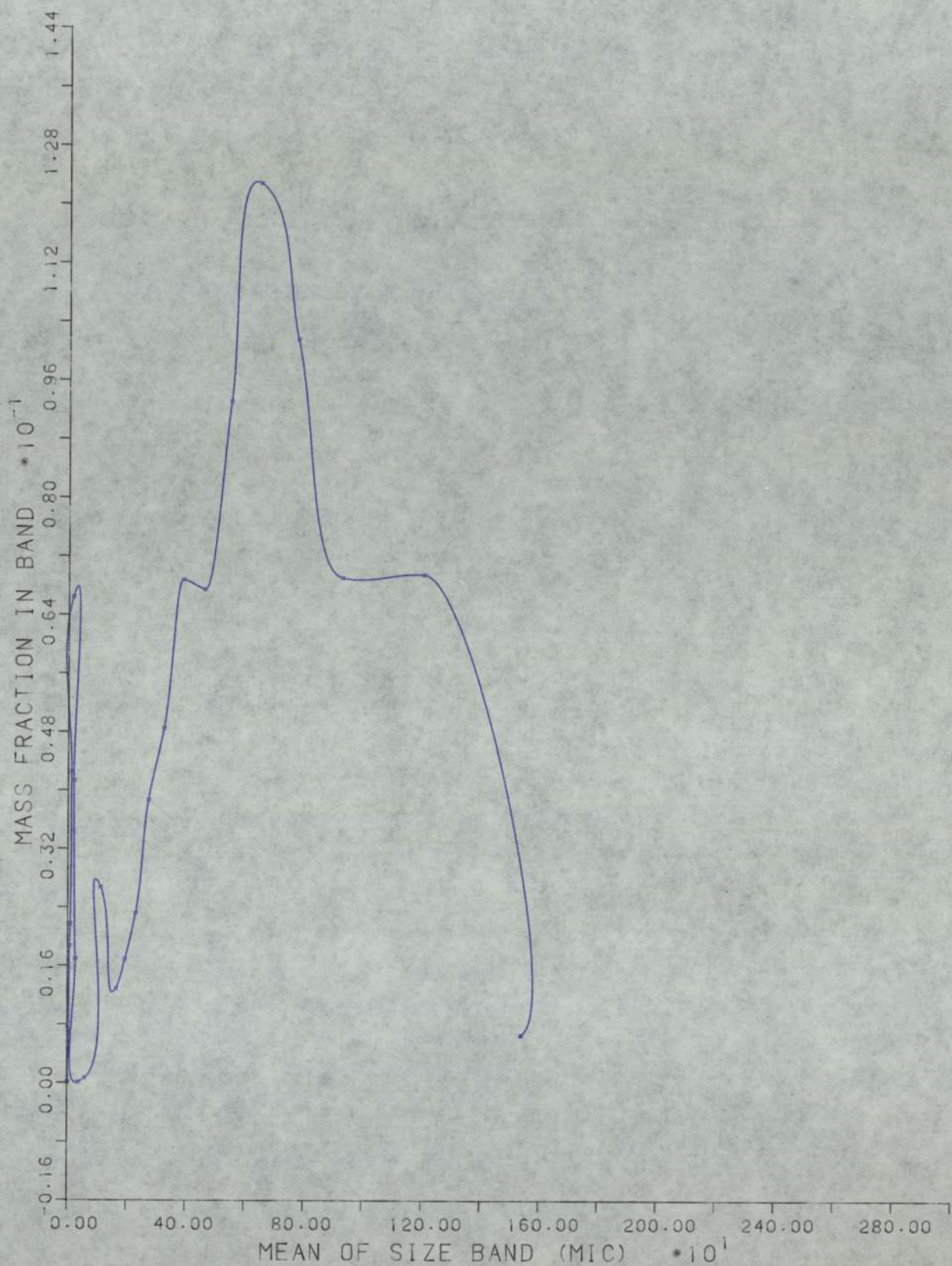


FIGURE A10.5

GRAPH FOR RUN NUMBER 55

MASS FRACTION IN BAND VS. MEAN OF BAND

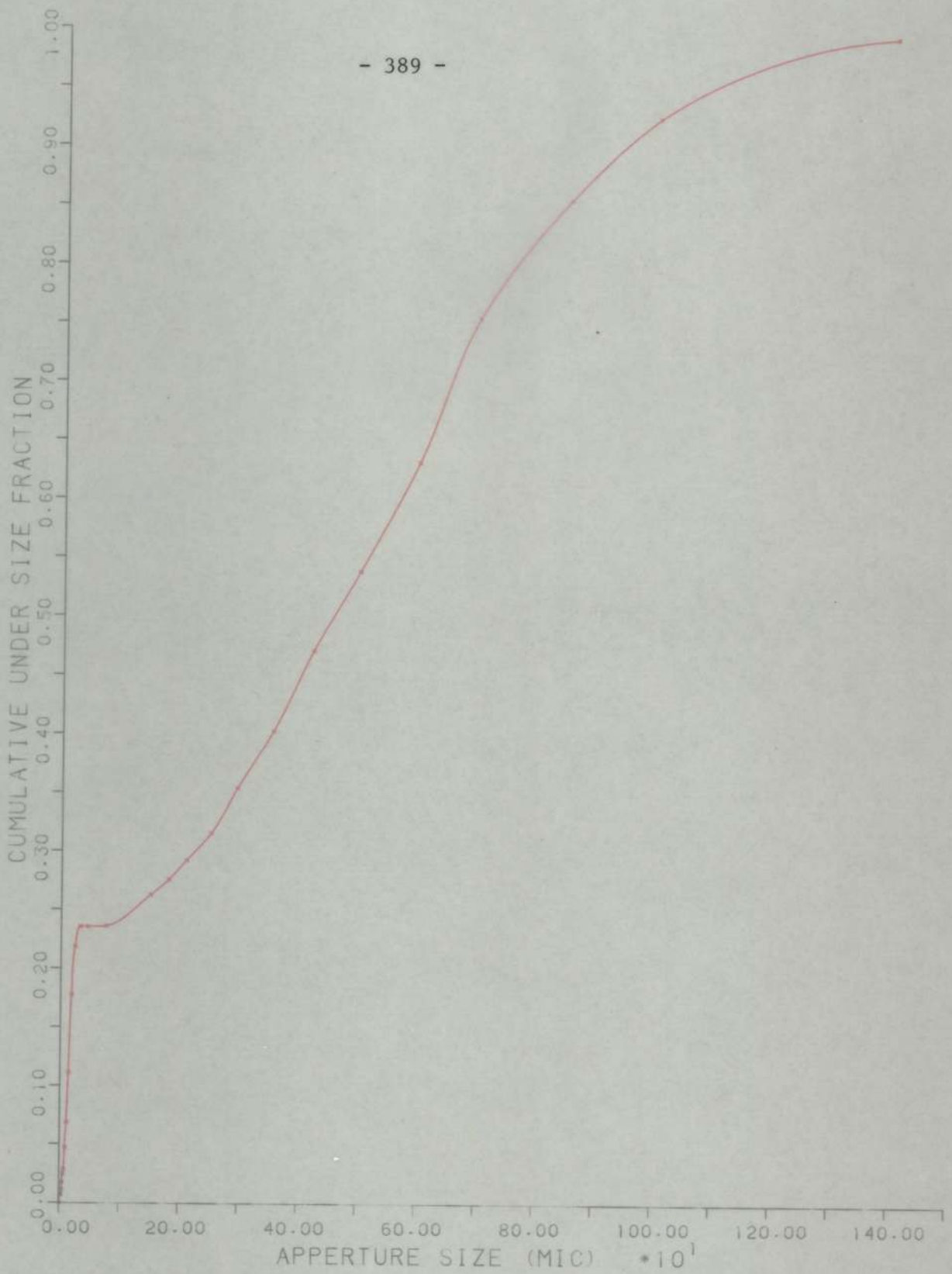


FIGURE A 10 . 6

GRAPH FOR RUN NUMBER 55

CUMULATIVE UNDER SIZE FRACTION VS. APPERTURE SIZE

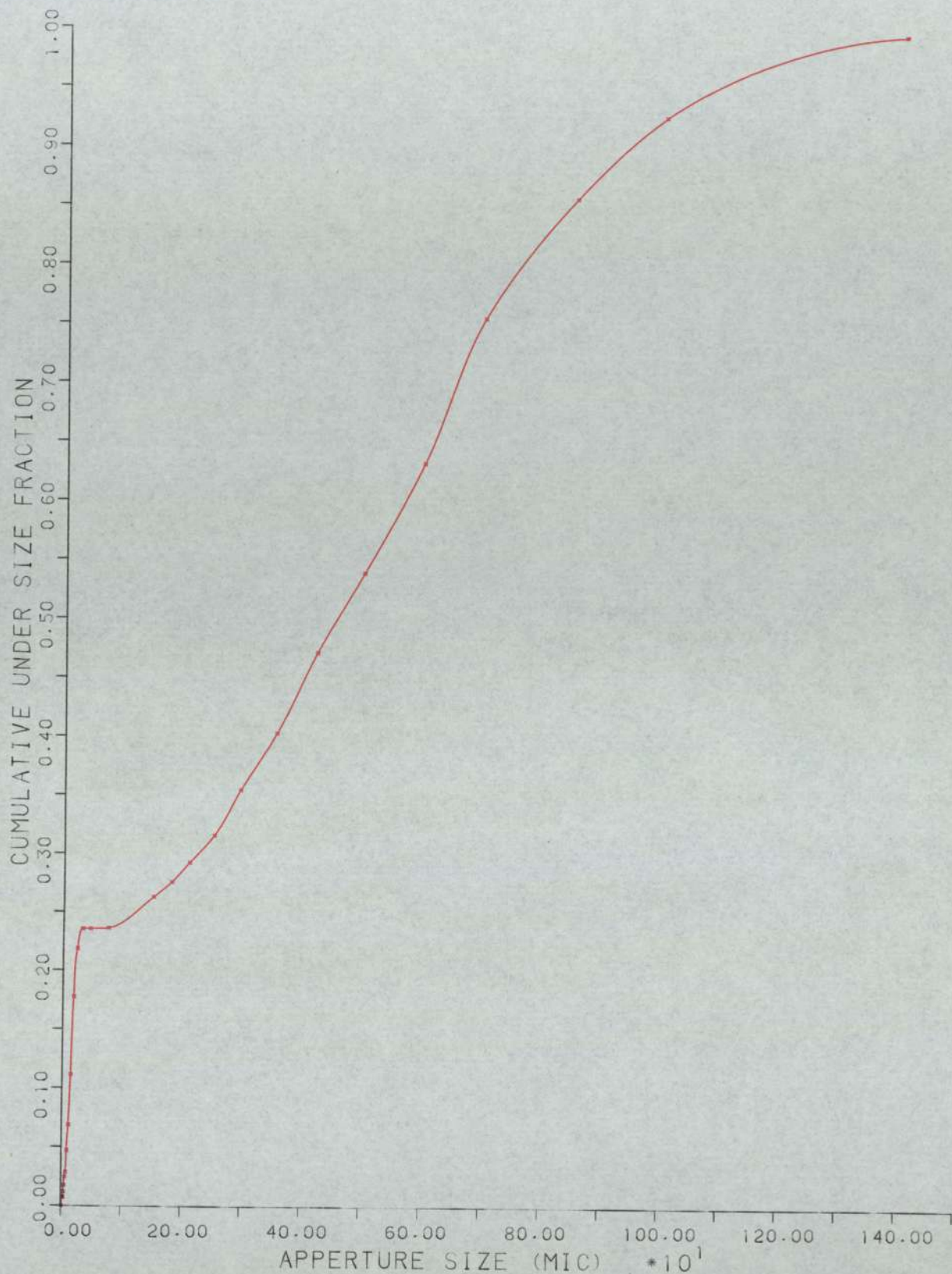


FIGURE A 1 0 . 6

GRAPH FOR RUN NUMBER 55

CUMULATIVE UNDER SIZE FRACTION VS. APPERTURE SIZE

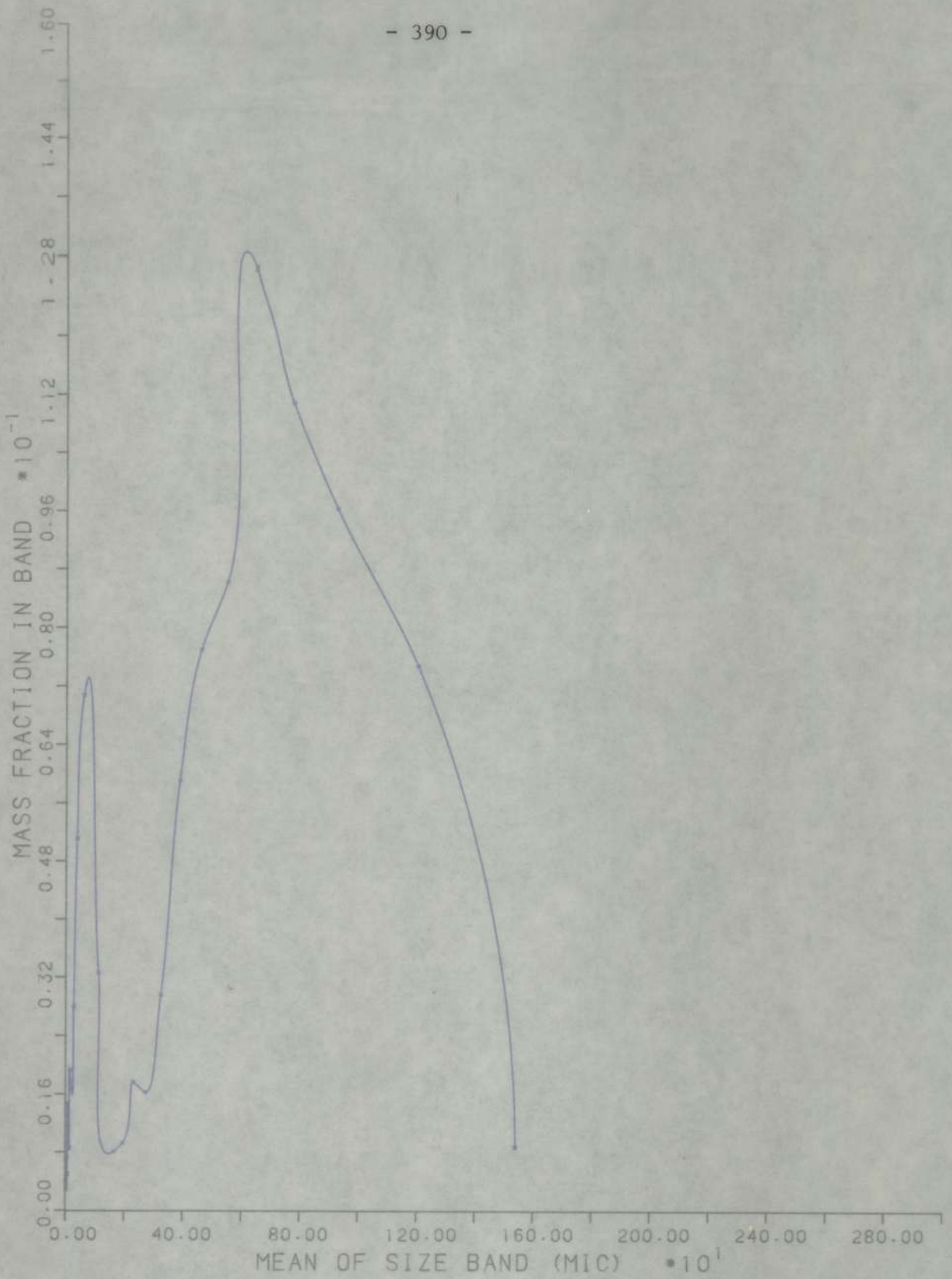


FIGURE A10.7

GRAPH FOR RUN NUMBER 59

MASS FRACTION IN BAND VS. MEAN OF BAND

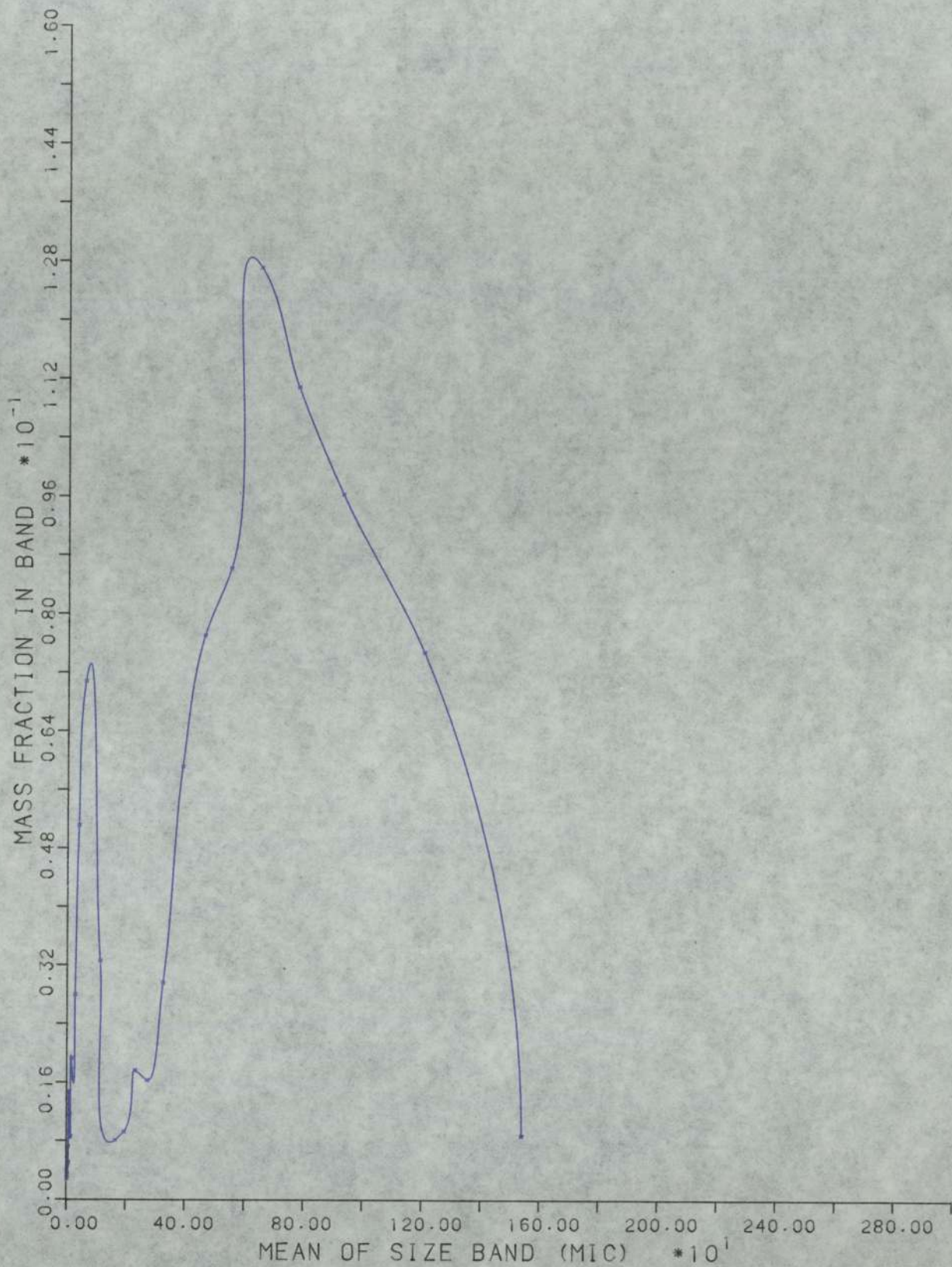


FIGURE A10 - 7

GRAPH FOR RUN NUMBER 59

MASS FRACTION IN BAND VS. MEAN OF BAND

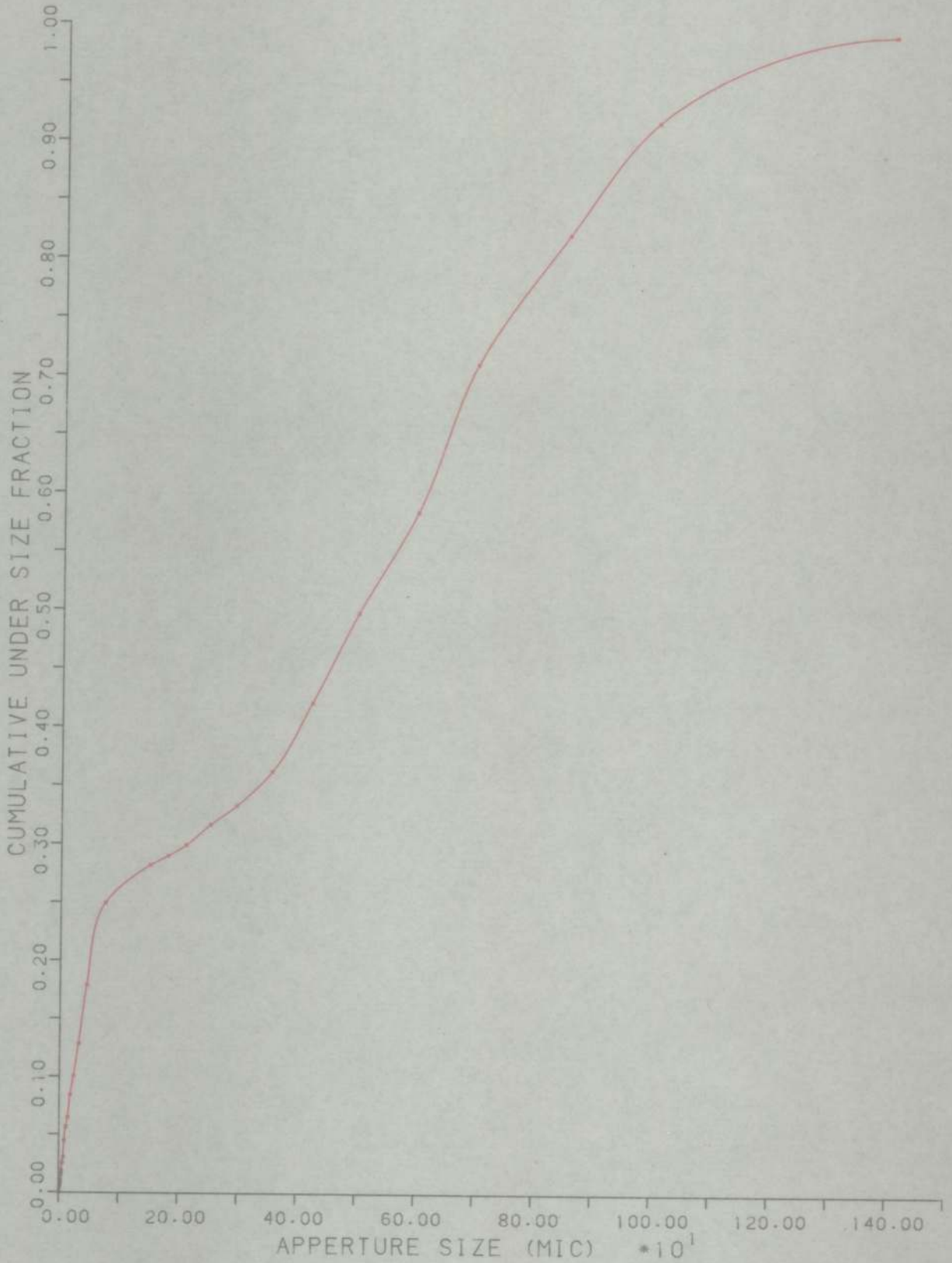


FIGURE A10 .{ }

GRAPH FOR RUN NUMBER 59

CUMULATIVE UNDER SIZE FRACTION VS. APPERTURE SIZE

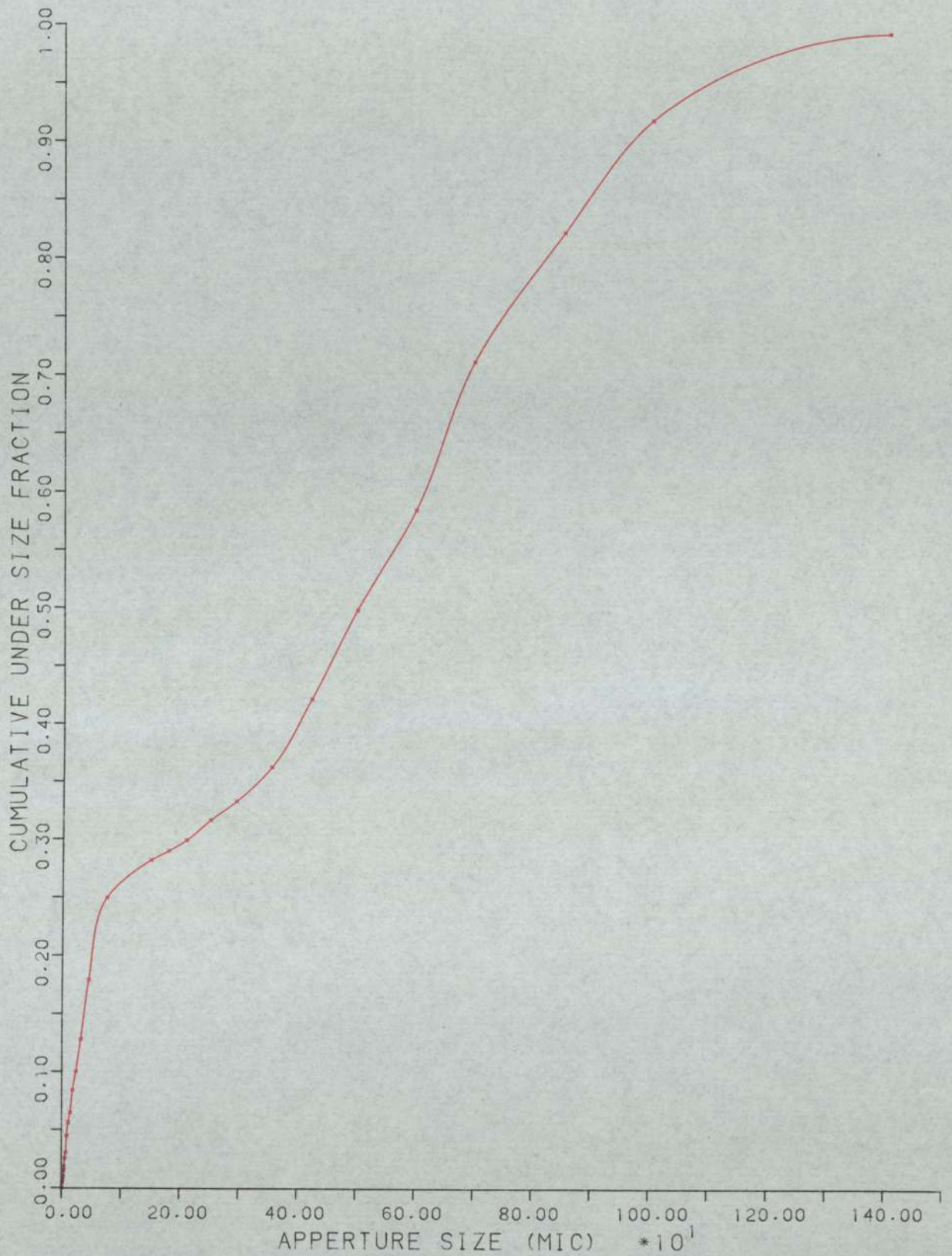


FIGURE A10 - { }

GRAPH FOR RUN NUMBER 59

CUMULATIVE UNDER SIZE FRACTION VS. APPERTURE SIZE

APPENDIX 11

MICROSCOPE PHOTOGRAPHS OF THE DISPERSANT PRODUCT FROM DIFFERENT PRODUCTION RUNS

An attempt was made to photograph samples of the dispersant additive obtained from different runs using the optical microscope in search of the presence of very fine pentaerythritol particles even in the final product. Some of these photographs are presented in this appendix. The magnification obtained was the same in all the photographs and was about 1700 times as can be seen from Figure All.1 in which each scale subdivision represents $10\mu\text{m}$, hence each subdivision of the superimposed scale represents $1.175\mu\text{m}$. These photographs were taken after a very long storage period at ambient temperature, ranging from four months for run 59 product to more than one year for the industrial Fawley batch.

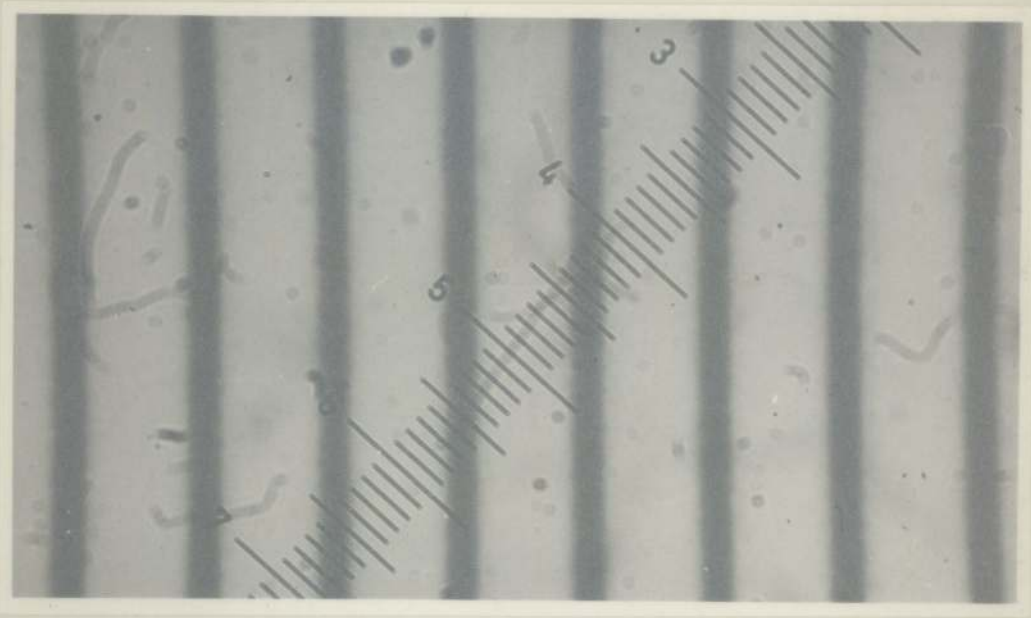


Figure All.1: A 1 mm scale of 0.01 mm subdivision. Magnification is about 1700 times, each subdivision of the superimposed scale represents 1.175 μm

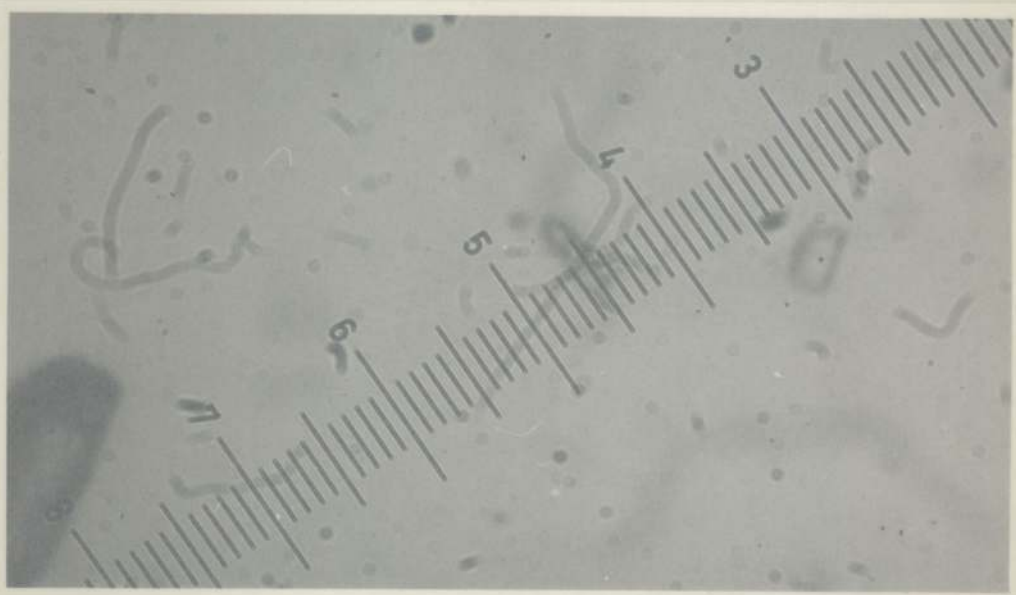
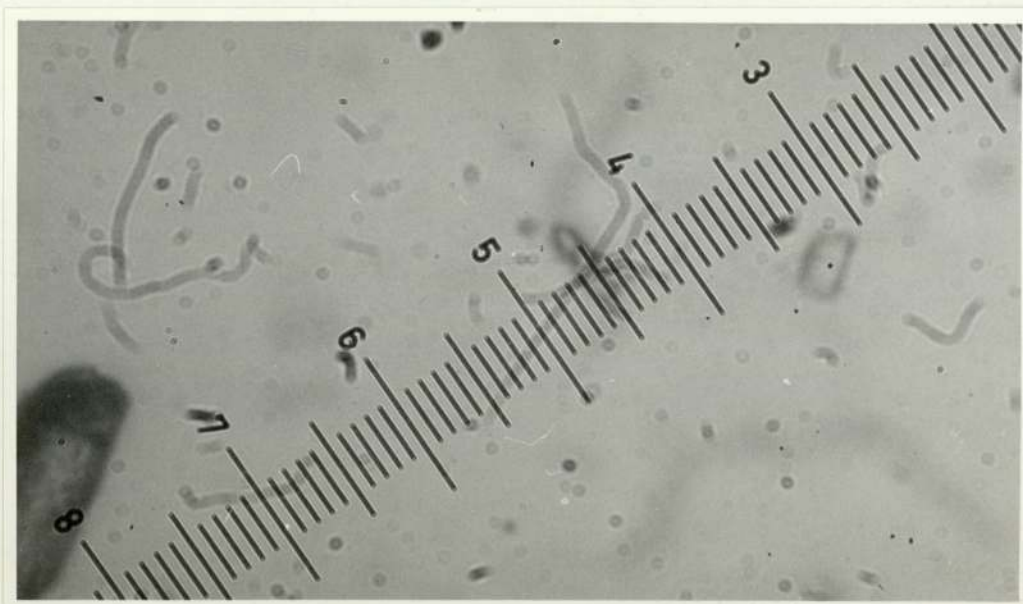
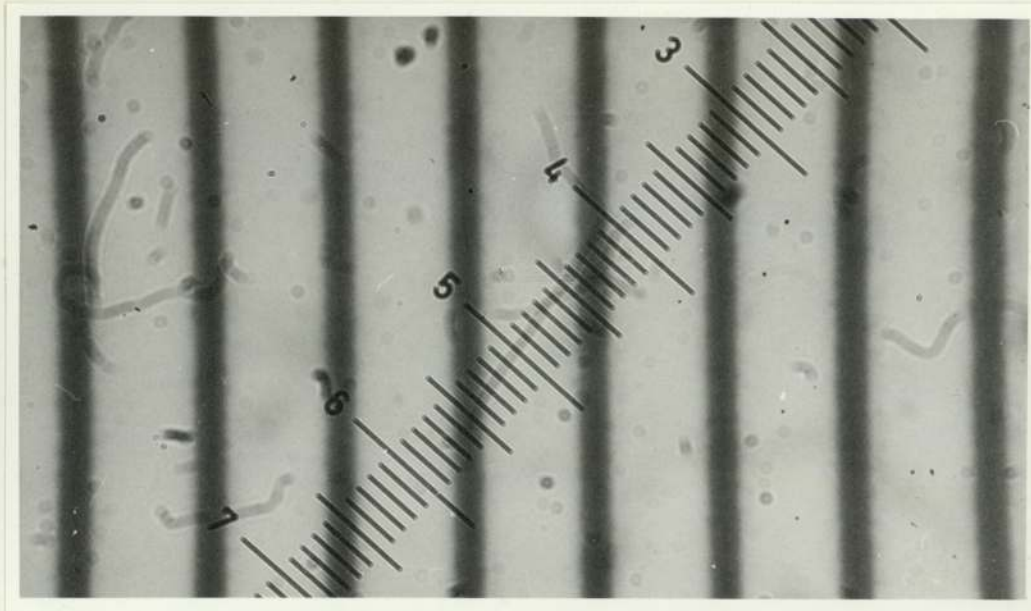


Figure All.2: Run 33 product sample, each subdivision represents 1.175 μm



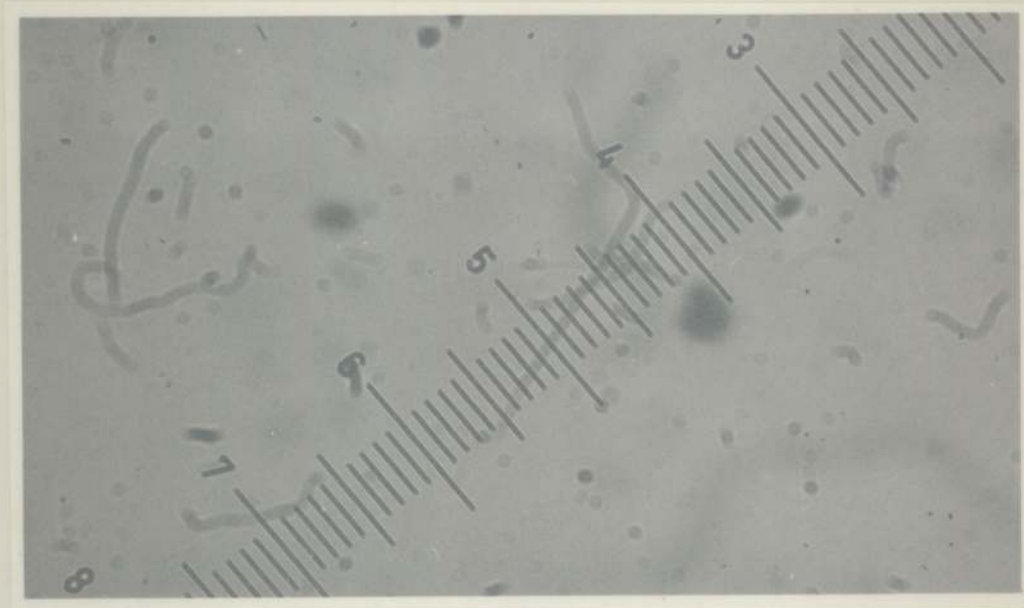


Figure All.3: Run 33 reheated product sample, each subdivision represents 1.175 μm

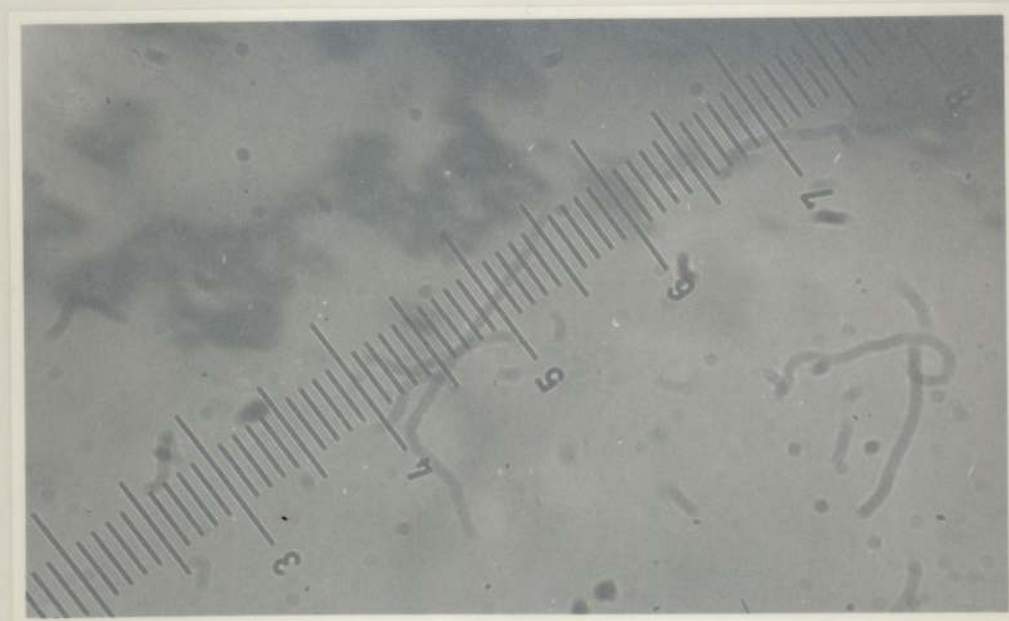
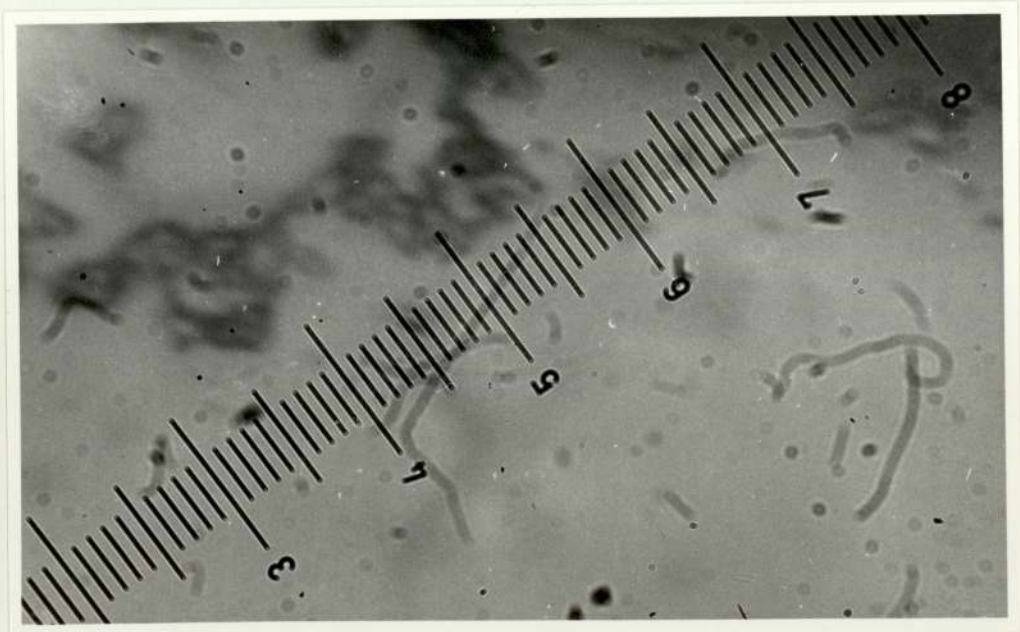
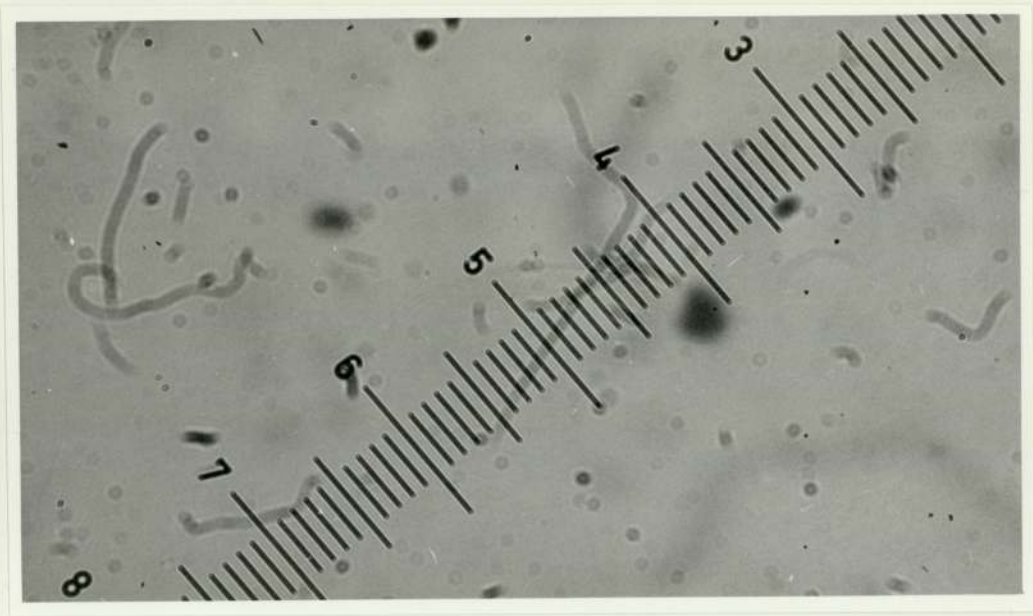


Figure All.4: Run 35 product sample, showing agglomerates of Fe_2O_3 , each subdivision represents 1.175 μm



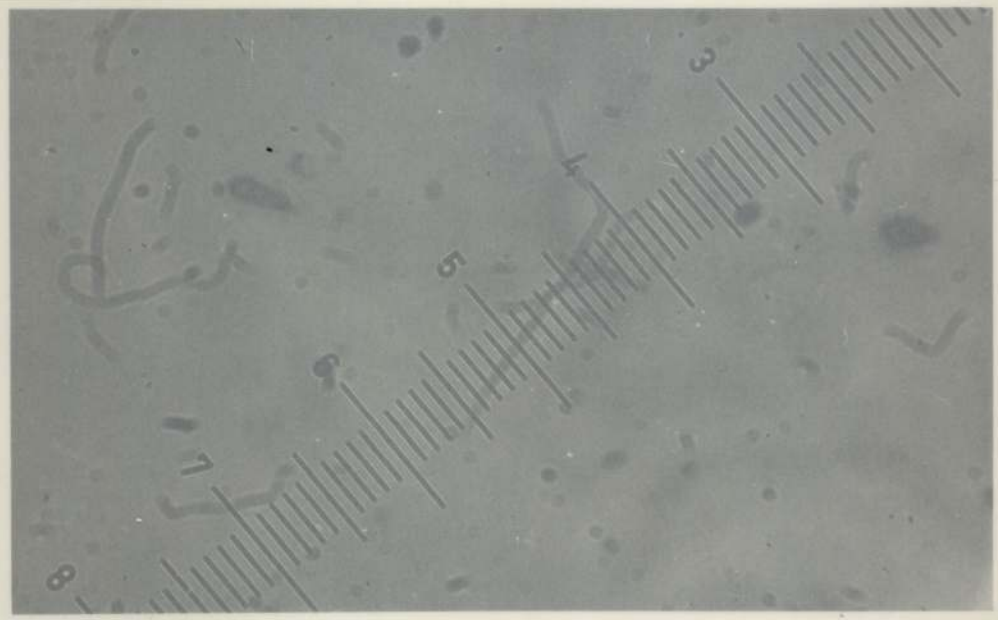


Figure All.5: Run 55 product sample, each subdivision represents 1.175 μm

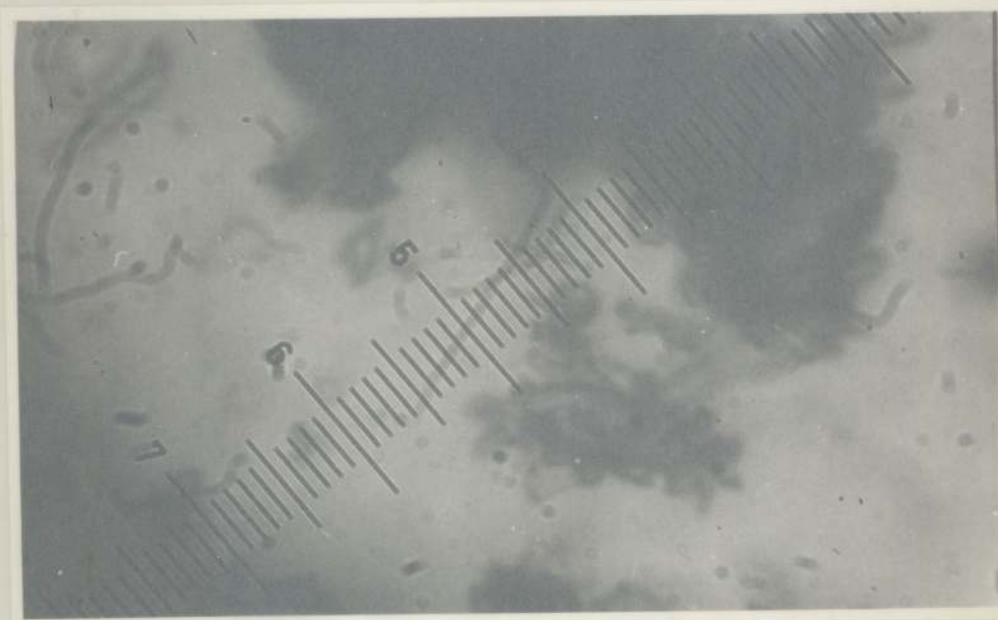
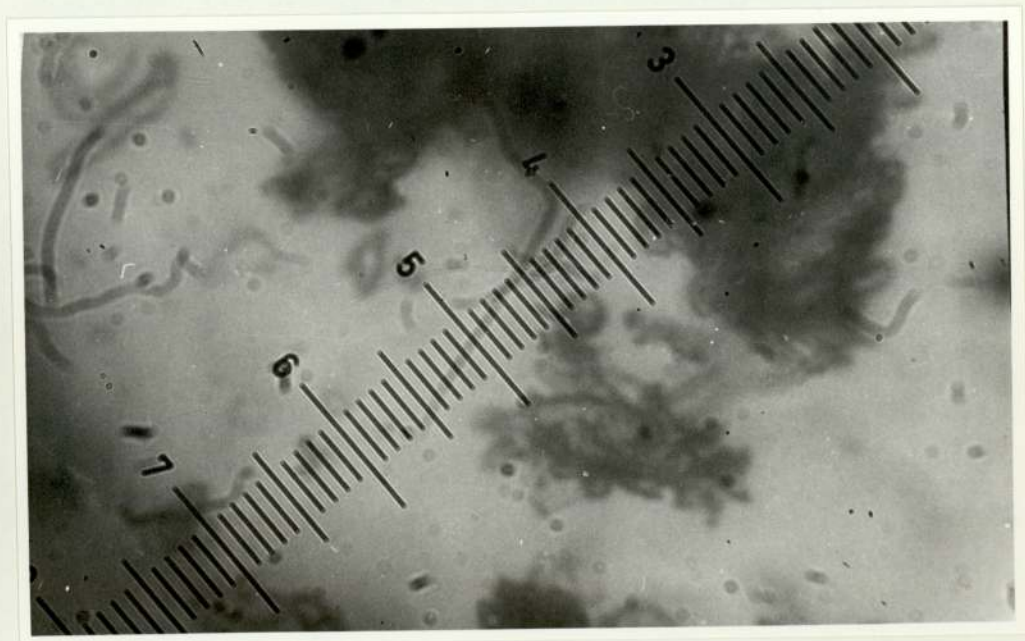
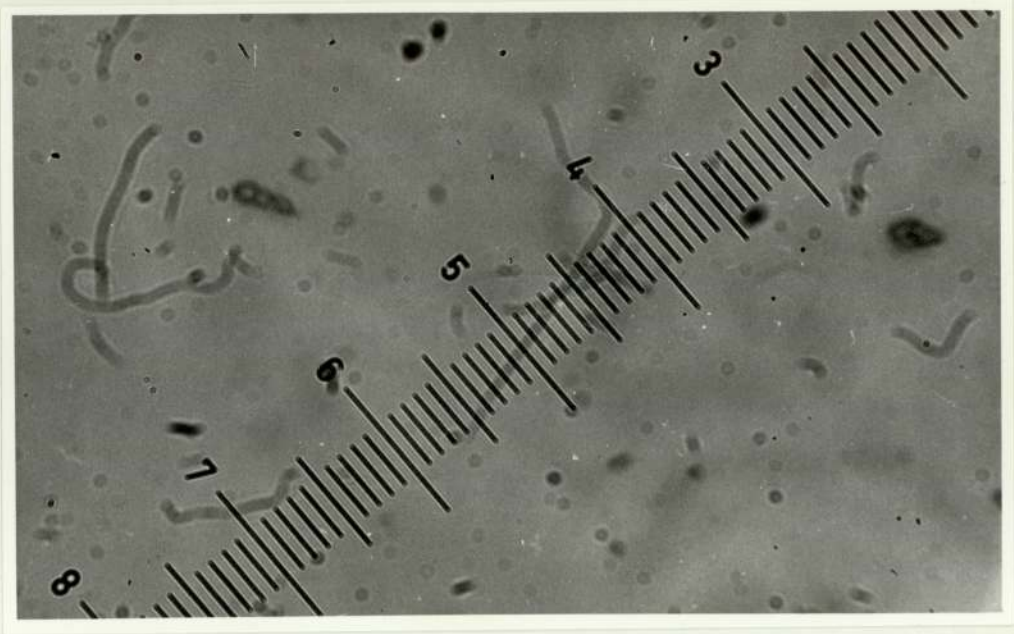


Figure All.6: Run 59 product sample, showing agglomerates of PE crystals, each subdivision represents 1.175 μm



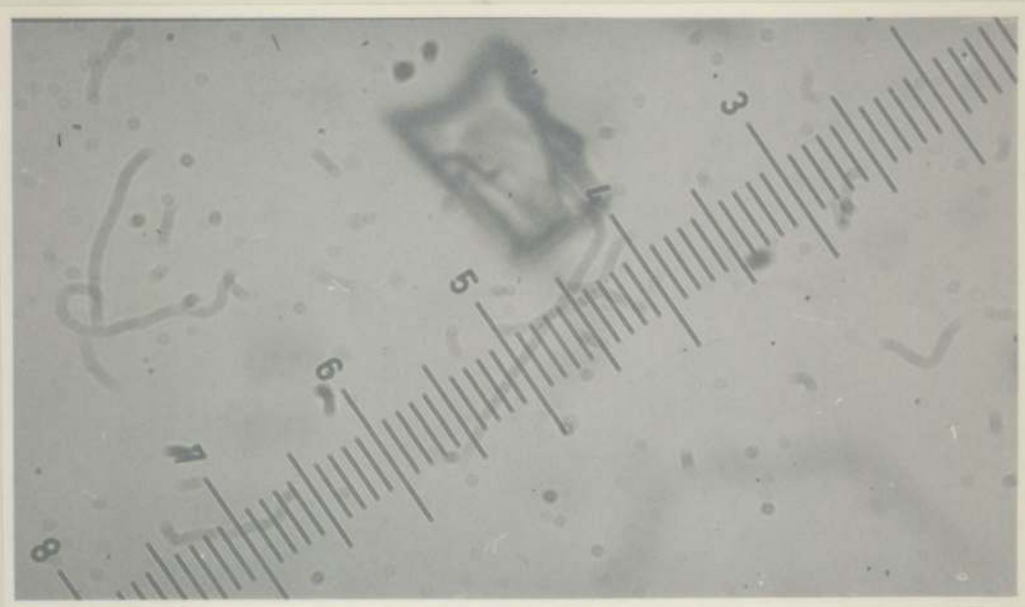
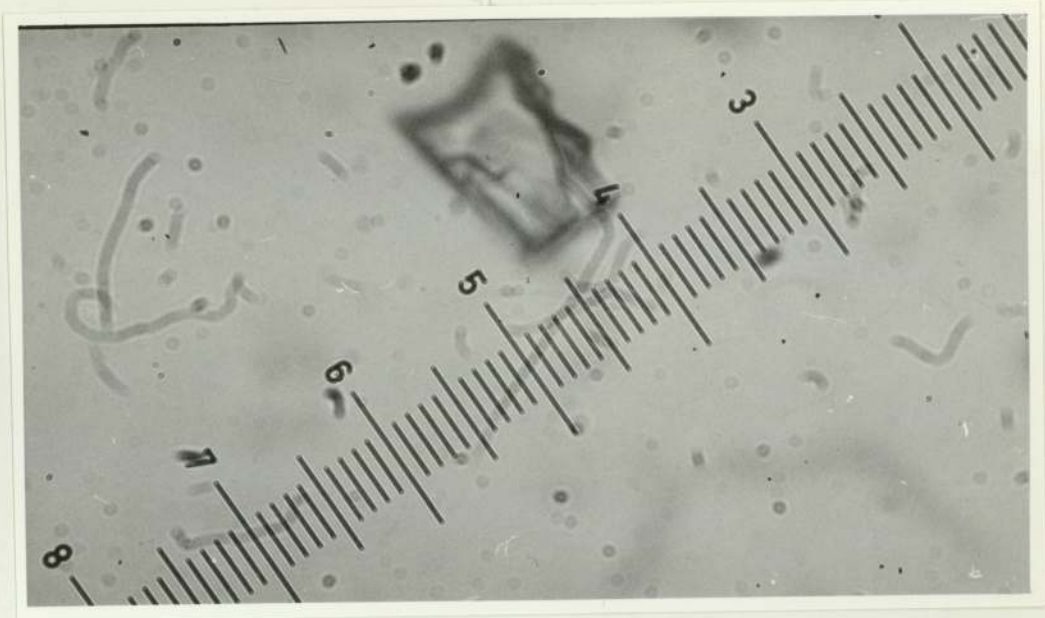


Figure All.7: Fawley batch product sample, each subdivision represents 1.175 μm



APPENDIX 12

ELECTRON MICROSCOPE PHOTOGRAPHS OF THE SEDIMENT FROM DIFFERENT PRODUCTION RUNS

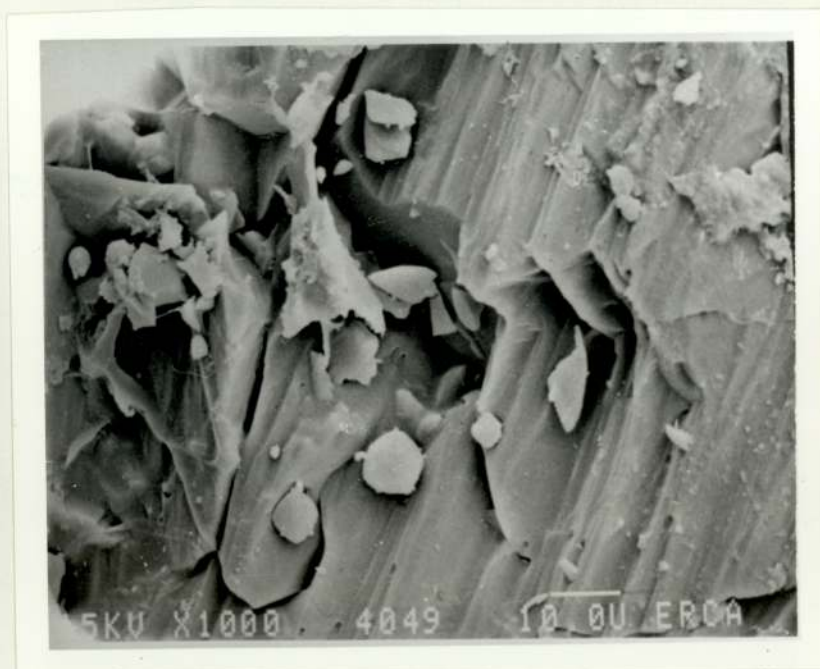
The sediment obtained at the end of many production runs covering a wide cross section of the experimental work was photographed using the electron microscope at Esso Research Centre in Abingdon. This was to check the effect of many production conditions on the type of crystal habit obtained and its relation to filtrability of the product. Some of the photographs obtained are presented in this appendix. The magnification used is given separately on each of the photographs.



Figure A12.1: Run 33 large crystals fraction sediment



Figure A12.2: Run 33 large crystals fraction sediment



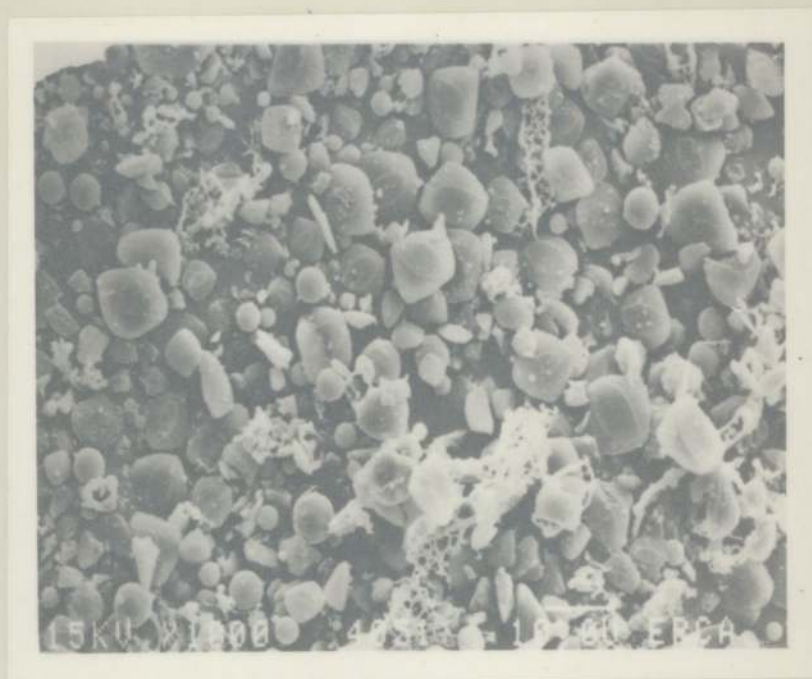


Figure A12.3: Run 33 fine crystals fraction sediment

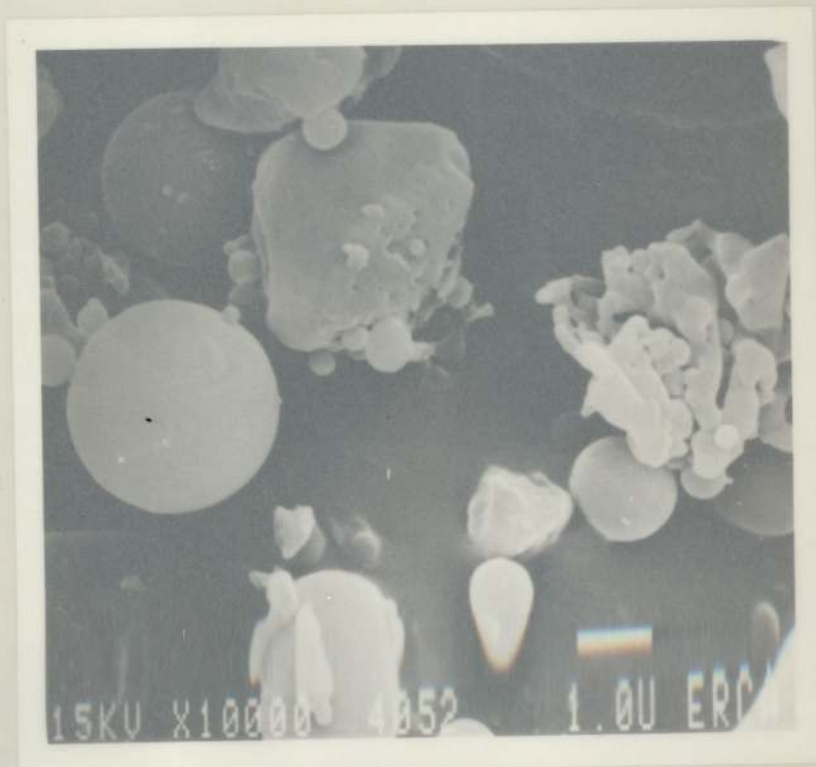


Figure A12.4: Run 33 fine crystals fraction sediment

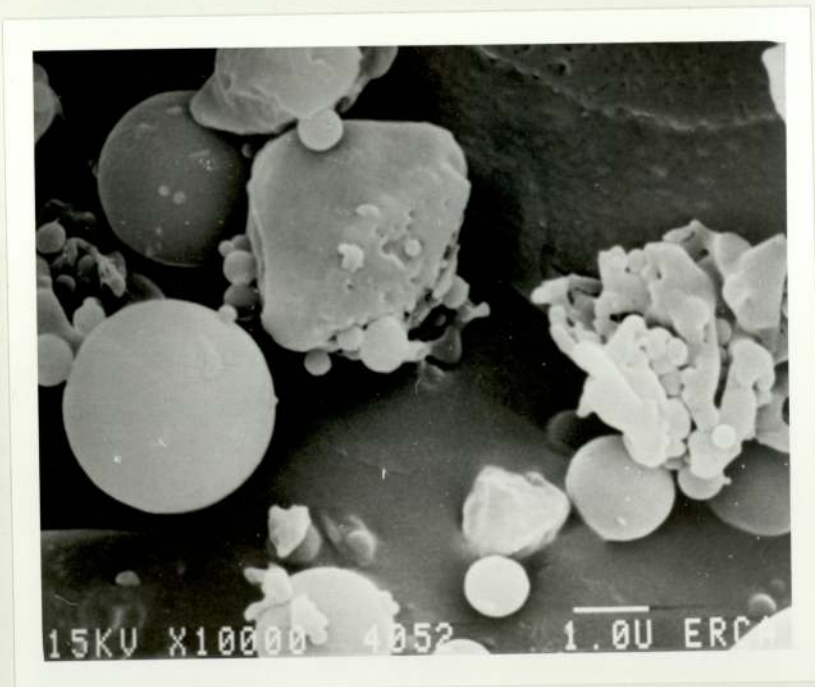
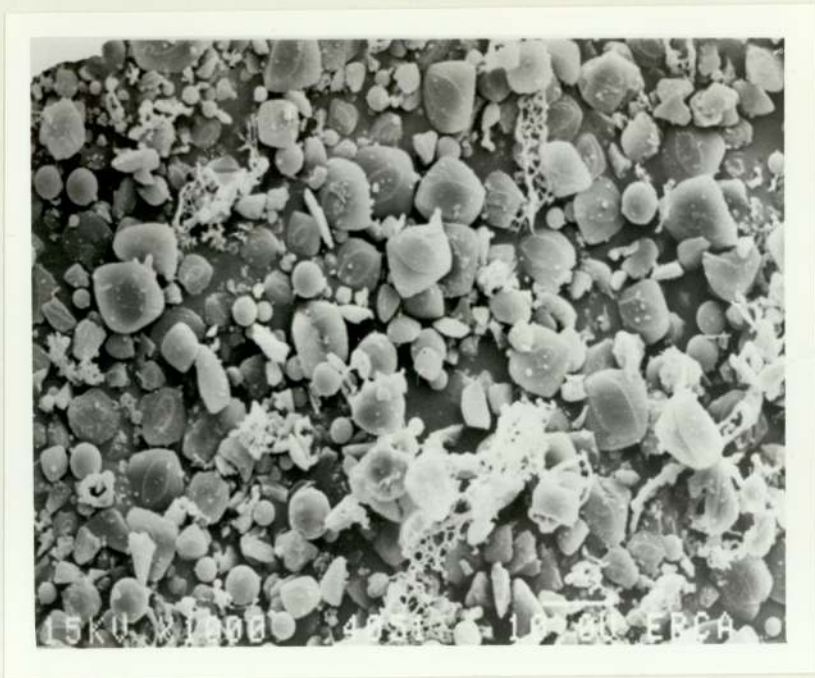




Figure A12.5: Run 51 large crystals fraction sediment



Figure A12.6: Run 51 large crystals fraction sediment

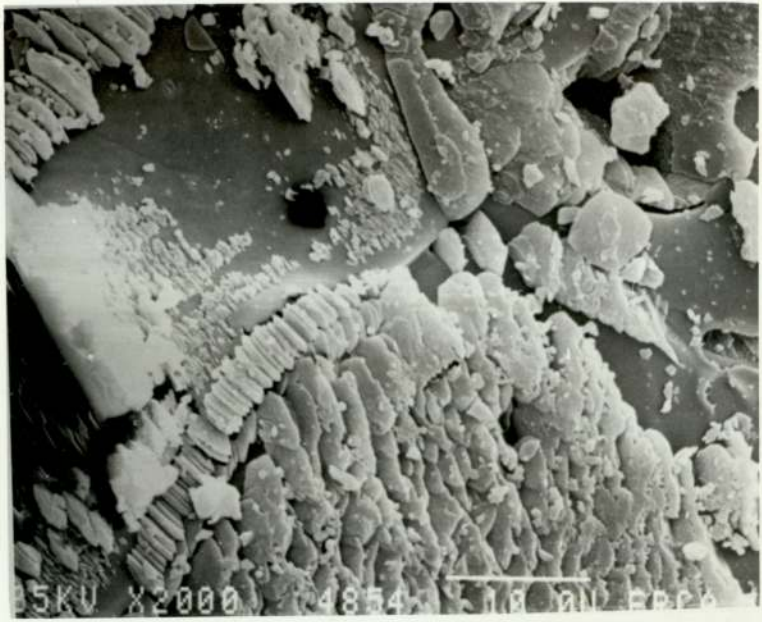




Figure A12.7: Run 51 large crystals fraction sediment



Figure A12.8: Run 51 large crystals fraction sediment



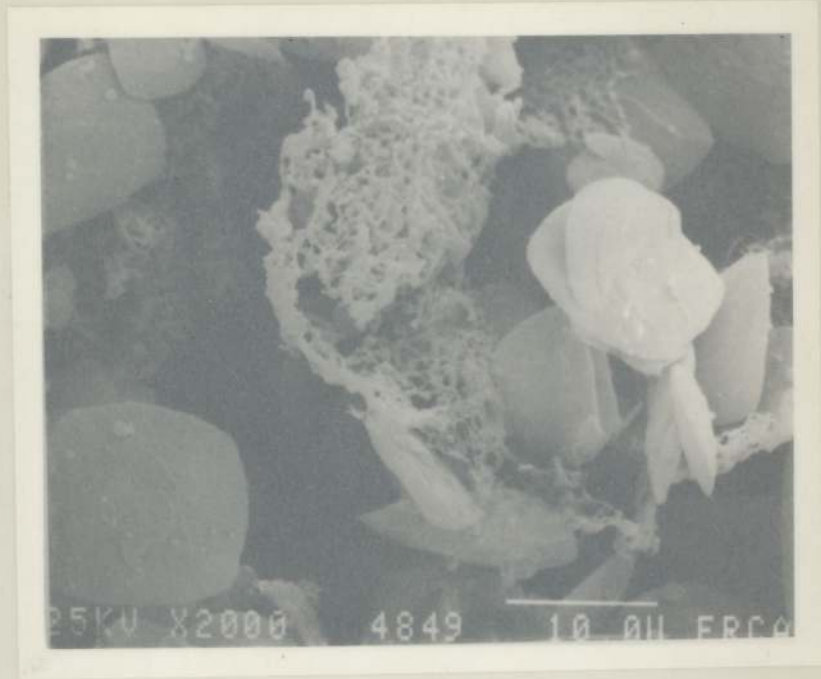


Figure A12.9: Run 51 fine crystals fraction sediment



Figure A12.10: Run 52 fine crystals fraction sediment



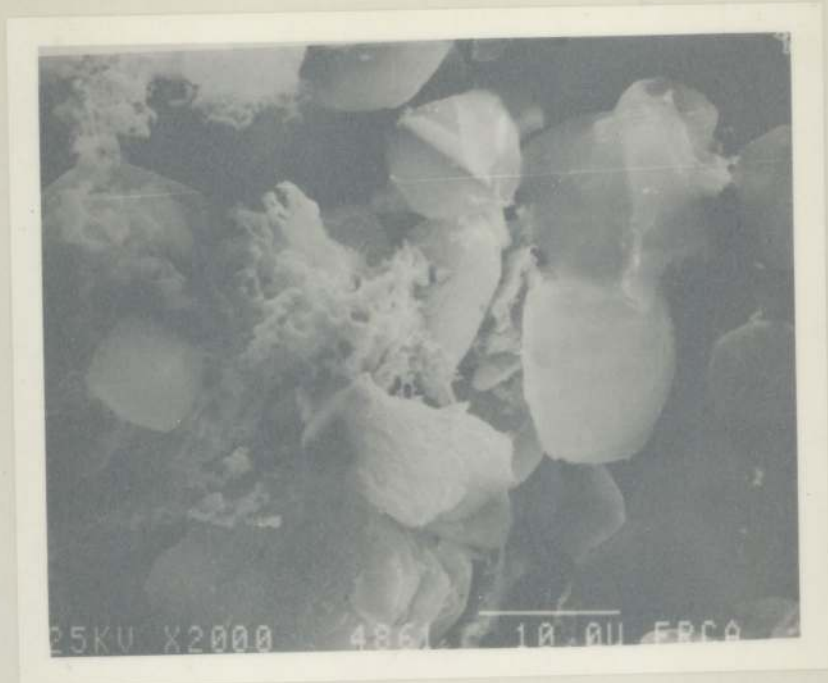


Figure A12.11: Run 53 fine crystals fraction sediment



Figure A12.12: Run 54 fine crystals fraction sediment

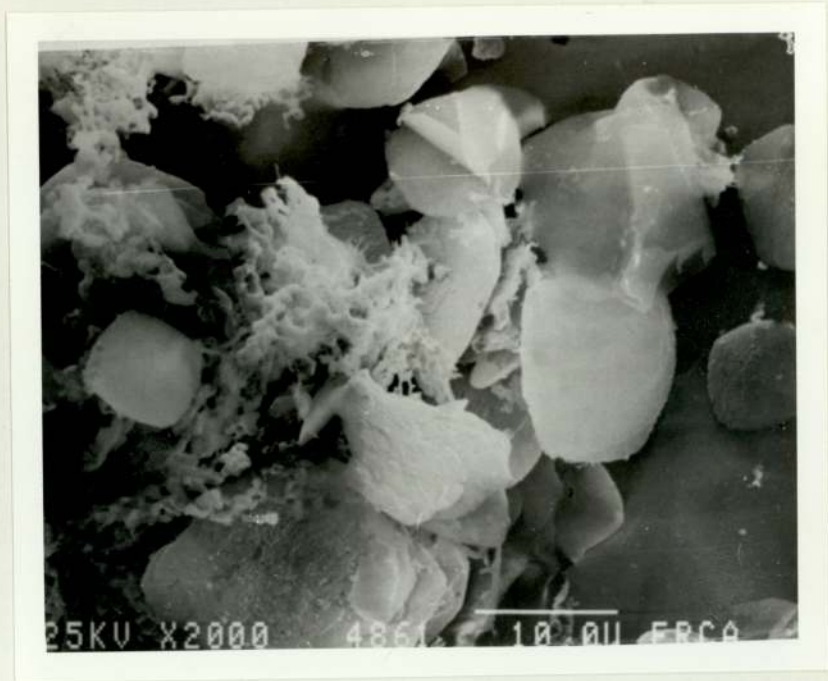




Figure A12.13 Run 55 fine crystals fraction sediment

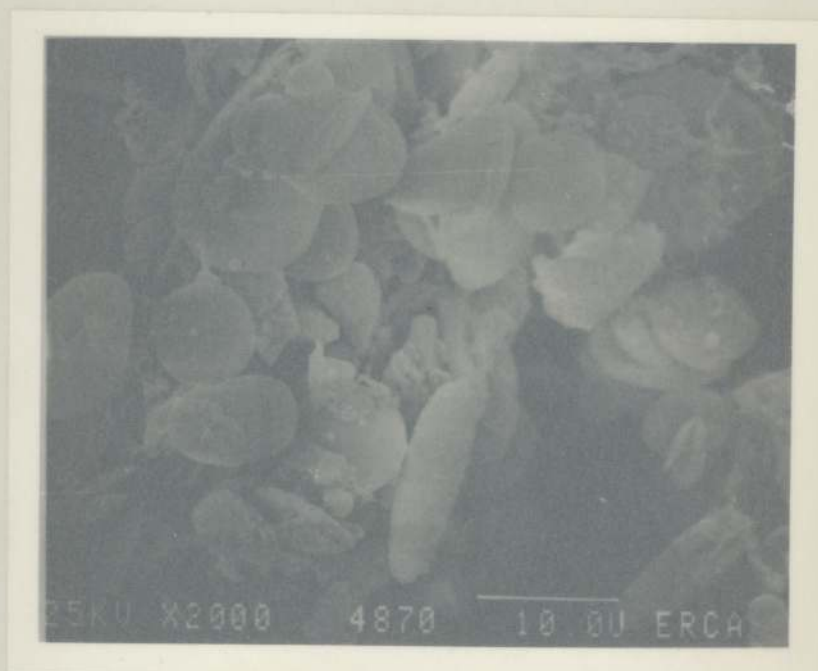


Figure A12.14: Run 56 fine crystals fraction sediment





Figure A12.15: Run 57 fine crystals fraction sediment

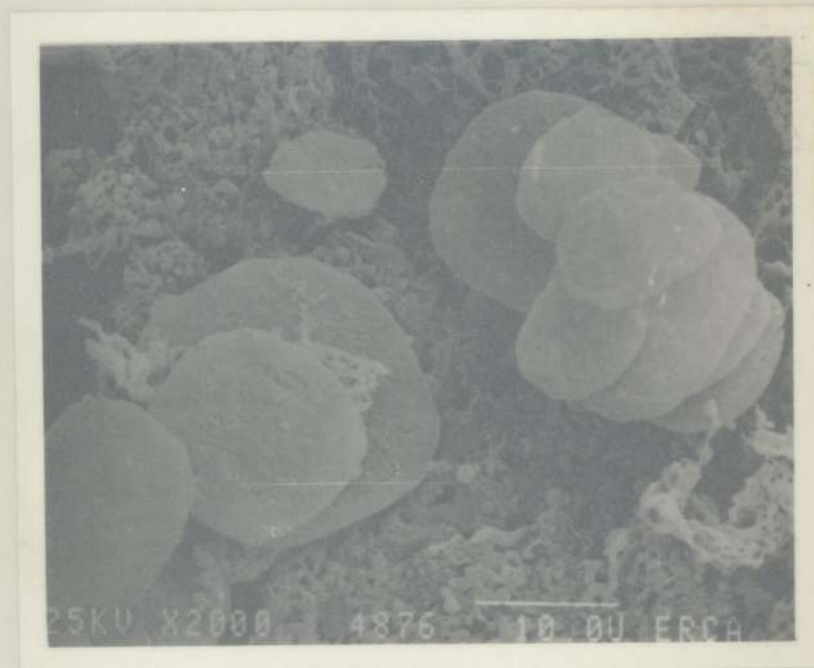


Figure A12.16: Run 58 fine crystals fraction sediment





Figure A12.17: Run 59 fine crystals fraction sediment

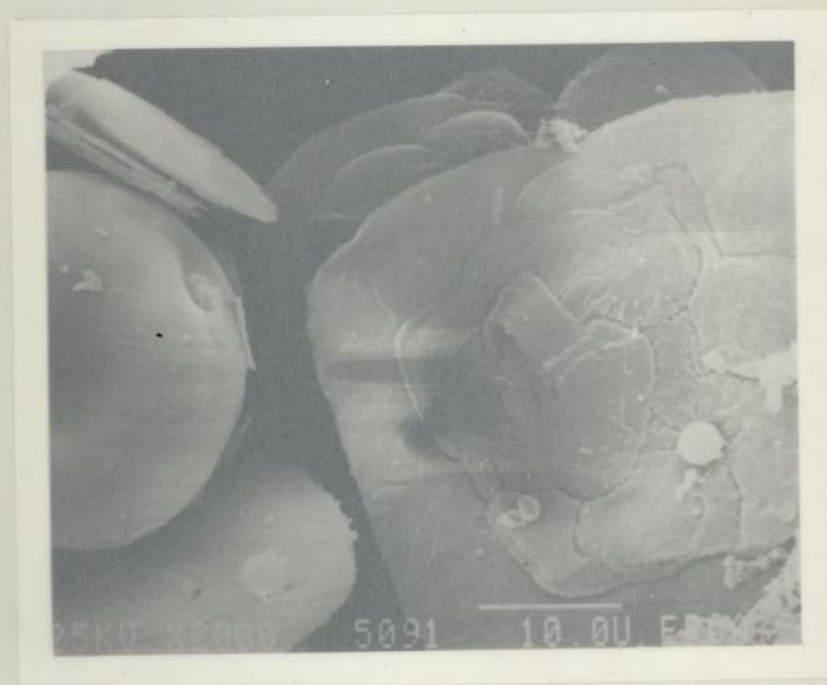


Figure A12.18: Run 59 fine crystals fraction sediment





Figure A12.19: Run 59 large crystals fraction sediment

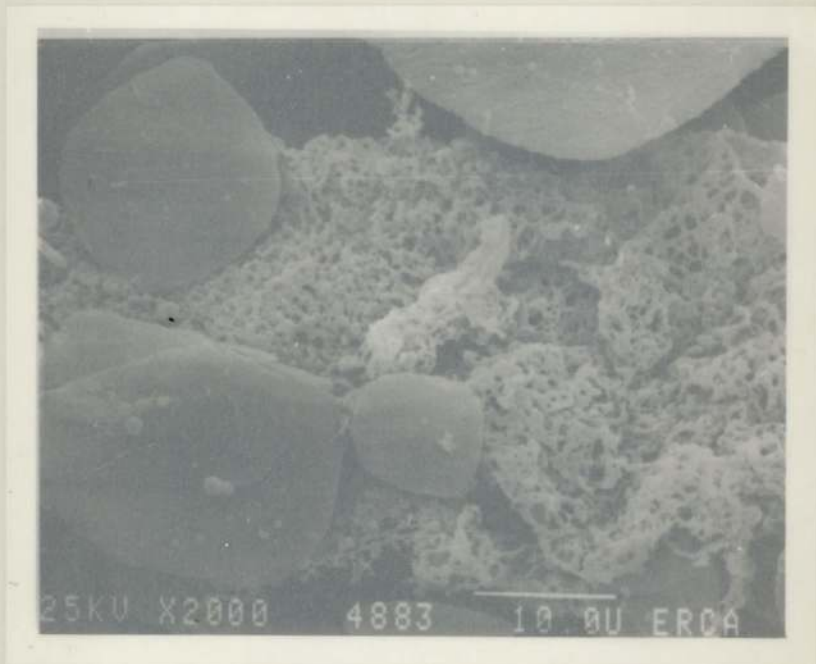


Figure A12.20: Run 60 fine crystals fraction sediment

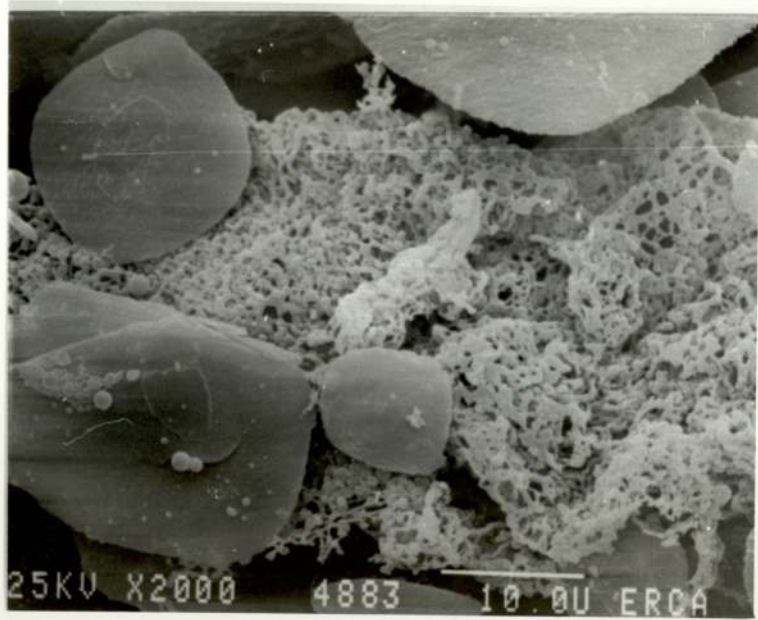
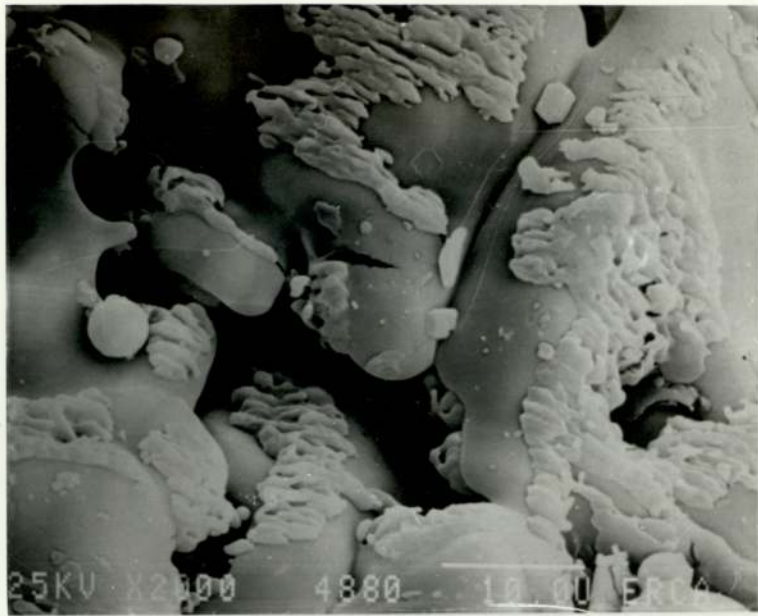




Figure A12.21: Sediment collected from centrifuge tubes after centrifuge tests were carried out on stored product samples

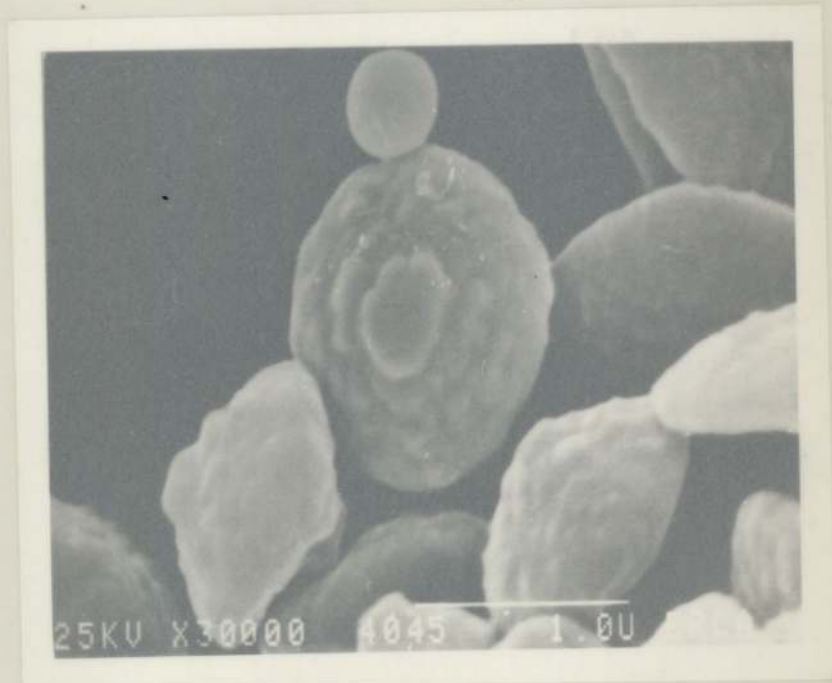
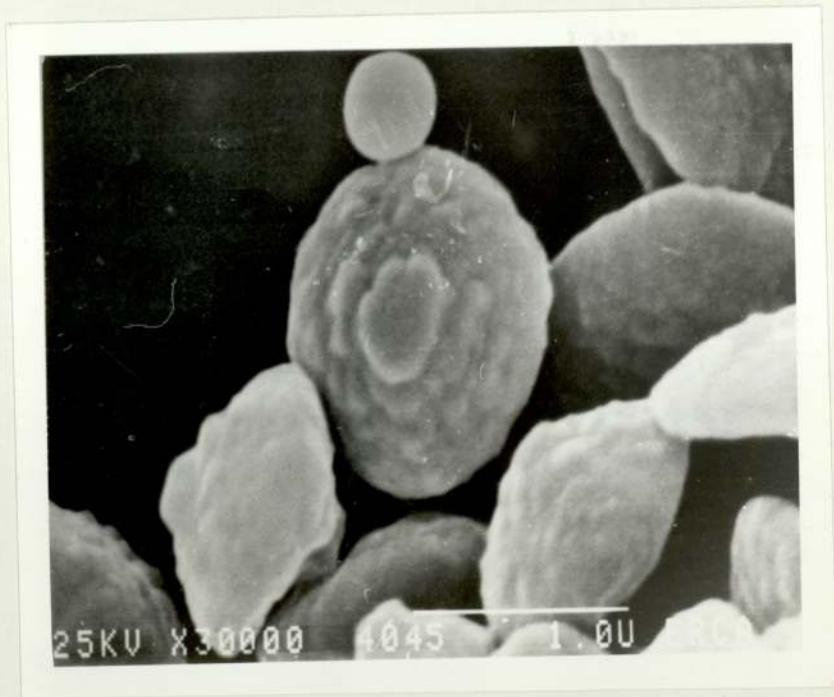
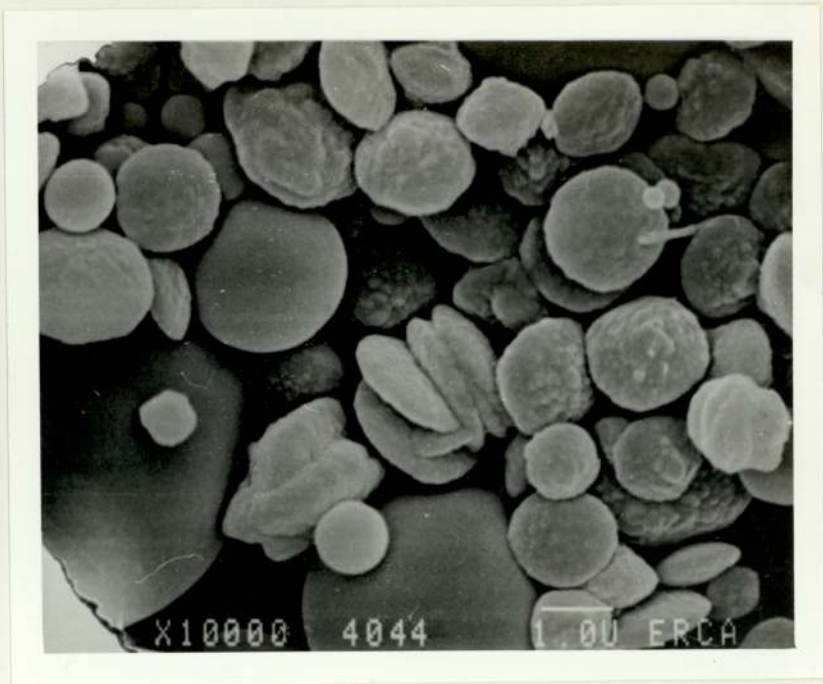


Figure A12.22: Sediment collected from centrifuge tubes after centrifuge tests were carried out on stored product samples



APPENDIX 13

NOMENCLATURE USED IN THE THESIS

The symbols that were used in the main text and in the appendices of this thesis were all defined specifically at the time of their use in the appropriate equations and sections. However, they are all listed in this appendix together with a brief description of their meaning and units. These meanings are to be taken unless otherwise stated in the proper equation or section.

<u>SYMBOL</u>	<u>DESCRIPTION</u>
A, A_T	The surface of a crystal face, single crystal, or a whole population of crystals (m^2).
A	The absorbance of a component, in equation (8.28) in the IR analysis section.
a	The order of the reaction with respect to PIBSA.
a_n	The surface area occupied by a single nucleus.
B	A complex temperature dependent constant in the BCF growth model, equation (2.25)
B_H	Homogeneous nucleation rate ($\frac{1}{s}$).
B_N	Numerical nucleation rate ($\frac{1}{s}$).
B_P	Primary heterogeneous nucleation rate ($\frac{1}{s}$)
b	The order of reaction with respect to PE.
b	The volume of the TBAH base needed for a blank titration, used in equation (A3.1) in Appendix 3, (cm^3)
C	Concentration of a component in solution, ($kmole/m^3$, or $moles/dm^3$, or $equivalents/dm^3$).
C_A	Concentration of PIBSA (or the anhydride) in the reaction mixture ($equivalents/dm^3$).

<u>SYMBOL</u>	<u>DESCRIPTION</u>
C_A^0	The initial concentration of PIBSA in the reaction mixture (equivalent/dm ³).
C_B	Concentration of PE in the reaction mixture (equivalents/dm ³).
C_B^0	The initial concentration of PE in the reaction mixture (equivalents/dm ³).
C_e	Concentration of the esters in the reaction mixture (equivalents/dm ³).
C_i	The solute concentration at the crystal-solution interface (kmole./m ³ , kg/m ³).
C_r	Solubility of spherical particles of radius r, (kmole/m ³).
C_∞	The solubility of large particle (as $r \rightarrow \infty$), (kmole/m ³).
C^*	The equilibrium solubility of the solute, (kmole/m ³ , kg/m ³ , kg/kg).
C_r^*	The maximum solubility of spherical particles at the critical radius r^* , (kmole/m ³).
ΔC	The concentration deriving force ($C-C^*$) in crystallization, (kmole/m ³ , kg/m ³).
d	Equivalent diameter of a particle, (μm).
d_{crit}	Critical diameter of nucleus, in primary homogeneous nucleation (μm , \AA).
d_p	Projected area diameter of a particle, measured by lazer size analysis (μm).
d_s	The equivalent diameter of the particles, measured by sieve size analysis (μm).
E	Activation energy of reaction (kcal./mole).
F_1, F_2	Dimensionless constants in equation (2.33).
f_i	The crystal mass fraction in a given size range.
$\Delta G_{\text{crit.}}$	Critical free energy for homogeneous nucleation (kJ/kmol).

<u>SYMBOL</u>	<u>DESCRIPTION</u>
h	Height of a crystal growth step (μm).
I	Radiation or light intensity transmitted by the sample (Watt).
I_o	Radiation or light intensity incident upon the sample (Watt).
K_G	An overall crystal growth coefficient (its units depends on the order of the overall crystal growth process, for a first order process the units are m/s).
K_H	Homogeneous nucleation rate constant in the expression for the steady state homogeneous nucleation rate ($\frac{1}{S}$).
K_P	Primary heterogeneous nucleation rate constant ($\frac{1}{S}$ if the dependence of the primary nucleation rate on the supersaturation ratio is linear).
k	The reaction rate constant of the PIBSA/PE esterification reaction, $(\text{equivalent}/\text{dm}^3)^{1-n} \cdot \text{hr}^{-1}$, where n is the order of the reaction).
k_1, k_2, k_3, k_4	Reaction rate constants, their units depend on the order of the respective reaction.
k_o	The frequency factor of the rate expression.
k_a	Surface area shape factor for the crystals.
k_d	The mass transfer coefficient by diffusion (m/s).
k_m	Mass transfer coefficient (m/s).
k_r	The rate constant for the surface reaction step in crystallization (m/s for a first order reaction step).
k_v	Volumetric shape factor for the crystals.
L	The linear characteristic dimension of the particles (μm).
\bar{L}	An adjustable parameter of the particle size distribution, equals to the arithmetic mean for the normal distribution, and to the geometric mean for the log-normal distribution (μm).

<u>SYMBOL</u>	<u>DESCRIPTION</u>
$L_{0.5}$	The size corresponding to a value of 0.5 mass fraction on the cumulative distribution plot (μm).
$L_{0.159}$	The size corresponding to a value of 0.159 mass fraction on the cumulative distribution plot (μm).
$L_{0.841}$	The size corresponding to a value of 0.841 mass fraction on the cumulative distribution plot (μm).
l	The length of the absorption cell in IR analysis (m).
M_T	Total crystal mass in a crystal population (kg).
m	Mass of solute deposited on a crystal surface (kg).
m_p	The exponential of the concentration deriving force for the primary heterogeneous nucleation rate in equation (2.22).
m_r	The order of the surface reaction step for the crystallization process, equation (2.28).
m_s	The weight of one particle in a population (g).
N	A statistical quantity in equations (8.22) and (8.23) denoting the number of experimental points.
N	The normality of the TBAH base used in the titrations, in equation (A3.1) in Appendix 3, (equivalents/dm ³).
N_A	The number of equivalents of the PIBSA (or the anhydride) present in the reaction mixture at any time (equivalents).
n	The overall order of the PIBSA/PE esterification reaction, used as such in the whole bulk of the thesis.
n	The overall order of the crystal growth process, used as such only in equations (2.29) and (2.32).
$n(L)$	The population density of particles of size L in a system, (m ⁻⁴).
P_a	The total acid peak height, used in IR analysis (mm).

<u>SYMBOL</u>	<u>DESCRIPTION</u>
P_a^o	The initial total acid peak height (mm).
P_e	The ester peak height, in IR analysis (mm).
q	The electric charge on the surface of a particle (kJ.m).
R	The universal gas constant (kcal/gmole. o k).
Re	Reynolds number ($Re = \rho Lv/\mu$).
R_G	Crystal growth rate (kg/s, Kmole/s).
r	Radius of a particle (m, μ m).
r^*	The critical radius of a small particle corresponding to the maximum solubility (μ m).
$(-r_A)$	The rate of PIBSA conversion into esters (equivalents/dm 3 .hr).
(r_T)	The rate of esters formation (equivalents/dm 3 .hr).
$(-r_{H_2})$	The rate of hydrogen consumption (Kmole/m 3 .S, mole/dm 3 .S, mole/dm 3 .hr).
S	The absorptivity in, equation (8.27) in the IR analysis, (m 2 /Kmole, m 2 /mole, depends on the units of the concentration of the absorbing component).
S	Supersaturation ratio (C/C^*).
S_r	Relative supersaturation ($(C-C^*)/C^*$).
Sc	Schmidt number ($Sc = \mu/\rho D_v$).
Sh	Sherwood number ($Sh = k_L L/D_v$).
T	Absolute temperature (o K).
T	Transmittance, the fraction of incident radiation transmitted by the component, in equation (8.27) in the IR analysis.
TAN	Total Acid Number of the reaction mixture (mgkoH/g sample).
TAN o	The initial Total Acid Number of the reaction mixture (mgkoH/g).

<u>SYMBOL</u>	<u>DESCRIPTION</u>
TAN	The residual Total Acid Number of the reaction mixture (mgkoH/g).
TAN _R	The relative Total Acid Number of the reaction mixture (TAN _R = TAN - TAN [∞]), (mgkoH/g).
TAN _R ⁰	The initial relative Total Acid Number of the reaction mixture (mgkoH/g).
t	Time (hr, min, s).
t _s	The flow time of a standard fluid used in the calibration of a viscometer (used exclusively in Appendix 5), (s).
V	Volume of the reaction mixture (dm ³).
V	Volume of the TBAH base needed to titrate the reaction mixture sample, used in equation (A3.1) in Appendix 3 (cm ³).
V _m	Molar Volume of solute (m ³ /mole).
w	The weight of the reaction mixture sample to be analysed for TAN (g).
X _A	The fractional conversion of the PIBSA into esters.
X ₁	The mass fraction of pentaerythritol in solution, used exclusively in the solubility equation (3.1).
x _i	A statistical quantity used in equations (8.22) and (8.23) to denote the x-coordinate of a point.
y _i	A statistical quantity used in equations (8.22) and (8.23) to denote the y-coordinate of a point.
Z _a , Z _e	Proportionality constants in equations (8.30), and (8.29) respectively (equivalent/dm ³ .mm).
Z ₁ , Z ₂	Constant indices in equation (2.33).
α	PE/PIBSA initial equivalent ratio (C _B ⁰ /C _A ⁰).
γ	The ratio of the initial PIBSA concentration to the initial relative TAN (C _A ⁰ /TAN _R ⁰), [($\frac{\text{equivalent}}{\text{dm}^3}$) / ($\frac{\text{mgkoH}}{\text{g}}$)]

<u>SYMBOL</u>	<u>DESCRIPTION</u>
μ_i	The arithmetic mean for a given size band i (μm).
$\bar{\mu}$	The mass weighted mean diameter of the final crystal size distribution (μm).
ν	Kinematic viscosity of a fluid (m^2/s).
ν_s	Kinematic viscosity of a standard fluid ($\text{m}^2\bar{\text{s}}$).
ρ	Density of the material of the particle (kg/m^3).
σ	The standard deviation for the final CSD (μm).
σ_s	The surface energy of a nucleus or a particle (kJ/m^2).
ψ	The dielectric constant.

REFERENCES

1. Berlow, E., Barth, R.H., Snow, J.E.
'The Pentaerythritols'
Reinhold Publishing Corporation 1958
Chapman and Hall Ltd., London.
2. CHEMCELL S.A.
'Monopentaerythritol'
Specification bulletin
CA-22-9.
3. U.S. Patent No. 2, 371, 333
Shell Oil Company
March 13, 1945.
4. B.P. Chemicals
Hyvis Polybutenes Technical Service
Chemical Reactions 1.
5. Personal Communication
Esso Research Centre
Abingdon, 1981.
6. G.B. Patent No. 2, 062, 672A
Patented in U.K. 1980.
7. U.S. Patent No. 4, 234, 435
Lubrizol Corporation 1980.
8. U.S. Patent No. 3, 936, 480
Patented 1976.
9. U.S. Patent No. 3, 522, 179
Lubrizol Corporation 1970.
10. U.S. Patent No. 3, 542, 680
Lubrizol Corporation 1970.
11. Brit. Patent No. 1, 441, 600
1976.
12. U.S. Patent No. 4, 239, 633
1980.
13. U.S. Patent No. 3, 542, 678
Lubrizol Corporation 1970.
14. EUR. PAT. No. 0051998
1981.
15. Prigogine, I.
Struct. Dyn. Chem. Proc. Symp.
1977 (pub. 1978) 172-86.

16. Lewis, E. S.
Tech. Chem. (N.Y.)
1974, 6 (Invest. Rates Mech. React., 3rd Ed. pt.1), 1-12.
17. Pilling, M.T.
Oxford Chem. Ser.
1975, 22, 122pp.
18. Sharp, J.H.
Differential Therm. Anal.
1972, 2, 47-77.
19. Jones, J.R.
Annu. Rep. Progr. Chem. Sect. A.
1971 (pub. 1972) 68, 101-21.
20. Caneda, Rodolfo V.
Ser. Quim-Programa Reg. Desarrollo Cient. Tecnol.
1978, 18, 1114pp.
21. Townshend, Alen
proc. Anal. Div. Chem. Soc.
1975, 12(9), 241-3.
22. Lin, K.H.
Annu. Rev. Ind. Eng. Chem.
1974, 2, 296-344.
23. Levenspiel, O.
'Chemical Reaction Engineering'
2nd Ed. 1972, John Wiley & Son.
24. Denbigh, K.G.
'The Principles of Chemical Equilibrium'
Cambridge University Press 1955.
25. Olah, G.A.
Science, 168, 1298 (1970).
26. Rice, F.O. and Herzfield, K.F.
J. Am. Chem. Soc.,
56, 284 (1934).
27. Lindemann, F.A.
Trans. Faraday Soc.
17, 598 (1922).
28. Laidler, K.J.
'Chemical Kinetics'
2nd Ed. 1965, McGraw-Hill, New York.
29. Words, S. and Ahlberg, P.
Acta Chem. Scand.
1970, 24, 618.

30. Ahlberg, P.
Acta Chem. Scand.
1970, 24, 1883.
31. Word, S.
Acta Chem. Scand.
1971, 25, 336.
32. Bodenstein, M. and Lind, S.C.
z. Physik. Chem.
(Leipzig), 57, 168 (1906).
33. Levenspiel, O., Weinstein, N.J. and Li, J.C.R.
Ind. Eng. Chem.
48, 324 (1956).
34. Walpole, R.E. and Myers, R.H.
"Probability and Statistics for Engineers and Scientists".
2nd Edition, Macmillan Publishing Co. Inc., New York, 1978.
35. Orudzheva, T.M., Guseinov, N.F., Gasarova, sh.D.
Issled. V obl. Sinteza Polimer. i Monomern.
Produktov 1977, 52-7.
36. Belov, P.S., Zavorotnyi, V.A., Korenev, K.D.
Neftepererab, Neftekhim
1980 (10), 32-3.
37. Arranz, F, Sanchezchares, M, Gil, F.
Angew Makromol Chem.
1980, 92, 121-32.
38. Sadovnikov, A.I., Kuritsyn, L.V.
Izu. Vyssh. Uchebn. Zaved., Khim. Khim. Teknol.
1981, 24(7), 847-50.
39. Khardin, A.P., Novakov, I.A., Radchenko, S.S., Voskresenskaya, I.A.
Zh. Orgkhim
1981, 17(8), 1674-7.
40. Bouvier, Jean Marie; Bruneau, Claude Marcel.
Bull. Soc. Chim. Fr.
1977, (11-12, pt. 1), 1093-8.
41. Fadeev, E.M., Livshits, R.M., Klygina, R.V.
Lokokras. Mater. Ikh. Primen
1981, (1), 10-11.
42. Ostrizhko, F.N., Yuminov, V.S., Panshin, Yu.A.
Sintez Pentaplasta, L.
1979, 5-8.
43. Popov, A.A., Nazarov, V.I., Kuznetsova, M.N., Leshchiner, D.R.
Pererab. Nefti
1980, 36, 41-5.

44. Popov, A.A., Nazarov, V.I., Kuz netsova, M.N., Leshchiner, D.R.
Sintetich. Smazoch Masla, Rabochie Zhidkosti
i ikh kom ponenty, M. 1980, 41-5.
45. Allen, R.H. et al.
 - (a) J. Am. Chem. Soc.
81, 42 (1959)
 - (b) *ibid.* 81, 5289 (1959)
 - (c) *ibid.* 82, 4853 (1960)
 - (d) *ibid.* 82, 4856 (1960)
46. Meguerian, G. and Clapp, L.B.
J. Am. Chem. Soc.
73, 2121 (1951).
47. Taft, R.W. and Cook, E.H.
J. Am. Chem. Soc.
81, 46 (1959).
48. Kubulu, G. and Matell, A.E.
J. Am. Chem. Soc.
1982, 104, 6602-6609.
49. Ostwald, W.
'Lehrbuck' Vol. II
Leipzig, Englemann 1896-1902.
50. Mullin J.W.
"Crystallization" 2nd Ed.
Butterworths, London 1972.
51. Miers, H.A.
J. Inst. Metals
37, 331, 1927.
52. Nyvlt, J.
J. Crystal Growth
3/4, p377, 1968.
53. Nyvlt, J., Rychly, R., Gottfried, J. and Wurzelova, J.
J. Cryst. Growth
Vol. 6, 151-162, 1970.
54. Storm, T.D., Hazelton, R.A. and Lahti, L.E.
J. Cryst. Growth
Vol. 7, 55-60, 1970.
55. Mullin, J.W. and Jancic, S.J.
Trans. Instn. Chem. Engrs.
Vol. 57, 188-193, 1979.
56. Freundlich, H.
"Colloid and Capillary Chemistry", p155,
New York, Duttan & Co., 1922.

57. Knapp, L.F.
Trans. Faraday Soc.
17, 457, (1922).
58. Dundon, M.L.
J. Amer. Chem. Soc.,
45, 2658, (1923).
59. Roller, J.
Phys. Chem.
35, 1133, 1931.
60. Hulett, G.A.
J. Am. Chem. Soc.
27 (1905), 49.
61. Glew, D.H. and Hildebrand, J.H.
J. Phys. Chem.
60, 616 (1956).
62. Kertes, A.S., Levy, O. and Markovits, G.Y.
in 'Experimental Thermodynamics'. Vol. 2, Eds. Le Neindre, B.
and Vodar, B. Butterworths, London, p.725-748, 1975.
63. Zimmerman, Howard K, Jr.
Chem. Rev.
51 (1952), 25-65.
64. James, A.M.
Practical Physical Chemistry 2nd Edition.
Churchill, London, p.116-128, 1967.
65. Rao, C.N.R.
'Ultraviolet and Visible Spectroscopy' 3rd Edition.
Butterworths, London 1975.
66. Falangas, E.
Ph.D. Thesis.
University of Aston in Birmingham 1980.
67. DeJong Esso J.
in: Proc. 7th Symp. Ind. Cryst., Ed.: DeJong, E.J. and Jancic, S.J.
North Holland, p.3-17, 1979.
68. Mullin J.W.
Chem. Ind.
No. 8 (3, May) p.372-377, 1980.
69. Nielsen A.E.
"Kinetics of Precipitation"
Pergamon Press 1964.
70. Ohara M and Reid R.C.
"Modeling Crystal Growth Rates from Solution"
Prentice-Hall, New Jersey 1973.

71. R. F. Strickland-Constable
The Chemical Engineer
Dec. 1973, p.603.
72. R. F. Strickland-Constable
AIChE Symp. Ser.
Vol. 68, (121), p.1-7, 1972.
73. Garside and Davey
Chem. Eng. Commun.
Vol. 4, p.393-424, 1980.
74. Botsaris, G.D.
in: Proc. 6th Symp. Ind. Cryst., Ed.: Mullin J.W.
Plenum Press, New York. p.3-22, 1976.
75. Nyvlt, J.
"Industrial Crystallization from Solution"
Butterworths, London, 1971.
76. R. F. Strickland-Constable
in: Proc. 6th Symp. Ind. Cryst., Ed.: Mullin, J.W.,
p.33-40, 1976.
77. Khambaty, S. and Larson, M.A.
Ind. Eng. Chem. Fundam.
Vol. 17, No. 3, p.160-164, 1978.
78. Denk, E.G.Jr. and Botsaris, G.D.
J. Crystal Growth
13/14 (1972), 493-499.
79. R. F. Strickland-Constable
J. Chem. Soc., Farad. Trans. I.,
75, 921 (1979).
80. Ottens, E.P.K., Janse, A.H. and DeJong E.J.
J. Crystal Growth
13/14 (1972) 500-505.
81. Garabedian, H and Strickland-Constable, R.F.
J. Crystal Growth
13/14 (1972) 506-509.
82. Garabedian, H. and Strickland-Constable, R.F.
J. Crystal Growth
12, (1972) 53-56.
83. Rusli, Larson and Garside
AIChE Symp. Ser.
No. 193, Vol. 76, p.52-58, 1980.
84. Bujac, P.D.B.
in: Proc. 6th Symp. Ind. Cryst., Ed.: Mullin J.W.,
p.23-31, 1976.

85. Van't Land, C.M. and Wienk, B.G.
in: Proc. 6th Symp. Ind. Cryst.,
ed.: Mullin, J.W., p.51-60, 1976.
86. Garside, J.
in: Proc. 7th Symp. Ind. Cryst.,
ed.: De Jong, E.J. and Jancic, S.J.
North Holland, p. 143-151, 1979.
87. Mullin, J.W.
in: Proc. 7th Symp. Ind. Cryst.,
ed: De Jong, E.J. and Jancic, S.J.
North Holland, p.93-103 (1979).
88. Bennema, P.
in Proc. 6th Symp. Ind. Cryst.,
ed.: Mullin, J.W., p.91-112, 1976.
89. Bennema, P.
in Proc. 7th Symp. Ind. Cryst.,
ed.: De Jong, E.J. and Jancic, S.J.
North Holland, p. 115-133, 1979.
90. Walton, A.G.,
"The Formation and Properties of Precipitates"
Interscience, New York, 1967.
91. Burton, W.K., Capreva, N. and Frank, F.C.
Phil. Trans. Roy. Soc.
Vol. 243, p.299-358, 1951.
92. Nielsen, A.E.
CROATICA CHEMICA ACTA
53(2), 255-79, 1980.
93. Garside, J.
Chem. Eng. Sci.
Vol. 26, p.1425-1431, 1971.
94. Ranz, W.E. and Marshall, W.R.
Chem. Eng. Progr.
Vol. 48(3), p.141-146, 1952.
95. Ranz, W.E. and Marshall, W.R.
Chem. Eng. Progr.
Vol. 48(4), p.173-180, 1952.
96. Karpinski, P.H.,
Chem. Eng. Sci.
Vol. 35, p.2321-2324, 1980.
97. Row, P.N., Claxton, K.T. and Lewis, J.B.
Trans. Inst. Chem. Engrs.
Vol. 43, p.14-31, 1965.

98. Levins, D.M. and Glastonbury, J.R.,
Trans. Inst. Chem. Engrs.
Vol. 50, p.132-146, 1972.
99. Bourne, J.R. and Davey, R.J.
J. Crystal Growth
36, 278-286 (1976).
100. Bourne, J.R. and Davey, R.J.
J. Crystal Growth
36, p.287-296, (1976).
101. Bourne, J.R. and Davey, R.J.
J. Crystal Growth
39, p.267-274, (1977).
102. Bourne, J.R.
AIChE Symposium Series
No. 193, Vol. 76, p.59-64, 1980.
103. Tavare, N.S, Garside, J. and Chivate, M.R.
Ind. End. Chem. Process Des. Dev.
19(4), p.653-65, 1980.
104. Tavare, N.S. and Chivate, M.R.
J. Chem. Eng. of Japan
Vol. 13, No. 5, p.371-379, 1980.
105. Mullin, J.W. and Nyvlt, J.
Chem. Eng. Sci.
26, p.369-77, 1971.
106. Jones, A.G.
Chem. Eng. Sci.
Vol. 29, p.1075-1087, 1974.
107. Blackadder, D.A.
Chem. Engr. p.303-320, Dec. 1964.
108. Nienow, A.W., Bujac, P.D.B. and Mullin, J.W.
J. Crystal Growth
Vol. 13/14, p.488-492, 1972.
109. Nienow, A.W.
in: Continuing Education Course,
Industrial Crystallization - Current developments and trends -
31 March-2 April 1982, University College, London.
110. Nienow, A.W.
Trans. Instn. Chem. Engrs.,
Vol. 54, p.205-207, 1976.
111. Botsaris, G.D.
in: Proc. 8th Symp. Ind. Cryst.,
ed.: Jancic, S.J. and De Jong, E.J.
North Holland, p.109-116, 1982.

112. Rehmatallah, S., Clatworthy, B., Wahab, A. and Creasy, D.E.
J. Appl. Chem. Biotechnol.
26, p.30-36, 1976.
113. Ziak, J.
Chem. prum.
33(6), p.300-2, 1983.
114. Rogers, J.F. and Creasy, D.E.
J. Appl. Chem. Biotechnology
24, p.171-180, 1974.
115. Wyckoff, R.W.G.
'Crystal Structure'
Wiley, Chichester, 2nd edn., 5, 7, 1966.
116. Nitta, I. and Watanabe, T.
Nature, 140, p.364 (1937).
117. Marrinan, H.J. and Mann, J.
J. Appl. Chem., 4, Part 4, p. 204-11, (1954).
118. Wells, A.F.,
Phil. Mag., 37, p.184 (1946).
119. Frevel, L.K. et al.,
Ind. Eng. Chem. (Analy.),
18, 83 (1946).
120. NAJIM, N.A.R.,
M.Sc. Thesis
University of Aston in Birmingham (1981).
121. Rogers, J.F.
Ph.D. thesis
University of Aston in Birmingham (1969).
122. Thomas, J.M. and Evans, J.R.N.,
Solid State Communications
9, (13), 1163 (1971).
123. U.S. Patent No. 2,299,048.
by: Wyler, J.A. and Warnett, E.A.,
(Trojan Powder Company), 1942.
124. Cook, E.G.,
Paint Manufacture, 18, 125 (1948).
125. Kuznetsova, L.I. and Gavrilova, I.V.,
'Growth of Crystals'
Consultant Bureau, New York, 3, 203 (1962).
126. Rogers, J.F., Farazmand, H. and Creasy, D.E.,
J. Chem. Eng. Data, 19, p.118, 1974.
127. Bradley, R.S. and Cotson, S.,
J. Chem. Soc., p.1684-88, 1953.
128. Nitta, I., Seki, S. and Suzuki, K.,
Bull. Chem. Soc. Japan
24, p.63-39, (1951).

129. Llewellyn, F.J. et al.,
J. Chem. Soc., 140, p.883, (1937).
130. Woolf, L.A.,
J. Phys. Chem., Wash.
67, p.273, 1963.
131. Sporek, K. and Williams, A.F.,
Analyst, 80, p.29-36, (1955).
132. Exxon Research and Engineering Company
Esso Research Centre, Abingdon
Analytical Method-Specification
'Analysis of pentaerythritol by gas chromatography'.
133. Rehmatullah, S.,
Ph.D. thesis
University of Aston in Birmingham 1973.
134. Whetstone, J.,
Research Supplement, 2-4, p.194, (1949).
135. Esso Chemical Research Centre,
Abingdon, June 1979
"The updated version of the ECA 7540X process data package".
136. Dicalite Industrial Filtration Manual
Technical Bulletin B-15E.
137. Brit. UK Patent No. 2,002,393.
by Cane, C. and Yeomans, B.
(Orbis Ltd.), 1979.
138. Exxon Chemical Company
"Process Development Work on PIBSA/PE Esters".
Rep. No. EAL-3M-69.
by G. J. Snell, 1969.
139. Exxon Chemical Company, Technology Division,
"PIBSA/PE Chemistry"
Doc. No. 79 PM 1750, 1979.
140. Hawksley, P.G.W.
B.C.U.R.A. Bulletin
Vol. 15(4), p.105-146, (1951).
141. Hawksley, P.G.W.
B.C.U.R.A. Bulletin
Vol. 16(4), p.117-147, (1952).
142. Hawksley, P.G.W.
B.C.U.R.A. Bulletin
Vol. 16(5), p.181-209, (1952).
143. Allen, T.
'Particle Size Measurement', 3rd edition
Chapman and Hall, London, 1980.

144. Allen, T.
Lab. Equip. Digest,
p.81-87, Feb. 1980.
145. Heywood, H.
Proc. Inst. Mech. Eng.,
Vol. 140, p.257-347, 1938.
146. Coulson, J.M. and Richardson, J.F.
'Chemical Engineering' Vol. 2, 3rd edition.
Pergamon, Oxford, 1978.
147. Leschonski, K.
Powder Tech.,
Vol. 24, p.115-124, 1979.
148. British Standards Institution
Specification for Test Sieves
BS 410, (1969).
149. British Standards Institution
Test Sieving,
BS 1796, (1976).
150. Coulter Electronic Ltd.
Instruction Manual for Coulter Counter
Model Z_B (Industrial), 1975
151. Allen, T. and Marshall, K.
'The Electronic Sensing Zone Method of Particle Size Measurement'.
University of Bradford, 1972.
152. De Silva, R.
Ph.D. Thesis
University of Aston in Birmingham 1982.
153. Randolph, A.D., White, E.T. and Che, C.D.L.
Ind. Eng. Chem. Process. Des. Dev.
20, p.296-503, 1981.
154. Brown, D.J., Dysart, S. and Felton, P.G.,
I. Chem. E. Jubilee Symp.
"Direct Measurement of Crystal Concentration and size using
Laser Light".
155. Malvern Particle Sizer Hand Book
(model 2200/3300), Version 1.3.
Malvern Instruments.
156. Kendall, D.N.
'Applied Infra-Red Spectroscopy'
Reinhold Publishing Corporation 1966.
157. Exxon Chemical Company
Esso Research Centre (Abingdon)
Inter-office correspondence
Job No. 18730220, 1975.
"Saponification Value of PIBSA".

158. Exxon Chemical Company
Paramin Technology Division
Esso Chemical Research Centre (Abingdon)
ECA 4461 Process technology attachment (II), 1975.
159. Exxon Chemical Company
Paramin Technology Division
Esso Chemical Research Centre (Abingdon).
ECA 4461 process technology attachment (I), 1975.
160. Perry, J.H. and Chilton, C.H.
'Chemical Engineering Handbook', 4th edition.
McGraw-Hill Book Company 1963.
161. Kot, Yu. D., Vdasenko, A.V., Savich, A.N. and Kravchuk, A.F.
Sakh. Prom. St. (8), p.31-2, 1982.
162. Shaw, D.J.,
'Introduction to colloid and surface chemistry'
2nd Edition, Butterworths, 1970.
163. Sheludko, A.,
'Colloid Chemistry',
New revised English Edition
Elsevier Publishing Company 1966.
164. Alexander, A.E. and Johnson, P.
'Colloid Science' Vol. I.
Clarendon Press, Oxford, 1949.
165. Boistelle, R.
NATO Adv. Study Inst. Ser., Ser. C.,
87 (Interfacial aspects phase transforms),
p.531-57,1982.
166. Pimentel and McClellan
'The hydrogen bond'
Freeman-San Francisco, 1960.
167. Vinogradov, S.N. and Linnell, R.H.
'Hydrogen bonding'
Van Norstrand Reinhold Company, 1971.
168. Covington, A.K. and Jones, P.
Proceedings of a symposium on equilibria and reaction
kinetics in hydrogen bonded solvent systems, 1968
169. Randolph, A.D. and Larson, M.A.,
"Theory of particulate processes".
Academic Press - New York and London 1971.
170. Fasoli, U. and Conti, R.
in: Proc. 6th Symp. Ind. Cryst.,
ed: Mullin, J.W., p.77-87, 1976.

171. Larson, M.A.
in: Proc. 8th Symp. Ind. Cryst.,
ed: Jancic, S.J. and De Jong, E.J.
North Holland, p.55-60, 1982.
172. Grootscholten, P.A.M., Asselbergs, C.J. and De Jong, E.J.
in: Proc. 8th Symp. Ind. Cryst.,
ed: Jancic, S.J. and De Jong, E.J.
North Holland, p.61-69, 1982.
173. Exxon Research and Engineering Company
Analytical Method - Specification
(a) 160.27, 1975.
(b) 77.081 revised 1977.
(c) 78.002 revised 1978.
(d) AM-S 160.25 (modified).